A Model for Calculating the Effective Diffusion Coefficient of Water Vapour in Snow

Rev Gavriliev
Melnikov Permafrost Institute SB RAS, Yakutsk, Russia

Abstract

A model is proposed for calculating the effective diffusion coefficient of water vapour for snow to account for its particulate structure. This is an improvement of the model presented in Gavriliev (2004), based on more adequate treatment of heat and mass transfer in snow. The model considers a cubic cell containing a spherical particle with point contacts on the apexes. The vapour concentration distribution on the particle surface is controlled by its temperature field. The temperature field is calculated based on generalized conduction theory for composite bodies, represented in the model by ice and vapour-air mixture. A quantitative relation between the diffusion coefficient of water vapour in snow and the snow density is established which provides a good explanation for the large scatter of experimental data. Because of the particulate structure of snow, the diffusion coefficient of vapour in snow is several times greater than the molecular diffusion coefficient of vapour in air (six times for compact snow).

Keywords: air; diffusion coefficient; snow; vapour flux.

Introduction

Experimental values for the vapour diffusion coefficient in snow, D_s, reported in the literature (Yosida 1950, Pavlov 1962, Kuvaeva 1966, Morozov 1967, Saveliev et al. 1967, Kolomyts 1971, Sommerfeld et al. 1986, Fedoseeva & Fedoseev 1988, Nikolenko 1988, Voitkovskii et al. 1988) scatter widely. There is also no agreement among authors whether this parameter depends on snow temperature, density or structure. The average D_s values measured in experiments vary from 0.17 to 1.20 cm^2/s, although the authors used the same standard methods, a crystallizer pan or cans. Some writers (Woodside 1958, Dyunin 1961) adopted the air diffusion coefficient of 0.20 cm^2/s at 0°C in their theoretical analyses of the heat and mass transfer in snow, assuming that the coefficients for vapour and air are approximately equal. The experimental results indicate, however, that the measured coefficients of diffusion of water vapour in snow are much larger than the molecular diffusion coefficient in air (4 to 6 times in Yosida [1950] and Pavlov [1962]). Yosida and Pavlov attribute this to the fact that in snow the water vapour is transferred not only by microscopic diffusion across the pores (free diffusion in air), but also by the passage through snow flakes, in which vapour is condensed on one side and evaporates from the other (macroscopic or hand-to-hand diffusion). In both cases, however, the mechanism of vapour transfer through the pore space is the same, namely, the molecular (free) diffusion of vapour-air mixture. Vapour is transferred in the pore space of snow due to the temperature gradient which establishes a vapour pressure gradient. The present author is of the opinion that the large differences in the diffusion coefficients of vapour in snow and in air are due to the particulate structure of snow, because actually vapour evaporates from the entire particle surface. Previous investigators estimated the vapour flux caused by the temperature gradient based on the plane area of a particle (the crystallizer model), which is evidently less than the area of its evaporating surface, i.e., as if the vapour flux is artificially increased. It should be borne in mind that instrumental measurements give the effective values of vapour diffusion coefficient in a unit area.

In order to prove this idea, a model for calculating the vapour diffusion coefficient was proposed by the author (Gavriliev 2004) which took into account the particulate structure of snow. The first attempt of model representation of snow structure to study vapour diffusion in snow was undertaken by Auracher (1978). Auracher's model consisted of plates of ice oriented either perpendicular or parallel to the flow, and the results were very dependent on the assumptions made. More recently, Colbeck (1993) proposed a particle-to-particle model. He considered a cubic packing of non-contacting, equally spaced spheres of ice in the air space. The vapour flux between particles was estimated using the electrostatic analogy. Colbeck found that the effective coefficient of vapour diffusion in snow D_s is related to the porosity of snow m according to

$$D_s = D_m \left[m^n + 10.0 \left(1 - m\right)^{0.51} \right] \quad (1)$$

where D_m is the coefficient of vapour diffusion in air and n is the exponent (n = 0, 1, 2, …). The D_s expression is highly insensitive to the exponent n and for practical purposes it can be taken equal to zero.

There are, however, several objections to the particle-to-particle model of Colbeck. First, the model virtually neglects the effect of vapour bypass around the particles through the free pore space, because by analogy with the electric force lines, the vapour flow lines close on the particles. So, Colbeck had to introduce the first term in Eq. (1) in order to obtain the coefficient of vapour diffusion in air D_m, when the particles disappear, i.e., at m = 1. Second, Colbeck's model assumes that the particles are isothermal, resulting in increased temperature gradients across the pores. The vapour flux is thus overestimated.

The model proposed in Gavriliev (2004) develops a very different approach to accounting for the vapour flow and temperature distribution, although it is outwardly similar to Colbeck's model in that it considers a cubic packing of spherical particles, but the particles have point contacts. Based on this model, a linear relation was found between the vapour diffusion coefficient in snow and snow porosity. Clearly some simplifying assumptions have to be made, as in any model investigation. The purpose of this paper is to improve my earlier model by treating heat transfer in snow in a more adequate way.

A Revised Model of Vapour Diffusion Flux in Snow

An outline of the proposed model is as follows. Since snow is cooled from above, the vapour concentration increases downwards. The vapour and heat flows move in the same direction, from the soil to the snow surface (upward). Snow has a complex multi-branch openwork structure with numerous contacts between particles. Modeling of this structure is a difficult task. However, some important advances have recently been made in three-dimensional modeling of snow structure, based on X-ray microtomopgraphic images of snow samples. Two lines of modeling research can be identified. The first one involves the development of simple physical models, based on Kelvin and Langmuir-Knudsen equations, to describe the isothermal and temperature gradient metamorphism of snow (Flin et al. 2003, 2005). Another approach is discrete element modeling (DEM) (Kaempfer et al. 2005, 2007). This snow model has an explicit geometric structure composed of large aggregate of discrete, individual snow grains with axisymmetric particle shapes, including spheres, tapered cylinders, and elongated or oblate spheroids and ellipsoids. The model was used by Kaempfer et al. to reproduce experimentally the radiative and heat transfer in snow. The above models provide realistic representation of the snow structure. However their application to the analysis of heat and mass transfer involves some difficulties. Usually in such a case, the model schemes are simplified; for example, the random structure is replaced by an ordered structure. The simplest models of mixture structure are based on the following rule (from chaos to order) (Dulnev & Zarichnyak 1974): the effective generalized conduction coefficients are equal for the ordered and chaotic systems, if their structures are similar and the properties and volumetric concentrations of the components are the same. This is the case for the model with changing particle shapes developed by the present author to calculate the thermal conductivity of snow (Gavriliev 1996, 1998). The model consists of three intersecting ellipsoids of revolution in a cubic cell and adequately reflects the main features of metamorphic changes in snow structure through the whole cycle from deposition to the glacial state. Depending on snow porosity, particles attain a large variety of shapes, such as stellar, needle, irregular, rounded, faceted and rounded cubical. It is a three-dimensional, ordered and rigid model with coordinate number 6. Contact spots exist where the model figure contacts with the planes of the cubic cell. The size of contact spots and the model porosity are determined by the semi-axes ratio of the ellipsoids of revolution. The model porosity ranges from 0 to 1. The model is purely geometrical and the system's porosity is changed by assigning ellipsoid parameters with no consideration of snow metamorphism.

For the vapour diffusion study, we have restricted ourselves to the special case of the model where the particles have a spherical shape (Gavriliev 2004), and are arranged cubically. In snow, the vapour evaporates from the upper surface of a lower-lying particle and, due to the temperature gradient, moves upward to the lower surface of a higher particle where it condenses in nearly the same amount according to the thermodynamic equilibrium condition. Therefore it is sufficient to consider one of the two processes, evaporation or condensation (the hemisphere scheme in the model). Evaporation has been chosen for the present research. The temperature field in the snow cover gives rise to concentration gradients, thus controlling the rate of vapour diffusion. There is no reverse transport of vapour in snow.

The earlier work (Gavriliev 2004) considered the scheme shown in Figure 1 for a hemisphere in a semicubical cell. At the tops, the particle has a plane of contact with other particles. The bottom *(y = 0)* and the top *(y = R)* of the sphere are maintained at constant temperatures t_1 and t_2 $(t_1 > t_2)$, which cause constant vapour concentrations c_1 and c_2 $(c_1 > c_2)$. Since vapour evaporation is a surface phenomenon, along the heat flow axis *oy* the vapour concentration distribution on the sphere's surface *c(y)* or *c(x)* is given over a range from c_1 to c_2.

Snow sublimation is a diffusive process and can be described by Fick's Law. According to the principles of Maxwell's diffusional theory of evaporation (Dyunin 1961), the general equation for the rate of evaporation of a body of arbitrary shape is

$$\frac{d\,M}{d\,t} = -\int_S D_o \; grad\; c\; \overline{d\,S} \qquad (2)$$

where dM/dt is the diffusive flux of vapour from the surface; D_o is the general coefficient of diffusion of vapour which depends on molecular diffusion and the character of medium movement relative the body; S is the surface area; $\overline{dS}$ is the vector element of surface area; and c is the weight concentration of vapour in air.

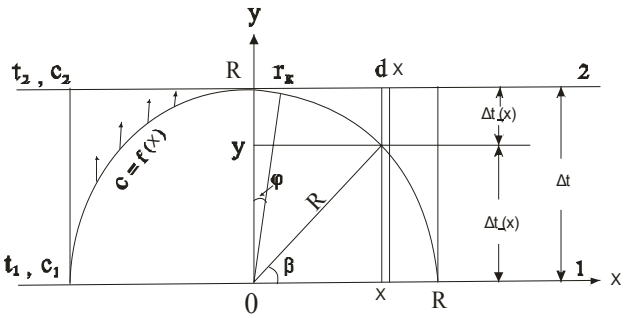

Figure 1. Schematic model of evaporation, vapour diffusion and snow temperature (Gavriliev 2004).

Since the exact theory of evaporation of solids is extremely complex, it is common to consider only the case of steady-state evaporation: $i = dM/dt$ = const. From Eq. (2) it follows that the amount of vapour in the space above the hemisphere depends on the surface area of evaporation and the vapour concentration gradient. The larger is the specific surface area, the more vapour is formed. The particulate structure of a body facilitates water evaporation. This can explain the great difference between the vapour diffusion coefficient in snow and that in air.

For the scheme shown in Figure 1, the concentration gradient in Eq. (2) is taken to be that outside the sphere, i.e., in the region R-y, and considered are the external surface of the sphere S and its differential dS. In the previous work (Gavriliev 2004), an error was made in selecting these parameters when y was taken instead of R-y and the differential dS was calculated from the bottom area of the sphere, i.e., the vapour flux within the sphere was computed.

The differential of the external surface of the sphere is $dS = 2\pi x dl$ (here $dl = (dy^2 + dx^2)^{1/2}$ is the arc length of the sphere's external surface intercepted by an inclined ring with radii x and $x+dx$). Taking into account that $y = (R^2 - x^2)^{1/2}$, we obtain

$$dS = \frac{2\pi R\, x\, dx}{\sqrt{R^2 - x^2}} \quad .$$

Considering the above remarks, the vapour flux i through the cylindrical region of the model is written:

$$i = -D_m \int_{S_c}^{S} \frac{c(y) - c_2}{R - y}\, dS =$$

$$= 2\pi R\, D_m \int_{r_c}^{R} \frac{[c(x) - c_2]\, x\, dx}{\left(R - \sqrt{R^2 - x^2}\right)\sqrt{R^2 - x^2}} \qquad (3)$$

where r_c and S_c are the radius and the area of the contact spot at the top of the sphere. In this equation, the concentration gradient is reckoned from c_2.

The distribution of vapour concentration on the particle surface, $c(x)$, is controlled by temperature. For an approximate estimate of this parameter, Kaganer's (1966) solution for the sphere with two contact areas was used in Gavriliev (2004) (see Fig. 1). The problem assumes that heat is transferred only through the contact surfaces of the particles, i.e., there is no heat transport across the pore space. This assumption is not entirely correct for snow and is only valid for very low temperatures (about -20°C or lower) when the diffusive transport of vapour is comparatively small and heat is predominantly transferred by conduction.

In the general case, calculation of the temperature distribution on the surface of a snow grain should account the additional heat convection by vapour diffusion due to a temperature gradient. This can be done by using the effective thermal conductivity of air λ_{ae}, which incorporates the thermal effect of vapour transfer in snow by thermal diffusion (Gavriliev 1998).

$$\lambda_{ae} = \lambda_a + \frac{L\, D_s\, e_o}{R_v\, T^2}\left(\frac{L}{R_v\, E} - 1\right)\exp\left[\frac{L\,(T - T_o)}{R_v\, T_o\, T}\right] \qquad (4)$$

where λ_a is the thermal conductivity of calm air; $e_o = 6.1 \cdot 10^2$ Pa is the saturation vapour pressure at 0°C (T_o = 273 K); R_v = $4.6 \cdot 10^2$ J/(kg·K) is the gas constant of water vapour; T is the absolute temperature; L is the latent heat of ice sublimation; and D_s is the diffusion coefficient of water vapour in snow.

For calculating λ_{ae} within the model space, however, the molecular diffusion coefficient of vapour, D_m, should be used in Eq. (4). The equation for the temperature dependence of D_m at atmospheric pressure (1 atm) given by Kikoin (1976) is

$$D_m = D_0 \left(\frac{T}{273}\right)^{1.5} \qquad (5)$$

where D_0 is the diffusion coefficient for vapour at 0°C (T_0 = 273 K).

The D_0 values for water vapour in air reported in the literature (see references in Gavriliev 2004) vary from 0.205 to 0.277 cm²/s, the more frequent values being within the range of 0.230 to 0.277 cm²/s. Jumikis (1962) gives D_0 = 0.426 cm²/s, the value which was obtained in a test with similar conditions to the crystallizer experiments but stands out of the common range. In this study, the value chosen for D_0 is 0.25 cm²/s.

The thermal conductivity of air in relation to temperature may be calculated by an equation given by Vargaftik (1963)

$$\lambda_a = \lambda_0 \left(\frac{T}{273}\right)^{0.82} \qquad (6)$$

where $\lambda_0 = 0.0244$ W/(m·K) is the thermal conductivity of air at 0°C (T_0 = 273 K).

The temperature dependence of the effective thermal conductivity of air, based on Eqs. (5) and (6), is shown in Figure 2.

An approximate estimation for the temperature distribution on the surface of a snow particle can be obtained based on the theory of generalized conductivity of composite bodies. The distortion of flow lines in the system components is usually neglected, which introduces some errors into the calculations. However, these errors are largely removed by fragmenting the elementary cell by adiabatic and isothermal planes and by using the arithmetic means of thermal conductivity (Dulnev & Zarichnyak 1974).

Let us consider the scheme in Figure 1, assuming that only point contacts exist between the spherical particles. Select a circular ring with width dx and inner radius x. The heat flux Q is the same across the particle (1) and the medium (2):

$$dQ = -\lambda_1 \frac{\Delta t_R}{y}\, dS = -\lambda_2 \frac{\Delta t_2}{R - y}\, dS \qquad (7)$$

where λ_1 and $\lambda_2 = \lambda_{ae}$ are the thermal conductivities of the ice particle and the air with water vapour, respectively (the effective coefficient); dS is the cross-section area of the ring; $\Delta t_R(x) = t_R(x) - t_1$ and $\Delta t_2(x) = t_2 - t_R(x)$ are the temperature

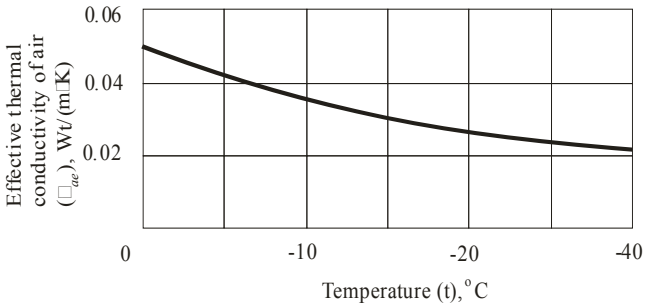

Figure 2. The effective thermal conductivity of air in snow versus temperature.

differences on the particle surface and in the air space of the circular ring, respectively; $\Delta t_R(x)$ is the temperature of the sphere's surface at points (x and y) of intersection with the cylindrical ring. Eq. (7) is valid for any radius x.

Considering expressions $y = (R^2 - x^2)^{1/2}$ and $\Delta t_R(x) + \Delta t_2(x) = \Delta t$ (the total temperature difference in the cell $t_2 - t_1$), the equation

$$\frac{\Delta t_R(x)}{\Delta t} = \frac{1}{1 + \frac{\lambda_1}{\lambda_2}\left(\frac{1}{\sqrt{1 - x^2/R^2}} - 1\right)} \tag{8}$$

is obtained from Eq. (7) for the relative temperature difference over the particle surface.

Hence it follows that the temperature distribution on the particle surface depends on the ratio between the thermal conductivities of the particle and the pore medium (Fig. 3). Taking into account the effective thermal conductivity of air, curves 6–8 fit for snow over a temperature range 0 to -10°C.

Because the vapour in snow is saturated, its concentration is determined using the well-known equation

$$c = \frac{c_0\, T_0}{T} \exp\left(\frac{22.46\, t}{T}\right) \tag{9}$$

where $c_0 = e_0 \mu_l / R_v T_0$ is the vapour concentration at T_0; μ_l is the molecular weight of the vapour.

When the temperature distribution at the particle surface is given by curves 6-8 (Fig. 3) (within the temperature range of 0 to -10°C), the calculations of vapour concentration with Eq. (9) result in a single curve (with few departures) relating the relative difference in vapour concentration over the sphere, $\Delta C_R(x)/\Delta C$, and the dimensionless coordinate x/R (Fig. 4). For convenience of integration in Eq. (3), this curve is expressed by the equation

$$\frac{\Delta C_R(x)}{\Delta C} = 2.4\frac{x}{R} - 1.4\frac{x^2}{R^2} \tag{10}$$

where $\Delta C = C_1 - C_2$ is the maximum difference in vapour concentration between the equatorial and vertex planes of the spherical particle; $\Delta C_R(x) = C_R(x) - C_2$ is the vapour concentration difference over the particle surface relative the vertex plane.

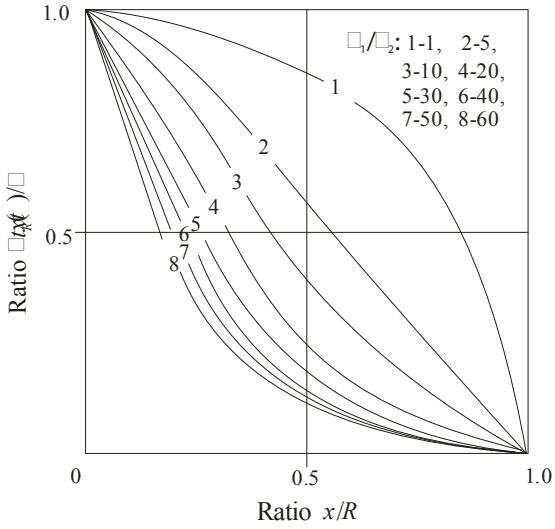

Figure 3. The distribution of the relative temperature difference over a spherical particle at various ratios between thermal conductivities of ice (1) and pore space (2).

Since the particles have only point contacts ($r_c = 0$), Eq. (43) is integrated over dx from 0 to R. Then the vapour flux in the cylindrical region of the model will be calculated using the equation:

$$i = -2\pi R\, D_m \left(C_1 - C_2\right) \int_0^R \frac{\left(2.4\,\frac{x}{R} - 1.4\,\frac{x^2}{R^2}\right) x\, dx}{\sqrt{R^2 - x^2}\left(R - \sqrt{R^2 - x^2}\right)} =$$

$$= -2\,\pi R\, D_m \left(C_1 - C_2\right)\left(1.2\,\pi + 0.3\right). \tag{11}$$

Effective Diffusion Coefficient of Vapour in Snow

The effect of the particulate structure of snow on the vapour diffusion coefficient is estimated as above by comparing the vapour flux calculated by Eq. (11) and the flux through the bottom of the cylindrical region $i_{fl} = -\pi R D_s'(c_1 - c_2)$ where D_s' is the effective diffusion coefficient for vapour in the cylindrical region of the snow model. Then we obtain, as above, the equation

$$D_s' = K\, D_m \tag{12}$$

where $K = 2(1.2\pi + 0.3)$ is a parameter for the particulate structure of snow which shows how many times the vapour diffusion coefficient in snow is greater than that in air due to the increased evaporation area of snow particles.

For the considered case of the vapour concentration distribution near the surface of the spherical snow particle, we have a different value of K which is equal to 8.2.

When the contribution of a through space to vapour diffusion is taken into account, the total diffusion coefficient is calculated by the equation in Gavriliev (2004)

$$D_s = D_m \left[1 + 1.5\left(K - 1\right)\left(1 - m\right)\right] \tag{13}$$

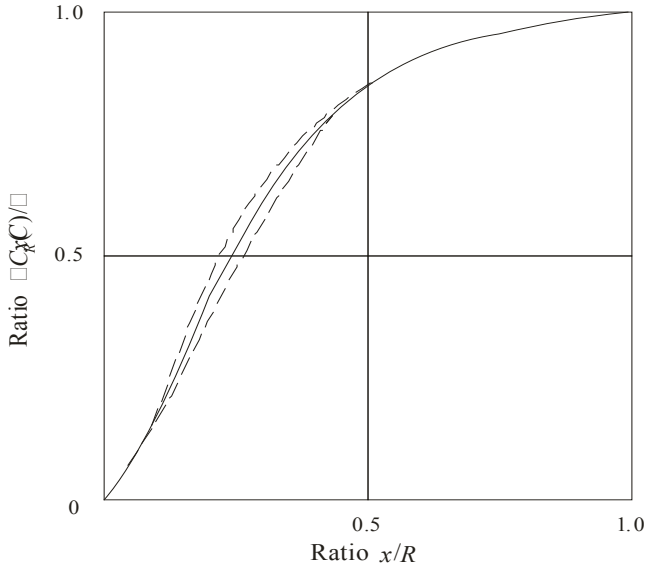

Figure 4. The distribution of the relative vapour concentration difference on the surface of a spherical snow particle.

where $0.33 \le m \le 1$. At $m = 1$, we have $D_s = D_m$, and at $m = 0.33$, $D_m = K D_m$.

Thus the diffusion coefficient of water vapour in snow depends on porosity (density).

Discussion of Results

Computations have been made for snow densities varying from 0.1 to 0.4 g/cm^3 ($m = 0.56 \div 0.89$). The obtained values of the diffusion coefficient for snow, D_m (cm^2/s), range from 0.55 to 1.45 and are compatible with the experimental results of most workers. It is interesting to compare the relative effective coefficients of vapour diffusion in snow (D_s/D_m) calculated by Eq. (1) (Colbeck 1993) and Eq. (13) (Gavriliev 2004). Figure 5 shows that the D_s/D_m ratio values from Colbeck's equation are invariably higher than those obtained by Eq. (13). The possible explanation is that calculations with the particle-to-particle model use the overestimated vapour flux due to the increased temperature gradient across the pores and the adding of the first term in Eq. (1) which leads to the results higher by unity. Curve 2′ for the results obtained without adding the first term in Eq. (1) agree better with our results (curve 1). It should be noted that actual computations with the particle-to-particle model led Colbeck to Eq. (1) that did not include the first term which was added later so that the logical reasoning would be complied for $m = 1$. Colbeck (1993) admitted that, because of the above reasons, the D_s/D_m values obtained by Eq. (1) were higher (4 to 7) than the D_s/D_m range (3.5 to 5) found by Yosida (1950).

Figure 5 also shows the experimental results of the authors mentioned in this paper. It is evident that there is no clear relationship between D_s/D_m and snow density and that the data scatter from 0.6 to 5.1. This is probably due to the effect of snow temperature on the measured coefficient of vapour diffusion in snow observed in the experimental data of Morozov (1967), Kolomyts (1971) and Nikolenko

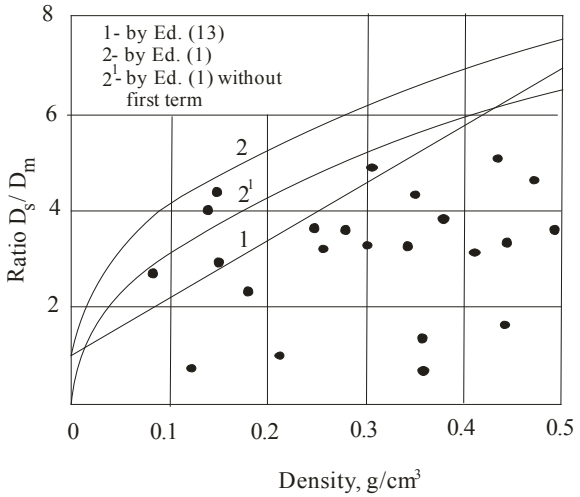

Figure 5. D_s/D_m ratio vs. snow density.

(1988). Most of the experimental data are lower than the theoretical results. Further investigations will be made to find an explanation.

It is interesting to note that, according to the proposed model, the diffusion coefficient of vapour in snow can reach a maximum of 2.06 cm^2/s at a porosity of 0.33, or a porosity of about 0.62 g/cm^3. This can be considered to be a purely theoretical value for dry snow which is hardly possible in real situations.

Conclusions

A model was developed to describe the process of water vapour diffusion in snow which takes into account the particulate structure of snow. Based on this model, a linear relation was found between the vapour diffusion coefficient and snow density. It has been theoretically established that because of the particulate structure of snow, the effective diffusion coefficient of vapour in snow is many times that of water vapour in air (up to six times for compacted snow).

Acknowledgments

The author is grateful to the Associate Editor of the Conference Proceedings and two anonymous reviewers for their valuable comments. The work described here was supported by the Russian Foundation for Basic Research (Grant 06-05-96126).

References

Auracher, H. 1978. Heat transfer in frost and snow. *International Heat Transfer Conference*. Washington, D.C.: Hemisphere, 25-30.

Colbeck, S.C. 1993. The vapor diffusion coefficient for snow. *Water Resources Research* 29(1): 109-115.

Dulnev, G.N. & Zarichnyak, Y.P. 1974. *Thermal Conductivity of Mixtures and Composite Materials (Teploprovodnost smesei I kompozitsionnykh materialov)* (in Russian). Leningrad: Energia, 263 pp.

Dyunin, A.K. 1961. *Snow Evaporation (Isparenie snega)* (in Russian). Novosibirsk: Izd-vo SO AN SSSR, 119 pp.

Fedoseeva, V.I. & Fedoseev, N.F. 1988. Estimation of the diffusion coefficient of water vapour in snow (in Russian). *Meteorologia i Gidrogeologia* 2: 132-136.

Flin, F., Brzoska, J.-B., Lesaffre, B., Coleou, C. & Pieritz, R.A. 2003. Full three-dimensional modeling of curvature-dependent snow metamorphism: first results and comparison with experimental tomographic data. *Journal of Physics D: Applied Physics* XXXVI(10): 49-54.

Flin, F., Brzoska, J.-B., Pieritz, R.A., Lesaffre, B., Coleou, C. & Furukawa, Y. 2006. A tentative model for the temperature gradient snow metamorphism and its first validations on X-ray microtomographic data. *Proceedings of the 8th International Conference on X-Ray Microscopy, Institute of Pure and Applied Physics Conference Series 7*: 306-308.

Gavriliev, R.I. 1996. A mathematical model for calculating thermal conductivity of snow subject to metamorphism. *Proceedings of the Fifth International Symposium on Thermal Engineering and Science for Cold Regions, Ottawa, Canada, May 19-22, 1996*: 516-521.

Gavriliev, R.I. 1998. *Thermal Properties of Soils and Ground Covers in Permafrost Areas (Teplofizicheskie svoistva gornykh porod I napochvennykh pokrovov)* (in Russian). Novosibirsk: Izd-vo SO RAN, 280 pp.

Gavriliev, R.I. 2004. On the diffusion coefficient of water vapour in snow cover (in Russian). *Kriosfera Zemli* VIII(2): 74-81.

Jumikis, A. 1962. Vapor diffusion in freezing soil systems of very large porosities. *Highway Research Board Bulletin* 331: 28-45.

Kaempfer, T.U., Hopkins, M.A. & Perovich, D.K. 2007. A three-dimensional microstructure-based photon-tracking model of radiative transfer in snow. *Journal of Geophysical Research* 112, D24113, doi: 10.1029/2006JD008239.

Kaempfer, T.U., Schneebeli, M. & Sokratov, S.A. 2005. A microstructural approach to model heat transfer in snow. *Geophysical Research Letters* 32, L21503, doi: 1029/2005GL023873.

Kaganer, M.G. 1966. Contact heat transfer in granular material under vacuum (in Russian). *Inzhenerno-Fizicheskiy Zhurnal* II(1): 30-37.

Kikoin, I.K. (ed.). 1976. *Handbook of Physical Quantities (Tablitsy fizichekikh velichin)* (in Russian). Moscow: Atomizdat, 1008 pp.

Kolomyts, E.G. 1971. *The Snow Structure and Regime in West-Siberian Taiga (Struktura I rezhim snezhnoi tolshi Zapadno-Sibirskoi taigi)* (in Russian). Leningrad: Nauka, 174 pp.

Kuvaeva, G.M. 1966. Determination of the coefficient of water vapour diffusion in snow. *Proceedings of the Third Trans-Caucasian Conference on Snow Cover, Avalanches and Glaciers in the Caucasian Mountains (in Russian)*: 75-79.

Morozov, G.A. 1967. Calculation of snow density changes due to water vapour diffusion, convection and sublimation (in Russian). *Meteorologia i Gidrologia* 6: 98-104.

Nikolenko, A.V. 1988. Laboratory-determined characteristics of water vapour diffusion in snow cover (in Russian). *Materialy Gliatsiologicheskikh Issledovanij* 62: 90-96.

Pavlov, A.V. 1962. Thermophysical properties and thermal balance of snow cover in the Moscow area. In: *Materials for the Study of Frozen Zones in the Earth Crust (Materialy k ucheniu o merzlykh zonakh zemnoi kory)* (in Russian). Moscow: Izd-vo AN SSSR, 3-35.

Saveliev, B.A., Laptev, M.P. & Lapteva, N.I. 1967. The structure, composition and physical-mechanical properties of snow in the Khibin mountains and their changes during metamorphism. In: *Snow and Avalanches in the Khibin (Sneg i laviny Khibin)* (in Russian). Moscow: Izd-vo MGU, 201-239.

Sommerfeld, R.A., Friedman, I. & Nilles, M. 1986. The fractionation of natural isotopes during temperature gradient metamorphism of snow. In: H.G. Jones & W.J. Orville-Thomas (eds.), *Seasonal Snowcovers: Physics, Chemistry, Hydrology*. Dordrecht: D. Reidel Publishing Company, 95-106.

Vargaftik, N.B. 1963. *Reference Book on Thermophysical Properties of Gases and Fluids Spravochnik po teplofizicheskim svoistvam gazov I zhidkostei)* (in Russian). Moscow: Fizmatgiz, 708 pp.

Voitkovskii, K.F., Golubev, V.N., Sazonov, A.V. & Sokratov, S.A. 1988. New data on the water vapour diffusion coefficient in snow (in Russian). *Materialy Gliatsiologicheskikh Issledovanij* 63: 76-81.

Woodside, W. 1958. Calculation of the thermal conductivity of porous media. *Canadian Journal of Physics* 37(7): 112-118.

Yosida, Z. 1950. Heat transfer by water vapour in snow cover. *Teion Kagaki* 5: 93-100.

Recent and Projected River Runoff Changes in Permafrost Regions of Eastern Siberia (Lena River Basin)

A.G. Georgiadi
Institute of Geography RAS, Moscow, Russia
I.P. Milyukova
Institute of Geography RAS, Moscow, Russia
E.A. Kashutina
Institute of Geography RAS, Moscow, Russia

Abstract

During the last decades the permafrost regions in the Lena River basin, Eastern Siberia, have experienced substantial climate warming. The analysis of long climatic and hydrological series revealed an inhomogeneous distribution of climate warming over the territory. Climate warming is shown to be accompanied by pronounced runoff changes, particularly in the cold season, that also exhibit significant space-time inhomogeneity. According to the hydrological modeling results, the expected anthropogenic climate warming in the 21st century can cause more perceptible runoff changes in the Lena River basin, as compared with the recent climate change. The hydrology-related consequences of climate warming are evaluated from a macro-scale monthly water-balance model (Georgiadi & Milyukova 2002, 2006).

Keywords: eastern Siberia; monthly water-balance model; permafrost; river runoff changes; scenarios of global climate warming.

Introduction

The river flow forming in the cryolithic zone of Eurasia, especially within the largest river basins (Lena, Enisey, Ob'), has a strong effect on the regional climate and the surrounding seas, affecting the chemical composition of water, the sea ice formation, and the circulation in the Arctic Ocean and the North Atlantic. Changes of the river runoff can have a pronounced effect on the processes involved.

During the recent decades significant global climate warming has been observed. Climate warming has been the largest in Northern Eurasia, particularly in the permafrost regions of Eastern Siberia (IPCC 2001). These changes include the winter air temperature and overall soil temperature rise (Varlamov et al. 2002). Regional climate changes are accompanied by river runoff changes in Eastern Siberia (Georgievsky et al. 1999, Savelieva, et al. 2000, Yang et al. 2002, Simonov & Khristoforov 2005, Berezovskaya et al. 2005, Georgiadi et al. 2006).

According to model forecasts of the climate change caused by the increased atmospheric greenhouse gases, the most perceptible changes take place in the permafrost regions of Eastern Siberia (IPCC 2001). Regional climate warming will cause a considerable increase in soil temperature and consequent permafrost thawing (Anisimov et al. 1997, Demchenko et al. 2002, Malevsky-Malevich et al. 2000). Such changes can alter the river runoff, particularly its intra-annual distribution (Georgiadi & Milyukova 2006). Possible changes of freshwater and heat flows going into the Arctic Ocean have potentially important implications for the ocean circulation and climate outside the region.

Until now, the processes regulating the river runoff in the large basins of the cryolitho zone have not been well studied, particularly the geographical (spatial and temporal) structure of their response to recent and projected global climate warming.

The Lena River basin in Eastern Siberia was selected as the main subject of investigation. It is one of the world's largest basins and occupies the area of 2,488,000 km^2 and extends as far as 4400 km. The basin is almost completely covered with deep permafrost ground whose upper active layer thaws out during the short summer season. In addition, the Lena basin is characterized by a small anthropogenic influence owing to a low population density. Analysis of the Lena basin is also facilitated by large intensive research programs carried out by Russian, bilateral, and international teams in the last 15 years.

The main objectives of this investigation is to analyze spatial and temporal heterogeneities of the recent river runoff changes over the Lena River basin, as well as to compute river runoff changes caused by the projected global climate warming.

Recent River Runoff Changes

The investigation of a spatial-temporal structure of the long-term runoff changes in the Lena River basin is based on the analysis of long-term series of hydrometric observations which are conducted on the national network of gage stations. Long-term series of annual, seasonal, and monthly runoff values for large, medium, and small representative river basins and annual and monthly series of air temperatures and precipitation are analyzed for characteristic zonal-landscape conditions. At the initial stage, the following methods were used:

1) Method to compare the characteristics of mean annual, seasonal, and monthly values of hydrological and climatic changes for the two periods: from the start of records to 1980 and from 1981 to the end of the 1990s and the beginning of the 2000s. It is the latter period alone, when the regional climate warming is most intensive.

2) Method of cumulative sum of normalized values which was traditionally used in the USSR and Russia to study the cycles of long-term changes in hydrological and climatic elements.

$$C_{si} = \sum (K_i - 1) / C_v \,,\; K_i = E_i / E_m \,, \qquad (1)$$

where C_v is the coefficient of variation, E_i is the value of the element for the i-year, E_m is the mean value of the element, K_i is the modulus coefficient of the element, C_{si} is the cumulative sum of the normalized values of the hydrological and climatic element.

Climatic changes

It follows from the calculations performed that in the period of the intensive regional climate warming, the annual air temperature rises considerably, with the temperature rise being distributed inhomogeneously over the territory of the Lena River basin. The maximal rise is registered in the central, eastern, and southern parts of the basin.

The character of the basin-averaged air temperature changes (provided that we do not consider the features of their spatial distribution) agrees with the classical idea, i.e. the most noticeable changes occur in the cold season of the year and insignificant warming and even temperatures fall in the summer-autumn period are observed. At the same time considerable spatial variation of changes throughout the year is typical for the basin.

Considerable spatial variation is also characteristic of the changes in average monthly precipitation values, especially in the summer.

The analysis of the cumulative sum curves of annual air temperatures indicates that beginning in the 1980s, the climate warming, which was synchronous enough in different parts of the Lena River basin, was recorded. The change of precipitation in this period is less homogeneous over the basin's territory.

River runoff changes

According to the analysis of the cumulative sum curves of the annual river runoff in different parts of the Lena River basin, the phase of the increase in the annual river runoff is observed in most of the basin during the last 15-25 years.

Only in some of the rivers, in the southern left-bank basin and in the upper course of the Lena, is the trend for the runoff decrease revealed.

The comparison of cumulative sum curves of annual and winter (November-April) river runoffs for the long period of observations (1935-2005) yields three types of their combinations (the list and the position of gage stations are shown in Figure 1):

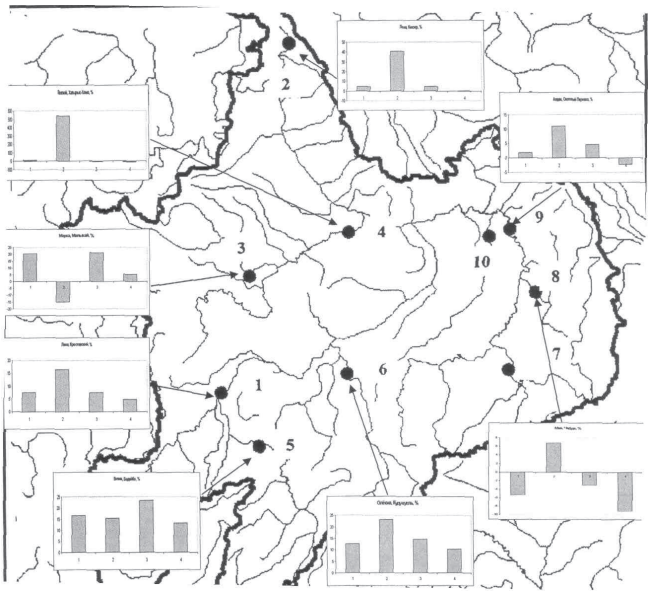

Figure 1. Deviations of mean annual and seasonal runoff for the period 1981-2005 and the period from the start of records to 1980 (in percent). Designations of diagram columns: 1 is the annual runoff; 2 is the winter (November-December) runoff; 3 is the flood (May-June); 4 is the low water (July-October). 1) Lena, Krestovsky; 2) Lena, Kyusyur; 3) Markha, Malyukai; 4) Vilyui, Khatyryk-Khomo; 5) Vitim, Bodaibo; 6) Olekma, Kudu Kuel; 7) Uchur, Chyul'byu; 9) Aldan, Okhotsky Perevoz; 10) Amga, Buyaga.

1) Phases of the annual and winter river runoff increase and decrease are almost synchronous, but for the winter runoff, these are usually better defined (Lena, Krestovsky; Vitim, Bodaibo; Olekma, Kudu Kuel; Aldan, Okhotsky Perevoz; Uchur, Chyul'byu; etc.).

2) Phases of the annual and winter runoff increase and decrease during the long period of observations can coincide or be asynchronous (Markha, Malyukai).

3) Relatively short and less intensive phases of the annual runoff increase and decrease are observed against the background of the long phases of increasing and decreasing winter runoffs (Lena, Kyusyur; Amga, Buyaga).

The comparison of intra-annual runoff changes in the Lena River basin for the periods considered shows the following (Fig. 1):

1) In the downstream of the Lena River, the most noticeable runoff increase occurs in the cold season of the year, while in the southern and southwestern mountain parts of the basin (with discontinuous and sporadic permafrost and more pronounced underground flow), the changes in runoff intra-annual distribution are more homogeneous and normally more intensive in all seasons of the year, as compared with the other parts of the basin.

2) The most noticeable increase in the Lena River runoff in the cold season is observed in the downstream of the Aldan and Vilyui rivers confluence.

3) The increase in the river runoff during the cold season in the downstream of the Aldan River can be related to the change of climatic conditions in its basin.

4) The considerable runoff increase in the lower portion of the Vilyui River in many respects can be connected with its artificial regulation as a result of the dam construction. This factor plays the main role in the winter runoff increase in the downstream of the Lena River.

Projected River Runoff Changes

Monthly water-balance model (MWBM)

The monthly water-balance model (MWBM), developed by the Institute of Geography of RAS to calculate hydrological consequences of the expected global climatic changes, was used to evaluate the large-scale hydrological changes (Georgiadi & Milyukova 2002, 2006). It can be referred to the category of macro-scale hydrological models with monthly resolution which are actively developed in the recent years (Willmott et al. 1985, Yates & Strzepek K. 1994, etc).

The model describes the main processes of the land hydrological cycle: infiltration and accumulation of water in the active layer; evaporation (based on the modified Tornthwite method (Willmott et al. 1985)); freezing and thawing of ground by using the Pavlov (1979) and the Belchikov & V.I.Koren methods (1979) which have been established as a simplified solution of the classical Stefan problem as applied to permafrost grounds; snow accumulation and snowmelt based on the Komarov method (Manual… 1989); formation of the surface flow and runoff from the active layer; and formation of the ground flow and river runoff.

The model allows for macro-scale inhomogeneity of hydrometeorological fields and other characteristics of the territory (permafrost, soil, hydrogeology). Such an approach provides the required accuracy in modeling climate changes that is achieved in the experiments with general atmosphere and ocean circulation models. The model calculations are performed in the regular grid cells. The existing version of the model employs a uniform spatial grid whose change makes it possible to take into account the main macro-scale inhomogeneity of the relief, the features of permafrost grounds including their active layer and hydrometeorological characteristics. The model is elaborated to estimate the changes of multi-year average characteristics of the water balance.

The principal approach to the account of inhomogeneity of the hydrogeological structure is to divide the underground zone into layers and calculate the runoff from each of them using our scheme of income and discharge of water for these layers.

The results of numerical experiments with ECHAM4/OPYC3 (Max Plank Meteorological Institute, Germany) and GFDL-R30 (Geophysical Laboratory of Hydrodynamics of the Princeton University, USA) were used based on the A2 family scenarios of global socio-economic changes in the 21st century from the last SRES scenario series accepted in the IPCC program. Calculations were made for the averaged conditions of the two periods (2010-2039, 2040-2069).

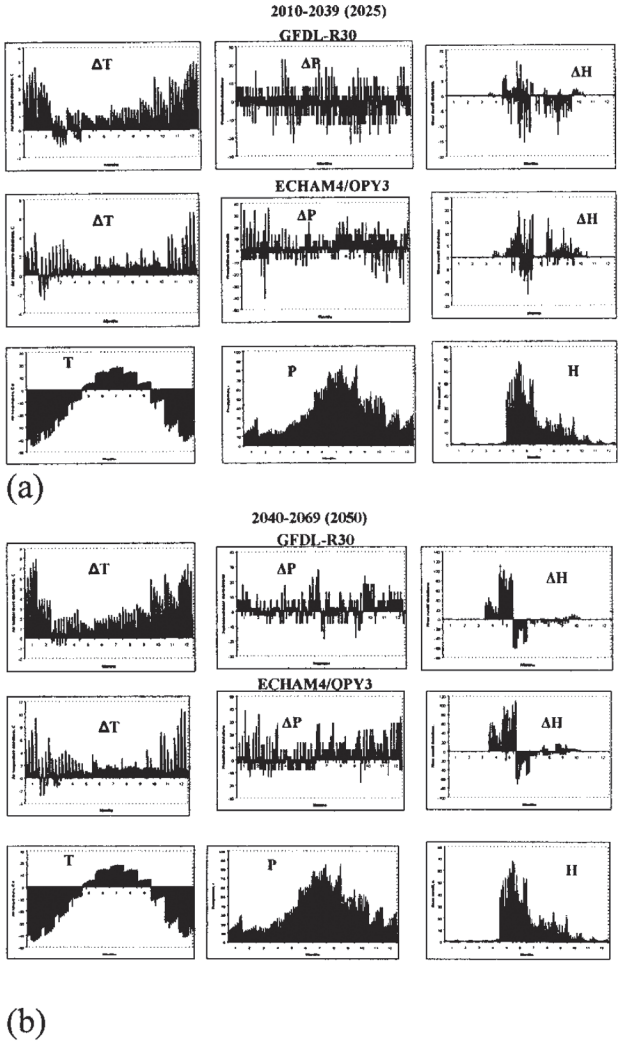

Figure 2. Deviations of mean monthly air temperatures (ΔT, °C), atmospheric precipitation (ΔP, mm) and river runoff (ΔH, mm) from their modern values generalized in the regular grid cells covering the plain part of the Lena basin, with regard for climate warming in 2010-2039 (a) and in 2040-2069 (b) by using scenarios of the Geophysical Laboratory of Hydrodynamics of the Princeton University (USA) and the Max Plank Meteorological Institute (Germany). The last line of figures shows mean monthly air temperatures (T, °C), atmospheric precipitation (P, mm), and stream flow (H, mm) under the modern climate conditions.

Discussion of modeling results for the plain part of the Lena River basin

Climatic conditions are shown in Figure 2. According to the considered scenarios for a plain in the central part of the Lena River basin, the climate is expected to warm essentially and more intensive in the middle of the 21st century.

Thus according to the scenario of the Max Plank Meteorological Institute, the climate warming can be more perceptible. Both scenarios predict a better pronounced air temperature increase in the cold period of the year, which is likely to lead to its duration reduction. The character of changes in atmospheric precipitation is more complicated. According to the both scenarios, the tendency towards the

precipitation increase is to be evident as late as the mid-21st century.

It should be noted that the character of annual distribution of scenario changes of monthly average air temperatures and precipitation is very similar to the appropriate changes observed in this region during the last decades of the modern climate warming, though it differs from the current changes in scale.

Hydrological conditions are also shown in Figure 2. According to the climatic scenarios developed by the Geophysical Laboratory of Hydrodynamics, Princeton University and the Max Plank Meteorological Institute for the plain part of the Lena River basin, during the first thirty years of the current century it is not likely to expect any noticeable increase in both annual river runoff and river runoff for the spring-summer flood period (three months with the greatest monthly flow). For the two scenarios realized, a significant increase in annual and spring flood runoffs is expected to occur by the middle of the 21st century.

It should be noted that the distribution of the possible changes in the river runoff over this part of the basin is characterized by essential spatial inhomogeneity which is to be reduced appreciably by the middle of the century.

Both scenarios suggest significant changes in the intra-annual stream-flow distribution. Thus in the first third of the century, both scenarios give similar changes in the wave of the spring-summer flood, whereas the river runoff changes following the main wave of high water may be of absolutely opposite character. By the middle of the century, both scenarios give, in essence, the same pattern of changes in the intra-annual stream-flow distribution: the wave of spring-summer high water is to be shifted (with the form and volume of water nearly unchanged) one month backward, as compared with the current situation. By the way, the character of changes in the intra-annual stream-flow distribution in the Lena River basin is identical to the similar changes in the Volga River basin with the probable global climate warming in the current century.

The following conclusions can be made as to the probable impacts of the predicted climate warming in the central plain part of the Lena River basin.

1. According to the considered scenarios, the essential climate warming is likely to be expected, and in the middle of the 21st century this is to be even more intensive.

2. The character of the intra-annual distribution of the scenario changes in monthly mean air temperatures and precipitation is rather similar to the appropriate alterations observed in this region during the last decades of the modern climate warming, but differs from the recent climate warming in scale.

3. According to the climatic scenarios, a significant increase, both in annual runoff and in spring-summer flood runoff, is likely to be expected by the middle of the current century.

4. Quite a significant change in the character of the annual stream-flow distribution may take place. By the middle of the century, the both scenarios give, in essence, the same pattern of changes in the intra-annual stream-flow distribution: the wave of spring-summer high water is to be shifted one month backward, as compared with the current situation.

This study was supported by NASA grant NNG06GH41G and the Russian Fund on Basic Research grant 07-05-12085-ofi.

Acknowledgments

The authors are grateful to Dr. R. Leemans, who contributed global a database on the modern climate, prepared in the International Institute of Applied System Analysis, Laxenburg, Austria.

References

Anisimov, O.A., Shiklomanov, N.I. & Nelson, F.E. 1997. Effects of global warming on permafrost and active-layer thickness: results from transient general circulation models. *Global and Planetary Change* 15(2): 61-77.

Belchikov, V.A. & Koren, V.I. 1979. Model of snow melting and rain runoff forming for forest watersheds. *Proc. of Hydrometeocenter of the USSR* issue 218: 3-21. (in Russian)

Berezovskaya, S., Yang D. & Hinzman, L. 2005. Long-term annual water balance analysis of the Lena River. *Global and Planetary Change* 48: 84-95

Demchenko, P.F., Velichko, A.A., Eliseev, A.V. Mokhov, I.I. & Nechaev, V.P. 2002. Dependence of permafrost conditions on global warming: comparison of models, scenarios, and paleoclimatic reconstructions. *Izvestiya, Atmospheric and Oceanic Physics* 38(2): 143-151. Translated from Izvestiya AN. Fizika Atmosfery i Okeana, Vol. 38, No. 2, 2002, 165–174. English Translation Copyright © 2002 by AIK

Georgiadi, A.G. & Milyukova, I.P. 2002. Possible scales of hydrological changes in the Volga river basin during anthropogenic climate warming. *Meteorology and Hydrology* No. 2: 72-79. (in Russian)

Georgiadi, A.G. & Milyukova, I.P. 2006. Possible river runoff changes in the largest river basins of the Russian Plain in the 21st century. *Water management complex of Russia* No. 1: 62-77. (in Russian)

Georgievsky, V.Yu., Ezhov, A.V., Shalygin, A.L., Shiklomanov, I.A. & Shiklomanov, A.I. 1999. Evaluation of possible climate change impact on hydrological regime and water resources of the former USSR rivers. *Meteorology and Hydrology* No. 11: 89-99. (in Russian).

IPCC 2001. *Climate Change 2001: The Scientific Basis. Contribution of Working Group I to the Third Assessment Report of the Intergovernmental Panel on Climate Change* (J.T. Houghton, Y. Ding, D.J. Griggs, M. Noguer, P.J. van der Linden, X. Dai, K. Maskell & C.A. Johnson [eds.]). Cambridge, UK, and New York, NY: Cambridge University Press, 881 pp.

Malevsky-Malevich, S.P., Molkentin, E.K, Nadyozhina, E.D. & Shklyarevich, O.B. 2001. Numerical simulation of permafrost parameters distribution in Russia. *Cold Regions Science and Technology* 32: 1-11.

*Manual on hydrological forecasts. Issue 1: Long-term forecasts of water regime of rivers, lakes and water reserve*s. 1989. Leningrad: Gidrometeoizdat, 358 pp. (in Russian).

Pavlov, A.V. 1979. *Thermophysics of Landscapes*. Novosibirsk: Nauka, 285 pp. (in Russian).

Savelieva, N.I., Semiletov, I.P., Vasilevskaya, L.N. & Pugach, S.P. 2000. A climate shift in seasonal values of meteorological and hydrological parameters for Northeastern Asia. *Progress in Oceanography* 47(2-4): 279-297.

Simonov, Yu.A. & Khristoforov, A.V. 2005. Analysis of long-term stream-flow variability in the Arctic Ocean basin rivers. *Water Resources* 32(6): 645-652. (in Russian).

Varlamov, S.P., Skachkov, Yu.B. & Skryabin, P.N. 2002. *Ground Temperature Regime of Central Yakutia Permafrost Landscapes*. Yakutsk: SB RAS, 218 pp. (in Russian).

Willmott, C.J., Rowe, C.M. & Mintz, Y. 1985. Climatology of the terrestrial seasonal water cycle. *Journal of Climatology* 5: 589-606.

Yang, D., Kane, D.L., Hinzman, L.D., Zhang, X., Zhang, T. & Ye, H. 2002. Siberian Lena River hydrologic regime and recent change. *Journal of Geophysical Research* 107(d 23, 4694): 14-4 – 14-10.

Yates, D. & Strzepek, K. 1994. *Comparison of Models for Climate Change Assessment of River Basin Runoff*. WP-94-45, IIASA, Laxenburg, Austria. 48 pp.

Permafrost Analogues of Martian Habitats

David A. Gilichinsky
Soil Cryology Laboratory, Institute of Physicochemical and Biological Problems in Soil Sciences, Russian Academy of Sciences, Pushchino, Russia

Abstract

Terrestrial permafrost, inhabited by viable microorganisms, represents a range of possible extraterrestrial cryogenic ecosystems on Earth-like planets without obvious surface ice, such as Mars. In a balanced permafrost environment, cells survive significantly longer than in other habitats. If life existed during the early stages of Martian development, then remnants of primitive forms may be found within frozen material that protects them against unfavorable conditions. This paper considers (a) the suggested age of Antarctic permafrost as an analogue somewhat closer to that of Mars than Arctic permafrost, (b) that free water can only exist on Mars in the form of cryopegs, as formed when Mars became dry and cold, (c) volcano-ice interactions in permafrost areas as one way to have liquid water on Mars, and (d) soil cover as a distant model of the Martian active layer.

Keywords: astrobiology; cryopegs; Mars; microorganisms; permafrost; volcanoes.

Introduction

Temperature is the fundamental aspect of the environment, where it acts as a regulator of physicochemical reactions and forms the basis of biological processes. Hard data indicate that biota survive over geological periods at temperatures <0°C within permafrost (for a recent overview, see Steven et al. 2006) down to -27°C (Gilichinsky et al. 2007a), and in ice sheets in Greenland (Miteva et al. 2004), the Tibetan Plateau (Christner et al. 2003), and in Antarctica down to -50°C (Abyzov 1993). In such environments, the dehydration leads to a considerable decrease of biochemical activities. This allows the survival of an ancient microbial lineage that can physiologically and biochemically adapt much longer than it would in any other known habitat.

The ability of microorganisms to survive on a geological scale forces us to redefine the spatiotemporal limits of the terrestrial and extraterrestrial biospheres and suggests that mechanisms of such adaptation might operate for millions of years. The long-term subzero temperature regime of the cryosphere is not limiting but rather a stabilizing factor. Organisms adapted to such balanced conditions represent a significant part of the biosphere—the cryobiosphere.

The cells, their metabolic by-products and bio-signatures (bio-minerals, bio-molecules, bio-gases), found in the Earth's cryosphere provide a range of analogues that could be used in the search for possible ecosystems and potential inhabitants on extraterrestrial cryogenic bodies. If life ever existed on other planets during the early stages of development, then its traces may consist of primitive cell forms. Similar to the Earth, they might have been preserved and could be found at depths within the ice or permafrost.

Microorganisms isolated from the ice cores of both hemispheres have been interpreted to be Earth's most representative analogues of icy inhabitants on Jupiter's ice-covered moon Europa, icy moon in Saturn's system Enceladus, and ice caps on Martian poles. Because ice thaws under geostatic pressure even at subzero temperatures, the existence of very old microorganisms is unlikely on the mentioned moons and caps.

The most inhabited and ancient part of the cryobiosphere's permafrost, being up to several hundred meters deep, harbors significant numbers of viable microorganisms, adhered on soil particles, and represents a wide range of possible cryogenic ecosystems for planets without obvious surface ice. Most intriguing are the traces of past or existing life on Mars, of interest due to upcoming missions. Because of unfavorable factors, life is unlikely to exist on the surface, and no terrestrial habitats duplicate Martian conditions. Anderson et al. (1972) and Cameron & Morelli (1974) first advanced the idea of using the terrestrial permafrost analogues, and the present paper considers these analogues as a bridge to Martian habitat and possible life forms. "Mars-Odyssey" observations of neutron fluxes that found water in the subsurface layer (Boyton et al. 2002) indicated Mars as a "water-rich planet." Hence, the requisite conditions for life have a place that makes the analogous models more or less realistic.

Soil Cover

Water ice within the top meters of the high-latitude regolith, as well as visual similarities on the Earth's and Martian surface—polygons formed by frost cracking—leads to consideration of the frost affected, seasonally thawed soil cover with mean annual temperature below 0°C underlain by permafrost as an extraterrestrial model. The leading factor in differentiation of these soils, named Cryosol, is temperature crossing through 0°C, resulting in freezing-thawing processes and ice-water phase exchange. The temperature oscillations crossing through the freezing point are also observed on the Martian surface. With respect to Mars, it is important to note that cryosol microbial communities, formed under the impact of multi-time freezing-thawing stress, did not change under such stress. Their maximal number and biodiversity correlate with the horizon A, decrease with

depth to the surface beneath the seasonal thaw layer, and have the accumulative sharp peak on the permafrost table. In spite of the tundra, the day surface is under the influence of solar radiation; the snow and vegetation covers decrease and minimize this impact, as well as temperature oscillations. Thus, Arctic cryosol has
distant similarities with the Martian surface.

The surface conditions in the Antarctic desert (the intensive level of solar radiation, the absence of snow and vegetation covers, and on account of the ultra-low subzero temperatures which can be as low as -60°C) and on Mars are closer. At elevations above 1500 m, there are no summer air temperatures above freezing. However, the surface temperatures of soil or rock can be 15°C warmer than the air due to solar heating; they may exceed 0°C for several hours (McKay et al. 1998), and for short periods even reach 10°C (Campbell & Claridge 1987). In addition to sharp temperature oscillations and high insolation, the main similarity between the Antarctic Dry Valleys and Mars is the vertical structure of their "active layers." In the Dry Valleys the upper 10–25-cm-thick sandy layer does not form a stable soil cover on the ice-cemented permafrost table. It is dry (W~2%) and lacks ice-cement due to sublimation. This dry-frozen permafrost—frosty, in the present author's terms—throughout the upper 100 cm (including the active layer) covers ~60% of the Dry Valleys area (Bockheim et al. 2007). The overcooled ground, with no water and thus no ice, is often mobilized by storm winds similar to the instability of Martian dunes. Such layering structure and distribution of water ice within the first surface meter on Mars is proposed according to HEND/Odyssey and MOLA/MGS data (Mitrofanov et al. 2007).

The upper ~2 cm layer of the Dry Valley surface often contains a low number of viable cells in comparison with the underlying horizons (Horowitz et al. 1972). In some cases, these microorganisms cannot be isolated on agar plates, correlating with a poor diversity of bacterial phylotypes, a low number of mycelia fungi strains, and a minimum of chlorophyll content. The occurrence and biodiversity of microorganisms is higher at depth than in the top of the active layer, and suggests that a search for life on Mars should not sample the surface but the bottom of the "active layer." In particular, because the upper horizons contain low cell counts, Antarctic frosty soils are useful for testing equipment for searching for life on Mars.

Cryolithosphere

It has been established that numerous (up to a dozen millions cells/g) and various ecological and morphological viable microbial groups have survived under permafrost conditions since the time the permafrost formed. They are the only known living organisms preserved over a geologically significant time. This approach is relevant to questions concerning the protective properties of permafrost, especially for astrobiology, because the Odyssey's discovery of water ice within the top meters of the high-latitude regolith points to the existence of near-surface permafrost on Mars. It also raises the question of liquid water presence as a necessary condition for life forms. Unfrozen water films play the leading role in the preservation of microorganisms. These films coat the soil particles and protect the viable cells adhered onto their surface from mechanical destruction by growing crystals of intrusive ice, and make possible the mass transfer of microbial metabolic by-products in permafrost, thus preventing the cells biochemical death (Gilichinsky et al. 1993). Therefore, the unfrozen water might be considered as a main ecological niche where the microorganisms might survive. In fine dispersed Arctic permanently frozen sediments at temperatures -3 to -12°C, the amount of unfrozen water can be estimated as 3–8% by weight. Because of temperatures below -20°C in the coarse Antarctic Valley's sands, the unfrozen water values are so small that the instrumental methods fail to record them. The unfrozen water must, therefore, only be firmly bound "liquid" water with binding molecules, and indicates a "biologically dry" environment. Based on experiments, Jakosky et al. (2003) calculate that liquid water can exist at ice grain-dust grain and ice grain-ice grain contacts above about -20°C. Below this temperature, water would not be present in soils in sufficient thickness and amount to physically allow the presence of microorganisms; i.e., this temperature is the lowest at which life can function. Both conclusions are not fully clear at this moment and not quite correct: First, R. Sletten has determined that, for Victoria Valley, the unfrozen water is ~2% at -20°C and ~1.5% at -30°C due to the salt content. The same amount of unfrozen water is expected in Beacon Valley, where the soil has a higher salt content (Gilichinsky et al. 2007). Second, considerable research has shown that microorganisms metabolize at extremely low temperatures in ice and permafrost—between -10 and -20°C (Rivkina et al. 2000, 2004; Carpenter et al. 2000; Bakermans et al. 2003; Junge et al. 2004), and down to -28 and -35°C (Gilichinsky et al. 2007a; Panikov & Sizova 2007). Mars polar and high-latitude temperatures rise above this level (up to 0°C for hours), and similar to cryptoendolithic microbial communities within Antarctic sandstone (Friedmann 1982) make the near-surface past and present permafrost layers potentially favorable sites to search for evidence of life. Probably, in such ecological niches, thin brine films might be formed within Martian permafrost as proposed by Dickinson & Rosen (2003) through their studies of minerals and accumulation of ground ice on Table Mountain, Sirius Group sediments.

From the astrobiological point, it is important that the permafrost, where 92–98% of water is in solid state, and subzero temperatures slack off the cumulative effects of background terrestrial gamma radiation on cells for thousands and millions of years. The lower the water content and the rate of metabolic processes, the less is the radio lesions of biological objects. This is why the irradiation sensitivity of soil microorganisms at temperatures above 0°C, differs from the sensitivity of microorganisms preserved in permafrost. Responses of the permafrost microbial complex to irradiation in nonfrozen and frozen states is different. At the irradiation

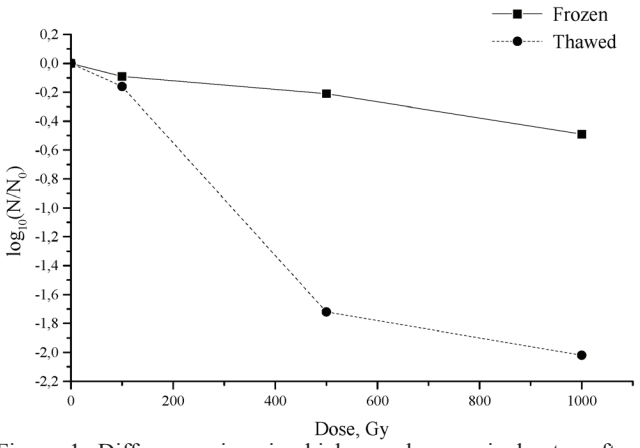

Figure 1. Differences in microbial complex survival rates after γ-irradiation in frozen or thawed state.

dose of 1 kGy, there is one magnitude difference in the number of viable cells between the nonfrozen and frozen samples (Gilichinsky et al. 2007b), and the cell survival rate was estimated to be, respectively, 1% and 10% from the initial number (Fig. 1). In the model γ-irradiation, the dose of 5 kGy was lethal for microorganisms in the nonfrozen samples.

The *in situ* measurements in the boreholes on the Eurasian northeast showed that the dose received by the immured bacteria in frozen sands and loams is about 2 mGy per year. Taking into account the oldest, ~3 Myr, late Pliocene age of permafrost and bacteria, the total dose received by cells would be 5–6 kGy. Under these conditions, most of the cells survived. This fact shows that freezing increased the cells' resistance to radiation and uniqueness of permafrost as an environment, where microorganisms display a high resistance to radiation. From these data the doze from radionuclides diffused through the permafrost is not fatal, but should be large enough to destroy the DNA of ancient viable cells. Their viability and growth implies the capacity for DNA repair, probably in the frozen environment; i.e., at the stable rate of damage accumulation, a comparable rate of repair also exists (Gilichinsky 2002). This is why the "biologically dry" (at temperatures deep below -20°C) Antarctic permafrost, with extremely low and inaccessible organic matter, is nevertheless inhabited by up to 10^4–10^5 viable cells/g, providing an analogue for the Martian ecosystem.

Antarctic Permafrost

Antarctic desert deposits beneath the frosty active layer are unexpectedly icy (Table 1); that is, of the same order as the more humid Arctic. This means that ground ice instability due to the processes of sublimation at ultra low humidity and air temperature is in a very thin surface layer only, and revises the earlier thesis of dry Antarctic permafrost. This is why we can also expect the existence of high icy subsurface layers on Mars.

Permafrost on Earth and Mars vary in age, from a few million years found on the Earth to a few billion years

Table 1. Ice content (I, %) in Taylor Valley permafrost sands.

depth, m	1	3	6	8.8	10	12	15	18
I, %	50	30	26	30	27	30	34	52

on Mars (Carr 2000, Baker 2004, Tokano 2005). Such a difference in time scale would have a significant impact on the possibility of preserving life on Mars because the number and biodiversity of microorganisms decrease with increasing permafrost age. This is why the longevity of life forms preserved within the Arctic permafrost can only work as an approximate analogue for Mars. The suggested age of Antarctic permafrost (~30 Myr) is somewhat closer to that of Mars. A number of studies indicates that the Antarctic cryosphere began to develop soon after the final breakup of Gondwana and the isolation of the Antarctic continent. It is believed to have been started on the Eocene-Oligocene boundary (Barrett 1996, Wilson et al. 1996, DeConto & Pollard 2003). The discussion of Neogene stability has focused mainly on the state of the ice sheet, which is the most variable part of the cryosphere. Permafrost is the more stable end-member of the cryosphere, and the conditions needed for ice degradation, even if they existed in the climatic optimum, are not enough to thaw the permafrost. Permafrost degradation is only possible when mean annual ground temperatures, -28°C now, rise above freezing; i.e., a significant warming, 25°C or more, is required to degrade the permafrost once formed. There is no evidence to date of such significant temperature variation, which indicates that the Antarctic climatic and geological history was favorable for the formation and persistence of pre-Pliocene permafrost. Antarctic permafrost may, therefore, be more than 30 Myr old (Gilichinsky et al. 2007a) and date from Antarctic ice sheets predicted in early Oligocene times (Zachos et al. 2001).

Viable microorganisms were isolated from the cores taken in Beacon Valley from beneath an 8.1 Myr volcanic ash layer that has been interpreted as a direct air-fall deposit (Sudgen et al. 1995), and this age is supported by several studies (Schäfer et al. 2000). The age of isolated communities remains controversial because the recent investigation has questioned this age relation, and the calculations indicate that sublimation rates would be too high for the ice to persist for 8.1 Myr (Ng et al. 2005). However, the last paper of Bidle et al. (2007) isolated microorganisms from the ice beneath this ash; these authors again affirm the 8.1 Myr age. From an age perspective, the Glacigene Sirius Group sediments on Mount Feather may be even older. They were estimated to be at least 2 Myr in age (Webb & Harwood 1991) and possibly as old as 15 Myr (Marchant et al. 1996). The ages for the superficial deposits, where bacteria were sampled in the permafrost, are 5 Myr (Wilson et al. 2002). If this age is correct, these are, to date, the oldest confirmed viable microorganisms discovered in permafrost and the oldest viable communities reported on the Earth (Gilichinsky et al. 2007a).

Permafrost distribution in Antarctica is well described by Bockheim (1995). It would be advantageous to locate relics of the oldest Antarctic permafrost. These are possibly to be

found at the high hypsometric levels of ice-free areas such as the Dry Valleys, along the Polar Plato and Trans-Antarctic mountains, on Northern Victoria Land. It is desirable to date the layers within them and test for the presence of viable cells. The limiting age, if one exists, within the most ancient Antarctic permafrost cores, where the viable organisms were no longer present, could be established as the age limit for life preservation within permafrost at subzero temperatures. Any positive results obtained from the Antarctic microbial data will extend the geological scale and increase the known temporal limits of Cryobiosphere; i.e., duration of life preservation. The author proposes this activity in accordance with the resolution of the International Workshop on Antarctic Permafrost and Soils (Madison 2004) and in the frame of the IPY ANTPAGE project, which has the following objectives:

- To integrate existing geological records and produce a thematic map of areas where climate and geological history of the last dozens of millions years were favorable for formation and persistence of early Oligocene permafrost and identify the most suitable drilling sites.
- To develop the hand-carried equipment for sterile drilling and sampling, and use these boreholes and cores for ground radiation and temperature measurements, cosmogony dating, ice and organic content, textural and chemical composition, microbial, pollen, diatom, and microfauna analysis.
- To develop the methods of direct dating of permafrost using the cosmogony radionuclides in ice-cement and segregated ice as a natural chronometer and biological clock, based on the racemization rates and differences of microbial communities immured in permafrost.
- To provide arguments that the Antarctic permafrost may have existed earlier than the Arctic permafrost by a factor of ten, and present the Earth's model with only one cold pole in the Southern Hemisphere during this period.
- To define the limit of dormancy of frozen life on Earth and in ancient permafrost on other planets and, potentially, provide a model for Martian ecosystems.

Volcanoes

Despite active volcanism, permafrost often exists on slopes of high-elevation or high-latitude volcanoes in places such as Hawaii, Iceland, Mexico, Peru, North America, and Antarctica. One way to have liquid water on Mars at shallow depths would be through subglacial volcanism. Such volcano-ice interactions could be going on beneath the polar caps of Mars today, or even within the adjacent permafrost around the margins of the ice caps. Basalt lava fields are common on Martian surfaces and some cinder cones have been found near the polar caps. The rover traces on the terrestrial ash fields and Martian surface, as well as the chemical composition of basalts on Earth and Mars, are similar (Squyres et al. 2006). This is why permafrost research on terrestrial volcanoes is expected to be a valuable step in understanding extraterrestrial volcanoes as one of the Earth's analogue. The main question is whether such ecological niches as volcanoes and associated environments contain microbial communities. The task is to find thermophylic microorganisms associated with volcanoes that have been deposited with products of eruption, and that have then survived in permafrost after the freezing of scoria and ash. Our study was carried out on the Kluchevskaya Volcano Group (Kamchatka Peninsula) which was formed starting from the late Pleistocene (Braitseva et al. 1995). The mean annual ground temperature decreases from -1°C on the lower boundary of permafrost (~900 m) to -7°C at 2500 m (Abramov et al. 2007). During the volcano eruptions in the last 2000–3000 yr, the thick (12–16 m) layers of volcanic ash, sand, and scoria accumulated on the elevations occupied by permafrost and at that time became frozen. The last eruption was in 1975–76, and ~500 km^2 were covered by scoria and ash (Fedotov & Markhinim 1983). The cores extracted from the borehole crossing these young volcano deposits contained biogenic CH_4 (up to 1900 µl/kg) and viable bacteria, including thermophilic anaerobes (10^3 cells/g), and among them, methanogens growing on CO_2+H_2. Because thermophiles have not previously been found before in permafrost, the only way for these bacteria to appear within frozen volcanic horizons is through the eruption of a volcano or its surrounding associated strata. The important conclusion is that thermophiles might survive in permafrost and even produce the biogenic gases. For future space missions, the permafrost volcano areas are promising test sites and provide opportunities to study analogues of possible Martian ecosystems. Their original microbial communities represent an analogue for Martian communities. The methanogenic bacteria found at such sites can likely adapt to temperatures <0°C as compared to other studied groups of anaerobes.

Cryopegs

Microorganisms have survived in natural conditions at subzero temperatures in ice and permafrost, but also have been reported to survive at above zero temperatures for dozens to hundreds of millions of years in amber (Cano & Borucki 1995) and saliniferous sediments (Vreeland et al. 2000), respectively. All these very different environments have common features: complete isolation, stability, aridity, and waterproof-ness, and represent the niches where microorganisms retain viability in the absence of free water. Based on the present study, it is possible that microorganisms might also survive in closed ancient aquatic ecosystems. Such habitats have overcooled water lenses formed during the Quaternary when the dynamics (transgression and regressions) of the Polar Ocean of the High Arctic favored the formation of overcooled brines (cryopegs) against a cold climatic background. Freezing in cryopegs is prevented by freezing-point depression due to the dissolved-solids content of the pore water. The cryopegs are embedded in permanently frozen coastal Pleistocene/Holocene marine strata. They are the only hydrological systems on the Earth with permanent subzero temperatures, high salinity, and isolation from

external factors throughout their geologic history.

Cryopegs were exposed by boreholes along the Polar Ocean coastal zone with mean annual ground temperatures varying between -2 and -12°C on Cape Barrow (Alaska), the Barents Sea coast, the Yamal Peninsula (surrounded by the Kara Sea), and the Kolyma lowland (East Siberian Sea). At the last site the cryopegs are confined to a 20-m-thick marine horizon, sandwiched between non-saline terrigenous layers at depths of 40–50 m below the tundra surface (the mean annual ground temperature varying -9 to -11°C). Finely dispersed sand and sandy loams were deposited in shallow lagoons at temperatures slightly above 0°C. After regression of the Polar Ocean, the water-bottom sediments were exposed sub-aerially and froze. Because of the pressure caused by freezing, water was released as the freezing front penetrated downward. This was accompanied by a freezing out of salts in the water to form lenses of overcooled sodium chloride brines with salinities of 170–300 g/L. Later, the marine horizon was buried by a 15–20–m-thick unit of lacustrine-alluvial late Pleistocene icy complex that was built up under harsh climate conditions, was syngenetically frozen and has never thawed. Within the marine horizon, the lenses occur at different depths, their thickness varying 0.5–1.5 m and their width 3–5 m. Some of them represent non-artesian water, and some exist under low pressure with a hydrostatic head. Different salinities of the brines confirm their lenticular nature and isolated bedding.

Bacteria isolated from cryopegs not only were adapted to subzero temperatures, but also were tolerant to the high salt concentrations. What is more, detected microorganisms are both halophilic and psychrophilic organisms, and have never been isolated from natural habitats. In the cold saline conditions of cryopegs, special communities were formed. Active adaptation to low temperatures of already-studied bacteria gives hope that fully active and reproducing bacteria can be discovered in saline habitats at subzero temperature. Biotic survival in the aquatic environment on a geological time scale indicates unknown bacterial adaptations. The microbial activity detected in cryopegs at temperatures as low as -15°C documents the fact that subzero temperatures themselves do not exclude biochemical reactions and provides reason to conclude that in overcooled water the metabolic strategy of microbial survival operates, and that this strategy does not accept that cells can multiply *in situ* (Gilichinsky et al. 2005).

The salt tolerance may be associated with cold tolerance. Experimental data showed that in the presence of 25% NaCl halophiles survive better than non-halophiles under low (-20 to -80°C) temperatures (Mancinelli et al. 2002). Mars is a cryogenic planet where free water only has the opportunity to exist in the presence of high solute content, probably as brine lenses within permafrost. These brines, like their terrestrial analogues, may contain microorganisms adapted to low temperature and high salinity. This is why unique halo/psychrophilic communities preserved hundreds of thousands of years in mineral-enriched Arctic cryopegs provide the plausible prototype for Martian microbial life (Gilichinsky et al. 2003), either as an "oasis" for an extant, or the last refuge of an extinct biota (Mancinelli et al. 2002).

Conclusion

The future mission priorities for the search for life on Mars must be based on studies of the most probable environments in which the life might be found, and the maximum period of time over which such life could be preserved. This is why terrestrial subsurface frozen layers represent the analogues of extraterrestrial cryobiosphere, where the probability of finding life is the highest. Hemolithotrophic psychrotolerant anaerobes with their unique mechanisms to assimilate CO_2 are more like life- forms on Mars, which has no free oxygen; as well, cryopeg halo/psychrophilic communities provide the other prototype for Martian microbial life.

Acknowledgments

This research was supported by the Russian Fund for Basic Research (grant: 07-05-00953) and NASA Astrobiology Institute. Special thanks to Dr. Sandra Ponder (Australian Antarctic Center) for editing the manuscript.

References

Abramov, A., Gruber, S. & Gilichinsky, D. 2008. Mountain permafrost on active volcanoes: Field data and statistical mapping, Kluchevskaya Volcano group (Kamchatka). *Permafrost and Periglacial Processes* (in press).

Abyzov, S. 1993. Microorganisms in the Antarctic ice. In: E.I. Friedmann (ed.), *Antarctic Microbiology*. New York: Wiley-Liss, Inc., 265-296.

Anderson, D., Gatto, L. & Ugolini, F. 1972. An Antarctic analog of Martian permafrost terrain. *Antarctic J. USA* 7: 114-116.

Baker, V. 2004. A brief geological history of water on Mars. In: *Origin, Genesis, Evolution and Diversity of Life*. Dordrecht, The Netherlands: Kluwer Publishers, 619-631.

Bakermans, C. et al. 2003. Reproduction and metabolism at -10°C of bacteria isolated from Siberian permafrost. *Environmental Microbiology* 5(4): 321-326.

Barrett, P. 1996. Antarctic paleoenvironment through Cenozoic times: A review. *Terra Antarctica* 3: 103-119.

Bidle, K., Lee, S., Marchant, D. & Falkowski, P. 2007. Fossil genes and microbes in the oldest ice on Earth. / *PNAS* 104 (33), 13455-13460.

Bockheim, J.G. 1995. Permafrost distribution in the southern circumpolar region and its relation to the environment: A review and recommendations for further research. *Permafrost Periglacial Processes* 6: 27-45.

Bockheim, J., Campbell, I. & McLeod, M. 2007. Permafrost distribution and active-layer depths in the McMurdo Dry Valleys, Antarctica. *Permafrost and Periglacial Processes* 18: 217-227.

Braitseva, O. et al. 1995. Ages of calderas, large explosives craters and active volcanoes in the Kuril-Kamchatka region, Russia. *Bulletin Volcanology* 57: 383-402.

Cameron, R. & Morelli, F. 1974. Viable microorganisms from ancient Ross Island and Taylor Valley drill core. *Antarctic J. USA* 9: 113-116.

Campbell, I. & Claridge, G. 1987. *Antarctica: Soils, Weathering Processes and Environment.* Amsterdam: Elsevier Science Publishers, 368 pp.

Cano, R. & Borucki, M. 1995. Revival and identification of bacterial spores in 25 to 40 million year old Dominican amber. *Science* 268(5213): 1060-1064.

Carpenter, E., Lin, S. & Capone, D. 2000. Bacterial activity in South Pole snow. *Applied Environmental Microbiology* 66(10): 4514-4517.

Carr, M. 2000. Martian oceans, valleys and climate. *Astron. Geophys.* 41(3):20-26.

Christner, B. et al. (2003). Bacterial recovery from ancient glacial ice. *Environmental Microbiology* 5: 433-436.

DeConto, R. & Pollard, D. 2003. Rapid Cenozoic glaciation of Antarctica induced by declining atmospheric CO_2. *Nature* 421(6920): 245-249.

Dickinson, W. & Rosen, M. 2003. Antarctic permafrost: An analogue for water and diagenetic minerals on Mars. *Geology* 31(3): 199-202.

Fedotov, S. & Markhinim, Y. 1983. *The Great Tolbachik Fissure Eruption:Geological and Geophysical Data 1975-1976.* England: Cambridge University Press.

Friedmann, E.I. 1982. Endolithic microorganisms in the Antarctic cold desert. *Science* 215: 1045-1053.

Gilichinsky, D., Soina, V. & Petrova, M. 1993. Cryoprotective properties of water in the Earth cryolithosphere and its role in exobiology. *Origin of Life & Evol. Biosph*. 23(1): 65-75.

Gilichinsky, D. et al. 2003. Supercooled water brines within permafrost–an unknown ecological niche for microorganisms: A model for astrobiology. *Astrobiology* 3(2): 331–341.

Gilichinsky, D. et al. 2005. Biodiversity of cryopegs in permafrost. *FEMS Microbioogy Ecology* 53(1): 117-128

Gilichinsky, D.G. et al. 2007a. Microbial populations in Antarctic permafrost: Biodiversity, state, age, and implication for astrobiology. *Astrobiology* 7(2): 275-311.

Gilichinsky, D. et al. 2007b. Bacteria in permafrost. In: R. Margesin, F. Schinner, J-C. Marx, & C. Gerday (eds.) *Psychrophiles: From Biodiversity to Biotechnology,* Chapter 6. Springer Verlag, 83-102.

Horowitz, N., Hubbard, J., & Cameron, R. 1972. Microbiology of Dry Valleys of Antarctica. *Science* 176: 242-245.

Jakosky, B. et al. (2003). Subfreezing activity of microorganisms and the potential habitability of Mars polar regions. *Astrobiology* 3(2): 343-350.

Junge, K., Eicken, H. & Deming, J. 2004. Bacterial activity at -20°C in Arctic wintertime sea ice. *Applied Environmental Microbiology* 70: 550-557.

Kapitsa, A. et al. 1996. A large deep freshwater lake beneath the ice of central East Antarctica. *Nature* 381: 684–686.

Mancinelli, R. et al. 2004. Brines and evaporates: Analogs for Martian life. *Advances Space Research* 33(8): 1244-1246.

Marchant, D. et al. 1996. Late Cenozoic Antarctic paleoclimate reconstructed from volcanic ashes in the Dry Valleys region of southern Victoria Land. *GSA Bulletin* 108: 181-194.

McKay, C. et al. 1998. Soil temperatures and stability of ice-cemented ground in the McMurdo Dry Valleys. *Antarctic Science* 10(1): 31-38.

Miteva, V. et al. 2004. Phylogenetic and physiological diversity of microorganisms isolated from a deep Greenland glacier ice core. Applied Environmental Microbiology 70(1): 202-213.

Mitrofanov, I. et al. 2007. Water ice permafrost on Mars: The layering structure and surface distribution according to HEND/Odyssey & MOLA/MGS data. *Geophysical Research Letters* 34, L18102.

Ng, F. et al. 2005. Fast growing till over ancient ice in Beacon Valley, Antarctica. *Geology* 33: 121-124.

Priscu, J. et al. 2000. Perennial Antarctic lake ice: An oasis for life in a polar desert. *Science* 280: 2095-2098.

Rivkina, E. et al. 2000. Metabolic activity of permafrost bacteria below the freezing point. *Applied Environmental Microbiology* 66(8): 3230-3233.

Rivkina, E. et al. 2004. Microbial life in permafrost. Advances Space Research 33(8): 1215-1221.

Schaefer, J. et al. 2000. The oldest ice on Earth in Beacon Valley, Antarctica: New evidence from surface exposure dating. *Earth Planetary Science Letters* 179: 91-99.

Squyres, S. et al. 2006. The Opportunity Rover's Athena science investigation at Meridian Planum, Mars. *Science* 306: 1698-1703.

Steven, B. et al. 2006. Microbial ecology and biodiversity in permafrost. *Extremophiles* 10: 259-267.

Sugden, D. et al. 1995. Preservation of Miocene glacier ice in East Antarctica. *Nature* 376: 412-414.

Tokano, T. (ed.) 2005. *Water on Mars and Life.* Springer.

Vreeland, R., Rosenzweig, W. & Powers, D. 2000. Isolation of a 250 million-year-old halotolerant bacterium from a primary salt crystal. *Nature* 407(6806): 897-900.

Webb, P-N. & Harwood, D 1991. Late Cenozoic glacial history of the Ross Embayment, Antarctica. *Quaternary Science Review* 10: 215-223.

Wilson, G. et al. 1996. Coring for microbial records of Antarctic climate. *Antarctic J. USA* 31: 83-86.

Wilson, G. et al. 2002. The Mount Feather diamicton of the Sirius Group: An accumulation of indicators of Neogene Antarctic glacial and climatic history. *PALEO* 182: 117-131.

Zachos, J. et al. 2001. Trends, rhythms, and aberrations in global climate 65 Myr to present. *Science* 292(5517): 686-693.

Microbial Diversity in a Permafrost Environment of a Volcanic-Sedimentary Mars Analog: Imuruk Lake, Alaska

Felipe Gómez, Olga Prieto-Ballesteros, David Fernández-Remolar, José Antonio Rodríguez-Manfredi, Maite Fernández-Sampedro, Marina Postigo Cacho, Josefina Torres Redondo, Javier Gómez-Elvira
Centro de Astrobiologia (CAB) INTA-CSIC. Carretera de Ajalvir Km 4 Torrejón de Ardoz Madrid 28850, Spain
Ricardo Amils
Centro de Astrobiologia (CAB) INTA-CSIC. Carretera de Ajalvir Km 4 Torrejón de Ardoz Madrid 28850, Spain and Centro de *Biología Molecular (UAM-CSIC), Universidad Autónoma de Madrid, Cantoblanco, Madrid 28049, Spain*

Abstract

Permafrost has attracted considerable interest from an astrobiological point of view (Wynn-Williams & Edwards 2000), due to the recently reported results from the Mars Exploration Rovers. The possible existence of past or present water in the subsurface of the red planet increases the probabilities of life existence on Mars. Considerable studies have been developed on extreme ecosystems and permafrost, in particular, to evaluate the possibility of life on Mars. The biodiversity of permafrost located on the Bering Bridge National Preserve has been studied. Different conventional (enrichment, isolation) and molecular ecology techniques (cloning, fluorescence in situ probe hybridization-FISH) have been used for isolation and bacterial identification.

Keywords: Alaska; astrobiology; biodiversity; Imuruk Lake; permafrost.

Introduction

Due to reported Mars surface environmental conditions (Klein 1978) (oxidative stress, high UV radiation levels, etc.) the possibility for life development in the surface of the red planet is very small. The identification of water-ice on the subsurface on Mars by the Thermal Emission Spectrometer onboard the Mars Odyssey (Kieffer & Titus 2001) and from the High Energy Neutron Detector (Litvak et al. 2006) has important astrobiological connotations, because in addition to being a potential source for water, these locations are shielding habitats against the harsh conditions existing on the planet, like UV radiation (Gomez, et al. 2004, Gomez et al. 2007).

Several authors have discussed similarities between Earth and Martian permafrost (Frolov 2003) and the structures that could play a protective role for subsurface ecosystems (Gilichinsky et al. 2007).

Chemolithotrophic microorganisms have the ability to use inorganic compounds, like reduced minerals, as energy sources for metabolism in isolated environments of the subsurface. Better understanding of permafrost ecosystems on Earth is needed to evaluate the possibilities that life could have developed in these types of structures on Mars. Permafrost on Earth is located at circumpolar latitudes. Of special interest is the permafrost on volcanic areas due to their similarities with Mars geology (Dyar & Schaefer 2004).

Future space missions will be focused on searching for life on the subsurface of Mars. New techniques and methodologies for studying these putative habitats need to be developed (Frolov 2003).

Material and Methods

Imuruk Lake campaign

We identified an interesting volcanic area associated with permafrost in the region of Imuruk Lake (Alaska). An exploration campaign was developed during July 2005 to study the geology and microbiology of the area. Imuruk Lake is located at 65.6ºN, 163ºW. This region is a volcanic area in the Bering Land Bridge National Preserve (Fig. 1).

The 2005 campaign was developed in the eastern part of the lake, near Nimrod Hill. Previous geologic studies (Hopkins 1963) of the area have been reported. The area is characterized by volcanic formations with basaltic composition. Some basalt lava flows are present. Over the lava structures there are two covers with different composition: the first is a wind blown silt layer, and the second is a peat cover at the top. Some intermediate terraces can be found around the hill with sedimentary material.

With the idea of future development of instrumentation for automated remote life detection systems on permafrost, three main objectives were considered during the expedition: (1) permafrost localization by geophysical techniques and drilling; (2) microbial diversity analysis, with special interest on deeper parts of the column, the oldest part of the permafrost (pattern preservation of biosignatures in cold environment is of extraordinary astrobiological interest); and (3) understanding cold ecosystems to facilitate permafrost niche detection and mapping.

An Arctic area has been selected for permafrost characterization. Field camping was developed on the Bering Land Bridge National Preserve (Fig. 1). Permafrost was localized using geophysical sounding techniques over several traverse lines on the Imuruk Lake area. A particular place for sampling was chosen, and a borehole 4 m deep

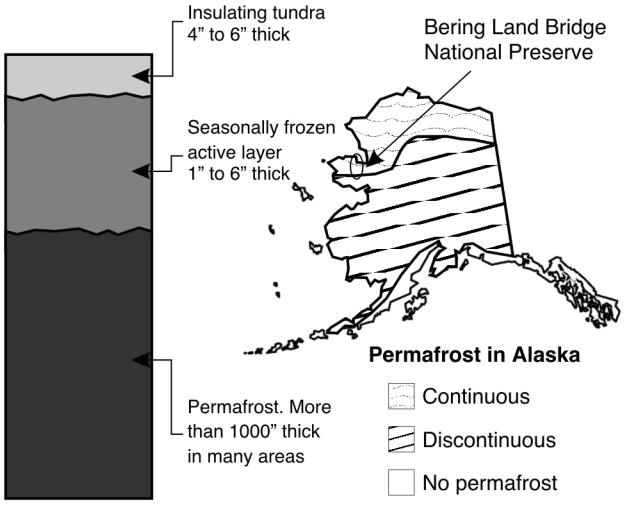

Figure 1. Bering Land Bridge National Preserve situation. Imuruk Lake is located on a volcanic area.

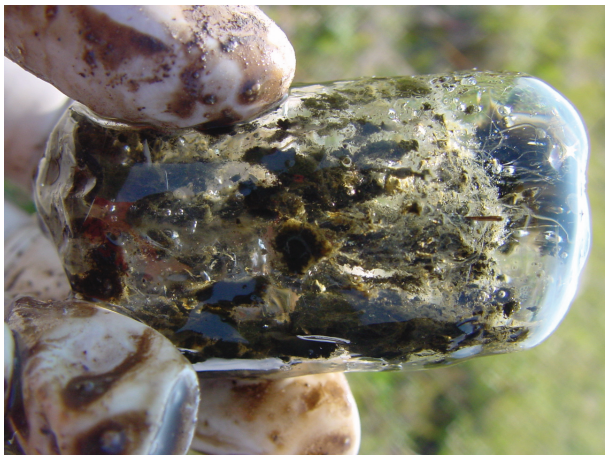

Figure 2. An 0.8 m deep sample from tomographic Line 11.

was drilled for sampling along the soil column. The active layer at the surface and subsequent permafrost were sampled at several depths. Samples were used for biodiversity determination using complementary techniques.

Geophysical studies

Permafrost depth was identified by geophysical techniques (electric tomography sounding, ERT). *Syscal KID Swich-24* equipment was used. Thirteen parallel lines were deployed from the lake to the top of the hill (see Prieto et al. in this issue for details). Each tomographic line was 48 mm long, separation between electrodes was 2 m, and the space between lines was 15 m.

Temperature recording during core sampling indicated a permafrost depth of around 30 cm, but tomographic data indicated that permafrost began at a mean depth of 0.50 m from the surface. After tomographic data interpretation a place for drilling was chosen.

Stratigraphic column

A portable drilling system was used for stratigraphic sampling at different depths. A Cardi E-400 fuel-powered system was adapted for core retrieval. The dimension of the pits was 0.5 long and 50 mm diameter. Pits could joint each other to obtain a maximum depth core of 4 m. Microbiological studies were performed over tomographic Line 11 core. Maximum depth on this drill was 3.6 m.

Microbial diversity studies

From ERT studies, a particular place was chosen for drilling and sampling at several depths. Proximity of permafrost to the surface was the criterion chosen for drilling. Several core depths were chosen for microbiological analysis (Table 1). Some ice pockets were detected in Line 11 (Fig. 2). From every core depth selected for sampling, two aliquots were used: the first for direct media inoculation, and the second for hybridization analysis. In the second case, the first step was to fix the sample with formaldehyde as soon as possible in order to maintain the structure of the microbial population without any alteration. These fixed samples were transported to the laboratory for further processing and hybridization with DNA probes of different specificity (species, genus, and phylum).

Two different methodologies for microbial population analysis were used:

(1) media inoculation for microbial enrichment: Three different media were chosen for microbial growth: chemolithotrophic media enriched with ferrous iron, heterotrophic organic media and several anaerobic specific media enriched with different energy sources (methanol, formate, proteolytic and volatile fatty acid). Growth was followed by optical density at 580 nm in a WPA Lightwave spectrophotometer. Qualitative values for growth were assigned depending on the slope of the growth curve. After growth, microbial populations were identified by 16S rRNA amplification of DNA, cloning, and sequencing.

(2) Fluorescence in situ hybridization techniques (FISH) with specific DNA probes, used for microorganism identification: The DNA probes used on this study were specific for *Bacteria* and *Archaea* domains, Alfa-, Beta-, and Gamma-proteobacteria subclasses, a CF (Cytophaga-Flavobacterium cluster) and a HGC (High G+C content bacterial cluster) specific group probes. Samples were directly fixed on the field with formaldehyde (4% v/v) and incubated at 4°C for 2 h. After incubation, samples were washed twice with PBS and filtered. Filters were stored under frozen conditions in PBS-ethanol (1:1). Samples from several depths were chosen for further analysis with different DNA-specific probes. Cell density was determined by cell counting with a microscope. Filters were dried and maintained at low temperature until further processing in the lab.

Results and Discussion

Thirteen transects along Nimrod Hill were chosen for electrical resistivity tomography studies, and thirteen tomography lines were obtained. The existence of different

resistivity values along the lines at different depth determined the presence of several units. Typical resistivity values of pits and sedimentary units were recorded. The tomography diagrams obtained from the 13 lines were used for permafrost localization (Fig. 3) to determine the drilling points (vertical arrow in Fig. 3) and the sampling depths for microbiology analysis. Samples were taken at 30 cm, 1 m, 1.5 m, 2.1 m, 3.1 m, and 3.6 m. From every sample, two aliquots were taken.

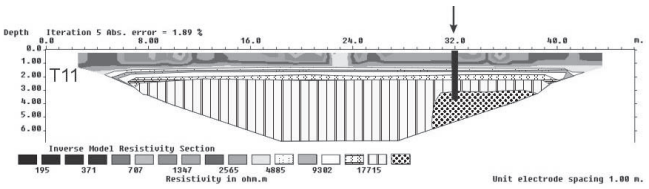

Figure 3. Electrical Resistivity Tomography for Line 11. This section was chosen for drilling a 4 m deep borehole for microbial sampling.

Microbial growth was observed in most of the media. Table 1 shows the results obtained on the inoculated media after 72 h of incubation at 12°C: - is no growth; +/- is less growth to +++, much growth; *Gas* indicates gas production during growth); Fe^{2+} indicates basal media enriched with ferrous iron on aerobic conditions; *Het.* indicates enriched media for heterotrophic bacteria cultures under aerobic conditions; *P* indicates media enriched with peptone and yeast extract for proteolytic bacteria and cultured under anaerobic conditions; *M* indicates methanol-enriched media under anaerobic conditions; *F* indicates formaldehyde-enriched media under anaerobic conditions; and *VFA* indicates volatile fatty acid (C2 plus C4) enriched media under anaerobic conditions.

The most efficient growth (Table 1) was obtained using

Table 1. Growth obtained on different inoculated media after 72 h of incubation at 12°C.

	Fe^{2+}	Het.	P	M	F	VFA
T11-1 (30 cm)	-	+++	+++ Gas	+++	++	++ Gas
T11-2 (1 m)	+/-	Gas	Gas	++	+	+
T11-3 (1.5 m)	+/-	++	+	++	++	++
T11-4 (2.1 m)	+/-	+++	++	+	+	+
T11-5 (3.1 m)	+/-	++	++	+	+	+
T11-6 (3.6 m)	+	+++	+++	++	++	++

Table 2. Biodiversity from sample point T11-1 after microbial enrichment in several media and cloning and sequencing the 16S rDNA from total extracted DNA. T11-1 is the 30 cm. deep sample from transect T11. Media: VFA Minimal media enriched with Volatile Fatty Acids. F: minimal media enriched with Formaldehyde. P: minimal media enriched with Peptone and Yeast Extract, M: minimal media enriched with Methanol, LB: Organic media for heterotrophic aerobic bacteria. Fe^{2+}: minimal media enriched with ferrous iron. N.D.: no data.

Culture	Blast result (NCBI database)	Gene Bank ID number	Query coverage	Max. Ident
T11-1 VFA	Unc. Proteobacterium	EF699933.1	100%	99%
	*Shigella flexneri*FBD002	EU009187.1	100%	99%
	Unc. Archaeon SPS46	AJ606292.1	10%	100%
	Unc. Propionibacterium 402C1	AM420143.1	100%	100%
T11-1 F	*Psychrobacter sp*. 9B	AY689064.1	100%	98%
	Antarctic sea water bac. BSW10170	DQ064630.1	100%	98%
T11-1 P	Unc. Archaeon SPS33	AJ606279.1	19%	100%
T11-1 M	*Citrobacter koseri* CP000822.1	CP000822.1	100%	92%
T11-1 LB	*Psychrobacter sp*. 9B	AY689064.1	100%	98%
	Antarctic sea water bac. BSW10170	DQ064630.1	100%	98%
T11-1 Fe^{2+}	N.D.			

heterotrophic media under aerobic and anaerobic conditions inoculated with samples from all along the column. There was no obvious relationship between depth and bacterial growth, indicating that viable bacteria are present along the column at all depths. Chemolithotrophic media produced less efficient growth, indicating that chemolithotrophs were not present in high numbers on these ecosystems. The opposite was observed for heterotrophic microorganisms, which have both aerobic and anaerobic representatives. Different microorganisms are present in the Imuruk Lake permafrost, since different media gave positive growth. In the case of sample T11-1, growth was observed in heterotrophic media under aerobic conditions and in the basal media under anaerobic conditions enriched with peptone plus yeast extract, methanol, formaldehyde, and volatile fatty acids. There was also gas production in the media enriched with peptone and yeast extract and VFA. These cultures inoculated with sample T11-1 were used for total DNA extraction, amplification, cloning and sequencing of the 16S rRNA gene (Table 2). Gas production could be congruent with the presence of methanogenic bacteria (Kotsyurbenko 2005). Amplification, cloning, and sequencing of the 16S rRNA confirmed this observation.

The 16S rDNA amplification from DNA extracted from cultures allowed identification of the presence of members of the *Psychrobacter* genus (Table 2). Also, the presence of some members of *Propionibacterium* genus, characterized by anaerobic growth using fatty acids for energy uptakes with production of propionic acid, was confirmed. Some uncultured Antarctic sea water representatives were also identified by 16S rRNA sequencing.

Soil samples from several depths were hybridized with specie- or genera-specific DNA probes and compared with universal staining (DAPI) for cell counting and evaluation of cell density along the column. Figure 4 shows a universal stained microbial preparation of a sample from tomographic Line 11 obtained at a depth of 2 m. Bacterial counting by light microscopy was used for cell density quantification. Figure 4 shows the population gradient (cells/gr of soil) with depth.

The presence of active bacteria on frost soil was determined by FISH techniques (Fig. 5). Hybridization of the RNA probe is done over the 16S rRNA, thus only active bacteria, which are sometimes uncultivable, can be detected. This technique requires the sample to be fixed at the moment of sampling to ensure the viability of the 16S rRNA molecule population.

Population gradient along the core (Fig. 5) was determined by direct counting of stained samples from 30 cm, 1 m, 1.5 m, 2.1 m, 3.1 m, and 3.6 m depth. Hybridized samples with genera- and group-specific DNA probes were counted to evaluate the correspondent percentage of the cell population (Fig. 5).

Bacterial density decreased with depth (Fig. 5), which is congruent with a permafrost model. An active layer develops during the summer on the first 50 cm cross section of the crust, and soil became completely frost down to this depth all through the year. This active layer develops a dense active bacterial population that is reduced during winter due to lower temperatures. The permafrost model is congruent with lower bacterial density on soil frosted year-round. An interesting result was the location of active bacteria under 50 cm depth. 16S rRNA sequencing results confirmed the presence *Psychrobacter* gen. representatives, corroborating the results obtained in culture experiments and underlying the identification of active microorganisms on the frosted layer of the soil.

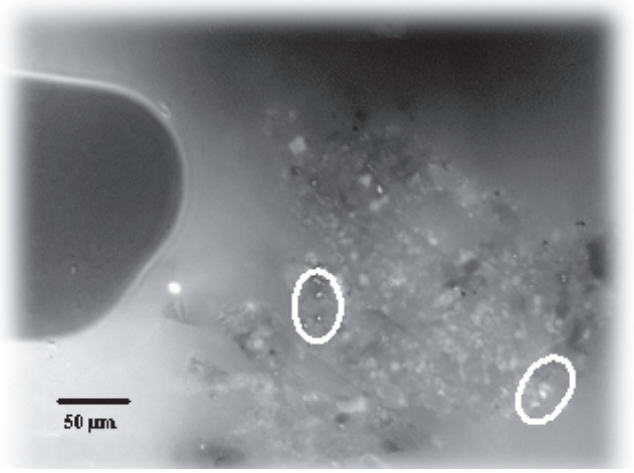

Figure 4. Soil sample from tomographic Line T11 stained with DAPI and used for cell quantification. Bacteria are the white spots inside the circle.

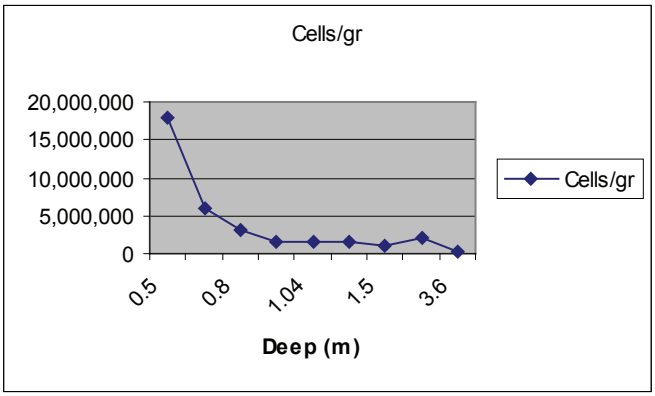

Figure 5. Population density (cells per gram of soil) gradient along the borehole from tomographic Line 11.

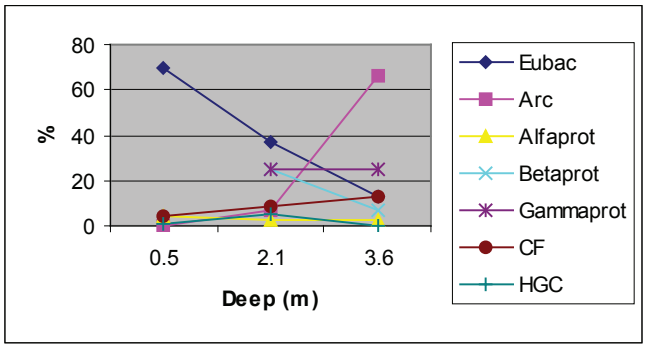

Figure 6. Percentage of different group pf microorganisms along the T11-1. Column identified by FISH techniques.

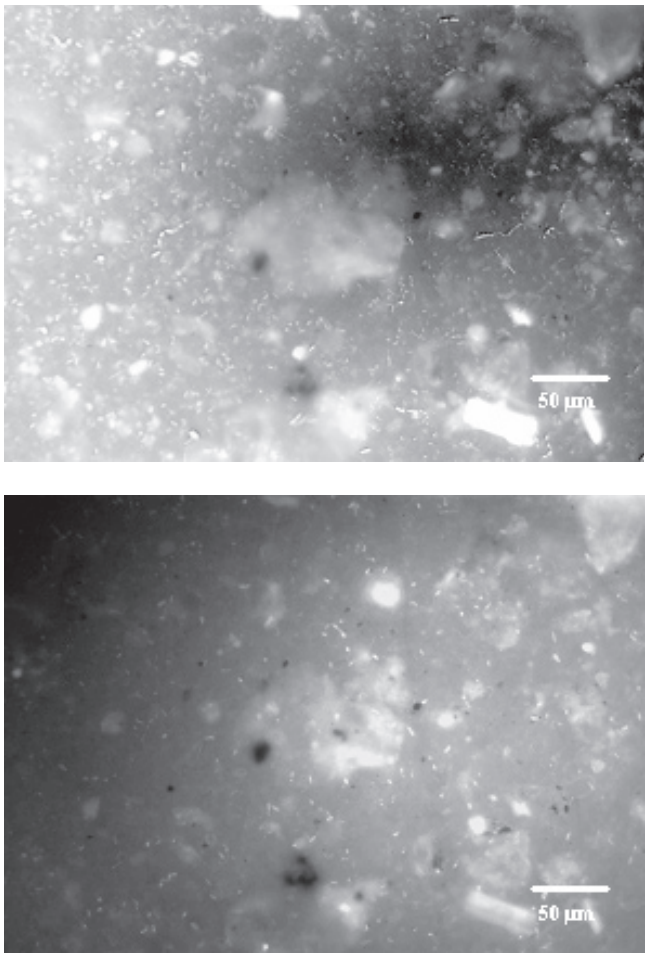

Figure 7. Universal staining DAPI preparation of a sample from the culture T-11-6 soil in heterotrophic media (top). Same culture preparation hybridized with *Alfaproteobacteria*-specific DNA probe labeled with CY3 fluorophore. Bacteria are small white spots.

The cell density decreased with depth; the lower the depth, the lower the bacterial population—a consequence of the harsh conditions of permafrost environments. Not only is reduction of the bacterial number the interesting data reported by these experiments, but also the fact that several microorganism groups were detected all along the column (Fig. 6). The percentage of every group varied with depth. On the first 50 cm of the soil column the main microbial population was composed by *Bacteria*. The presence of this type of microorganisms is constantly reduced with depth. While members of the domain *Archaea* have a low representation in the upper part of the column, its population increased with depth.

The Archaea identified on the grown media T11-1 P and T11-1 VFA (Table 2) are closely related to acetoclastic and hydrogenotrophic methanogens (Kotsyurbenko 2003).

The viability of microorganisms on the permafrost was tested by sample inoculation on growth media and following the growth of the cultures. Figure 7 shows bacteria preparation from the aerobic heterotrophic media inoculated with a 3.6 m deep sample from T11 borehole. The quantification of every metabolic group of bacteria was done by comparison of the total bacteria stained with the universal stain DAPI (Fig. 7, top) and the positive hybridization signals with group specific DNA probes (Fig. 7, bottom).

Conclusions

Abundant cells per mg of sample were detected in the first 60–70 cm of the column (the permafrost active layer). Accordingly to in situ hybridization and metabolic analysis, an active microbial layer was detected on the first 60–70 cm. Hybridization with specific 16S rRNA probes reported the presence of a high number of microorganisms from the *Bacteria* domain in the upper part of the column, which is congruent with the higher temperature reached at this depth during the summer. In contrast, deeper samples gave decreasing numbers for members of the bacterial domain, while the cell density for *Archaea* started to grow. From 2.1 m depth to the 3.6 m, the *Archaea* are the most abundant, and it correlates with the fact that, at this depth, the soil is permanently frozen. The production of gas and the identification of archaeal-related sequences on the T11-1 enrichment cultures are congruent with the presence of methanogenic *Archaea* and with the permafrost model.

These results are congruent with a putative ecosystem completely isolated from the surface and protected against possible harsh atmospheric conditions with the production of methane. The detection of this type of ecosystem in permafrost increases the possibility of existence of life in other planetary bodies like planet Mars, especially after the detection of methane in the Mars atmosphere by the Mars Express Planetary Fourier Spectrometer (Formisano et al. 2004).

Acknowledgments

The 2005 expedition to Imuruk Lake was supported by Centro de Astrobiologia-INTA (Spain). The laboratory experimental procedures were supported by Grant ESP 2006-06640 “Desarrollo de Tecnología para la identificación de vida de forma automática” from the Spanish Government. We thank the Bering Land Preserve staff (U.S. National Parks) for their help, especially Dr. Chris Young and INTA and Dr. Juan Pérez-Mercader for helping us during the campaign and later experimental work development.

References

Dyar, M.D. & Schaefer, M.W. 2004 Moessbauer spectroscopy on the surface of Mars: Constraints and expectations. *Earth and Planetary Science Letters* 218: 243-259.

Formisano, V., Atreya, S., Encrenaz, T., Ignatiev, N. & Giuranna, M. 2004 Detection of methane in the atmosphere of Mars. *Science 306*: 1758-1761.

Frolov, A. 2003 A review of the nature and geophysical studies of the thick permafrost in Siberia: Relevance to exploration on Mars. *J. Geoph. Res.* 108(E4): 8039-8046. doi:10.1029/2002je001881.

Gilichinsky, D.A., Wilson, G.S., Friedmann, E.I., McKay, C.P., Sletten, R.S., Rivkina, R.M., Vishnivetskaya, T.A., Erokhina, L.G., Ivanushkina, N.E., Kochkina, G.A., Shcherbakova, V.A., Soina, V.S., Spirina, E.V., Vorobyova, E.A., Fyodorov-davydov, D.G., Hallet, B., Ozerskaya, S.M., Sorokovikov, V.A., Laurinavichyus, K.S., Shatilovich, A.Y., Chanton, J.P., Ostroumov, V.E. & Tiedje, J.M. 2007. Microbial populations in Antarctic permafrost: Biodiversity, state, age, and implication for astrobiology. *Astrobiolog* 7(2): 275-311.

Gomez, F., Grau-Carles, A., Vázquez, L. & Amils, R. 2004 UV radiation effects over microorganisms and study of protective agents. *ESA SP-545*: 21-25.

Gómez, F., Aguilera, A. & Amils, R. 2007. Soluble ferric iron as an effective protective agent against UV radiation: Implications for early life. *Icarus.* doi:10.1016/j.icarus.2007.04.008

Hopkins, D.M. 1963 Geology of the Imuruk Lake area, Seward Peninsula, Alaska. *U.S. Geological Survey Bulletin* 1141-C: C1-C101.

Kieffer, H.H. & Titus, T.N. 2001 TES mapping of Mars' north seasonal cap. *Icarus* 154: 162-180.

Klein, H.P. 1978. The Viking biological experiments on Mars. *Icarus* 34: 666-674.

Kotsyurbenko, O.R. 2005. Trophic interactions in the methanogenic microbial community of low-temperature terrestrial ecosystems. *FEMS Microbial. Ecol.* 53: 3-13.

Kotsyurbenko, O.R., Chin, K.J., Glagolev, M.V., Stubner, S., Simankova, M.V., Nozhevnikova, A.N. & Conrad, R. 2003. Acetoclastic and hydrogenotrophic methane production and methanogenic populations in an acidic West-Siberian peat bog. *GenBank ID number: AJ606292 (s*ubmitted 08-Nov-2003). Unpublished.

Litvak, M.L., Mitrofanov, I.G., Kozyrev, A.S., Sanin, A.B., Tretyakov, V.I., Boynton, W.V., Kelly, N.J., Hamara, D., Shinohara, C. & Saunders, R.S. 2006. Comparison between polar regions of Mars from HEND/Odyssey data. *Icarus* 180(1): 23-37.

Prieto-Ballesteros, O., Fernández-Remolar, D.C., Gómez, F., Torres Redondo, J., Fernández-Sampedro, M., Martín Redondo, M.P., Rodriguez-Manfredi, J.A., Gómez-Elvira, J. & Gómez-Ortíz, D. 2008. Astrobiological applications of the studies on the permafrost of the Imuruk Lake basaltic field area (Alaska). *Proceedings of the Ninth International Conference on Permafrost, Fairbanks, Alaska, June 29–July 3, 2008* (this proceedings).

Wynn-Williams, D.D. & Edwards, H.G.M. 2000. Antarctic ecosystems as models for extraterrestrial surface habitats. *Planetary and Space Science* 48: 1065-1075.

Thermal Dynamics of the Active Layer Along a Hydrologic Gradient Bordering Lakes in the McMurdo Dry Valleys, Antarctica

Michael N. Gooseff
Department of Civil & Environmental Engineering, Pennsylvania State University, University Park, PA 16802
J. E. Barrett
Department of Biological Sciences, Virginia Polytechnic Institute, Blacksburg, VA 24061
Scott Ikard
Geology & Geological Engineering Department, Colorado School of Mines, Golden, CO 80401
Melissa Northcott
Geology & Geological Engineering Department, Colorado School of Mines, Golden, CO 80401
Cristina Vesbach
Department of Biology, University of New Mexico, Albuquerque, NM 87108
Lydia Zeglin
Department of Biology, University of New Mexico, Albuquerque, NM 87108

Abstract

With little precipitation (<10 cm water equivalent annually as snow), soils of the McMurdo Dry Valleys (MDV) have limited water available to support hydrological or biogeochemical processes. Active layer depths across most of this landscape are <1 m. Saturated sediments are obvious in wetted margins on the shorelines of lakes, extending for up to ~10 m into a zone where typically arid MDV soils prevail. We propose that wetted margins of MDV lakes will differ from arid soils across the rest of the landscape in their active layer depth and temperature regimes because of the consistent presence of water within these wetted margins. We have monitored temperatures along a wetted margin of Lakes Fryxell, Bonney, and Joyce. During the austral summer, we found that drier soils promoted shallower thaw depths and that, at the same depths, wet soils generally had lower temperatures and smaller diurnal fluctuations than dry soils.

Keywords: active layer; Antarctica; McMurdo Dry Valleys; temperature time series.

Introduction

Soil temperature dictates physiological constraints on biological activity (Kirshbaum 1994) and is especially important in the McMurdo Dry Valleys (MDV) of Antarctica (Fig. 1) where temperature is a primary control over biogeochemical cycling and biotic communities (Doran et al. 2002b, Parsons et al. 2004, Aislabie et al. 2006). Similarly, soil moisture is a limiting factor in Antarctic soil ecosystems where low temperatures severely limit the availability of liquid water (Kennedy 1993). Most soil studies in the MDV have emphasized the top 10 cm of the soil profile, within the active layer that is generally 60 cm thick (Campbell et al. 1998).

There has been extensive research on active layer thermal dynamics in the Arctic, with emphasis on numerical modeling of these dynamics (Hinkel 1997), and their response to changing climate (Hinkel et al. 2001). Arctic active layer soils exhibit seasonal changes in surface energy balances comparable to those in the MDV, though the magnitudes and types of energy exchange differ greatly due to the presence of extensive vegetation in the Arctic, as well as substantial spring snowmelt infiltration and rain infiltration during the summer. There have been several studies of permafrost and active layer processes in the Victoria Land (Bockheim et al. 2007, Guglielmin 2006), but little attention has been paid to active layer thermal dynamics on floors of the MDV, particularly with respect to dependence upon soil moisture. Bockheim and Tarnocai (1998) note that most of the surficial permafrost in the MDV is dry permafrost, which has very low water content (<5%), and Pringle et al. (2003) have documented thermal properties of MDV permafrost and active layer from two fairly high elevation sites in the region.

The shores of MDV water bodies are continually proximal to liquid water during the austral summer, and wick water from the lake and stream edges to the dry mineral soil. These wetted margins are visually apparent, and represent a hydrologic gradient in soil moisture from saturated at the water body to dry conditions at distal locations. Around lakes, Gooseff et al. (2007) found that the dimensions of these wetted margins vary as a function of both shore slope and depth of the active layer. We propose that, because these wetted margins represent an obvious gradient of soil moisture, the active layer thermal dynamics across these wetted margins should vary, with general soil moisture condition, due to the differences in thermal conductivity and heat capacity of the soil matrix with changes in soil moisture status.

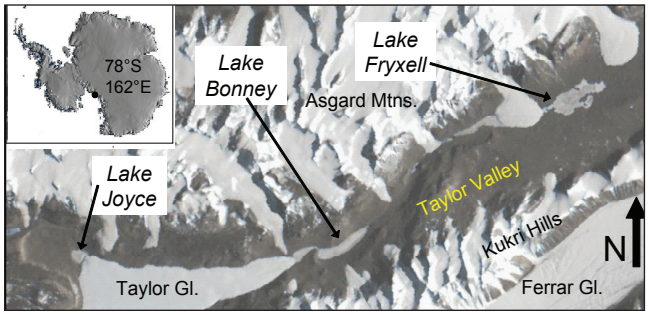

Figure 1. Map of Taylor Valley, Antarctica and Lakes Joyce, Bonney and Fryxell.

Table 1. Distances to thermocouple strings from the edge of the lake, in meters (XX), and depth of deepest thermocouple, in meters (YY), in the format XX,YY. All thermocouples are spaced by 10 cm vertically on a string. The number of thermocouples at a location is determined by the depth of penetration possible when deployed, with a maximum of 0.5 m depth.

	Study Plot		
String	*Lk. Fryxell*	*Lk. Bonney*	*Lk. Joyce*
I	0.0, 0.50	0.0, 0.35	0.0, 0.35
II	0.2, 0.50	0.20, 0.32	0.2, 0.30
III	5.1, 0.45	1.89, 0.50	1.75, 0.40
IV	10.3, 0.45	3.64, 0.50	3.20, 0.33
V	11.3, 0.33	5.42, 0.50	3.80, 0.17

Site Description and Methods

Site description

The MDV are located on the western edge of the Ross Sea, at approximately 78°S 162°E. The climate is cold, with annual mean temperatures of -20°C, and dry, with <10 cm precipitation (all as snow) annually (Doran et al. 2002a). The water balance of closed-basin lakes on the valley floors are maintained by incoming glacial meltwater stream flow and losses due to annual ablation of perennial ice covers, and evaporation of open water "moats" that form along the lake shores during the austral summer. Thus, lake shore soils and sediments are immediately adjacent to liquid water for approximately 2.5 months annually. Due to the dry nature of the MDV and the presence of continuous permafrost, these shoreline sediments wick lake water several meters inland from the shoreline.

Methods

In January 2005, we deployed thermocouple strings with 10 cm vertical spacing along transects across wetted margins of the north shore of Lake Joyce, the south shore of the east lobe of Lake Bonney, and the north shore of Lake Fryxell (Fig. 1). Five thermocouple strings were deployed at each lake-side location (Fig. 2A): String I at the water edge, String II 20 cm from the shoreline, String III at a point bisecting the wetted margin, String IV just before the outside edge of the wetted margin, and String V outside of the wetted margin (Fig. 2B, Table 1). Thus we collected active layer temperature data across three hydrologic gradients, from saturated conditions at String I to dry conditions at

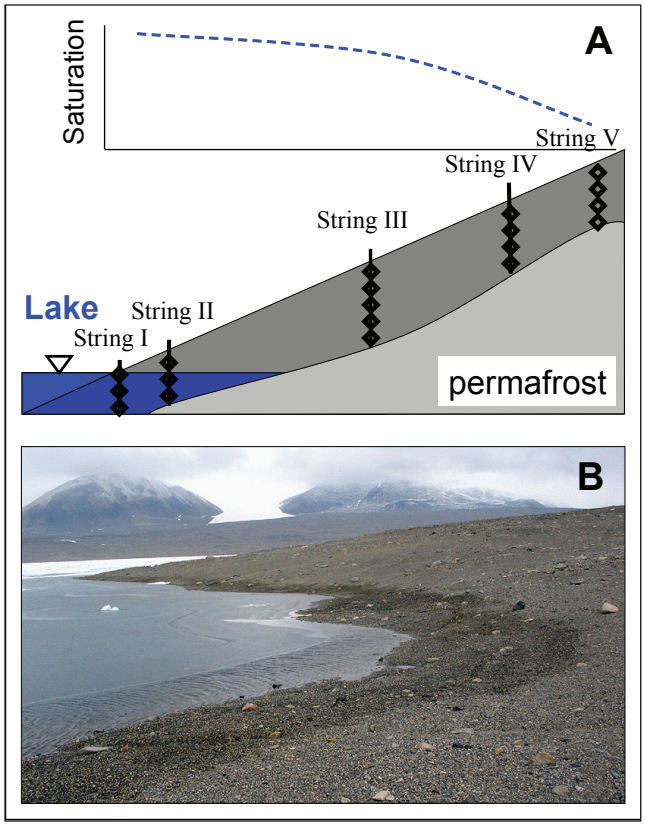

Figure 2. (A) General layout of thermocouples along transects, across wetted margins, (B) wetted margin around Lake Fryxell, extending ~10 m from shoreline.

String V. Thermocouple strings were built in a lab prior to deployment and then inserted into the ground using a thin steel rod attached to the end of the thermocouple string. The rod was subsequently removed after being inserted to the point of refusal.

At each transect, thermocouple data was collected by a Campbell Scientific CR-10XT datalogger via an AM-25T multiplexer. In addition, a thermistor was also deployed which collected air temperature data near the soil surface, in a shaded location. During the 2004-05 and 2005-06 field seasons, we were able to visit the dataloggers intermittently. Records are not continuous for the entire time of deployment due to datalogger failures. At Lake Joyce, data was collected on a 4 h interval from 18–22 Jan. 2005, from 12 Jul. to 15 Dec. 2005, and on a 15 min interval from 27 Dec. 2005 to 04 Jan. 2006. At Lake Fryxell, data was collected on a 15 min interval from 18–25 Jan. 2005, on a 4 h from 02 Jul. to 05 Dec. 2005, on a 1 h interval from 07 Jan. to 01 Feb. 2006, and on a 4 h interval from 01 Feb. to 30 Jan. 2007. At Lake Bonney, data was collected on a 15 min interval from 15–22 Jan. 2005, and on a 4 h interval from 03–30 Jan. 2006, and from 14 Dec. 2006 to 02 Feb. 2007.

We analyzed the collected subsurface temperature data by calculating 1) total degree-days of thaw (DDT) for each thermocouple record and 2) the daily amplitudes of temperature at every site, for days on which complete data collection was available (539 d at Lake Fryxell, 81 d at

Lake Bonney, and 166 d at Lake Joyce). We then computed frequency-duration curves (FDCs) using these data to illustrate comparisons among the thermocouple strings at each site, along the hydrologic gradients. Temperature FDCs that plot to the right on such graphs indicate a greater proportion of large diurnal cycles compared to those that plot toward the left. Our expectation is that thermocouple records in the drier shore sediments (i.e., Strings IV and V) will have greater diurnal variation than strings in more saturated conditions (Strings I-III). Because each thermocouple string is not deployed to a common depth, we cannot compare all FDCs on the same plot. Thus, for a more fair comparison, we have only plotted FDCs for thermocouple strings that have common or very similar depths (within 3 cm of each other). From Lakes Fryxell and Bonney, we plot only Strings III, IV and V. From Lake Joyce, we plot only Strings II, III, and IV.

Results and Discussion

Temperatures in the subsurface vary throughout the year from -50°C to just above 10°C. At Lake Fryxell, the time series data indicate a tight coupling of the temperature records near the shore (Strings I and II) and increasing vertical temperature gradients at more distal locations (Strings III, IV, and V) (Fig. 3). Similar patterns are evident from data collected at Lake Bonney (Fig. 4) and Lake Joyce (Fig. 5). It is worth noting that none of these locations appear to go through an extensive periods of zero-curtain condition during thawing (Figs. 3–5), as has been observed in arctic active layers (Hinkel et al. 2001). The only freeze-up data available is from Lake Fryxell, which does indicate a few days of zero-curtain condition close to the shorelines (Strings I and II) at Lake Fryxell (Fig. 3).

The vertical temperature gradients (Figs. 3–5) are not perfectly comparable as the thermocouples are deployed at different absolute depths along each thermocouple string. Despite these differences, these gradients are approximately comparable for Strings I-IV at Lake Fryxell, as the penetration depths are 50 cm, 50 cm, 45 cm, and 45 cm, respectively. At Lake Bonney, Strings III, IV, and V are all deployed to the same depths, and it is evident that String IV appears to have the greatest diurnal fluctuation in temperature, at the 10 cm depth (Fig. 4). At Lake Joyce, String IV is offset by 3 cm from Strings II and III (Fig. 5).

To compare integrated heating among locations along the soil moisture gradients, the DDT values are presented in Table 2. As expected, there is a pattern of diminishing degree-days above freezing with increasing depth. Similar to the analyses of temperature time series, these data are not ideally comparable among thermocouple strings within a site because of different absolute depths. The vertical pattern exceptions are String II and String V at Lake Fryxell, and String I at Lake Bonney. These unexpected results are likely due to one of three explanations: (1) surface evaporation which may drive cooling in the upper layers of the soil, (2) longitudinal movement of cool water from

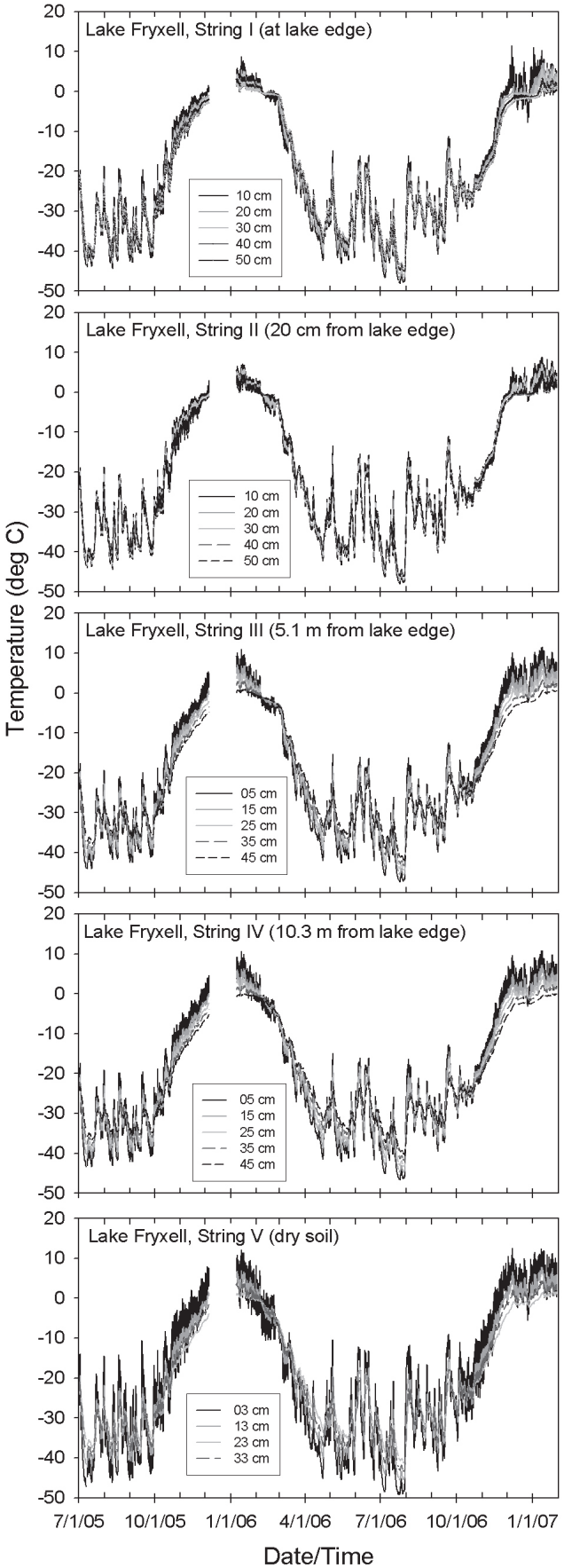

Figure 3. Lake shore soil temperatures from thermocouple strings I through V at Lake Fryxell.

Table 2. Degree-days of thaw (DDT, °C·d) for entire temperature records of thermocouples and thermistors. The table is organized by thermocouple string and position along the string with 1 = shallowest and 5 = deepest.

	Thermocouple String				
TC#	I	II	III	IV	V
			Lake Fryxell		
Air			274.8		
1	264.7	230.0	427.5	384.2	543.0
2	173.2	178.8	292.5	245.5	300.9
3	140.4	162.7	173.1	126.4	39.2
4	83.3	99.0	92.7	53.7	140.8
5	41.0	114.9	16.9	0.00	-
			Lake Bonney		
Air			234.4		
1	40.0	100.8	348.0	425.3	447.7
2	60.5	110.9	240.2	327.4	312.8
3	67.7	78.0	146.4	203.1	190.8
4	64.9	78.1	74.0	118.4	107.5
5	-	-	16.8	60.0	39.0
			Lake Joyce		
Air			53.5		
1	97.4	86.0	134.3	160.3	157.5
2	83.5	81.0	84.3	81.8	104.1
3	35.4	49.1	47.1	36.5	-
4	10.0	15.2	20.7	13.3	-
5	-	-	3.6	-	-

the shoreline outward toward the dry soils, or (3) change in surface conditions. String I at Lake Bonney was found to be inundated at the surface in Jan. 2006, due to rising lake levels. Thus the temperature signal at this location becomes more representative of benthic interaction with a water column than a soil exposed to atmosphere. The longitudinal movement of water is a possibility at String II at Lake Fryxell, given that the water at the lake shore (String I) is generally cooler within the same ~depths (positions 4 and 5).

The comparisons of temperature dynamics are also informed by the frequency analysis of diurnal temperature amplitudes (Fig. 6). At the Lake Fryxell transect, the diurnal amplitudes of temperatures increase for near-surface thermocouples from String III to IV to V, with similarities between III and IV, and much more variable overall at V (red curves, Fig. 6A). The same pattern exists at the thermocouples in the 2nd position (green curves, Fig. 6A), but changes at the 3rd thermocouple position, with Strings III and V similar in their FDC curves, and that of IV being generally less variable (blue curves, Fig. 6A). This is unexpected, and may be due to (1) the fact that these mid-transect locations are buffered at depth because of greater soil moisture or (2) lateral movement of water (i.e., along a direction that is parallel to the shoreline), which was not investigated here. At Lake Bonney, String IV is more variable at thermocouple positions 1 and 2, than Strings III and V (red and green curves, Fig. 6B). Similar to the patterns observed at Lake Fryxell, this sequence changes at position 3, and String IV becomes generally less variable than Strings III and V (blue curves, Fig. 6B). This

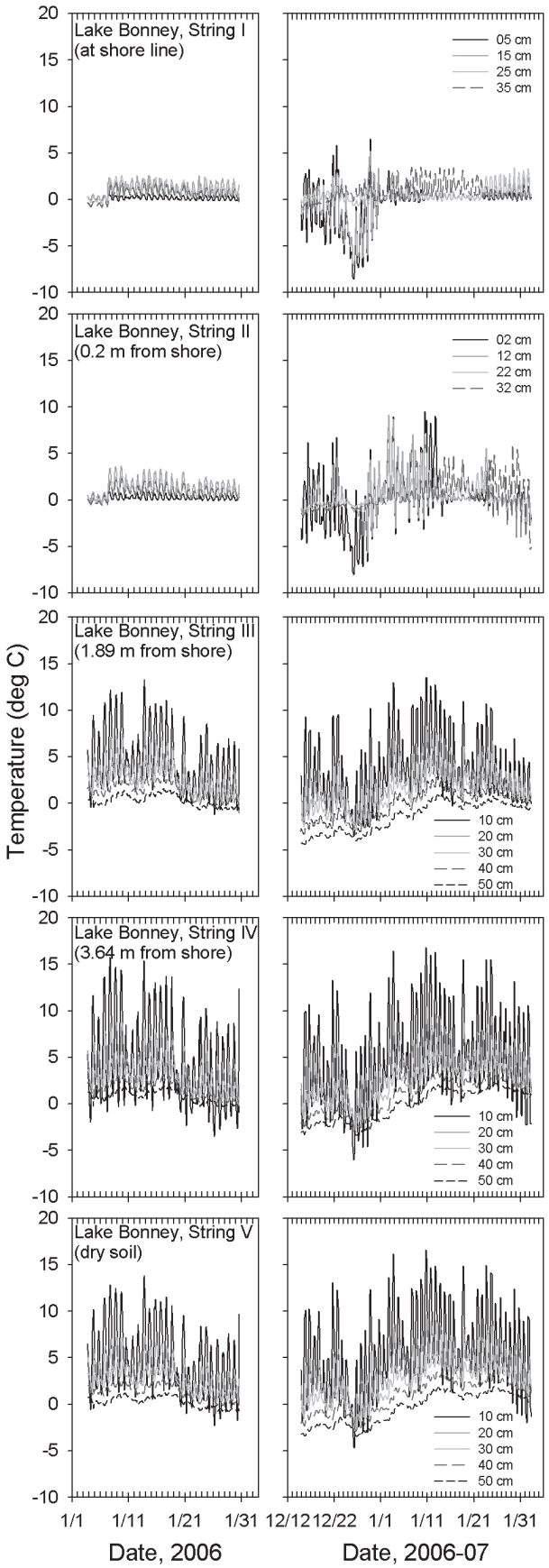

Figure 4. Lake shore soil temperatures from thermocouple strings I through V at Lake Bonney.

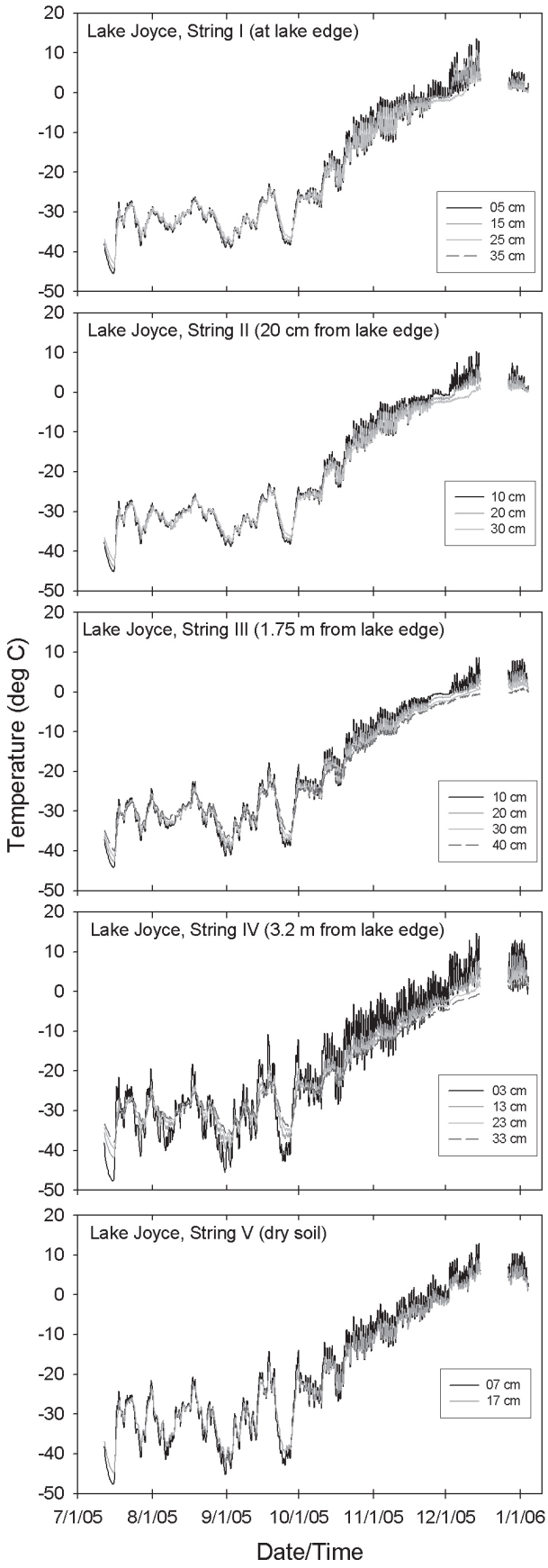

Figure 5. Lake shore subsurface temperatures from thermocouple strings I through V at Lake Joyce.

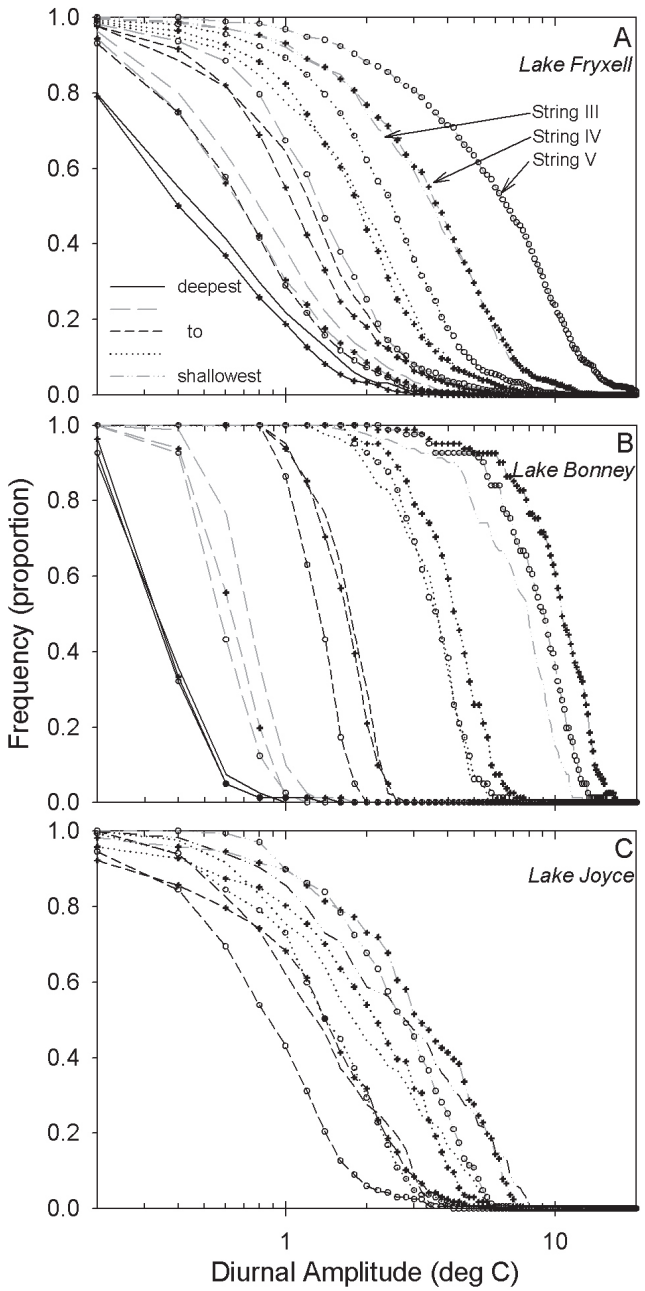

Figure 6. Frequency-duration curves (FDCs) for daily amplitudes in soil temperatures at A) Lake Fryxell, B) Lake Bonney, and C) Lake Joyce. Each curve represents the entire record for a single thermocouple. Strings with comparable depths of thermocouple deployments are presented for comparison. Strings are distinguished by symbols on the curves: nearest the lake has no symbol, the next one out has a cross symbol, and the furthest an open circle. Similar depths are indicated by pattern.

may indicate here too that String III is well buffered because of (1) enhanced soil moisture at depth at this position, (2) this mid-transect location is a transition point between the influence of convected heat from either longitudinal (i.e., away from the shoreline) flowing water from the shore to the dry soils, or (3) the influence of lateral flow of water not investigated here. At Lake Joyce, there is a consistent pattern of String IV having greater diurnal variability, in

general, than String V at thermocouple positions 1, 2, and 3 (red, green, and blue lines, respectively, Fig. 6C). At the 4th thermocouple position (next to deepest), String V is much more variable in daily temperature fluctuation than String III at Lake Fryxell (black curves, Fig. 6A), and very similar for Strings III-V at Lake Bonney (gray curves, Fig. 6B). At the deepest thermocouple location (positions 5) temperature amplitudes are similarly buffered at Strings III and IV at both Lake Fryxell (Fig. 6A) and Lake Bonney (Fig. 6B).

These three sets of results generally support our expectation, that drier soils would be warmer and more variable than wetter soils. In particular, this notion is supported by the evident temperature time series magnitudes, which are greater at the distal thermocouple strings than at the near-shore strings, as well as by the general patterns of increased DDF at the distal locations compared to the nearshore locations. Finally, for the most part, locations that have less soil moisture are more variable in daily temperature amplitude than more saturated soils.

Conclusions

We found that, in general, soils with little soil moisture were warmer and more variable in temperature than wetter soils. This investigation focused on locations of soil moisture gradients near three lakes in the MDV, which may host variable microbial communities due to potential dependence upon habitat conditions, namely soil temperature and water content. These factors also influence biogeochemical processes across these hydrologic gradients.

Acknowledgments

The authors gratefully acknowledge Raytheon Polar Services Corp., Petroleum Helicopters, Inc., and UNAVCO for logistical and field support, and the McMurdo Long Term Ecological Research project. This research was funded by the National Science Foundation under collaborative research grants OPP 03-38267, 03-36970, and 03-38174. Any opinions, findings, and conclusions or recommendations expressed in this material are those of the author(s) and do not necessarily reflect the views of the National Science Foundation.

References

Aislabie, J.M., Chhour, K.L., Saul, D.J., Miyauchi, S., Ayton, J., Paetzold, R.F. & Balks, M.R. 2006. Dominant bacteria in soils of Marble Point and Wright Valley, Victoria Land, Antarctica. *Soil Biology & Biochemistry* 38: 3041-3056.

Bockheim, J.G. & Tarnocai, C. 1998. Nature, occurrence and origin of dry permafrost. *Proceedings of the Seventh International Permafrost Conference*, 57-63.

Bockheim, J.G., Campbell, I.B. & McLeod, M. 2007. Permafrost distribution and active-layer depths in the McMurdo dry valleys, Antarctica. *Permafrost and Periglacial Processes* 18(3): 217-227.

Campbell, I.B., Claridge, G.G.C., Campbell, D.I. & Balks, M.R. 1998. Permafrost properties in the McMurdo Sound-Dry Valley region of Antarctica. *Proceedings of the Seventh International Permafrost Conference*, 121-126.

Doran, P.T., McKay, C.P., Clow, G.D., Dana, G.L., Fountain, A.G., Nylen, T. & Lyons, W.B. 2002a. Valley floor climate observations from the McMurdo dry valleys, Antarctica, 1986–2000. *Journal of Geophysical Research* 107(D24): 4772, doi:10.1029/2001JD002045.

Doran, P.T., Priscu, J.C., Lyons, W.B., Walsh, J.E., Fountain, A.G., McKnight, D.M., Moorhead, D.L., Virginia, R.A., Wall, D.H., Clow, G.D., Fritsen, C.H., McKay, C.P. & Parsons, A.N. 2002b. Antarctic climate cooling and terrestrial ecosystem response. *Nature* 415: 517-520.

Gooseff, M.N., Barrett, J.E., Northcott, M.L., Bate, D.B., Hill, K., Zeglin, L., Bobb, M. & Takacs-Vesbach, C. 2007. Controls on soil water dynamics in near-shore lake environments in an Antarctic polar desert. *Vadose Zone Journal* 6: 841-848.

Guglielmin, M. 2006. Ground surface temperature (GST), active layer and permafrost monitoring in continental Antarctica. *Permafrost and Periglacial Processes* 17(2): 133-143.

Hinkel, K.M. 1997. Estimating seasonal values of thermal diffusivity in thawed and frozen soils using temperature time series. *Cold Regions Science and Technology* 26(1): 1-15.

Hinkel, K.M., Paetzold, F., Nelson, F.E. & Bockheim, J.G. 2001. Patterns of soil temperature and moisture in the active layer and upper permafrost at Barrow, Alaska: 1993–1999. *Global and Planetary Change* 29(3–4): 293-309.

Kennedy, A.D. 1993. Water as a limiting factor in the Antarctic terrestrial environment: A biogeographical synthesis. *Arctic and Alpine Research* 25(4): 308-315.

Kirschbaum, M.U.F. 1995. The temperature-dependence of soil organic-matter decomposition, and the effect of global warming on soil organic-C storage. *Soil Biology & Biochemistry* 27: 753-760.

Parsons, A.N., Barrett, J.E., Wall, D.H., & Virginia, R.A. 2004. Soil carbon dioxide flux from Antarctic Dry Valley soils. *Ecosystems* 7(3): 286-295.

Pringle, D.J., Dickinson, W.W., Trodahl, H.J. & Pyne A.R. 2003. Depth and seasonal variations in the thermal properties of Antarctic Dry Valley permafrost from temperature time series analysis. *Journal of Geophysical Research* 108(B10): 2474, doe:10.1029/2002JB002364.

The Mechanism of Ice Formation in Connection with Deformation of the Freezing Layer

J.B. Gorelik
Earth Cryosphere Institute SB RAS, Tyumen, Russia

Abstract

The freezing of a closed volume of water-saturated sands is considered in this report. The separate clay body may be situated inside sand. Only the freezing layer may be deformed under action of cryogenic pressure. It is shown that a layer of ice may be formed in the volume. For its formation, it is necessary that the effective radius of the water-supplying area be more than some critical value. In this condition, the frozen layer is similar to the frozen part of a pingo with a water lens in its base. In the opposite case, only the frozen soil with different ice content may be formed. If the vertical length of the clay body is less than some limit, it will be pulled out from its sandy environment or it will be broken along some of its horizontal cross section.

Keywords: cryogenic pressure; deformations; frozen layer; ice content.

Introduction

Thick ice bodies are spectacular features of the permafrost environment. The mechanisms of formation of some of them are still debatable and there are ten hypotheses concerning their formation. They are subdivided into two groups: a) ice body formed inside the ground; b) ice body formed on the surface of the ground and then buried by alluvium. Different viewpoints on this problem are reflected in several books and in numerous articles. Recently some articles were published where mechanisms from both of these groups are discussed and differences in ideas are not resolved.

The idea of ice body formation as a result of segregation or injection is mostly found among hypotheses of the first group. The burial of glacial ice is the most recognized hypothesis of the second group. Existing approaches cannot completely explain ice body formation under certain conditions, as well as structure ice and structure of the enclosing sediments.

The mechanism of ice body formation is proposed in this paper. It attempts to explain a number of important characteristics of the structure of ice body deposits.

Deformations of Freezing Layer

Let us consider the freezing of a closed volume of water-saturated soil which includes clay and sand. The bottom and sides of this volume are formed by dense clay with sand inside it. It is assumed that a separate clay body may be situated inside the sand (Fig. 1). Additional assumptions are: 1) the freezing layer is connected rigidly with clay sides of the volume and 2) the additional water supply of the considered volume may be realized from the sands which are outside of the clay sides. Thus, only the freezing layer may be deformed in such a system. These deformations are caused by cryogenic pressure which arises in a closed system, with increase in the volume of freezing water due to a difference in the density of water and ice.

During freezing of a closed volume, the cryogenic pressure increases, causing the plate of freezing ground to curve upwards. The upward-directed force acts on the central clay body while it is freezing; simultaneously the opposite direction force acts on the freezing layer and holds it back from deformations. The force causes tension stresses in the horizontal direction at the unfrozen part of the clay body. These stresses have a maximum at the contact of frozen and unfrozen parts, and they increase in time. When the cohesion value of the unfrozen material is reached, then the clay body is broken along this frozen/unfrozen contact. The crack between broken parts is filled with water which freezes, resulting in ice body formation. For analysis of the transformations in the system, it is necessary to consider the deformation process of the freezing layer first.

For general consideration, let us introduce the "closing" depth of the volume h_0. It determines the freezing depth at which surface water is not connected with freezing soil. The source of surface water in Figure 1 is nonessential anymore. It is assumed that the deformations of the freezing layer at all clay bodies and at the peripheral water-supplying zone are negligible. We use R_w and R_f for the effective radii of the water-supplying zone and of the rigid connection contour accordingly. The inequality takes place in general: $R_w \geq R_f$ (Fig. 1). Assuming that the thickness of the frozen layer, h, is much less than the value of R_f, its mechanical behavior may be described as deformations of the thin plate. Real configuration of all the elements of the considered system is very complicated. Theoretical analysis may be realized for the system with any symmetry. Later on, we shall use the mechanical analog of the Figure 1 scheme,where all vertical walls are cylindrical. This analog has the axis symmetry. In this analog, the vertical deformation of freezing layer ζ_r is the function of the radial coordinate r and time t.

It is considered that the deformations of the freezing layer are started after freezing of the surface sources of water. These deformations are limited if the acting stresses are smaller than the long-term strength of frozen sands, and they are increased with no limit in the opposite case. The attenuated deformations are described by the equation of

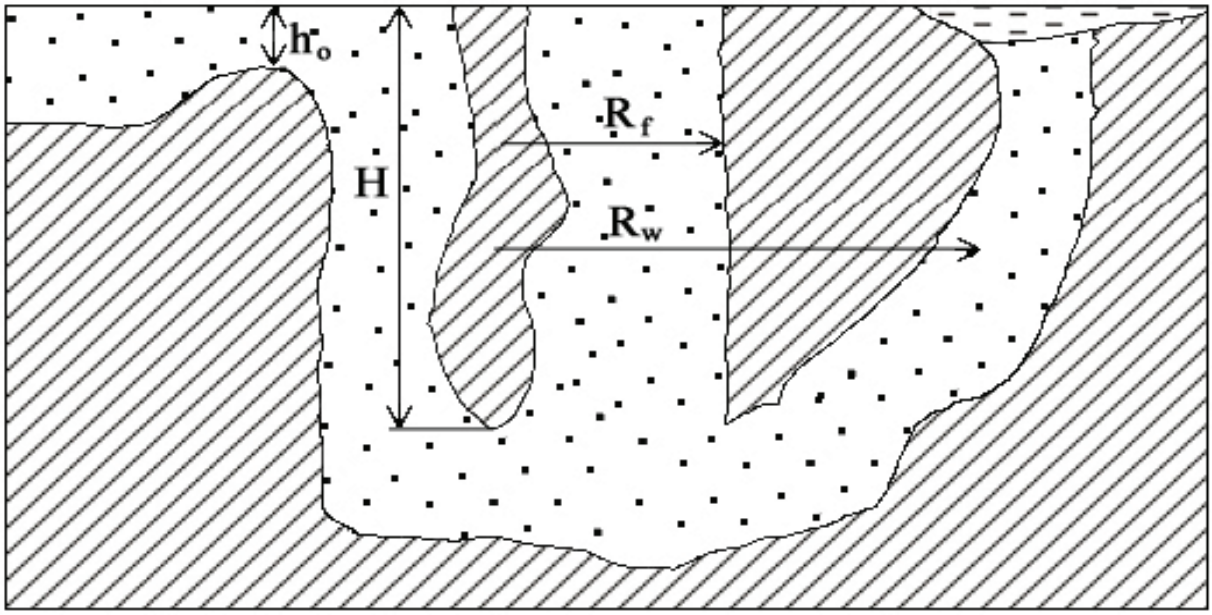

Figure 1. The scheme of closed volume before freezing. - clay, - sands, - surface basin. The notation of the values is in the text.

hereditary creep theory (the instantaneous deformations are negligible):

$$\varsigma_r(t) = t_r^{-1}\int_0^t \varsigma_r^u(\tau)\cdot\exp\left[-(t-\tau)/t_r\right]d\tau \qquad (1)$$

where E, v, η are elastic modulus, the Poisson ratio and viscosity coefficient of frozen sand; $t_r = 2(1+v)\eta/E$ is relaxation time; $\zeta_r^u(t)$ is elastic solution of the task (its change in the time is due to the slow change of cryogenic pressure and of the thickness of the freezing layer at the same time). The characteristics of frozen soils should be defined from the tests with attenuated deformations. Methods and results of the frozen soils tests, both for the attenuated and for no-limited deformations are fully presented by Grechishev (1963). The constant E should be defined at the stabilized state in the tests of frozen sample and constant η should be defined by measuring the deformations rate through the same tests in the beginning of the test. Then equation (1) describes satisfactorily these experimental data of frozen sand attenuated deformations in time. For frozen sands, the relaxation time is not more than 15 days as a rule. For a closed system, the elastic bend, ζ_r^u, is defined by equation:

$$D\cdot\Delta^2\varsigma_r^u = -\rho_s g h + P_c - \rho_w g\varsigma_r^u \qquad (2)$$

where P_c is the value of cryogenic pressure; ρ_s, ρ_w are the densities of frozen soil and of pore water; $D=Eh^3/12(1-v^2)$ – plate rigidity; Δ is the Laplasian operator; g is acceleration of gravity. The term $\rho_s gh$ is the pressure associated with weight of the freezing layer and the term $\rho_w g\zeta_r^u$ is pressure due to Archimedean force. The last arises owing to deformations inequality of the plate as it takes place for floating plates (Timoshenko 1967). It is important that the elastic reaction from the sandy bed to the freezing plate is absent because the effective stresses are equal to zero in a closed system (Gorelik 2007b). The last statement is true for the uniform loadings acting on the plate, considered here. The value $P=P_c-\rho_s gh$ defines the prevalence of cryogenic pressure over pressure of the freezing layer weight. It is always positive in a closed system, and it is upward-directed.

We shall consider the non-limit deformations only at the stage of stationary creep. These deformations may be described by the viscous-plastic soil flow model. The scheme of this flow is analogous to the flow of the viscous-plastic liquid in the cylindrical tube. At the stage of stationary creep, the freezing layer is shifted continuously relative to the clay walls of the volume. The elastic deformations are negligible, and the kern of the flow may be considered as rigid. Near the walls, there is a thin layer which is deformed as viscous uncompressible liquid. The beginning of the creep stage occurs when the intensity of the stress at the attenuated deformations stage reaches the value of long-term strength of frozen sands on the contour of the rigid connection. The definite values of abundance P_s and of freezing depth h_s correspond to execution of this criterion. The rigid kern velocity of the flow v_s for $h\geq h_s$, $P\geq P_s$ is defined by expression:

$$v_s = -\frac{\tau_s}{\eta}(R_f - r_s) + \frac{P}{4\eta h}(R_f^2 - r_s^2) \qquad (3)$$

where r_s is rigid kern radius. For running values of h and P it is defined by $r_s=2\tau_s h/P$; τ_s is long-term strength of frozen sands defined under shear-tests of the samples. The viscosity coefficient, η, in equation (3) is different than its value in equation (1) in general, and it must be defined under the same shear-tests during stationary creep stage. The shear-test may be realized by the rotation of a frozen soil tube with acting axial force as presented by Grechishev (1963).

Both cryogenic pressure P_c in equation (2) and the abundance P in equation (3) are not determined up to now. For its determination it is necessary to use the equation of water mass conservation in a closed system:

$$\frac{1}{\pi R_f^2}\int_0^{R_f}\varsigma_r 2\pi r dr = \\ = (\frac{\rho_w n_u - \rho_i n_f}{\rho_w\sqrt{n_u n_f}} + \frac{\Delta\rho_{wi}}{\rho_w}(\alpha^2 - 1))(h - h_0) \quad (4)$$

Here: ρ_i is the density of ice; $\Delta\rho_{wi}=\rho_w-\rho_i$; n_u, n_f are the soil porosities at the unfrozen and frozen states (they are constants here); $\alpha=R_w/R_i\geq 1$; $h\geq h_0$. For the determination the value of P in equation (3) it is necessary to derive the relation (4) over t taking into account $v_s=\partial\zeta_r/\partial t$ for the creep stage. In the equation (4) the average deformation of freezing layer (left part) is proportional to its thickness after closing the system. It occurs because of change it porosity migration of water from peripheral parts of the system (right part). These deformations are purely connected with nonzero densities difference $\Delta\rho_{wi}$. It may be shown that $\zeta_r=0$ for all r if we shall take on formally $\Delta\rho_{wi}=0$ in equation (4). Later on, we take the simple form of the relation between frozen depth and time: $h=(\beta t)^{0.5}$, where β is a constant proportional annual mean surface temperature and to the value of n_f^{-1}.

The written equations and the formulated additional conditions are sufficient to determine cryogenic pressure and deformations of the freezing layer in time. The behavior of the value P as a function of the freezing depth is shown on Figure 2a at the following initial data: $E=10^8$ *Pa*, $\eta=10^{13}$ *Pa·sec*, $\tau_s=1.8\cdot10^5$ *Pa*, $R_f=300$ *m*, $h_0=0$ *m*, $n_u=0.3$, $n_f=1.5n_u$, $\beta=1.3\cdot10^{-7}$ *m²/sec*, $\alpha^2=7$. It can be seen that the value of P has a bend at the deformations transition to the stationary creep stage.

The criterion of breaking of the central clay body may be written as: $P=cR_c/R_f$. Here c is the cohesion of the unfrozen clay and R_c is the radius of the central clay body. The clay bodies may be broken at any deforming stage (if, of course, the freezing depth will reach the needed value). For example, the dotted line on Figure 2a demonstrates the breaking stress with the parameters: $c=0.5\cdot10^5$ *Pa*, $R_f=300$ *m*, $R_c=50$ *m*. Figure 2b shows the correlation between bend lines of the freezing layer before and after breaking of the central clay body. At the breaking at the attenuated deformations stage, the bend line from double convex is transforming to the convex one. The experimental modeling of this process shows that this transformation is accompanied by increasing of the temperature and abrupt falling of the cryogenic pressure. Electromagnetic emission and crack formation in the freezing layer were observed during the process. But the frozen layer was unbroken as whole (Gorelik 2007a).

The further fluent lifting of the broken (upper) clay body part is possible, together with the frozen layer itself, for breaking at the stationary creep stage.

The breaking criterion does not take into account the vertical length of the clay body, H. But such interval of values H exists ($0\leq H\leq H^*$) that for every H from this interval the clay body will be pulled out from its sandy couch before it will be broken. The limiting value H^* is defined by two conditions: 1) the vertical stress at the contact of frozen and unfrozen parts reaches the value of c and 2) the upward-directed force is equal to the sum of the unfrozen part weight and the friction force at its lateral contact with sands. The expression for H^* is:

$$H^* = h^* + \frac{cR_c}{\Delta\rho_{sw} g R_c + 2\tau_t}; \quad (5)$$

where τ_t is the lateral stress of the friction; h^* is the freezing depth at which the unlimited in vertical direction clay body is broken. Similar conditions can be used to develop the equation for the freezing depth h^{**} at which the pulling out takes place at any H from the interval.

The ice body must be formed directly under the base of the clay body on its pulling out. The main tendencies in the deformation of the freezing layer under this process will be the same as at its breaking.

Water Flows and Ice Accumulation

All deformations of the freezing layer in a water-saturated closed system are connected with water inside this system. So, the deformations are negligible near the points of the rigid connection contour, and water is driven away from the freezing front here. The water flows to the freezing front in this area. It means that the porosity, n_f, is a function of radial coordinate r in general and it cannot take arbitrary values (as it is considered above approximately). The function $n_f(r)$ characterizes the local ice accumulation along the freezing layer by coordinate r. As it was noticed above, the constant β is proportional to n_f^{-1}; then the freezing layer thickness h_r at any radial point is connected with it at the points of the rigid connection contour h by dependence: $h_r=h(n_u/n_f(r))^{0.5}$. To find the function $n_f(r)$ it is necessary to use an additional correlation as the local equation of the skeleton's mass conservation (Gorelik 2007b):

$$(n_f - n_u)\partial z_f / \partial t = -(1 - n_f)v_f \quad (6)$$

where $\partial z_f/\partial t$, v_f are the rates of the freezing front movement and lifting of the upper surface of freezing layer relatively to the unfrozen part of the volume ($v_f=\partial\zeta_r/\partial t$ at the attenuated deformations stage and $v_f=v_s$ at the stationary creep stage). Between values of $\partial z_f/\partial t$, v_f and $\partial h_r/\partial t$ the connection exists: $v_f-\partial z_f/\partial t=\partial h_r/\partial t$ (Fig, 2c).

The rate v_s does not depend on r at the stationary creep stage and the values of n_f, v_s and $\partial z_f/\partial t$ may be calculated as functions of parameter α (Fig. 2d). Such critical value α^* exists that for $\alpha<\alpha^*$ $n_f<1$ and $n_f=1$ in the opposite case (for $n_u\approx0.25$ we have $\alpha^*\approx4.5$). With the increasing of α from one to α^* the value of n_f increases to one monotonously. The rate $\partial z_f/\partial t$ is less than zero always in this case. For $\alpha\rightarrow\alpha^*$ we have $n_f\rightarrow1$ and very icy soil is formed. For $\alpha\geq\alpha^*$ only

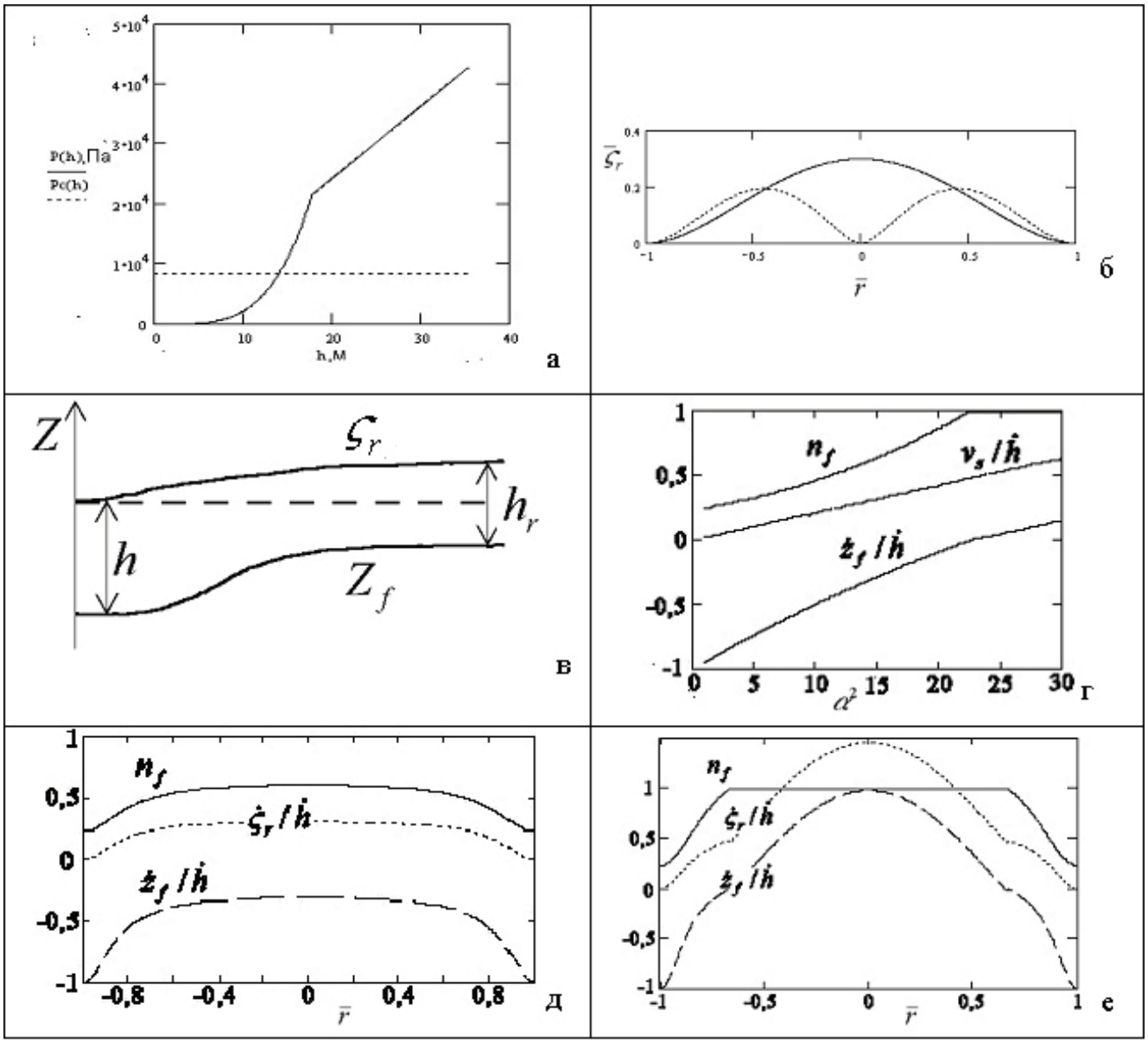

Figure 2. The characteristics of cryogenic pressure, deformations and ice accumulation at the freezing of closed volume: a) the dependence of cryogenic pressure abundance on freezing depth (continuous line), dotted line is the breaking stress in the central clay body; b) the bend lines before (dotted line) and after (continuous line) the break of the central clay body (in non-dimensional coordinates); c) the scheme of frozen layer near the points of rigid connection; dotted line is the initial position of the ground surface; d) the dependences of frozen soil porosity, relative velocities of deformations and of freezing on value of α at the stationary creep stage; e) the dependences of frozen soil porosity, relative velocities of deformations and of freezing on non-dimensional coordinate r at attenuated deformations stage (α=3.5<α^*); f) the dependences of frozen soil porosity, relative velocities of deformations and of freezing on non-dimensional coordinate r at attenuated deformations stage (α=4.8>α^*).

clear ice is formed and rate $\partial z_f/\partial t$ is more than zero. The last means that the freezing front is retired from the unfrozen soil, and a clear water lens is formed under the ice body. The vertical thickness of the lens should increase with time. All these transformations may be interpreted as changes in the character of ice accumulation at the variation of the radius R_w and at fixed radius R_f.

At the attenuated deformations stage, the value of n_f is a function of r. In this case the critical value α^* exists also: if $\alpha<\alpha^*$, we always have $n_f<1$ for all values of r from the deformations zone, and if $\alpha>\alpha^*$, the area with radius R_α exists inside the deformations zone ($R_\alpha<R_f$) where n_f=1 for all the values of r from this area (for $n_u\approx0.25$ we have $\alpha^*\approx4.2$). For $\alpha=\alpha^*$, we have R_α=0 and the value of R_α is increased with increasing of α.

The dependence of the functions n_f, v_s and $\partial z_f/\partial t$ on r for $\alpha<\alpha^*$ is shown on Figure 2e. In this case we have $n_f<1$, $\partial z_f/\partial t<0$ for all $r\le R_f$. For $\alpha>\alpha^*$ the limited area with n_f=1 and $\partial z_f/\partial t>0$ is present inside the deformations zone (Fig. 2f). It means that the kern of the clear ice is formed in the freezing layer. This kern is surrounded by very icy soil, and the water lens underlies the kern. This structure of the frozen layer is

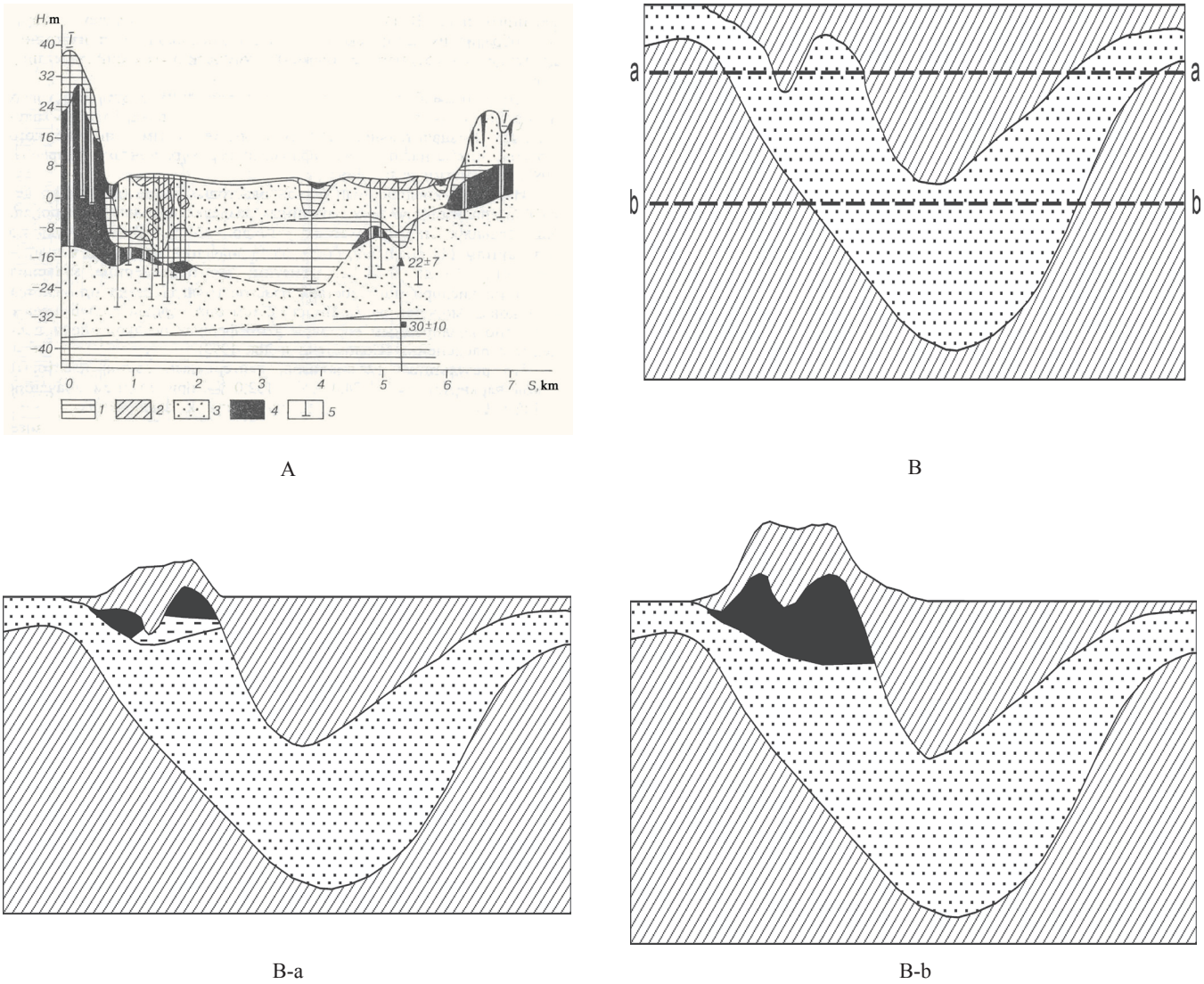

A B

B-a B-b

Figure 3. The sections of ice body deposits: A) the cross section of the Se-Yaha river valley, 1-clay, 2-clay loam, 3-sand, 4-ice, 5-borehalls (Solomatin & Konyahin 1997); B), B-a), B-b) the hypothetic section for different stages of the freezing, ■ -ice, ‾ ‾ ‾ -water lens. The other notations and clarifications are on the Figure 1 and in the text.

analogous to the structure of a pingo, which is presented by Mackay (1978). The likeness of the structures of some ice body deposits and a pingo is noted by Fotiev (2003).

Geological Aspects of the Considered Problem

The soil section in Figure 1 has a specific structure characterized by the certain combination of sand and clay. The important role in a ice body formation belongs to the lower clay layer which forms bottom and walls of the volume. Continuous bodies of massive ice widely occur on the Yamal Peninsula. It is interesting to compare their occurrence and relationship with the surrounding soil with a soil section in Figure 1? Although field descriptions and photographs of the sections with ice bodies are presented in many publications, information about soil beneath ice bodies is limited. However, the clay layer is found under sands, which underlain ice (Velikotsky 1987, Baulin et al. 1996, Solomatin & Konyahin 1997, Dubikov 2002, Streletskaya & Leibman 2002, Fotiev 2003, Shpolanskaya et al. 2006). The role of the lower clay layer in an ice body formation has not been previously discussed. All the sections described in these papers have had a three-layer structure before ice formation: clays, sand, and clay. It created the conditions for freezing of the sands in a closed system. For example, Figure 3A shows such a section presented by Solomatin and Konyahin (1997). It shows that the ice bodies are covered by clay, and they have sand in its bedding everywhere, but under these sands, the clay layer is present. Without ice (before freezing), the section has a three-layer structure. It is of interest to deduce the role of each of the layers in the ice body formation. Let us consider the question for the hypothetic section presented in Figures 3B, 3B-a, and 3B-b for different stages of freezing (the small and big tongues in upper clay layer are analogs of small and big clay bodies in the sands of Figure 1). Figure 3B shows this section before

freezing. The dotted lines a-a and b-b are the positions of the freezing front at intermediate and final stages of freezing (in assumption that mass transfer processes are absent in the system). Figure 3B-a shows separate fragments of the ice body, water lens, and deformations of the separate layer boundaries and the surface of the massif at the intermediate stage. Figure 3B-b shows the final form of the ice body and final deformations of the layers and boundaries.

In this process, the lower clay layer is a confining layer at the bottom and walls of the closed volume. There is a solid connection between the freezing layer and these walls. Without this connection, the cryogenic pressure that occurs will not be enough to deform the upper layers. The lower clay layer is not deformed at ice body formation process as a rule.

The sandy layer is the main water-containing and water-conductive layer. The ice accumulation and deformations of the upper layer and the structure and composition of the ice body are essentially connected with an extension of this layer in horizontal and vertical directions. At the deforming of the upper layer, the fractures and cavities are formed between the upper and sandy layers. As far as cohesion of sand is equal to zero and under an impact of the water flow, sand partially fills these defects. Hence, the upper boundary of the sands has to take on a subhorizontal position under the water lens and ice bodies (Figs. 3A, 3B-a, 3B-b).

The upper clay layer is the main layer which is subjected to transformations during ice body formation. Configuration of the ice body depends on size and configuration of this clay layer. The only clay composition of this layer is not obligated, but if clay is present here, the freezing layer moves its unfrozen parts upwards. Deformations arise and expand at mostly weak parts of the layer (Figs. 3B, 3B-a). Its more solid parts (as the big tongue on Fig. 3B-a) hold the freezing layer from deformations. (On the real section of Fig. 3A it is the central clay body. It is possible that the upper left part of the clay layer on this section is broken during ice body formation.) At the final stage, the solid parts of the layer may be deformed, too. For example, the big tongue of Figure 3B-b has some rotation to the right. It may be cracks formation in the tongue's body at this rotation. The upper boundary of the ice takes over the configuration of the lower boundary of the upper clay layer (Fig. 3B-b).

Acknowledgments

The author is indebted to Professor S.E. Grechishchev and to Professor S.M. Fotiev for discussing the problem and for their useful criticisms.

References

Baulin, V.V., Aksenov, V.I. & Dubikov, G.I. 1996. Permafrost conditions of development of Bovanenkovo gas-field. In: V. Tsibulsky (ed.), *Geotechnical Monitoring of Yamal Oil- and Gas-Fields*. Tyumen: Institute of Northern Development SB RAS, 3-238.

Dubikov, G.I. 2002. *Composition and Cryogenic Structure of Permafrost in West Siberia*. Moscow: GEOS Publishing House, 248 pp.

Fotiev, S.M. 2003. Ice bed genesis in the Yamal marine deposits. *Earth's Cryosphere* 1, VII: 63-75.

Gorelik, J.B. 2007a. Shift in ice cover deformations under freezing in a closed system. *Proceedings of the International Conference "Cryogenic Resources of Polar Regions," Salechard, Russia, June 17–21, 2007*: 125-128.

Gorelik, J.B. 2007b. On regimes of ice formation during freezing of the ground. *Earth's Cryosphere* 4(XI): 42-49.

Grechishchev, S.E. 1963. Creep of the frozen soils under complex stressed state. In: K. Voytkovsky (ed.), *Strength and Creep of Frozen Soils*. Moscow: USSR Academy of Sciences

Mackay, J.R. 1978. Sub-pingo water lenses, Tuktoyaktuk Peninsula . *Canadian Journal of Earth Sciences* 8(15): 1219-1297.

Shpolanskaya, N.A., Streletskaya, I.D. & Surkov, A.V. 2006. Cryolithogenesis in Arctic shelf (recent and relict). *Earth's Cryosphere* 3(X): 49-60.

Solomatin, V.I. & Konyahin, M.A. 1997. Cryolithogenesis and stratigraphy of the Central Yamal frozen soils formation. In: E. Melnikov (ed.), *Results of the Earth's Cryosphere Fundamental Researches in Arctic and Sub-Arctic*. Novosibirsk: Nauka, 173-182.

Streletskaya, I.D. & Leibman, M.O. 2002. Cryogeochemical interrelation of massif ground ice, cryopegs, and enclosing deposits of Central Yamal. *Earth's Cryosphere* 3(VI): 15-24.

Timoshenko, S.P. 1967. *Plates and Shells*. Moscow: Nauka, 626 pp.

Velikotsky, M.A. 1987. Dislocations and ice bodies in quaternary sediments of the Yamal Peninsula. In: A. Popov (ed.), *Cryogenic Processes*. Moscow: Moscow State University, 48-59.

Technocryogenesis Controls on the Permafrost Environment and Geotechnical Factors in Towns of the Permafrost Zone

V.I. Grebenets
Geographical Faculty, Lomonosov State University, Moscow, Russia

Abstract

Currently, due to the significant landscape modification that alters the thermal and mass exchange between permafrost and the atmosphere, special geocryological conditions are formed in urbanized areas of the permafrost zone. It is suggested that the specificity of changes in geocryological, landscape, geoecological and geotechnical environments should be delineated with the technocryogenesis concept, which has four basic features. Technocryogenesis is the specific exogenous process taking place in urbanized areas of the cryolithozone (1); it occurs at the contact of technogenic loads and the permafrost environment (2); it has an irreversible character (3); and appears as specific natural geocryological complexes (4). Regional studies of technocryogenesis revealed its varied influence on permafrost and ecological environments and geotechnical condition.

Keywords: cryogenic processes; deformation; permafrost degradation; technocryogenesis; temperature regime.

Introduction

Currently, due to significant landscape modifications that have altered the thermal and mass balance between the permafrost and the atmosphere, special geocryological conditions are developed in urbanized areas of permafrost. In addition, engineering and mechanical loads force permafrost soils to change physical, thermal, and mechanical properties. Consequently, the soil temperature beneath the affected surface rises and dangerous cryogenic processes are activated. This results in the overall reduction of geotechnically stable areas.

Methods

To study the relation between the permafrost conditions and geotechnical environments, we measured the temperature of permafrost in boreholes. This was done in built-up areas, and the results were compared to the thermal field that existed before construction. Geodetic survey data of the surface prior to embankment construction was also analyzed to determine the trends and rates of cryogenic processes taking place at the study sites. Visual and instrumental observations of the state of buildings and constructions were collected.

Results

There are several types of forces acting on permafrost soils in urban basements, as described below:

Mechanical disturbance

Exploitation of soils for basement construction, borrowing and excavation, and mining and tunneling, alter the strength capacity and continuity of the permafrost. Dirt piles, montons, and embankments favor either formation of permafrost bodies or permafrost degradation.

Technogenic inundation and salinization

The release of unrefined effluents on the daylight surface, accidental release from sewerage, and penetration of contaminants into the active layer notably alter the geochemistry of soils. This has been observed in Yakutsk, Vorkuta, Igarka, and many others towns in the permafrost zone. For instance, soil water of the active layer in Norilsk (where there exist the largest nonferrous-metal industries in the world) is rich in sulfates and chlorides, making the environment aggressive to the foundation concrete. The maximal salinity is found in areas being built up at the outset of the Northern exploration– up to 21 mg/l is the concentration of salts in sands under the Nickel Plant built in 1940 (Grebenets 1988). Chemical contamination of soils lowers the freezing temperature, increases active layer thickness, and favors thawing of ice-rich sediments with consequent thermokarst.

Alteration of surface thermal conditions

The vast majority of both domestic and rural areas of northern towns are free of vegetation and covered with asphalt. Asphalt allows soil heat flow to increase due to summer heating and winter cooling from snow clearing. Observations showed that the snow collecting areas have warmer (by 2–3°C) permafrost than that under the snow cleared roads. Ventilating cellars lower the soil temperature due to shading in summer and protection from snow accumulation in winter. Correct operation of a ventilating cellar could lower the permafrost temperature by 2–4°C. However, multiple failures in service were found and include the following: missing the solid waterproof cover and catch-water drains; malfunctioning of the sanitation system; insufficient number of weep holes in ventilating cellars or weep holes covered with snow; and low altitude of ventilating cellars turning them into encatchments. Serious service failures were found in 85% of the buildings in Dudinka. Failures favored degradation of permafrost, resulting in local taliks or warmer soil body formation as well as formation of non-anchored permafrost bodies. Bedding courses without lateral watertight faces have a generally negative influence on permafrost (Grebenets 2003). The bedding courses consist

of roughly sorted coarse grained wastes including crushed rock, pebble, and sand that could be easily supplemented with construction debris or snow. Moss and vegetation is covered, consequently increasing heat flux into the soils. Moreover, due to high filtration coefficient of 10 to 50 m/day, the bedding course material is permeable for surface waters. For example, residential 9-storey buildings on Laureatov st., Norilsk were constructed in 1975–1980 having 2–3 m to 8–10 m of the bedding course in the basement damaged several years after due to a reduction in the soil bearing capacity. The soil temperature under the bedding courses changes in range from -2.5°C to +2°C (Grebenets 2001).

Thermal forcing

Enhanced flow of heat into the soil from industries, residential buildings and communications, water released in rural areas or accidentally, lack of storm canalization, will all lead to permafrost degradation. Large heat-emitting utility collectors contribute most to permafrost warming. The collectors in Talnakh, Vorkuta, Dudinka, and other populated towns represent a distributed net of technogenic systems dug 4 to 6 m into the soil. We recorded above zero temperatures in the annual thermal regime of the collectors, which is the reason the thaw bulb is expanding. There were icings found in winter, while snow melt water and effluents flow in summer. The thermal forcing could be prevented if the collectors were laid on the ground like those in the Yamburg and Novozapolyarnyi settlements.

We suggest that technogenic impacts are the reason for the change in the soil temperature profile. Measurements in a deep borehole in downtown Norilsk evidence the temperature increase at a depth of 20–60 m by 0.5°C to 1°C during the period 1955–1985. Geothermal studies in a 135 m borehole in the suburbs of Norilsk revealed a increase of temperature over the last 50 years from -3.5 or -4°C to -1.5 or -2°C at a depth of 20 to 90 m. It is thought that temperature changes below the 15–20 m layer is not controlled by seasonal changes in climate parameters, and thus are associated with continuous technogenic pressure. It is confirmed by air temperature data recorded at meteorological stations in Norilsk during the period 1933–2005 and at Dikson (1917–2003); the data do not evidence any regional air temperature warming. However, the permafrost temperature before the construction in the 1940s varied from -0.1 or -0.5°C to -6 or -7°C, and the soil temperature in domestic areas was -3°C (Sheveleva & Khomichevskaya 1967). By the year 2005, it had risen up to -2.5°C. Consequently, great warmed areas appeared and hugh technogenic taliks formed over about 30% of the territory. Thermokarst is indicated as the asphalt breaks up, and due to the increase in the active layer depth, the frost heaving of soils and foundations is widespread in built-up areas.

The temperature regime changes, with subsequent lowering of the bearing capacity of the soils and activation of dangerous cryogenic processes. This has led to a growing number of deformed buildings and constructions. More than 75% of buildings in the permafrost zone of Russia are built on frozen basements, with permafrost supporting the basement. Under the tendency for permafrost degradation in the largest towns of the permafrost zone (Grebenets & Sadovsky 1993, Grebenets 2003), the increase of the soil temperature, often supplemented by ground thaw, consequently lowers the bearing capacity of the frozen foundation. The deepening of seasonal thaw expands the zone of cryogenic weathering of concrete. Acting together, these processes lead to mass destruction of buildings and constructions. Currently, 60% of buildings are deformed in Igarka, Dikson, and Vilyuysk; literally 100% in tribal settlements of Taymyr Autonomous District; and around 40% in Vorkuta. The number of deformed constructions in Norilsk Region of northern Siberia during the last 10 years has markedly exceeded that of the last 50 years. Currently, there are nearly 300 large buildings in towns of the Norilsk Industrial Region that are significantly deformed due to unfavorable permafrost, and geological consequences arose. More than 100 objects were in the state of failure, with 50 of the 9-storey and 5-storey buildings constructed during 1960–1980 recently being deconstructed.

A growing number of building breakdown, constructions, water lines, oil lines, and industries causes increased technogenic pressures on permafrost in urbanized areas, leading to new changes in the permafrost and forming a new geocryological environmental reality. Due to the factors of physical and economical geography, industrial exploration of permafrost is spotty. Permafrost in urbanized areas can be characterized by the altered intensity of cryogenic processes that have taken place in the region, or even a new set of processes. Occurrence, activity, intensity, reversibility, the formation of a paragenic series of geocryological phenomena, together with other characteristics of the cryogenic processes on urbanized areas, significantly differ from that of natural areas or those having no analogues in the natural environment.

Specific naturally-technogenic geocryological complexes form in urbanized areas. Each identity has various permafrost dynamics that differ from that under natural conditions. There were thirteen (13) basic identities marked in the territory of Norilsk Industrial Region (Grebenets 2001), ranging from technogenic badlands (tailing dams, waste and ash disposal areas) where permafrost is disturbed and the natural landscape destroyed, to relatively weakly modified sites in tundra and forest tundra where the active layer deepens due to an increase in thermal conductivity of soils impacted by acid rains and technogenic salinization. Listed below are the natural-technogenic geocryological identities allocated for Yamburg gas-condensate field:

1) sites currently occupied with gas-preparation facilities; having water drains; systems for basement soil cooling; with the geotechnical state and engineering geocryological conditions being stable;

2) urban areas having water drains in operation; regular snow removal; on-ground utilities; maintained with ventilating cellars; with a tendency for aggradation of permafrost and controlled damping of cryogenic processes;

and lacking deformation of buildings or constructions;

3) sites with residential and service buildings built during the 1980–1990s, among which are many that are heat emitting; these are areas with degrading permafrost and multiple deformation of buildings and constructions;

4) sites of the infrastructural objects including rural areas where the objects are being used on disturbed permafrost; having extensive warming and thawing areas; intensive thermokarst and frost heaving; with a number of objects being destroyed or even being in the breakdown state;

5) areas occupied with coarse wastes and where rubbish accumulation takes place; where permafrost warming occurs due to chemical reactions;

6) linear zones along multiple pipelines where the conditions of heat exchange on the surface are significantly modified; with active frost heaving of pipeline supports; thermokarst and thermoerosion development;

7) relatively stable tundra areas of thermokarst, thermoerosion, and gully expansion along heavy vehicle pathways.

Nonstandard permafrost-ecological problems arise under housing compaction or reconstruction of objects in areas of continuous (years to decades) technogenic loading on permafrost basements. For example, in Talnakh in northern Siberia, to provide stable building constructions on the spot where old buildings were located for 25–30 years and then demolished, the pile footing depth needed to be increased by 50 to 75%. Rebuilding the areas of recently deconstructed buildings in Yakuts and Norilsk resulted in tackled the serious problem connected with anthropogenic cryopegs. The aggressive medium actively corroded ferroconcrete piles of the new buildings.

Conclusions

Permafrost dynamics in towns, involving the state, temperature, bearing capacity, seasonal thaw depth, and activity of cryogenic processes is controlled by the following factors: 1) geocryological (features and properties of permafrost before construction); 2) geotechnical (town-planning parameters, technogenic impact type, intensity and effective area); and 3) temporal (duration of influence and climate changes). Factors could often act multi-directionally, at various scales, and asynchronously; this results in spotty pattern of permafrost change in the urbanized areas.

It is suggested that the specificity of changes in geocryological, landscape, geoecological and geotechnical environments should be delineated with the technocryogenesis concept having four basic features. Technocryogenesis is the specific exogenous process taking place in urbanized areas of the cryolithozone (1); occurring at the contact of technogenic loads and the permafrost environment (2); having irreversible character (3); and appearing as specific natural geocryological complexes (4). Regional studies of technocryogenesis revealed its varied influence on permafrost and ecological environments and geotechnical condition.

The study of technocryogenesis accounting for the size of the town system, number of elements involved and duration of interaction with nature, and permafrost stability is thought to present interest. The important issue is to assess technocryogenesis interaction with climate change trends at the regional scale for permafrost areas.

Acknowledgments

This work was funded by the Russian Programme of Scientific Schools Support, grant 4861.2006.5.

References

Grebenets, V.I. 2003. Geocryological-geoecological problems occurring in urbanised territories in Northern Russia and methods for improvement of foundations. *Proceedings of the Eighth International Conference on Permafrost, Zurich, Switzerland, July 21–25, 2003* 1: 303-307.

Grebenets, V.I. & Sadovskii, A.V. 1993. Climate warming vs thermal regime of the northern city basements. *Osnovaniya, fundamenty i mekhanika gruntov* (*Basements, Foundations, and Soil Mechanics)* 5: 27-30.

Grebenets, V.I. 2001. Specific technogenic ecosystems formation in Norilsk Industrial Region. *Proceedings of the Second Russian Conference on Geocryology, Moscow, June 1—3, 2005* 4. Engineering Geocryology: 59—65.

Grebenets, V.I. 1998. Study of technogenic inundation and salinization in Norilsk Industrial Region. *Kriosfera Zemli* (*Earth Cryosphere)* 2 (1): 44-48.

Sheveleva, N.S. & Khomichevskaya, L.S. 1967. *Geocryology of Northern Yenisei Region*. Moscow: Nauka, pp.

A Study of High Arctic Retrogressive Thaw Slump Dynamics, Eureka Sound Lowlands, Ellesmere Island

J.D. Grom
McGill University, Montreal, Canada
W. H. Pollard
McGill University, Montreal, Canada

Abstract

To better understand retrogressive thaw slump dynamics and their potential response to a warming climate, this study investigates the form and process of a thaw slump located in the Eureka area of Ellesmere Island in the Canadian High Arctic and attempts to identify microclimatic variation induced by its morphology. Preliminary analysis indicates that microclimates develop at the ablating ice face and within the mudflow that potentially create a feedback process for headwall retreat. Furthermore, trends in development indicate spatial variation in energy input and morphological influence on the landform.

Keywords: massive ground ice; retrogressive thaw slump; thermokarst.

Introduction

Polar regions are expected to exhibit a strong response to projected warming trends, and a significant concern is the expansion of thermokarst—land surface affected by permafrost degradation—and the resulting terrain instability throughout the Arctic. Retrogressive thaw slumps, a type of erosional backwasting resulting from the exposure of ice-rich permafrost, are a prominent thermokarst feature in arctic landscapes and have a profound potential for landscape alteration (Fig. 1). They consist of three main structural components: 1) a nearly vertical "headwall" made up of permafrost soil; 2) a steeply inclined (20°–80°) "headscarp" of ice-rich sediment acting as a thermal erosion belt; and 3) the slump floor, consisting of a low-angle (1°–10°) mud pool expanding to form a lobate pattern at the base of the slump (Burn & Lewkowicz 1990, de Krom 1990, Lantuit & Pollard 2005). The headwall and headscarp are the most dynamic components of the thaw slump and contribute the thaw material, flow deposits, and water accumulation of the mud pool. The landform often has a characteristic "horse-shoe" or linear shape and typically ranges from tens to hundreds of meters in length and width (Barry 1992, Lantuit & Pollard 2005). Retrogressive thaw slumps are initiated by various activities and are sensitive to climate and morphology, providing for periods of activity and stabilization (Burn & Lewkowicz 1990).

Rates of retreat for active retrogressive thaw slumps are variable and dependent upon climate and morphology, including slope, rate and patterns of erosion, and ground ice distribution and quantity (McRoberts & Morgenstern 1974). Radiation and sensible heat transfer have been identified as the principal energy sources for ice face ablation (Burn & Lewkowicz 1990, Lewkowicz 1986a, b, Robinson 2000); therefore, warm and clear days are the most conducive to retrogressive thaw slump activity and headwall retreat.

In an attempt to further define controlling parameters on retrogressive thaw slump development, this study investigates the potential formation of a microclimate existent within the retrogressive thaw slump as compared to the surrounding area, with increased temperatures developing at the ice face during periods of high incoming shortwave radiation (↓K), creating a positive feedback for melt of the ice face and headwall retreat. This paper also describes the methodology used to quantitatively define associated process and morphology. Field activities, including the collection of microclimate and morphologic data, were performed at a retrogressive thaw slump near Eureka, Ellesmere Island, Nunavut, Canada, over a 17-day period. Data were then analyzed to describe retrogressive thaw slump activity and characterize the development of a microclimate unique to the landform.

Study Area

Field observations were conducted from July 3–22, 2007, in the Eureka Sound Lowlands, located at the Fosheim Peninsula of Ellesmere Island, in the Nunavut Territory of Northern Canada (Fig. 2). Specific data collection focused

Figure 1. Photograph of retrogressive thaw slump, July 4, 2007.

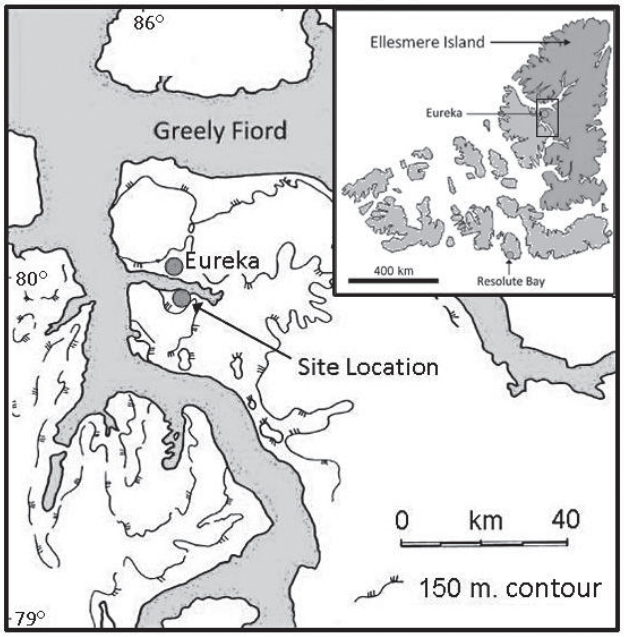

Figure 2. Map of site location and Canadian Archipelago. (150 m contour obtained from Pollard & Bell 1998).

on a southerly-oriented, active, retrogressive thaw slump located at 79°53.782′N, 85°59.357′W, approximately 10 km southeast of Eureka. This region is a polar desert, experiencing an average mean annual air temperature (MAAT) of -19.7°C and an average of 64 mm of precipitation per year, 60% of which is snow (Pollard & Bell 1998, Pollard 2000). Permafrost thickness can exceed depths of 500 m, with active layer depths ranging from 0.15–0.9 m and an extrapolated mean ground surface temperature of -20.8°C (Robinson 1993, Robinson 2000). Regional topography consists of broad, undulating lowlands.

Massive ground ice up to 17 m thick is present throughout the Eureka Sound Lowlands, and as such, substantial thermokarst activity is found along slopes experiencing active erosion and/or former thermokarst events (Robinson 2000). Ice exposures, the majority of which are overlain by marine sediments of varying thickness, are often up to 8 m thick and result in retrogressive thaw slump activity and development. Field studies performed in 1991/1992 at the nearby Hot Weather Creek revealed at least 20 active thaw slumps within an 80 km^2 area (Robinson 2000). Average rates of retreat for the duration of the study ranged from 8–14 m/year for high-angle slumps and 5–9 m/year for low-angle slumps, indicating the importance of morphology in ablation of the ice face. Additionally, several active and inactive retrogressive thaw slumps were observed in the vicinity of the studied thaw slump during the recent site reconnaissance.

Field Methods

Morphology

The outline of the headwall was identified on July 12, 2007, using differential global positioning satellite (DGPS), and aerial photographs were obtained for the site. Headwall retreat was obtained manually by installing a series of 10 coupled stakes along the headwall and measuring the change in distance between the stakes and headwall using a 50-m tape measure. Measurements were recorded to the nearest millimeter; however, accuracy was possible to the nearest centimeter.

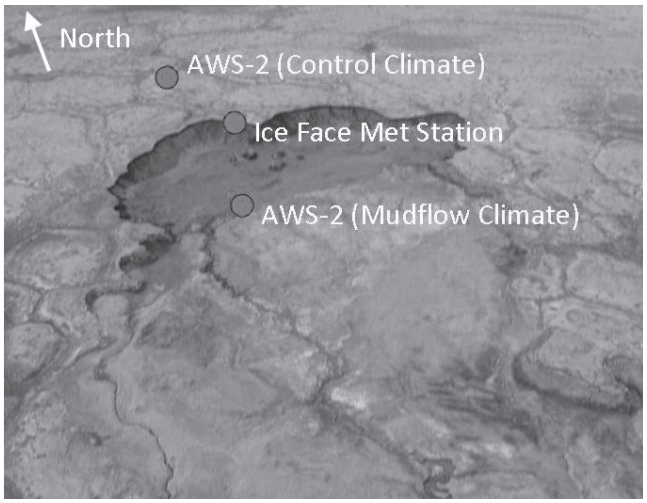

Figure 3. Oblique overhead photograph of retrogressive thaw slump investigated in study, including headwall, mudflow, micrometeorological equipment.

Additionally, headwall retreat was obtained for the portion of the headwall situated directly above the ice face meteorological station in order to integrate morphologic and climatic data impacting the landform. The headwall was measured 4 times over the 17-day period, including July 5, July 6, July 12, and July 22. Surface angles were obtained at the beginning of the site investigation using a handheld abney level for the inactive portion of the slump mudflow and the surrounding terrain in addition to 10 points along the ice face corresponding to the aforementioned locations of headwall retreat measurement.

A profile of the ice face was obtained in the vicinity of the ice face meteorological station in order to characterize ground ice and stratigraphy. Additional samples were obtained from the ice face for the laboratory determination of gravimetric moisture-content in order to determine the volumetric latent heat of the ice to be applied in future analysis in conjunction with the ice face meteorological weather station data to gain insight to the energy balance at the ablating ice face.

Microclimate

In order to investigate the potential formation of a microclimate induced by retrogressive thaw slump morphology, two automatic weather stations were strategically placed at the site; one weather station was placed within the slump mudflow (AWS-1), approximately 78 m from the ice face and headwall, and the second was placed atop the slump (AWS-2), approximately 67 m upslope of the headwall, in order to represent the control climate (Fig. 3). It should be noted that AWS-1 could not be placed closer to the headwall as originally intended due to the viscous nature of the mudflow, making it inaccessible to installation and repeated access. The placement of these stations was

Figure 4. Ice face meteorological station.

intended to capture the microclimates within the thaw slump in comparison to the surrounding area, or the control climate, using the data collected from AWS-1 and AWS-2, respectively. Both of the stations were equipped with an SP-LITE silicon pyranometer (measuring ↓K), an HMP45C shielded thermistor and relative humidity probe (measuring ambient temperature and atmospheric relative humidity), an RM Young wind monitor (measuring wind speed and direction), and a barometric pressure sensor. AWS-2 was also equipped with a temperature sensor, measuring subsurface temperatures at depths of 50 and 70 cm below surface grade. It should be noted that the temperature sensors and SP-LITE, which provide the basis of data for this analysis, are considered accurate within ±0.35°C and approximately ±2 W/m^2, respectively. Climate data were scanned at 60-second intervals and compiled to produce 1-hour averages. Data output was stored on automated data loggers (AWS-1 and -2: Campbell Scientific CR10X; ice face station: Campbell Scientific CR10).

Additional instrumentation was suspended approximately 0.5 to 1 m above the ice face in order to provide additional quantification to retrogressive thaw slump microclimate development, in addition to defining the microclimate and energy activity at the ablating ice face (Fig. 4). This station was equipped with an NR–LITE (measuring net radiation), an HMP45C shielded thermistor and relative humidity probe, and a model 014A wind speed sensor.

Results and Discussion

Morphology

The observed retrogressive thaw slump consisted of 2 well-developed units, consisting of a layer of massive ice with an average surface exposure of approximately 4 m, overlain by massive sandy/clayey silt with a depth of 0.8–1.0 m; refer to Figure 1. The massive ice unit consisted of an intersedimental ice unit with exposed ice wedges embedded throughout.

The headwall of the retrogressive thaw slump was horseshoe-shaped and approximately 240 m along its perimeter. Retreat was variable among the points of

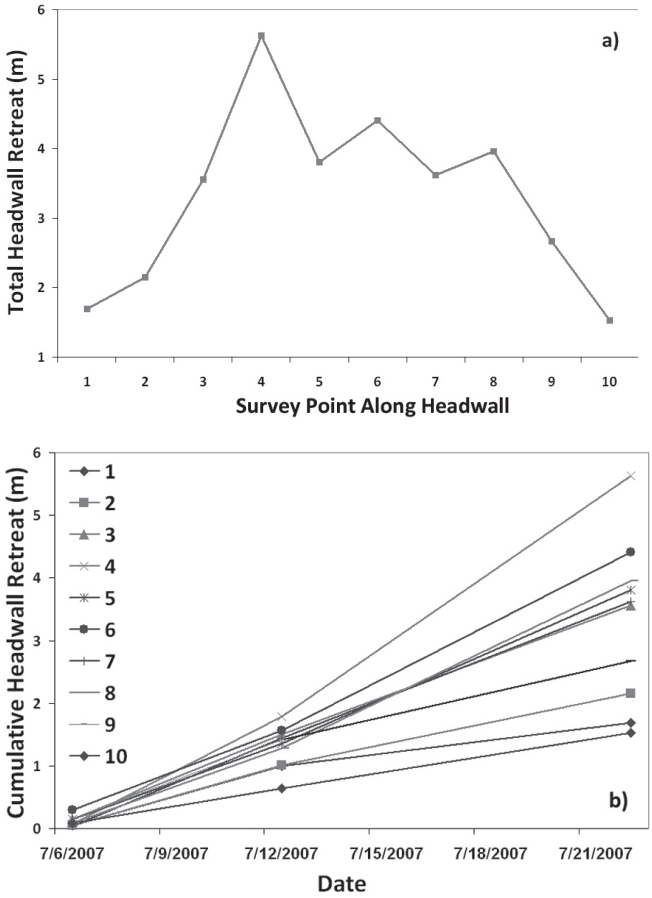

Figure 5. a) Total headwall retreat observed at studied retrogressive thaw slump, with each number representing a survey point spaced in 24-m intervals, moving west to east along the headwall. b) Retreat at all 10 survey points along the headwall over time.

measurement along the headwall - spaced at 24-m intervals along the perimeter, ranging from 1.5–5.6 m over the 17-day period (Fig. 5). Greater retreat was observed along the central portion of the headwall as opposed to the sidewalls, further contributing to its horseshoe-shaped morphology. This trend reflects the characteristic pinching of the sidewall attributed to lower ice angles, as identified in previous investigations (Barry 1992). However, it should be noted that no significant trend was observed between ice angle and cumulative headwall retreat in this study. Therefore, the spatial variation in headwall potentially reflects differences in ablation of the underlying massive ice in response to differences in energy distribution and morphology, including both depths of the overburden and ice and terrain angles.

Microclimate

Previous studies have identified solar radiation as providing a primary energy contribution to ablation, and therefore headwall retreat, of retrogressive thaw slumps (Lewkowicz 1985, Pufahl & Morgenstern 1980). It has been noted that net radiation alone can accurately capture approximately 60% of the variation in energy available for ablation (Lewkowicz 1986b) and that ice face orientation, which impacts periods of direct ↓K exposure, influences ablation rates (Lewkowicz

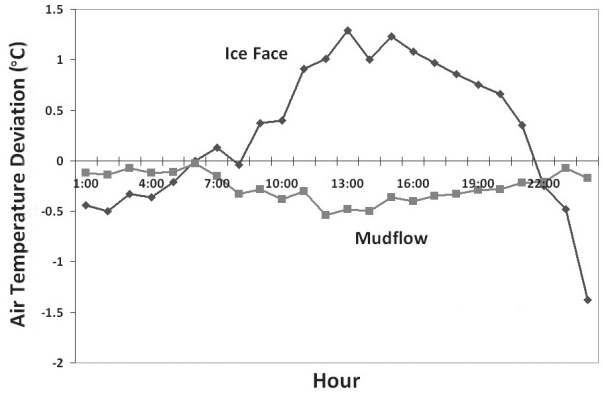

Figure 6. Air temperature deviation from control climate at ice face and within mudflow on a sunny day.

1988). An additional study also observed relatively high near-surface temperatures within the active portion of a retrogressive thaw slump (Mackay 1978). Data provided by the current study indicate that the influence of ↓K, which is inherently related to net radiation, is potentially further exaggerated by a feedback process that induces increased temperatures within the thaw slump, specifically at the ice face, during periods of high ↓K.

Initial analysis suggests the potential creation of unique microclimates existing near the ice face and in the mudflow in comparison with the surrounding climate. Temperatures appear to be heightened at the ice face in response to increased amounts of ↓K, whereas the temperatures are simultaneously slightly dampened at the automatic weather station located within the mudflow, potentially due to increased evaporation. In 119 of the hourly cases in which the ice face air temperature was greater than the control temperature by at least 0.35°C, 117 (98%) were under conditions of ↓K exceeding 250 W/m^2. In addition, of the 28 hourly cases in which mudflow air temperature was at least 0.35°C less than the control temperature, 27 (96%) were accompanied by a ↓K greater than 250 W/m^2.

Figure 6 displays a characteristic response of these spatial temperature differences on July 19, 2007, a relatively sunny day, characterized as having an average daily ↓K exceeding 250 W/m^2. As displayed, temperatures are increased up to 1.3°C at the ice face as compared to the control temperature and are decreased by 0.5°C within the mudflow, with an average increase of 0.29°C at the ice face and an average decrease of 0.26°C within the mudflow for the day. ↓K on July 19, 2007, averaged 315.6 W/m^2 (min 141.2 W/m^2, max 500.6 W/m^2), and the studied portion of the ice face received direct solar radiation from approximately 10:00–20:00, which strongly correlates to the period of observed increase in ice face air temperature. Winds were northerly/northeasterly with an average speed of 3.4 m/s, and air temperatures averaged 12.5°C ± 6.4°C (Fig. 7).

In contrast, the above air temperature deviations are not displayed during periods of low ↓K. Under these conditions, temperature deviations at the ice face and within the mudflow are minor, supporting the hypothesis that ↓K is a controlling factor in microclimate development. These

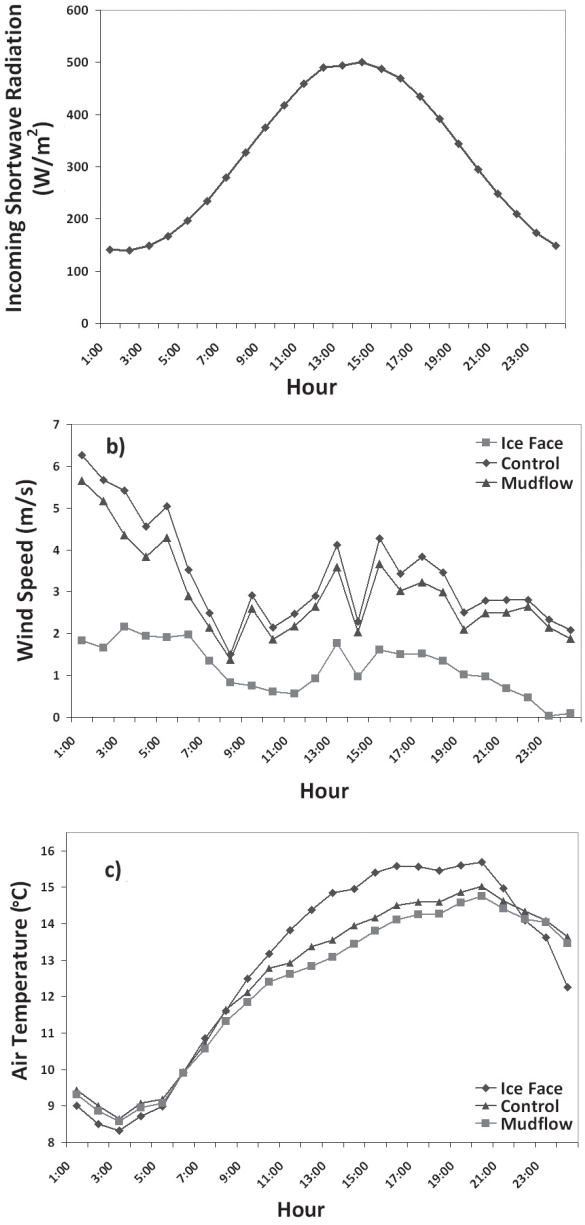

Figure 7. a) ↓K (measured at AWS-2), b) wind speed, and c) air temperature trends for July 19, 2007.

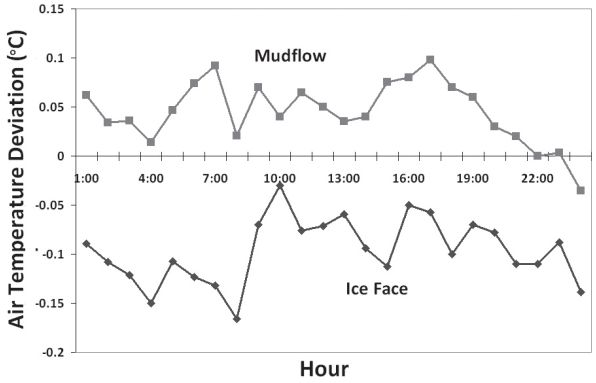

Figure 8. Air temperature deviation from control climate at ice face and within mudflow on a cloudy day.

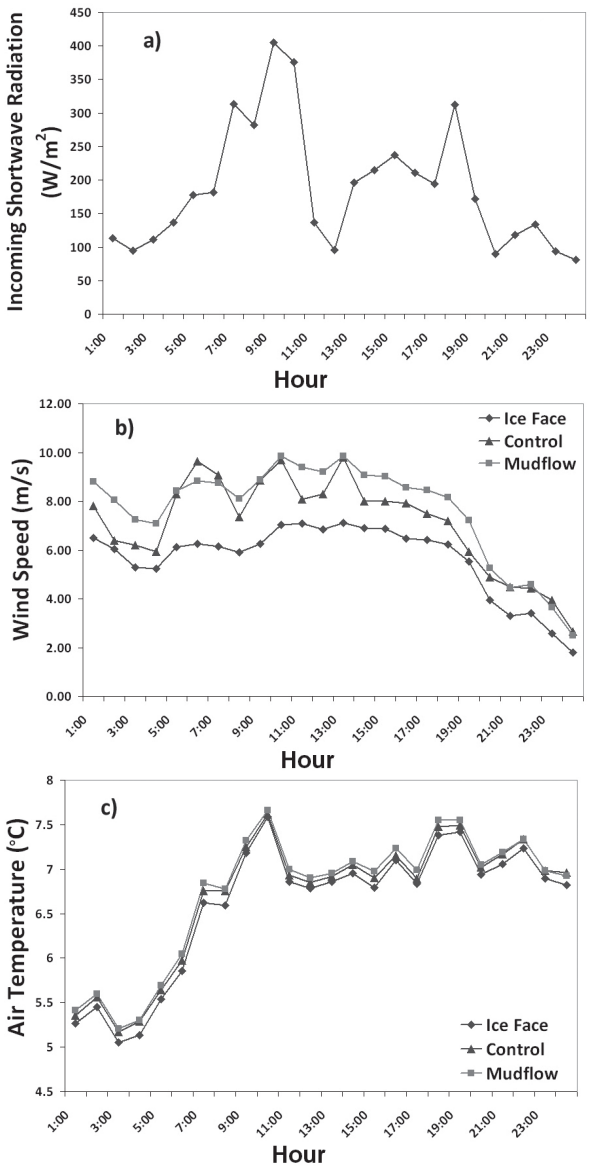

Figure 9. a) ↓K (measured at AWS-2), b) wind speed, and c) air temperature trends for July 7, 2007.

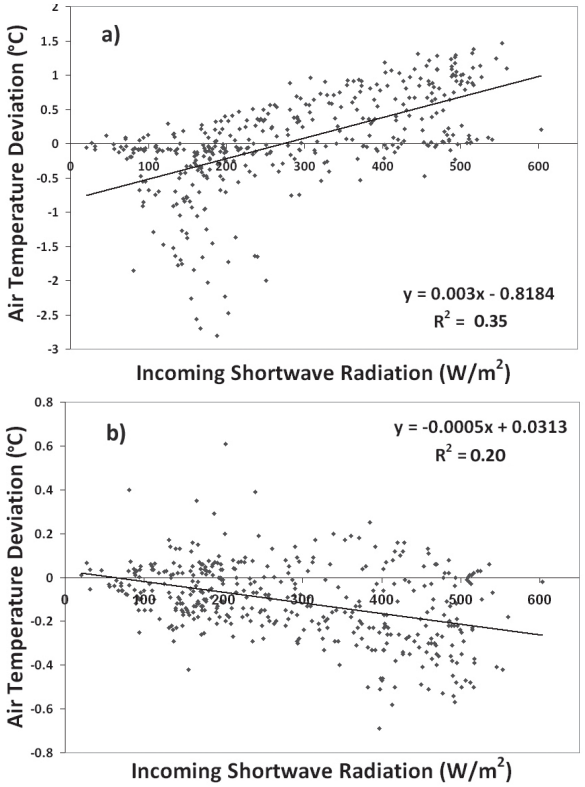

Figure 10. a) Ice face air temperature deviation versus ↓K, and b) mudflow air temperature versus ↓K; July 6–22, 2007.

trends are displayed in Figure 8, which displays temperature deviation trends on July 7, 2007, a relatively cloudy day, characterized by an average ↓K of 186.6 W/m^2. Additionally, southerly winds with an average speed of 7.1 m/s and an average daily air temperature of 6.7°C were observed on this day (Fig. 9). Under these circumstances, average daily air temperature deviations are -0.1°C and 0.0°C for the ice face and mudflow, respectively. It should be noted that trends within this range are considered relatively insignificant due to the aforementioned accuracy of the temperature sensor.

In order to further support the formation of spatial microclimates within the retrogressive thaw slump, a regression analysis was performed on the full dataset of temperature deviations and ↓K (Fig. 10). This analysis reveals significant trends between air temperature deviations from the control temperature under increasing ↓K conditions, identifying an overall positive trend in air temperature difference at the ice face ($p < 0.001$) and a significant but slight decrease in mudflow air temperature ($p < 0.001$). It should be noted that the r^2 values are relatively low for the ice face air temperature ($r^2 = 0.35$) and mudflow ($r^2 = 0.20$); however, this indicates the influence of additional factors in the formation of the observed microclimates and supports the need for additional investigation.

It is suspected that these deviations are the result of retrogressive thaw slump morphology (i.e., ice angle, sediment content, slump shape) and the associated differences in parameters such as albedo and wind speed. This could also be related to spatial differences in ablation rate previously identified, in which microvariations in energy input were identified as the most likely factor contributing to these conditions (Lewkowicz 1985). Additional investigation of available microclimate data is required in order to further define the conditions observed in field data.

It should be noted that climate data were also obtained from the nearby Eureka Weather Station and compared to the data obtained at the site. Previous studies have displayed that temperatures are typically significantly warmer in the Fosheim Peninsula as compared to the nearby Eureka Weather Station (Atkinson 2000). The site control station recorded temperatures in average exceedance of 4°C as compared to measurements reported from Eureka, and measured and reported temperatures rarely coincided with one another (Fig. 11). These differences, in addition to the microscale variations measured at the site, display the need for location-specific on-site weather measurements when investigating process-based dynamics of a landform.

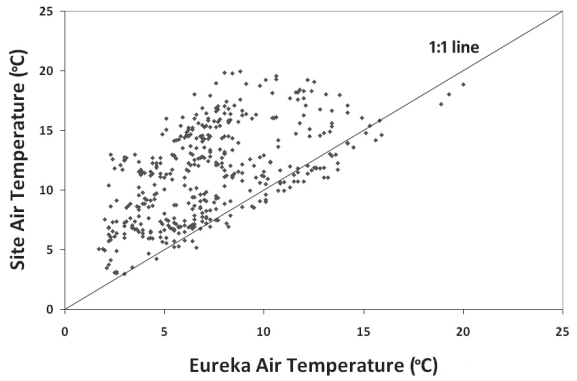

Figure 11. Recorded site air temperature vs. air temperature recorded at the Eureka Weather Station, July 4–22, 2007.

Summary and Conclusions

This study describes the methodology developed to capture and explore the dynamic interaction of climate and morphology in retrogressive thaw slump activity. The 17-day study period represents the most annually active period of ablation and headwall retreat, which was variable along various points of the headwall. These variations have previously been linked to changes in angle of the underlying ice face. However, this study does not support the sole influence of ice angle and indicates that additional investigation addressing the interplay of morphology and surficial energy activity is required.

Additionally, significant temperature variations in microclimates were identified at the site, specifically in the vicinity of the ice face. Preliminary analysis indicates that ↓K influences these conditions and further supports the importance of solar radiation on ablation and retrogressive thaw slump activity, as identified in previous studies. Further definition of these temperature variations is required to understand their formation and impact on retrogressive thaw slump morphology.

Microclimate data derived at the ablating ice face during this study are also being analyzed to further quantify the energy balance. These investigations will provide important information into retrogressive thaw slump process and provide the foundation for understanding the potential responses under altering climate conditions.

Acknowledgments

This research was supported by the Natural Science and Engineering Research Council of Canada (W. Pollard) and ArcticNet (W. Pollard). Exceptional logistic support was provided by Polar Continental Shelf Project (PCSP). J.D. Grom is supported by the Natural Science and Engineering Research Council of Canada (W. Pollard), ArcticNet (W. Pollard), and McGill University. Aerial photographs and DGPS data were generously performed by T. Haltigin, and excellent and much appreciated field assistance was provided by P. Budkewitsch, M. Ecclestone, and T. Haltigin. Dr. I. Strachan also contributed to helpful discussions in developing research methods. This manuscript has been enhanced by the insightful recommendations of three anonymous reviewers.

References

Atkinson, D.E. 2000. Modelling July mean temperatures on Fosheim Peninsula, Ellesmere Island, Nunavut. *Geological Survey of Canada* 529: 99-111.

Barry, P. 1992. *Ground Ice Characteristics in Permafrost on the Fosheim Peninsula, Ellesmere Island, N.W.T.: A Study Utilizing Ground-Probing Radar and Geomorphological Techniques*. M.Sc. thesis, Montreal, Quebec: McGill University, 135 pp.

Burn, C.R. & Lewkowicz, A.G. 1990. Retrogressive thaw slumps. *The Canadian Geographer* 34: 273-276.

de Krom, V. 1990. *A Geomorphic Investigation of Retrogressive Thaw Slumps and Active Layer Slides on Herschel Island, Yukon Territory.* M.Sc. thesis, Montreal, Quebec: McGill University, 157 pp.

Lantuit, H. & Pollard, W.H. 2005. Temporal stereophotogrammetric analysis of retrogressive thaw slumps on Herschel Island, Yukon Territory. *Natural Hazards and Earth System Sciences* 5: 413-423.

Lewkowicz, A.G. 1985. Use of an ablatometer to measure short-term ablation of exposed ground ice. *Canadian Journal of Earth Sciences* 22: 1767-1763.

Lewkowicz, A.G. 1986a. Headwall retreat of ground-ice slumps, Banks Island, Northwest Territories. *Canadian Journal of Earth Sciences* 24: 1077-1085.

Lewkowicz, A.G. 1986b. Rate of short-term ablation of exposed ground ice, Banks Island, Northwest Territories, Canada. *J. of Glaciology* 32: 511-519.

Lewkowicz, A.G. 1988. Ablation of massive ground ice, Mackenzie Delta. *Proceedings of the Fifth International Conference on Permafrost, Trondheim, Norway. August 1988*: 605-610.

Mackay, R.J. 1978. The surface temperature of an ice-rich melting permafrost exposure, Garry Island, Northwest Territories. *Geological Survey of Canada*. 78-1A: 521-522.

McRoberts, E.C. & Morgenstern, N.R. 1974. The stability of thawing slopes. *Canadian Geotechnical J.* 11: 447-269.

Pollard, W.H. 2000. Ground ice aggradation on Fosheim Peninsula, Ellesmere Island, Nunavut. *Geological Survey of Canada* 529: 325-333.

Pollard, W.H. & Bell, T. 1998. Massive ice formation in the Eureka Sound Lowlands: a landscape model. *Proceedings of the Seventh Canadian Permafrost Conference, Yellowknife, NWT, June 1998*: 903-908.

Pufahl, D.E. & Morgenstern, N.R. 1980. The energetics of an ablating headscarp in permafrost. *Canadian Geotechnical Journal* 17: 487-497.

Robinson, S.D. 1993. *Geophysical and Geomorphological Investigations of Massive Ground Ice, Fosheim Peninsula, Ellesmere Island, Northwest Territories*. M.Sc. thesis, Kingston, Ontario: Queen's University, 171 pp.

Robinson, S.D. 2000. Thaw-slump-derived thermokarst near Hot Weather Creek, Ellesmere Island, Nunavut. *Geological Survey of Canada* 529: 335-345.

Distribution of Thermokarst Lakes and Ponds at Three Yedoma Sites in Siberia

Guido Grosse
Geophysical Institute, University of Alaska Fairbanks, USA
Vladimir Romanovsky
Geophysical Institute, University of Alaska Fairbanks, USA
Katey Walter
Institute of Northern Engineering / International Arctic Research Center, University of Alaska Fairbanks, USA
Anne Morgenstern
Alfred Wegener Institute for Polar and Marine Research, Potsdam, Germany
Hugues Lantuit
Alfred Wegener Institute for Polar and Marine Research, Potsdam, Germany
Sergei Zimov
Northeast Science Station, Cherskii, Russia

Abstract

Thermokarst lake formation in ice-rich yedoma deposits in north Siberia has a major impact on regional landscape morphology, hydrology, and biogeochemistry. Detailed assessment of lake distribution characteristics is critical for understanding spatial and temporal lake dynamics and quantifying their impacts. The distribution of thermokarst ponds and lakes at three different sites with ice-rich permafrost (Bykovsky Peninsula, SW Lena Delta, and Cherskii) in northeast Siberia was analysed using high-resolution remote sensing and geographical information system (GIS) tools. Despite similarities in geocryological characteristics, the distribution of thermokarst lakes differs strongly among the study regions and is heavily influenced by the overall hydrological and geomorphologic situation as a result of past lake-landscape dynamics. By comparing our high-resolution water body dataset with existing lake inventories, we find major discrepancies in lake distribution and total coverage. The use of low-resolution lake inventories for upscaling of thermokarst lake-related environmental processes like methane emissions would result in a strong underestimation of the environmental impacts of thermokarst lakes and ponds in Arctic lowlands.

Keywords: lake distribution; remote sensing; Siberia; thermokarst lakes; yedoma.

Introduction

Global lake inventories currently used in Earth system modeling contain only lakes larger than 10 ha (Lehner & Döll 2004, Downing et al. 2006). Most of these lakes are found in the Northern Hemisphere; that is, in permafrost-influenced or formerly glaciated regions. In permafrost regions with unconsolidated sediments most of the lakes are thermokarst lakes or ponds which formed due to the melting of massive or segregated ground ice and subsequent surface settlement. Thermokarst lakes are a major component of vast arctic and subarctic landscapes in Siberia, Alaska, and Canada. Thermokarst lakes and ponds can laterally expand by thermo-erosion and thaw slumping along shores. Usually a positive relation is established between thaw subsidence, horizontal basin extension, and water body growth, resulting in continued thawing of underlying permafrost and thermo-erosion on its margins. This runaway effect is mostly dependent on ground ice content in the underlying permafrost, and it continues going until thawed-out sediments form an insulating layer preventing further thawing and subsidence. Consequently, ice-rich unconsolidated permafrost deposits like those of the widespread Late Pleistocene Yedoma Suite in northeast Siberia (Schirrmeister et al. 2008) are especially vulnerable to thermokarst development initiated by natural or anthropogenic environmental change.

Regional medium-resolution studies aimed at the classification and spatial analysis of thermokarst lakes in Arctic regions were mostly based on Landsat satellite imagery, which has proven valuable for water body detection (e.g., Frazier & Page 2000). Such studies were conducted for the North Alaska Coastal Plain (Sellmann et al. 1975, Frohn et al. 2005, Hinkel et al. 2005), the Siberian Lena Delta (Morgenstern et al. 2008), the Lena-Anabar Lowland (Grosse et al. 2006), and the Tuktoyaktuk Peninsula (Côté & Burn 2002). These and other works reveal a very large number of lakes and ponds between 1–10 ha for most permafrost lowland areas. Based on field experience and spatially limited aerial surveys, it is known that there is very likely an even larger number of thermokarst ponds smaller than 1 ha.

The lacking representation of small lakes and thus bias towards large lakes in existing global lake inventories might result in a strong underestimation of the environmental impact of thermokarst lakes, which would seriously hamper the understanding of their role in the Arctic hydrological cycle and global biogeochemical cycles. First qualitative and quantitative studies on the environmental impact of thermokarst lakes over both geological and historical time frames suggest a potentially large role of such lakes in the

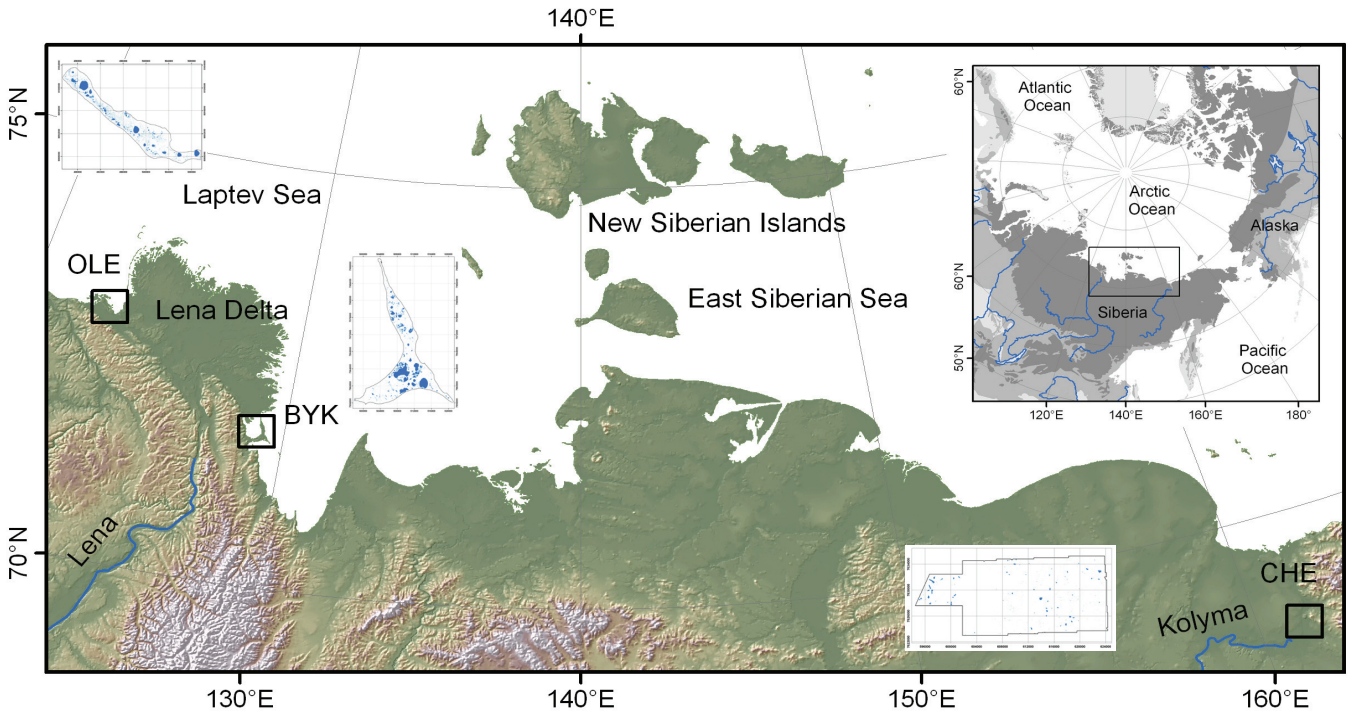

Figure 1. Relief map showing the location of the three study sites: Olenek Channel (OLE), Bykovsky Peninsula (BYK), and Cherskii (CHE) in NE Siberia including maps showing the lake distribution. Small inset in upper right indicates the location of the large map (black rectangle) in Siberia and the distribution of continuous (dark grey) and discontinuous permafrost (medium grey) after Brown et al. (1998).

arctic carbon cycle by unlocking vast amounts of permafrost-stored organic carbon and thus also for global climate dynamics (Zimov et al. 1997, Walter et al. 2006, Walter et al. 2007). Other studies indicate e.g., the impact of arctic wetland and lake distribution on atmospheric circulation patterns (Gutowski et al. 2007). Many studies also show that small water bodies in permafrost lowlands, e.g., polygonal ponds, are an important component for methane emissions from tundra wetlands (e.g., Wagner et al. 2003, Schneider et al. in review). To quantify the environmental impact of such arctic lakes and ponds it is necessary to have detailed information on their distribution and extent.

Several studies suggest a direct connection between thermokarst lake distribution and underlying permafrost characteristics, as well as between lake dynamics and permafrost dynamics. Widespread lake drainage in the discontinuous permafrost zone is related to a beginning disappearance of permafrost due to current climate warming (Yoshikawa & Hinzman 2003, Smith et al. 2005, Riordan et al. 2006). On the contrary, in the continuous permafrost zone an increase in lake area was observed in Western (Smith et al. 2005) and Eastern Siberia (Walter et al. 2006), but not on the Alaskan North Slope (Riordan et al. 2006, Hinkel et al. 2007). Most of these studies are based on the medium-resolution (30–80 m) Landsat satellite data record spanning about 35 years and some additionally involve historical aerial photography. However, although Landsat data may be sufficient to detect complete drainage and drying of some large lakes or the formation of new large lakes, it has serious limitations in detecting changes in lake extent due to thaw slumping and thermo-erosion. A high-resolution dataset of recent lake and pond distribution in combination with historical imagery would form an excellent base for studying change in lake extent and link these changes to permafrost or climate dynamics.

In this study a dataset of recent thermokarst lake and pond distribution on ice-rich yedoma deposits is developed based on high-resolution (1–2.5 m) satellite remote sensing data for three sites in Northeast Siberia and then compared with data from the Global Lake and Wetland Database (GLWD: Lehner & Döll 2004).

Study Region

All three study sites are situated in the continuous permafrost region of northeast Siberia (Fig. 1). The size of the study areas, a set of basic environmental characteristics, and information about the geocryology are provided in Table 1. The Bykovsky Peninsula (BYK) is situated southeast of the Lena River Delta. The peninsula is surrounded on three sides by large bays and the Laptev Sea. It is an erosional remnant of a Late Pleistocene accumulation plain consisting predominantly of silty to sandy ice-rich permafrost deposits of the yedoma (Grosse et al. 2007). Lakes, predominantly of early Holocene thermokarstic origin, are abundant at BYK (Grosse et al. 2005). They are located either on the yedoma uplands or as lake remnants and polygonal ponds in drained lake basins. These basins were formed by large thermokarst lakes during the early Holocene climate warming. They subsequently shrunk or drained after the middle Holocene due to climate deterioration and coastal erosion, leaving behind lake remnants and drained lake basins, which upon freezing

Table 1. General environmental characteristics of the study areas.

Parameter	OLE	BYK	CHE
Location	72.94°N 122.90°E	71.80°N 129.30°E	68.75°N 161.33°E
Study area (ha)	7982	17 009	28 897
Permafrost depth (m)	200–600	500–600	400–500
Active layer depth (m)	0.3–0.6	0.3–0.6	0.3–1.5
Annual ground temperature (20 m depth) (°C)	-9– -11	-9 – -11	-3 – -11
Climate data for closest weather station (Rivas-Martínez 2008):			
Station name	Tiumyati	Bukhta Tiksi	Nizhniye Kresty
Measurement period	1948–60	1984–94	1984–94
Annual air temperature (°C)	-14.5	-13.2	-11.6
Annual precipitation (mm)	206	427	294
Vegetation zone	Tundra	Tundra	Taiga / Tundra
Yedoma thickness (m)	~ 8[d]	< 50[b]	< 40
Gravimetric ice content (%)	88[c]	116[c]	< 80[a]
Ice wedge width / length (m)	3-5 / 9	6 / 40	3 / 40
Organic carbon content (%)	3.0[c]	4.7[c]	~2[a]

[a] Zimov et al. 1997
[b] Grosse et al. 2007
[c] Schirrmeister et al. 2003
[d] Schirrmeister et al. 2008

could support formation of polygonal ponds (Grosse et al. 2007). The land surface at BYK ranges from 0–45 m a.s.l. The study area around Cherskii (CHE) is part of the Kolyma fluvial lowland and located in the surroundings of the Rodinka hill (351 m a.s.l.). The wide, undulating slopes of this hill are mantled by ice-rich deposits of the yedoma stretching down to the banks and flood plain of the Kolyma River.

The study area in the southwest Lena River Delta along the Olenek channel (OLE) is part of an erosional remnant of Late Pleistocene sediments incorporated into the Holocene river delta architecture. It has the form of a peninsula and is bordered by the Laptev Sea and the wide channels of the delta. The permafrost deposits consist of ice-poor fluvial sands (ca. 0–17 m a.s.l.) overlain by yedoma (Schirrmeister et al. 2003) (Table 1). The topography is dominated by a flat plain with some thermo-erosional valleys and thermokarst basins. Water bodies are abundant in sizes ranging from polygonal ponds to large thermokarst lakes.

Remote Sensing Data

Spatially high-resolution recent satellite imagery was acquired from all three study sites to study thermokarst lake distribution and extent (Table 2). All images are from the snow-free early summer period.

For the BYK and the OLE sites two Spot-5 images were georeferenced to topographic maps of scale 1:100,000, for CHE several Ikonos-2 images were ortho-rectified (Table 2). All imagery used in this study is panchromatic and showed excellent contrasts for land-water separation.

Table 2. Satellite imagery used for mapping lake distribution.

Site	Platform	Date	Ground Resolution
BYK	Spot-5	2006-07-09	2.5m
OLE	Spot-5	2006-07-08	2.5m
CHE	Ikonos-2	2002-07-09	1.0m

Table 3. Main parameters of lakes and ponds in the study areas.

Parameter	OLE	BYK	CHE
Number of water bodies N	15,012	13,001	1348
Total water body area A (ha)	1059.6	2622.1	242.3
Limnicity (%)	13.3	15.4	0.8
Largest lake size (ha)	196.19	605.00	16.71
Mean water body size (ha)	0.0706	0.2017	0.1797
Median water body size (ha)	0.0088	0.0075	0.0115
Normalized per 10 000 ha:			
Number of water bodies N	18,808	7644	466
Total water body area A (ha)	1327.6	1541.6	83.8

Methods

A simple density slice classification was applied to the most recent images at each site to distinguish water and land in the panchromatic imagery. A threshold that best separated image pixel values (Digital Numbers, DN) of water from land was chosen. Usually, there is a strong difference in reflectance between water bodies (dark or black, low DN) and bare or vegetated land surfaces (bright, high DN). A visual comparison was conducted to verify the classification. The DN of some lakes was found to be influenced by either very shallow water levels (probably less than 1 m), resulting in higher DN due to reflectance of the lake bottom, or turbid water with high sediment suspension, resulting in higher DN from the sediment load. On some lakes remaining lake ice (highly reflective, very high DN) resulted in misclassification. Additional misclassifications occurred for pixels associated with deep thermo-erosional valleys and steep north-facing cliffs or slopes. In both cases shadows were misclassified as water. These misclassifications were corrected by applying manually generated masks in ArcGIS™ to either exclude pixel (shadows, stream water bodies, man made structures) or to include pixel (lake ice, turbid and shallow water) from the lake dataset. Based on our visual examination and manual correction the resulting datasets can be considered a conservative minimum of standing water bodies in the study areas.

Based on the ground resolution of the available imagery, a minimum of 5 pixels was considered acceptable for successful water body detection. For better comparison between all study areas we therefore only included and analyzed standing water bodies larger than 0.003 ha. Since our classification approach was conservative and aiming at open water surfaces, we assume to have missed especially small ponds overgrown by vegetation in our inventory. At BYK, three thermokarst lagoons were included in the dataset, since they morphologically belong to the peninsula. Eventually, ArcGIS™ was used to analyze the spatial distribution of water bodies in the resulting datasets. The resulting dataset was then compared with the GLWD dataset (Lehner & Doell 2004) for all study areas.

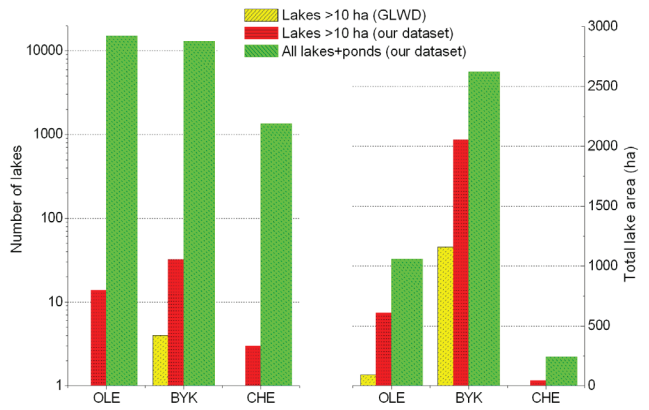

Figure 2. Comparison between GLWD (Lehner & Döll 2004) and high-resolution lake inventory for all study sites.

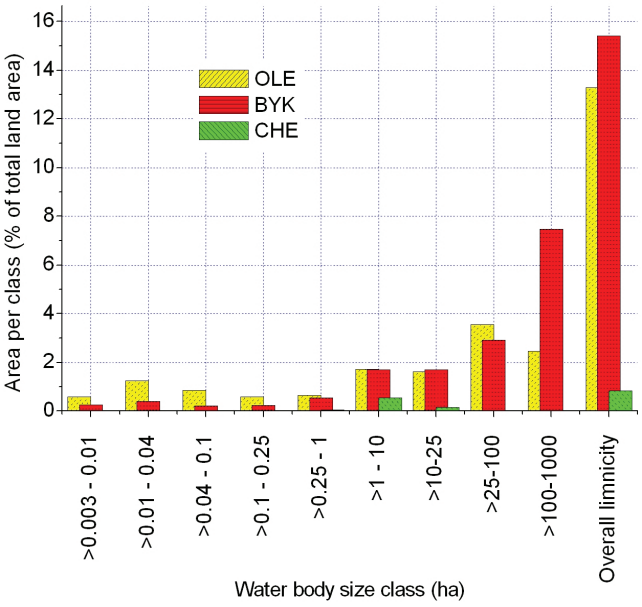

Figure 3. Histogram of total water body surface area for various sizes classes. Last bar shows the overall limnicity in the study areas.

Results

Despite similar basic geocryological conditions at all three sites (ice-rich yedoma deposits), the distribution of thermokarst lakes strongly differs among them. A total number of 29,361 lakes >0.003 ha were classified in the study areas (Table 3). The highest lake cover by land area (limnicity) was found at BYK (15.4%), closely followed by OLE (13.3%). Though CHE is the largest study area, its lake portion is lower than at both other sites by more than one order of magnitude (0.8 %).

Of the lakes >10 ha (49 lakes), 14 belong to OLE (609 ha), 32 to BYK (2053 ha), and 3 to CHE (44 ha) (Fig. 2). When comparing the water body distribution in various size classes, strong differences between the three study sites become even more obvious (Fig. 3). The OLE region has more than double the number of small ponds (0.003–0.01 ha) when compared to the BYK region, and almost 50-fold that of the CHE region. This disparity is also expressed in the low mean lake size for

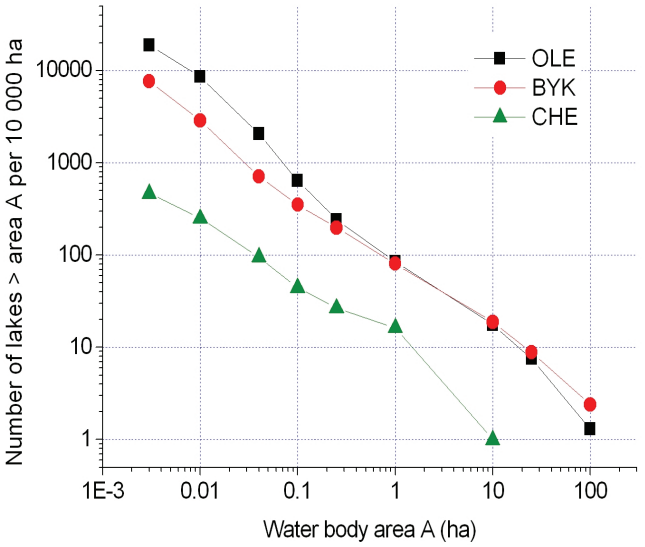

Figure 4. Area-normalized distribution of water bodies per 10,000 ha in the study areas as total number N of water bodies > area A.

OLE. The dominance of lake numbers in the OLE area is true for all size classes except the three largest (>5 ha), where BYK dominates.

Comparing the area-normalized (per 10,000 ha) number N of water bodies larger than area A versus the area A in a logarithmic scaled diagram reveals an almost linear trend for the lake size distribution in all three study sites (Fig. 2). The possibility of describing a lake distribution with such a power law function of type $y=ax^b$ is well known from investigations of other large lake inventories (Lehner & Döll 2004, Downing et al. 2006). It seems to be also applicable to the NE Siberian dataset of comparably small-sized thermokarst lakes investigated in this study. However, obviously for the CHE water bodies the trendline is situated about one order of magnitude below BYK and OLE.

Comparison of lake density between the sites shows a generally highly dense water body population at OLE due to a large amount of small ponds, the clustering of water bodies and thus lake density at BYK, and the overall sparse lake cover at CHE. At CHE, the presence of Rodinka hill in the study area and the lack of lakes on the bedrock hill itself creates an additional cause for the scarcity of lakes. However, it appears not to be the main reason, since flat areas with unconsolidated yedoma farther away from the hill also have much lower lake densities then OLE or BYK. Image analysis and ground truthing reveal that the large lakes in the BYK area usually occur in deep thermokarst basins (subsided up to 40 m below surrounding surface) and often are only the lake remnants of previously partially drained lakes. Many polygonal ponds are situated in these drained basins. Small ponds and medium lakes are found on the yedoma uplands with poor drainage. Yedoma uplands with many thermo-erosional valleys do not contain many lakes. At OLE, most of the numerous, small ponds are found on the yedoma upland. There are only a few large, drained thermokarst basins. Remarkably, the OLE area is relatively homogeneously covered with numerous small ponds, while these small water bodies occur in irregular patterns at BYK and CHE. There are comparably few small thermokarst lakes at CHE. Many of

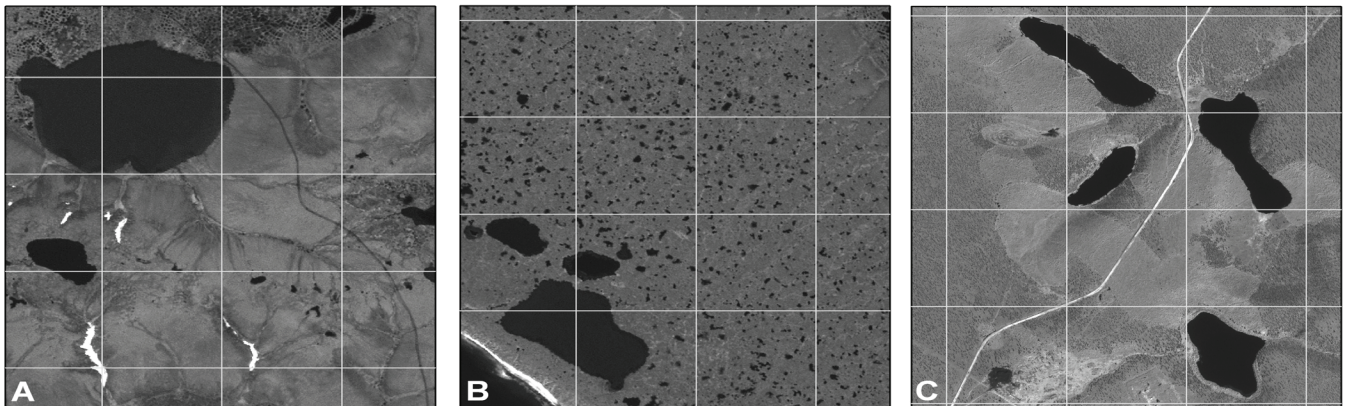

Figure 5. Subsets of study areas displaying characteristic landscape and lake patterns for all three sites. A – BYK; B – OLE; C – CHE. Image grid spacing is 600 m.

these were formed due to human activity in the area around the settlement of Cherskii, adding an artificial component to the natural lake distribution. Similar, at BYK human impact resulted in the drainage of several small lakes along vehicle tracks in the tundra. In contrary to CHE, the overall lake population is very high at BYK and therefore the human influence on the lake distribution characteristics is probably negligible here.

A comparison of our detailed water body dataset with the lakes in the GLWD (Lehner & Döll 2004) reveals large discrepancies in number and area of thermokarst lakes larger than 10 ha (minimum size GLWD) (Fig. 2). As a result, GLWD limnicity at OLE (1.1%), BYK (6.8%), and CHE (0.0%) is significantly lower than in our dataset for the same lake size category (7.6%, 12.1%, and 0.2% respectively). A large percentage of the total water body area (<10 ha) that is important for hydrological and biogeochemical cycles is currently not inventoried and used in environmental modeling (not inventoried water body area per 10 000 ha land area at OLE: 42.7%, BYK: 21.6%, and CHE: 82.2%).

Discussion

Thermokarst lake distribution in our study areas seems to be strongly connected to hydrological and geomorpho-logical factors rather than to geocryology alone. At BYK, a strong thermokarst relief developed during the Late Pleistocene-Holocene transition and many first-generation thermokarst basins and thermo-erosional valleys were formed (Fig. 5A). A large number of second-generation lakes appeared during the Holocene in drained basins. OLE is dominated by a flat yedoma surface with only some thermokarst basins and valleys. Also, yedoma thickness is considerably less than at both other sites with possibly impacts on lake expansion dynamics. The poorly drained upland plain is densely and relatively homogeneously packed with a large number of first generation lakes (Fig. 5B). At CHE (Fig. 5C) the yedoma is mantling the rolling slopes around Rodinka Hill. Comparably few small water bodies occur, but proportionally many medium-sized first-generation lakes. Compared to both other study sites, lakes are less abundant, most likely due to better overall drainage. However, there are plain regions east of Rodinka Hill with the same deposits but still very low lake density.

Vegetation either growing or floating in the lake can pose a challenge for any water-land classification method, be it manual or fully automated. Careful image interpretation, field experience, and in some cases ground truthing are required. We estimate the effect of unclassified water due to vegetation on the order of <2% of the overall water body area for some lakes. Seasonal hydroclimatology can also have an effect on lake surface area especially for lakes with shallow basin topography. While many of the ponds certainly fall into this category, many of the typical thermokarst lakes in ice-rich permafrost do not. These usually have steep banks and a more pronounced basin morphology resulting predominantly in vertical lake level changes rather than lateral lake area changes during seasonal water level variations. Many of the larger lake basins have subsided tens of meters below the surrounding land surface and are surrounded by steep banks. Lake extent changes for such thermokarst lakes are more related to thermoerosion, thaw slumping, or drainage than just seasonal water level changes.

A lake change study for the study areas is still in progress. The time series of lake extent for the BYK site will range for the period from 1951–2008, providing an observational high-resolution dataset for 57 years. For OLE and CHE the time series span a period of 42 and 37 years, respectively.

Conclusions

High-resolution satellite imagery provides the opportunity to characterize the distribution of thermokarst lakes on yedoma deposits in high detail. Spatial analysis of thermokarst features plays an important role in understanding thermokarst dynamics in northern regions and impacts on the global hydrological and biogeochemical cycles. It was shown that thermokarst lake distributions at three yedoma sites differ greatly. Lake distribution is distinguishable for areas with first and second generation lakes. Our comparison with the GLWD lake dataset demonstrates the necessity to quantify northern lakes; that is, thermokarst lakes, in a much higher detail than currently available. Any quantification and upscaling of thermokarst lake-related parameters like methane emission might be biased due to the exclusion of a large number of small lakes and ponds not represented in current global databases. This highlights the need for more intense research on thermokarst distribution and lake dynamics.

Acknowledgments

Grosse and Walter were partially funded by University of Alaska IPY fellowships. Spot imagery for OLE and BYK was provided through the OASIS program. Ikonos imagery for CHE was provided through the NSF AON project.

References

Brown, J., Ferrians, O.J., Jr., Heginbottom, J.A. & Melnikov, E. 1998. Circum-Arctic Map of Permafrost and Ground-Ice Conditions. In: M. Parsons & T. Zhang (eds.), International Permafrost Association Standing Committee on Data Information and Communication (comp.). 2003. *Circumpolar Active-Layer Permafrost System, Version 2.0.* Boulder, CO: National Snow and Ice Data Center/World Data Center for Glaciology. CD-ROM.

Côté, M.M. & Burn, C.R. 2002. The oriented lakes of Tuktoyaktuk Peninsula, Western Arctic Coast, Canada: A GIS-based analysis. *Permafrost and Periglacial Processes* 13: 61–70.

Downing, J.A., Prairie, Y.T, Cole, J.J., Duarte, C.M., Tranvik, L.J., Striegl, R.G., McDowell, W.H., Kortelainen, P., Caraco, N.F., Melack, J.M. & Middelburg, J.J. 2006. The global abundance and size distribution of lakes, ponds, and impoundments. *Limnology and Oceanography* 51(5): 2388–2397.

Frazier, P.S. & Page, K.J. 2000. Water Body Detection and Delineation with Landsat TM Data. *Photogrammetric Engineering & Remote Sensing* 66(12): 1461-1467.

Frohn, R.C., Hinkel, K.M. & Eisner, W.R. 2005. Satellite remote sensing classification of thaw lakes and drained thaw lake basins on the North Slope of Alaska. *Remote Sensing of Environment* 97: 116-126.

Grosse, G., Schirrmeister, L., Kunitsky, V.V. & Hubberten, H.-W. 2005. The use of CORONA images in Remote Sensing of periglacial geomorphology: An illustration from the NE Siberian coast. *Permafrost & Periglacial Processes* 16: 163-172.

Grosse, G., Schirrmeister, L., Malthus, T.J. 2006a. Application of Landsat-7 satellite data and a DEM for the quantification of thermokarst-affected terrain types in the periglacial Lena-Anabar coastal lowland, *Polar Research* 25(1): 51-67.

Grosse, G., Schirrmeister, L., Siegert, Ch., Kunitsky, V.V., Slagoda, E.A., Andreev, A.A. & Dereviagyn, A.Y. 2007. Geological and geomorphological evolution of a sedimentary periglacial landscape in Northeast Siberia during the Late Quaternary, *Geomorphology* 86(1-2): 25-51.

Gutowski, W.J., Wei, H., Vörösmarty, C.J. & Fekete, B.M. 2007. Influence of Arctic Wetlands on Arctic Atmospheric Circulation. *Journal of Climate* 20: 4243–4254.

Hinkel, K.M., Frohn, R.C., Nelson, F.E., Eisner, W.R. & Beck, R.A. 2005. Morphometric and Spatial analysis of thaw lakes and drained thaw lake basins in the western arctic coastal plain, Alaska. *Permafrost & Periglacial Processes* 16: 327-41.

Hinkel, K.M., Jones, B.M., Eisner, W.R., Cuomo, C.J., Beck, R.A. & Frohn, R. 2007. Methods to assess natural and anthropogenic thaw lake drainage on the western arctic coastal plain of northern Alaska. *Journal of Geophysical Research* 112: F02S16.

Lehner, B. & Döll, P. 2004. Development and validation of a global database of lakes, reservoirs and wetlands. *Journal of Hydrology* 296: 1–22.

Morgenstern, A., Grosse, G. & Schirrmeister, L. 2008. Genetical, Morphological, and Statistical Classification of Lakes in the Permafrost-dominated Lena Delta. *Proceedings of the Ninth International Conference on Permafrost, Fairbanks, Alaska, June 29–July 3, 2008* (this proceedings).

Riordan, B., Verbyla, D. & McGuire, A.D. 2006. Shrinking ponds in subarctic Alaska based on 1950–2002 remotely sensed images. *Journal of Geophysical Research* 111: G04002.

Rivas-Martínez, S. 2008. Worldwide Bioclimatic Classification System. Phytosociological Research Center, Spain. Online database, http://www.globalbioclimatics.org

Schirrmeister, L., Kunitsky, V.V., Grosse, G., Kuznetsova, T., Meyer, H., Derevyagin, A., Wetterich, S. & Siegert, Ch. 2008. The Yedoma Suite of the northeastern Siberian shelf region – characteristics and concept of formation. *Proceedings of the Ninth International Conference on Permafrost, Fairbanks, Alaska, June 29–July 3, 2008* (this proceedings).

Schirrmeister, L., Kunitsky, V.V., Grosse, G., Schwamborn, G., Andreev, A.A., Meyer, H., Kuznetsova, T., Bobrov, A. & Oezen, D. 2003. Late Quaternary history of the accumulation plain north of the Chekanovsky Ridge (Lena Delta, Russia) - a multidisciplinary approach. *Polar Geography* 27: 277-319.

Schneider, J., Grosse, G. & Wagner, D. (in review). Land cover classification of tundra environments in the arctic Lena Delta based on Landsat 7 ETM+ data and its application for upscaling of methane emissions. *Remote Sensing of Environment.*

Sellmann, P.V., Brown, J., Lewellen, R.I., McKim, H. & Merry, C. 1975. *The Classification and Geomorphic Implications of Thaw Lakes on the Arctic Coastal Plain, Alaska.* United States Army, CRREL Research Report 344, 21 pp.

Smith, L.C., Sheng, Y., MacDonald, G.M. & Hinzman, L. D. 2005. Disappearing Arctic Lakes. *Science* 308: 1429.

Wagner, D., Kobabe, S., Pfeiffer, E.-M. & Hubberten, H.-W. 2003. Microbial controls on methane fluxes from a polygonal tundra of the Lena Delta, Siberia. *Permafrost and Periglacial Processes* 14: 173-185.

Walter, K.M., Edwards, M.E., Grosse, G., Zimov, S.A. & Chapin, F.S., III. 2007. Thermokarst lakes as a source of atmospheric CH4 during the last deglaciation. *Science* 318: 633-636.

Walter, K.M., Zimov, S.A., Chanton, J.P., Verbyla, D. & Chapin, F.S., III. 2006. Methane bubbling from Siberian thaw lakes as a positive feedback to climate warming. *Nature* 443: 71-75.

Yoshikawa, K. & Hinzman, L.D. 2003. Shrinking thermokarst ponds and groundwater dynamics in discontinuous permafrost near Council, Alaska. *Permafrost & Periglacial Processes* 14: 151-160.

Zimov, S.A., Voropaev, Y.V., Semiletov, I.P., Davidov, S.P., Prosiannikov, S.F., Chapin, F.S., III, Chapin, M.C., Trumbore, S. & Tyler, S. 1997. North Siberian lakes: a methane source fueled by Pleistocene carbon. *Science* 277: 800-802.

The Cooling Effect of Coarse Blocks Revisited: A Modeling Study of a Purely Conductive Mechanism

Stephan Gruber, Martin Hoelzle
Glaciology, Geomorphodynamics and Geochronology, Geography Department, University of Zurich, Switzerland

Abstract

Coarse blocks are a widespread ground cover in cold mountain areas. They have been recognized to exert a cooling influence on subsurface temperatures in comparison with other types of surface material and are employed in man-made structures for ground cooling and permafrost protection. The contrast in heat transfer between the atmosphere and the ground caused by thermally driven convection in winter and stable stratification of interstitial air during summer is usually invoked to explain this "thermal diode" effect. Based on measurements and model calculations, we propose an additional cooling mechanism, which is independent of convection, and solely functions based on the interplay of a winter snow cover and a layer of coarse blocks with low thermal conductivity. The thermal conductivity of a block layer with a porosity of 0.4 is reduced by about an order of magnitude compared to solid rock. We use a simple and purely conductive model experiment to demonstrate that low-conductivity layers reduce the temperature below the winter snow cover as well as mean annual ground temperatures by comparison with other ground materials. Coarse block layers reduce the warming effect of the snow cover and can result in cooling of blocky surfaces in comparison with surrounding areas in the order of one or several degrees. The characteristics of this mechanism correspond to existing measurements.

Keywords: coarse blocks; heat transfer; mountain permafrost; rock glacier; snow cover; thermal offset.

Introduction

Coarse blocks are a common surface cover in many cold and temperate mountain ranges. They have a cooling influence on ground temperatures compared with fine-grained soil or bedrock in otherwise similar settings (cf. Haeberli 1973, Harris 1996, Gorbunov et al. 2004, Juliussen & Humlum 2008). This cooling effect makes blocky substrates interesting for construction in cold regions (e.g., Goering & Kumar 1996, Guodong et al. 2007) and it is a significant factor influencing the distribution and characteristics of permafrost (Haeberli 1975). Therefore, the understanding and quantification of this cooling effect is important for spatial modeling of permafrost, estimation of its characteristics, and assessment of its temporal evolution.

Measurements in coarse blocky substrate as well as their interpretation are faced with a number of difficulties. To begin with, it is difficult to define the surface of a blocky substrate. Point measurements are bound to either the interstitial air or large clasts and integral macroscopic properties of the blocky material, such as temperature or albedo, are difficult to determine. Similarly, on a macroscopic scale, snow is partly deposited in a volume rather than on a discrete surface because the geometric surface roughness and the depth of voids can have the same order of magnitude as snow thickness itself. Despite these difficulties, a number of processes that may be responsible for the cooling effect of coarse blocks have been proposed and analyzed (e.g., Hanson & Hoelzle 2004, Juliussen & Humlum 2008, see Herz 2006 for a comprehensive review).

These processes are: (a) free convection; (b) forced convection; (c) chimney effect; (d) evaporation/sublimation/ice melt; (e) snow deposition deep into the active layer; and (f) protruding blocks reducing the insulating effect of the snow cover. While all of these processes are plausible, little is known about their relative importance and about the dependence of this importance on environmental conditions. However, understanding the importance of each process is vital to further progress.

One way to achieve this is the joint analysis of model results and measured data. The deviation between model and measurements is bound to contain (among other errors) the error produced by not including an important process in the model. Using such experiments, we were surprised to find that the thermal conductivity of the near-surface material decisively controls ground temperatures below the snow cover. For example, the depression of winter temperatures measured on coarse block fields (cf. BTS on coarse blocks, Haeberli 1973, 1975) in the Murtèl/Corvatsch area (Fig. 1) could be reproduced with two models (TEBAL, Gruber 2005; SNOWPACK, Bartelt & Lehning 2002) that do not include the process of air movement in blocks (cf. Frey 2007). This suggests that at this site, either convection is of secondary importance after an effect related to thermal conductivity, or, that errors in both models resulted in temperature depressions similar to those measured.

In this paper we explore and describe this combined effect of near-surface thermal conductivity and snow pack using a simplified model. While subject to strong generalization with respect to the measured situation, the simple model used here allows to isolate and properly demonstrate the relevant process in a framework that is easily traceable. The cooling mechanism, which we propose, does not contradict existing and well-established research on convective heat transport in coarse blocks (e.g., Goering & Kumar 1996, Guodong et al. 2007). Instead, it offers an explanation of measured cooling where snow cover is thick and signs of significant convection are absent.

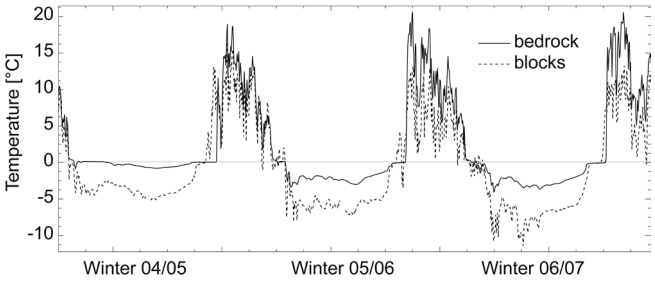

Figure 1. Near-surface temperatures at the rock glacier Murtèl. The solid line shows average daily temperatures 10 cm deep in bedrock adjacent to the rock glacier front. The dashed line shows daily temperature measurements about 50 cm deep within the blocky surface of the rock glacier. These measurements were taken around midnight and therefore have a cold bias during the snow-free time when significant diurnal amplitudes exist.

Model Experiment with Synthetic Data

Based on a model experiment, we intend to illustrate that a lower thermal conductivity of near-surface material causes lower temperatures below the winter snow cover and that this also affects mean temperatures at greater depth. The model is reduced to only conductive components and effects of, e.g., water percolation or phase change are neglected. That way, this mechanism can be studied in isolation from other effects.

Model description

The model contains a finite-difference Crank-Nicolson solution of the heat conduction equation with no treatment of phase change or advective heat transport. The snow pack and the uppermost 5 m of the ground are discretized with a spacing of 0.1 m. Below, the interval gradually increases down to 15 m. The snow cover is added and depleted in steps of 0.1 m. Available model parameters are: maximum snow cover thickness (H_{max}), duration of the accumulation (D_{acc}) and ablation (D_{abl}) periods, date of maximum snow cover thickness (J_{max}), phase lag of temperature cycle (L), mean surface temperature (M), surface temperature amplitude (A), and the thickness of the block layer (B).

Equation (1) describes the temporal evolution of the snow cover thickness H (Fig. 2). The parameter Δt ranges from 0 to 1 and describes the relative distance to J_{max}, where Δt=0 at the date of J_{max} and Δt=1 at the dates of D_{acc}.and D_{abl}.

$$H = H_{\max} \cdot \left(1 - \left(\frac{e^{-\Delta t^{2.5}} - 1}{e - 1}\right)\right) \quad (1)$$

The influence of the snow cover on ground temperatures in nature has three main causes: (a) thermal insulation; (b) reduction in albedo; and (c) advection of latent heat because melt energy is required to remove the snow. In this model, only (a) is considered because the effect of thermal insulation is of interest here.

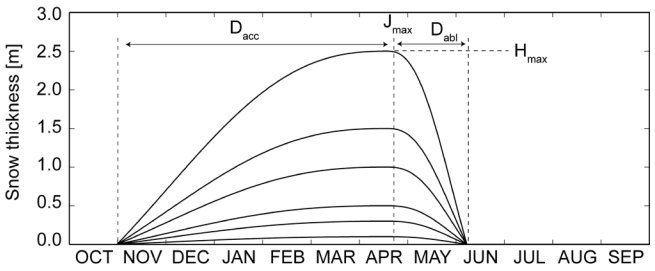

Figure 2. Synthetic snow cover evolution using H_{max} of 2.5, 1.5, 1.0, 0.5, 0.3, and 0.1 m.

Ground properties

The snow cover has a uniform density of 280 kg m^{-3}, a thermal conductivity of $k_S = 0.13$ W m^{-1} K^{-1}, and a volumetric heat capacity of $c_S = 5.4\times10^5$. The thermal conductivity of the ground is $k_G = 2.5$ W m^{-1} K^{-1} and the volumetric heat capacities of the ground and block layers are $c_G = 1.6\times10^6$ J m^{-3} K^{-1} and $c_B = 0.8\times10^6$ J m^{-3} K^{-1}. This is based on typical rock thermo-physical properties (Cermák & Rybach 1982) and a porosity of the block layer, which is assumed to be 0.4–0.5. For the block layer, different thermal conductivities k_B are considered between that of pure rock (2.5 W m^{-1} K^{-1}) and a rather low estimate (0.2 W m^{-1} K^{-1}). The low values of thermal conductivity for the block layer are in accordance with values in the range of 0.3 W m^{-1} K^{-1} published for dry sand and for theoretical values when calculating a mixture of rock and air using the geometric mean that usually approximates random aggregates rather well.

Boundary conditions

A harmonic temperature boundary condition (Dirichlet) representing seasonal variation drives the heat conduction scheme at its upper boundary for the duration of several hundred years. This condition ($T_{surface}$) is prescibed at the snow surface during winter and at the ground surface during summer. It is described by Equation (2), where φ is the duration of one seasonal cycle (one year). Similar to conditions at Murtèl/Corvatsch, we assume M = -2.5°C, A = 10°C, L = 45, J_{max} = 105, D_{abl} = 50, D_{acc} = 170, where $D_{abl/acc}$, J and L are given in days and days of the year, respectively.

$$T_{surface} = \sin\left(-(t+L)\frac{2\pi}{\varphi}\right) \cdot A \cdot M \quad (2)$$

Results

The insulating influence of the winter snow cover increases with thicker snow cover (Fig. 3). The temperature T_0 refers to the temperature at the ground surface. Changing the thermal conductivity of the block layer modifies the warming influence of the snow cover (Fig. 4A) and, in accordance with observations (Fig. 1), lower temperatures are modeled under the snow when using lower thermal conductivities of the near-surface, which are characteristic of the block layer. During winter, the heat conduction through the snow pack is very small and, as a consequence, the heat conduction from deeper ground layers

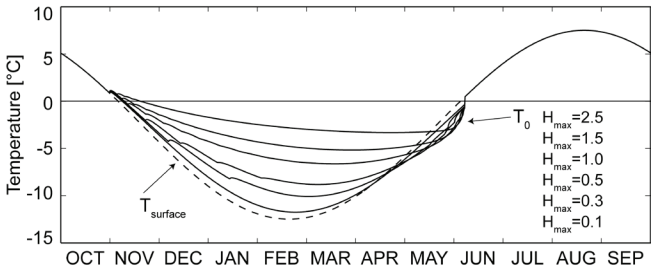

Figure 3. Temperature evolution at the ground surface during one year and for diverse snow cover conditions defined by H_{max}. All cases have a thickness of the block layer B = 3 m and a thermal conductivity of the block layer $k_B = 0.2$ W m^{-1} K^{-1}. The dashed line represents the prescribed surface temperature $T_{surface}$. In the cooling phase, slight kinks are visible in the temperature curve. These are unimportant artifacts from the simple modeling scheme in which discrete elements of 0.1 m are added or removed as the snow pack evolves.

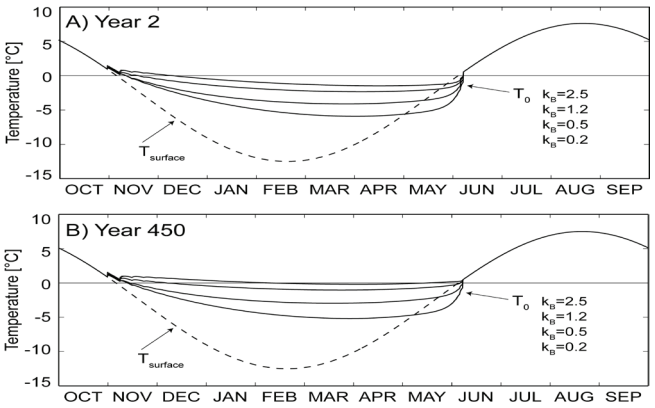

Figure 4. Temperature evolution at the ground surface during two different model years for a maximum snow thickness $H_{max} = 1.5$ m and a thickness of the blocky layer of B = 3 m. Different curves refer to different thermal conductivities of the block layer k_B.

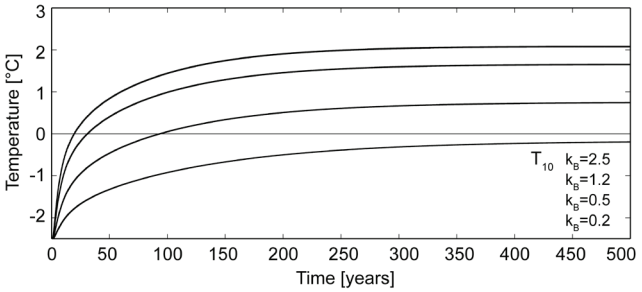

Figure 5. Temperature evolution at a depth of 10 m below the ground surface (T_{10}) during 500 model years for a maximum snow thickness $H_{max} = 1.5$ m and a thickness of the blocky layer of B = 3 m. Different curves refer to different thermal conductivities of the block layer k_B.

dominates the temperatures at the snow/ground interface. The BTS method (Haeberli 1973) exploits this effect. If the thermal conductivity of the near-surface ground layer is significantly lower, then the relative importance of heat transfer through the snow increases and temperature at the snow/ground interface will respond more to atmospheric forcing. This is also visible in Fig. 1, where both time series contain similar temperature fluctuations in winter and where these fluctuations are more pronounced in the blocks.

It is now important to know whether this effect only results in lower temperatures under the snow cover, or, whether it also influences mean ground temperatures. In Fig. 4B we can see that over the course of about 450 modeled years, all temperatures have warmed with respect to Figure 4A, indicating exactly this effect over the longer term. This is also visible in the transient response of temperatures at 10 m depth (Fig. 5). After initialization with a temperature of M = –2.5°C and constant boundary conditions having the same mean, temperatures equilibrate at much higher levels due to the insulating effect of the winter snow. This insulating effect is modulated by the thermal conductivity of the blocky layer. These results can be explained as follows: The mean annual ground temperature (at some shallow depth) in first approximation contains a weighted average of surface temperatures. The weight and relative importance of winter temperatures in this average is reduced by the insulating effect of the snow cover (cf. Zhang et al. 2001) that impedes the heat transfer between the (snow) surface and the ground. Where the thermal conductivity of the near surface is low, the heat transfer in snow-free conditions is already slow. As a consequence, the contrast between summer and winter conditions is smaller than for situations with high thermal conductivity of the subsurface. The relative cooling effect of blocky material (compared to many other surfaces) is essentially an effect of reduced warming. This effect is a thermal filter with an effectiveness that is dependent on the thermal contrast between summer and winter conditions. A block layer reduces the overall thermal conductivity of the ground-atmosphere interface and thus reduces the contrast between summer and winter.

Discussion

This experiment illustrates that the temperature below the winter snow cover as well as mean annual ground temperatures at greater depth can be significantly reduced solely based on the low thermal conductivity of blocky material. The use of a one-dimensional scheme together with macroscopic properties of block layers is a challenging concept because the size of individual clasts can exceed the vertical discretization interval by far. Nevertheless, as long as the majority of clasts do not exceed the thickness of the block layer, this approximation should produce acceptable results, because the overall conductive heat transfer is impeded by the small surface of the contacts between individual pieces of rock. The comparison of modeling results with measurements, however, has to employ either spatial averaging or deeper measurements in order to average lateral variability (cf. Frey 2007, Hoelzle & Gruber 2008). Using the geometric average as an approximate mixing model (Clauser & Huenges 1995), the thermal conductivities of coarse blocks (cf. Binxiang et al. 2004) and sand should be the same because both materials have similar constituents and a similar porosity. This is only true for completely dry material because sand or other soil material usually holds significant amounts of water due to capillary forces in the more abundant small pores. This likely

Table 1. Example of the net effect of diverse near-surface layers.

Block layer thermal conductivity	Heat flux at lower boundary condition 0.0 W m^{-2}	0.06 W m^{-2}
k_B=2.5 W m^{-1} K^{-1}	4.6 °C	4.7 °C
k_B=1.2 W m^{-1} K^{-1}	4.1 (0.5) °C	4.3 (0.4) °C
k_B=0.5 W m^{-1} K^{-1}	3.2 (1.4) °C	3.5 (1.2) °C
k_B=0.2 W m^{-1} K^{-1}	2.3 (2.3) °C	3.2 (1.5) °C

Subsurface warming for a 3 m thick near-surface layer with diverse thermal conductivities and two different lower boundary conditions. The second column (zero heat flux) represents the conditions shown in Fig. 5. Warming values refer to final subsurface warming at a depth of 3 m with respect to the mean (prescribed) surface temperature (M). Numbers in brackets express this warming as relative cooling with respect to pure rock (2.5 W m^{-1} K^{-1}).

results in a distinctively higher overall thermal conductivity in fine-grained soil than in coarse material.

In many publications, the effect of ground cooling in block slopes is referred to as thermal offset, in analogy to common terminology in the Arctic. The thermal offset described in the Arctic is caused by seasonal differences in the properties of the active layer, which are due to the contrast in thermal conductivity between water and ice. This usually results in a curved temperature profile and a marked temperature difference between the top and bottom of the active layer. Convection of air would be similar to a temporary increase in the thermal conductivity and resembles this pattern. The mechanism we propose here, produces no temperature difference between the top and bottom of the active layer, and this behavior corresponds with several existing measurements (Juliussen & Humlum 2008, Hoelzle & Gruber 2008).

A block layer of very low thermal conductivity results in a strong thermal gradient with depth in the presence of a geothermal heat flux. This effect can reduce the relative ground cooling (Table 1) and varies with the thickness of the block layer and with the heat flux across it. In mountain areas, the deeper heat flux is usually reduced (Kohl 1999) and spatially highly variable (Gruber at al. 2004). Additionally, the advection of subsurface ice (moving rock glacier) and transient effects can reduce or even invert the heat flux in the uppermost tens of meters.

The effect of reduced warming by the snow cover as proposed here does not preclude the presence of additional processes that lead to relative ground cooling. Depending on environmental conditions, other processes may even be more important. The most prominent other process that is described in the literature is the circulation of air caused by temperature-driven free convection. This effect and the effect proposed in this paper are complementary in some way: conditions of little snow cover favor the effect of advection and reduce the purely conductive mechanism described here, whereas a thick snow cover inhibits convection and gives rise to the full effect of low thermal conductivity. Conditions may vary on a continental scale (low/high precipitation areas), locally (wind-swept ridge or snow-filled depression) or with time (dry winter, climate change). Because the proposed effect is "relative cooling by reduced warming," it cannot result in ground temperatures significantly below the MAAT as has been observed for block surfaces with strong air movement (e.g., Gorbunov et al. 2004, Delaloye et al. 2003).

Conclusion and Outlook

We have presented a simple and purely conductive mechanism that can cause lower temperatures at the snow/ground interface as well as lower mean ground temperatures in coarse blocky surfaces as compared to bedrock or fine-grained material. This mechanism is not an alternative but rather an extension of existing theory, and it can at least partly clarify previously unexplained measurement results.

The quantitative understanding of the influence of each proposed mechanism and its sensitivity to material properties and environmental conditions is an important topic for future research. This will determine, for instance, which processes have to be included in a specific model and which are of secondary importance, only. The creative combination of both modeling and measurements is expected to be a viable means to achieve this. Additionally, methods for the delineation of block fields (cf. Heiner et al. 2003, Gruber & Hoelzle 2001) are important because this can strongly improve the quality of simulations, even with simple methods.

Acknowledgments

We are grateful to S. Bircher and E. Frey who contributed to the ideas presented here with their MSc theses as well as many discussions and experiments. Three anonymous reviewers have provided valuable feedback—the question of the lower boundary condition being our favorite by far.

References

Bartelt, P. & Lehning M. 2002. A physical SNOWPACK model for the Swiss avalanche warning. Part I: numerical model. *Cold Regions Science and Technology* 35: 123-145.

Binxiang, S., Xuezu, X., Yuanming, L,, Dongqing, L., Shuangjie, W. & Zhang, J. 2004. Experimental researches of thermal diffusivity and conductivity in embankment ballast under periodically fluctuating temperature. *Cold Regions Science and Technology* 38: 219-227.

Cermák, V. & Rybach, L. 1982. Thermal conductivity and specific heat of minerals and rocks. In: G. Angeneister (ed.), *Landolt-Börnstein Zahlenwerte und Funktionen aus Naturwissenschaften und Technik, Physikalische Eigenschaften der Gesteine (V/1a)*, Berlin: Springer, 305-343.

Clauser, C. & Huenges, E. 1995. Thermal conductivity of rocks and minerals. In: T.J. Ahrens (ed.), *Rock Physics and Phase Relationsóa Handbook of Physical Constants*, *AGU Reference Shelf,* 3: 105-126.

Delaloye, R., Reynard, E., Lambiel, C., Marescot, L. & Monnet, R. 2003. Thermal anomaly in a cold scree slope, Creux du Van, Switzerland. *Proceedings of the 8th International Conference on Permafrost, Zurich, 2003*, Vol. 1: 175-180.

Frey, E.A. 2007. *Messung und Modelllierung der Basistemperatur der alpinen Schneedecke*. Unpublished MSc thesis, Department of Geography, University of Zürich, Switzerland, 95 pp.

Goering, D.J. & Kumar, P. 1996. Winter-time convection in open-graded embankments. *Cold Regions Science and Technology* 24: 57-74.

Gorbunov, A.P., Marchenko, S.S. & Seversky, E.V. 2004. The thermal environment of blocky materials in the mountains of Central Asia. *Permafrost and Periglacial Processes* 15: 95-98.

Gruber, S. 2005. *Mountain permafrost: transient spatial modeling, model verification and the use of remote sensing*. PhD thesis, Department of Geography, University of Zurich, Switzerland, 123 pp.

Gruber, S. & Hoelzle, M. 2001. Statistical modelling of mountain permafrost distribution – local calibration and incorporation of remotely sensed data. *Permafrost and Periglacial Processes* 12: 69-77.

Gruber, S., King, L., Kohl, T., Herz, T., Haeberli, W. & Hoelzle, M. 2004. Interpretation of geothermal profiles perturbed by topography: The Alpine permafrost boreholes at Stockhorn Plateau, Switzerland. *Permafrost and Periglacial Processes* 15: 349-357.

Guodong, C., Yuanming, L., Zhizhong, S. & Fan, J. 2007. The "thermal semi-conductor" effect of crushed rock. *Permafrost and Periglacial Processes* 18: 151-160.

Haeberli, W. 1973. Die Basis-Temperatur der winterlichen Schneedecke als möglicher Indikator für die Verbreitung von Permafrost in den Alpen. *Zeitschrift für Gletscherkunde und Glazialgeologie* 9: 221-227.

Haeberli, W. 1975. Untersuchungen zur Verbreitung von Permafrost zwischen Flüelapass und Piz Grialetsch (Graubünden). Zürich, *Mitteilungen der Versuchsanstalt für Wasserbau, Hydrologie und Glaziologie* 17: 221pp.

Hanson, S. & Hoelzle, M. 2004. The thermal regime of the active layer at the Murtèl rock glacier based on data from 2002. *Permafrost and Periglacial Processes* 15: 273-282.

Harris, S.A. 1996. Lower mean annual ground temperature beneath a block stream in the Kunlun Pass, Qinghai Province, China. *Proceedings of the 5th Chinese Permafrost Conference, Lanzhou, 1996*: 227-237.

Heiner, S., Gruber, S. & Meier, E. 2003. The spatial extend and characteristics of block fields in alpine areas: evaluation of aerial photography, LIDAR and SAR as data sources. *Extended abstract volume of the 8th International Conference on Permafrost, Zurich, 2003*: 59-60.

Herz, T. 2006. *Das Mikroklima grobblockiger Schutthalden der alpinen Periglazialstufe und seine Auswirkungen auf Energieaustauschprozesse zwischen Atmosphäre und Lithosphäre*. PhD thesis, Department of Geography, University of Giessen, Germany, 207 pp.

Hoelzle, M. & Gruber, S. 2008. Borehole and ground surface temperatures and their relationship to meteorological conditions in the Swiss Alps. *Proceedings of the 9th International Conference on Permafrost 2008*, Fairbanks, Alaska, USA.

Juliussen, H. & Humlum, O. 2008. Thermal regime of openwork block fields on the mountains Elgåhogna and Sølen, central-eastern Norway. *Permafrost and Periglacial Processes* 19: 1-18.

Kohl, T. 1999. Transient thermal effects at complex topographies, *Tectonophysics* 306: 311-324.

Zhang, T., Barry, R.G. & Haeberli, W. 2001. Numerical simulations of the influence of the seasonal snow cover on the occurrence of permafrost at high latitudes. *Norwegian Journal of Geography* 55: 261-266.

Interrelation of Cryogenic and Hydrologic Processes on Small Streams and Catchments of Central Yamal

A.A. Gubarkov
Tyumen Oil and Gas University, Tyumen, Russia
M.O. Leibman
Earth Cryosphere Institute SB RAS, Tyumen, Russia

Abstract

Small streams of the Yamal Peninsula provide the best opportunity to study the interrelation of cryogenic and hydrologic processes. A case study on the test river Panzananayakha was undertaken to assess catchment morphogenesis, water flow, and sediment transport in relation to cryogenic processes. Which dominating cryogenic processes most affect the river channel depends on channel morphology. In V-shaped valleys the low valley slopes end directly in the channel, and the influence of cryogenic landsliding on hydrologic processes dominates. Ice wedges close to the surface produce bead-shaped channels that slow the stream velocity. Cryogenic processes directly affect sediment transport as well. The complex cryogenic and hydrologic processes which are characteristic for upper, middle, and lower stream courses in the small catchments are specified. Channel processes include bottom and lateral thermoerosion. Trans-catchment processes include transitional landslides, earth flows, and ravine thermoerosion.

Keywords: bead-shaped channel; cryogenic processes; hydrologic processes; landslides; thermoerosion.

Introduction

More than 90% of the rivers in tundra regions can be considered as small rivers less than 10 km in length. These small rivers comprise more than 80% of the total length of all rivers. Small rivers in the cryolithozone are characterized by the interaction and interrelation of cryogenic and hydrologic processes. These processes result in specific valley slopes and bottom shape, stream mode and transport of sediments. The same scale of cryogenic and hydrologic processes in these small catchments is the main reason for such a relation. On middle-length and long rivers, the impact of cryogenic processes on a channel is not observed as the mass waste processes are not capable of changing the stream direction, or creating a full or even partial damming of the water flow.

The main cryogenic process affecting water and sediment runoff of these small rivers is thermoerosion, cryogenic landslides (active-layer detachments and earth flows), and thermokarst.

Thermoerosion studies have been carried out since the middle of 19th century. The Yamal Peninsula is discussed in numerous publications including: Kosov & Konstantinova (1973), Malinovskiy (1980), Dan'ko (1982), Sidorchuk (1999), Voskresensky (2001). Typically thermoerosion occurs only at the end of summer or in the fall when the active layer reaches its maximum depth. Dan'ko (1982) suggests that thermoerosion is possible during different periods of warm time of the year. Malinovskiy (1980) measured the ability of water flow to carry sediment load and bottom sediments under thermoerosion and found typical values of 700 g/l.

Sidorchuk (1999) conducted observations on the Bovanenkovo gas field at Central Yamal in 1987–1995 and found the hydrologic and morphometry factors of ravine erosion and thermoerosion in both natural and anthropogenic environments. Voskresenskiy (2001) emphasized the need to consider the complex interactions between thermoerosion and thermokarst. These studies showed an obvious relationship between the density of ravines and thermokarst distribution on the Yamal Peninsula.

The interrelation of thermoerosion and thermokarst is also discussed by Romanovsky (1961) who concluded that lake thermokarst and thermoerosion in alases result in a united system of erosion-thermokarst depressions, through which runoff of water and sediment takes place. Romanenko (1997) studied tundra lakes in the Siberian Arctic. He has showed that the proportion of erosion-thermokarst lakes at the Bovanenkovo gas field is maximal in all of northern Siberia and accounts for 15% of the total lake distribution of this region.

Study of the cryogenic landsliding (Leibman & Kizyakov 2007) shows that the greatest influence on water and sediment runoff, and the evolution of channels and valleys of small rivers is induced by landslides (both active-layer detachments and earth flows). Important features of landslides are the speed of descent, volume of the landslide body, and position on the valley slope. This last feature determines whether the landslide body has the potential to block the valley and small stream channel, and therefore, creates a temporary lake in the stream channel or valley. The duration of cryogenic landslides varies from several hours to minutes, while the lifetime of a resulting dammed lake depends on the time needed for the stream to cut through the dam formed by the landslide body. One directly observed dammed lake drained 11 years after a landslide event.

The level of activity of the erosion, transport and accumulation during the warm period in relation to a complex of natural factors can vary considerably from year to year. As determined from theoretical assumptions, laboratory tests and field observations, thermoerosion is most active in the

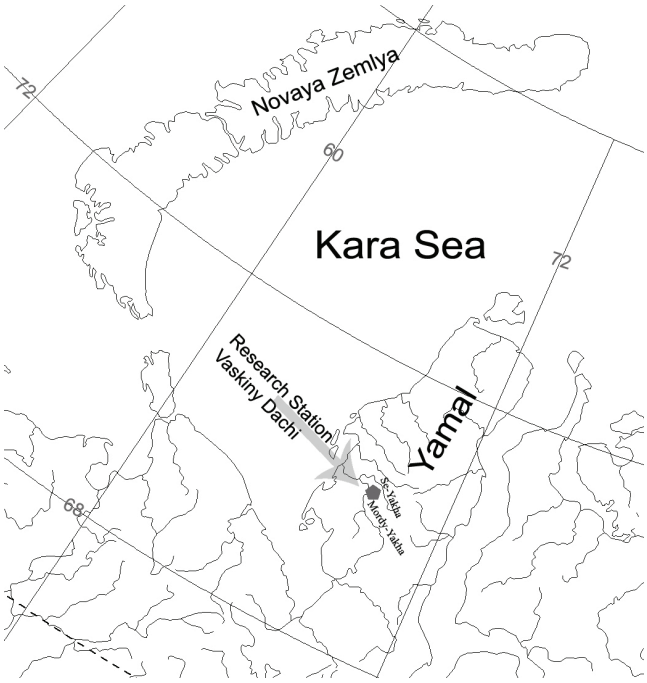

Figure 1. The study area on Central Yamal in the vicinity of Research station Vaskiny Dachi.

summer-fall, when air temperature and , water temperature are the highest. The heat energy of the flow is enough to melt permafrost under such conditions. This is especially true in cases where there is sufficient energy of flow to erode the thawed active layer soils first. However on Central Yamal in summer-fall, the slopes are protected by vegetative cover and thus are hard to erode. The active layer deposits consolidate and aggregate with time while the thaw depth increases, reducing the ability of the erosion of the active layer as well as underlying permafrost. Erosion of sands is easier compared to clayey and organic soils but the active-layer depth in sands is much higher. Consequently to promote thermoerosion in permafrost, intensive rains are required to provide the power of flow sufficient to erode the active-layer deposits. According to Russian Hydrometeorological Service records very intense rainstorms in these tundra regions occur once in 30 years, and intense showers occur only once in 10-20 years. More typical are drizzling rain, which do not increase streamflow sufficiently to allow intensive thermoerosion. Thermoerosion in summer-fall period most likely occurs in interrelation with cryogenic landslides and thermal denudation or other slope displacements forming cracks or bare surface.

Methods and Study Area

Both remote-sensing and land-based data were used to obtain information on cryogenic and hydrologic features in the study area. Both 1:25000 topographic maps and 1:10000 aerial photos were digitized and interpreted. Interpretation included counting and measuring both hydrological and cryogenic features. These features were then evaluated by field measurements.

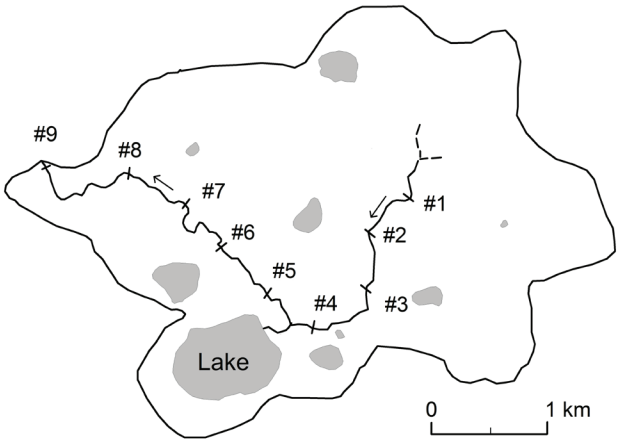

Figure 2. Panzananayakha river catchment. Numbers refer to section lines where water discharge was measured.

The test river Panzananayakha, which is 7 km in length and has a catchment area of 8 km^2, is representative of small rivers of the Central Yamal as shown from analysis of maps of various scale and field studies in the basin of Se-Yakha and Mordy-Yakha rivers and their tributaries. Average river length in this region is 5.99 km.

Land-based studies were used to determine features of beam-shaped river-channel forms, including width, length and depth, as well as stream velocity. Turbidity was measured in both middle and small sized rivers. This was done by water sampling, filtering, drying, and weighing the dried solids.

Field studies at the research station "Vaskiny Dachi" (Fig. 1) were undertaken in 2005–2007, considered the regime and morphology of temporary non-channel and channel streams, small rivers with catchment area under 10 km^2, and a middle-length river (catchment area about 3000 km^2).

The temporary non-channel and channel streams were located on 25 shear surfaces of landslides, in 3 thermocirques, and 3 ravines. Channel features, as well as water and sediment runoff were observed in 4 small and 1 middle-length rivers. On the Panzananayakha test river, all morphometry features of its channel, including landslides, thermokarst forms, erosion, and hydrology were measured (Fig. 2). In addition, alternation of erosive and accumulation zones, and channel shape along the crosscuts were studied in the test river valley.

Results and Discussion

In some years, the slope erosion in the spring may account for up to 75% of annual erosion (Dan'ko 1982). This suggests that most of the erosion is confined to frozen deposits (thermoerosion), including both active-layer deposits and permafrost that are in a frozen state. In the late summer–fall period, as mentioned above, thermoerosion and erosion are limited by active-layer properties and vegetative cover. However, according to our observations, the processes of cryogenic landsliding promoting thermoerosion and erosion events are most active during this period.

Table 1. Depth of shear surface against surrounding slope, and depth of thermoerosion landforms against the landslide shear surface at the upper, middle and lower portions of the landslide slope.

Landslide #	Depth of shear surface, m			Depth of thermoerosion landforms, m		
	upper	middle	lower	upper	middle	lower
1	-3.3	-3.8	-9.5	-1.2	-1.2	-0.2
2	-0.5	-3.1	2.5	-0.5	-2.1	-0.4
3	-3.5	-2.5	-0.5	-1	-1.1	-0.8
4	-4.2	-3.4	-2.2	-1.2	-1.2	-0.3
5	-5.7	-5.7		-0.2	-1.5	
6	-2.1	-1.8		0	-0.2	
7	-1.7	-2.3		-0.2	-1.7	
8	-3.7	-5.8		-1.2	-0.1	
9	-5.3	-6.2		-0.1	-1	
10	-3.7			-1		
11	-5.3			-0.9		
Average	-3.5	-3.8	-3.9	-0.7	-1.1	-0.4

After landslide shear surfaces are exposed, they are susceptible to heavy erosion and thermoerosion, and as a result a significant quantity of sediments are often delivered into the stream network (Leibman & Streletskaya 1997). Under the influence of temporary stream erosion/thermoerosion, troughs develop in a specific sequence. We subdivide these into three zones of down slope thermoerosion: sediment mobilization (upper), sediment transition (middle), and sediment accumulation (lower). All three zones are developed only when the landslide body entirely moves away from the shear surface.

Cross-sections were set and slope morphology measured in the upper, middle, and lower portions of slope. Results are presented in Table 1.

Analysis of Table 1 shows that there is a relation between the depth of thermoerosion against the landslide shear surface and the depth of shear surface against the surrounding slope or hilltop edges. This relation is directly proportional in the sediment mobilization zone, and inversely proportional in the accumulation zone as shown on cross-sections of the landslide shear surfaces and erosion troughs (Fig. 3). In the upper portion of the landslide shear surface, the increase of the erosion trough depth is observed when landslide shear surface is deeper than the slope surface. This is due to the higher relief potential energy when the shear surface is deeper. At the same time, runoff from the catchment does not contain a high sediment load due to the vegetation coverage. That is why the erosional ability of the water flow in the sediment mobilization zone of a landslide shear surface is the highest.

In the lower portions of the landslide slope, the depth of the erosion troughs is less when the shear surface is deeper. This is a result of increased input of sediment from the higher shear surface rim. For this reason, maximum runoff observed in the lower portion of the shear surface performs minimal erosion because the sediment load

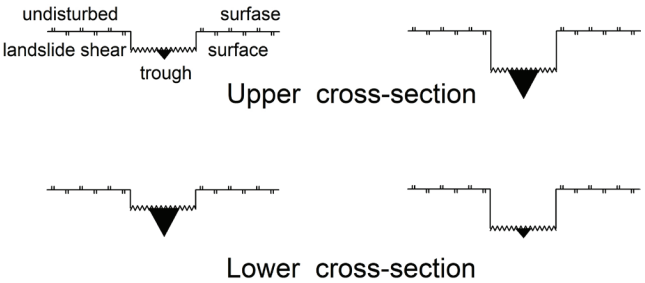

Figure 3. Erosion/thermoerosion trough in relation to the depth of cryogenic landslide shear surface cut into a slope surface in the zones of sediment mobilization (upper cross-section) and sediment accumulation (lower cross-section).

exceeds the potential eroding ability of the water flow.

In the middle portion of the slope, the depth of the shear surface cutting does not affect the erosion trough depths because up slope and down slope patterns compensate for each other.

Water runoff is higher here than at the upper cross section but erosion potential is used to transport larger sediment load (Fig. 3).

The most pronounced combined effect of cryogenic and hydrologic processes is the formation of thermoerosion pits and "tunnel thermoerosion" (term introduced by Poznanin 1995) in headwater gullies. Our observations are generalized in Figure 4. At the initial stage of snowmelt at the gully headwater, water flow and thermoerosion occur (Fig. 4, I). During melt, a thermal pit forms at the uppermost point of the headwater. These pits gradually increase in depth. Our measurements show that the depth of thermal pits changes from 2 to 6 m. Since the active-layer at the gully slopes is typically oversaturated with meltwater, they often start to creep, resulting in the formation of an earthflow. The snow surface may be dammed by the landslide mass, and thermoerosion may continue beneath the snowpatch undersurface as tunnel erosion (Fig. 4, II). It often takes 5–10 days for the landslide mass to cover the snow patch surface, and therefore exclude surface runoff. Finally the water-cut pit may be filled by collapsed pit walls and landslide masses so that runoff is forced back to the surface (Fig. 4, III). The entire cycle of thermal pit-tunnel thermoerosion process starting with spring snowmelt takes approximately one month.

In the upper cross-section (Fig. 4, I–III-A) both the depth and width of the gully can change from stage I through to stage III. However, in the lower cross-section (Fig. 4, I–III-B) only the width of the gully increases with time and the proportion of snow and silt deposits on top the snow change, with the ratio of snow decreasing.

River sediment transport is affected by processes in the inflowing ravines. In the ravine networks, the influence of erosion and thermoerosion on the river sediment transport is determined by the river length. The shorter the river, the greater the impact. Turbidity of the river may change twice depending on the remoteness of the inflowing ravine. This effect is much less significant in the middle-length rivers. For instance, our measurements in Se-Yakha river, a middle-

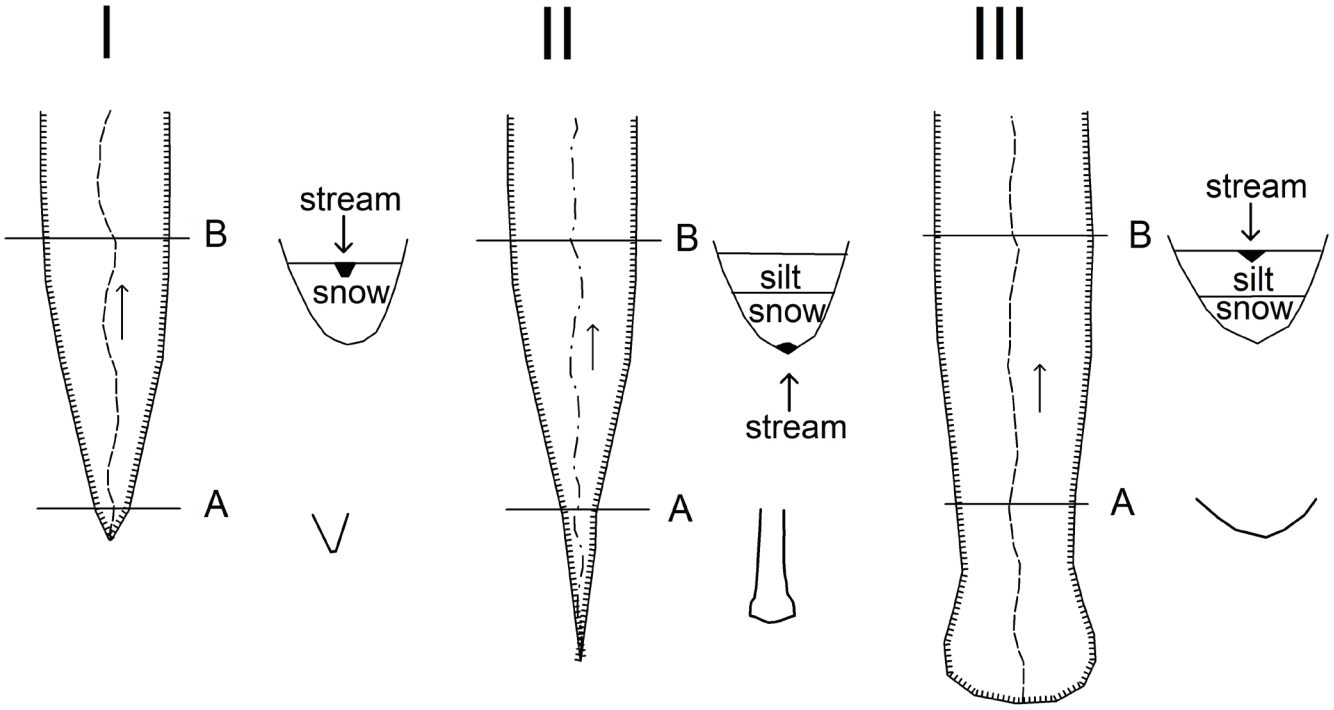

Figure 4. Stages of gully development and formation of thermoerosion water-cut pit: I, initial period of snowmelt on top of the surface of snow patch in the gully; II, the period thermoerosion water-cut pit formation and of meltwater flow below the snow patch; III, collapse of thermoerosion water-cut pit walls; A, plan (left) and cross-section (right) in the upper course of the gully; B, the same in the lower course.

length river in Central Yamal, showed that at the end of August 2007 turbidity was as high as 90 g/m^3, which is several orders of value higher than sediment runoff measured at the same time in the majority of small rivers-tributaries of Se-Yakha.

The cryogenic factors not only increase the sediment runoff, but also reduce it. Reduction of the sediment runoff in small rivers occurs when bead-shaped and dammed river channel features are formed. These can result first from polygonal structures and second from landsliding. In the upper stream of Panzananayakha river in August 2007, sediment runoff was as high as 5120 g/m^3 resulting from activation of erosion and thermoerosion. But in the middle course, sediment runoff reduced to 3 g/m^3 because of precipitation of sediments in the bead-shaped features. Analysis of aerial photography allows us to conclude that for the majority of small rivers with active cryogenic processes at the river banks sediment fans are formed at the ravine mouths, and landslide bodies often descend to the valley bottom and into the channel. Erosion and thermoerosion fans are comparable in size with the width of the valley bottom and river channel, and the lifetime of these fans is longer when compared to dammed lakes resulting from landslide activity.

Dams formed out of landslide bodies loaded in the valley bottom and small river channel may be 2–3 m high. They prevent any sediment transport downriver. After the dams' breakout on former flooded valley bottom, sheet runoff prevails over linear runoff that does not promote erosion, and also slows the sediment transport. The upper course of the test river Panzananayakha and river Halmeryakha at the study area show such features.

Mouth areas of small rivers inflowing into bigger rivers are separated from the river channel of a higher grade by the flood plain with numerous lakes. So, on the way to this channel small river sediment load precipitates within the flood plain lakes.

In small river catchments interrelation of channel and cryogenic processes is common. Depending on slope gradient, lengths and shape, as well as cryogenic features, different cryogenic slope and thermokarst processes are controlling the river runoff.

Small rivers with intensive linear and side erosion trigger landsliding to produce dammed lakes. The lifetime of these lakes is several years, thus prolonging the water cycle time by two to four orders of magnitude (Tab. 1). Thus on small streams even a single landslide event may affect river runoff for several years.

Polygonal ice-wedge features occurring close to the surface and subject to thermokarst, produce bead-shaped channels which last much longer compared to the dammed lakes. Being larger in volume, these channel features have a major impact on the water cycle. They reduce water runoff in the channel by three to four orders of magnitude as follows from measurements presented in Table 2.

Cryogenic processes determine the particularities of the sediment transport through the channel depending on their location at the upper, middle or lower course. Cryogenic landsliding at the upper course expose surface deposits which are eroded into the channel. Prior to the removal of dammed lakes, as mentioned above, the sediment load settles in these lakes, but after the dammed

Table 2. Cryogenic and hydrometric features measured in the upper, middle and lower course of Panzananayakha River.

Distance of the section line from the river head, km	River course	Water discharge, m^3/s	Volume of bead-shaped forms, m^3	Volume of dammed lakes, m^3	Time of water cycle, hour	Cryogenic/ hydrological features observed upstream from the section line
1.5	Upper	0.005	0	0	3	None
1.5	Upper	0.005	205	0	11	Ice wedges/Bead-shaped forms
1.5	Upper	0.005	0	50	3	Landslides/Dammed lakes
1.5	Upper	0.005	0	1700	94	Landslides/Dammed lakes
3	Middle	0.0075	2800	0	104	Ice wedges/Bead-shaped forms
5	Lower	0.015	1185	0	22	Ice wedges/Bead-shaped forms
	Total		4190	1700	220	

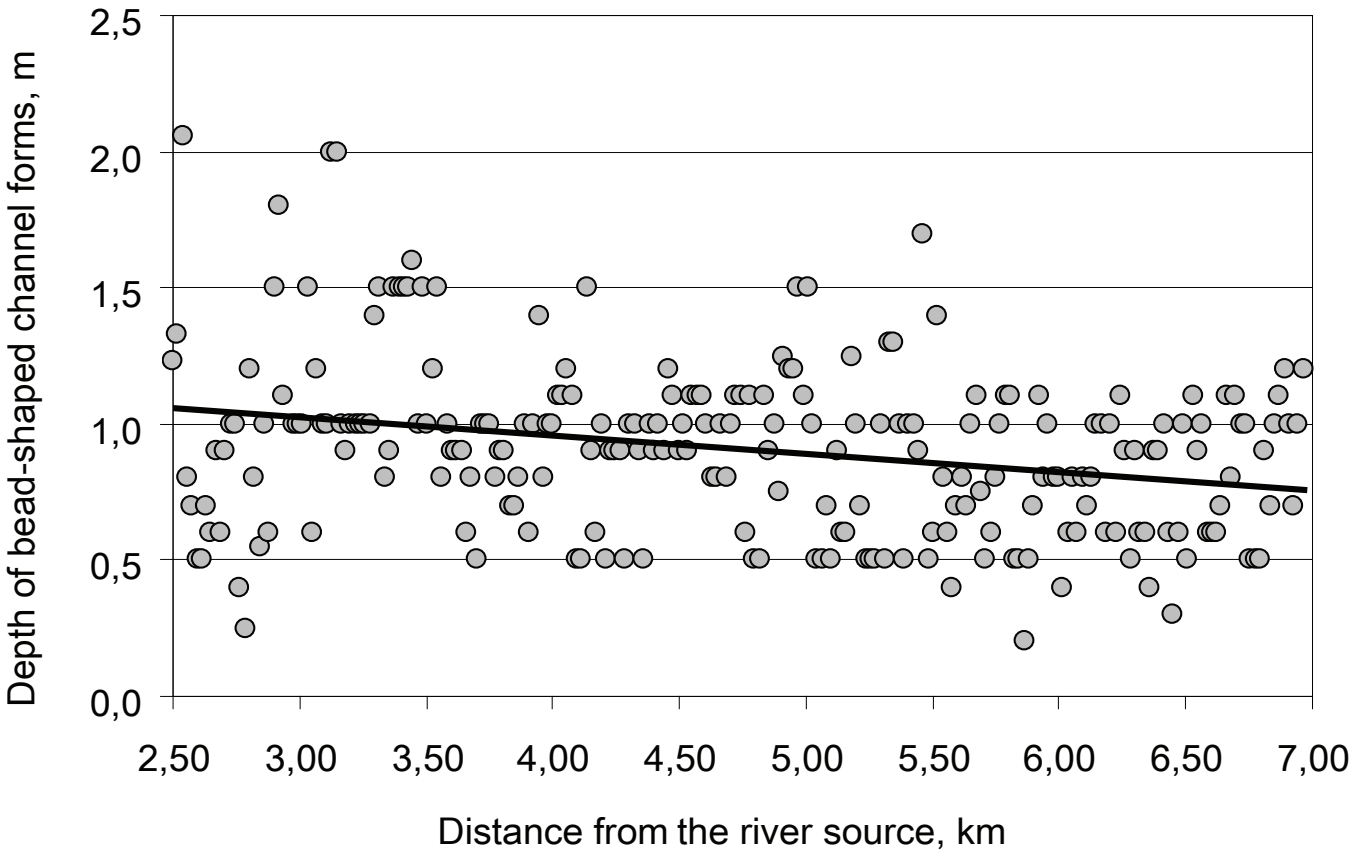

Figure 5. Depth of bead-shaped channel forms in the middle and lower courses of Panzananayakha River in relation to the distance from the river source.

lakes drain the sediment is transported downstream to fill in the bead-shaped forms of the middle course. In the lower course though there are no bare surfaces produced by landsliding, the water discharge is much higher than in the upper course, sediment load is reduced by middle-course bead shaped forms, so that the water flow can produce both thermokarst and erosive work in the lower course. Bead-shaped forms appear due to heat transfer, and sediment runoff increases due to erosive work in the sides and bottom of the valley. As a result, bead-shaped forms are filled in with the sediment and their depth reduces downstream as measured in the lower course of the test river (Fig. 5).

Conclusions

Interrelation of hydrologic and cryogenic processes in the small river catchments differs spatially. Valley slopes can be subdivided by temporary streams and small river banks and channels in the upper, middle and lower portions of the river valley. Activity of the erosion and thermoerosion in temporary stream network on slopes of the river valleys is determined by domination of landslide processes. Concave bare or sparsely vegetated landslide shear surfaces concentrate water runoff into temporary channels that are easier to erode. Hydrological processes depend on the position against the landslide headwall and on the depth of shear surface cutting into the surrounding slopes. Temporary streams on landslide affected slopes are

important sources of sediment runoff in the small rivers.

In a small river catchment, interrelation of the hydrologic and cryogenic processes occurs in many locations. Depending on the catchment morphometry, the dominating cryogenic process affecting the river channel differs. In the V-shaped valley slopes, the influence of cryogenic landsliding on hydrologic processes dominates: dammed lakes are formed, which may exist from many years and increase the storage time of the water cycle.

In the U-shaped valleys, ice wedges are found close to the surface, and bead-shaped channels are formed. These bead-shaped channels may slow down the water cycle in the streams, exceeding the effect of dammed lakes as bead-shaped channels occur more regularly. All together they store a greater volume of water, and may exist much longer.

Cryogenic landsliding results in the active sediment washout from the exposed landslide shear surfaces into a channel, and the "bead" forms, occurring on adjacent portions of the channel are filled with these sediments. However when landslide bodies still dam the channels, they interfere with sediment transport and thus promote longer existence of bead-shaped channels downstream.

The complexes of cryogenic and hydrologic processes, characteristic for upper, middle and lower stream courses in the small catchments are: (1) a landslide complex in the upper course with subsidiary bottom thermoerosion and the prevalence of accumulation instead of sediment erosion; (2) thermokarst complex of the middle course with an equilibrium of accumulation and sediment erosion; and (3) thermoerosion complex of the lower course with subsidiary thermokarst, and a prevalence of sediment erosion over sediment accumulation.

Cryogenic and hydrologic processes are important drivers in the formation of the Arctic landscapes. Therefore, understanding the interrelation of these processes is a prerequisite for successful maintenance of infrastructure in the Arctic.

References

Dan'ko, V.K. 1982. *The regularities of the thermoerosion process development in the north of West Siberia.* Candidate dissertation. Moscow: PNIIIS Publisher, 20 pp. (in Russian)

Kosov, B.F.& Konstantinova, G.S. 1973. Ravine density in the north of West Siberia. In: *Natural conditions of the West Siberia*. Moscow: Moscow University Press, 104-115 (in Russian).

Leibman, M.O. & Kizyakov, A.I. 2007. *Cryogenic landslides of the Yamal and Yugorsky peninsular*. Moscow-Tyumen: IKZ SO RAN, 206 pp. (In Russian).

Leibman, M.O. & Streletskaya, I.D. 1997. Land-slide induced changes in the chemical composition of active layer soils and surface-water run-off, Yamal Peninsula, Russia. *Proceedings of the International Symposium on Physics, Chemistry, and Ecology of Seasonally Frozen Soils, Fairbanks, Alaska, 1997:* 120-126.

Malinovskiy, D.V. 1981. The particularities of the thermoerosion development on western Yamal peninsula. In: *Natural conditions of the West Siberia*. Moscow: Moscow University Press, 130-137 (in Russian).

Poznanin, V.L. 1995. *Nature of ravine thermoerosion.* Doctor of science dissertation. Moscow: Moscow University Press, 33 pp. (in Russian).

Romanenko, F.A. 1997. *Formation of the lake basins on Siberian Arctic plains*. Candidate dissertation. Moscow: Moscow University Press, 25 pp. (in Russian).

Romanovskiy N.N. 1961. Erosion-thermokarst depressions in the North of Maritime lowlands of Yakutiya and Novosibirsk islands. In: *Permafrost Studies (Merzlotnye Issledovaniya)* 1. Moscow: Moscow University Press, 124-144 (in Russian).

Sidorchuk, A.Yu. 1999. The sediment balance on ravine catchments. In: A.Yu. Sidorchuk & A.V. Ram (eds.), *Erosion Processes at Central Yamal.* Saint-Petersburg: 242-252 (in Russian).

Voskresenskiy, K.S. 2001. *The Modern Relief-Forming Processes on Plains of the Northern Russia*. Moscow: Moscow University Press: 264 pp. (in Russian).

Periglacial and Permafrost Map of Signy Island, South Orkney Islands, Maritime Antarctica

M. Guglielmin
Insubria University, Via Dunant, 3, 21100 Varese, Italy
D. Boschi
Insubria University, Via Dunant, 3, Varese, Italy
Carlo D'Agata
Milano University, Earth Sc. Dep., Via Mangiagalli 34, Milano, Italy
C. Ellis-Evans and M.R. Worland
British Antarctic Survey, Natural Environment Research Council, Madingley Road, Cambridge CB3 0ET, United Kingdom

Abstract

Signy Island was one of the first Antarctic locations to be the subject of a detailed periglacial landform study which was completed in the 1960s. Several periglacial features such as patterned ground, block stripes, and gelifluction lobes have been analysed and monitored. More recently, the relationships between different vegetation coverage, soil type, and the underlying permafrost have also been studied. In this paper we present a geomorphological map of Signy Island that has been mapped with particular reference to the occurrence of periglacial landforms. Geomorphological features were mapped at 1:10,000 scale during the austral summer of 2004/05. A highly simplified permafrost model (PERMDEM) based on the digital elevation model and the air lapse temperature have been here presented and tested by comparing the distribution of some periglacial features together with thermal profiles and trenches excavated in the main geomorphological areas of interest.

Keywords: gelifluction; Maritime Antarctica; modeling; patterned ground; periglacial features; permafrost.

Introduction

Studies of permafrost distribution in Antarctica have recently been developed through the IPY–ANTPAS initiative and other linked research programs (Bockheim et al. 2008). Nevertheless in the South Orkneys, as in other parts of the maritime Antarctic, permafrost is still poorly understood. As far as we are aware, no permafrost maps of Maritime Antarctica have been produced, although some papers have presented information related to permafrost distribution such as; models of net radiation balance (Vieira & Ramos 2003), permafrost thermal profiles (e.g., Chen 1993), and active layer thermal regimes (Ramos & Vieira 2003, Cannone et al. 2006, Guglielmin et al. in press). Periglacial landforms have received more attention resulting in the production of maps for the South Shetlands (e.g., Serrano & Lopez Martinez 2000, Serrano et al. 1996, Zhu et al. 1996) and other islands (i.e., Mori et al. 2007, Strelin & Sone 1998). Investigations by Chambers (1966a, b, 1967, 1970) into periglacial processes such as frost heave, frost creep, and solifluction would have benefited from both permafrost and periglacial geomorphology maps. Signy Island, South Orkney Islands, provides a unique opportunity in Antarctica to compare new data on the active layer thermal regime with previous Signy Island data collected in 1963 by Chambers (1966b).

The main aims of this paper are to provide a preliminary permafrost and periglacial map of Signy Island and to analyze possible relationships between the mapped periglacial features, permafrost distribution, and some climatic factors such as air temperature, global radiation, and snow cover.

Study Area

Climatic and geological constraints

Signy Island (60°43′S, 45°38′W) in the South Orkney Islands is located in the maritime Antarctic and is characterized by a cold oceanic climate with a mean annual air temperature of around -3.5°C; mean monthly air temperature above 0°C for at least one, but up to three months each summer; and annual precipitation of around 400 mm, primarily in the form of summer rain and cloud cover of 6–7 okta year-round. The climatic records indicate a progressive warming of air temperatures of 2°C ± 1 over the past 50 years (Turner et al. 2005).

The substrate is mainly quartz-mica-schist, although in some parts of the island there are small marble outcrops (Matthews & Maling 1967). Half of the island is covered by an ice cap that is currently rapidly shrinking.

Glacial evolution

According to Sudgen & Clapperton (1977), during the Last Glacial Maximum (17,000–18,000 years BP) Signy Island was completely covered by the South Orkneys ice cap with the former coastline extended to the actual 130-150 contour b.s.l. The reduction of the ice cap has not been investigated in detail although some authors indicate a major period of shrinkage between 9000 and 6000 years BP (e.g., Nakada & Lambeck 1988), while others suggest that the disappearance of the ice cap occurred some time before 7000 yr BP (Herron and Anderson 1990).

Deglaciation has been confirmed by lake formation dated

Figure 1. Location of the study area. The black dot indicates the CALM grid. The black thick line indicates the extent of the glacier in 2004.

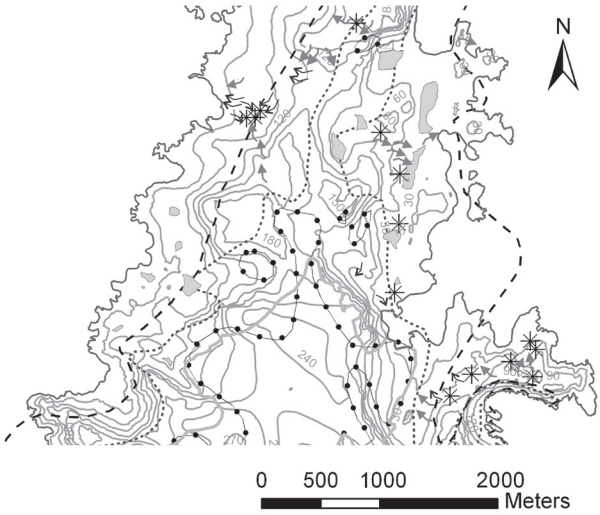

Figure 2. Geomorphological sketch of the center part of the Signy Island. Legend: 1) rock glacier; 2) gelifluction lobes; 3) soil stripes; 4) patterned ground; 5) glacier boundary 5000–3000 BC; 6) glacier boundary 400–600; 850–1000; 1150–1300 AD; 7) glacier boundary 600–850; 1000–1150; 1300–1450 AD; 8) extent of the glacier in 2004. The glacier limits at point 5–7 are suggested by Smith (1990).

between 5890 ± 60 14C yr BP at Heywood Lake and c. 5700 yr BP at Sombre Lake (Jones et al. 2000) and later by the oldest moss banks developed at c. 5500 yr BP (Smith 1990). During the middle and upper Holocene, different phases of cooling and warming occurred as established by proxy data. Radiocarbon data from the moss banks indicate several glacial advances between 1250 and 1600 AD and two advances between 1700 and 1850 AD (Smith 1990). Paleolimnological studies carried out particularly on Sombre and Heywood lakes suggest a different Holocene evolution characterized by cool conditions and slow sedimentation and colonization rates between c. 5900-3800 yr BP, followed by evidence for a late "Holocene climate optimum" (c. 3300–1200 yr BP) and finally a cooling period (Jones et al. 2000). More recently there is evidence of a strong reduction in size of the glaciers with an increase in new deglaciated areas of 35% between 1949 and 1989, (Jones et al. 2000) and an even faster shrinkage in the last 20 years.

Permafrost distribution and periglacial landforms

Permafrost on Signy Island was considered discontinuous by Chambers (1966b) with variable active layer thicknesses ranging from 40 cm in moss sites to more than 2 m in well-drained coarse deposits.

Most of the island is covered by cryptogamic vegetation which has a distinct influence on the ground surface temperature (GST) and also in some cases on the active layer thickness (Cannone et al. 2006, Guglielmin et al. in press).

During the austral summer of 2004/2005 a permanent CALM grid (40 x 50 m with the nodes every 10 m) was installed under the auspices of the framework of the project "Permafrost and Global Change in Antarctica II (PGCAII)" established by the Insubria University and the British Antarctic Survey (BAS) with logistical support by PNRA and BAS. An automatic station monitored the temperature of the active layer at 4 different points within a CALM grid located on a flat summit behind the Signy research station (Fig. 1). The system also recorded the main climatic elements at the site.

Despite the clear and innovative studies on the periglacial processes involved in the production of sorted and unsorted circles, sorted stripes and "stone streams" carried out here in the 1960s by Chambers (Chambers 1966a, b, 1967, 1970) few geomorphological studies have been conducted since. However there have been a few studies investigating weathering processes (e.g., Hall 1986, 1987, 1988, 1990).

Chambers emphasized in his works that only the upper part of the active layer (40-60 cm) was involved in sorting, gelifluction, and ice segregation.

Methods

During the austral summer of 2004/2005, two of the authors made a geomorphological survey of the island at the scale of 1:10,000 with particular attention to the periglacial and permafrost features. Transversal trenches were dug at the site of some selected periglacial features to explore their internal structure and to sample soils and underlying deposits.

Additionally, some trenches and pits were excavated to measure the active thermal profile and describe the main soil characteristics in different geomorphological areas and in different quaternary deposits.

Each trench and pit was included in a GIS system with the geomorphological map. Boreholes were drilled down to 2.5

m at Spin Drift Col and on the upper part of the Backslope close to the Signy research station (Fig. 1) to sample frozen ground. The digital elevation model (DEM) developed by BAS has a pixel of 7.5 m.

The permafrost model (PERMDEM) has been developed to obtain a mean annual GST (MAGST) using the available DEM of the island as an input to produce a map of the mean annual air temperature (MAAT) and a map of the global annual radiation (direct plus diffuse short wave).

The first map was achieved by applying the adiabatic lapse rate calculated between the only two available automatic weather stations (AWS) (Fig. 1). The lapse rate for 2006 was 0.011°C/m.

The solar radiation analysis tools calculate insolation across a landscape or for specific locations, based on methods from the hemispherical viewshed algorithm (Rich 1990), as further developed by Fu & Rich (2002). The total amount of radiation calculated for a particular location or area is given as global radiation.

Considering that snow/ice-free ground surfaces suffer GST almost always warmer than the air temperature we used the annual global radiation map (calculated for 2006) to compute a correction factor *Ir* to add to the obtained MAAT value according to the equation:

$$MAGST = MAAT + Ir \quad (1)$$

where *Ir* is calculated as the regression between the difference ΔT (MAGST-MAAT) of two monitored points of the CALM grid (bare grounds) and the global annual radiation compiled in the same points.

Finally, the permafrost map was tested comparing the obtained modeled results with the temperatures measured in the excavated trenches and in the monitored boreholes.

Results

Geomorphological mapping

An example of a very simplified geomorphological map is shown in Figure 2. The symbols that represent periglacial features (patterned ground; soil stripes; gelifluction lobes) indicate the areas in which more than 10 single features occur. Neither patterned ground nor soil stripes are differentiated between sorted and unsorted in this simplified sketch. In the field, low-centered sorted circles, sorted stripes and stone-banked lobes are the most widespread. Low-centered sorted circles are the most widespread form of patterned ground and show a high level of size variability with diameter ranging between 2 and 5 m.

Low-centered sorted circles occur preferentially in flat and depressed areas at altitudes lower than 80 m. High-centered sorted circles are less frequent than smaller ones (ranging between 10 and 150 cm) and generally occur on flat summits at higher altitudes. Unsorted circles occur quite often and generally have a size similar to the high-centered sorted circles, but do not show a clear distribution pattern. In some depressed and peaty areas, frost boils also occur with a diameter of between 0.2 and 0.7 m. No ice wedge

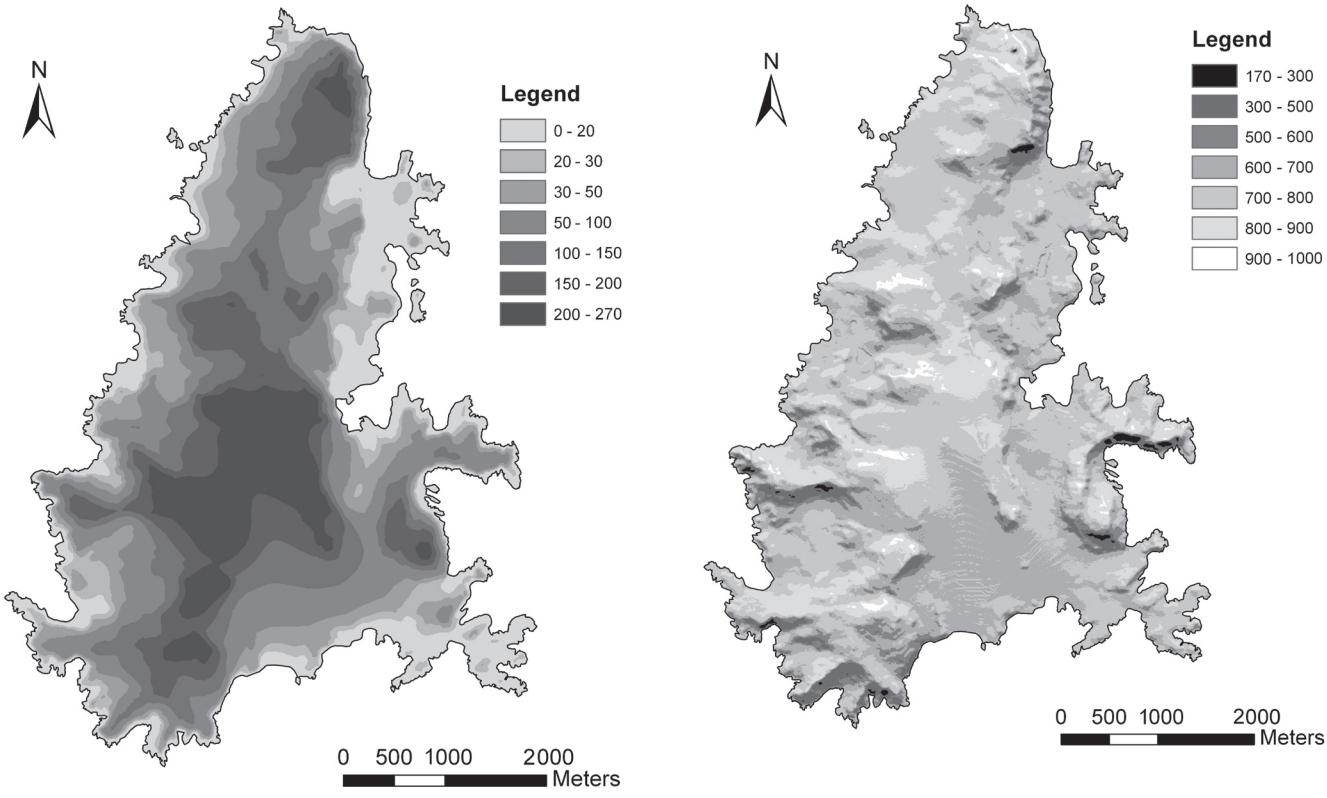

Figure 3. a) DEM classified according the elevation (m a.s.l.); b) global radiation (W/m^2) for the austral summer 2005/2006 (December 2005–February 2006).

polygons or sand wedge polygons were found. Only some poorly defined frost fissure polygons occur on the flat and highest ice-free areas of the island. Soil stripes are mainly sorted with a width ranging from 10 to 210 cm at the same site. Soil stripes are developed on glacial till and on colluvial deposits with slopes greater than 4°-6°. Transitional features from low-centered circles to sorted stripes are also present. Usually the coarse bands are raised with respect to the fine ones although sometimes can occur the opposite as unsorted stripes can occur very close to the sorted ones. Also soil stripes frequently end with low lobes (less than 1 m).

Gelifluction lobes are the most common periglacial feature which often occur on the same slope with a high variability of shape and dimension from stone-banked terracettes to lobes and stone streams (in Chambers *sensu*) and sometimes combine to form sheets. The gelifluction features are almost all stone-banked and develop on a wide range of slopes, but always greater than 4°-5° and show frontal ramps between 0.5 to 3 m in height. On the western side of the island moss-banked lobes which can be over 3 m high at the frontal ramp are quite widespread.

Only one active rock glacier has been detected on the island just northward of Sombre Lake. The rock glacier shows a convex profile along the flow direction and a very steep frontal scarp indicating the presence ice within it.

Permafrost distribution and modeling

PERMDEM is a very simplified model (derived by PERMACLIM, Guglielmin et al. 2003) which uses available climatic data (air temperature) and data automatically achievable by DEM that can influence the GST and consequently the permafrost distribution.

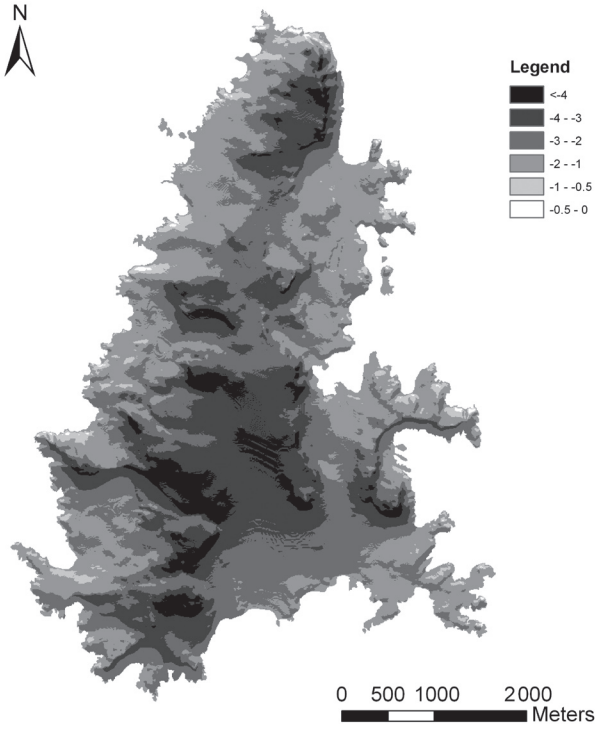

Figure 4. PERMDEM map of the Signy Island. The results MAGST are always negative, and only in less than 0.2% of the total area MAGST is between 0 and -0.%°C.

Figure 3 shows the DEM (classified according to the altitude 3a) and an example of the global radiation for the austral summer of 2005/2006 (3b).

From these layers and applying equation (1), a MAGST map has been obtained (Fig. 4). This model shows that permafrost conditions in 2006 (MAGST < 0°C) occur over the entire island from the sea shoreline upward. The model also shows that aspect and slope are important factors when considering global radiation and therefore the radiative balance and the energy balance of the surface. The major part of the ice-free areas of the island have a MAGST between -1°C and -2°C (41%) and between -2° and -3°C (34%), while only 4% have a temperature greater than -1°C.

The known effects of vegetation cover (Cannone et al. 2006, Guglielmin et al. in press) are not considered here, but the extensive cover of some mosses like *Sanionia* can significantly cool the surfaces. In contrast, the widespread black lichens (*Usnea*) and the patchy grasses can warm the surfaces compared to levels predicted by the model. Moreover, due to a lack of data on snow cover, thickness, and permanence on the island, its effect is also disregarded. The estimation of the snow cover from the preliminary observations of the available aerial and satellite images is difficult due to the high degree of cloud cover present for the majority of the time. From historical records and field data the depressions on the west side and on the south side of the island have the maximum snow accumulation and are more protected from the catabatic winds coming from Coronation Island. In 2006 the CALM grid remained completely snow free for all of the year suggesting that, at least for the year under study, the surface energy balance was not influenced on the exposed summit of the island and reasonably on the northward slopes.

The trenches carried out between December 2004 and the beginning of January 2005 had a target depth of 1 m. In several cases it was not possible to achieve this depth because (a) the water flow above the frost table filled the trench or (b) the presence of large boulders which prevented the holes from being dug. In the case of (a) above and where trenches could be dug to 1m depth, the frost table was found to be between 20 and 60 cm in depth. In all other cases, the 0° isotherm depth was estimated from the thermal profile according to Guglielmin (2006) and was estimated to range between 50 and 250 cm. Where the trenches were deeper than frost table, ice-cemented permafrost and subordinately ground ice (segregated ice) was found.

Discussion and Conclusions

The field excavations and the permafrost model indicate that permafrost does occur everywhere, although the periglacial features occurring on Signy Island do not provide conclusive evidence of permafrost because there is a lack of permafrost indicators such as ice wedge or sand wedge polygons and frost mounds. The gelifluction features do

Table 1. Distribution of the investigated periglacial features respect the MAGST classes calculated by PERMDEM for 2006. Legend: 1) -1<MAGST<1.5; 2) -1.5<MAGST<-2; 3) -2<MAGST<-2.5; 4) -2.5<MAGST<-3; 5) -3<MAGST<-3.5; 6) -3.5<MAGST<-4.

	N	1	2	3	4	5	6
Patterned Ground	14	28.5	43	28.5	0	0	0
Un/sorted Stripes	11	0	36	46	18	0	0
Gelifluction Lobes	23	30.5	30.5	17	4	9	9

not show any clear pattern with aspect and seem to prefer the areas where MAGST is higher (Table 1) confirming the conclusion of Vieira and Ramos (2003) for Livingston Island. The distribution of the different types of patterned ground seems to reflect their different genetic processes.

PERMDEM appears to be appropriate for use in Maritime Antarctica to model permafrost distribution because it requires only a minimum of air temperature data and a reasonably good DEM. The results obtained could certainly be improved by the inclusion of the effects of vegetation and snow cover. On the other hand PERMDEM indicates clearly that permafrost conditions are actually present everywhere on the Island even in the beach deposits.

The major limit of the model is that the *Ir* factor is actually calculated using only two points (the only two points located on bare ground and monitored all year round). It may be that the quite strong difference between the measured MAGST for the two areas of bare ground studied are related not only to the incoming radiation but also to difference of latent heat. The two sites were located less than 60 m apart and at the same altitude, but one had a southwestern aspect and the other a northeastern aspect.

The success of the model (more than 90% of accuracy) for the particular year studied may partly be due to the low snow cover for that year. As there was actually little snow cover, the lack of data on snow conditions had little effect on the predictions of the model.

It seems reasonable to conclude that, in any case, there are no altitudinal boundaries for permafrost occurrence at Signy Island as suggested by Serrano & Lopez Martinez (2000) for the South Shetlands and that permafrost is continuous and not discontinuous as suggested by Chambers (1966a). Further developments are required to improve the model and its calibration, especially to model active layer and permafrost thickness. Also more detailed geomorphological analyses of the periglacial features occurring on this unique island are required in order to understand their genesis and evolution in this period of climatic change.

Acknowledgments

We thank BAS and PNRA for their logistic and financial support of this research in the frame of the joint project "Permafrost and Global Change in Antarctica II (PGCAII)." We thank also BAS for permission to use and elaborate on the DEM data of Signy Island. Special thanks to James Bockheim, whose comments and suggestions allowed us to improve this paper significantly.

References

Bockheim, J.G., Campbell, I.B., Guglielmin, M. & López-Martínez J. 2008. Distribution of permafrost and ground ice in the Antarctic region. *Proceedings of the Ninth International Conference on Permafrost, Fairbanks, Alaska, June 29-July 3, 2008* (this proceedings).

Cannone, N., Ellis Evans, J.C., Strachan, R. & Guglielmin, M. 2006. Interactions between climate, vegetation and active layer in Maritime Antarctica. *Antarctic Science*,18(3): 323-333.

Chambers, M.J.G. 1966a. Investigations of patterned ground at Signy Island, South Orkney Islands: I. Interpretation and mechanical analyses. *Brit. Antarct. Surv. Bull.* 9: 21-40.

Chambers, M.J.G. 1966b. Investigations of patterned ground at Signy Island, South Orkney Islands: II. Temperature regimes in the active layer. *Brit. Antarct. Surv. Bull.* 10: 71-83.

Chambers, M.J.G. 1967. Investigations of patterned ground at Signy Island, South Orkney Islands: III. Miniature patterns, frost heaving and general conclusions. *Brit. Antarct. Surv. Bull.* 12: 1-22.

Chambers, M.J.G. 1970. Investigations of patterned ground at Signy Island, South Orkney Islands: IV. Long-term experiments. *Brit. Antarct. Surv. Bull.* 23: 93-100.

Chen, X. 1993. Permafrost around CGWS, Antarctica. *Proceedings of the Sixth International Conference on Permafrost, Beijing, China. July 5-9, 1993:* 84-88.

Fu, P. & Rich, P.M. 2002. A geometric solar radiation model with applications in agriculture and forestry. *Computers and Electronics in Agriculture* 37: 25-35.

Guglielmin, M. 2006. Ground surface temperature (GST), active layer, and permafrost monitoring in continental Antarctica. *Permafrost and Periglacial Processes* 17(2): 133-143.

Guglielmin, M., Aldighieri, B. & Testa, B. 2003. PERMACLIM: a model for the distribution of mountain permafrost, based on climatic observations. *Geomorphology* 51: 245-257.

Guglielmin, M., Ellis Evans, C.J. & Cannone, N. in press. Active layer thermal regime under different vegetation conditions in permafrost areas. A case study at Signy Island (Maritime Antarctica). *Geoderma*.

Hall, K. 1986. Rock moisture content in the field and the laboratory and its relationship to mechanical weathering studies. *Earth Surf. Proc. Landf.* 11: 131-142.

Hall, K. 1987. The physical properties of quartz-micaschist and their relationship to mechanical weathering studies. *Earth Surf. Proc. Landf.* 12: 137-149.

Hall, K. 1988. A laboratory simulation of rock breakdown due to freeze–thaw in a maritime Antarctic environment. *Earth Surf. Proc. Landf.* 13: 369-382.

Hall, K. 1990. Mechanical weathering rates on Signy Island, maritime Antarctic. *Perm. Perigl. Proc.* 1: 61- 67.

Herron, M.J. & Anderson, J.B. 1990. Late Quaternary glacial history of the South Orkney Plateau, Antarctica. *Quaternary Research* 33: 265-275.

Jones, V.J., Hodgson, D.A. & Chepstow-Lusty, A. 2000. Palaeolimnological evidence for marked Holocene environmental changes on Signy Island, Antarctica, *The Holocene* 10(1): 43-60.

Matthews, D.H. & Maling, D.H. 1967. The geology of the South Orkney Islands: I Signy Island. *Falkland Islands Dependencies Survey Scientific Reports* 25: 32 pp.

Mori, J., Fukui, K., Sone, T., Strelin, J. & Torielli, C. 2007. Internal structure of stone−banked lobes and terraces on rink plateau, James Ross Island, Antarctic peninsula region. *Polish Polar Research* 28(1): 23-30.

Nakada, M. & Lambeck, K. 1988. The melting history of the late Pleistocene Antarctic ice sheet. *Nature* 333 (6168): 36-40.

Ramos, M. & Vieira, G. 2003. Active layer and permafrost monitoring in Livingston Island, Antarctic. First results from 2000 to 2001. In: M. Phillips, S.M. Springman, L. Arenson (eds.), *Proceedings of the 8th International Conference on Permafrost, Zurich, Switzerland.* Lisse: Balkema Publishers, 929-933.

Rich, P.M. 1990. Characterizing plant canopies with hemispherical photography. In: N.S. Goel & J.M. Norman (eds.), Instrumentation for studying vegetation canopies for remote sensing in optical and thermal infrared regions. *Remote Sensing Reviews* 5: 13-29.

Serrano, E. & Lopez-Martinez, J. 2000. Rock glaciers in the South Shetland Islands, Western Antarctica. *Geomorphology* 35: 145-162.

Serrano, E., Martınez de Pison, E. & Lopez-Martınez, J., 1996. Periglacial and nival landforms and deposits. In: J. Lopez-Martınez, M.R.A. Thomson & J. Thomson (eds.), *Geomorphological Map of Byers Peninsula, Livingston Island, BAS Geomap Series, 5A*. Cambridge: British Antarctic Survey, 28–34.

Strelin, J.A. & Sone, T. 1998. Rock glaciers on James Ross Island, Antarctica. *Proceedings of the Seventh International Conference on Permafrost*, *Yellowknife, Canada, 23–27June, 1998:* 1027-1032.

Sugden, D.E. & Clapperton, C.M. 1977. The maximum ice extent on island groups in the Scotia Sea, Antarctica. *Quaternary Research* 7: 268-282.

Smith, R.I.L. 1990. Signy Island as a paradigm of biological and environmental change in Antarctic terrestrial ecosystems. In K.R. Kerry & G. Hempel (eds.), *Antarctic ecosystems. Ecological change and conservation*. Berlin: Springer-Verlag, 32-50.

Turner, J., Colwell, S.R., Marshall, G.J., Lachlan-Cope, T.A., Carleton, A.M., Jones, P.D., Lagun, V., Reid, P.A. & Iagovkina, S. 2005. Antarctic climate change during the last 50 years. *International Journal Climatology*, 25: 279-294.

Vieira, G. & Ramos, M. 2003 Geographic factors and geocryological activity in Livingston Island, Antarctica. Preliminary Results. *Proceedings of the Eighth International Conference on Permafrost, Zurich, Switzerland, 21–25 July 2003:* 1183-1188.

Development and Initial Evaluation of a Daily DEM-Based Active Layer Heave and Subsidence Model

Davor Gugolj
Terrapoint Canada Inc., Calgary, AB, Canada
Brian J. Moorman
Department of Geography, University of Calgary, Calgary, AB, Canada
Matthew P. Tait
Department of Geomatics Engineering, University of Calgary, Calgary, AB, Canada

Abstract

Daily permafrost active layer heave and subsidence was simulated for a 1 km^2 study area in the Mackenzie Delta, NWT for a period of one year. This study involved the development and application of a simplified methodology for assessing the dynamic nature of the active layer. It is based on the adaptation and integration of previously developed empirical and theoretical relationships related to the formation of segregated ice within frozen soil. The model requires a limited dataset including: general soil characteristics, a representation of the terrain in form of a digital elevation model, and regional weather records. The model was able to simulate the active layer thermal regime, yielding thaw depth values well within the range of measured observations. Likewise, daily changes in ground surface elevation across the study area due to formation or melt of segregated ice lenses agreed with direct measurements.

Keywords: heave; permafrost; segregation ice; subsidence; thermal modeling.

Introduction

Freezing and thawing of the active layer and the resultant heaving and subsidence of the ground surface are of particular significance in the Arctic regions, as the vertical movement of the ground surface throughout the year presents a hazard for the infrastructure. With an expected increase in the production of oil and natural gas in the Canadian Arctic, and associated infrastructure development, frost heaving may become a significant engineering issue, as well as a safety hazard (Bergquist et al. 2003, Palmer & Williams 2003). Various efforts have been made to predict and prevent active layer heave and subsidence from an engineering point of view, especially for prevention of gas pipeline buckling and road pavement heave (Konrad 1994, Palmer & Williams 2003). The dynamic nature of the active layer also presents challenges in assessing the subsidence caused by the oil and natural gas extraction in the permafrost-rich Arctic regions. Precise monitoring of terrain deformation through methods such as differential interferometric synthetic aperture radar (DInSAR) requires an accurate assessment of the state of the active layer at the date of acquisition. To address this issue, an active layer heave and subsidence model was developed that provides daily estimates of the thermal state of active layer, cumulative active layer heave or subsidence and the resulting ground surface elevation change.

To enable easy application of the model in a variety of permafrost terrain, the model complexity is reduced to require minimal input parameters. These parameters include a single sampling of terrain (elevation) and soils data, as well as regional weather data or that from nearby weather stations. All other required parameters are derived from such inputs based on empirical and theoretical relationships.

Study area

The model was tested at a site approximately two kilometers upland from Reindeer Station, NWT on the East Channel of the Mackenzie River (68.68°N, 134.06°W), and forty kilometers north of Inuvik, NWT, as shown in Figure 1. The site is one square kilometer of rolling tundra in the Caribou Hills, with a local relief of 20 meters, on an elevated bench overlooking the Mackenzie Delta. This hummocky upland terrain features a variety of soil types, ranging from peat to clayey silt colluvium derived from carbonate tills. The vegetation in the area is typified by dwarf shrubs, sedges, and herbs characteristic of a tundra environment, with willow and ground birch occupying the transitional zone between the tree-line and the tundra. The climate of the area can be characterized as very cold and dry, with a mean yearly temperature of -8.8°C and mean annual precipitation of 248.4 mm at Inuvik, for the years 1971-2000. Snowfall can occur in any month of the year, contributing an average of 167.9 mm SWE annually, and remaining on the ground for up to 8 months of the year (Environment Canada 2005).

Data

Minimizing the amount of input data required to simulate the active layer heave and subsidence is pertinent to providing a very simple, yet accurate model that can be applied in a variety of scales and environments. Weather data can be obtained from a climatological record at a nearby station, or from an in-situ weather station set up in the study area. For this study, climatological records for Environment Canada station *Inuvik A*, at Inuvik, NWT were used. Daily air temperature, precipitation, wind, and snow records for the years 1995 to 2006 were used (Environment Canada 2005). Terrain is represented in form of a digital

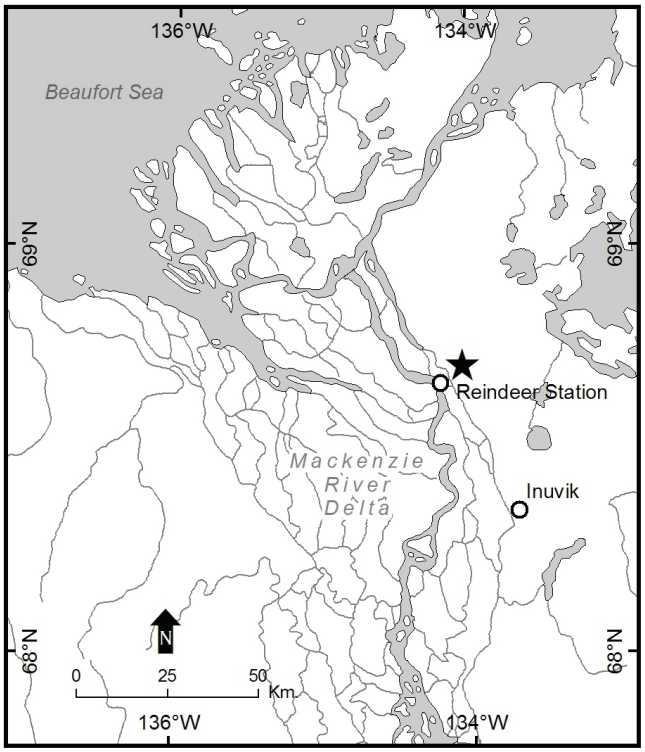

Figure 1. The star indicates the location of the study site in the Mackenzie Delta.

elevation model (DEM), which was created from a leveling survey conducted in the summer of 2004. A DEM with a 50-m resolution was generated from a dataset of 3962 points uniformly distributed across the study area. In addition, soil properties, water content, the presence and depth of the organics/peat layer, and active layer depth were obtained from a dataset of 36 sampling points also collected in the summer of 2004. Particle size analysis and moisture measurements were performed on the soil data, to obtain the necessary input parameters for the model. A 30-sample set of snow depth measurements was obtained at the study site in March of 2006, to be used to verify the predictions of the snow model.

Methodology

The simulation of the motion of the active layer was comprised of three sub-models. A snow distribution model was developed to predict the snow depth at the study site, in order to estimate the upper boundary (surface) thermal condition to be used in the thermal regime model, a thermal regime model estimated the temperature of the soil at different depths and so provided the location and character of the frost and thaw fronts, and an active layer heave/subsidence model calculated the amount of segregation ice formed or melted, and therefore the daily change in surface elevation

Snow distribution model

Spatial distribution of snow is fundamental for predicting the extent of permafrost in Arctic environments. Since snow acts as an insulator to the ground below, areas with long periods of thick snow cover usually remain permafrost free, while lack of snow cover promotes cooling of the soil and thus the growth of permafrost. Historically, the modeling of snow movement has been done through a variety of approaches, including empirical relationships between snow and wind, wind-tunnel testing, as well as one-dimensional and two-dimensional numerical models that predict the patterns of snow erosion and accumulation in a specified area (Liston & Sturm 1998, Pomeroy et al. 1993, 1997, Pomeroy & Li 2000).

Using a DEM of the study area in a geographic information system (GIS) environment, as well as the daily snowfall records and prevailing wind direction data from the weather station, the accumulation and redistribution of snow on the site was calculated. Implementation into a raster-based GIS environment was done through an iterative process using a 3 x 3 cell kernel which calculated the erosion or accumulation of snow in a given raster cell based on the above empirical relationships, as well as terrain characteristics. The results of this snow distribution model were then input into the thermal regime model.

Thermal regime model

Numerical models are generally the most popular approach to simulating and forecasting the thermal regime of active layer and permafrost (Miller 1979, Kane et al. 1991, Pustovoit 2000, Woo et al. 2004).

Determination of the thermal regime in this model was done using a simplified finite difference function (Rankinen et al. 2004) for calculating the ground temperature at a given depth. This calculation is based on a minimal set of environmental parameters, which include air temperature, snow depth, deep layer soil temperature at a known depth, and soil characteristics from field measurements. The thermal regime at each sampling point was calculated daily for each sample point for a period from July 1, 2002 to December 31, 2005. Allowing the model to stabilize for approximately 550 days before the needed values (years 2004-2005), the initial conditions were set sufficiently.

In order to provide an accurate estimate of the position of the freezing front within the soil, soil temperature was calculated at 1.0 cm increments to a maximum depth of 1.0 meter. Assuming a continuous flux between the soil surface and the air, through the snowpack and peat layers, surface temperature for every point was determined on a daily basis. Thermal properties of snow and peat were assumed to be constant over the study period.

Although snow becomes denser after snowfall, there was no practical solution to account for this change in density and thermal properties. However, on the tundra where considerable wind speeds are found at the ground surface, fresh snow quickly becomes reworked and reaches a steady state dense snow pack. Snow density value of 250 kg m^{-3} was used to represent tundra snowpack that was a few days to a week old. The thermal properties of snow used in this study reflect this density value (Williams & Smith 1989).

The model assumes that the soil properties below the

surface (or peat layer where present) are homogeneous and do not vary with depth. This simplification of natural processes is necessary as the thermal properties of soil data at varying depths were not available for this study. Future versions of the model could include such variability.

The presence of water and ice close to the freezing temperature has significant effect on the thermal properties of frozen soils (Williams & Smith 1989). Therefore, thermal properties of soils must be modified accordingly for the proper interpretation and analysis of thermal conditions in the ground and for carrying out thermal calculations. Since the thermal conductivity and heat capacity of the soil were not measured for the soil samples, representative value for silty clay was obtained from Williams & Smith (1989) and used for all sampling locations. Silty clay, as defined in Williams & Smith (1989), was chosen as it was fairly representative of the soil samples obtained in the study area. The model accounts for the variability in thermal conductivity of soil with change in temperature, as well as adjusting for the variability of heat capacity due to influences from the ratio of unfrozen water and ice content in the soil, as well as those from the soil temperature.

It is argued that the water in soils freezes over a range of temperatures, depending on the chemical and geological properties of the host soil (Williams & Smith 1989). The frost front, defined as the location within the soil where the segregation ice will begin to form, often occurs close to the 0ºC isotherm, and the exact temperature varies with the aforementioned soil properties. Konrad & Morgenstern (1981) argue that the frost front for fine sands or coarse silts occurs very close to the 0°C isotherm. The present study therefore assumes that the frost front coincides with the 0°C isotherm based on the amount of fines present in the soil samples.

To identify the location of the frost front within the calculated thermal regime, the model identifies the location of the 0°C isotherm within the soil for each day, and returns the depth at which the frost front resides. The algorithm automatically recognizes the upper and lower temperatures on either side of the freezing front, and calculates the temperature gradient at the location. Since the thickness of the frozen fringe is fairly small (1.0 cm) it is assumed that the temperature gradient is linear. The model is robust enough to account for dual frost fronts that may occur as the freezing descends from the surface, and ascends from the underlying permafrost. In such situations, both depths and associated temperature gradients are used for the calculation of heave. The same function is used to identify the depth of thaw, as the soil is thawing during the warmer months. The location of the thaw front is identified, as well as the temperature gradient across it, and is used for subsidence calculations.

Heave and subsidence model

In its simplest form, the theory of frost heave is based on the freezing of water that is arriving at the freezing front in a saturated soil, as well as freezing of in-situ pore water. Formation of segregated ice lenses in the soil due to these two phenomena cause significant structural disturbances in the soil. Segregated ice occurs as pure ice layers or lenses, millimeters to meters thick, within the soil. When ice lenses form, the overlying soil is pushed up (heaved) to accommodate for the volume of the ice itself, thus causing heaving at the ground surface. During the melt season, the disappearance of the ice lenses through melting causes weakening of the soil structure, which is often followed by collapsing of the ground surface (Konrad 1999).

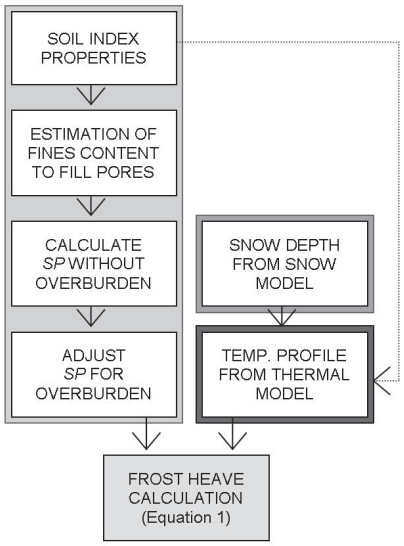

Figure 2. Model flowchart for calculating frost heave.

The segregation potential model developed by Konrad & Morgenstern (1980) offers a very simple, but highly sensitive approach to simulating frost heave using a minimal set of input variables and is based on the concept of a segregation potential parameter (*SP*). Konrad (1999) defined a relationship between the *SP* parameter and four key soil properties (fines content, clay mineralogy, soil fabric, overburden pressure) and created a simple, soil index-based derivation of the *SP* parameter and the resulting frost heave. The amount of frost heave Δh (mm) that occurs during a given time interval Δt (s), is therefore defined as:

$$\frac{\Delta h}{\Delta t} = 1.09(SP gradT) \quad (1)$$

where *SP* is the calculated segregation potential value, and *gradT* defines the temperature gradient across the frozen fringe, as derived in the thermal regime model. Figure 2 summarizes this approach.

Required soil index properties were calculated for each sampling point from the samples obtained at the study site. Daily segregated ice content was calculated for each of 110 points across the study site and the depth at which it formed was identified. In situations where dual frost fronts occurred, both depths were identified and the amount of segregated ice was summed for a daily total. The calculations were performed for all days where freezing occurred, until the two freezing fronts converged and the soil was completely frozen.

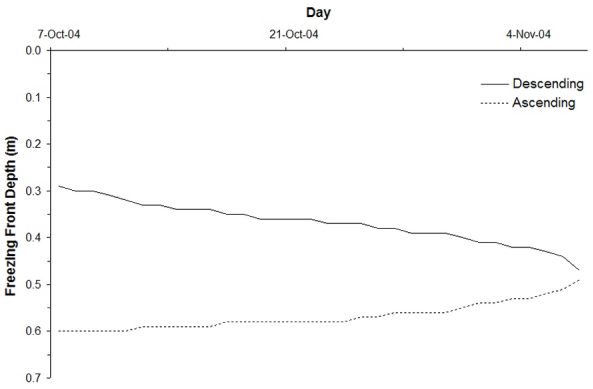

Figure 3. The progression of freezing front with time, for the end of the freeze-up period in year 2004.

During the thaw season, the amount of subsidence was calculated as the thaw front descended through the segregated ice formed during the previous year's freezing period. If the thaw depth coincided with the location of an ice lens, it was assumed that the entire ice lens that formed at that given depth will be melted and the ground surface will subside by the thickness of the lens. Changes in thermal properties of the soil due to presence of ice lenses were not accounted for. Elevation of each sampling point was modified daily, based on the amount of heave or subsidence that occurred. Heave and subsidence amounts were output into a database to be used in further spatial analyses.

Results and Discussion

Snow distribution model

The simplified approach to snow modeling provided a sufficient snow surface to be used in this model. Statistical comparison of the predicted snow surface and the set of 30 observed snow points show that the minimum and maximum snow depths are within one centimeter of each other, and the model overestimates the mean by 0.11 cm. The standard deviations of the two datasets are within 0.69 cm, indicating a similar variance of snow depths throughout the study area. The estimated snow distribution displayed the expected pattern, with thicker snow found in sheltered areas and thin snowpack on exposed slopes.

While having a more complex snow model (e.g., Liston & Sturm 1998, Pomeroy et al. 1993) would possibly be beneficial to accurately assess the daily snow cover over the study area, the method presented here is suitable for predicting the snow cover based on a minimal number of input parameters.

Thermal regime model

The thermal regime for all 110 locations was calculated for the test period (January 1, 2002, to December 31, 2005). In order to assess the change in elevation at each point due to heave and subsidence, the test period was considered to be from the first day of freeze-up in 2004 to the last day of thaw in 2005, thereby providing one full cycle of heave and thaw. Through the thermal model, these days were found to be October 7, 2004, and September 24, 2005, respectively.

As expected, the temperatures at depth respond well to the oscillations in air temperature, but with diminishing amplitude and an increasing phase lag with increasing depth. Figure 3 illustrates the depth of the frost fronts predicted for a selected station over time. The model successfully simulates the convergence of the descending and ascending freeze fronts in the soil, to completely freeze up the active layer.

Averaged across all locations, the depth of thaw for 2004 was found to be 56 cm. This is within the range of values measured in the Mackenzie Delta area. Kokelj & Burn (2005) estimate the thaw depth on the uplands near Inuvik to be between 30 and 100 cm. The thaw results also were validated by frost probing conducted through the summer.

To achieve a complete freeze-up the soil took an average of 40 days, starting on October 7, 2004. The soil was found to remain completely frozen for most locations until between May 15, 2005, and June 5, 2005. The average depth of thaw in 2005 was found to be 52 cm, with most locations achieving their maximum thaw depth by mid-September, approximately a week prior to the first day of freeze-up.

Heave and subsidence model

The amount of segregated ice, and therefore the amount of surface upheaval, was found to be an average of 10.33 cm per station during the freeze-up period in 2004. Approximately 78% of segregation ice formed at the descending frost front, at depths less than 30 cm below ground. This facilitated a fairly fast melt of the bulk of the segregated ice, as on average, the thaw front achieved a depth of 30 cm in approximately 35 to 40 days. Ignoring possible resultant alterations to the soil fabric and any factors that may inhibit the soil from returning to its original state, the subsidence due to melt of segregated ice has been modeled to be an average 9.10 cm. This therefore suggests that the soil does not return to its baseline elevation, and that an average of 1.24 cm of segregated ice remains into the next freeze-up season. This is a function of colder temperatures experienced in the second model year.

Figure 4a depicts the predicted progression of segregated ice formation through time at one sampling point. As the ground begins to freeze, the steep thermal gradient across the freezing front initially causes a significant amount of segregated ice to form. With a decrease in the gradient, less ice is formed, reaching a minimum at zero as either all water in the soil is frozen, or the two freezing fronts converge. Due to the lag time in the response to surface temperature changes at depth, the thermal gradient across the descending freezing front is always much steeper than that moving upwards from the permafrost below. Thus, the amount of segregated ice formed at the descending freezing front contributes much more to the total ice content, while leaving the majority of ice lenses within the first few tens of centimeters below the surface. This is also supported by the results presented in Figure 4b, showing the progression of the thaw front though the soil, as well as the associated subsidence due to melt of

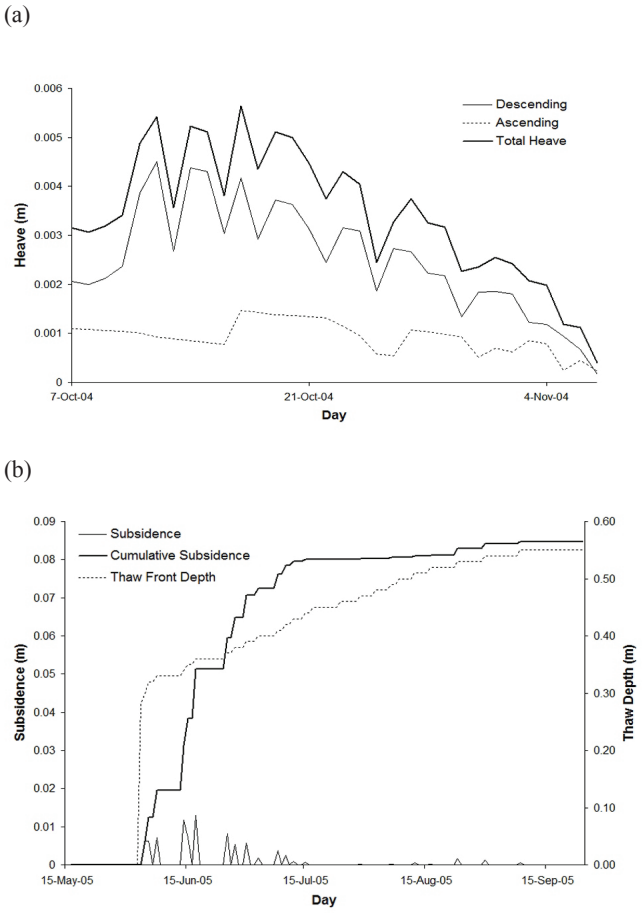

Figure 4. (a) Generation of segregated ice lenses (and therefore heave) at the descending and ascending freezing fronts at point #54, during the freeze-up season in 2004 (b) Progression of the thaw front during the melt season in 2005 and the consequent subsidence due to melt of ice lenses, for point #54.

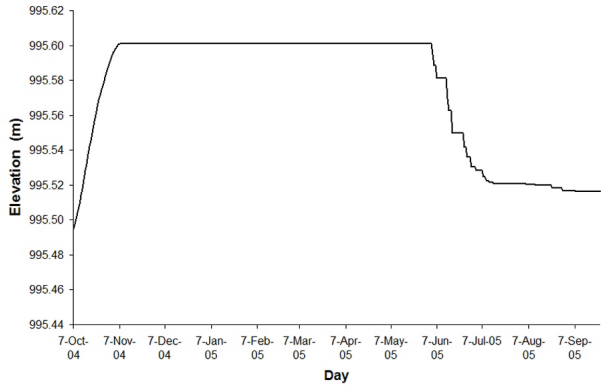

Figure 5. Predicted elevation changes during the study period (2004-2005) due to formation and melting of segregated ice at point #54.

ice lenses. Figure 5 illustrates the annual cycle of ground surface heave and subsidence due to formation and melt of segregated ice for a single sampling point, during the testing period. The overall change in elevation at the end of the melt period in 2005 is shown in Figure 6. As the thaw depths in 2005 did not reach all of the segregated ice that was formed

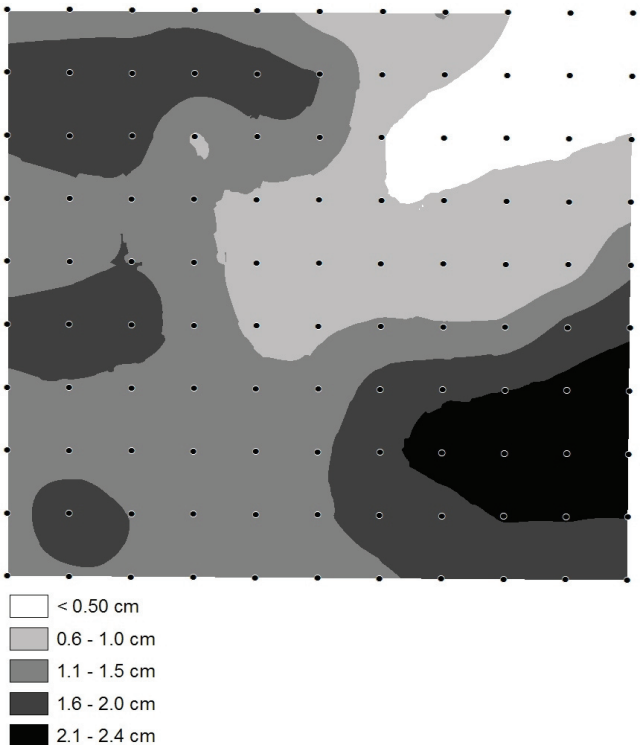

Figure 6. Total predicted change in elevation for the study area, after the melt season of 2005.

in 2004, a lift in the ground surface is observed across the whole study area. Biggest elevation changes are seen in the northeastern quadrant of the study area, where the ground has been raised by up to 2.4 cm.

Conclusions

This work provides a simplified methodology for predicting active layer heave and subsidence on a daily basis based on a limited number of parameters. The approach integrated and modified a number of previously developed methodologies for snow distribution modeling, calculation of freezing soil thermal regimes and the formation of segregated ice within frozen soil.

The snow distribution and thermal models produced estimates that closely matched measured values at the test site. Based on the predicted frost and thaw front depths, the heave/subsidence model was able to simulate the daily changes in the surface elevation due to formation and melt of segregated ice lenses, also yielding values within the expected ranges for the area.

The model is also able to take into account inter-annual weather variability and the resultant changes in the depth of thaw and longer term surface elevation change resulting from changes to the active layer.

Future refinements of the active layer motion model presented in this study will focus on capturing the characteristics of layered soils. As well, implementation of lateral exchanges of heat and water would allow for full

three-dimensional predictions of the thermal regime and have characteristics, thereby accounting for natural variations in microclimatic and terrain conditions that may play a role in the formation of segregated ice.

Acknowledgments

The authors would like to express gratitude to Jeff Williams for field data collection and analyses, as well as to Imperial Oil Limited and NSERC for financial assistance and Steve Solomon and the Geological Survey of Canada for logistical assistance.

References

Bergquist, C.L., Graham, P.P., Johnston, D.H. & Rawlinson, K.R. 2003. Canada's Mackenzie Delta: fresh look at an emerging basin. *Oil and Gas Journal* 101: 42-46.

Environment Canada. 2005. National Climate Data and Information Archives. *Online.* <http://www.climate.weatheroffice.ec.gc.ca/climateData/canada_e.html> Accessed December 15, 2005.

Kane, D.L., Hinzman, L.D. & Zarling, J.P. 1991. Thermal response of the active layer to climate warming in permafrost environment. *Cold Regions Science and Technology* 19: 111-122.

Kokelj, S.V. & Burn, C.R. 2005. Geochemistry of the active layer and near-surface permafrost, Mackenzie delta region, Northwest Territories, Canada. *Canadian Journal of Earth Sciences* 42: 37-48.

Konrad, J.M. 1994. Sixteenth Canadian Geotechnical Colloquium: Frost heave in soils: concepts and engineering. *Canadian Geotechnical Journal* 31: 223-245.

Konrad, J.M. 1999. Frost susceptibility related to soil index properties. *Canadian Geotechnical Journal* 36: 403-417.

Konrad, J.M. & Morgenstern, N.R. 1980. A mechanistic theory of ice lens formation in fine grained soils. *Canadian Geotechnical Journal* 17: 473-486.

Konrad, J.M. & Morgenstern, N.R. 1981. The segregation potential of a freezing soil. *Canadian Geotechnical Journal* 18: 482-491.

Liston, G.E. & Sturm, M. 1998. A snow-transport model for complex terrain. *Journal of Glaciology* 44: 498-516.

Miller, T.W. 1979. The surface heat balance in simulations of permafrost behaviour. *Journal of Energy Resources Technology* 101: 240-250.

Palmer, A.C. & Williams, P.J. 2003. Frost heave and pipeline upheaval buckling. *Canadian Geotechnical Journal* 40: 1033-1038.

Pomeroy, J.W., Gray, D.M. & Landine, P.G. 1993. The prairie blowing snow model: characteristics, validation, operation. *Journal of Hydrology* 144: 165 - 192.

Pomeroy, J.W. & Li, L. 2000. Prairie and Arctic aerial snow cover mass balance using a blowing snow model. *Journal of Geophysical Research* 105: 26619-26634.

Pomeroy, J.W., Marsh, P. & Gray, D.M. 1997. Application of a distributed blowing snow model to the Arctic. *Hydrological Processes* 11: 1451-1464.

Pustovoit, G.P. 2000. Calculation of permafrost temperature. *Soil Mechanics and Foundation Engineering* 37: 27-31.

Rankinen, K., Karvonen, T. & Butterfield, D. 2004. A simple model for predicting soil temperature in snow-covered and seasonally frozen soil: Model description and testing. *Hydrology and Earth System Sciences* 8(4): 706-716.

Williams, P.J. & Smith, M.W. 1989. *The Frozen Earth: Fundamentals of Geocryology*. Cambridge: Cambridge University Press, 306 pp.

Woo, M.K., Arain, M.A., Mollinga, M. & Yi, S. 2004. A two-directional freeze and thaw algorithm for hydrologic and land surface modeling. *Geophysical Research Letters* 31: L12501.

Shear Strength of Ice-Filled Rock Joints

Friederike K Günzel
University of Brighton, Brighton, UK

Abstract

Ice-filled rock joints are a common feature of high mountain permafrost areas. Warming of these joints in rock can lead to instabilities and rockfall events. In the following study, a series of direct shear tests was performed with artificial samples simulating ice-filled rock joints. The direct shear tests were carried out in two testing modes: constant strain and constant stress. In constant stress tests, the ice-filled joints show a parabolic relationship between normal stress and shear stress unlike the linear relationship usually found in mineral filled rock joints (Barton 1974). Constant stress tests were also conducted in which the samples were allowed to warm up until failure occurred while a constant normal stress and a constant shear stress were applied. Different failure modes could be identified, either driven by breaking the connection of ice and concrete or ductile deformation of the ice or a combination of both.

Keywords: direct shear; ice strength; rock joints; rock slopes; shear strength.

Introduction

In recent years, increased numbers of landslide and rockfall events have been reported in high mountain areas (Gruber et al. 2004). A connection between the landslide events and the warming of permafrost due to increasing mean annual air temperatures was observed in landslide events, such as the Val Pola Landslide in 1987 (Dramis et al. 1995).

Earlier laboratory experiments, carried out on a geotechnical centrifuge (Davies et al. 2003 and Günzel & Davies 2006) showed that ice-filled joints in rock are stable as long as the temperature of the ice is low (below about 2°C); however, both the strength and stiffness of ice in the joint reduce if the temperature rises closer to melting point. This leads to a reduction in strength of the rock joint which, if it is critical to maintaining slope stability, can result in slope failure or rockfall. However, the stability increases again when the ice from the joint melts and the rock surfaces come into contact with each other. That means that slope failure can occur at a joint during warming of the permafrost ice, even if a slope is stable both when the rock joints contain "cold" ice and when no ice is present. Slope failure might be avoided if these critical joints can be identified and stabilised temporarily during the period when the ice is warming and when the shear capacity of the joint is below that required for stability.

The current study systematically uses direct shear testing to investigate the shear strength of an ice-filled rock joint during warming of permafrost.

Laboratory Methods

Preparation of samples

In the study, artificial samples made of high-strength concrete (Densit Ducorit D4) were used. To simulate the roughness of the rock joint surfaces, a regular saw-tooth surface was used with the dimensions as shown in Figure 1. Regular, saw-toothed surfaces are a commonly used idealisation of rough rock surfaces in the literature (de Toledo & de Freitas 1993). The dimensions of the samples were 59mm x 59mm to fit inside a 60mm square shear box.

A thermocouple was cast into the concrete samples with the sensitive tip in a small cavity at the centre of the sample surface (Fig. 2). This allowed the temperature of the ice to be measured during the shear tests.

Initial tests were carried out without ice to establish the friction of the concrete surface. Then two different types of ice-filled samples were prepared: concrete-ice samples (Fig. 3) and sandwich samples (Fig. 4).

The concrete-ice samples consist of a concrete block with saw-toothed surface overlaid by an equally thick ice block (Fig. 3). This sample type simulates an ice-filled joint, with

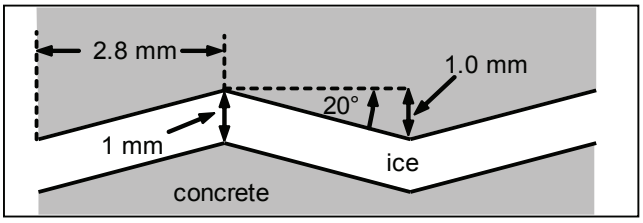

Figure 1. Dimensions of the saw-tooth surface.

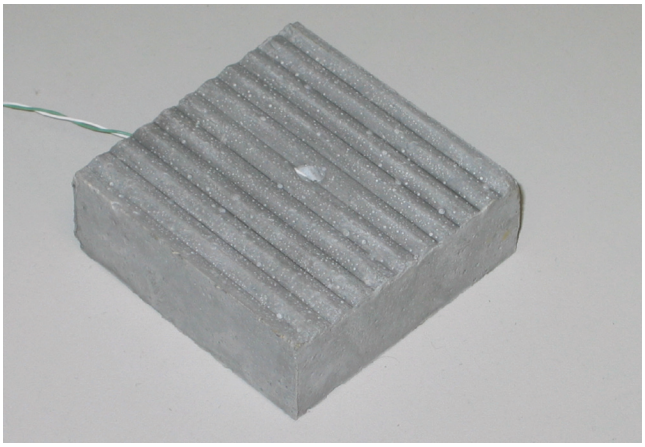

Figure 2. Concrete block with cast saw-tooth surface; the small cavity in the center holds the tip of the thermocouple.

Figure 3. Concrete-ice sample after a constant strain test with normal stress = 207 kPa.

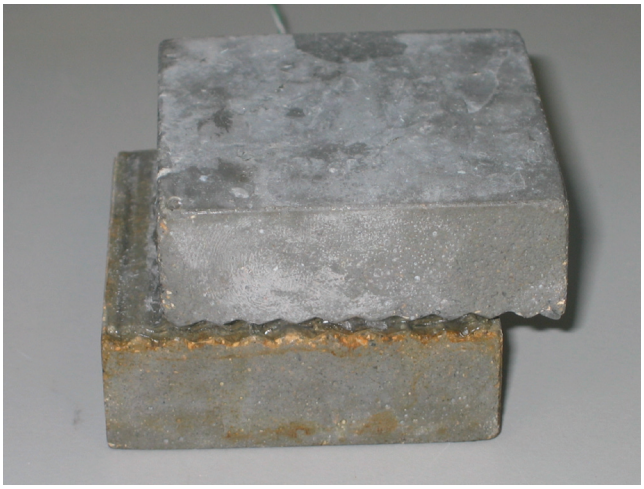

Figure 4. Sandwich sample after a constant stress test with normal stress = 207 kPa.

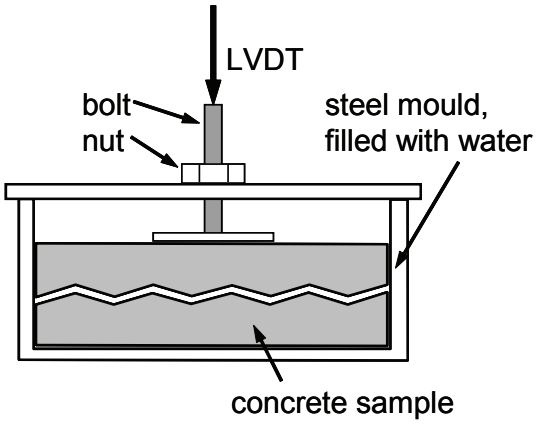

Figure 5. Preparation of sandwich sample.

the ice thickness being much larger than the amplitude of the surface roughness. The concrete-ice samples are prepared by placing concrete blocks into moulds filled with water and allowing them to freeze.

The sandwich samples consist of two saw-toothed concrete blocks with a 1mm thick layer of ice in-between

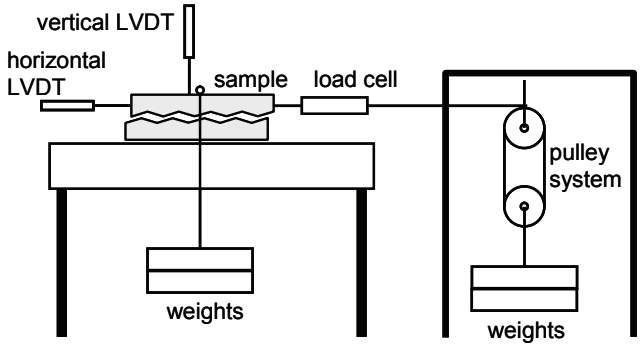

Figure 6. Schematic overview over experimental set-up of the constant strain test.

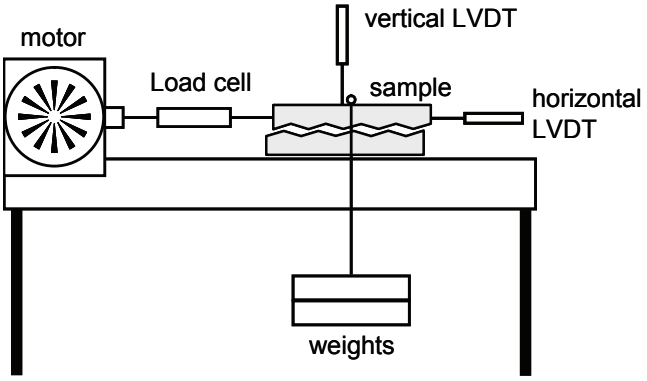

Figure 7. Schematic overview over experimental set-up of the constant stress tests.

(Fig. 4). This sample type simulates an ice thickness equal to the amplitude of the surface roughness. These samples are prepared as illustrated in Figure 5. The two concrete blocks are immersed in water in a mould. A bolt is glued to the top block. The top block is then lifted by turning the nut against the lid of the mould while the movement is measured with an LVDT (Linear Variable Displacement Transducer). After that, the surplus water on top of the sample is drained, and the sample is frozen.

Direct shear tests

Two different modes of direct shear tests were carried out in this study: constant strain tests and constant stress tests. Schematic overviews of both testing modes are shown in Figures 6 and 7. Normal stress is provided by hanging weights. Horizontal and vertical displacements are measured with LVDTs.

In the constant strain tests, shear stress is applied by an electric motor pushing the upper part of the sample while the lower part remains stationary. The shear stress is measured with a load cell. These tests were carried out at -2°C and -4°C, with normal stresses ranging between 135 kPa and 620 kPa. This is equivalent to a depth of 5–25 m below ground. This depth is above the range of the annual freeze-thaw depth of 5±2 m in the Alpine periglacial belt reported by Matsuoka et al. (1998). However, with increasing air temperatures, the freeze-thaw depth can be

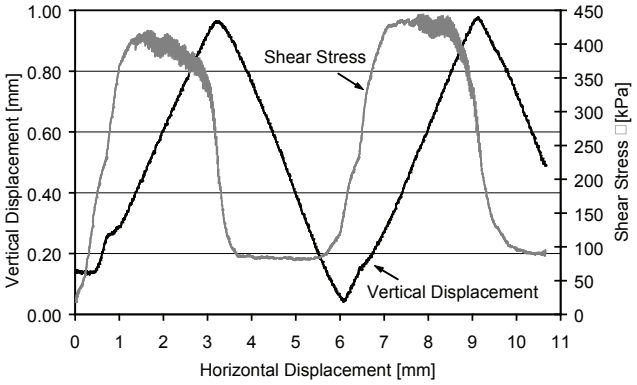

Figure 8. Vertical displacement and shear stress vs. horizontal displacement of a shear experiment without ice (normal stress = 207 kPa).

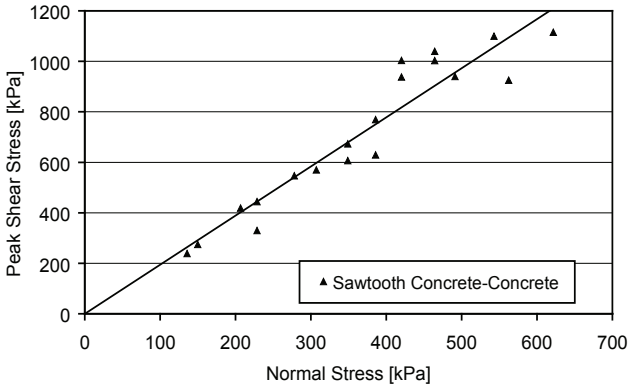

Figure 9. Overview of peak shear test results of concrete samples.

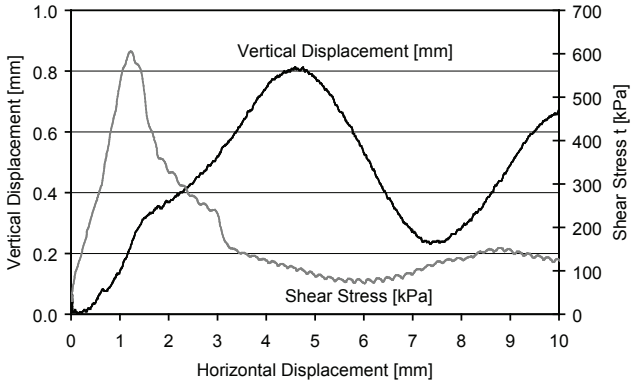

Figure 10. Results of a constant strain shear experiment with a concrete-ice sample at -2°C (normal stress = 207 kPa).

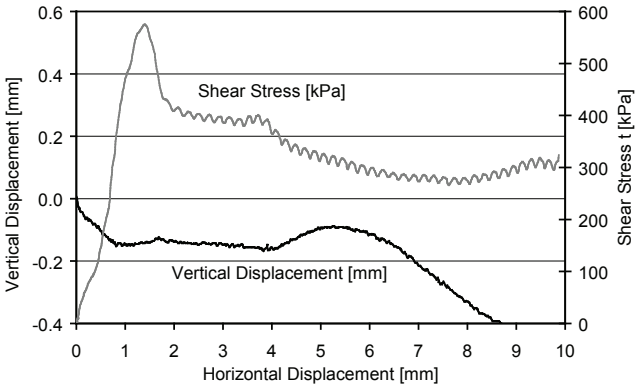

Figure 11. Results of a shear experiment at constant strain with a concrete-ice sample. Temperature = -4°C, normal stress = 562 kPa.

expected to increase.

A constant horizontal displacement rate of 0.47 mm/hour was used for all tests. However, earlier studies (Barnes et al. 1971) found that not only the temperature, but also the strain rate, has a significant effect on the shear strength of an ice-granite interface. Also, failure of a rock slope is not controlled by constant strain, but rather by constant stress.

Therefore the shear box was modified to be able to apply a constant shear stress rather than a constant strain onto the concrete ice samples and the sandwich samples. Here, the motor was replaced by a pulley system and weights to apply a constant shear stress to the samples. The sample temperature was then increased slowly until the sample failed.

Cold room

The experiments were carried out in a cold room. To ensure a constant temperature of the sample during the defrosting cycles of the cooling element, the shear box was encased inside a Styrofoam box with 100 mm wall thickness. However, the electric motor of the shear box apparatus caused the temperature inside the Styrofoam box to increase during the constant strain tests. Therefore it was very difficult to control the temperature of the sample and subsequently the temperatures at failure varied by about 0.5 C.

Experimental Results

Samples without ice

To establish the frictional resistance of the concrete samples without ice, direct shear tests were carried out with normal stresses between 135 kPa and 620 kPa. The typical response of a sample is shown in Figure 8. Here the shape of the saw tooth surface is clearly visible from the vertical displacement. The development of the shear stress follows the same pattern with the maximum shear stress during the uplift of the top sample.

Figure 9 shows the maximum measured shear stresses of all concrete samples plotted against the normal stress applied to the sample. As expected, there is a clear linear relationship between the normal stress and the shear stress. The scatter of data above a normal stress of 400 kPa is due to abrasion of the concrete samples during the test.

Constant strain tests with concrete-ice samples

A total number of 26 constant strain tests were carried out at two different temperatures: -2°C and -4°C. Depending on the normal stress, the vertical displacement during the test showed different behaviour (Figs 10,11): at low normal stresses, the vertical displacement clearly reproduces the shape of the saw-toothed surface, albeit with a slightly reduced amplitude (Fig. 10). This behaviour can be

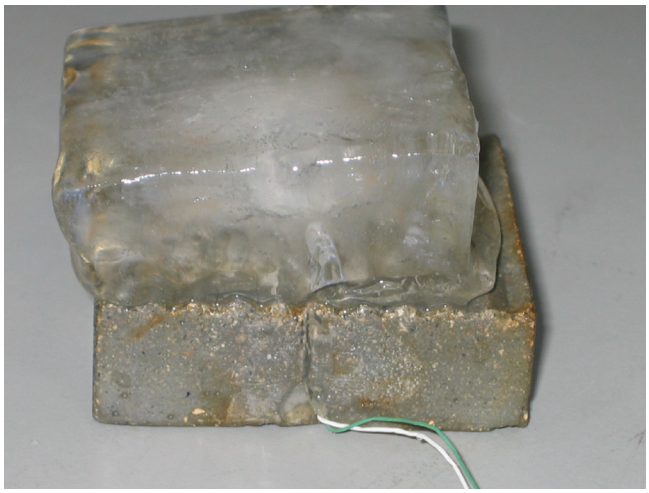

Figure 12. Shear deformation of a concrete-ice sample after a constant strain test with normal stress = 490 kPa.

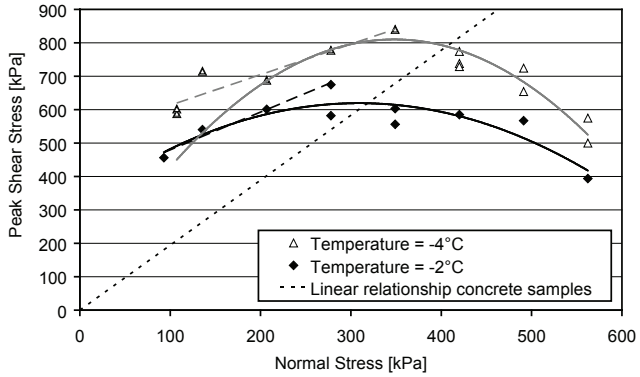

Figure 13. Peak shear test results from concrete-ice samples in constant strain tests.

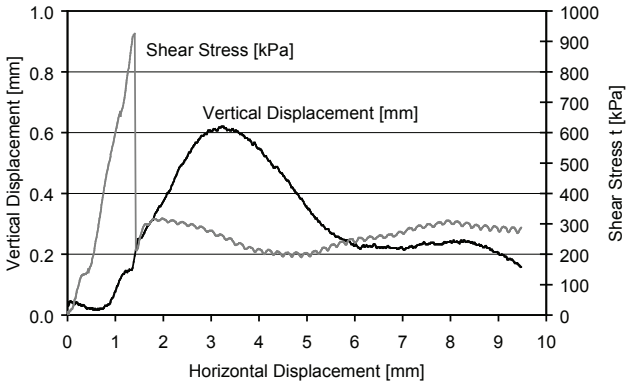

Figure 14. Results of a constant strain shear experiment with a sandwich sample at -5°C (normal stress = 490 kPa).

interpreted as the ice becoming detached from the concrete surface, and the behaviour of the sample is mainly defined by the friction between surfaces of the ice and the concrete (Fig. 3). However, at high normal stresses, no dilation of the sample was observed (Fig. 11). Here the deformation of the sample is mostly due to a shear deformation of the ice itself rather than the sliding of ice over concrete. At the end of these tests, the ice was still firmly attached to the concrete surface (Fig. 12). No granularisation of the ice comparable

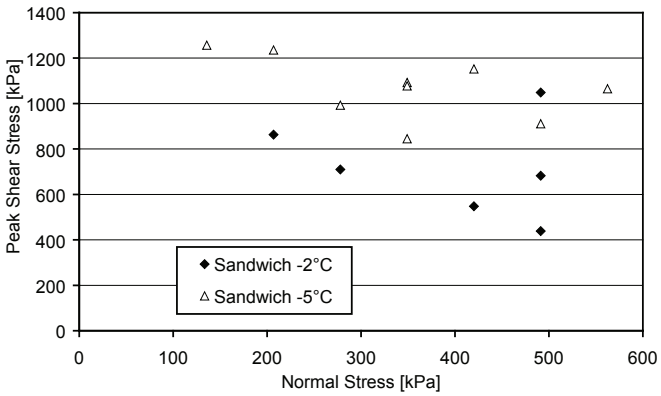

Figure 15. Overview of peak shear test results of sandwich samples in constant strain tests.

to the "rubblisation" reported by Yasufuku et al. (2003) was observed. It should be noted, that the initial stiffness of the samples is approximately the same, irrespective of the type of deformation.

The two different mechanisms of deformation also become apparent in the relationship of maximum shear stresses and normal stresses at failure (Fig. 13): at low normal stresses, the relationship between maximum shear stress and maximum normal stress appears to be linear (dashed lines in Fig. 13), which is in agreement with the behaviour of mineral-filled rock joints (Barton 1974). However, at normal stresses, above 220 kPa and 300 kPa for -2°C and -4°C, respectively, this relationship becomes parabolic. This result agrees with the parabolic strength envelopes of ice found by Fish & Zaretsky (1997).

Constant strain tests with sandwich samples

The constant strain tests with sandwich samples were carried out at -2°C and -5°C. Unlike the concrete-ice samples, the sandwich samples dilated even at high normal stresses (Fig. 14). It is also noticeable that the shear stress maximum forms a very sharp peak with a sudden drop when the ice becomes detached from the concrete surface. Again, the initial stiffness of the sample is very similar to the stiffness of the concrete-ice samples. Due to the sharp peak, a considerable scatter of the maximum strength at failure is to be expected (Fig. 15). It is unlikely that the scatter is enhanced to a large extent by the sampling rate: the shear stress increased with a rate of approximately 10 kPa per minute, so that with a one-minute sampling rate, the error would be not more than 10 kPa. Despite the large scatter, a decrease of the maximum shear stress with increasing normal stress can be observed.

Constant stress test

The tests were started at an ice temperature of approximately -5°C, and then the temperature was increased at a rate of about 0.3°C per hour until failure occurred. These shear tests were carried out at normal stresses between 136 kPa and 630 kPa. The typical result of a constant stress shear test with a concrete-ice sample is shown in Figure

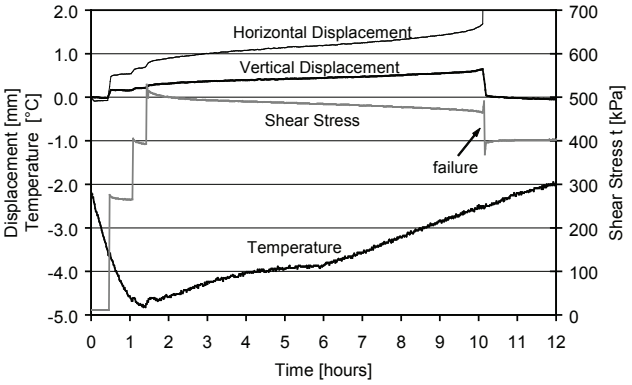

Figure 16. Results of a constant stress experiment (concrete-ice sample, normal stress = 207 kPa) plotted against time.

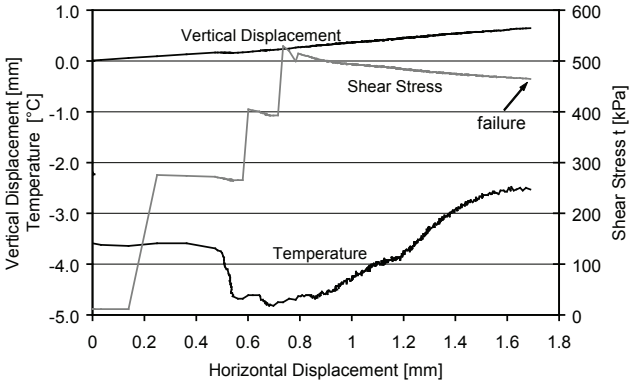

Figure 17. Results of a constant stress experiment (concrete-ice sample, normal stress = 207 kPa) plotted against horizontal displacement.

16 (plotted against time) and Figure 17 (plotted against horizontal displacement). The results for concrete-ice samples and sandwich samples are very similar. The steps of the shear stress at the beginning of the test correspond to adding weights to the pulley system. The decrease of stress during the test is due to friction in the pulley system: the tension in the nylon rope connecting the sample with the weight slackens slightly as the sample deforms, due to creep in the ice prior to failure. The apparent change of the rate of temperature increase is due to the increasing rate of horizontal deformation immediately before failure of the sample.

The horizontal displacement during the constant stress tests was considerably slower than during the constant strain tests; it varied between 0.002 mm/hour and 0.06 mm/hour. The deformation rate increased with increasing shear stress, but no significant change could be observed for increasing normal stress or temperature. The horizontal displacement at failure was between 1.5 mm and 2.5 mm, similar to the displacement at failure of the constant strain tests. The vertical displacement decreased with increasing normal stress.

Figure 18 shows the variation of failure temperature depending on normal stress and shear stress for concrete-ice samples and sandwich samples. The data points represent the shear stress at failure versus the normal stress acting on the sample. The temperature distribution for both sample types is very similar, with the only difference being that the failure temperatures of the sandwich samples were about 0.5°C lower than the concrete-ice samples. The data show decreasing failure temperatures with increasing shear stresses. However, the failure temperatures increase with increasing normal stresses throughout the test series up to normal stresses of 630 kPa. This behaviour differs from the constant strain experiment where, at normal stresses above 300 kPa, a decrease of failing temperature with increasing normal stress was observed (Fig. 13).

Figure 18 also shows the failure envelope of the concrete samples. It can be seen that, at low temperatures and low normal stresses, the ice-filled joints have a higher shear strength than joints without ice-filling.

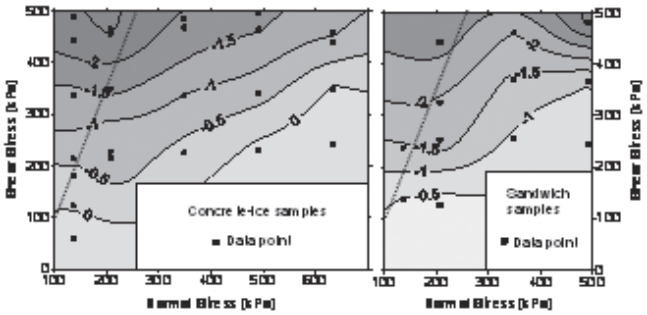

Figure 18. Temperatures at failure (measured by the sensor in the middle of the sample) during constant stress tests with concrete-ice samples (left) and sandwich samples (right). The dotted lines represent the linear relationship between shear stress and normal stress obtained for the concrete samples.

Discussion

Depending on sample type (concrete-ice or sandwich) and test type (constant stress or constant strain), three different types of deformation could be identified:

1. Deformation driven by breaking of the connection between the ice and the concrete surface;
2. Deformation driven by shear deformation of the ice itself; and
3. Combination of the deformation types 1 and 2.

In the constant strain tests with concrete-ice samples at low normal stresses, the first type of deformation is predominant. Indicators for this type of failure are the extent of the dilation of the samples during the test (Fig.10) and the visual examination of the sample after the test (Fig. 3) that clearly shows the ice being detached from the concrete surface. However, the same sample type shows ductile deformation of the ice at high normal stresses. Here the samples show no net dilation during the test (Fig. 11); any local dilation that may be present in the sample is counteracted by the ductile deformation of the ice, which is clearly visible in the sample after the test (Fig. 12).

In the constant-strain tests of the sandwich samples, a

combination of the first two failure modes is observed. Visual examination of the samples showed the ice detached from one of the concrete surfaces. However, these samples show a reduced dilation of 0.4mm–0.6mm (Fig. 14) indicating that sliding of the ice over the concrete surface is not the only type of deformation in these samples. The other type of deformation may be shear deformation of the ice itself. The maximum shear strength reduces with increasing normal stress (Fig. 15), again indicating shear deformation of the ice.

Constant-stress experiments with both sample types show that here the predominant type of deformation is breaking the connection between the ice and the concrete. This observation is consistent with the data shown in Figure 18, where the shear stress at failure increases rather than decreases with normal stress for a constant temperature.

Conclusions and Outlook

In this study, three different failure modes of ice-filled joints could be distinguished. This adds to the understanding of the failure mechanisms of rock slopes in warming permafrost conditions.

Several issues that have not been considered to date will be addressed in the near future:

- The strength of ice depends on the strain rate; constant strain tests need to be carried out with the same strain rate as observed in the constant stress tests.
- Creep measurements of ice at constant temperatures, rather than increasing temperatures, need to be conducted.
- The strain rate measured in the laboratory needs to be compared with strain rates measured in full scale rock slopes rather than small-scale centrifuge model tests.

Acknowledgments

All experiments were carried out at the geotechnical laboratories of the University of Dundee, UK.

References

Barnes, P., Tabor, D. & Walker, J.C.F. 1971: The friction and creep of polycrystalline ice. *Proceedings of the Royal Society, London (Series A)* 324: 127-155.

Davies, M.C.R., Hamza, O. & Harris, C. 2003: Physical modelling of permafrost warming in rock slopes. *Proceedings of the Eighth International Conference on Permafrost, Zürich, Switzerland, July 21-25, 2003:* 169-174.

de Toledo, P.E.C. & de Freitas, M.H. 1993: Laboratory testing and parameters controlling the shear strength of filled rock joints. *Géotechnique* 42(1): 1-19.

Dramis, F., Govi, M., Guglielmin, M. & Mortara, G. 1995: Mountain permafrost and slope instability in the Italian Alps: the Val Pola Landslide. *Permafrost and Periglacial Processes* 6: 73-82.

Fish, A.M. & Zaretsky, Y.K. 1997: Ice strength as a function of hydrostatic pressure and temperature. *CRREL Report 97-6.*

Gruber, S., Hoelzle, M. & Haeberli, W. 2004: Permafrost thaw and destabilization of Alpine rock walls in the hot summer of 2003. *Geophysical Research Letters* 31:L13504.

Günzel, F.K. & Davies, M.C.R. 2006: Influence of Warming Permafrost on the Stability of Ice Filled Rock Joints. *Proceedings of the Sixth International Conference on Physical Modelling in Geotechnics, Hong Kong, August 4-6, 2006:* 343-348.

Matsuoka, N., Hirakawa, K., Watanabe, T., Haeberli, W. & Keller, F. 1998: The role of diurnal, annual and millennial freeze-thaw cycles in controlling Alpine slope instability. *Proceedings of the Seventh International Conference on Permafrost, Yellowknife, Canada, June 20-24, 1998:* 711-717.

Yasufuku, N., Springman, S.M., Arenson, L.U. & Ramholt, T. 2003: Stress-dilatancy behaviour of frozen sand in direct shear. *Proceedings of the Eighth International Conference on Permafrost, Zürich, Switzerland, July 21-25, 2003:* 1253-1258.

An Analysis of Land Suitability for Urban Construction in Permafrost Regions

Igor E.Guryanov
Melnikov Permafrost Institute, SB RAS, Yakutsk, 677010, Russia

Abstract

Natural conditions of sites varying in favorability for urban construction are discussed, based on the example of Yakutsk, northeastern Russia. Their role in overall land suitability is shown. Relationships between the initial land suitability level and the resulting ecological situation at the townsite are analyzed, with particular reference to the permafrost region.

Keywords: conditions; ecological situation; factors; land suitability; permafrost; urban construction.

Problem Statement

The common feature of community infrastructures in permafrost regions is the lower structural and maintenance safety of buildings and facilities compared to more temperate regions, and the frequent performance problems resulting from permafrost thawing due to anthropogenic changes. It is, therefore, important to determine to what extent these deficiencies are related to the design and construction solutions, the choice of which is dictated indispensably by considerations of economics.

Construction Area Quality Factors

Depending on the favorability of environmental conditions, areas vary in suitability for urban development. Development of the areas of limited suitability results in an additional burden on the urban environment. Development of unsuitable areas aggravates the situation, producing complex engineering and ecological problems.

The suitability of any area for urban land use is predetermined by five basic factors characterizing the general conditions for construction:

1) The geology of the area and the geological processes and features anticipated to occur beneath buildings and structures.

2) The topography of the area which affects the convenience of service lines.

3) The hydrogeology and the surface and subsurface drainage conditions.

4) The hydrology of rivers and lakes.

5) The thermal regime and the air and water quality.

These factors are analyzed during the planning process in order to create the most favorable conditions and control the quality of construction sites. Inadequate consideration or neglect of any of these environmental factors reduces the overall suitability of the construction area. Since the factor combinations are always specific, suitability evaluations are only made for specific areas.

Factor Assessment Criteria

First factor (geological conditions)

- Favorable conditions: Homogenous soils or rocks that are good foundation material for conventional foundation types; the stability and adequate performance of engineering structures are guaranteed;
- Provisionally favorable conditions: Ground properties that call for some restrictions of the effects from buildings and other structures to ensure their stability and good performance; special foundation types, soil improvement, and other measures can be applied;
- Unfavorable conditions: Weak soils that require special foundation designs, soil improvement, structural measures. and stringent controls on construction and maintenance.

Second factor (topography)

- Favorable conditions: Lowlands with slopes of 0.5 to 10%, local relief of up to 10 m, and low horizontal dissection (erosional incisions spaced at least 2 to 5 km apart).
- Provisionally favorable conditions: Slopes less than 0.5% and 10 to 20% in the lowlands and up to 30% in the mountains; 10 to 25 m local relief; moderate horizontal dissection with incisions spaced at 0.5 to 2 km.
- Unfavorable conditions: Slopes greater than 20% in the lowlands and greater than 30% in the mountains; local relief greater than 25 m; and high horizontal dissection with less than 0.5 km spacing between incisions (Solodukhin 1985).

Third factor (hydrogeology and drainage)

- Favorable conditions: Groundwater occurs lower than the foundation bottom; no protective measures against the influence of groundwater are required.
- Provisionally favorable conditions: Special precautions are required to ensure adequate construction and maintenance of buildings and structures (water proofing, drawdowning, drainage, corrosion control, etc.).
- Unfavorable conditions: A complex system of special measures must be taken to prevent the adverse effect of groundwater on the construction and maintenance of engineering structures and their performance.

Fourth factor (flooding hazard):

- Favorable conditions: Areas unflooded by 1% probability flood events (one in one hundred years).
- Provisionally favorable conditions: Areas that are not

flooded in a 4% probability flood event (one in 25 years).

- Unfavorable conditions: Areas liable to flooding during >4% probability flood events (more than one in 25 years) (Lomtadze 1978).

Fifth factor (temperatures and water and air quality)

Only two categories—favorable conditions and unfavorable conditions—are identified, based on the atmospheric circulation patterns and the environmental quality standards.

In accordance with favorability, provisional favorability, and unfavorability of each factor, study areas are categorized as suitable, limited suitable, and unsuitable.

Analysis of Land Suitability for Construction

The actual approaches to urban development in permafrost regions will be illustrated below, using the example of Yakutsk which faces the typical problems.

Considering the first factor of land suitability for urban construction which characterizes the geological structure and related geological processes, it should be noted that the special design and construction methods for engineering work in permafrost areas have less than one century of history (USSR Building Code 2.02.04-88, 1990). Based on technical experience, special-purpose permafrost zonation of Russia has been made, and special requirements for design and construction of foundations and buildings have been elaborated. However, the need for special foundation types and structural improvements, as well as the special considerations for construction and operation stages, imply the overall unfavorability of engineering-geological conditions. It means that any permafrost area is essentially unsuited for urban construction, and strict solutions to the problems posed by the first factor require that in each specific case, proper weight should be given to the other factors in order to prevent them from adding to adverse effects on the engineering geological conditions.

By the second factor (topography), the townsite of Yakutsk located on the first and second terraces of the Lena River has a general slope of much less than 0.5% per 10 km or more, and the distance between frequent oxbow depressions is about 1 km. These conditions are provisionally favorable, making the townsite limited suitable by the second factor which affects the quality of utility lines and roads.

Moreover, because of the flatness of the townsite, surface and subsurface (active layer) drainage is in fact lacking. In other words, the area is unsuited for urban development in terms of the third factor, since the problems of inundation and salinization remain unsolved due to the technical complexity. The 370 years of continuous anthropogenic saturation and salinization of the soils, as well as leaking service pipes, have resulted in cryopegs in the low-lying areas with salinities of up to 10 g/l. These cryopegs contain Na and Mg chlorides aggressive to foundation concrete.

Within the city limits, the first river terrace is from 93–95 m to 97 m in elevation. Surface runoff and drainage occur very slowly, from Lermontov Street to Khabarov and Chernyshevsky Streets. The lack of drainage results in frost jacking of the structures and frost cracking beneath the buildings. With the construction of a new residential district, Mirkorayon 202, on the Lena floodplain filled to a 97-m elevation, the first-terrace area between Lermontov and Khabarov Streets has become a depression, and drainage in the active layer has been disrupted.

The fourth factor (hydrological conditions) is of prime importance for Yakutsk, as it lies in the Lena Valley. Floods to levels between 1% and 4% probability make the area that of limited suitability for urban development, while the zones with levels of less than 4% probability are classified as unsuited. Flood levels of the Lena River in the Yakutsk area are 96.36 for 1% probability events and 95.46 for 4% floods. Since the level at Khabarov Street near the town dam is 95.5 m, the first terrace is entirely an area of limited suitability for construction.

Filling of the floodplain area for new construction is estimated by the project designer, Giprokomminstroy, to add 40 cm to flood levels, and a 4% probability flood thus would reach 95.86 m. As a result, the first terrace has become a flood-risk area, making the developed parts of the city unsuited in terms of the building standard. This change in the situation has already resulted, in that every spring flood-control action has to be taken along the first-terrace slope.

By the fifth factor, atmospheric quality, the urban land-use suitability is not evaluated. However, its ecological implications should be given consideration, because, being located in the river valley, Yakutsk is influenced by temperature inversion during the winter. The inversion is several hundreds of meters in vertical extent and up to 10º in temperature difference; the number of days with fog is up to 56 during the winter months. Weak air movement results in heavy air pollution with the maximum permissible concentrations exceeded by 10 to 20 times. The average maximum exceeding of the standards is 3–8 for SO_2, 9 for CO, 5 for NO_2, and 10–17 for H_2S. These levels are above high and harmful air pollution thresholds (Central Research and Design Institute on Urban Development 1986). The development of the floodplain has increased trapping of pollution emissions within the city area.

According to the recommended environmental criteria for urban areas (Central Research and Design Institute on Urban Development 1986), Yakutsk is now an extremely unfavorable (critical) zone in terms of air and water quality, as well as soil and vegetation conditions.

Osipov (2004), in his analysis of environmental problems in Russia, presents environmental degradation zonation of the country. The map shows that in the permafrost zone, local areas of degradation are those affected by mining activities. No degradation is indicated for the Yakutsk area. However, the above discussion makes us conclude that Yakutsk appears to be the only community in the permafrost zone where the arduous situation has resulted solely from the absence of an orderly pattern of development. The oldest city erected on

permafrost has been an experimental plot with both building successes and failures.

Construction and Maintenance Problems at Yakutsk

The critical engineering and ecological situation has resulted in significant negative consequences, which are listed below in a decreasing order of the number of affected buildings and structures.

1. Anthropogenic salinization of the foundation materials and related reduction in the frozen soil strength and bearing capacity.

2. Warming and thawing of the underlying frozen ground due to insufficient heights of air space between the buildings and the ground surface, primarily due to overall saturation of the townsite soils resulting from the lack of surface runoff and hydraulic discharge of the active layer.

3. Repeated or contingent leaks from the internal, external, district and main water and heat lines into the ground near or below the buildings. Leakage results in large thaw bulbs, foundation settlement, and structural damage.

4. Concrete deterioration in the foundation sections within the layer of seasonal thaw due to frost and chemical action. Capillary suction of groundwater from the active layer to the masonry walls of the mid-20th century or older buildings (a demolished building on Ordzhonikidze Square, a number of buildings on Lenin, Khabarov, and Bestuzhev-Marlinsky Streets) and gradual damage to the bearing walls leading to complete failure.

5. Frost cracking in the foundation soil during the winter months resulting in damage to the basement walls.

Of about 500 residential and public buildings examined at Yakutsk, 182 buildings, or 36.4% of major infrastructure, show various levels of deformation. It is not surprising, since Yakutsk, which initially had no sanitary or storm sewer systems, is the oldest community on permafrost.

The current situation on the Yakutsk townsite calls for the following immediate measures:

1. Prohibit new construction in the floodplain areas. Develop measures aimed at minimizing the adverse effects of the built-up floodplain sections on the remainder of the townsite.

2. Establish, by the city of Yakutsk Department of Housing and Municipal Services, a special supervisory service for performance control, repair, and reconstruction of the district utility systems and the sewage main.

3. Prepare alternative reconstruction plans for the areas of sporadic construction, providing for green recreational zones to reduce the total burden on the city.

4. Enforce the re-opening of the Yakutsk permafrost station which would, at the initial stage, be subordinate to the Federal Emergency Management Department's Monitoring and Prediction Centre. Based on the existing experience (USSR Committee for Construction's Institute of Foundations and Underground Structures 1982), this station should be charged with developing a single network of thermal and level monitoring network of the city area and building sites. In the first years, the station should prepare regular reports on the permafrost conditions at the city and the performance of the existing infrastructure.

The recommended measures are certainly of regulative character and cannot be expected to solve the general problem. Land quality remediation is a task for many decades to come. City expansion should be diverted away from the inversion-affected valley (an ecological objective) and the low terraces of the Lena River (a planning objective). It is evidently the only way to improve the urban land use quality.

General Evaluation of Permafrost-Affected Infrastructure

Despite the diversity of construction conditions in northern communities, it is of interest to compare the infrastructure conditions survey data, since these figures provide some indication of the general situation. At Norilsk, for example, about 300 of the 1000 buildings examined required foundation stabilization; about 40 buildings are reconstructed and repaired annually by a specialized engineering company. At Chita, 132 of 526 buildings investigated (25.1%) are damaged or distressed. In the communities located on the Arctic coasts, 30% of the buildings show signs of deformation. Mosgiptotrans, the railroad design company of Moscow, reports that 27.4% of the northern railroad embankments show deformation. With Yakutsk, these findings indicate that, on average, 30% of the infrastructure in the permafrost areas is in distress, irrespective of its type.

An analysis of the survey results for 114 damaged buildings in Magadan Province showed that 25% of the cases were due to improper site investigation and design, 17% due to inadequate site preparation and poor foundation construction, and 58% due to maintenance deficiencies. It follows that at least 83% of the problems are caused by errors in evaluation of construction conditions, and this corresponds to the lower level of the probable number of problem buildings. Thus, neglect of the urban construction quality of an area as a whole and individual construction sites produces a practically exact range: 25–30% damaged buildings. This range means that the precision of achieving a design purpose, expressed as the confidence probability of a target result, corresponds to the square root of variance. Hence urban development can be viewed as a stochastic process characterized by a normal distribution; i.e., the system control of the urban design and construction process is entirely absent. This is the reality of the urban development process in the permafrost regions.

Conclusions

The neglect of technical requirements in the construction practice in the North has no objective reasons. The northern communities that came into existence in recent decades are characterized by the same failure rate as Yakutsk with its 375-year history. The only way to solve the problem is enact into law and enforce the current urban construction regulations for permafrost areas discussed above.

References

Central Research and Design Institute on Urban Development. 1986. *Recommendations on Environmental Protection in Regional Planning*. Moscow: Stroyizdat, 160 pp.

Lomtadze, V.D. 1978. *Engineering Geology. Special Engineering Geology*. Leningrad: Nedra Publ., 496 pp.

Osipov, V.I. 2004. Ecological problems in Russia. *J. Geoecology. Engineering Geology, Hydrogeology and Geocryology* 1: 5-12.

Solodukhin, M.A. 1985. *Engineering-Geological Investigations for Industrial and Civil Construction.* Moscow: Nedra Publ., 225 pp.

USSR Building Code 2.02.04-88. Foundations in Permafrost. 1990. Moscow: USSR Committee for Construction Press, 56 pp.

USSR Committee for Construction's Institute of Foundations and Underground Structures. 1982. Recommendations on Monitoring of Foundations in Permafrost. Moscow: Stroyizdat, 33 pp.

A New Permafrost Map of Quebec-Labrador Derived from Near-Surface Temperature Data of the Moderate Resolution Imaging Spectroradiometer (MODIS)

Sonia Hachem
Centre d'Études Nordiques, Département de Géographie, Université Laval, Quebec, Quebec, Canada
Michel Allard
Centre d'Études Nordiques, Département de Géographie, Université Laval, Quebec, Quebec, Canada
Claude Duguay
Department of Geography, Faculty of Environmental Studies, University of Waterloo, Waterloo, Ontario, Canada

Abstract

Data obtained from spaceborne platforms offer a significant advantage for studies conducted in arctic and subarctic areas where measurement stations are geographically scattered. The Land Surface (skin) Temperature (LST) products of the Moderate Resolution Imaging Spectroradiometer (MODIS), aboard NASA's Terra and Aqua satellite platforms, were retrieved over continuous and discontinuous permafrost zones. A temporal interpolating model was applied to fill gaps due to extensive periods of cloudiness (more than 50% of cloudy days per year were observed from 2000 to 2005). Mean annual and monthly near-surface temperatures, as well as freezing (Fi) and thawing indices (Ti) and the ratio (Ti/Fi), were calculated pixel by pixel over the six complete annual temperature cycles for large geographical areas. This approach provides a new and original view of surface temperature patterns over Quebec-Labrador. It is suggested that conditions favourable for permafrost have recently moved northward.

Keywords: freezing index; land surface temperature; MODIS; permafrost boundaries; thawing index.

Introduction

Many authors have mapped the spatial distribution of permafrost in the past using various climatological and terrain parameters. For this purpose, different methods for interpolating climate data between dispersed stations were used. The first maps used mean annual air temperature isotherms (Brown 1960, 1970, Heginbottom 1984, Johnston 1981), some added mean July air temperatures (Allard & Séguin 1987), and included typical permafrost landform reconnaissance (Allard & Séguin 1987, Brown 1979, Harris 1982, Jorgenson & Kreig 1988, Rochefort & Payette 2001). Others have used thawing and freezing indices to delineate permafrost zones (Hinkel et al. 2001, Nelson 1986, Nelson & Outcalt 1987, Riseborough & Smith 1998). Recently, active layer thaw depth has also been mapped from these indices (Hinkel & Nicholas 1995, Riseborough 2003, Shiklomanov & Nelson 1999, 2002), and improved by n-factors (Klene et al. 2001, Riseborough 2004, Shur & Slavin-Borovskiy 1993).

The arctic and the subarctic regions are remote areas where to install and maintain measurement stations is technically difficult and excessively expensive. Even so, it remains necessary to assess surface temperatures over the landscape to monitor the climate. The large swath scanned by satellite sensors allows for broad-scale mapping in a single satellite overpass. As satellite sensors measure radiative temperatures at the atmosphere/surface boundary. The satellite temperatures are called "skin" surface temperatures or near-surface temperatures. Mapping at a regional scale a subsurface phenomenon such as permafrost using satellites is hence a challenge. But since permafrost owes its existence basically to the surface temperature regime, mapping this controlling variable seems to be the most logical approach. Hence, this type of measurement is physically different from those collected with temperature sensors (thermistors) either in the air or in the ground, usually at depths of 2 to 10 cm.

The MODIS sensor aboard the Terra and Aqua satellites was chosen for three main reasons. First, the Land Surface Temperature (LST) product is distributed online where it is easily and rapidly accessible. Second, this product is retrieved by two satellites that overpass the same region twice daily: in the morning and in the evening. Third, the spatial resolution chosen (pixel size of 1 km²), on one hand, is coarse enough to compute and store regional mapping, and on the other hand, is small enough to keep an acceptable accuracy for delimiting boundaries over vast landscapes. The LSTs are tile-shape distributed. Each tile is a piece about 1113 km by 1113 km in 1200 rows by 1200 columns, in a sinusoidal map projection. Three tiles (h14v02, h14v03 and h13v03) are needed to cover the entire Quebec-Labrador area. The LSTs used herein start on February 24, 2000, for Terra, and from July 4, 2002, for Aqua, and end on May 31, 2005, for both satellites.

Skin temperature validations were made previously for different landscapes, Lake Titicaca (Wan et al. 2002), rice fields (Coll et al. 2005) and homogeneous landscapes on the Tibetan Plateau (Wang et al. 2007), using field radiance measurements. Stations used for each of these studies were comprised within 1 km². The amount of radiation reaching the satellite radiometer is modified by both atmospheric water vapour effects and surface emissivity effects (spectral

Table 1. Comparison between TM, Ti and Fi from Reference calculation with the ones calculated from the fitted sinusoidal equations Tair_sin et LST_sin.

	Mean annual TM		Degree-days of thawing (Ti)		Degree-days of freezing (Fi)	
	REF/ Tair_sin	REF/ LST_sin	REF/ Tair_sin	REF/ LST_sin	REF/ Tair_sin	REF/ LST_sin
R^2	0.90447021	0.4955715	0.47103442	0.20069824	0.85643988	0.83075603
rmse	0.656	1.6044	189.6851	370.4642	232.7709	251.3852
P-value	0.0001	0.0001	0.0001	0.0101	0.0001	0.0001

and angular) over the land. The very complex (e.g,., heterogeneity of mixed land covers) effect produced suggest that for them accuracy can only be done in a few special cases, when surface and atmospheric properties are very well known (Prata 2000). For the present study, instead of radiance measurements, the available stations, which were far apart from each other, collected ground temperatures and meteorological data. As these stations represent several tundra landscapes (low and sparse vegetation), comparisons between LST pixel values and ground station temperatures cannot be used to validate LST for a particular square kilometer. Nevertheless, the evaluation of the level of agreement between MODIS LST (LST data) and near-surface air temperature measurements (Tair data) at 2–3 m above ground, at ground-based stations located in the continuous permafrost zones of northern Quebec and Alaska, yielded a very good correlation ($R^2 > 0.81$; $4.41 < RMSE < 6.89$; $-3.58 <$ mean bias < 5.92). From this first assessment, it was deemed feasible to try to use MODIS LST products to map the surface temperatures dictating the presence of permafrost and its thermal regime (Hachem 2007).

Temporal Interpolation

The Arctic is known for its high cloudiness weather regime. This persistent cloudiness is evident through the analysis of measurements from 15 stations in Alaska and northern Quebec. The year had been divided in two parts to simplify calculations. As summer begins on June 1 and ends on September 30, it is composed of the four warmest months of the year. The additional months are defined as winter, i.e., from October 1 to May 31. All stations taken together showed a number of cloudless days of 23 (19%) during summer and of 88 (36%) during winter, summing to slightly more than a hundred days per year. As LSTs are measured at cloud-sensitive Earth-emitted thermal infrared wavelengths, for each cloudy day, LSTs are missing. Over a year, there are many weeks during which the presence of a cloud cover prohibited the determination of surface temperatures by space-based thermal infrared sensors. This setback was partly overcome through developing a statistical model of the temporal LSTs distribution.

Mathematically, the annual distribution of temperatures can be expressed by the following sinusoidal function:

$$T_t = T_m - A_0 . \cos\left(\frac{2\pi t}{P} - \phi\right) \quad (1)$$

where T_t is the measured temperature at time t, T_m is the mean annual temperature, A_0 is the amplitude, P is the period (a constant equal to 365 days), and ϕ is the phase (Williams & Smith 1989).

From this equation mean annual temperature (T_m) is directly given, freezing (F_i) and thawing indices (T_i) are obtained by calculating the integrals under the sinusoidal curve, corresponding to the sum of negative temperatures (freezing degree-days) and positive temperatures (thawing degree-days), respectively (i.e., consecutive winter and summer). The sinusoidal curve was calculated to fit to LSTs and Tair data. Results from this calculus were named LST_sin, and Tair_sin, the sin abbreviation refer to the fitted sinusoidal equation.

As Tair were measured at field stations, we also calculated the Tm, Fi, and Ti as it is usually done, and named the results from these calculations REF.

We compared Tm, Fi, and Ti calculated with the year-by-year fitted equations from LSTs (LST_sin) and Tair (Tair_sin) data with Tm, Fi, and Ti calculated the usual way from Tair (REF). The LSTs used for comparison were taken from pixels which coordinates include a meteorological station in the field.

Table 1 shows statistical analyses of the different calculated Tm, Ti, and Fi. There are very good correlations between Tm and Fi, calculated from the LST dataset and recorded air temperatures, and a good correlation between the two sets for Ti (Hachem 2008). The statistical model gives excellent results for the two Tair datasets (REF and Tair_sin), which validates the use of this model. It still provides good results when REF is compared with LST_sin. Nevertheless, Ti correlations are very low (Table1). This is not necessarily related to the model used or to the absence of cloudy day values. Actually, Ti is known to be a highly variable parameter, as well as between two consecutive years than between stations only a few meters apart (Klene 2000).

The statistical algorithm was devised to derive the equation of the sinusoidal curve that best fits MODIS LST for each year of data and for each image pixel. Through applying that relationship to LST data over the pixels, Fi and Ti maps were drawn.

A New View of Quebec-Labrador Permafrost Distribution

Tm, Fi, and Ti maps description

The Tm, Fi, and Ti maps (not presented here) are an average over six years, from 2000 to 2005, and correspond to

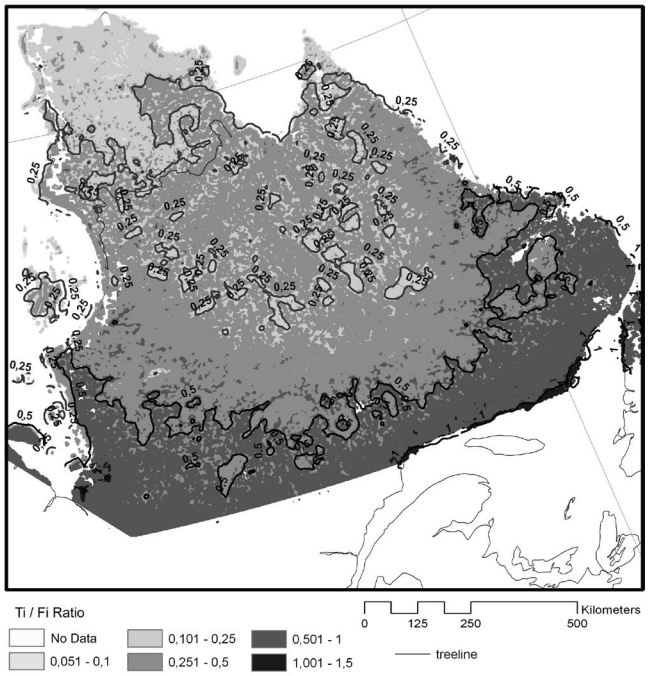

Figure 1. Ti/Fi ratio map.

Figure 2. After Payette & Rochefort (2001). A: continuous permafrost zone. B: discontinuous permafrost zone; B^1: more than 50% of permafrost; B^2: less than 50% of permafrost; B^3: maximal concentration of cryogene hillock and plateaus formed in Tyrrell Sea loamy silt. C: sporadic permafrost (less than 2%). D: annual frozen soils. Otish (1) mounts and Groulx mounts (2) are two high summit permafrost enclaves in sporadic permafrost zone. Chic-Choc mounts (3) and Lac des Cygnes mount (4) are high summit permafrost enclaves in annual frozen soil zone. (R. is used to indicate "reservoir," i.e., La Grande Reservoir.)

a mixture of temperatures from different cover types included within a single pixel (1 km^2). They all show a similar climate pattern (latitudinal, altitudinal, continental distribution, and large lakes). Colder areas are northernmost. The central section of northern Quebec is colder than coastal areas–a poorly documented observation until now as no stations are located on the high central plateaus of the peninsula. Also, due to Hudson Bay influence and barrier effects by the Torngat Mountains, the east coast of the Quebec-Labrador peninsula is colder than the west coast. Moreover, the maps show that large water bodies produce colder microclimates that influence the surrounding land areas (within 2 pixels of water bodies). However, in the continuous permafrost zone, large river basins show warmer temperatures than the surrounding plateaus (Hachem 2008). The high elevated topography is easily identifiable because of the cold tops which are colder than the plains.

The Ti/Fi ratio map

Anisimov & Nelson (1997) used Fi and Ti ratios to estimate the presence or absence of permafrost. If F_i is greater than T_i, it means that the mean annual temperature is below 0°C, suggesting that permafrost is likely to be present. Whereas if F_i is less than T_i, then the heat gain in summer is large enough to counterbalance the heat loss in winter, hindering permafrost to form, or in areas where it is present, leading to its disappearance over time. In addition, if T_i increases over time and remains greater than F_i, it can be deduced that the active layer is thickening, leading to the progressive disappearance of permafrost from the top downward. Here, we used the T_i/F_i ratio (Fig. 1) to provide a first estimate of the presence or absence of permafrost.

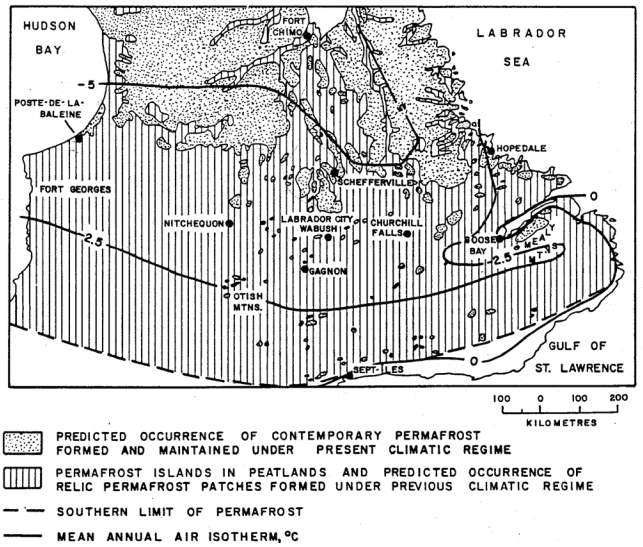

Figure 3. Discontinuous permafrost (Brown 1979).

However, this estimate could be improved either by calculating the frost number (Nelson & Outcalt 1987) or by including the "buffer" information (Riseborough 2004). The frost number is defined by Nelson & Outcalt (1987) as a dimensionless ratio using freezing and thawing degree-day

sums and gives a device for portraying the distribution of contemporary permafrost at continental scales. The "buffer layer" effect, often integrated in the n-factor, corresponds to the impact of factors affecting heat exchanges between the atmosphere and the ground surface (i.e., vegetation, organic layer, snow cover).

The Ti/Fi ratio map (Fig. 1) is divided into three main parts, by two isolines. The 0.25 isoline (i.e., when Fi is four times as large as Ti) corresponds and follows nearly the southern limit of the continuous permafrost drawn by Payette & Rochefort (2001), based on general knowledge of landforms and vegetation zones (Fig. 2), which corresponds also to the +10°C isotherm of the mean air temperature of the warmest month of the year (Allard & Séguin 1987). Herein, July was used as the warmest.

The 0.5 isoline (i.e., when F_i is twice as large as T_i)

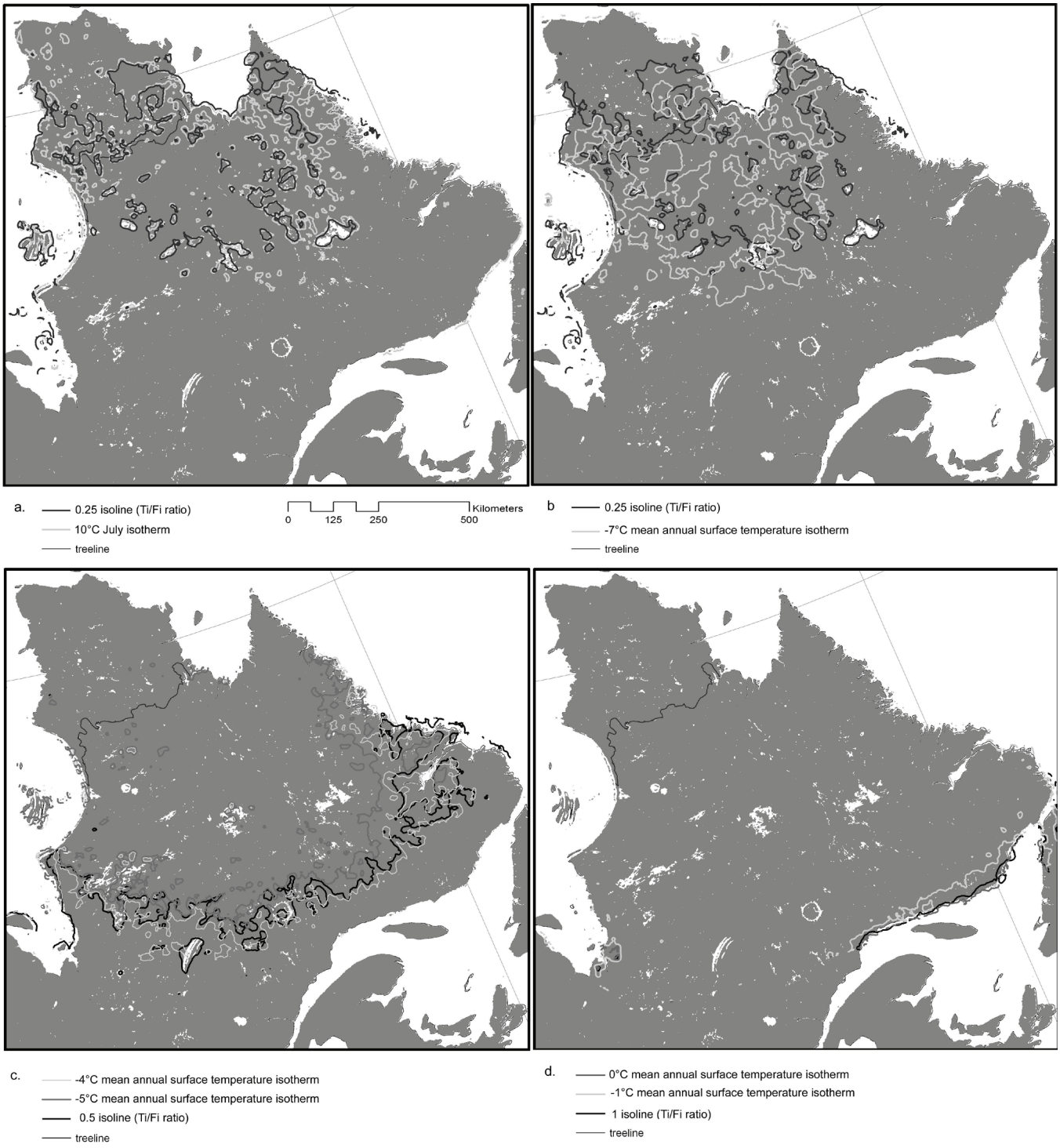

Figure 4. Comparisons of different potential limits of permafrost.

corresponds rather well to the known southern limit of the Brown's (1979) sporadic permafrost zone drawn by Figure 3.

Therefore, this first map is a promising starting point to pursue the next mapping steps.

Northern Quebec-Labrador permafrost limits

A consensus exists in the literature that permafrost extent can be mapped in three categories: continuous, discontinuous, and sporadic or isolated patches. The categories are not perfectly established and depend on what characteristics are mapped (e.g., percentage of frozen soil actually related to ground ice conditions, or air isotherms) and on mapping scale (Heginbottom 2002). While mapping the northern Quebec-Labrador peninsula one limiting criteria chosen by Allard & Séguin (1987) was the +10°C isotherm for the warmest month of the year (corresponding to the tree line) as the boundary between discontinuous and continuous permafrost. The limit between discontinuous and sporadic permafrost was roughly the -−1°C isotherm of mean annual air temperature. Inclusion of other information such as topography, physiography, surface geology, soil moisture, content vegetation, and snow cover would help to better define boundaries and map distribution of permafrost patches in greater detail.

A relatively good correspondence appears between key Ti/Fi ratio contour lines and key isotherms that are generally used for interpreting the boundaries of permafrost zones. For instance, Figure 4a shows the excellent correspondence between the 0.25 Ti/Fi ratio contour line and the +10°C July isotherm, both measured with the MODIS sensor, therefore supporting the idea that this contour fits roughly with the boundary between continuous and discontinuous permafrost. It is to be noted, however, that this line was further north than the tree line during the period 2000–2005, which agrees with observed recent climate warming. This suggests that climate conditions propitious for continuous permafrost are currently moving northward. The -7°C mean annual surface temperature (MAAT) isotherm derived by MODIS on Figure 4b is likely a better approximation of the diffuse boundary between widespread (>50%) and scattered discontinuous permafrost (<50%) than what was previously estimated. The overlapping 0.5 Ti/Fi ratio contour line and -5°C MAAT isotherm in Figure 4c can be associated with the southern limit of discontinuous permafrost. Finally, sporadic occurrences of permafrost can occur as far south as the 0°C MAAT isotherm, in good correspondence with Brown's permafrost map (Fig. 4d).

Conclusion

We developed a statistical model that uses MODIS LST to map mean monthly and annual surface temperatures as well as freezing and thawing indices, as an alternative to conventional ground-based measurements which are spatially limited. Thermal permafrost limits were added through the calculation and mapping of the Ti/Fi ratio contour lines. These maps compare rather well with maps drawn by previous authors based on ground-collected data. They can be used only as a first approximation since other (local) factors such as snow cover, vegetation, and organic layers—variable with moisture content—create a "buffer" effect between the atmosphere and the surface which is not included in the Ti/Fi ratio.

These maps bring in new knowledge regarding the spatial distribution of temperatures across northern Quebec-Labrador. In an upcoming study, maps similar to the ones presented in this paper will be produced to encompass the entire pan-arcticArctic domain. They could be improved if n-factors are available. Also it would be possible to input the Ti in different models calculating active layer thickness (TTOP [Riseborough 2003], the frost number [Nelson & Outcalt 1987], or the GIPL model [Sazonova & Romanovsky 2003]). This approach with MODIS data is also a new tool available for monitoring surface temperature changes at a high spatial resolution.

References

Allard, M. & Séguin M.K. 1987. Le pergélisol au Québec nordique: bilan et perspectives. *Géographie physique et quaternaire* 41(1): 141-152.

Anisimov, O.A. & Reneva, S. 2006. Permafrost and Changing Climate: The Russian Perspective. *Ambio* 35(4): 7 pp.

Brown, R.J.E. 1960. The distribution of permafrost and its relation to air temperature in Canada and the USSR. *Arctic* 13(3): 163-177.

Brown, R.J.E. 1970. *Permafrost in Canada, Its Influence on Northern Development.* Toronto: University of Toronto Press.

Brown, R.J.E. 1979. Permafrost distribution in the southern part of the discontinuous zone in Québec and Labrador. *Géographie physique et quaternaire* 33(3-4): 279-289.

Coll, C., Caselles, V., Galve, J.M., Valor, E., Niclos, R., Sanchez, J.M. & Rivas, R. 2005. Ground measurements for the validation of land surface temperatures derived from AATSR and MODIS data. *Remote Sensing of Environment* 97: 288-300.

Hachem S. 2008. *Cartographie des températures de surface, des indices de gel et de dégel de la répartition spatiale du pergélisol, à l'aide du Moderate Resolution imaging Spectroradiometer (MODIS)*. Thèse de Doctorat. Département de Géographie, Université Laval, 144 pp.

Hachem, S., Duguay, C.R. & Allard, M. 2007. Comparison of MODIS-derived Land Surface Temperatures with Near-Surface Soil and Air Temperature Measurements in Continuous Permafrost Terrain. (submitted)

Harris, S.A. 1982. Identification of permafrost zones using selected permafrost landforms. *Proceedings of the Fourth Canadian Permafrost Conference, Calgary, Alberta, March 2–6, 1981*: 49–57.

Heginbottom, J.A. 1984. The Mapping of Permafrost. *Canadian Geographer* 28(1): 78-82.

Heginbottom, J.A. 2002. Permafrost mapping: a review. *Progress in Physical Geography* 26(4): 623-642.

Hinkel, K.M. &Nicholas, J.R. 1995. Active layer thaw rate at a boreal forest site in Central Alaska, USA. *Arctic and Alpine Research* 27(1): 72-80.

Hinkel, K.M., F. Paetzold, F.E. Nelson &Bockheim, J.G. 2001. Patterns of soil temperature and moisture in the active layer and upper permafrost at Barrow, Alaska 1993-1999. *Global and Planetary Change* 29(3-4): 293-309(17).

Johnston, G.H. 1981. *Permafrost, Engineering Design and Construction.* Toronto:Wiley, 540 pp.

Jorgenson, M.T. & Kreig, R.A. 1988. A model of mapping permafrost distribution based on landscape component maps and climatic variables. *Fifth International Conference on Permafrost, August 2–5, 1988, Trondheim, Norway.* Tapir.

Klene, A.E. 2000. *The N-Factor in Natural Landscapes: Relations between Air and Soil-Surface Temperatures in the Kuparuk River Basin, Northern Alaska.* Publications in Climatology 53. Newark: University of Delaware, Center for Climatic Research, 85 pp.

Klene, A.E., Nelson, F.E. & Shiklomanov, N.I. 2001. The n-factor as a tool in geocryological mapping: seasonal thaw in Kuparuk River basin, Alaska. *Physical Geography* 22(6): 449-466.

Nelson, F.E. 1986. Permafrost distribution in central Canada: applications of a climate-based predictive model. *Annals of the Association of American Geographers* 76: 550-569.

Nelson, F.E. & Outcalt, S.I. 1987. A computational method for prediction and regionalization of premafrost. *Arctic and Alpine Research* 19(3): 279-288.

Payette, S. & Rochefort, L. 2001. *Ecologie des tourbières du Québec-Labrador.* Québec: Presse de l'Université Laval.

Prata, A.J. 2000. The proposed global land surface temperature product for ENVISAT's AATSR: Scientific basis, algorithm description and validation protocol. *ERS-ENVISAT Symposium, 16-20 October, 2000, Gothenburg, Sweden.*

Riseborough, D.W. 2003. Thawing and freezing indices in the active layer. *8th International Conference on Permafrost, 22-25 July, 2003, Zurich, Switzerland.* Lisse: Swets and Zeitlinger.

Riseborough, D.W. 2004. *Exploring the Pparameters of a Simple Model of the Ppermafrost Relationship. Geography and Environmental Studies.* Ottawa: Carleton, 310 pp.

Riseborough, D.W. & Smith, M.W. 1998. Exploring the limits of permafrost. *Seventh International Conference on Permafrost, Yellowknife, Canada.* Québec, Québec, Canada: Université Laval, Centre d'Etudes Nordiques.

Sazonova, T.S. & Romanovsky, V.E. 2003. A model for regional estimation of temporal and spatial variability of active layer thickness and mean annual ground temperatures. *Permafrost and Periglacial Processes* 14: 125-139.

Shiklomanov, N.I. & Nelson, F.E. 1999. Analytic representation of the active layer thickness field, Kuparuk River Basin, Alaska. *Ecological Modelling* 123: 105-125.

Shiklomanov, N.I. & Nelson, F.E. 2002. Active layer mapping at regional scales: a 13 year spatial time series for Kuparuk Region, North Central Alaska. *Permafrost and Periglacial Processes* 13: 219-230.

Shur, Y.L. & Slavin-Borovskiy, V.B. 1993. N-factor maps of Russian permafrost region. *Sixth International Conference on Permafrost, July, 1993, Wushan Guangzhou, China.* Beijing: South China University of Technology Press.

Wan, Z., Zhang, Y.-L., Zhang, Q.-C. & Li, Z.-L. 2002, Validation of the land surface temperature products retrieved from terra moderate resolution imaging spectroradiometer data. *Remote Sensing of Environment* 83(1-2): 163-180.

Wang, K., Wan, Z., Wang, P., Liu, J. & Sparrow, M. 2007. Evaluation and improvement of the MODIS land surface temperature/emissivity products using ground-based measurements at a semi-desert site on the western Tibetan Plateau. *International Journal of Remote Sensing* 28: 2549-2565.

Williams, P.J. & Smith, M.W. 1989. *The Frozen Earth: Fundamentals of Geocryology.* Cambridge: Cambridge University Press, 306 pp.

—Plenary Paper—

Research Challenges for Permafrost in Steep and Cold Terrain: An Alpine Perspective

Wilfried Haeberli
Glaciology, Geomorphodynamics & Geochronology, Geography Department, University of Zurich, Switzerland
Stephan Gruber
Glaciology, Geomorphodynamics & Geochronology, Geography Department, University of Zurich, Switzerland

Abstract

The past few decades have seen a rapid development and progress in research on permafrost in mountain areas with complex and rugged topography such as the European Alps. At the same time, it becomes increasingly clear that climate change impacts have the potential to severely affect future living conditions in areas with steep and cold terrain by influencing the chain of surface processes that link debris production via rock fall to talus/moraine formation, creep deformation of frozen deposits, and material evacuation by debris flows and fluvial transport. Key scientific challenges relate to special aspects induced by complex topography. Corresponding aspects are briefly outlined concerning the relation between the atmosphere and the permafrost in areas with highly variable snow cover and potentially strong lateral energy fluxes, permafrost thermal conditions in mountains with pronounced microclimatic asymmetries, the destabilization of steep to near-vertical rock walls and degrading permafrost, the flow and stability of ice-rich frozen debris with increasing subsurface temperature and melt water availability, interactions between glaciers and permafrost under conditions of rapid if not accelerating change, 4D-evolution of permafrost in rugged mountain topography, and hazards from permafrost slopes in densely populated high-mountain chains.

Keywords: climate change; cold regions; mountains; natural hazards; permafrost; slope stability.

Introduction

The first contributions in the Proceedings of the International Permafrost Conferences about permafrost in mid-latitude, high-altitude mountain regions started to appear in the late 1970s (e.g., Barsch 1978, Fuji & Higuchi 1978, Gorbunov 1978, Haeberli 1978, Harris & Brown 1978). This indicates the essential beginning of systematic research on permafrost in high-mountain areas and led to a first visibility peak at the International Workshop on Mountain Permafrost in Interlaken 1991 with a first set of overview papers (cf. situation reports by Barsch 1992, Guodong & Dramis 1992, Haeberli 1992, Harris & Corte 1992, King et al. 1992, Lautridou et al. 1992). During its rather young history, research on permafrost in steep and cold terrain developed and expanded rapidly. Perhaps the most important impulse was the EU-funded PACE project (Permafrost and Climate in Europe, Harris et al. 2001). The subsequent progress and increase in visibility is impressing: high-mountain permafrost is now described for many regions (for instance, Isaksen et al. 2007, Jin et al. 2000, Marchenko 2007, Trombotto 2000) and is regularly included in international assessments on cryospheric conditions, especially as related to climate change (IPCC 2007, UNEP 2007, cf. also Harris 2008).

Climate change indeed constitutes a major challenge for the science of mountain permafrost as it concerns a phenomenon that depends on atmospheric conditions in a complex way, is not directly accessible through visual observation, often involves logistic problems with difficult access and strikingly lacks observational series over extended time periods. As a consequence, even key questions are still open for detailed investigations. The present contribution focuses on special aspects related to rugged topography and steep terrain. It is primarily built on experience from the European Alps as summarized in recent reviews (Harris et al. 2008, Gruber & Haeberli 2008, Haeberli & Gruber 2008) and briefly outlines a set of high-priority research topics covering process understanding, numerical modeling and the anticipation/assessment of potential climate change impacts. The basic structure of the considered geo-system (Fig. 1) as is characteristic for mountain ranges with transitional to continental climate—where glacier equilibrium lines are far above the 0°C-annual isotherm—is the process chain leading from debris production via rock fall to debris cone or moraine formation, creep deformation of frozen deposits and sediment evacuation to larger valleys by fluvial transportation and debris flows.

In the following discussion, the most important conclusions based on existing knowledge are briefly outlined and major challenges concerning research on mountain permafrost are discussed. We thereby distinguish seven major topics: (1) atmosphere-permafrost coupling in complex topography; (2) permafrost thermal conditions inside mountains; (3) destabilization of permafrost rock walls; (4) flow and stability of ice-rich frozen debris; (5) glacier/permafrost interactions; (6) 4D-evolution of permafrost in mountain topography; and (7) hazards related to rock falls and debris flows from permafrost slopes.

Topics (1) to (5) are related to necessary improvements of our process understanding. The spatio-temporal consideration, on the other hand, is more and more urgently needed for realistically assessing consequences and impacts from continued atmospheric warming. The discussion

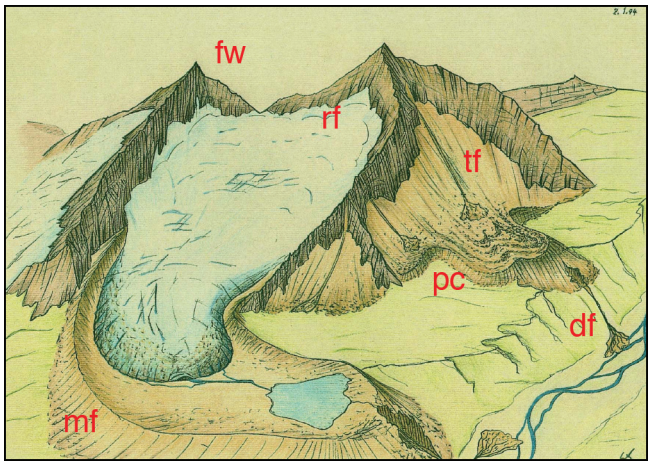

Figure 1. Scheme of the characteristic process chain in cold mountain areas: frost weathering (fw) and debris production, rock fall (rf), talus (tf) or moraine formation (mf), permafrost creep (pc), evacuation by fluvial transport and debris flows (df). Adapted from Haeberli (1996).

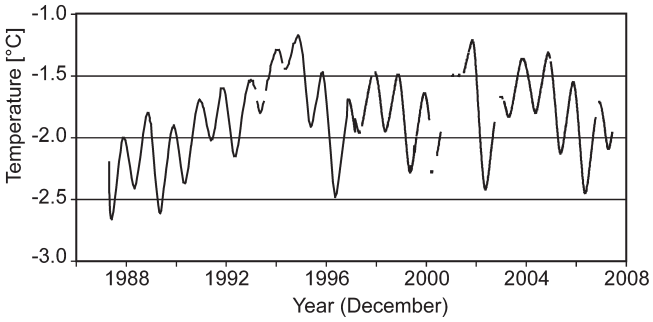

Figure 2. Borehole temperatures in the active Murtèl rock glacier. The winters of 1996, 2002 and 2006 had thin snow cover causing strong ground cooling despite relatively warm air temperatures.

therefore also includes two central aspects—topics (6) and (7)—related to the assessment of local, regional and global impacts of climate change and the anticipation of corresponding hazard potentials.

Atmosphere-Permafrost Coupling in Complex Topography

The now 20 years old series of borehole temperatures in the Murtèl rock glacier (Fig. 2) clearly shows the important influence of the winter snow cover on near-surface ground temperatures. This effect of snow on relations between the atmosphere and the permafrost has been investigated using measurements (Keller & Gubler 1993) and snow/permafrost models (e.g., Lütschg et al. 2003). A number of studies also address the cooling influence that coarse blocks exert on ground temperatures when compared with lower porosity or finer-grained surface materials (Hanson & Hoelzle 2004, Hoelzle & Gruber 2008).

The effect of topography on temperatures in steep rock has been investigated with measurements (Gruber et al. 2003) and model experiments (Gruber et al, 2004 a, b, Noetzli et al. 2007, Salzmann et al. 2007). Despite significant progress in understanding these processes of atmosphere-permafrost coupling, the high spatial variability of surface micro-climatology and subsurface properties in mountain terrain makes the generalization of findings to larger areas difficult. One example is the thermal effect of thin and intermittent snow cover in rock faces that has not been quantified to date.

The role of heat advection by moving water or air in sediments or in cleft systems is a further set of processes that is little understood but that bears high relevance for the anticipation of climate change impacts (fast thaw along frozen joint systems and corresponding rock fall) and for the understanding of permafrost dynamics (Gruber & Haeberli 2007). Especially lateral transfer of sensible as well as latent heat through ventilation effects in steep, coarse-grained debris or by melt water in heavily fissured, near-vertical rock walls appear to be essential.

Permafrost Thermal Conditions Inside Steep Mountains

Measured borehole temperatures (Harris et al. 2003, Gruber et al. 2004c, Isaksen et al. 2007) and combined time-dependent energy balance and heat diffusion modeling for complex topography (Noetzli et al. 2007) now document the main thermal characteristics of cold mountains. Summits can be frozen to depths of nearly 1000 m, and often have strongly asymmetrical thermal fields with steeply inclined isotherm configurations and predominant lateral heat flow from warmer to colder outer rock walls. The uppermost parts of such ridges and summits are essentially decoupled from geothermal heat and, due to their geometry, enable thermal disturbances to penetrate from two or more sides. Atmospheric warming during the 20th century has caused pronounced thermal anomalies to depths of about 50–70 m below surface. In perennially frozen debris (talus, moraines, rock glaciers) with high ice contents near the lower boundary of local permafrost occurrence, temperatures below the depth of zero annual amplitude have, in places, reached phase equilibrium condition (pressure melting) throughout (zero or near-zero heat flow).

The formation and existence of unfrozen zones within permafrost (taliks) as documented, for instance, in the borehole through Murtèl rock glacier in the Swiss Alps (Vonder Mühll et al. 2003), constitutes a disturbance and heterogeneity for subsurface heat and energy flow. Positive feedback between energy input and hydraulic permeability most likely causes such effects to be widespread in warm permafrost, to increase in importance with continued warming and often to dominate over heat conduction through extended subsurface layers.

The occurrence and intensity of corresponding processes, however, are hardly known and most difficult to predict. Individual observations at high-mountain railway and cable car stations (Fig. 3) point to the importance of the

Figure 3. A roof protects tourists from melt water that only recently began to percolate through the rock mass above the tunnel inside the Jungfraujoch rock crest, 3500 m asl, Swiss Alps.

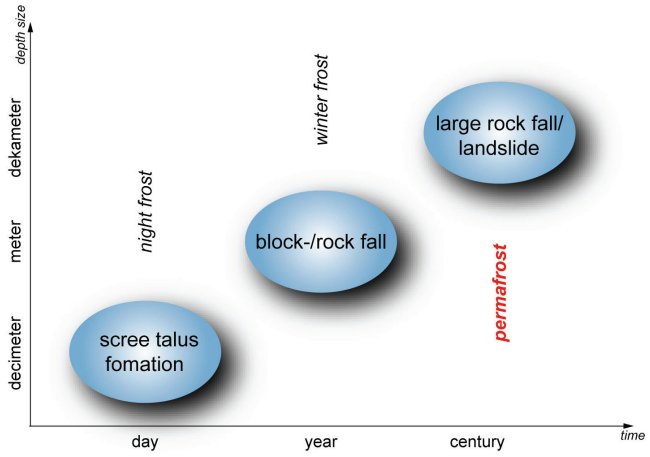

Figure 4. Scales of frost weathering and gravity driven mass wasting in rock walls.

phenomenon (Gruber & Haeberli 2007) and approaches to scientifically investigate these phenomena are now being developed (Hasler et al. 2008). Geophysical tomography (seismic refraction, electrical resistivity, Hauck & Vonder Mühll 2003, Krautblatter et al. 2007, Sass 2003), drilling/borehole temperature monitoring in fissured rock with warm permafrost (cf. Vonder Mühll et al. 2008) and the combination of heat diffusion modeling with other sources of information (Noetzli et al. 2008) for defining the conductive part of changes in the subsurface thermal field appear to be the most viable research avenue.

Destabilization of Permafrost Rock Walls

It is now quite well understood that frost-induced processes of rock destruction act on scales of time and depth that are often—but not always—connected via heat diffusion (Fig. 4). Seasonal to perennial frost, strong spatial temperature gradients in ridges and the availability of snowmelt water in active layers are likely to promote ice segregation involving depth scales of decimeters to tens of meters. Laboratory investigations (Davies et al. 2001) indicate that critical temperatures for the destabilization of frozen rocks with ice-filled cracks on steep slopes can also be reached at temperatures of -1 or -2°C. With continued warming, permafrost in cold mountains reaches such critical temperatures over more and more extended areas and over increasing depths. As a consequence, the probability of large rock falls from warming permafrost in steep to near-vertical rock walls is increasing. The process of rock destabilization by permafrost thaw is supported by observational evidence and theoretical consideration (Gruber & Haeberli 2007). However, we know little about the dominant processes responsible. Frequent rock fall during the extremely hot and dry summer 2003 in the Alps occurred in July, long before the active layer reached its maximum depth and long before it exceeded maximum thaw depths of previous years based on pure heat conduction modeling (Gruber et al. 2004c). Failure is therefore likely to have taken place under the influence of factors other than pure thaw to excessive depths. This finding points to the role of fast linear thaw along joint systems by heat advection during water transport. The influence of melt water penetrating into partially frozen rock may also be a reason for the strikingly high proportion of detachment zones from partially or at last strongly asymmetrically frozen summits and crests with marginal or even absent permafrost on the warm side. Reanalysis of recent rock falls (cf. Fischer et al. 2006, Noetzli et al. 2003) using energy balance modeling for defining pre-failure thermal conditions in the detachment zones is presently being undertaken in the Swiss Alps. International collaboration and exchange of information is important in order to expand the sample size and to enable reliable statistical analysis.

Flow and Stability of Ice-Rich Frozen Debris

The number of observations concerning flow phenomena in mountain permafrost using high-precision photogrammetry, geodesy and borehole measurements as combined with relative and absolute age dating and numerical modeling is rapidly increasing. The corresponding evidence now provides a quite coherent image of the processes, which govern cumulative long-term deformation of perennially frozen debris (talus, moraines etc.) containing ice in excess of the pore volume available between the rock particles under unfrozen conditions (Haeberli et al. 2006). Corresponding steady-state creep of ice-supersaturated debris over millennia —most probably since the end of the last Ice Age—led to the formation of the widespread and spectacular landforms called (active) rock glaciers. A major part of the straining obviously takes part within discrete shear horizons. The deforming fine-grained material from the upper part of talus cones thereby carries large blocks at its surface, which were deposited at the foot of the same talus cones, ride along the flow trajectory with maximum (surface) speed and, therefore, fall over the rock glacier front (where the creeping fine-grained material is exposed again), are overridden and

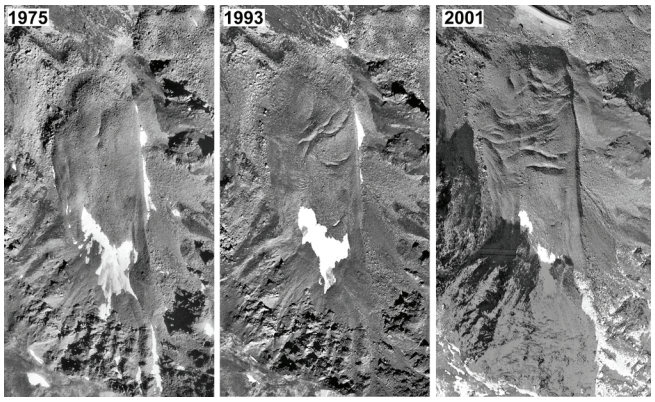

Figure 5. Grueo 1 rock glacier in the Turtmann Valley (Swiss Alps) showing signs of accelerating flow and intense crevasse formation (from Roer 2007).

form a saturated "structured" permafrost layer at depth with damped creep behavior. Seasonal and inter-annual variations of surface velocity can be observed where the permafrost base is not in bedrock but in non-frozen sediments.

The most surprising recent observation concerns the spectacular inter-annual variations of flow velocity as documented over wide areas in the European Alps in connection with the extremely hot/dry summer of 2003 (Delaloye et al. 2008, Kääb et al. 2006). Many rock glaciers with fronts near the local boundary of permafrost occurrence accelerated their flow speed almost simultaneously in the same year 2003 by a factor of two to five or even more and then more steadily decelerated to average long-term flow rates over the following about three years with less extreme conditions. The processes explaining this striking regional-scale phenomenon still remain to be explained (Roer et al. 2008). Rheological softening of ice/rock-mixtures by permafrost warming at temperatures close to phase equilibrium and at depths close to the expected shear horizons may have been part of the answer (Kääb et al. 2007). Increased melt water infiltration into already "temperate" or at least very warm permafrost may have been another contribution (Ikeda et al. 2007). Higher water pressure causing softening of subpermafrost sediments may also have come into play and enhanced mobility within the shear horizon itself cannot be excluded either. Continued high-resolution flow observations will help clearing the difficult question about corresponding interactions between the processes mentioned. Already now, however, the stability problem connected with warm permafrost in rock glaciers on steep mountain slopes received a new dimension. With the formation of striking crevasse patterns as a result of accelerated flow (Fig. 5, Roer et al. 2005), strong heterogeneities with respect to cohesion, hydraulic permeability and stress distribution developed within the creeping permafrost: possibilities for the triggering of debris flows and even landslides in such cases is no more restricted to the over-steepened frontal parts of rock glaciers alone (cf. Arenson et al. 2002).

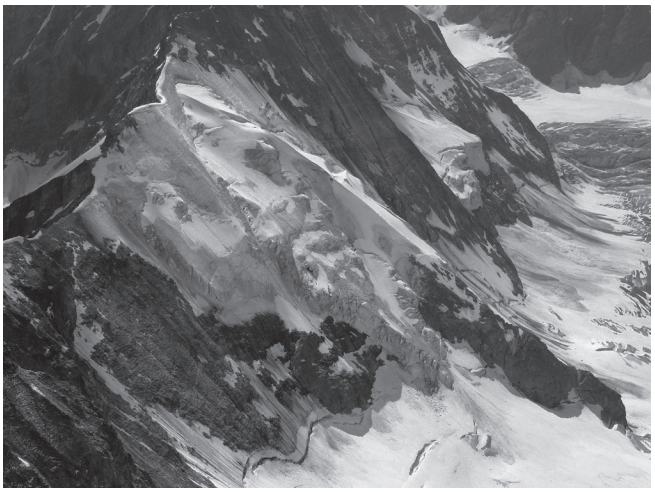
Figure 6. Hanging glaciers and ice faces on the northern side of the ridge extending between the Matterhorn and the Dent d'Herens along the border between Switzerland and Italy. Interactions between polythermal surface ice and subsurface permafrost are complex, especially with conditions of rapid atmospheric warming. Photo by S. Gruber.

Glacier-Permafrost Interactions

Interactions between glaciers and permafrost are widespread in regions with moderately to strongly continental climate, because the equilibrium line on glaciers is situated inside zones and altitudinal belts with discontinuous and continuous permafrost occurrence. Information concerning this important aspect is sparse at present (Haeberli 2005), especially because the scientific communities involved in permafrost and glacier research still communicate far too little. Results from geophysical soundings, miniature temperature data-logging, shallow borehole observations and photogrammetric movement determinations show that subsurface ice in glacier forefields successively exposed since the end of the Little Ice Age is often polygenetic (Kneisel 2003). It is most likely derived from recent ground freezing in cold microclimates of formerly temperate bed parts after glacier retreat, preservation of former subglacial permafrost underneath cold marginal parts of polythermal glaciers, burial of "dead ice" from the glacier itself or a combination of these processes. Ice-containing parts of morainic deposits commonly show signs of lateral flow and vertical displacements (heave, subsidence, cf. Kääb & Kneisel 2006).

Most important questions concern the evolution of permafrost in recently deglaciated moraines under the influence of changing surface conditions and continued atmospheric warming at lower altitudes and the thermal structure and stability of high-altitude hanging glaciers in steep, perennially frozen rock walls at higher elevations (cf. Gruber & Haeberli 2007). The stability of often polythermal hanging glaciers with temperate and permeable firn behind and above cold and rather impermeable cliffs (Fig. 6) and their thermal and hydraulic interaction with the permafrost inside the underlying rock walls (Lüthi & Funk 1997) may indeed

constitute a key factor concerning large ice/rock avalanches with extremely far runout (Haeberli et al. 2004, Huggel et al. 2005). At a different level of process understanding, another common phenomenon deserves much more attention: basal regelation layers of glaciers are nothing else than epigenetic permafrost in fine grained sediments—often with large amounts of excess ice and ice lenses—attached to the base and deforming under peak stresses and at maximum strain rates of the corresponding glaciers. Improved knowledge about the rheology of the involved creep phenomena would provide essential insights with respect to non-isotropic flow characteristics of ice sheets, glaciers and rock glaciers.

Spatial Patterns and 4D-Evolution of Permafrost in Mountain Topography

Spatial distribution patterns of permafrost in complex high-mountain topography can be estimated by distributed modeling of the surface energy balance and sub-surface heat transfer. However, this implies knowledge of surface and sub-surface characteristics, proper initialization techniques, as well as methods for snow redistribution by wind and avalanches (Gruber 2007). Full energy balance models (e.g., Lehning et al. 2002) can make use of high (hourly or more frequent) time resolution, and thus resolve effects like the diurnal variability of convective cloud formation that often can have an essential influence on spatial ground temperature distribution.

A variety of models from empirical-statistical to more process-oriented approaches have so far been used with considerable success (Etzelmüller et al. 2001, Gruber & Hoelzle 2001). The Swiss Federal authorities have now produced a 1:50,000 map of permafrost distribution for the entire Swiss Alps. The model used for producing this map is more empirical-statistical but includes a discrimination between steep rock faces with little snow and less inclined slopes with thick winter snow (Gruber et al. 2006). First experiments with coupling regional climate models and GIS-based impact models indicate that warming trends are stronger in north-facing (shadow) than on sunny south-exposed slopes, because the relative influence of sensible heat effects in comparison to solar radiation is stronger (Salzmann et al. 2007). First successful attempts have also been made to couple surface energy balance with heat diffusion at depth for high mountains (Noetzli et al. 2007).

The main steps to follow this successful development consist in expanding such spatial modeling to all cold mountains on earth based, for instance, on SRTM or ASTER digital elevation and global climate data or model scenarios. Another important progress would be to further improve and validate modeling also on less inclined slopes covered by thicker and more irregular snow cover including cases with high ice contents using transient modeling. A possible result could be the coupling of thermal and geomorphic spatial models such as the modeling of creep phenomena as demonstrated in first encouraging attempts by Frauenfelder (2005). There is, undoubtedly, a long way to go for even partially reaching such research goals. However, already relatively rough approaches and early accomplishments could help with making it clear to scientists as well as policymakers and the public that permafrost belongs to the primary characteristics of cold mountain areas, that it relates to many other phenomena like snow, glaciers, erosion or slope stability, and that atmospheric warming causes growing disequilibria already now but even much more so in the foreseeable future.

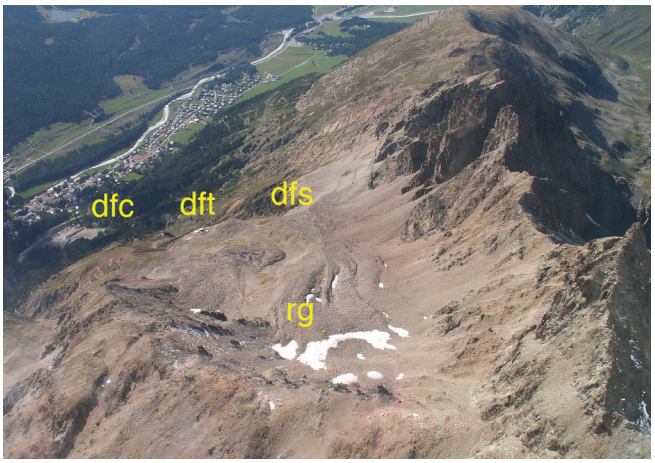

Figure 7. Creeping permafrost (rock glaciers rg) and debris flow starting zone (dfs), trajectory (dft) and cone (dfc) above Potresina (Swiss Alps). Note recently constructed avalanche and debris flow retention dam on cone. Photo by C. Rothenbühler.

Hazards Related to Rock Falls and Debris Flows from Permafrost Slopes

Debris flows from rock glaciers and moraines in permafrost areas (Fig. 7) can be among the largest debris flow events in mountain areas and cause devastating damage to settlements and infrastructure in valley bottoms.

Large-scale rock falls from steep to near-vertical rock faces seem to take place at increasing frequency and can propagate to areas far below timberline. They can dangerously erode or mobilize thick snow packs, glaciers, or water bodies, thereby undergo process changes, transform into high-speed flows or trigger flood waves which can reach extremely far runout distances and cause severe damage to human lives and economy. In the Swiss Alps, for instance, the 500,000 m^3 debris flow at Guttannen in 2005—probably the largest during decades back in time—started from a large moraine accumulation where (rather marginal) permafrost may have helped to transfer the water runoff from extreme precipitation to cross the flat cirque floor and to reach the steep outer moraine slopes. In the valley bottom, the large deposited debris volume dammed the Aare river which itself had peak flood discharge and soon started to overflow the debris dam and to cut a new bed on the other side of the principal road. As a logical consequence, the large river reached and damaged the village before heavy machines could cut an opening through the road and force the river back into its abandoned bed.

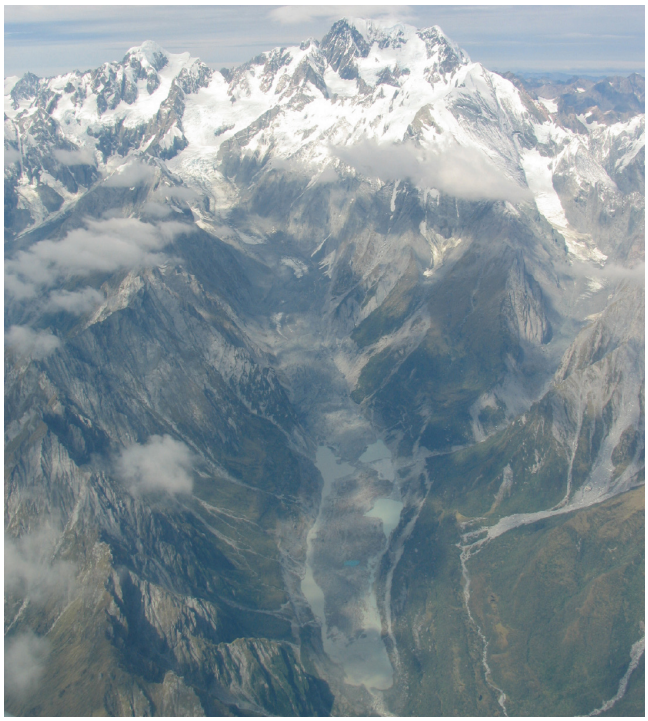

Figure 8. Disintegrating glacier tongue and formation of a large lake in the New Zealand Alps. Such lakes constitute an increasing hazard potential with respect to flood-waves triggered by rock falls from deglaciated slopes and/or slopes with warming and degrading permafrost. Photo by M. Hoelzle.

In the Caucasus, a combined ice/rock avalanche from the perennially frozen north wall of Dzimarai Khkok near Kazbek volcano eroded a medium size debris-covered glacier almost entirely. The mobilized mass squeezed out large amounts of probably subglacial water, turned into a high-speed two-phase mass flow and traveled over a runout distance of about 33 kilometers. Rivers from tributary valleys were dammed by the deposits to form lakes drowning parts of a local village and constituting a flood wave threat to people even in settlements situated far downstream (Haeberli et al. 2004, Huggel et al. 2005). Despite large uncertainties involved with the present understanding about the exact triggering and flow mechanisms of such events, hazard potentials from similar future phenomena must be anticipated and assessed at the best possible level of experience and knowledge.

GIS-based models to estimate flow paths and runout distances of ice/rock avalanches and debris flows in rugged high-mountain topography exist and can be applied already now (Huggel et al. 2003, Noetzli et al. 2006). Perhaps the most urgent need concerns the possibility of large ice/rock falls into existing lakes or lakes that newly form as a consequence of glacier retreat and downwasting (Haeberli & Hohmann 2008, Fig. 8). Debuttressing of formerly glacierized valley walls in combination with permafrost warming could thereby be an especially critical condition. In fact, primary factors influencing the stability of steep permafrost slopes are:

- slope inclination and topographically unsupported parts;
- geological structure (layer dipping, crack density and orientation);
- permafrost conditions (temperature, ice content, hydraulic permeability); and
- topographic evolution (erosion, glacier vanishing, earlier events).

Among these factors, permafrost and glacier conditions are changing most rapidly. Together with slope inclination, they can be spatially modeled in order to find most critical factor combinations. In a second step, possible flow trajectories of avalanches from such sites and their potential interactions and process chains involving snow, glaciers and/or water bodies could be modeled in order to detect places of highest risk. Such preliminary analyses over large areas would help to direct more detailed geological investigations and to establish focused monitoring or adequate protection measures. Integrative hazard assessment is far more than an academic idea: the potential for very large catastrophes is neither negligible nor undetectable. It rises at an accelerating rate with continued deep warming of high mountain permafrost, rapid glacier vanishing and drastic changing of alpine landscapes and habitats.

Further Issues and Perspectives

Besides the concrete challenges mentioned with respect to the described specific topics, three important challenges can be envisaged for future research on mountain permafrost: (a) holistic understanding; (b) increasingly quantitative methods; and (c) applied research. Holistic understanding is the broad understanding of all permafrost and its role in mountain landscapes. Our understanding at present is largely focused on special cases such as rock glaciers or steep bedrock but in fact, most permafrost has characteristics that lie in between these two cases and that are poorly constrained. Also, the transient interaction between permafrost and glaciers or the long-term influence of permafrost on the evolution of mountain topography remains largely unknown. Quantitative methods are necessary in order to understand and disentangle processes of increasing complexity. This requires not only infrastructure (such as data and models), but also novel concepts for the validation of models and for the analysis of uncertainty and scale issues that are among the most prominent characteristics of quantitative research in mountain areas. Applied research, for example in collaboration with public authorities or operators of high-elevation infrastructure, helps to transfer knowledge and evidence between researchers and people who work in permafrost environments on a daily basis, and, it is important in order to remain focused on research areas of direct importance to society.

Acknowledgments

Our special thanks go to all friends and colleagues who share with us the fascination and learning process related to mountain permafrost research. Their scientific progress, open discussions and feedbacks formed the basis of this review. An anonymous reviewer provided constructive comments.

References

Arenson L.U. 2002. Unstable Alpine permafrost: a potentially important natural hazard: Variations of geotechnical behaviour with time and temperature. Ph.D. Thesis No 14801, Inst. for Geotechnical Engineering, ETH, Zurich, 271.

Barsch, D. 1978. Active rock glaciers as indicators for discontinuous alpine permafrost – an example from the Swiss Alps. *Proceedings of the Third International Conference on Permafrost*, NRC Ottawa, 1, 349-3353.

Barsch, D. 1992. Permafrost creep and rock glaciers. *Permafrost and Periglacial Processes* 3/3: 175-188.

Davies, M., Hamza, O. & Harris, C. 2001. The effect of rise in mean annual temperature on the stability of rock slopes containing ice-filled discontinuities, *Permafrost Periglacial Processes* 12(1): 137-144.

Delaloye, R., Perruchoud, E., Avian, M., Kaufmann, V., Bodin, X., Hausmann, H., Ikeda, A., Kääb, A., Kellerer-Pirklbauer, A., Krainer, K., Lambiel, C., Mihajlovic, D., Staub, B., Roer, I. & Thibert. E. 2008. Recent interannual variations of rock glaciers creep in the European Alps. Proceedings of the 9th International Conference on Permafrost 2008, Fairbanks, Alaska, USA. This volume.

Etzelmüller, B., Hoelzle, M., Soldjørg, Flo, Heggem, E., Isaksen, K., Mittaz, C., Vonder Mühll, D., Ødegard, R.S., Haeberli, W. & Sollid, J.L. 2001. Mapping and modelling the occurrence and distribution of mountain permafrost. *Norsk Geografisk Tidsskrift* 55: 186-194.

Fischer, L., Kääb, A., Huggel, C. & Noetzli, J. 2006. Geology, glacier changes, permafrost and related slope instabilities in a high-mountain rock wall: Monte Rosa east face, Italian Alps. *Natural Hazards and Earth System Science* 6: 761-772.

Frauenfelder, R. 2005. Regional-scale modeling of the occurrence and dynamics of rockglaciers and the distribution of paleopermafrrost. Schriftenreihe Physische Geographie: Glaziologie und Geomorphodynamik 45, University of Zurich, 202 pp.

Fujii, Y. & Higuchi, K. 1978. Distribution of alpine permafrost in the northern hemisphere and its relation to air temperature. *Proceedings of the Third International Conference on Permafrost*, NRC Ottawa, 1, 367-371.

Gorbunov, A.P. 1978. Permafrost in the mountains of central Asia. *Proceedings of the Third International Conference on Permafrost*, NRC Ottawa, 1, 372-377 (in Russian).

Gruber, S. 2007. MTD: a mass-conserving algorithm to parameterize gravitational transport and deposition processes using digital elevation models. *Water Resources Research* 43, W06412, doi:10.1029/2006WR004868.

Gruber, S. & Haeberli, W. 2007. Permafrost in steep bedrock slopes and its temperature-related destabilization following climate change. *Journal of Geophysical Research* 112: F02S18, doi:10.1029/2006JF000547.

Gruber, S. & Haeberli, W. 2008. (in press) Mountain permafrost. Mountain Permafrost. In: *Permafrost Soils,* edited by: Margesin, R., Biology Series, Springer.

Gruber, S. & Hoelzle, M. 2001. Statistical modelling of mountain permafrost distribution – local calibration and incorporation of remotely sensed data. *Permafrost and Periglacial Processes* 12(1): 69-77, doi: 10.1002/ppp.374.

Gruber, S., Haeberli, W., Krummenacher, B., Keller, F., Mani, P., Hunziker, G., Hölzle, M., Vonder Mühll, D., Zimmermann, M., Keusen, H.-R., Götz, A. & Rätzo, H. 2006. Erläuterungen zur Hinweiskarte der potentiellen Permafrostverbreitung in der Schweiz 1:50'000. Bundesamt für Umwelt (BAFU) / Swiss Federal Office for the Environment.

Gruber, S., Hoelzle, M. & Haeberli, W. 2004a. Permafrost thaw and destabilization of Alpine rock walls in the hot summer of 2003. *Geophysical Research Letters* 31: L13504, 4pp, doi:10.1029/2006JF000547.

Gruber, S., Hoelzle, M. & Haeberli, W. 2004b. Rock wall temperatures in the Alps – modelling their topographic distribution and regional differences. *Permafrost and Periglacial Processes* 15(3): 299-307, doi: 10.1002/ppp.501.

Gruber, S., King, L., Kohl, T., Herz, T., Haeberli, W. & Hoelzle, M. 2004c. Interpretation of geothermal profiles perturbed by topography: the Alpine permafrost boreholes at Stockhorn Plateau, Switzerland. *Permafrost and Periglacial Processes* 15(4): 349-357, doi:10.1002/ppp.503.

Gruber, S., Peter, M., Hoelzle, M., Woodhatch, I. & Haeberli, W. 2003. Surface temperatures in steep Alpine rock faces: a strategy for regional-scale measurement and modelling. *Proceedings of the 8th International Conference on Permafrost 2003*, Zurich, Switzerland: 325-330.

Guodong, Ch. & Dramis, F. 1992. Distribution of mountain permafrost and climate. *Permafrost and Periglacial Processes* 3/2: 83-91.

Haeberli, W. 1978. Special aspects of high mountain permafrost methodology and zonation in the Alps. *Proceedings of the Third International Conference on Permafrost*, NRC Ottawa, 1: 379-384.

Haeberli, W. 1992. Construction, environmental problems and natural hazards in periglacial mountain belts. *Permafrost and Periglacial Processes* 3/2: 111-124.

Haeberli, W. 1996. On the morphodynamics of ice/debris-transport systems in cold mountain areas. *Norsk Geografisk Tidsskrift* 50: 3-9.

Haeberli, W. 2005. Investigating glacier-permafrost relationships in high-mountain areas: historical background, selected examples and research needs. In: Harris, C. & Murton, J. B. (eds): Cryospheric Systems: Glaciers and Permafrost, The Geological Society of London, Special Publication 242, 29-37.

Haeberli, W. & Gruber, S. 2008. (in press) Global warming and mountain permafrost. In: *Permafrost Soils,* edited by: Margesin, R., Biology Series, Springer.

Haeberli, W. & Hohmann, R. 2008. Climate, glaciers and permafrost in the Swiss Alps 2050: scenarios, consequences and recommendations. Proceedings of the 9th International Conference on Permafrost 2008, Fairbanks, Alaska, USA. This volume.

Haeberli, W., Hallet, B., Arenson, L., Elconin, R., Humlum, O., Kääb, A., Kaufmann, V., Ladanyi, B., Matsuoka, N., Springman, S. & Vonder Mühll, D. 2006. Permafrost creep and rock glacier dynamics. *Permafrost and Periglacial Processes* 17/3: 189-214. (doi: 10.1002/ppp).

Haeberli, W., Huggel, C., Kääb, A., Zgraggen-Oswald, S., Polkvoj, A., Galushkin, I., Zotikov, I. & Osokin, N. 2004. The Kolka-Karmadon rock/ice slide of 20 September 2002: an extraordinary event of historical dimensions in North Ossetia, Russian Caucasus, *Journal of Glaciology* 50/171: 533-546.

Hanson, S. & Hoelzle, M. 2004. The thermal regime of the active layer at the Murtèl rock glacier based on data from 2002. *Permafrost Periglacial Processes* 15(3): 273-282.

Harris, C. 2008. (Plenary presentation), Proceedings of the 9th International Conference on Permafrost 2008, Fairbanks, Alaska, USA. This volume.

Harris, C., Haeberli, W., Vonder Muehll, D. & King, L. 2001. Permafrost monitoring in the high mountains of Europe: the PACE Project in its global context. *Permafrost and Periglacial Processes* 12(1): 3-11

Harris, C., Arenson, L.U., Christiansen, H.H., Etzelmüller, B., Frauenfelder, R., Gruber, S., Haeberli, W., Hauck, C., Hölzle, M., Humlum, O., Isaksen, K., Kääb, A., Lehning, M., Lütschg, M.A., Matsuoka, N., Murton, J.B., Nötzli, J., Phillips, M., Ross, N., Seppälä, M., Springman, S.M. & Vonder Mühll, D. 2007. (In review.) Permafrost and climate in Europe: geomorphological impacts, hazard assessment and geotechnical response. *Earth Science Reviews.*

Harris, C., Vonder Mühll, D., Isaksen, K., Haeberli, W., Sollid, J., King, L., Holmlund, P., Dramis, F., Guglielmin, M. & Palacios, D. 2003. Warming permafrost in European mountains. *Global and Planetary Change* 39: 215–225.

Harris, S. & Brown, R.J.E. 1978. Plateau Mountain: a case study of alpine permafrost in the Canadian Rocky Mountains. *Proceedings of the Third International Conference on Permafrost*, NRC Ottawa, 1, 386-391.

Harris, S. & Corte, A. 1992. Interactions and relations between mountain permafrost, glaciers, snow and water. *Permafrost and Periglacial Processes* 3/2: 103-110.

Hasler, A., Talzi, I., Beutel, J., Tschudin, C. & Gruber, S. 2008. Wireless sensor networks in permafrost research – concept, requirements, implementation and challenges, Proceedings of the 9th International Conference on Permafrost 2008, Fairbanks, Alaska, USA. This volume.

Hauck, C., & Vonder Mühll, D. 2003. Inversion and interpretation of two-dimensional geoelectrical measurements for detecting permafrost in mountainous regions. *Permafrost Periglacial Processes* 14: 305-318.

Hoelzle, M. & Gruber, S. 2008. Borehole and ground surface temperatures and their relationship to meteorological conditions in the Swiss Alps, Proceedings of the 9th International Conference on Permafrost 2008, Fairbanks, Alaska, USA. This volume.

Huggel, C., Kääb, A., Haeberli, W. & Krummenacher, B. 2003. Regional-scale GIS-models for assessment of hazards from glacier lake outbursts: evaluation and application in the Swiss Alps. *Natural Hazards and Earth System Sciences* 3 (6): 647-662.

Huggel, C., Zgraggen-Oswald, S., Haeberli, W., Kääb, A., Polkvoj, A., Galushkin, I. & Evans, S.G. 2005. The 2002 rock/ice avalanche at Kolka/Karmadon, Russian Caucasus: assessment of extraordinary avalanche formation and mobility, and application of QuickBird satellite imagery. *Natural Hazards and Earth System Sciences* 5: 173-187.

Ikeda, A., Matsuoka, N. & Kääb, A. 2008 (in press). The role of liquid water in the fast deformation of perennially frozen ground. A case study on a rock glacier in the Swiss Alps. *Journal of Geophysical Research.*

IPCC 2007. Climate Change 2007. Intergovernmental Panel on Climate Change, Cambridge and New York. Various reports.

Isaksen, K., Sollid, J., Holmlund, P. & Harris, C. 2007. Recent warming of mountain permafrost in Svalbard and Scandinavia. *Journal of Geophysical Research* 112: F02S04, doi:10.1029/2006/F000522.

Jin, H., Li, S., Cheng, G., Wang, S. & Li, X. 2000. Permafrost and climate change in China. *Global and Planetary Change*. 26 (4), 387-404.

Kääb, A., Frauenfelder, R. & Roer, I. 2006. On the response of rockglacier creep to surface temperature increases. *Global and Planetary Change* 56(1-2): 172-187.

Kääb, A. & Kneisel, C. 2006. Permafrost creep within a recently deglaciated glacier forefield: Muragl, Swiss Alps. *Permafrost and Periglacial Processes* 17(1): 79-85.

Keller, F. & Gubler, H.U. 1993. Interaction between snow cover and high mountain permafrost at Murtèl/ Corvatsch, Swiss Alps. *Proceedings of the 6th International Conference on Permafrost (Bejing, China),* South China University of Technology Press, 332-337.

King, L., Gorbunov, A.P. & Evin, M. 1992. Prospecting and mapping of mountain permafrost and associated phenomena. *Permafrost and Periglacial Processes* 3/2: 73-81.

Kneisel, C. 2003. Permafrost in recently deglaciated glacier forefields – measurements and observations in the eastern Swiss Alps and in northern Sweden. Zeitschrift für Geomorphologie 47, 289-305.

Krautblatter, M. & Hauck, C. 2007. Electrical resistivity tomography monitoring of permafrost in solid rock walls. *Journal of Geophysical Research* 112, F02S20. doi:10.1029/2006JF000546.

Lautridou, J.P., Francou, B. & Hall, K. 1992. Present-day periglacial processes and landforms in mountain areas. *Permafrost and Periglacial Processes* 3/2: 93-101.

Lehning, M., Bartelt, P.B., Brown, R.L., Fierz, C. & Satyawali, P. 2002. A physical SNOWPACK model for the Swiss Avalanche Warning Services. Part III: meteorological boundary conditions, thin layer formation and evaluation. *Cold Reg. Sci. Technol.*, 35: 169-184.

Lüthi, M. & Funk, M. 1997. Wie stabil ist der Hängegletscher am Eiger? *Spektrum der Wissenschaft* 97(5): 21-24.

Lütschg, M., Bartelt, P., Lehning, M., Stoeckli, V. & Haeberli, W. 2003. Numerical simulation of the interaction processes between snow cover and alpine permafrost. *Proceedings of the 8th International Conference on Permafrost 2003*, Zurich, Switzerland, 697-702

Marchenko, S.S., Gorbunov, A.P. & Romanovsky, V.E. 2007. Permafrost warming in the Tien Shan mountains, Central Asia. *Global and Planetary Change* 56 (3-4): 311-327.

Noetzli, J., Gruber, S., Kohl, T., Salzmann, N. & Haeberli, W. 2007. Three-dimensional distribution and evolution of permafrost temperatures in idealized high-mountain topography. *Journal of Geophysical Research* 112, F02S13, doi:10.1029/2006JF000545.

Noetzli, J., Hoelzle, M. & Haeberli, W. 2003. Mountain permafrost and recent Alpine rock-fall events: a GIS-based approach to determine critical factors. *Proceedings of the 8th International Conference on Permafrost 2003*, Zurich, Switzerland, 827-832.

Noetzli, J., Hilbich, C., Hoelzle, M., Hauck, C., Gruber, S. & Krauer, M. 2008. Comparison of transient 2D temperature fields with time-lapse electrical resistivity data at the Schilthorn Crest, Switzerland, Proceedings of the 9th International Conference on Permafrost 2008, Fairbanks, Alaska, USA. This volume.

Noetzli, J., Huggel, C., Hoelzle, M. & Haeberli, W. 2006. GIS-based modelling of rock-ice avalanches from Alpine permafrost areas. *Computational Geosciences* 10: 161-178 (doi: 10.1007/s10596-005-9017z).

Roer, I. 2007. Rockglacier kinematics in a high mountain geosystem. Bonner Geographische Abhandlungen 117.

Roer, I., 2008. Observations and considerations on destabilizing active rockglaciers in the European Alps. Proceedings of the 9th International Conference on Permafrost 2008, Fairbanks, Alaska, USA. This volume.

Roer, I., Kääb, A. & Dikau, R., 2005. Rockglacier acceleration in the Turtmann valley (Swiss Alps) - probable controls. *Norwegian Journal of Geography* 59 (2), 157-163.

Sass, O. 2003. Moisture distribution in rockwalls derived from 2D-resistivity measurements. *Z. Geomorph. Suppl.* 132: 51- 69.

Salzmann, N., Noetzli, J., Hauck, C., Gruber, S. & Hoelzle, M. 2007. RCM-based ground surface temperature scenarios in high-mountain topography and their uncertainty ranges. *Journal of Geophysical Research* 112, F02S12, doi:10.1029/2006JF000527.

Trombotto, D. 2000. Survey of cryogenic processe, periglacial forms and permafrost conditions in South America. *Revista Instituto Geologico* 21(1/2): 35-55.

UNEP 2007. Global Outlook for Ice & Snow, UNEP, Nairobi, Kenya.

Vonder Mühll, D., Arenson, L.U. & Springman, S.M. 2003. Temperature conditions in two Alpine rock glaciers. *Proceedings of the 8th International Conference on Permafrost 2003*, Zurich, Switzerland, 1195-1200.

Vonder Mühll, D., Noetzli, J. & Roer, I. 2008. PERMOS – a comprehensive monitoring network of mountain permafrost in the Swiss Alps, Proceedings of the 9th International Conference on Permafrost 2008, Fairbanks, Alaska, USA. This volume.

Climate, Glaciers, and Permafrost in the Swiss Alps 2050: Scenarios, Consequences, and Recommendations

Wilfried Haeberli
Glaciology, Geomorphodynamics & Geochronology, Geography Department, University of Zurich, Switzerland
Roland Hohmann
Environment, Traffic and Energy Division, B,S,S. Economic Consultants, Basel, Switzerland

Abstract

Climate scenarios for the time horizon of 2050 in the Swiss Alps, as simulated by using high-resolution ensemble modeling, indicate most likely changes in temperature/precipitation by + 2°C / + 10% in winter and + 3°C / - 20% in summer. Such a development would lead to the vanishing of about 75% of the existing glacier surface and deep warming of permafrost in mountain peaks. Corresponding impacts would mainly concern rather dramatic changes in landscape appearance, slope stability, and the water cycle. The formation of lakes in the forefields of retreating or even collapsing glaciers, together with the decreasing stability of rock walls, leads to an increasing probability of major rockfalls impacting onto water bodies and triggering dangerous flood waves. A special recommendation was therefore provided to systematically assess the safety of natural, artificial, and newly forming lakes in the Alps.

Keywords: climate change; cold mountains; glaciers; permafrost; slope stability.

Introduction

Climate change in cold mountain areas is faster than on the global average and strongly affects one of their most characteristic aspects – surface and subsurface ice (UNEP 2007). Increasing concentrations of greenhouse gases are likely to cause accelerating rates of change, which would lead within decades to environmental conditions far beyond historical and Holocene precedence and to commitments for the future probably lasting for centuries if not millennia. A primary challenge to cope with such a rather clearly foreseeable development is the anticipation of impacts from the reaction of complex, highly interconnected, and more and more disequilibrated natural systems (Watson & Haeberli 2004).

In March 2007, the Advisory Body on Climate Change created in 1996 by the Swiss Academy of Sciences on behalf of the Swiss Federal Government published a report on climate change and Switzerland for the year 2050 (OcCC 2007). Based on corresponding assessments for various sectors of the environment, the economy and the society, recommendations were prepared for the Swiss Federal Government. The present contribution deals with glaciers and permafrost in the Swiss Alps as an example of corresponding analyses and assessments relating to cold high-mountain regions at lower latitudes. It briefly summarizes the now-available knowledge based on climate projection and glacier and permafrost changes, and possibly resulting impacts. An example (Stein Glacier) is provided to emphasize the importance of combined glacier/permafrost considerations within the framework of recommendations to governmental policy makers.

Projections

Climate

Excellent data document the climate and its recent change in Switzerland. Atmospheric temperature rise during the 20th century was > 1°C and, hence, about twice the global average of 0.6°C. During the same time period, annual precipitation increased by some 8%. Due to the fact that evaporation also increased, river runoff remained more or less constant. The topography of the Alpine Mountain Chain only introduces relatively minor spatial variability of these changes with time.

Regional and seasonal climate change scenarios for Switzerland and the years 2030, 2050, and 2070 (Fig. 1) were calculated by Frei (2004) on the basis of the results from the EU-funded PRUDENCE project (Christensen et al. 2002). Uncertainties were estimated based on the distribution of the results from 16 model chains representing different combinations of 2 emission scenarios, 4 global, and 8 regional climate models. The estimates are based on the assumption that mitigation policies will only have a major influence in the second part of the 21st century and that the time horizon of 2050 could mark a transition to much more severe conditions at later stages. According to the applied scenario, temperatures will increase until 2050 with respect to 1990 by 1.8°C in winter (95% interval 0.9°C to 3.4°C) and 2.8°C (1.4°C to 4.9°C) in summer, both, north and south of the Alps. As a result the 0°C-isotherm will rise during winter by about 360 m (180 m to 680 m). Precipitation will increase by about 10% (-1% to +26%) in winter and decrease by about 20% (-36% to -6%) in summer. A trend towards more frequent and intense heat waves, probably also droughts, is expected in summertime. Cold waves in wintertime will probably decrease in number and intensity.

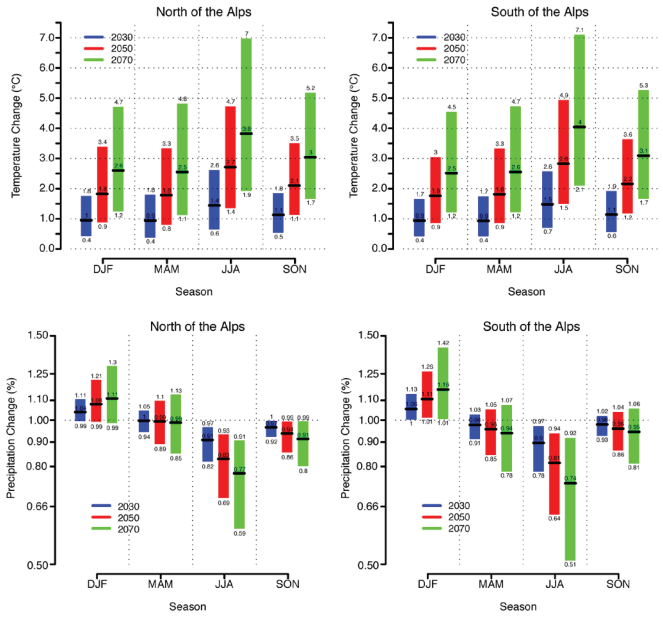

Figure 1. Seasonal climate scenarios (top: temperature, bottom: precipitation) for Switzerland and the years 2030, 2050, and 2070 for the parts north and south of the Alps (from OcCC 2007).

Glaciers

In the European Alps, a comprehensive database on glaciers and their long-term fluctuations has been built up over more than a century. This now enables the integration of *in situ* measurements (length change, mass balance), remote sensing (glacier inventories), digital terrain information, and numerical modeling for the entire mountain chain (Haeberli et al. 2007). The average loss in overall glacier volume was about 0.5% per year between 1850—the end of the Little Ice Age—and 1975, then increased to about 1% per year of the remaining volume between 1975 and 2000; and since the turn of the millennium, has accelerated to about 2–3% per year. The extremely hot and dry summer of 2003 alone eliminated some 8% of the remaining ice volume. Many glaciers started to waste down or even collapse and disintegrate rather than to actively retreat (Paul et al. 2007).

Alpine-wide estimates of future glacier evolution had first been made by Haeberli and Hoelzle (1995; cf. also Maisch et al. 2000, Maisch 2001) and proved to be rather robust. The latest and most differentiated model uses statistically calibrated relations between equilibrium line altitude as measured in long-term mass balance observations, summer temperature, and annual precipitation together with glacier inventory data and the SRTM3 digital elevation model (Zemp et al. 2006). Combination with the climate scenario applied for 2050 shows that the glacier surface area in the European Alps could be reduced with respect to conditions in 1971–1990 by a further 75% (50% to 95%) as soon as by 2050 (Fig. 2). Slightly smaller losses can be assumed for the Swiss Alps, where the largest glaciers exist. A remarkable part—roughly one-third—of this anticipated development has already taken place by now (in 2007).

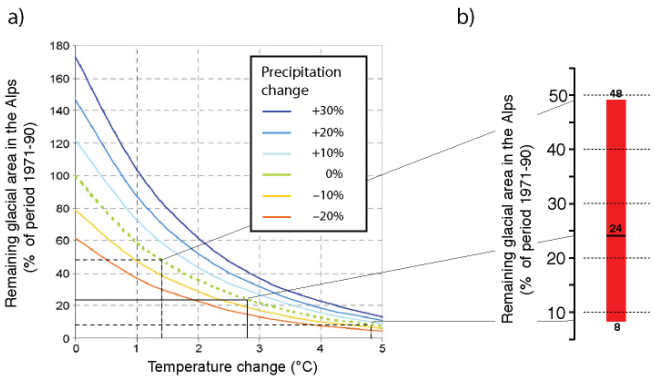

Figure 2. Glacier area in the Alps as a function of temperature and precipitation change: (a) as combined with the assumed climate scenario for 2050; (b) after Zemp et al. 2006, from OcCC 2007.

Permafrost

Systematic research on permafrost in the Alps only started well after World War II. First attempts to establish a long-term monitoring program began with the observation of borehole temperatures in the ice-rich debris of Murtèl rock glacier (Vonder Mühll & Haeberli 1991) and photogrammetric rock glacier monitoring (Haeberli et al. 1993). A decisive step forward was the installation of 100-m-deep bedrock boreholes in the permafrost of European mountains within the Permafrost and Climate in Europe (PACE) project (Harris et al. 2003). Numerical models for estimating spatial permafrost distribution patterns in the Swiss Alps were first applied by Keller et al. (1998). Most recently, a model simulation was done at a 1:50,000 scale for the entire Swiss Alps on behalf of the Federal Office for the Environment (FOEN). Permafrost in the Swiss Alps is now known to occupy a surface area, which is roughly twice as large as the glacierized area. Its development is observed within the framework of PERMOS (Permafrost Monitoring Switzerland; Vonder Mühll et al., 2008), one of the first networks of this kind.

Thermal conditions in commonly ice-rich permafrost in talus and moraines strongly depend on snow cover conditions and are thus difficult to predict. Because of latent heat effects, complete thawing of such frozen debris in any case takes many decades to centuries, even with warming to 0°C. Permafrost evolution in bedrock of steep mountain peaks with highly complex topography is less snow-dependent. The PACE boreholes indicate surface warming during the 20th century by about 0.5 to 1°C, and corresponding thermal anomalies (heat flow reduction) down to 50 70 m below surface. Future scenarios can be simulated using 3-dimensional transient heat diffusion models.

Corresponding calculations for idealized topographies (Noetzli et al. 2007) illustrate that the uppermost peaks are largely decoupled from the geothermal heat flow because of predominant lateral fluxes in strongly asymmetrical thermal fields and that warming trends can penetrate from two or more sides (Fig. 3). Due to the slow process of heat diffusion at depth, permafrost inside the mountains still persists after centuries, but with warmer if not near 0°C temperatures over wide altitudinal ranges and at great depths.

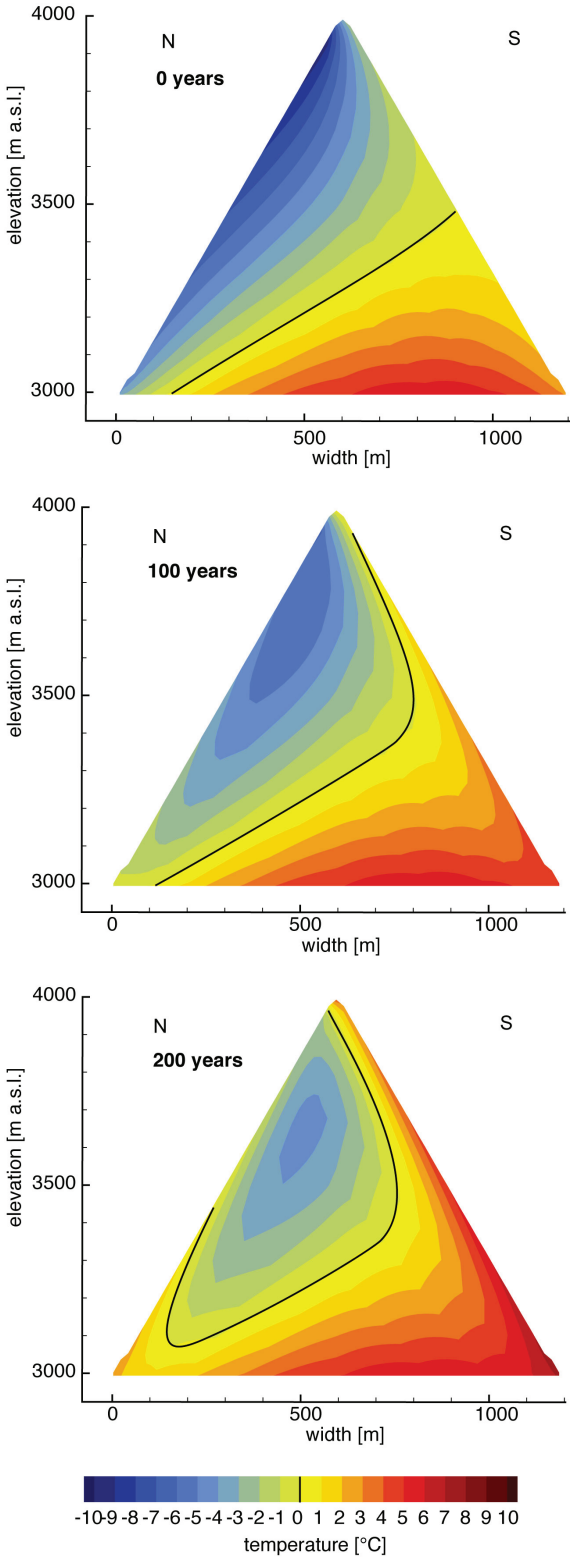

Figure 3. Model simulation (heat diffusion only) of the thermal field within a high Alpine mountain peak with realistic permafrost occurrence (from energy balance modeling), assumed centennial warming and idealized topography (after Noetzli et al. 2007; cf. OcCC 2007).

Impacts

Landscape and surface processes

Rapid glacier shrinkage is among the most obvious and visible phenomena related to ongoing warming trends. Already today, the perception of high-mountain landscapes is changing: the vanishing beauty of firn and ice as a symbol of an intact environment is more and more seen as a clear and easily understood indication of human-induced disturbance. In areas with a moderately humid to relatively dry climate, revegetation of newly exposed terrain is a slow process. For generations to come, therefore, deglaciated high-mountain chains will predominantly remain as areas of bare rock and debris without closed forests and mature soils (Egli et al. 2006). This will affect the attractiveness and touristic value of the respective landscape. Entire geo- and ecosystems as well as their individual parts have strongly different characteristics and time scales of response to fast climate change. This will undoubtedly lead to growing distances from conditions of dynamic equilibrium, which were able to form during the Holocene with its relatively stable climate.

One remarkable landscape element developing with continued atmospheric warming is the formation of new lakes with further glacier retreat and disintegration. Potential sites for future lake formation in over-deepened bed parts can be modeled by assuming constant basal shear stress along the central flow line, constant width-to-depth ratio of channel-type valley cross sections, and compressive flow connected with negative bed slopes. New lakes will thus most likely form where present-day low-slope ice surfaces, free of crevasses, have an enlarged width and grade into a narrower, steeper, and more or less heavily crevassed part in the flow direction (Fig. 4). Such lakes will be landforms of considerable attractiveness and, hence, to some degree compensate for the loss in landscape attractiveness from glacier disappearance. In many instances, however, they will be situated within an over-steepened and destabilized surrounding topography with enhanced periglacial-geomorphological activity. Corresponding slope stability problems would cause hazardous situations not known from the past. One example out of the number of possibilities is outlined below.

Natural hazards

Most critical stability conditions in perennially frozen rock walls are expected to be found in areas with warm permafrost (Davis et al. 2001, Noetzli et al. 2003, Gruber et al. 2004, Gruber & Haeberli 2007). Deep long-term warming of perennially frozen mountain peaks has the potential to bring steeply inclined rock layers to critical temperatures, not only over more extended vertical ranges but also to greater depths. As a consequence, the probability of large rockfalls is slowly increasing. Loss of support of steep slopes due to glacier disappearance leads to a reorientation of the stress field in adjacent slopes, and further contributes to the destabilization of rock walls above newly forming lakes. The possibility of flood waves from impacts of large rock, ice, snow or mixed avalanches must, therefore, be seriously considered.

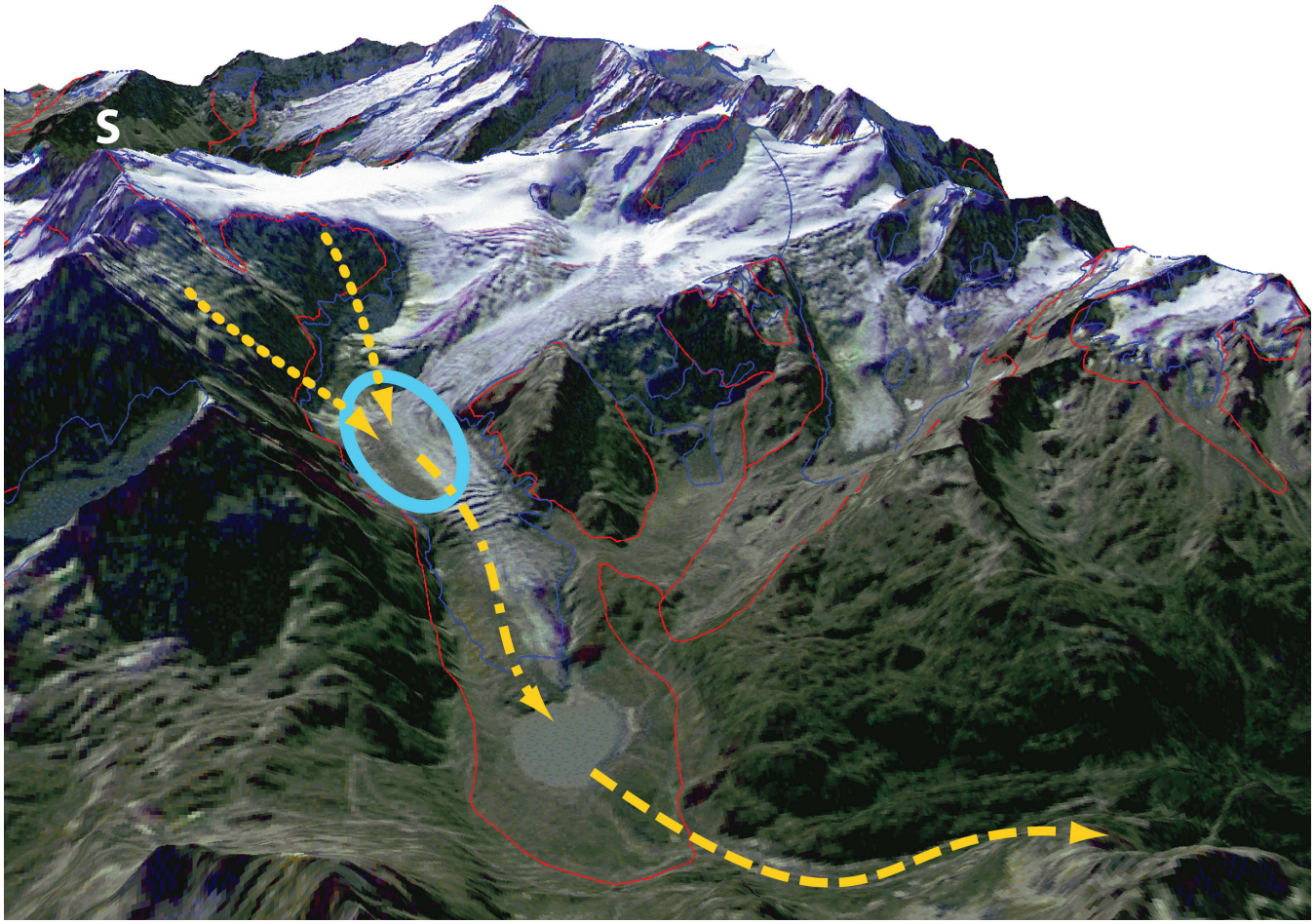

Figure 4: Modeled future development of a lake in an assumed overdeepened bed part of the Stein glacier near Sustenpass, Bernese Alps. Dotted lines indicate potential rock/ice avalanches from warming permafrost in the rock walls of Sustenhorn (S), dashed-dotted line related flood wave into the existing proglacial lake Steinsee, dashed line resulting flood wave from both lakes. Satellite image (combined SPOT/Landsat, September 1992) drawn over a DEM from swisstopo, image by F.Paul). Thin lines are former glacier margins (red 1850, blue 1973). Reproduced by permission of swisstopo (BA081042).

GIS-based models of trajectories from rock/ice avalanches can be applied for realistic assessments (Noetzli et al. 2006). The timing of the events, however, can involve long delays and is hardly predictable. The same is true, in principle, for debris flows, which can be triggered by intense convective summer precipitation events in, so far, glacier-covered starting zones with newly exposed moraine material. Examples of corresponding assessments for the Bernina group in the Upper Engadin were calculated by Rothen-Bühler (2006) within the framework of an integrative 4-dimensional geo-information system, which was built up as a tool for environmental planning in high mountain areas. Another case of a future hazard potential from flood waves caused by rock/ice avalanches from high/steep rock walls with warming permafrost into a modeled future lake replacing the now existing glacier surface is illustrated for Steingletscher/Sustenhorn (Bernese Alps) in Figure 4.

Water cycle

As a result of climate change, the maximum in river discharge will occur earlier in the year and will be less pronounced. The combined effect of increased precipitation and 0°C-isotherms at higher elevations will lead to a growing risk of winter flooding in lowlands surrounding the Alps, because greater percentages of liquid precipitation must be expected to runoff directly instead of being temporarily stored as snow. Drier summers, on the other hand, will lead to more frequent and especially more severe droughts. With conditions like in summer 2003 (stable high pressure over central Europe during several months) becoming near average in the second part of the century, the combination of missing precipitation, earlier snowmelt, and strongly reduced meltwater from disappearing glaciers could lower runoff to critical levels even in large Alpine rivers (Rhine, Rhone).

Despite the large water resources in the Alpine region, water stress could become a problem in some parts of Switzerland during the hot/dry season because of the decreasing availability of river water and its interconnection with soil humidity, water temperatures, lake/groundwater levels and aquatic ecosystems (fish, algae, etc.) and the increasing demands for domestic freshwater supply,

Figure 5: Detail of the map 1:50,000 with numerically simulated permafrost distribution as compiled for the entire Swiss Alps on behalf of the Federal Office for the Environment (BAFU/FOEN). The area is the same as on Figure 4. Yellow colors indicate relatively warm/thin, violet colors relatively cold/thick permafrost.

agriculture (irrigation), hydropower production, cooling of nuclear power plants, or even firefighting in desiccated forests. Conflicts about water use are likely to grow and options for adaptation—for instance, redefinition of the use of reservoirs at high-altitude (irrigation and summer power production rather than winter power production)—should be investigated as early as possible.

Conclusions and Recommendations

The "experiment with the global climate" has started. It cannot be stopped, but only be influenced. Grave consequences for cold mountain areas are unavoidable and are already developing at accelerating rates. Corresponding mitigation and adaptation measures must be planned. This primarily requires early and realistic anticipation of future developments and potential system reactions. The time scale to be considered involves several coming decades. As a consequence, rapid action is necessary. With modern digital terrain information, numerical and GIS-based models, and satellite imagery, all necessary technical means are available.

As a follow-up to the report on the climate in 2050 (OcCC 2007), a set of recommendations with respect to climate change impacts was provided to the Swiss Federal Government. Concerning Alpine glaciers and permafrost, the importance of adequate monitoring and the need for a systematic safety assessment of all existing natural and artificial lakes, as well as of all newly forming lakes, was emphasized. Perhaps the most important and most far-reaching statement, however, relates to the rights for the use of water, an aspect which may well become a central focus of living conditions and economic development in a rather near future.

At a national level, first steps have already been undertaken. The numerically modeled 1:50,000 permafrost map of the Swiss Alps, prepared on behalf of the Federal Office for the Environment (FOEN, Fig. 5), greatly helps with providing transparent information to authorities and raising public awareness. The Swiss Academy of Sciences, the Federal Office for the Environment, and MeteoSuisse, together, now definitely established the highly developed network Permafrost Monitoring in Switzerland (PERMOS), and the glacier monitoring network is being reorganized in order to integrate modern technologies and strategies according to international climate-related observing systems (GCOS 2003, 2004).

Acknowledgments

We thank all the numerous colleagues and experts who contributed to the original assessment reports. The interest, support, and excellent collaboration of the Swiss Academy of Sciences, the Federal Office for the Environment, and MeteoSuisse are gratefully acknowledged. Stephan Gruber, Jeannette Noetzli, Max Maisch, Frank Paul, and Isabelle Roer critically read an early draft of the present paper.

References

Christensen, J.H., Carter, T. & Giorgi, F. 2002. PRUDENCE employs new methods to assess European climate change. *EOS* 82: 147.

Davies, M., Hamza, O. & Harris, C. 2001. The effect of rise in mean annual air temperature on the stability of rock slopes containing ice-filled discontinuities. *Permafrost and Periglacial Processes* 12: 137-144.

Egli, M., Wernli, M., Kneisel, C., Biegger, S. & Haeberli, W. 2006. Melting glaciers and soil development in the proglacial area Morteratsch (Swiss Alps): II. Modeling the present and future soil state. *Arctic, Antarctic, and Alpine Research* 38/4: 510-521.

FOEN. 2007. Klimaänderung in der Schweiz – Indikatoren zu Ursachen, Auswirkungen, Massnahmen. Federal Office for the Environment, Switzerland.

Frei, C. 2004. Klimazukunft der Schweiz – eine probabilistische Projektion. (www.occc.ch/products/CH20250/CH2050-Scenarien.pdf).

GCOS. 2003. Second report on the adequacy of the Global Observing Systems for Climate in support of the UNFCCC. GCOS-82, WMO, Geneva.

GCOS. 2004. Implementation plan for the Global Observing System for Climate in support of the UNFCCC. GCOS-92, WMO, Geneva.

Gruber, S. & Haeberli, W. 2007. Permafrost in steep bedrock slopes and its temperature-related destabilization following climate change. *Journal of Geophysical Research* 112: F02S18 (doi:10.1029/2006JF000547).

Gruber, S., Hoelzle, M. and Haeberli W. 2004. Permafrost thaw and destabilization of Alpine rock walls in the hot summer of 2003. *Geophysical Research Letters*, 31/L13504.

Haeberli, W. & Hoelzle, M. 1995. Application of inventory data for estimating characteristics of and regional climate-change effects on mountain glaciers: a pilot study with the European Alps. *Annals of Glaciology* 21: 206-212. Russian translation in: *Data of Glaciological Studies*, Moscow, 82: 116-124.

Haeberli, W., Hoelzle, M., Keller, F., Schmid, W., Vonder Mühll, D. & Wagner, S. 1993. Monitoring the long-term evolution of mountain permafrost in the Swiss Alps. *Proceedings of the Sixth International Conference on Permafrost* 1: 214-219.

Haeberli, W., Hoelzle, M., Paul, F. & Zemp, M. 2007. Integrated monitoring of mountain glaciers as key indicators of global climate change: the European Alps. *Annals of Glaciology* 46: 150-160.

Harris, C., Vonder Mühll, D., Isaksen, K., Haeberli, W., Sollid, J.L., King, L., Holmlund, P., Dramis, F., Guglielmin, M. & Palacios D. 2003. Warming permafrost in European mountains. *Global and Planetary Change* 39: 215-225.

Keller, F., Frauenfelder, R., Gardaz, J.M., Hoelzle, M., Kneisel, C., Lugon, R., Phillips, M., Reynard, E. & Wenker, L. 1998. Permafrost map of Switzerland. *Proceedings of the 7th International Conference on Permafrost*, Yellowknife, Canada: 557-562.

Maisch, M., Wipf, A., Denneler, B., Battaglia, J. & Benz, Chr. 2000. Die Gletscher der Schweizer Alpen. Gletscherhochstand 1850, Aktuelle Vergletscherung, Gletscherschwund-Szenarien 21. Jahrhundert. NFP 31-Schlussbericht Teilprojekt 4031-033412, (1. Auflage 1999), 2. Auflage, 373p.

Maisch, M. 2001. The longterm signal of climate change in the Swiss Alps: Glacier retreat since the end of the Little Ice Age and future ice decay scenarios. *Geografia Fisisca e Dinamica Quaternaria* 23/2000, 139-151.

Noetzli, J., Gruber, S., Kohl. T., Salzmann, N. & Haeberli, W. 2007. Three-dimensional distribution and evolution of permafrost temperatures in idealized high-mountain topography. *Journal of Geophysical Research* 112: F02S13 (doi: 10.1029/2006JF000545).

Noetzli, J., Hoelzle, M. and Haeberli W. 2003. Mountain permafrost and recent Alpine rock-fall events: a GIS-based approach to determine critical factors. ICOP 2003 Permafrost: *Proceedings of the Eighth International Conference on Permafrost*, 21-25 July 2003, Zurich, Switzerland, A.A. Balkema Publishers 2, 827-832.

Noetzli, J., Huggel, C., Hoelzle, M. & Haeberli W. 2006. GIS-based modelling of rock-ice avalanches from Alpine permafrost areas. *Computational Geosciences* 10: 161-178 (doi: 10.1007/s10596-005-9017z).

OcCC. 2007. Klimaänderung und die Schweiz 2050 – erwartete Auswirkungen auf Umwelt, Gesellschaft und Wirtschaft. OcCC and ProClim, Swiss Academy of Sciences (Ed. R. Hohmann).

Paul. F., Kääb, A. & Haeberli, W. 2007. Recent glacier changes in the Alps observed by satellite: Consequences for future monitoring strategies. *Global and Planetary Change* 56: 111-122.

Rothenbühler, C. 2006. GISALP – räumlich-zeitliche Modellierung der klimasensitiven Hochgebirgslandschaft des Oberengadins. Schriftenreihe Physische Geographie (Universität Zürich), Glaziologie und Geomorphodynamik 50, 179p.

UNEP. 2007. Global outlook for ice and snow. United Nations Environment Programme, Nairobi (Kenya), Birkeland Trykkerri, Birkeland, Norway, 235 p.

Vonder Mühll, D. & Haeberli, W. 1990. Thermal characteristics of the permafrost within an active rock glacier (Murtèl/Corvatsch, Grisons, Swiss Alps). *Journal of Glaciology* 36/123: 151-158.

Vonder Mühll, D., Noetzli, J. and Roer, I. 2008. PERMOS: A comprehensive monitoring network of mountain permafrost in the Swiss Alps. This volume.

Watson, R. T. & Haeberli, W. 2004. Environmental threats, mitigation strategies and high-mountain areas. In: Royal Colloquium: Mountain Areas – a Global Resource; *Ambio* Special Report 13: 2-10.

Zemp, M., Haeberli, W., Hoelzle, M. & Paul, F. 2006. Alpine glaciers to disappear within decades? *Geophysical Research Letters* 33: L13504 (doi: 10.1029/2006GL026319).

Frost Boil Dynamics Using ^{210}Pb as a Tracer for Soil Movement

Birgit Hagedorn
University of Alaska Anchorage, Environment and Natural Resources Institute
Rolf Aalto
University of Exeter, Department of Geography
Ronald S. Sletten
University of Washington, Quaternary Research Center
Bernard Hallet
University of Washington, Quaternary Research Center

Abstract

Frost boils, also known as plugs or non-sorted circles, are non-sorted mineral soil centers surrounded by vegetation and occur throughout the Arctic. They influence surface albedo, soil temperature, soil stability, and consequently the distribution of vegetation; thus they are an important environmental factor in arctic landscapes. Numerous mechanisms for their initiation and maintenance have been proposed including: differential frost heave, convection cell-like cryoturbation, diapirism, and load casting; however, there are few techniques for direct observations. In this paper, we evaluate the natural, atmospheric-derived, radioactive isotope ^{210}Pb as a novel tracer of frost boil kinematics in a case study in northwestern Greenland, Pituffik Peninsula (76°N, 68°W). Once deposited, ^{210}Pb is strongly adsorbed to particle surfaces and decays with a half-life of 22.3 years; thus it is an excellent tracer for sediment motion up to approximately 80 years. Our first results confirm the usefulness of this tracer but also highlight necessary measurements and sampling strategies to fully interpret the ^{210}Pb distribution in frost boils.

Keywords: frost boil; High Arctic; patterned ground; ^{210}Pb tracer; plug.

Introduction

According to Washburn (1980:128), "Nonsorted circles are patterned ground whose mesh is dominantly circular and lacks a border of stones. The term mud-boil is frequently used in Canada for both nonsorted and sorted circles. Nonsorted circles are characteristically margined by vegetation, and occur singly or in groups…." Nonsorted circles, mudboils, or frost boils are found across the Arctic, where they are important environmental features (Walker et al. 2004). They influence microtopography, the abundance and distribution of vegetation, and therefore the temperature and moisture regime of the active layer (Roth & Boike 2001, Boike et al. 2002, Boike et al. 2007), which are important factors for the stability of permafrost as well as atmosphere-ground surface interaction. A thorough description of field observation and discussion of the diverse hypothesis of the genesis of plugs and plug circles is given by Washburn (1997).

From the 19 hypotheses for the formation of patterned ground reviewed by Washburn (1956), detailed descriptions during excavations and measurements of soil motion and soil physical parameters (Schmertmann & Taylor 1965, Washburn 1969, Nicholson 1976, Zoltai & Tarnocai 1981, Hallet & Prestrud 1986, Hallet et al. 1988, Washburn 1989, van Vliet-Lanoë 1991, Washburn 1997, Hallet 1998, Walker et al. 2004, Overduin & Kane 2006) as well as mathematical modeling approaches (Kessler et al. 2001, Kessler & Werner 2003, Peterson & Krantz 2003) indicate that cycles of freezing and thawing and of drying and wetting, inclined freezing fronts, buoyancy, and differential frost heave are the most important factors for the formation of circles, if sufficient fine soil (Goldthwait 1976) and water are present. In the case of unsorted circles (e.g., frost boils, mud boils, mud hummocks), gravity driven diapirism of water-oversaturated soil above permafrost has been suggested by Swanson et al. (1999) and Shilts (1978). Based on viscosity and density measurements, Swanson (1999) estimated that several decimeter of diapir movement could happen during a single thaw event (Swanson et al. 1999). Burial of organic rich surface material (e.g., Dyke & Zoltai 1980) along boil fringe suggests that some boils are closed systems where upward movement of soil in center causes lateral outward movement at surface and subsidence at the boil fringe (Mackay & MacKay 1976, Nicholson 1976, Dyke & Zoltai 1980, Mackay 1980, Zoltai & Tarnocai 1981, Washburn 1997). Such circulatory movement has mostly been attributed to inclining freezing front (Nicholson 1976), differential frost heave (Mortensen 1932, Hallet & Waddington 1991, van Vliet-Lanoë 1991), and freeze-thaw pumping (Mackay 1980, Veillette 1980). Dating of buried organic matter in three boils of central Canadian Arctic indicates subduction rates of organic material of ~1 mm yr^{-1} (Zoltai & Tarnocai 1981). However, even though distribution of organic material and radiocarbon dating gave indications of sediment motion, direct and detailed monitoring of sediment transport over longer (~100 years) time periods will greatly improve the understanding of the proposed mechanism.

Our study presents a new approach to trace sediment motion in frost boils using the radionuclide ^{210}Pb as tracer. ^{210}Pb is a natural product of the ^{238}U decay series and a direct

daughter of ^{222}Rn ($T_{1/2}$ 3.8 d). During ^{238}U decay in the soil, part of ^{222}Rn emanates into atmosphere where it decays to ^{210}Pb ($T_{1/2}$ 22.3 y). The ^{210}Pb is scavenged by aerosols, washed out by rain and snow, and deposited on the ground surface where it is strongly adsorbed to sediment grain surfaces. These chemical and physical characteristics of ^{210}Pb make it an excellent tracer of sediment transport processes in time and space. ^{210}Pb has been used in numerous applications including sedimentation and erosion processes in lacustrine, marine, and terrestrial environments (Appleby et al. 1979, Dörr 1995, Hagedorn et al. 1999, Walling et al. 2003, Aalto et al. 2008). To our knowledge, however, it has not been used in patterned ground studies. The half-life of ^{210}Pb limits its applications to ~100 years within which surface expressions become evident based on modeling studies from Peterson & Krantz (2003) and estimates from heave and motion measurements on sorted circles in Thule NW Greenland by Schmertmann & Taylor (1965).

Study Site and Methods

The study was conducted near Thule Airforce Base in northwest Greenland (76°N, 68°W). The base is located on a ~800 km^2 ice-free peninsula between the Greenland Ice Sheet to the west and Baffin Bay to the south and east. The sampling site is in Nordfjeld (North Mountain), a high valley with average elevation of 180 m. Proterozoic sedimentary rocks (Dundas formation) dominate among glacial drift and the last glaciation was initiated around >32 Ka ago (Davies et al. 1963). A more recent glacial advance either from the fjord or ice sheet is debated (Davies et al. 1963, Kelly et al. 1999). Annual average air temperature and precipitation measured by Thule Air Base since 1978 are -11.7±3°C with July temperatures at 5.3±1°C and 124 mm_{weq} precipitation of which ~40% falls as snow. For the years of sampling (2003 & 2004), the average annual air temperature was -9.2°C; average soil temperatures ranged from -9.1°C (surface) to -9.8°C (1.2 m) with a thaw depth reaching ~1.2 m in early August. Spring snow cover in 2003 and 2004 was 80 mm_{weq} and 30 mm_{weq}, and rain was 71 mm and 106 mm, respectively.

Patterned ground at the study site is nonsorted a priori and appears as irregular stripes and frost boils. The frost boils are ~0.5 m to 2 m in diameter; they show little micro-relief during the summer and are bordered with vegetation. Some boils show slight enrichment of pebbles towards their edges, but abundance of coarse material is generally sparse. During the early summer when the surface is thawed, desiccation cracks and salt precipitates develop at the surface of the central portion of the boils. Soil of distinctive color than surface has been observed near the center of several boils and appears to be recently injected from below the surface, suggesting that soil movement can be very rapidly, which has also been suggested by Swanson et al. (1999).

The central portion of the frost boil discussed here is 1.5 m in diameter. A few pebbles rest on the surface; they are more abundant towards the fringe (Fig. 1). Near

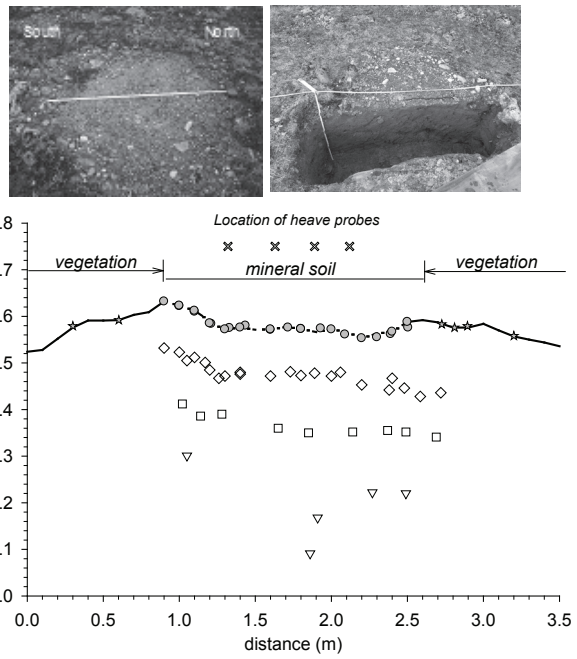

Figure 1. Upper: view of frost boil before and after excavation; note prominent crack in the image on the right developed after the excavation. Lower: detailed topography and position of samples. The different symbols refer to sampling depth in the following figures. Stars are in vegetation and dashed lines mark transition between mineral boil and vegetation. Circles with dots are measured elsewhere in vegetated areas close to frost boil. The dashed lines (Trans) mark transition from mineral soil to vegetated soil (see text). Location of boil: 78°33.241N, 68°33.596W.

the vegetated border, the mineral soil is covered with cryptogamic crust that locally forms small folds with axes paralleling the vegetation border. The center of boil consists of two apparent soil horizons: C1 (surface to 0.3 m depth) and C2 (>0.3 m depth). The C1-horizon tends to break into crumbs, shows silt caps, and has a weak platy structure. The C2- horizon has a well-developed platy structure. A few roots reach down to the frozen ground, which was at 0.69 m depth during time of excavation (June 29, 2004). A ~0.02 m O-horizon is developed in the vegetated area, and it is underlain by ~0.1 m A-horizon with weak crumb structure. A buried AB-horizon was found ~0.25 m below the vegetation. Surface samples were taken in 2003 without excavating the boil. After sampling, four heave probes were installed and left over winter, additional heave probes were installed in vegetated areas. The heave probes consist of 10 cm Plexiglas stick glued perpendicular on a 2.5 x 2.5 cm base. A Plexiglas sleeve is put over the stick and this ensemble is installed in the upper soil in the way that upper end of stick and sleeve are level with soil surface. Frost heave in upper soil will pull the sleeve up relative to the base buried deeper in the soil. The soil heave is then measured as distance between stick and outer sleeve. In 2004 the surface topography of boil was mapped and one half of boil was excavated and sampled in detail (Fig. 1). Most samples were collected undisturbed in 60 mL moisture cans to determine soil water content and bulk density gravimetrically. Dried samples were sieved to

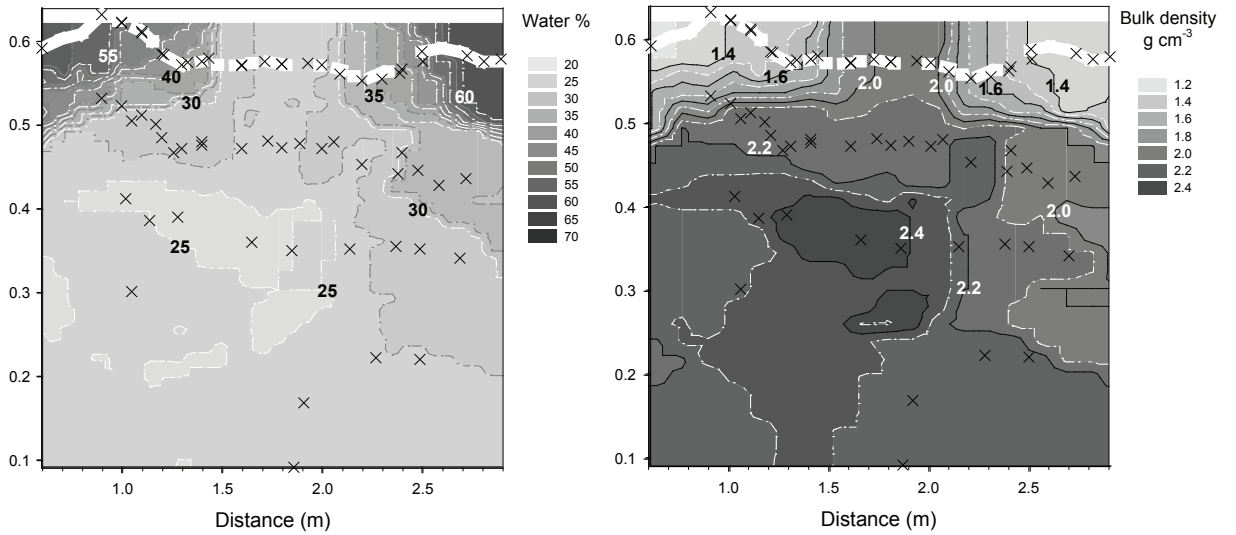

Figure 2. Vertical section through the frost boil showing contour maps of measured (A) water content and (B) wet bulk density in frost boil. Crosses mark position of measurements. The heavy white line shows the surface (topography) of the boil. Information above this line has no significance. The contours were generated by linear interpolation between nearest neighbor.

<2 mm and particle size distribution was determined by laser diffraction of the <2 mm fraction. Grain sizes of samples analyzed for ^{210}Pb were determined by Sedigraph 5100 on the <250 µm fraction. ^{210}Pb was analyzed on acid leachates of the <250 µm fraction by analyzing its granddaughter ^{210}Po using alpha spectroscopy (Aalto et al. 2008). This method only accounts for externally derived ^{210}Pb (adsorbed at grain surfaces) and the majority of it derives from atmospheric fallout. In addition to this excess unsupported ^{210}Pb, a smaller amount of supported ^{210}Pb is produced in situ by the decay of locally derived ^{222}Rn trapped in the soil atmosphere. This supported ^{210}Pb produces some background activity at depth.

Results and Discussion

Heave, grain size, and water content

Heave probes were installed in four positions (Fig. 1) across the mineral center on September 1, 2003. In addition, heave probes were also installed in vegetated areas in near proximity of the investigated frost boil. The total heave values on June 28, 2004 were 6, 12, 23, and 12 mm, while heaving rate measured in vegetated soil was <2 mm.

The grain size distribution of all samples (boil and vegetation) is loamy sand with sand: 59.5 ± 10%, silt: 30.1 ± 8.4%, and clay: 10.5 ± 4.7%. This grain size distribution is equal to low centered mud boils described by Zoltai and Tarnocai (1981) and has enough fine material to be suitable for frost heave and patterned ground formation (Goldthwait 1976). Although the frost boil appears as a nonsorted circle, there is a slight enrichment of pebbles towards the vegetated border and slight increase in the clay size fraction at depth.

The water content on June 29, 2004 is displayed in Figure 2A. It covers a range between 22 wt% and 78 wt% (on basis of wet weight) where surface samples from the center of the boil have lowest water content (22 wt% to 35 wt%). In contrast, surface samples close to surrounding vegetation are wetter (41-58 wt%) and the vegetated surfaces have highest water content (44-78 wt%). Volumetric water content calculated from bulk density and gravimetrical water content is between 13 vol% to 36 vol% indicating that soils are not water saturated at this time of the year.

The wet bulk density ranges between 990 kg m^{-3} to 2600 kg m^{-3} with lowest values below vegetation and cryptogamic crust-covered surfaces, and highest values in the bare central portion of the boil (Fig. 2A). The higher bulk density in the central portion of the boil and at depth is quite consistent with the theory that after thawing soil dries out and is compacted in center. The soil water distribution observed here is similar to water content measured in mud boils in Svalbard during and shortly after snowmelt (Boike et al. 2002). As shown by Boike et al. (2002) moisture content in these boils is quite dynamic during the season and it is difficult to draw conclusions from a single set of density/soil moisture measurements. However, using spatial distributed year-round measurements of soil moisture and soil temperature in the mud boil Boike et al. (2002) observed that moisture is transported to fringe in frozen ground and therefore leads to thawing and collapse of these regions (Boike et al. 2002). Such water dynamic seem to concurs well with freeze-thaw pumping as driving mechanism for boil development as discussed by Washburn (1997)

^{210}Pb systematics and distribution

Assuming that ^{210}Pb is deposited equally on the surface by continuous atmospheric flux, all surface samples should display the same activity if they have the same history of surface exposure. Due to its adsorption primarily on small grain sizes, lead will not infiltrate far into the ground (Stumm 1992) and therefore, surface samples collected from upper 0.1 m should contain almost all atmospheric deposited ^{210}Pb.

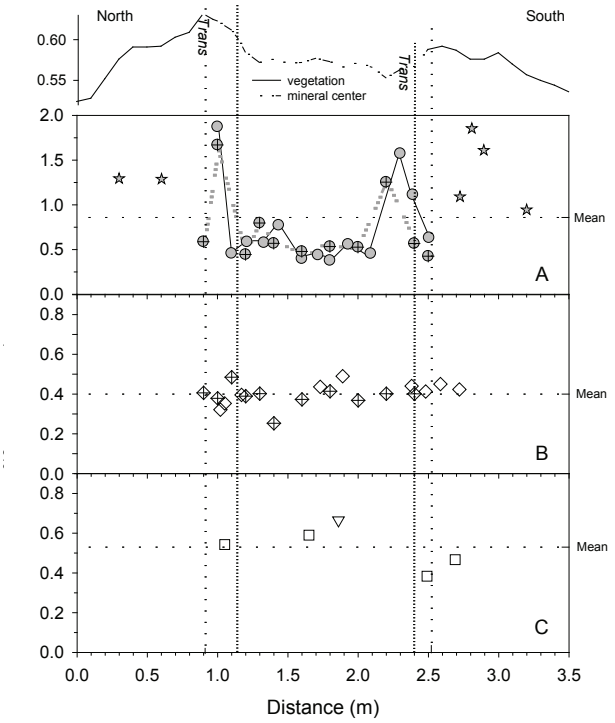

Figure 3. ^{210}Pb activity distribution in the investigated frost boil and surrounding area. The two lines delineate the transition between mineral surface and vegetation. (A) Surface samples, (B) Samples from ~0.1 to 0.15 m below surface, and (C) samples from >0.25 m below surface. Symbols refer to sampling depth (see Fig. 1); symbols with cross indicate samples collected in 2003.

If undisturbed, the ^{210}Pb activity in surface soil will begin to approach steady state conditions with ^{210}Pb deposition balanced by decay after $1/\lambda_{210}$ (τ_{210} residence time of ^{210}Pb, see Albarède (1996, p. 344 ff.)) which is 32.2 years. However, our alpha analytical techniques allow more accurate exposure determinations, or dating out to approximately $2.5/\lambda_{210}$. Hence, soil on surfaces that have been undisturbed for >80 years should closely approach the steady state ^{210}Pb activity. Furthermore, the ^{210}Pb activity at depth should be equal to background values from in situ decay of ^{222}Rn in soil atmosphere and will be lower than steady state ^{210}Pb activity at surface. Accepting that ^{210}Pb background flux is much lower than atmospheric flux, elevated ^{210}Pb values at depth indicate that surface material is transported to depth within the last 100 years and for these samples, the duration of burial can theoretically be estimated out to 80 years using the decay rate of ^{210}Pb. Following this line of reasoning, surface soil with ^{210}Pb activity lower than steady state activity has been at the surface less than 80 years.

^{210}Pb values of surface samples display a very distinct, almost symmetrical pattern with low values in center of the boil and higher values towards the vegetation border (Fig. 3A) and this pattern exists in samples collected in both years. The average ^{210}Pb activity in the inner center of the boil is 0.5 dpm g^{-1} and is much lower than the average ^{210}Pb in vegetation (1.65 dpm g^{-1}). Samples at ~0.10 to 0.15 m depth (Fig. 3B) have average ^{210}Pb values of 0.40 dpm g^{-1} with a range between 0.50 and 0.22 dpm g^{-1}. These samples do not show a systematic trend like the surface samples but scatter around the average activity. Samples collected from greater depth >0.25m (Fig. 3C) have slightly higher ^{210}Pb activity with average of 0.45 dpm g^{-1}. One sediment sample collected just above the permafrost table (triangle at ~ 60 cm in Fig. 1) has ^{210}Pb activity of 0.68 dpm g^{-1} higher than most samples at depth and higher than surface samples in the mineral center of the frost boil.

Following the ^{210}Pb systematics described above, the average ^{210}Pb activity in vegetation of 1.65 dpm g^{-1} reflects steady state. Since this surface is very stable the observed variability of ^{210}Pb activities may indicate accumulation processes due to topographic depressions or changes in plants which serve as natural sediment and dust traps.

Low ^{210}Pb activities in center part of boil suggest that sediments have recently been exposed to surface. As described above, freshly injected sediment in boil center has been observed during the thaw season on adjacent frost boils supporting the trend observed with the ^{210}Pb. Assuming that boil and its close perimeter is closed sediment system demands that the injected sediment is balanced by subduction; both motions have been assumed based on distribution of buried rocks and organic material (Dyke & Zoltai 1980) in non sorted circles. They lead to the assumption of a circulatory motion where soil subsides at boil fringe and rises from below in center of boil. According to this mechanism, the bottom of boil just above permafrost table would be replaced by material from the surface. If the circulation is fast enough (<80 years) the sediment at depth should have ^{210}Pb activity above background but lower than steady state activity. The subduction rates from Dyke and Zoltai (1980) on the order of 1 mm yr^{-1} infer that most of unsupported ^{210}Pb is decayed below a depth of 10 cm. The observed elevated ^{210}Pb activity in the one sediment sample at depth (at ~60 cm) may be due to remaining ^{210}Pb from subducted sediments and would suggest much higher subduction rates. However, elevated background activities can be reached at depth due to high moisture content which reduces ^{222}Rn diffusion out of soil and therefore, increases the in situ produced ^{210}Pb background activity. These results show the importance to accurately determine background levels of ^{210}Pb.

The fresh injected sediment in center of boil will be laterally transported towards fringe and therefore, accumulation of atmospheric ^{210}Pb with time would cause a constant increasing in ^{210}Pb activity toward the fringe. The slightly higher activity towards the northern fringe of boil could indicate lateral transport though this trend is missing in the southern part. Overall, a circularly motion in central mineral boil is not well documented by ^{210}Pb except for general low activities compared to stable surfaces which indicates that sediment has not been exposed to atmosphere for very long time and therefore, may have been injected recently from below.

In the area between stable vegetation and mineral boil, low ^{210}Pb activity in direct contact to stable vegetation also suggests injection of sediment from depth while the high

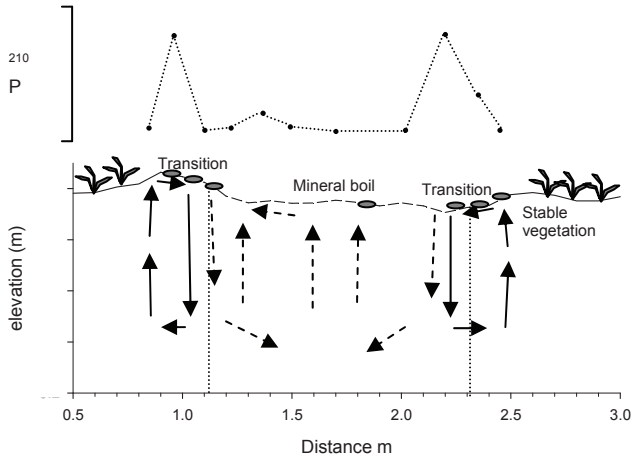

Figure 4. Schematic sketch of observed ^{210}Pb activity in surface sediments (upper) and possible sediment motion to produce observed ^{210}Pb activity trend (lower).

^{210}Pb activities in this area (Fig. 3A) indicate that sediment has been at surface for elevated time. A possible mechanism to create the observed ^{210}Pb distribution could be a circulatory cell opposite to that in mineral boil as indicated in Figure 4. The sediment is than subducted close to mineral center of boil (Fig. 4). Subduction at this location is supported by observed buried plant material (*Dryas spp.*) which was found in 12 cm depth at 1.21 m distance at north side of boil (X-axis, Fig. 3). Hallet and Prestrud (1986) proposed a similar circulatory motion ("rolling border") in the stone perimeter of sorted circles based on soil displacement measurements.

Conclusions and Outlook

The use of ^{210}Pb as a tracer for soil motion yields promising results. Compared to the radiocarbon tracer, ^{210}Pb is connected directly to sediment grains and not restricted to certain components in the sediment. It therefore can be sampled in as high resolution as needed for individual system. However, the time limit of ~80 years restricts its application to recent processes. Conclusions drawn from ^{210}Pb distribution in this study are in agreement with other field observations in this high Arctic site and with general mechanism proposed by other researchers for formation and sustainability of nonsorted circles. However, for developing this tracer to its full potential it is important to accurately determine the steady state and background ^{210}Pb activity, which are the upper and lower limits of unsupported ^{210}Pb activity within the frost boil system. Knowledge of these boundary values will allow more detailed interpretation of ^{210}Pb activities and their significance with respect to sediment motion. A way to do this would be to determine the ^{210}Pb inventory (dpm m^{-2}) by sampling continuous depth profiles rather than single points of activity. Together with boundary values sampling of continuous profiles will provide the opportunity to estimate sediment motion in time and space for the studied frost boil system.

Acknowledgments

We would like to thank Paul Overduin for his review of the manuscript, VECO, Thule Air Base for their logistical support, and A. Vigna for field assistance. This study was funded by the National Science Foundation Grant OPP-0221606 with partial support for dating by NSF EAR-0403722 and 0521774.

References

Aalto, R., Lauer, J.W. & Dietrich, W.E. 2008. Spatial and temporal dynamics of sediment accumulation and exchange along Strickland River floodplains (Papua New Guinea) over decadal-to-centennial timescales. *Journal of Geophysical Research* (in press).

Albarède, F. 1996. *Introduction to Geochemical Modeling*. Cambridge: Cambridge University Press.

Appleby, P.G., Oldfield, F., Thompson, R., Huttunen, P. & Tolonen, K. 1979. ^{210}Pb dating of annually laminated lake sediments from Finland. *Nature* 280: 53-55.

Boike, J., Ippisch, O., Overduin, P.P., Hagedorn, B. & Roth, K. 2007. Water, heat and solute dynamics of a mud boil, Spitsbergen. *Geomorphology* (in press).

Boike, J., Ippisch, O. & Roth, K. 2002. Thermal and hydrological dynamics of a mud boil - any clue about its formation? *Chinese Journal of Glaciology and Geocryology* 24 (5): 538-543.

Davies, W.E., Krinsley, D.B. & Nicol, A.H. 1963. Geology of the North Star Bugt area, northwest Greenland. *Meddelelser om Gronland* 12(162): 68.

Dörr, H. 1995. Application of ^{210}Pb in soils. *Journal of Paleolimnology* 13: 157-168.

Dyke, A.S. & Zoltai, S.C. 1980. *Radiocarbon-dated Mud-boils, Central Canadian Arctic.* Geological Survey of Canada, Current Research, Part B 80: 271-275.

Goldthwait, R.P. 1976. Frost sorted patterned ground: A review. *Quaternary Research* 6: 27-35.

Hagedorn, B., Harwart, S., van der Loeff, M.M.R. & Melles, M. 1999. *Lead-210 Dating and Heavy Metal Concentration in Recent Sediments of Lama Lake (Norilsk Area, Siberia)*. Berlin, Heidelberg: Springer Verlag.

Hallet, B. 1998. Measurements of soil motion in sorted circles, western Spitsbergen. *Seventh International Conference on Permafrost, Yellowstone, Collect. Nordicana.*

Hallet, B., Anderson, S.P., Stubbs, C.W. & Gregory, E.C. 1988. Surface soil displacements in sorted circles, Western Spitzbergen. *Permafrost, Fifth International Conference, Trondheim, Norway*: Tapir Publishers.

Hallet, B. & Prestrud, S. 1986. Dynamics of periglacial sorted circles in Western Spitzbergen. *Quaternary Research* 26: 81-99.

Hallet, B. & Waddington, E.D. 1991. Buoyancy forces induced by freeze-thaw in the active layer: implications for diapirism and soil circulation. *Periglacial Geomorphology*. J.C. Dixon & Abrahams, A.D. London: John Wiley and Sons Ltd., 251-279.

Kelly, M., Funder, S., Houmark-nielsen, M., Knudsen, K. L., Kronborg, C., Landvik, J. & Sorby, L. 1999. Quaternary glacial and marine environmental history of northwest Greenland: a review and reappraisal. *Quaternary Science Reviews* 18(3): 373-392.

Kessler, M.A., Murray, A.B., Werner, B.T. & Hallet, B. 2001. A model for sorted circles as self-organized patterns. *Journal of Geophysical Research* 107(B7): 13,287-13,306.

Kessler, M.A. & Werner, B.T. 2003. Self-organization of sorted pattern ground. *Science* 299: 380-383.

Mackay, J.R. 1980. The origin of hummocks, western arctic coast. *Canadian Journal of Earth Sciences* 17(8): 996-1006.

Mackay, J.R. & MacKay, D.K. 1976. Cryostatic pressure in nonsorted circles (mud hummocks), Inuvik, Northwest Territories. *Canadian Journal of Earth Sciences* 13: 889-897.

Mortensen, H. 1932. Über die physikalische Möglichkeit der 'Brodel'-Hypothese. *Neues Jahrbuch für Mineralogie, Geologie und Paläontologie, Monatshefte Part B*: 417-422.

Nicholson, F.H. 1976. Pattern ground formation and description as suggested by low Arctic and subarctic examples. *Arctic and Alpine Research* 8(4): 329-342.

Overduin, P.P. & Kane, D.L. 2006. Frost boils and soil ice content: Field Observations. *Permafrost and Periglacial Processes* 17: 291-307.

Peterson, R.A. & Krantz, W.B. 2003. A mechanism for differential frost heave and its implications for patterned-ground formation. *Journal of Glaciology* 49(164).

Roth, K. & Boike, J. 2001. Quantifying the thermal dynamics of a permafrost site near Ny-Alesund, Svalbard. *Water Resources Research* 37: 2901-2914.

Schmertmann, J. & Taylor, S.R. 1965. *Quantitative Data from a Pattern Ground Site over Permafrost.* Technical Report Hanover, N.H., U.S. Army Cold Regions and Engineering Laboratory.

Shilts, W.W. 1978. Nature and genesis of mudboils, central Keewatin, Canada. *Canadian Journal of Earth Sciences* 15: 1053-1068.

Stumm, W. 1992. *Chemistry of the Solid-Water Interface*. New York: Willey.

Swanson, D.K., Ping, C.-L. & Michaelson, G.J. 1999. Diapirism in soils due to thaw of ice-rich material near the permafrost table. *Permafrost and Periglacial Processes* 10(4): 349-367.

van Vliet-Lanoë, B. 1991. Differential frost heave, load casting and convection: Converging mechanisms; a discussion of the origin of cryoturbation. *Permafrost and Periglacial Processes* 2: 123-139.

Veillette, J.J. 1980. *Nonsorted Circles on Cohesionless Fine Silty Sand, North Central District Keewatin.* Paper 80-1B, Geological Survey of Canada: 259-267.

Walker, D.A., Epstein, H.E., Gould, W.A., Kelley, A.M., Kade, A.N., Knudson, J.A., Krantz, W.B., Michaelson, G., Peterson, R.A., Ping, C.-L., Raynolds, M.K., Romanovsky, V.E. & Shur, Y. 2004. Frost-boil ecosystems: Complex interactions between landforms, soils, vegetation and climate. *Permafrost and Periglacial Processes* 15: 171-188.

Walling, D.E., Collins, A.L. & Sichingabula, H.M. 2003. Using unsupported lead-210 measurements to investigate soil erosion and sediment delivery in a small Zimbian catchment. *Geomorphology* 52: 193-213.

Washburn, A.L. 1956. Classification of patterned ground and review of suggested origins. *Geological Society of America, Bulletin* 67: 823-865.

Washburn, A.L. 1969. Patterned ground in the Masters Vig district, Northeast Greenland. *Biuletyn Periglacjalna* 18: 259-330.

Washburn, A.L. 1980. *Geochryology: A Survey of Periglacial Processes and Environments.* New York: Halsted Press, John Willey & Sons, Inc.

Washburn, A.L. 1989. Near-surface soil displacement in sorted circles, Resolute area, Cornvallis Island, Canadian High Arctic. *Canadian Journal of Earth Sciences* 26: 941-955.

Washburn, A.L. 1997. Plugs, and plug circles: A basic form of patterned ground, Cornwallis Island, Arctic Canada - origin and implications. *Geological Society of America.*

Zoltai, S.C. & Tarnocai, C. 1981. Some nonsorted pattern ground types in northern Canada. *Arctic and Alpine Research* 13(2): 139-151.

“Pingo-Like” Deformation, Vilaine Estuary, Britanny

Bernard Hallégouët
Géographie, Université de Bretagne Occidentale, 29793 Brest, France
Brigitte Van Vliet-Lanoë
UMR 6538, Domaines Océaniques, IUEM, 29280 Plouzané, France
Christian Hibsch
UMR CNRS 7566 G2R, BP239, Université H. Poincaré, 54506 Vandoeuvre-lès-Nancy cedex, France

Abstract

The Pénestin section (southern Brittany, France) presents large diapiric deformations initially attributed to pingos by several authors. We present tectonic, petrographic and stratigraphic arguments leading to a mechanical interpretation of the deformations. The area corresponds to an upper Neogene paleoestuary of the Vilaine River, in middle terrace position, incised into a kaolinitic saprolite. There is no evidence for recent transpressive tectonics or for periglacial pingos, despite the presence of MIS 8 ice wedge casts. Shale diapirism does exist. Deformation is favoured by the liquefaction of saprolite and a seaward mass movement triggered by an earthquake around 280,000 yr. BP. This kind of deformations is common in tectonically active regions. The development of permafrost during MIS 8 (Saalian I) allowed ice segregation of the porosity in sediments, which froze younger reactivation of the shale diapirism.

Keywords: Brittany; earthquake; neotectonic; periglacial; saprolite; shale diapirism.

Introduction

Distinguishing between tectonic deformations and periglacial disturbances in the Quaternary is a prerequisite for seismic hazard assessment in former periglacial areas. Among these deformations, we discuss whether a specific “folds” succession can be related to neotectonic activity or, periglacial forms. Examples exist in the southern Pénestin section (Brittany, N.W. France, Fig. 1) and the Bovey Tracey basin (Devon, UK), where deformation was first interpreted as pingo scars (Jenkins & Vincent 1981, Rivière and Vernhet 1962) or as complex features in Germany attributed to permafrost by Eissman (1981) and Strunk (1983). Recently, these “fold trains” have been interpreted as induced by seismic shaking (Van Vliet-Lanoë et al. 2004) or as Quaternary tectonic folding (Brault et al. 2001). This paper presents tectonic, petrographic and stratigraphic arguments leading to a mechanical interpretation of the Quaternary deformation processes at Pénestin, located south of the Vilaine estuary southwest of Pénestin city. The morphologic convergence with classical deep-seated shale diapirism is explained on the basis of earthquake-induced transient transformation of a basal saprolite.

Geology

The section of “la Mine d’or” is a fluvio-marine middle terrace complex from the Vilaine River, perched about 15 m above the Hercynian basement cropping out along the shore cliff. The basement is faulted in several compartments and deeply weathered (kaolinitic saprolite). The water table is commonly above it. The section is oriented roughly north-south. At the top of the section, the topography slopes 0.5% to the north and 1% to the west (seaward).

Pénestin is located close to a southern branch of the South Armorican Shear Zone (Fig. 1). This structure is one of the major Variscan dextral strike-slip faults of the European plate (Gapais et al. 1993). The seismicity is moderately active with intensities MSK reaching VII or even VII-VIII (SIRENE database, Fig. 1). to:

- Unit B**:** Scattered blocks of sandstones observed at the contact between the saprolite and the sediments with some sandy gravel generally attributed to Oligocene deposition.
- Unit C1: A beach conglomerate, prograding from the south. At its base, it includes flat-lying blocks of Laderes sandstones and vertical frost-jacked cobbles (cryoexpulsion) stacked into the saprolite, forming cryogenic pattern ground. The truncation by abrasion of the soft but coherent saprolite, with the absence of scouring, also argues for shore face

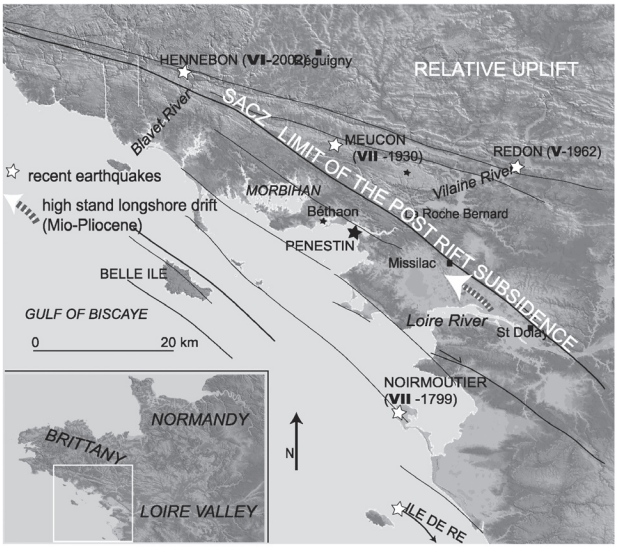

Figure 1. Location of the section.

deposition under a cold climate with block transportation by ice rafting (Van Vliet-Lanoë et al. in press). This unit yields an age of 6.7 ± 0.7 Ma by ESR. It is further locally consolidated by a hydromorphic ferricrete. This hard pan has a major impact on the deformations throughout the section by modifying the permeability and rheology above the saprolite.

- Unit C2: A prograding coarse sandy unit with an increasing charge of angular rock fragments constitutes a sedimentary progradation coming from the south. This unit is strongly rubified close to the surface by yellow-red podzolic pedogenesis. It corresponds to the top of a middle Pliocene estuarine, river-dominated braided fan formed during a major regression. It is covered by rhythmic red and grey silty clays, often wrinkled, unit C3; these tidalites represent the Gelasian/Pre-Tiglian high stand.

Unit D1: Unit C2 is eroded by a channel, consisting of fine-grained sands and clays lacking frost perturbation. This interglacial estuarine material has been dated at 445 ± 71 ka by ESR (Marine Isotope Stage 13) (Laurent 1994). The extent of the sands is visible at the base of some of the large "bowls.". This unit is practically never deformed where it is thick, but is susceptible to stretching where it is thin and is sometimes faulted.

Unit D2: This sandy gravel belongs to a braided channel system with large blocks and covers most of the section. Blocks are ice-rafted. This periglacial river corresponds to the Pleistocene "middle" terrace of the Vilaine and is further weathered by a polygenetic red-yellow podzolic soil. The sediment has been dated at 317 ± 53 ka (MIS 10 to 8) by ESR (Laurent 1994).

Locally, Unit E1 appears. This is a loess-like khaki silt infilling wedges. These wedges are developed in specific tensional positions and post-date unit D2 and the deformations. (Van Vliet-Lanoë et al. 1997a). They correspond to ice wedge casts, which are truncated by an erosional surface, some recent loesses and heads (unit E2), and by recent dune sands (unit F), Holocene in age.

The geometry of the section revealed a paleosurface shaped at least since the Oligocene and further incised by three successive channel generations. C1 crops out as a marine strand flat, corresponding to a periglacial low stand, Late Miocene to Lower Pliocene in age. C2 is a temperate tidal channel, ending in a mud flat and coming from the south, Middle to Late Pliocene in age. D1 is a temperate tidal channel, 420 ka old. D2 is a conglomerate with more sandy layers, corresponding to a periglacial braided river, 307 ka old; it pre-dates the fold-like deformations. This stratigraphic interpretation makes the age range of the basement deformations clear. North of the bay, the weathered micaschists are truncated by a marine abrasion reaching 8 m NGF. In the middle part of the section, the substratum is weathered in bleached soft clayish silt. The main Kerfalher fault is located 50 m south of Poulante Point, the southern end of the section. A satellite fault outcrops at Poulante Point. Its orientation is roughly N120°E and it does not seem to have suffered recent slip reaching the surface.

Quaternary deformations

The wavy, fold-like deformations affecting the saprolite and the sedimentary units have been interpreted as pingo traces or as evidence for recent strike-slip faulting of the Kerfalher fault system (Brault et al. 2001). Deformations do not present a regular wavelength or strike-slip faulting. Some sectors are devoid of deformation, although others close to Poulante Point are smaller and more clustered (Fig. 2). It seems clear from our data that the more intense deformational features are almost always developed above faults affecting the basement. These pre-existing faults acted as specific water pathways to fault-controlled water migration for potential seismic pumping. Few striations have been observed along the faults. The slip movements reveal normal-sinistral kinematics, compatible with sliding toward the sea-side and incompatible with the supposed strike-slip faulting.

Deformations mostly developed in thick bleached saprolite. These are much less intense when the preserved overburden sediments are thick and more permeable. To the south, the geometry of the deformations is more or less continuous and is elongated roughly N60°E, like the basement faults. Short, often asymmetric, irregular "bowls" have developed due to the presence of the thick white saprolite below units D1 and D2 (Fig. 3a). Usually 2-3 m below the base of D1, the saprolite is undisturbed and porous. No deformation has developed where the conglomeratic ferricrete exists. The deformations are smoother and "longer" in wavelength where the saprolite is coherent (A2), larger and stronger for A3, and smaller but strong where the alluvial complex is thin. Wrinkling developed in unit C3 is related to saprolite injections and has been interpreted as due to the interaction of *P* and Rayleigh waves (Van Vliet-Lanoë et al. 2004). Deformations are thus controlled by (i) pre-existing faults; (ii) the overburden sedimentary load; (iii) the characteristics of its porosity, and (iv) the mechanical properties of the saprolite and the absence of C1 conglomeratic ferricrete.

Liquefaction can develop in clayish sands (Ruxton 2004), allowing incipient doming that stretches the overburden conglomerate cover and pinches out the flanking sandy units, simulating syn-sedimentary deformation. Locally, the D1 sand unit shows stretching with listric microfaults and bending. At the level of maximal curvature of the doming, tension gashes are injected with liquefied kaolinitic silts. Where the saprolite bursts out, load casts deform the extruded saprolite mass, with local wrinkling (Fig. 3b). At the apex of saprolite upward injection, ice wedge casts filled with khaki loess (unit E1) were later centred on tension bulges connected with the large undulations (Fig. 3c). Differential frost heaves may have deformed the structures later (Van Vliet-Lanoë et al. 2004). The clay fraction consists essentially of neoformed, silt-sized kaolinite with about 10% illite, leading to a low density and high porosity in the undisturbed saprolite. Such material has a much lower plasticity index than the other clay minerals (illite, smectite) (Skempton 1953). According to our

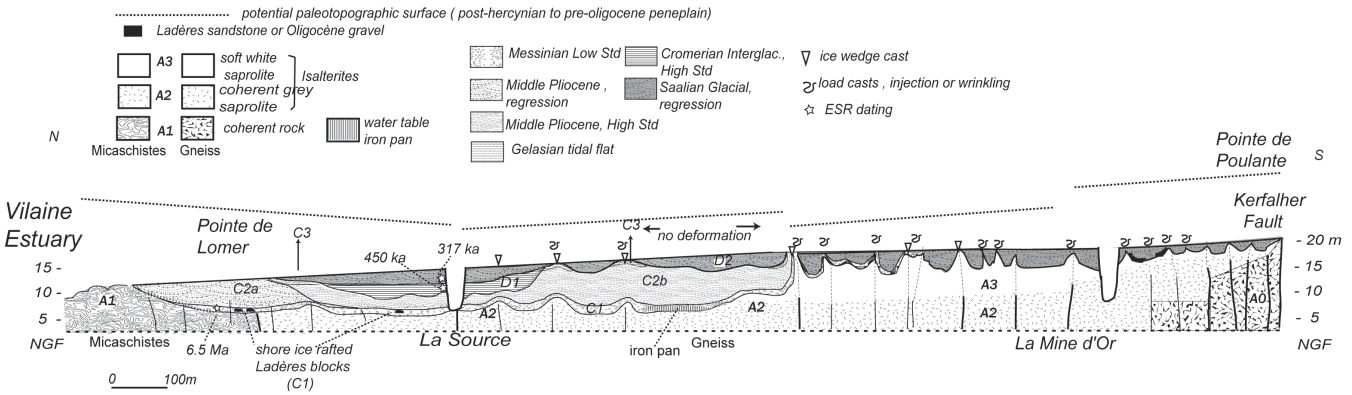

Figure 2. Global sketch of the main section at Pénestin.

laboratory data, the winter water content of unremoulded saprolite is around 23%, slightly above the water content at Atterberg plastic limit (20%, Cassagrande methodology). Liquefaction occurs above 30% in unremoulded sediment (28% at Atterberg liquid limit) where the water table seeps along most of the cliff. Shocks induced by storm waves can ease the collapse of original porous fabric of the saprolite, inducing mass wasting. The bulk density of the saprolite increases towards the surface. The undisturbed dark grey saprolite yields a 1.3 dry bulk density, which when slightly disturbed rises to 1.6, and for white, fully disturbed saprolite to 1.9. The dry bulk density of the coarse sand and the conglomerate are about 1.9 and 2.0, respectively. Cohesive kaolinitic silt is hard to liquefy in normal conditions (Skempton 1953); to destroy the fabric, we need an external trigger to induce liquefaction. To reach the liquid limit (30%) and equilibrate the pressure induced by the overburden conglomerates, we need to destroy the original porous fabric of the "light" saprolite to reach 23% water in the collapsed silt and to add at least 7% water without the possibility of water escape. The origin of this supplementary water supply is clearly connected to the basement faults. To induce mass movement, water needs to be confined in excess within the liquefied saprolite and oversaturation of the saprolite needs to be supplied with water for several days. Petrographic analysis of the saprolite is instructive, revealing no petrographic change in an undisturbed saprolite. The dense material with an unpreserved macro-fabric (A3) reveals interstitial porosity collapse. The material with a partly disturbed macro-fabric preserves most of the initial porosity, but deformed and partly crushed. At the contact with the D1 unit, the saprolite presents sliding planes, attesting to lateral movement of A3 mass with respect to D2. Other units, like C3 and D2, present late deep traces of ice lensing (paleopermafrostrelic permafrost). Frost-induced porosity usually promotes lateral drainage.

Discussion

Periglacial deformation

The deformations were first interpreted by Rivière and Vernhet (1962) as pingo scars relative to continuous permafrost, as indicated by ice wedge casts, but the clustered deformations do not fit the cone-in-cone internal fabric related to the ice-body collapse observed by De Gans (1995) and the isolated pingo. Other periglacial mounds like palsa occur in clustered locations, on wet silty or clayish surfaces, sometimes sloppy. The observed deformations do not fit those described by Pissart (1993). In pingo and palsa, scars, overturned layers exist inside the rims of the scars, sometimes disrupted by normal faults (pingo) with sedimentation or peat developed within the central depression.

Diapirs can also be induced at shallow depths with a residual thick ice cap decaying on oversaturated subglacial sediments like glacio-marine or glacio-lacustrine silts and clays (Brodzikowski & Van Loon 1980). This process is unrelated to the Pénestin paleoclimatic context, as the site is located at least 800 km from the southernmost extent of the British ice sheet. Hydrates diapirs in permafrost may also be responsible for those deformations but the section is too shallow to support this interpretation.

Liquefaction

In the southern section, liquefaction is evident from injections and the global geometry of the deposits reveals mostly a positive gradient in density with light unconsolidated saprolite overlain by dense gravely sedimentary units. However, the coarse-grained D2 unit shows mostly brittle behaviour, the sandy basal layer from D1 is stretched with brittle fracturing, and sliding planes exist close to the contact of the deformed saprolite. The occurrence of subsurface overconsolidation of the saprolite with reduction of microporosity, thin mud injection and fabric wrinkling suggests rapid deformation (Van Vliet-Lanoë et al. 2004) but the development of the large deformations with larger injections seems related to slower motion over several days. Liquefaction susceptibility reflects the relative resistance of soils to loss of strength when subjected to ground shaking. Co-seismic liquefaction is always associated with water-saturated sediments that can reach oversaturation by fabric collapse or with sediments oversaturated by co-seismic water supply (Muir-Wood & King 1993). Co-seismic liquefaction also leads to overconsolidated sediments at shallow depth, although the superficial layers are liquefied.

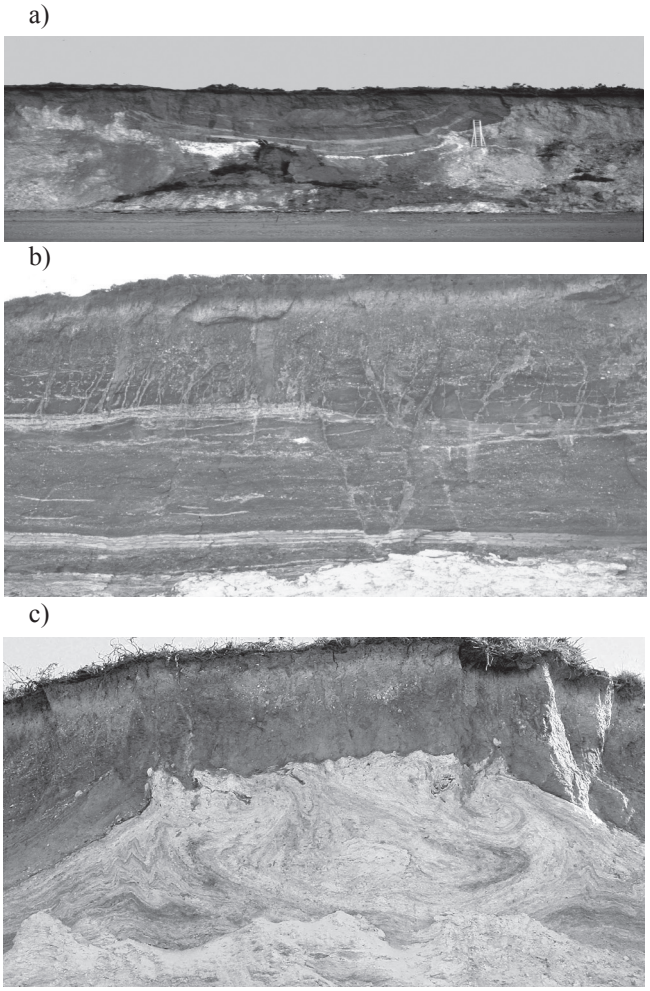

Figure 3. a): View of a "bowl" north of "la Mine d'or." Notice injection at the level of the ladder; b): Giant drop with lateral wrinkling in saprolite A3 (section height: 2 m); c): Clustered ice wedge casts above a diapir.

At Penestin, we interpret evidence of liquefaction and overconsolidation in initially cohesive sediments as resulting from fabric collapse and transient water supply. An external trigger for liquefaction and a complementary water supply is needed. As water is a non-compressible fluid, the alternating squeezing and suction from the local water table located in the faulted basement caused by P and Rayleigh waves caused a rise in excess pore water pressure in the overlying saprolite with subsequent liquefaction. This ejection of liquid mud is normally locked by overburden sediments. Here, the overburden weight of the D units is limited by erosional truncation so mud ejection was easier. Youd et al. (2004) observed that soil softening leads to a lengthening of the period of ground motion and that ground oscillation leads to a continued rise of pore water pressures after ground shaking ceases. The generated overpressure is confined at depth in the regional water table contained in a fractured substratum. An earthquake of strong magnitude can liquefy cohesive silty soils as demonstrated by recent major earthquakes. Liquefaction was also very important even on the gentle slope at the foot of the Turnagain hills with lateral spreading and sliding of a rafted suburb of Anchorage (Seed & Wilson 1967).

The remaining possible mechanisms are thus shale diapirism or folding. Tectonic transpressive folding does not fit our observations, as discussed previously. Disharmonic surface folding is difficult to apply to the geometry of deformation at Pénestin (apex of basement faults). After deformation, the whole system was truncated by a late erosional surface related to the periglacial regimes of MIS 8 and MIS 6, without younger evidence of "folding."

Shale diapirism

While often mimicking folding, shale diapirism usually develops in marine basin in association with fast sedimentation, the strong sedimentary overburden leading to water overpressure in unconsolidated sediments. Active shale diapirism occurs when the overburden layer is thinned by tension and the mobilized shales are pushed upward due to the rise in internal pressure (Vendeville & Jackson 1992). In these conditions, clay behaves as a fluid, with a very low viscosity, inducing hydraulic fracturing in the confining layer, with differential loading (Bolton & Maltman 1998). The initial diapir shape is modified by lateral or oblique upward migration of fluidized shales and may generate a network of clay dykes and sills, in the form of a ring or conical faults that help the rise of the diapir. When the hydraulic pressure drops, the diapirism stops, followed by drainage and consolidation with further collapse (Vendeville & Jackson 1992).

At Pénestin, there is no evidence of thick overburden sediments to justify confining, since sedimentation stopped at about 300 ka, prior to the main deformation. Most D1-D2 gravels behave as a confining system for the saturated saprolite. The extra pore-fluid was produced locally by seismic-induced water supply along the normal faults triggering the diapiric motion, as discussed above. This localized overpressure source induced a metric swell of the saprolite at the apex of the feeding fault, resulting in tension gashes at the apex of the bulging developed in the rigid and confining alluvial system. During the fracturing process, the inner hydraulic pressure gradient was probably involved in fracture opening, like in hydrofracturing. Nevertheless, it is difficult to determine if fracturing and fluidization were synchronous, although tension gashes were rapidly injected by the fluidised saprolite and locally extruded to the surface. The conical faulting developed further, marked and eased by injections of fluidized saprolite on the side of the diapirs; this has been confused with flower structures due to transpressive shear. In detail, shale diapirism should explain most of the deformational structures in the saprolite as well as deformation like stretching in D1 sands and sliding planes developed in the saprolite observed at the base of the bowl-like structures.

These mechanisms, co-seismic fluidization and diapiric motion, do not perfectly explain the elongation of the observed patterns and their higher frequency close to the summit of Poulante Point. The elongation develops in parallel with the

main slope (E-W 1%) of the Pénestin peninsula. During the Anchorage earthquake, sliding of the whole liquefied saprolite mass (Seed and Wilson 1967) induced buoyancy and rafting of sedimentary bodies. For Pénestin, two raft models can be proposed. In the first, the sliding is orthogonal to the positive ridges that correspond to local mud diapirs in stretched areas (Fig. 4c), while in the second, the raft structures are groove-shaped and each is separated by and strikes along mud diapirs (Fig. 4d). This last model agrees with the topographic slope towards the sea (marine low stand at the time of deformation) and with the kinematics observed in NE-SW slickensides in the deformed saprolite.

Reconstitution of Pénestin event

With this succession of mechanisms, nearly synchronous, we can reconstitute the entire story. A major earthquake occurred around 280-290 ka when the climate was periglacial and the Vilaine River was prograding, but sea level was not yet too low and permafrost was absent. The regional water table was high, and during the event, fluids probably escaped along basement fault nets, locally bulging the saprolite and consequently weakening the rigid confining alluvial body. During the earthquake, water was supplied by the fractured weathered substratum, except above the ferricrete. The whole saprolite surpassed the plastic limit and, in the upper layer, the liquid limit; it began to rise, rapidly deforming the base of deposits C3, D1 and D2. This process probably continued to evolve with the continuing rise in pore water pressure after ground shaking ceased. The diapir movement probably persisted for several hours after the event and generated lateral spreading. Displacement may have been mostly south-westward, following the main slope. The sliding was groove-shaped by differential loading of the D1 gravels, parallel to the diapirs separating the various corrugations. The "folds" in the northern part of the section trace thus aborted shale diapirism.

The date of the paleo-earthquake, roughly marking the onset of a regional relaxation event after a regional compressional event (circa 430-280 ka) is somewhat disturbed by the building of major ice sheets on Britain (MIS 12 and 10; Van Vliet-Lanoë et al. 1997, 2002). After this event, the saprolite probably dried out during the Saalian I (MIS 8; 280-240 ka), by segregated ice development in the permafrost, also responsible for the development of ice wedges, and by subsequent drainage of the alluvial body when it thawed. Today, the water table is perched on the densified saprolite A3.

Such a development in a tectonically active region is basically linked to the existence of an unconsolidated clay body (sedimentary or saprolite) and to the presence of a rather shallow water table and a confining surface layer like consolidated clayish conglomerate or even a lodgement till. In formerly glaciated region, the normal load of dead ice bodies can be traced on unconsolidated mud (Brodzikowki & Van Loon 1980); seismic activity induced by glacio-isostatic rebound also provides evidence (Hasegawa & Basham 1989). Outside the glacial limits, large undulations of so-called periglacial diapirs in places like the Rhine Graben (Strunk 1983) or basins like Bovey Tracey (Devon) are more likely due to seismically induced shale diapirism.

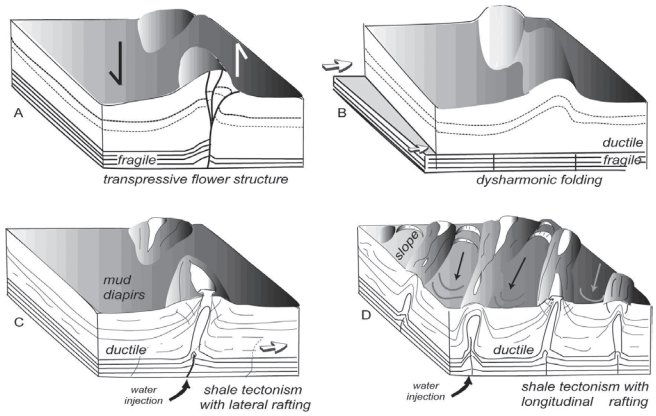

Figure 4. Hypothetic model of deformation at Pénestin. D is the most evident from field data.

Conclusions

The deformations observed along the Mine d'or section at Pénestin represent the evidence of successive events triggered by the distant effects of an earthquake. One major deformational process is shale diapirism, initially triggered by seismic water supply, loading and lateral spreading, favoured by liquefaction of the saprolite basement that allowed the shale diapirism to develop. Traces of periglacial pingo and palsa are not observed at Pénestin, despite the presence of a paleo-relic permafrost. Neither Quaternary transpressive tectonics nor local ruptures are identified at this precise site.

During the seismic event, the phenomenon could have developed further. This whole process resulted, especially at the Mine d'or, in a liquefied mud leaded to a local mega-load cast on top of the saprolite outbursting, with lateral shortening induced by pulsated motion (wrinkling). Post-seismic relaxation, drainage and normal collapse of the stretched saprolite allowed some normal tension faulting to develop, probably also related to mass wasting, especially near "La Source." Diapir motion probably persisted at a much lower rate for a few days or weeks, controlled by the main slope to the west, explaining the bulging of some of the diapirs exploited on the tension zone by younger ice wedge casts (260 ka), when permafrost developed and definitively blocked the motion. Seismically-induced shale diapirism seems to be frequent in active continental basins when a shallow water table is available to promote liquefaction.

References

Bolton, A. & Maltman, A., 1998. Fluid-flow pathways in actively deforming sediments: the role of pore fluid pressure and volume change. Mar.Petr.Geol., 15: 281-297.

Brault, N., Guillocheau, F., Proust, J.-N., Nalpas, T., Brun, J.-P., Bonnet, S. & Bourquin, S. 2001. Le système fluvio-estuarien Pléistocène moyen-supérieur de Pénestin (Morbihan): une Paléo-Loire? Bull. Soc. Géol. France 172: 563-572.

Brodzikowski, K. & Van Loon, A.J. 1980. Sedimentary deformations in Saalian glaciolimnic deposits near Wlostow (Zary area, W. Poland). Geol. Mijnb. 59: 250-272.

De Gans, W., 1988. Pingo scars and their identification. In: M.J. Clark (ed.), Advances in Periglacial Geomorphology. London: Wiley, 299-322.

Eissman, L., 1981. Periglaziäre Prozesse und Permafrost-strukturen aus sechs Kaltzeiten des Quartärs. Altenberger Naturwis. Forsch. 1: 171p.

Gapais, D., Lagarde, J.-L., Le Corre, C., Audren, C., Jegouzo, P., Casas Sainz, A. & Van Den Driessche, J. 1993. La zone de cisaillement de Quiberon. Témoin d'extension de la Chaîne Varisque en Bretagne méridionale au Carbonifère. C.R. Acad. Sci., Ser. II, 316: 1123-1129.

Hasegawa, H.S. & Basham, P.W. 1989. Spatial correlation between seismicity and postglacial rebound in Eastern Canada. In S. Gregersen,S. & P.W. Basham, P.W. (eds), Earthquakes at North-Atlantic Passive Margins: Neotectonics and Postglacial Rebound. Kluwer Acad. Publ., 483-500.

Jenkins, D.G. & Vincent, A. 1981. Periglacial features in the Bovey basin, south Devon. Proc. Ussher Soc. 5 : 201-205.

Laurent, M. 1993. Datation de quartz de formation quaternaires, comparaison avec le paléomagnétisme. PhD, MNHN, Paris, 104 p.

Muir-Wood, R. & King, G.C.P. 1993. Hydrologic signatures of earthquake strain, J. Geophys. Res. 98: 22035-22068.

Obermeier, S.F. 1996. Using liquefaction-induced features for paleoseismic analysis. In: J. McCalpin,J. (ed.), Paleo-Seismology. Acad.Press, 331-396.

Pissart, A. 1983. Remnants of periglacial mounds in the Hautes Fagnes, Belgique; structure and age of the ramparts. Geol. Mijnb. 62: 551-555.

Rivière, A., Vernhet, S. 1962. Accidents périglaciaires dans la région de Pénestin, (Morbihan). C.R. Acad.Sc. Paris, 255: 744-746.

Seed, H.B., Wilson, S.D. 1967. The Turnagain Heights landslide, Anchorage, Alaska. J Soil Mech. Found. Div., ASCE, 93 : 325-353.

SIRENE. 1996. Base de la macrosismicité française. CEA-IRSN-BRGM.

Skempton, A.W. 1953. The colloidal activity of clays. Proceedings of the 3rd International Conference on Soil Mech. & Found. Eng., Switzerland, 1: 57-61.

Strunk, H. 1983. Pleistocene diapiric upturnings of lignites and clayey sediments as periglacial phenomena in central Europe. Proceedings of the Fourth International Permafrost Conference, , Fairbanks, Alaska, July 17-22, 1983: ()1200-4.

Van Vliet-Lanoë, B., Bonnet, S., Hallégouët, B. & Laurent, M. 1997. Neotectonic and seismic activity in the Armorican and Cornubian Massifs: regional stress field with glacio-isostatic influence? J.O.Geodyn. 24: 219-239.

Van Vliet-Lanoë, B., Meilliez, F. & Maygari, A. 2004. Distinguishing between tectonic and periglacial deformations of Quaternary continental deposits in Europe. Glob.Planet.Ch. 43: 103-127.

Van Vliet-Lanoë, B., Hibsch, C., Csontos L., Jegouzo, S, Hallégouët, B, Laurent, M., Maygari, A., Mercier, D. & Voinchet, P., Seismically induced shale diapirism: the Mine d'or section, Vilaine estuary, southern Brittany. Int..J.Earth Sci., in press.

Vendeville, B.C. & Jackson, M.P.A. 1992. a) The rise of diapirs during thin skinned extension. b) The fall of diapirs during thin skinned extension. Mar. Petr. Geol. 9: 331-371.

Youd, T.L., Steidl, J.H., & Nigbor, R.L. 2004. Lessons learned and need for instrumented liquefaction sites. In: Soil Dynamics and Earthquake Engineering 24: 639-646.

The Rich Contributions of A.L. Washburn to Permafrost and Periglacial Studies

Bernard Hallet
Quaternary Research Center and Department of Earth and Space Sciences, University of Washington, Seattle

Abstract

Albert Lincoln Washburn, (1911–2007) contributed immensely to the fields of periglacial geomorphology and permafrost research through his studies, publications, leadership, and personal qualities. His deep interest in the "intimate workings of nature" is evident in his own meticulous and exhaustive field and laboratory studies of diverse types of periglacial processes, including patterned ground formation, slope movement, and ice growth in soils. This review focuses on these productive field studies in Greenland and on Cornwallis Island, and on his research in the Periglacial Laboratory at the University of Washington. Link's intense curiosity about periglacial processes and his untiring, generous effort to properly present the work and ideas of other researchers are clearly evident in his monographs and renowned books, which remain the standard references in the field decades after their publication (*Periglacial Processes and Environments* [1973], *Geocryology—A survey of periglacial processes and environments* [1979]). In addition, Link launched and directed research centers and scientific journals that have nurtured the study of cold landscapes. Significantly, his scientific legacy also includes an exceptional, more personal dimension: the emergence of the unusually cohesive and amiable permafrost/periglacial community, as it was fostered in part by Link and his wife Tahoe's warmth, generosity, and friendship, which graced many members of our worldwide community.

Keywords: active layer; frost heaving; frozen ground; patterned ground; periglacial geomorphology; periglacial processes; permafrost; upfreezing.

"To test the forefront of knowledge for even a brief period, particularly when the subject matter concerned the intimate workings of nature, provided both a motivation and challenge that ... are deep and real for me."

—From one of Lincoln Washburn's rare speeches, 1988

"Quietly content as we trotted beside the kamotik [large dog sled], I thought of some friends who would envy me, and others who would be at a loss to understand why I would wish to undergo what to them would be extreme hardship. I could not have explained my feeling to them then, nor can I do so now.... One is very close to the earth and one's companions but at the same time quite detached—an odd feeling of being free, yet an integral part of the nature of things. The Inuit know they belong to the Arctic. They are an integral part of the natural world around them. While, sadly, many of us have lost touch with it."

—From Tahoe Washburn's (1999) book relating experiences in the Canadian Arctic 1938–41

Introduction

Very sadly, Lincoln Washburn passed away on January 30, 2007, in Seattle; he was 95. He will be missed by many. We can, however, rejoice upon reflecting on his remarkably productive career.

Herein, I highlight his exceptional contributions to science and focus on his pioneering discoveries about processes shaping Arctic landscapes. I also mention his broader contributions to science, which extend well beyond his own research; they include his leadership role in the foundation of major interdisciplinary research centers and academic journals that have nurtured advances in understanding the Polar Regions, the Quaternary period, as well as permafrost and periglacial phenomena.

For more personal information about Link, as his many friends knew him, please refer to the thoughtful obituaries written by two of his long-term friends and colleagues, Steve Porter (2007) and Carl Benson (2007). Considerable material from these sources appears below.

Research Contributions: Field

Here, I focus on Link's productive field studies in Greenland and on Cornwallis Island. They comprise a wealth of detailed observations of surface exposures and excavations of diverse types of patterned ground, and extensive long-term studies of surface displacements to define quantitatively the kinematics of patterned ground activity and slope movement. It was Link's extensive fieldwork that provided the foundation and motivation for his unifying nomenclature and concept about periglacial soil patterns. He coined the term "patterned ground," provided rich and diverse examples, and summarized all ideas current at that time about their genesis (Washburn, 1950, 1956). Interestingly, "patterned ground" is now widely used not only by those working in periglacial features on Earth, but by the planetary community (e.g., Mangold et al. 2004), especially as the current stream of high-resolution images of Mars (e.g., Hi-Rise; http://hirise.lpl.arizona.edu) are revealing diverse forms of patterned ground, many of which resemble those in the hyper arid polar regions where, in contrast with Mars, the conditions and processes manifested in these patterns can be examined and monitored in detail.

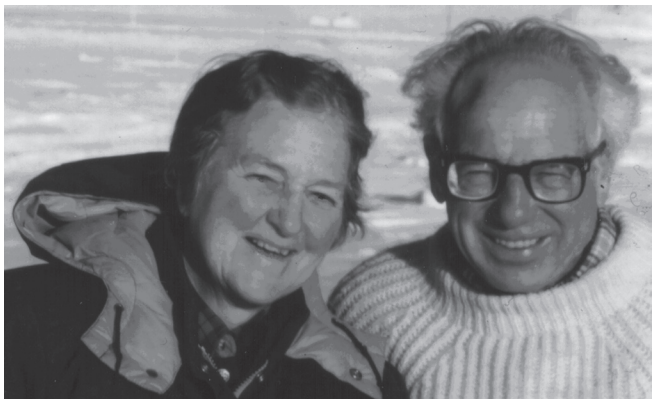

Figure 1. Link and Tahoe Washburn in the late 1980s, Resolute, Cornwalis Island, Canada.

Mesters Vig

Link launched his fieldwork on periglacial processes and features near Mesters Vig in the King Oscar Fjord region of East Greenland, which he had first visited during the Louise Boyd expedition in 1937. He conducted a reconnaissance study in the summer of 1955, established instrumented sites in 1957, and made observations each year from 1957 through 1961, and again in 1964. The results of his studies are presented in three substantial monographs that appear in separate issues of the Danish journal *Meddelelser om Grønland* (Washburn, 1965, 1967, 1969). Collectively, these volumes comprise over 600 pages that record in detail his observations and measurements at more than 20 experimental sites.

His research was comprehensive in addressing a diversity of landforms and periglacial phenomena with a persistent focus on better understanding the formative processes. For example, Washburn (1969) systematically considered 11 forms of weathering, and 12 types of patterned ground. At his experimental sites, he deployed arrays of markers and established detailed photographic records that enabled him to monitor soil motion and surface changes over a period of many years. Moreover, he did not limit himself to landscape features; his outlook was interdisciplinary and included the vegetation and climate of the region, as well as its history of isostatic uplift.

Antarctica

He conducted research in Antarctica in 1957 and 1958 and was involved in planning the multinational, interdisciplinary Dry Valley Drilling Project in 1972-75, which succeeded in drilling a number of deep boreholes into permafrost, which gave revealing glimpses at the subsurface ice distribution, stratigraphy and chemistry, as well as temperature gradient over a large sector of the Dry Valleys near McMurdo. Valuable $\delta^{18}O$ data from the cores at three sites (DVDP cores 8–12) in the Taylor Valley emerged from a study led by his close colleague, Minze Stuiver, in the Quaternary Research Center (QRC, Stuiver et al. 1981). These early isotopic data and chronology continue to help fuel research within the QRC. They now render this location an ideal validation and calibration site for an ongoing effort by QRC scientists, R. Sletten, B. Hagedorn, and me, to understand the existence of subsurface ice in hyper-arid cold regions and to model the isotopic evolution of ground ice.

Resolute

His fieldwork on Cornwallis Island, Arctic Canada, in what is now Nunavut Territory, extended from 1981 to 1995. There, Link focused on solifluction and patterned ground activity. In the former, he established arrays of surface markers that he resurveyed periodically. The patterned ground work consisted of detailed mapping of extensive areas of sorted circles, establishing arrays of markers across individual circles that were repeatedly measured to monitor soil motion, and "bed-frames" that enabled him to monitor the spatial variation in surface heave and settling across a ~5 m^2 area. Washburn (1989) summarized his findings on soil displacements in sorted circles in a comprehensive paper that examines the spatial pattern of changes in position and tilt of dowels inserted in the soil surface. His research results inspired and guided much subsequent field work in diverse Arctic regions by a number of researchers (e.g., Anderson 1988a, Hallet & Prestrud 1986, Hallet et al. 1988, Hallet 1990, Hallet & Waddington 1991)

The culmination of this work is his last major written contribution, a monograph, "Plugs and plug circles: A basic form of patterned ground. Cornwallis Island Arctic Canada—Origin and implications." Washburn (1997) presents the results of years of observations and countless excavations of these soil domains, which develop spontaneously and ascend progressively through the active layer, and are likely to transform into more distinct types of patterned ground. He combines lucid, accurate descriptions with thoughtful and careful interpretations that shed light on the complexity of the principal formative processes active in the early stage of patterned ground development. Interestingly, recent numerical modeling shows sorted patterned ground initiating as plugs much like those depicted by Link (Kessler et al., 2001).

Research Contributions: Laboratory

His research in the Periglacial Laboratory at the University of Washington was focused on the effects of ice growth/thaw and frost heaving/thaw settling on solifluction, vertical textural segregation (sorting), and the development of deformational structures in layered soils. With the competent assistance of researchers, C.M. Burrous and R.G. Rein, Link Washburn used his specially designed laboratory for a comprehensive, long-term study of processes and features of the active layer, including soil deformation on horizontal surfaces and slopes. This laboratory featured a unique tilting slab capable of accommodating soil up to 1 m thick and 9 m^2 in area overlying a simulated permafrost table or an unfrozen substrate.

Next, I will describe two experiments conducted in the 1973–76 period in some detail not only because they yielded interesting sets of useful and unparalleled results, but because

they illustrate the meticulous care taken in conducting the experiments in Link Washburn's Periglacial Laboratory, and in presenting the results. Unfortunately, these studies are essentially unpublished but considerable information is available in detailed internal QRC reports at the University of Washington. Two of these reports are used extensively here: "Soil deformation resulting from some laboratory freeze-thaw experiments" by A.L. Washburn, C.M. Burrous, and R.G. Rein, and "Experimental Upfreezing of Objects: Effects of Object Geometry" by C. M. Burrous. Few results from solifluction and horizontal slab experiments were published (Rein and Burrous 1980, Washburn et al. 1978).

Soil deformation, involutions

Through a number of well-designed, large-scale experiments, with thoroughly documented, simple initial conditions, Link and his co-workers were able to elucidate the rich interactions between soil texture, thermal regime, and soil deformation. Two comprehensive experiments were conducted using frost-susceptible silt on the 2.5 m by 3.6 m slab (Washburn et al. 1978). In experiment 2, for example, the slab was subdivided in plan view into 4 sectors differing in the nature of the upper 3 cm of material, but sharing the same base material, which consisted of 24 cm "clayey$_{12}$sandy$_{16}$silt$_{72}$ of predominantly eolian origin from eastern Washington" overlying 8 cm of "coarse, angular sand (Del Monte white sand) that served as a good basal aquifer. The upper 3 cm of each sector consisted, respectively, of A) clean gravel, B) silt mixed with gravel in the ratio of 6:4, C) white sand, and D) silt identical to base material. The slab was cycled through 10 freeze-thaw cycles, generally ranging from -15ºC to 15ºC while water was made available to the basal sand and remained unfrozen throughout most experiments with piezometric control at least at the onset of freezing

Figure 2 illustrates two sectors, C) with sand at the surface and D) all silt, viewed in a vertical cross-section. It demonstrates cleanly the important effect of surface soil texture on thermal behavior, and highlights the more rapid descent of the freezing front under the sand. This difference in thermal evolution, and associated surface heave, was well documented using a thermocouple probe and a displacement transducer in each sector (Fig. 3). These probes consisted of copper-constantan thermocouples spaced 2 cm apart.

The differential descent of the freezing front due to differences in soil texture results in an inclined freezing front (Fig. 4), which is important because it can induce lateral as well as vertical relative motion of relatively "large" particles in the soil. This lateral motion and inclined freezing fronts are widely recognized to be important in the development of sorted pattern ground. They also figure prominently in numerical models of patterned ground formation (Kessler et al., 2001; Kessler and Werner, 2003), and yet, with the notable exception of these poorly known results, there is a dearth of solid experimental or field data to guide the key assumptions that are required for realistic modeling of the texture-thermal feedbacks that are central to patterned ground formation.

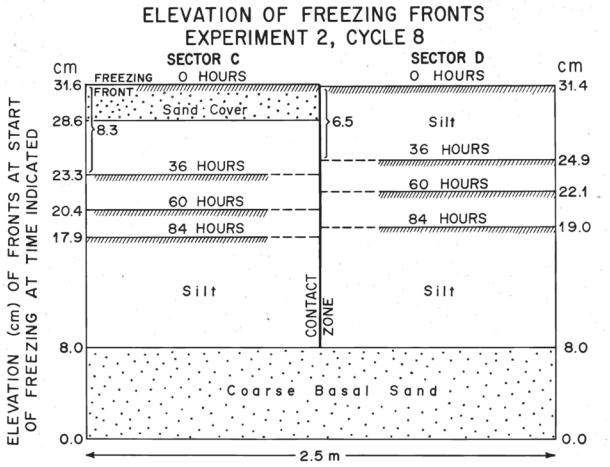

Figure 2. Initial configuration of soil in experiment 2, and descent of freezing front during a typical cooling period. After 36 hours the freezing front had descended 6.5 cm into the silt, and 8.3 cm below the sand cap. The freezing front depth was defined using temperature probes and frost tubes located in each sector, ~11 cm and 41 cm from the contact zone, respectively.

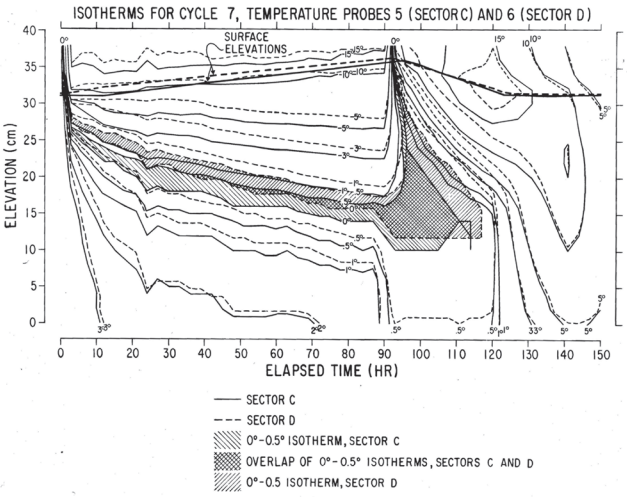

Figure 3. Contrasting thermal evolution and surface heave for the two soil sectors shown in Figure 2 through one representative freeze-thaw cycle.

Aside from important temperature data, these experiments also yielded a wealth of additional observations that were carefully described and interpreted. These are not new, but they gain importance because they arise in a system designed to be simple and uniform in terms of soil materials and moisture content at the onset, with initial conditions that are exceptionally well documented.

In a year-long study, experiment 3, Fairbanks silt, a well known frost-susceptible soil, was subjected to 32 controlled freeze-thaw cycles. The silt was underlain by 6 cm of sand that allowed for the controlled input of water at the base of the soil to fuel the ice lens growth and frost heaving. Typically, to begin freezing the surface temperature was lowered to -20ºC, while the base of the frost-susceptible soil was maintained at 2ºC. This thermal regime was maintained for 4 days, and then the soil was thawed over ~1.5 days by raising the room

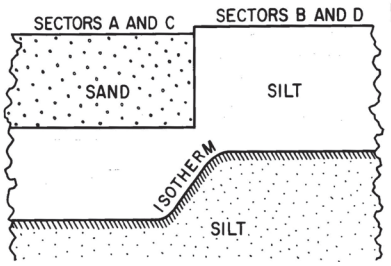

Figure 4. Hypothetical isotherm across the boundary between domains with contrasting surface materials.

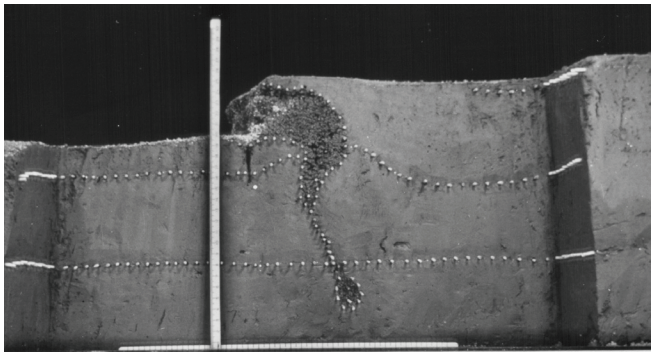

Figure 5. Vertical section at the end of 32 freeze-thaw cycles in experiment #3 highlighting a domain of sand that descended ~20 cm from the surface, a 6 cm-thick layer on the left side (removed before picture was taken). Arrays of white toothpicks delineate glitter surfaces in the soil that were initially horizontal at depths of 0.8, 8.5, and 16.6 cm. Scales are 32 cm long.

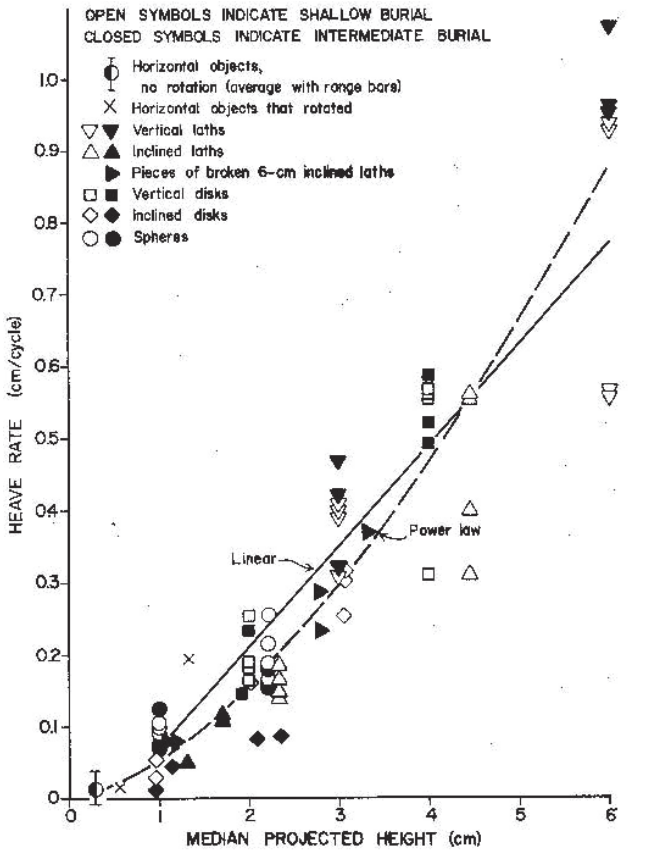

Figure 6. Combined upfreezing data as a function of median projected height of buried glass objects.

temperature and using infrared heaters above the soil surface. The silt surface generally heaved at a nearly uniform rate of 1.2 cm/day as the freezing front descended ~2.8 cm/day; the surface subsided 3.1 cm/day as it thawed. The total heave per cycle was roughly 5 cm, corresponding to a heaving strain of about 20%. Based on visual inspection, this strain is consistent with the volume ratio of visible ice lenses in cores that were taken of the frozen soil. Interesting phenomena developed largely at the boundary between domains with contrasting surface materials; they include A) involutions of sand that penetrated well below the surface, most probably during the thaw-settling phase of the experiments (Fig. 5), and B) shear displacement along a vertical surface and with limited descent of surface sand along this surface. In addition, Link and his co-workers noted details that are seldom mentioned, such as the tendency for bubbles to emerge at the soil surface near shallow up-freezing objects, and the appearance of a gleyed horizon at the silt base.

Upfreezing

Another exhaustive laboratory study examined systematically the dependence of size and shape of diverse objects on the rate at which they progressively ascend through the soil due to repeated cycles of heaving and settling. This was part of the year-long study just described, experiment 3. Prior to freezing, the Fairbanks silt was prepared carefully to permit the precise placement of 54 glass objects of different sizes and shapes (spheres, disks, and laths), with known initial position and orientation, on a 20 cm-grid at each of three levels in a silt layer ~25 cm thick.

A striking result (Fig. 6) is that the distance objects ascend through the silt per freeze/thaw cycle increases roughly linearly with their projected height. Surprisingly, the shape and orientation of the object have little effect. According to this clear result, larger stones are expected to move up toward the surface faster than smaller stones, and the upfreezing rate can be modeled as scaling with the product of the projected height of an object and the heaving strain of the soil. This powerful result inspired Anderson (1988a, b) to launch her own laboratory study of upfreezing, and guided her as she explored the role of upfreezing in sorted patterned ground. According to Figure 6, the net upfreezing of a stone with a projected height of 5 cm, for example, was ~0.6 cm per freeze/thaw cycle. This presumably resulted from an ascent of, at most, 1 cm (the product of the 20% heaving strain and the 5 cm projected height) during the freezing phase, followed by a descent of 0.4 cm during the thaw phase. Anderson (1988a) reported similar ascent/descent ratios during freeze-thaw experiments as long as the stones were well below the soil surface.

Several other findings from this study are noteworthy: 1) inclined tabular objects in these experiments rotated toward the horizontal, which was somewhat surprising in view of the common observation of steeply inclined stones emerging from the tundra that suggest a tendency for upfreezing to

rotate stones toward the vertical; 2) all long (6 cm) inclined laths broke, indicating that these objects were subjected to large torques, presumably during the freezing phase; 3) for objects of the same projected height, laths heaved slightly faster than disks, which in turn heaved faster than spheres; and 4) the depth below the ground surface had little effect, which is counterintuitive because heaving strains were larger at depth due to the slower freezing while the surface heaving rate remained roughly constant; evidently greater upward heave during freezing was offset by greater settling during thaw.

Books and Monographs

Link's deep interest in periglacial processes and his untiring generous effort to present the work and ideas of other researchers properly are clearly evident in his monographs and books, which remain the standard authoritative references worldwide decades after their publication (Washburn 1973, 1979). His books are esteemed for their being thorough and for presenting the fruit of deep scholarly searches, as well as his own research findings. In contrast with most modern journal publications, Link's manuscripts are rich with lengthy presentations of multiple hypotheses and interpretations of diverse periglacial features and processes from researchers worldwide. His recent comprehensive monograph on the multitude of origins that have been proposed for the Mima Mounds in western Washington (Washburn 1987) exemplifies these qualities.

A Leader and a Visionary

Lastly, I wish to highlight Link Washburn's considerable contribution to science through his exceptional leadership and vision. He gained much recognition and appreciation while serving as the first director of the Arctic Institute (Dunbar 1952). Later, but still decades before the emergence of "earth system science" and the widespread concern about global warming, Link envisioned and launched the Quaternary Research Center at the University of Washington to promote interdisciplinary research about the global environment during the Quaternary. This fascinating period features the evolution of humans and the advent of civilization as well as massive abrupt changes in climate, sea level, global biota, and ice extent that still challenge our understanding and remind us of the difficulty of predicting climate and environmental change. Sensing the need for a scientific journal devoted to this important field, Link launched *Quaternary Research*, which appeared in 1970. "He shepherded the journal through its first 5 years, establishing for it a reputation for breadth and excellence, and making it one of the most widely cited earth science publications" (Porter 2007).

Link has been recognized and honored nationally and internationally. A few apt words by Albert Pissart (personal communication from Liège, Belgium, 2007) capture the essence of this worldwide recognition; reflecting on his deceased friend, he wrote: "j'avais conservé un culte pour ses travaux, son honnêteté scientifique, sa modestie et son extrême amabilité." Loosely translated, Albert worshipped Link's work, his scientific honesty, his modesty, and his extreme kindness. Moreover, Albert noted that with his appetite for learning and unusual fluency in German and French, he read and understood essentially all published material, and on his frequent trips to meetings in Europe between 1959 and 1985, he exchanged ideas and information freely within the European as well as the American scientific community. This exceptionally rich background contributed to his monographs and books, which were the first important syntheses of worldwide knowledge to date about periglacial processes and landforms and their connections with fossil periglacial features.

Albert also stressed that Link had received the highest scientific recognition possible in Belgium as an elected associate member of the Royal Academy. Steve Porter (2007) provides a listing of the numerous honors he received and the committees and organizations for which Link served as a directing officer, both nationally and internationally.

Summary

Highlights of Link's career include unfailing scholarship, research, administration, and careful detailed planning. His books and monographs catalyzed the emergence of periglacial geomorphology as a distinct scientific field, and solidified the field internationally by assembling and generously distilling results from a multitude of studies scattered in diverse sources worldwide, across national and linguistic boundaries. In addition to the research centers he directed and the scientific journals he launched, his rich scientific legacy includes the unusually cohesive and amiable permafrost and periglacial community, the emergence of which was fostered in part by Link and Tahoe's warmth, generosity, and friendship, which reached many members of this worldwide community.

Acknowledgments

I thank Steve Porter and Carl Benson for their thoughtful and comprehensive obituaries, sections of which I have borrowed from liberally, Ross Mackay and Albert Pissart for helpful communications, and Land Washburn for permitting use of the photograph of Link and Tahoe.

References

Anderson, S.P. 1988a. Upfreezing in sorted circles, western Spitsbergen. *Proceedings of the 5th International Conference on Permafrost,* Trondheim, Norway.

Anderson, S.P. 1988b. The upfreezing process; experiments with a single clast. *Geological Society of America Bulletin* 100 (4): 609-621.

Benson, Carl S. 2007. Albert Lincoln Washburn (1911–2007). *Arctic* 60(2).

Dunbar, M.J. 1952. A.L. Washburn. *Arctic* 5(1): 3.

Hallet, B. 1990. Self organization in freezing soils: from microscopic ice lenses to patterned ground. *Canadian Journal of Physics* 68: 842-852.

Hallet, B. & Prestrud, S. 1986. Dynamics of periglacial sorted circles in Western Spitsbergen. *Quaternary Research* 26: 81-99.

Hallet, B. & Waddington, E.D. 1991. Buoyancy forces induced by freeze/thaw in the active layer: implications for diapirism and soil circulation. In: J.C. Dixon & A.D. Abrahams (eds.) *Periglacial Geomorphology.* Proceedings, 22nd Binghampton Geomorphology Symposium 1991. New York: J. Wiley and Sons, 251-279.

Hallet, B., Anderson, S., Stubbs, C.W. & Gregory, E.C. 1988. Surface soil displacements in sorted circles, western Spitsbergen. *Proceedings, Fifth International Conference on Permafrost,* Trondheim, Norway 1: 770-775.

Kessler, M., Werner, B., Murray, B. & Hallet, B. 2001. A model for sorted circles as self-organized patterns. *Journal of Geophysical Research-Solid Earth* 106 (B7): 13287-13306.

Kessler, M. & Werner, B. 2003. Self-organization of sorted patterned ground. *Science* 299(5605): 380-383.

Mangold, N., Maurice, S., Feldman, W.C., Costard, F. & Forget, F. 2004. Spatial relationships between patterned ground and ground ice detected by the Neutron Spectrometer on Mars. *Journal of Geophysical Research* 109(E08001), doi:10.1029/2004JE002235.

Porter, S.C. 2007. In memoriam: A. Lincoln Washburn (1911-2007). *Quaternary Research* 67: 311-312.

Rein, R.G. Jr. & Burrous, C.M. 1980. Laboratory measurements of subsurface displacements during thaw of low-angle slopes of a frost-susceptible soil. *Arctic and Alpine Research* 12(3): 349-358.

Stuiver, M., Yang, I.C., Denton, G.H. & Kellog, T.B. 1981. Oxygen isotope ratios of Antarctic permafrost and glacier ice. *Antarctic Research Series: Dry Valley Drilling Project*. L.D. McGinnis. Washington, D.C., American Geophysical Union 33: 131-139.

Washburn, A.L. 1947. Reconnaissance geology of portions of Victoria Island and adjacent regions, Arctic Canada. *Geological Society of America Memoir* 22, 142 pp.

Washburn, A.L. 1950. Patterned ground. *Revue Canadienne de Géographie* 4: 5-54.

Washburn, A.L. 1956. Classification of patterned ground and review of suggested origins. *Geological Society of America Bulletin* 67: 823-866.

Washburn, A.L. 1965. Geomorphic and vegetational studies in the Mesters Vig District, Northeast Greenland. *Meddelelser om Grønland* 166(1), 60 pp.

Washburn, A.L. 1967. Instrumental observations of mass-wasting in the Mesters Vig District, Northeast Greenland. *Meddelelser om Grønland* 166(4), 296 pp.

Washburn, A.L. 1969. Weathering, frost action, and patterned ground in the Mesters Vig District, Northeast Greenland. *Meddelelser om Grønland* 176(4), 303 pp.

Washburn, A.L. 1970. An approach to a genetic classification of patterned ground. *Acta Geographica Lodziensia* 24: 437-446.

Washburn, A.L. 1973. *Periglacial Processes and Environments.* London: Edward Arnold, 320 pp.

Washburn, A.L. 1979. *Geocryology: A Survey of Periglacial Processes and Environments*. London: Edward Arnold, 402 pp.

Washburn, A.L. 1980. Permafrost features as evidence of climatic change. *Earth Science Reviews* 15: 327-402.

Washburn, A.L. 1987. Mima mounds: An evaluation of proposed origins, with special reference to the Puget Lowland. Washington Department of Natural Resources. Division of Geology and Earth Resources. *Report of Investigations* 29, 53 pp.

Washburn, A.L. 1989. Near-surface soil displacement in sorted circles, Resolute area, Cornwallis Island, Canadian High Arctic. *Canadian Journal of Earth Sciences* 26: 941-955.

Washburn, A.L. 1997. Plugs and plug circles: A basic form of patterned ground. Cornwallis Island Arctic Canada: Origin and implications. *Geological Society of America Memoir* 190, 183 pp.

Washburn, A.L., Sanders, J.E. & Flint, R.F. 1964. A convenient nomenclature for poorly sorted sediments. *Journal of Sedimentary Petrology* 33: 478-480.

Washburn, A.L., Burrous, C.M. & Rein, R.G. Jr. 1978. Soil deformation resulting from some laboratory freeze-thaw experiments. *Proceedings 3rd International Conference on Permafrost,* Trondheim, Norway.

Washburn, T.T. 1999. *Under Polaris: An Arctic Quest*. Seattle: University of Washington Press.

—Plenary Paper—

Advances in Permafrost and Periglacial Research in the Dry Valleys, Antarctica

Bernard Hallet, Ronald S. Sletten, Jaakko Putkonen
Quaternary Research Center, University of Washington, Seattle WA 98195, USA

Abstract

Extremely dry and cold conditions in continental portions of Antarctica lead to permafrost properties and periglacial processes that merit special attention because they are quite distinct from those in the Arctic, which are generally more familiar. Moreover, they resemble most closely those on Mars, providing powerful analogues that are helpful in interpreting the surface of the planet and the dominant surficial processes, as well as evidence for major recent change in the climate of Mars. Herein, we review recent studies of periglacial processes and implications for understanding the hyper-arid, cryogenic landscape typical of the non-ice covered portions of the Antarctic continent and beyond. Our review is selective as it is limited to the research we are familiar with in the Dry Valleys region; it includes 1) thermal and moisture states of Antarctic permafrost 2) factors affecting the formation, stability and longevity of ice below the ground surface, 3) nature and rates of patterned ground processes with a focus on sand-wedge polygons, 4) rates and mechanisms of permafrost creep, hillslope processes and sediment transport, and 5) specific analogues pertinent to permafrost and periglacial activity on Mars, and related inferences about Martian climate change.

Keywords: Antarctica; contraction cracks; Dry Valleys; Mars; patterned ground; periglacial; permafrost.

Introduction

In comparison with the Arctic, the Antarctic continent is very cold and extremely dry. In addition to leading to distinct thermal conditions below the ground surface, the cold and hyper-arid conditions cause major differences in permafrost properties and processes between the polar regions. The dearth of water in the Dry Valleys profoundly affects a suite of periglacial processes that are fueled by large volumetric changes associated with freezing and thawing in water-rich systems. Frost heaving is very limited, which curtails a suite of processes that are directly linked to ice lens or needle ice growth: weathering of bedrock and sediments, frost-induced sorting of material, formation of sorted patterned ground, and downslope motion of debris. On the other hand, the large seasonal temperature fluctuations, and in particular the very low soil temperatures attained in the winter because of the lack of thick insulating blanket of snow, lead to large thermal stresses in the upper part of the permafrost; the resulting thermal contraction cracks in the permafrost render polygonal patterned ground pervasive and often the dominant surface texture of extensive areas. The dry conditions also lead to two characteristics unusual in wetter cold regions: the accumulation of salts at and below the ground surface, and the importance of eolian processes in shaping the periglacial landscape. Moreover, under the cold conditions that prevail in the Dry Valleys, subsurface ice can form and persist for long periods of time, and landscape evolution can be extremely slow.

The relatively slow periglacial processes and stable landscapes typical of Antarctica merit special attention because they contrast with those in the Arctic, which are generally more familiar, and they resemble those on Mars most closely, providing an informative analogue environment that is helpful in interpreting the surface of that planet. Moreover, diverse techniques that have been developed for studying permafrost and periglacial systems in the Antarctic may prove useful in other cold regions. They include 1) analyses of cosmogenic nuclide concentrations in bedrock, sediment, soil and ice for diverse objectives: determining rates of weathering and sublimation of buried ice, ages of deposition, and duration of exposure or burial; 2) isotopic, trace and major element studies of subsurface ice to examine the origin and evolution of the ice, and 3) ground displacements using in situ instrumentation as well as space borne techniques (GPS, SAR Interferometry) to document the magnitude of thermally or gravitationally driven regolith motion.

Permafrost and periglacial process studies in the Antarctic also complement those in the Arctic in addressing questions that seldom emerge in the wetter and more dynamic frozen landscape of the Arctic. Why is there ice below the surface in this dry environment? What is the longevity of buried ice? What is the rate of sublimation of that ice? What is the origin of salts and how do they affect H_2O transport, and ionic transport and isotopic exchange in the ice? How stable is the ground surface or a landform?

Herein, we do not attempt to provide a comprehensive review but rather summarize the more substantial advances in terms of new approaches, methodology, or insight gained into key processes largely in the Dry Valleys of southern Victoria Land, near McMurdo, which contain the largest non-ice covered area on the Antarctic continent (Campbell & Claridge 2006).

Thermal Properties of Dry Valley Soils

Two primary factors distinguish the soil thermal regime in the Dry Valleys from that of a typical Arctic site: 1) soils are extremely cold in the winter, often dropping below -40ºC (Fig. 1), and 2) the near surface soil (the upper ~0–20 cm) often lacks H_2O, making the soil an effective, cohesionless

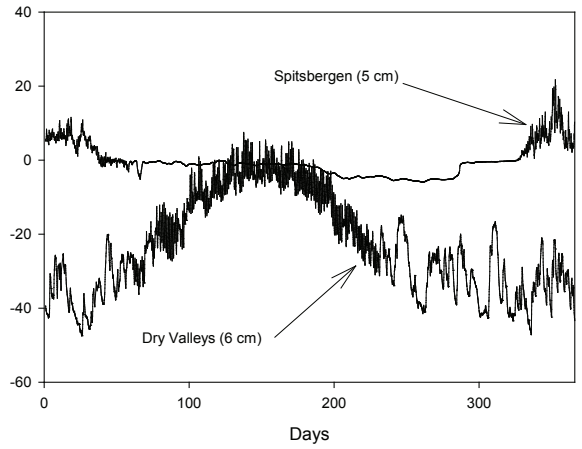

Figure 1. Soil temperatures 5 and 6 cm below the ground surface in Spitsbergen (Putkonen 1998), and in the Dry Valleys (Putkonen et al. 2003). The data span one year starting on the first of August. As the field sites are in opposite hemispheres, the summers are out of phase. Note very cold and variable conditions, and the conspicuous absence of the zero-degree curtain or other phase change effects close to 0ºC in the Dry Valleys.

insulator (Putkonen et al. 2003) with bulk soil thermal conductivities as low as 0.1–0.4 W m^{-1} K^{-1}. Laboratory measurements of typical dry surface soil samples, yield values of 0.3 W m^{-1} K^{-1} for the thermal conductivity 1000 J kg^{-1} K^{-1} for the heat capacity and 1200–1800 kg m^{-3} for the density; correspondingly, the thermal diffusivity is 0.17–0.25 x 10^{-6} m^2 s^{-1}

Such a low thermal conductivity promotes steep thermal gradients, which can reach 200 K m^{-1} near the soil surface, and limits the penetration of surface temperature variations (Putkonen et al. 2003). The dearth of near surface ice/water also eliminates all thermal effects related to the phase change of water that are characteristic of Arctic soils.

Due to the cold winters, short cool summers and low thermal conductivity of the dry soil, the active layer is thin, ranging from 30-60 cm for low altitude coastal sites to about 15 cm in the alpine valleys ~1400 m asl and about 70 km from the coast (Campbell et al. 1998, Putkonen et al. 2003). Snow may fall any time of the year, but the thin snow cover (typically less than 30 cm) lasts only days (Campbell et al. 1998, Hagedorn et al. 2007). Without the insulating snow cover, the near surface soil temperatures vary widely through the winter reflecting the large variations in atmospheric conditions.

Moisture State

Due to low precipitation and air temperatures, averaging around –20°C, in the Dry Valleys, liquid water is very limited; most snow sublimates and only a small amount melts, delivering little or no moisture to the ground (Gooseff et al. 2003, Hagedorn et al. 2007). Campbell and Claridge (1982) report that soil moisture moves mostly in the form of vapor with limited migration of snow melt. Nevertheless, salt horizons and salt crystallization beneath stones are prevalent in the Dry Valleys (Keys & Williams 1981); considering the limited solubility of the salts, these accumulations reflect significant long term fluxes of liquid water even under these extremely arid conditions.

Water persists in thin films on mineral surfaces to very low temperatures (Anderson & Morgenstern 1973, Yong et al. 1979, Fu et al. 1993) and considerable ion migration probably occurs along these films (Ugolini & Anderson 1973, Wettlaufer & Worster 1995, Claridge et al. 1996, Wettlaufer 1999, Wettlaufer 2001, Dickinson & Rosen 2003). The high solute content lowers the freezing point of water well below 0°C, and tends to increase the mobility of both water and solutes by thickening these films. To date only two studies of transport rates have been performed in the field. Using LiCl-tracers in Antarctic soils, Claridge et al. (1996) documented Li diffusion 15–25 cm into the soil and 5 m laterally in ≤ 3 years, with a strong dependence on the moisture content. Application of ^{36}Cl and ^{22}Na-labeled NaCl close to the ice-cemented permafrost in Wright Valley by Ugolini and Anderson (1973) revealed upward migration of both ions but significantly less movement of ^{22}Na than ^{36}Cl, presumably due to differences in diffusion coefficients and chemical behavior e.g., ion exchange and adsorption.

Subsurface Ice

Subsurface ice is pervasive in the Dry Valleys, where it occurs in various forms: pore ice, ice in permafrost cracks, and buried lake or buried glacial ice (Bockheim & Hall 2002, Campbell & Claridge 2006).

This ice is fundamental to diverse periglacial processes, including patterned ground activity and mass wasting, not only in Antarctica but also on Mars. Its existence within the top decimeters in soils that are 10^4 to 10^6 year old is enigmatic, however, since current models indicate that any ice within few meters of the surface would sublimate into atmosphere within several thousand years (van der Wateren & Hindmarsh 1995, Hindmarsh et al. 1998, Schorghofer 2005). Most recently, Hagedorn et al. (2007) explore mechanisms that slow or may reverse ice loss from the soil to the atmosphere, and incorporate them into a sublimation model that uses high-resolution climate and soil temperature data in Victoria Valley, where the surface is ~10 Ka old and the soil is ice cemented 0.22 m below the surface. According to this model, snow slows long-term sublimation but, due to the dearth of data on the duration and timing of snow cover, the potential of snow melt to offset vapor transport out of the soil cannot be assessed quantitatively at present. Studies of depth profiles of δD and $\delta^{18}O$ in pore ice are providing new insights into the origin and evolution of ground ice in the Dry Valleys (Hagedorn et al. 2003, Souchez & Lorrain 2006).

Massive subsurface ice occurs sporadically in the Dry Valleys. Much effort has been directed at dating and understanding the origin and longevity of this buried ice, especially in Beacon Valley where it has been interpreted as the oldest glacier ice on Earth. Such ancient ice would be of

considerable interest because it may contain an unparalleled archive of paleoenvironmental conditions and lyophilized bacteria. Sugden et al. (1995) reported an 8.1 Ma volcanic ash in the sublimation till overlying this ice, and viewed it as a direct air-fall deposit. This interpretation implies slow sublimation for the survival of both the ice and the delicate layer of ash and hence, a persistent cold climate, which has broad implications about global climate stability since the Miocene. This extreme stability is not, however, consistent with independent estimates of sublimation rates of 50 m Ma^{-1} and ~10^3 m Ma^{-1}, respectively from measurements of cosmogenic nuclides in a 19-m ice core (Stone et al. 2000) and from theory (e.g., Hindmarsh et al. 1998). Moreover the use of the ash to constrain the age of the ice has been questioned by Sletten et al. (2007) who reported old tephra erratics within the sublimation till.

One way to resolve this age controversy is to decipher the history of the till overlying the massive ice from cosmogenic nuclide measurements. The till is a residue of debris-laden ice that sublimed. Ng et al. (2005) reinterpreted published ^{3}He depth profiles through the sublimation till in Beacon Valley, Antarctica, to derive rigorous constraints on the till-thickness history and on the amount and rate of ice loss by sublimation. The ^{3}He profiles show that the lower 80% of the till formed in the past 310–43 ka under sublimation rates averaging >7 m Ma^{-1}. Such rapid, recent growth of the till contradicts previous interpretations that it is older than 8.1 Ma at an adjacent site, where it encloses volcanic ash of this age, casting additional doubt on the validity of the ash in constraining the age of the ice.

Soil Distribution and Characteristics, and Weathering

Relative to many well studied portions of the Arctic, the spatial distribution of soils in the Dry Valleys region has received little attention until recently (Bockheim et al. 2007). A new soil map is being developed for selected regions of the McMurdo Dry Valleys (McLeod et al. 2007). As mentioned earlier, the active layer tends to be relatively dry and shallow (Paetzold et al. 2003); it is often ice-free particularly at the higher elevation sites near the ice sheet (Bockheim et al. 2007).

The paucity of liquid water in the Dry Valleys leads to soils sharing many characteristics with soils of arid regions with considerable salt accumulation. The dominant salts are chlorides, nitrates, and sulfate, mostly of direct marine origin (Bao et al. 2008); the latter two reflect oxidation in the atmosphere prior to deposition (Bao et al. 2000). The abundance of salts influences soil moisture (Hagedorn et al. 2007), weathering (Dickinson & Grapes 1997), and biology (Barrett et al. 2006).

The Dry Valleys Long Term Ecological Research site in Taylor Valley has served as a focus for studies of soil processes related to the soil fauna (Barrett et al. 2006, Wall et al. 2006) and to chemical weathering, which influences the chemistry of soil water, as well as streams and lakes (Lyons et al. 2002, Gooseff et al. 2007). Publications on the soils, hydrology, and biota are listed on the LTER web site (www.mcmlter.org).

The cold, hyper-arid conditions lead to some of the lowest known bedrock erosion rates on Earth. A powerful means of determining these rates has been exposure age dating using cosmogenic nuclides. Such research in the Dry Valleys area has shown that 1) the bedrock surfaces have been exposed sub-aerially for millions of years; notably they have not been buried by ice sheets or covered by water or sediments, and 2) these bedrock surfaces erode at rates of ~1 m Ma^{-1} (Nishiizumi et al. 1991, Brook et al. 1995, Summerfield et al. 1999, Smith et al. 2001, Schoenbohm et al. 2004). These bedrock erosion rates are among the lowest recorded on Earth and are 1-3 orders of magnitude slower than, for example, ~10 m Ma^{-1} in the Sierra Nevada, USA (Stock et al. 2005).

Patterned Ground

Polygonal patterned ground is ubiquitous in the Dry Valleys, even on steep hillslopes. In this and other arid, cold regions, thermal contraction cracks tend to open at the ground surface during cold periods. In contrast with regions where moisture is abundant and the cracks tend to fill with water and ice, the Dry Valley cracks fill partially with wind-blown sand and other fine-grained debris. This infilling prevents the cracks from fully closing during warm periods. During subsequent cooling periods, each crack reopens, permitting more sand infilling, thereby, incrementally forming a wedge of sand. With time, the ground surface on either side of the crack is warped upward by the growing sand wedge to form symmetrical ridges separated by a trough over the crack (Péwé 1959). These sand-filled cracks interconnect to form polygons (Fig. 2) that have received very little attention compared to the thoroughly studied ice-wedge polygons (Mackay 1971, 2002).

The progressive growth of sand-wedges can be examined by monitoring the distance between markers installed across contraction cracks. Recent measurements of 417 pairs of steel rods, which were hammered vertically into the ground on opposite sides of contraction cracks at 13 sites established in the early 1960s by Robert Black, show steady divergence across the sand-wedges of patterned ground in the Dry

Figure 2. Polygonal patterned ground in upper Victoria Valley. These distinctive low-centered polygons form spontaneously from the recurrent opening and closing of cracks due to thermal strains, and the progressive addition of wind-blown sand into the cracks.

Valleys. Rod spacings were measured on several occasions from 1962 to 2002 (Berg & Black 1966, Black 1973, Black 1982, Malin & Rawine 1995, Sletten & Hallet 2004). Individual divergence rates between paired rods in lower Beacon Valley, for example, are highly variable, ranging from 0.1 to 1.8 mm a^{-1}. By 2002, the mean distance between rod tops increased 20–25 mm (std. dev. 16-18 mm) since their installation 39 years earlier. The rates are remarkably steady in time, and are essentially identical to those at sites recently established to continuously monitor contraction crack dynamics (Sletten et al. 2003).

The recurrent cracking and sustained addition of wind-blown sand to a depth of ~5 m generate long-term pervasive deformation in the permafrost and wedge material and net surface aggradation, or inflation, at rates of 0.05 to 0.1 mm a^{-1}. Evidence for both surface and sub-surface deformation includes the pair of ridges that commonly border each contraction crack (Fig. 2), and frozen soil layers that are often warped upward as they approach the wedge (Péwé 1959). Recent, high resolution instrumental measurements show significant thermally-induced permafrost deformation and are invaluable in studying the dynamics of this form of patterned ground (Fig. 3).

This soil deformation is complex, and constitutes a form of cryoturbation that is expected to pervasively disrupt geomorphic surfaces where sand-wedge polygons are active. The ratio of polygon size (~10 m) to typical sand-wedge growth rate (~1 mm a^{-1}) for lower Beacon Valley provides an indication of the time scale for the reworking of the ground surface, which is only ~10^4 years. Provided that the rates of wedge growth deduced from Black's data over the last few decades can be extrapolated to considerably longer time scales, they challenge the notion that similar nearby geomorphic surfaces have been stable for millions of years, as proposed by Sugden et al. (1995) and Marchant et al. (2002).

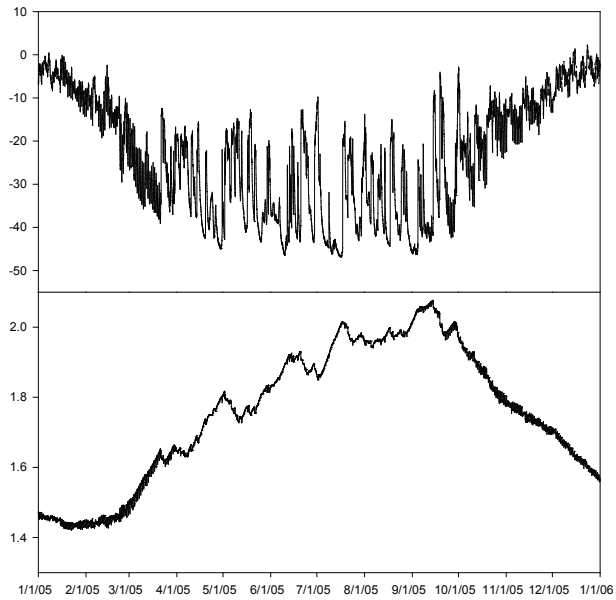

Figure 3. Air temperature (deg C) at 2 m and increase in distance between two markers (in cm) that are ~2 m apart across a contraction crack in central Beacon Valley. Displacements were measured with micrometer resolution using a linear motion transducer. Data were recorded hourly using a Campbell CR10X data logger.

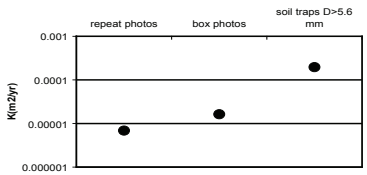

Figure 4. Mean topographic diffusivity for Dry Valleys determined using repeat photography and soil traps. These values approach the lowest known terrestrial values from hot deserts and they contrast strongly with those in the Arctic where regolith fluxes are among the highest on Earth. For additional details see (Putkonen et al. 2007).

Slope Processes

The stability of ground surfaces and preservation of deposits that record past events and environments are important to studies of the geologic and climatic history of Antarctica. Clear indications of downslope debris transport such as solifluction lobes and direct measurements of debris motion on slopes, which are common in the Arctic, are rare in the Dry Valleys; elongated polygons or sorted stripes, and solifluction terraces are uncommon. (Putkonen et al. in press).

Although the common occurrence of ancient volcanic ashes at or near ground surfaces suggests essentially perfect preservation of sedimentary deposits in the Dry Valleys (Marchant et al. 1993, Marchant & Denton 1996, Marchant et al. 1996) and negligible downslope debris motion, recent research suggests rates of downslope motion that approach those in hot deserts.

In contrast with the Arctic, all the downslope movement in the Dry Valleys is limited to the upper few centimeters of the dry soil (Putkonen et al. in press). Using repeat photographs, soil traps, and measurements of downslope displacements of rock fragments in the Dry Valleys, Putkonen et al. (2007) determined a sediment transport coefficient (topographic diffusivity) for the Dry Valleys that normalizes the debris flux per unit width of the slope for the local slope angle (Fig. 4). This contemporary diffusivity ranges from 10^{-5} to 10^{-4} m^2 a^{-1}; it is relatively low but approaches those previously reported from other sites worldwide (Oehm & Hallet 2005). Indirect observations in the Dry Valleys suggests that strong winds play a significant role in the downslope transport of dry debris as they can destabilize relatively large pebbles as evidenced by gravel dunes in the lower Wright valley and sediment recovered in soil traps (Lancaster 2002, Putkonen et al. 2007). The topographic diffusivities are highest in alpine valleys located farther inland from the coast, and lowest near the coast.

To determine the longer term downslope debris flux Putkonen et al. (2007) also analyzed concentrations of distinct rock fragments found downhill of eroding source boulders. These boulder trails yielded a lower limit for the

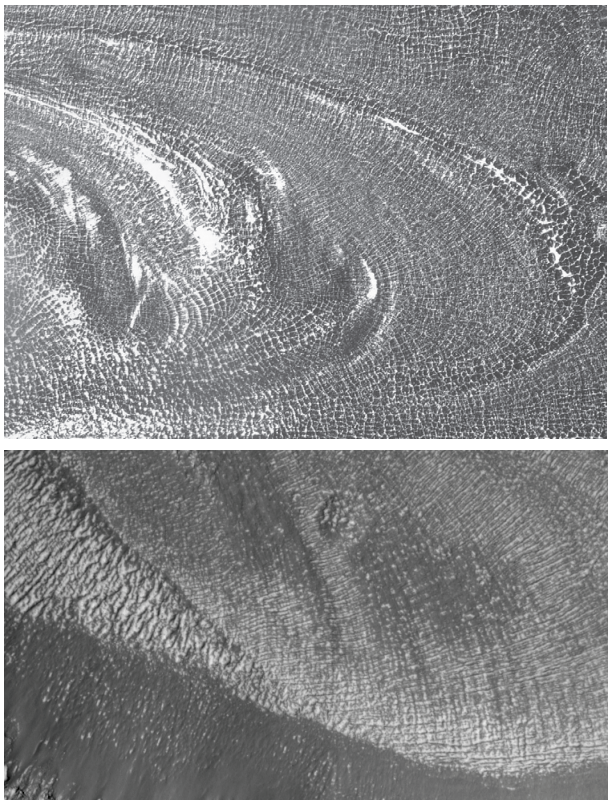

Figure 5. Upper picture shows accurate ridges and a pervasive system of near-orthogonal surface cracks on the rock glacier in upper Mullins, Valley, Antarctica. Similar terrain is observed on Mars (MOC S05-01603).

long term topographic diffusivity of order 10^{-8}–10^{-7} m^2 a^{-1}; actual diffusivities are likely much larger. Another source of information about the long-term mobility of surface debris can be extracted from braking blocks, which are partially exhumed boulders that have a typical bulge of regolith on the uphill side and a depression on the downhill side; they are ubiquitous in the Dry Valleys. Using a model of downslope motion governed by local slope, Morgan and Putkonen (2005) simulated the evolution of the microtopography toward a steady state, obtaining results resembling closely the microtopography observed in the field. They were able to assess minimum regolith transport rates; the corresponding topographic diffusivity was found to exceed 10^{-6} m^2 a^{-1}.

In conclusion, the rates at which debris moves downslope in Antarctica are generally the smallest known on earth; they strongly contrasts with those from wet Arctic that are among the highest. Despite these low rates, downslope debris transport can significantly alter landforms and disturb ancient deposits in the Dry valleys over a typical exposure time of millions of years.

Rock Glaciers – Permafrost Creep

The absence of vegetation, dearth of snow and stability of land surfaces in the Dry Valleys are ideal for the use of satellite-based Synthetic Aperture Radar studies of surface motion as the surface maintains excellent coherence of the radar returns over several years. Rignot et al. (2002) obtained a

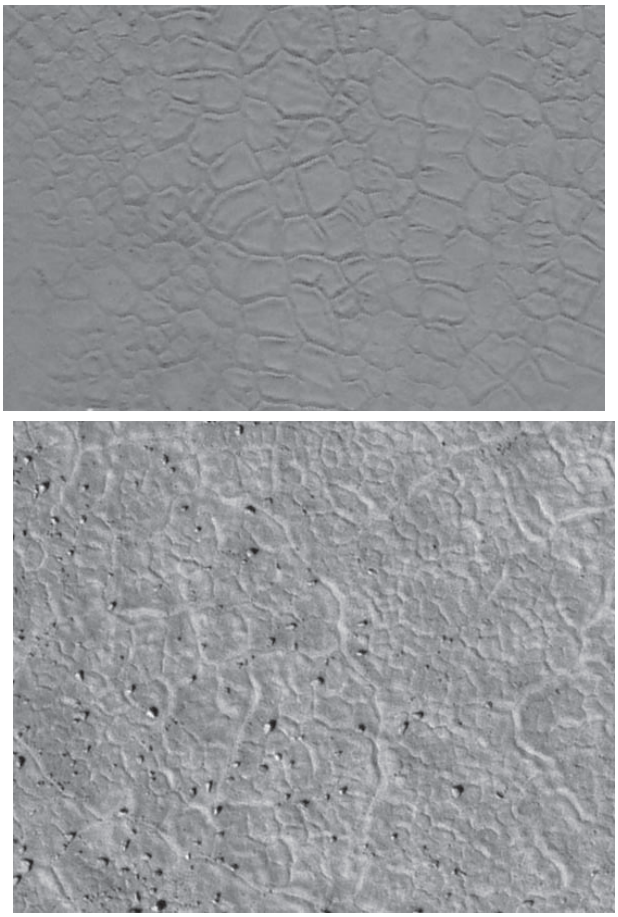

Figure 6. Aerial photograph of Victoria Valley (top) and analogous terrain on Mars (HiRise image TRA_000828_2495_IRB; illumination from the lower left). Shallow surface troughs outline polygons approximately 10–20 m across.

spatially continuous surface velocity field with a precision of fractions of a millimeter per year on rock glaciers (debris-covered glaciers) entering Beacon Valley. They found coherent velocity patterns, with peak velocities approaching 40 mm per year; these velocities are consistent with our unpublished GPS measurements of surface boulder motion.

The ice supply from these rock glaciers nourishes the central portion of Beacon Valley, where it sublimates. Interestingly, the ice supply balances the loss by sublimation provided sublimation rates are within the 0.02–0.2 mm a^{-1} range, which brackets the net sublimation rate of 0.05 mm a^{-1} obtained using cosmogenic isotopes in subsurface ice (Stone et al. 2000).

The surface of rock glaciers displays a series of features strikingly similar to those imaged on Mars suggesting the likely presence of debris-covered massive ice on Mars. Figure 5 illustrates many of these features including lobe-like forms, arcuate ridges, and complex dense patterns of surface cracks.

Studying Mars Using Antarctica Analogue

The cold and dry near-surface conditions typical of the Dry Valleys approach those on Mars. Studies of Antarctica

as a useful analogue were initiated in the 1970s after the first images were taken by the Mariner and Viking spacecraft (e.g., Anderson et al. 1972). With additional successful missions and the recent acquisition of much higher resolution images, along with compelling evidence for widespread ice in the upper ~1 m of permafrost (Boynton et al. 2002), there is a considerable resurgence in interest to use the Dry Valleys as a popular natural laboratory to study landforms and processes that occur or may occur on Mars. They include rock glaciers and moraines (Head & Marchant 2003), the sublimation of subsurface ice (McKay et al. 1998, Hagedorn et al. 2007) that has much in common with the identical process on Mars (Schorghofer 2005), the formation of polygonal patterned ground (Fig. 6) and associated micro-relief (Mellon 1997, Sletten & Hallet 2003), and the occurrence and preservation of simple life forms under extreme polar conditions (e.g., Gilichinsky et al. 2007).

Acknowledgments

We acknowledge C. McKay, B. Hagedorn, D. Gilichinsky, M. Mellon and A. Gillespie for assisting us in the field and/or for informative discussions pertinent to this review. This material is based upon work supported by the National Science Foundation under Grant No. 9726139 & 0636998, and by NASA Grant NNX06AC10G. The authors acknowledge the use of Mars Orbiter Camera (MOC) images processed by Malin Space Science Systems that are available at http://www.msss.com/moc_gallery/.

References

Anderson, D.M., Gatto, L.W. & Ugolini, F.C. 1972. An antarctic analog of Martian permafrost terrain. *Antarctic Journal of the U.S.* 7: 114-116.

Anderson, D.W. & Morgenstern, N.R. 1973. Physics, chemistry, and mechanics of frozen ground: a review. *Permafrost; Second International Conference, Proceedings*, Yakutsk, USSR, National Academy of Sciences Press, Washington, D.C., 257-288.

Bao, H.M., Barnes, J.D., Sharp, Z.D. & Marchant, D.R. 2008. Two chloride sources in soils of the McMurdo Dry Valleys, Antarctica. *Journal of Geophysical Research-Atmospheres* 113(D3).

Bao, H.M., Campbell, D.A., Bockheim, J.G. & Thiemens, M.H. 2000. Origins of sulphate in Antarctic dry-valley soils as deduced from anomalous ^{17}O compositions. *Nature* 407(6803): 499-502.

Barrett, J.E., Virginia, R.A., Hopkins, D.W., Aislabie, J., Bargagli, R., Bockheim, J.G., Campbell, I.B., Lyons, W. B., Moorhead, D., Nkem, J., Sletten, R.S., Steltzer, H., Wall, D.H. & Wallenstein, M. 2006. Terrestrial Ecosystem Processes of Victoria Land, Antarctica. *Soil Biology and Biochemistry* 38(10): 3019-3034.

Berg, T.E. & Black, R.F. 1966. Preliminary measurements of growth of nonsorted polygons, Victoria Land, Antarctica. *Antarctic Soils and Soil Forming Processes*. J.C.F. Tedrow. Washington, D.C., American Geophysical Union 8: 62-108.

Black, R.F. 1973. Growth of patterned ground in Victoria Land, Antarctica. *Permafrost: The North American Contribution to the 2nd International Conference*, Yakutsk, Siberia, National Academy of Sciences, 193-203.

Black, R.F. 1982. Patterned-ground studies in Victoria Land. *Antarctic Journal of the U.S.* 17(5): 53-54.

Bockheim, J.G., Campbell, I.B. & McLeod, M. 2007. Permafrost distribution and active-layer depths in the McMurdo Dry Valleys, Antarctica. *Permafrost and Periglacial Processes* 18(3): 217-227.

Bockheim, J.G. & Hall, K.J. 2002. Permafrost, active-layer dynamics and periglacial environments of continental Antarctica. *South African Journal of Science* 98(1-2): 82-90.

Boynton, W.V., Feldman, W.C., Squyres, S.W., Prettyman, T.H., Bruckner, J., Evans, L.G., Reedy, R.C., Starr, R., Arnold, J.R., Drake, D.M., Englert, P.A.J., Metzger, A.E., Mitrofanov, I., Trombka, J.I., d'Uston, C., Wanke, H., Gasnault, O., Hamara, D.K., Janes, D.M., Marcialis, R.L., Maurice, S., Mikheeva, I., Taylor, G.J., Tokar, R. & Shinohara, C. 2002. Distribution of hydrogen in the near surface of Mars: Evidence for subsurface ice deposits. *Science* 297(5578): 81-85.

Brook, E.J., Brown, E.T., Kurz, M.D., Ackert-Jr, R.P., Raisbeck, G.M. & Yiou, F. 1995. Constraints on age, erosion, and uplift of Neogene glacial deposits in the Transantarctic Mountains determined from in situ cosmogenic ^{10}Be and ^{26}Al. *Geology* 23(12): 1063-1066.

Campbell, I.B. & Claridge, G.G.C. 1982. The influence of moisture on the development of soils of the cold deserts of Antarctica. *Geoderma* 28: 221-238.

Campbell, I.B. & Claridge, G.G.C. 2006. Permafrost properties, patterns and processes in the transantarctic mountains region. *Permafrost and Periglacial Processes* 17(3): 215-232.

Campbell, I.B., Claridge, G.G.C., Campbell, D.I. & Balks, M.R. 1998. The soil environment of the McMurdo Dry Valleys, Antarctica. *Ecosystem dynamics in a polar desert, the McMurdo Dry Valleys, Antarctica*. J. Priscu. Washington, D.C., American Geophysical Union 72: 369.

Claridge, G.G.C., Campbell, I.B. & Balks, M.R. 1996. Ionic migration in soils of the Dry Valley region. *International Workshop on Polar Desert Ecosystems*, Christchurch, New Zealand, A.A. Balkema, Rotterdam.

Dickinson, W.W. & Grapes, R.H. 1997. Authigenic chabazite and implications for weathering in Sirius group diamictite, Table mountain, dry valleys, Antarctica. *Journal of Sedimentary Research* 67((5) Part A): 815-820.

Dickinson, W.W. & Rosen, M.R. 2003. Antarctic permafrost: An analogue for water and diagenetic minerals on Mars. *Geology* 31(3): 199-202.

Fu, H., Dash, J., Wilen, L. & Hallet, B. 1993. The physics of liquid water in frozen powders and soils. *Permafrost; Sixth International Conference, Proceedings*, Beijing, 1117-1119.

Gilichinsky, D.A., Wilson, G.S., Friedmann, E.I., McKay, C.P., Sletten, R.S., Rivkina, E.M., Vishnivetskaya, T.A., Erokhina, L.G., Ivanushkina, N.E., Kochkina, G.A., Shcherbakova, V.A., Soina, V.S., Spirina, E.V., Vorobyova, E.A., Fyodorov-Davydov, D.G., Hallet, B., Ozerskaya, S.M., Sorokovikov, V.A., Laurinavichyus, K.S., Shatilovich, A.V., Chanton, J.P., Ostroumov, V.E. & Tiedje, J.M. 2007. Microbial Populations in Antarctic Permafrost: Biodiversity, State, Age, and Implication for Astrobiology. *Astrobiology* 7(2): 275-311.

Gooseff, M.N., Barrett, J.E., Doran, P.T., Fountain, A.G., Lyons, W.B., Parsons, A.N., Porazinska, D.L., Virginia, R.A. & Wall, D.H. 2003. Snow-patch influence on soil biogeochemical processes and invertebrate distribution in the McMurdo Dry Valleys, Antarctica. *Arctic Antarctic and Alpine Research* 35(1): 91-99.

Gooseff, M.N., Barrett, J.E., Northcott, M.L., Bate, D.B., Hill, K.R., Zeglin, L.H., Bobb, M. & Takacs-Vesbach, C.D. 2007. Controls on the spatial dimensions of wetted hydrologic margins of two antarctic lakes. *Vadose Zone Journal* 6(4): 841-848.

Hagedorn, B., Sletten, R.S. & Hallet, B. 2007. Sublimation and ice condensation in hyperarid soils: Modeling results using field data from Victoria Valley, Antarctica. *Journal of Geophysical Research Earth Surfaces* 112: F03017, doi:10.1029/2006JF000580.

Hagedorn, B., Sletten, R.S., Hallet, B. & Steig, E. 2003. Formation and characterization of ice-cemented soils in Victoria Valley. *9th International Symposium on Antarctic Earth Sciences*, Potsdam, Germany.

Head, J.W. & Marchant, D.R. 2003. Cold-based mountain glaciers on Mars: Western Arsia Mons. *Geology* 31(7): 641-644.

Hindmarsh, R.C.A., Van Der Wateren, F.M. & Verbers, A.L.L.M. 1998. Sublimation of ice through sediment in Beacon Valley, Antarctica. *Geografiska Annaler Series A: Physical Geography* 80(3-4): 209-219.

Keys, J.R. & Williams, K. 1981. Origin of crystalline, cold desert salts in the McMurdo region, Antarctica. *Geochimica et Cosmochimica Acta* 45(12): 2299-2309.

Lancaster, N. 2002. Flux of eolian sediment in the McMurdo Dry Valleys, Antarctica: a preliminary assessment. *Arctic Antarctic and Alpine Research* 34(3): 318-323.

Lyons, W.B., Nezat, C.A., Benson, L.V., Bullen, T.D., Graham, E.Y., Kidd, J., Welch, K.A. & Thomas, J.M. 2002. Strontium isotopic signatures of the streams and lakes of Taylor Valley, southern Victoria Land, Antarctica: Chemical weathering in a polar climate. *Aquatic Geochemistry* 8(2): 75-95.

Mackay, J.R. 1971. The origin of massive icy beds in permafrost, western Arctic coast, Canada. *Canadian Journal of Earth Sciences* 8: 397-422.

Mackay, J.R. & Burn, C.R. 2002. The first 20 years (1978-1979 to 1998-1999) of ice-wedge growth at the Illisarvik experimental drained lake site, western Arctic coast, Canada. *Canadian Journal of Earth Sciences* 39(1): 95–111.

Malin, M.C. & Rawine, M.A. 1995. Thirty years of measurements of sand wedge growth in lower Wright, Antarctica. *Antarctic Journal* Review 1994: 19-20.

Marchant, D.R. & Denton, G.H. 1996. Miocene and Pliocene paleoclimate of the Dry Valleys region, southern Victoria Land: a geomorphological approach. *Marine Micropaleontology* 27(1-4): 253-271.

Marchant, D.R., Denton, G.H., Sugden, D.E. & Swisher, C.C. III. 1993. Miocene glacial stratigraphy and landscape evolution of the western Asgard Range, Antarctica. *Geografiska Annaler* Series A 75A(4): 303-330.

Marchant, D.R., Denton, G.H., Swisher, C.C. III. & Potter, N. Jr. 1996. Late Cenozoic Antarctic paleoclimate reconstructed from volcanic ashes in the Dry Valleys region of southern Victoria Land. *Geological Society of America Bulletin* 108(2): 181-194.

Marchant, D.R., Lewis, A.R., Phillips, W.M., Moore, E.J., Souchez, R.A., Denton, G.H., Sugden, D.E., Potter, N. Jr. & Landis, G.P. 2002. Formation of patterned ground and sublimation till over Miocene glacier ice in Beacon Valley, southern Victoria Land, Antarctica. *Geological Society of America Bulletin* 114(6): 718-730.

McKay, C.P., Mellon, M.T. & Friedmann, E.I. 1998. Soil temperatures and stability of ice-cemented ground in the McMurdo Dry Valleys, Antarctica. *Antarctic Science* 10(1): 31-38.

McLeod, M., Bockheim, J.G. & Balks, M. 2007. A fifth-order reconnaissance soil map of ice-free areas of the Transantarctic Mountains, Antarctica. *A Keystone in a Changing World: Online Proceedings of the 10th ISAES*. A. K. Cooper, C. R. Raymond & ISAES Editorial Team**:** Extended Abstract 116, 4 pp.

Mellon, M. 1997. Small-scale polygonal features on Mars: seasonal thermal contraction cracks in permafrost. *Journal of Geophysical Research* 102(E11): 25617-25628.

Morgan, D.J. & Putkonen, J. 2005. Sediment transport in the McMurdo Dry Valeys, Antarctica. *Geological Society of America Abstracts with Programs* 37(7): 304.

Ng, F., Hallet, B., Sletten, R.S. & Stone, J.O. 2005. Fast-growing till over ancient ice in Beacon Valley, Antarctica. *Geology* 33(2): 121-124.

Nishiizumi, K., Kohl, C.P., Arnold, J.R., Klein, J., Fink, D. & Middleton, R. 1991. Cosmic ray produced 10Be and 26Al in Antarctic rocks: exposure and erosion history. *Earth and Planetary Science Letters* 104(2-4): 440-454.

Oehm, B. & Hallet, B. 2005. Rates of soil creep, worldwide: weak climatic controls and potential feedback. *Zeitchrift fur Geomorphologie* 49(3): 353-372.

Paetzold, R.F., Balks, M.R., Aislabie, J. & Sletten, R.S. 2003. Active Layer Thickness of Soils In The Ross Sea Region, Antarctica. *EOS Transaction of the Am. Geophys. Union*, San Francisco. Fall Meet. Suppl., Abstract C21B-0810.

Péwé, T.L. 1959. Sand-wedge polygons (Tesselations) in the McMurdo sound region, Antarctica; a progress report. *American Journal of Science* 257: 545-552.

Putkonen, J., Balco, G. & Morgan, D. In Press. Slow regolith degradation determined by cosmogenic-nuclide concentrations in Arena Valley, Antarctica. *Quaternary Research*.

Putkonen, J., Rosales, M., Turpen, N., Morgan, D., Balco, G. & Donaldson, M. 2007. Regolith transport in the Dry Valleys of Antarctica. *ISAES 2007 Proceedings. USGS OFR-2007,* doi:10.3133.

Putkonen, J., Sletten, R.S. & Hallet, B. 2003. Atmosphere/ ice energy exchange through a thin debris cover in Beacon Valley, Antarctica. *Permafrost; Eighth International Conference, Proceedings* Zurich. 8: 913-915.

Putkonen, J.K. 1998. Soil Thermal Properties and Heat Transfer Processes Near Ny Alesund, Northwestern Spitsbergen, Svalbard. *Polar Research* 17: 165-179.

Rignot, E., Hallet, B. & Fountain, A. 2002. Rock glacier surface motion in Beacon Valley, Antarctica, from synthetic-aperture radar interferometry. *Geophysical Research Letters* 29(12): 13,494-7.

Schoenbohm, L., Kurz, M., Ackert, R., Brook, E. & Brown, E. 2004. Erosion history from cosmogenic ^{10}Be ^{26}Al, ^{3}He and ^{21}Ne depth profiles: Dry Valleys, Antarctica. *European Geosciences Union 1st General Assembly*, Nice, France.

Schorghofer, N. 2005. A physical mechanism for long-term survival of ground ice in Beacon Valley, Antarctica. *Geophysical Research Letters* 32: L19503, doi: 10.1029/2005GL023881.

Sletten, R.S. & Hallet, B. 2003. Surface stability and contraction crack development on various forms of ground ice in the Dry Valleys, Antarctica. *9th International Symposium on Antarctic Earth Sciences*, Potsdam, Germany.

Sletten, R.S. & Hallet, B. 2004. Extreme soil inflation in the Dry Valleys, Antarctica. *Geological Society of America Annual Meetings,* Invited Talk, Seattle.

Sletten, R.S., Hallet, B. & Fletcher, R.C. 2003. Resurfacing time of terrestrial surfaces by the formation and maturation of polygonal patterned ground. *Journal of Geophysical Research* 108(E4): 8044, doi:10.1029/2002JE001914.

Sletten, R.S., Mann, D.H., McIntosh, W.C., Dunbar, N.W., Prentice, M.L., Dickinson, W. & Stone, J. O. 2007. Possible redeposition of volcanic ashes in the Dry Valleys by glacier transport: in Antarctica. *A Keystone in a Changing World: Online Proceedings of the 10th ISAES*. A. K. Cooper, C. R. Raymond & ISAES Editorial Team**:** Extended Abstract 158, 4 pp.

Smith, M.E., Stone, J.O., Sletten, R. & Hallet, B. 2001. Cosmogenic Isotope Exposure Constraints on the Age and Sublimation Rate of Buried Ice in Beacon Valley, Antarctica. *Eos Transactions, American Geophysical Union,* Fall Meeting Supplement, 2001 82(47).

Souchez, R. & Lorrain, R. 2006. The environmental significance of deuterium excess in meteoric and non- meteoric Antarctic ice. *Glacier Science and Environmental Change*. P. Knight, Blackwell Publishing, 179-184.

Stock, G.M., Anderson, R.S. & Finkel, R.C. 2005. Rates of erosion and topographic evolution of the Sierra Nevada, California, inferred from cosmogenic 26Al and 10Be concentrations. *Earth Surface Processes and Landforms* 30: 985-1006.

Stone, J.O., Sletten, R.S. & Hallet, B. 2000. Old ice, going fast: Cosmogenic isotope measurements on ice beneath the floor of Beacon Valley, Antarctica. *Eos Transactions, American Geophysical Union, Fall Meeting Supplement,* Abstract H52C–21 81(48).

Sugden, D.E., Marchant, D.R., Potter, N., Jr., Souchez, R.A., Denton, G.H., Swisher, C.C., III & Tison, J.-L. 1995. Preservation of Miocene glacier ice in East Antarctica. *Nature* 376(6539): 412-414.

Summerfield, M.A., Stuart, F.M., Cockburn, H.A.P., Sugden, D.E., Denton, G.H., Dunai, T. & Marchant, D.R. 1999. Long-term rates of denudation in the Dry Valleys, Transantarctic Mountains, southern Victoria Land, Antarctica based on in-situ-produced cosmogenic ^{21}Ne. *Geomorphology* 27(1-2): 113-129.

Ugolini, F.C. & Anderson, D.M. 1973. Ionic migration and weathering in frozen Antarctic soils. *Soil Science* 115(6): 461-470.

van der Wateren, D. & Hindmarsh, R. 1995. Stabilists strike again. *Nature* 376(6539): 389-391.

Wall, D.H., Adams, B.J., Barrett, J.E., Virginia, R.A. & Hopkins, D.W. 2006. A synthesis of soil biodiversity and ecosystem functioning in Victoria Land, Antarctica. *Soil Biology & Biochemistry* 38(10): 3001-3002.

Wettlaufer, J.S. 1999. Impurity effects in the premelting of ice. *Physical Review Letters* 82(12): 2516-2519.

Wettlaufer, J.S. 2001. Dynamics of ice surfaces. *Interface Science* 9(1-2): 117-29.

Wettlaufer, J.S. & Worster, M.G. 1995. Dynamics of premelted films: frost heave in a capillary. *Physical Review E* 51(5): 4679-4689.

Yong, R.N., Cheung, C.H. & Sheeran, D.E. 1979. Prediction of salt influence on unfrozen water content in frozen soils. *Engineering Geology* 13: 137-155.

Spatial Analysis of Small-Scale Polygonal Terrain in Utopia Planitia, Mars: A Comparison with Terrestrial Analogues

T.W. Haltigin
Department of Geography, McGill University, Montreal, QC, Canada
W.H. Pollard
Department of Geography, McGill University, Montreal, QC, Canada
G.R. Osinski
Department of Earth Sciences, University of Western Ontario, London, ON, Canada
P. Dutilleul
Department of Plant Science, McGill University, Ste. Anne de Bellevue, QC, Canada
J.W. Seaquist
Department of Physical Geography, Lund University, Lund, Sweden

Abstract

This paper presents the results of a Spatial Point Pattern Analysis (SPPA) of small-scale polygonal terrain in Utopia Planitia, Mars, and draws comparisons with a number of terrestrial analogue sites. Utopia Planitia displays a wide variety of landforms interpreted as having periglacial origins, suggesting the past or present existence of large quantities of ground ice. Therefore, this region of Mars offers an excellent case study to assess the applicability of statistical analysis in quantifying and comparing terrestrial and Martian small-scale polygonal terrain, which in turn may yield insight about the processes responsible for their formation.

Keywords: Axel Heiberg Island; Canada; Mars analogues; polygonal terrain; spatial point pattern analysis.

Introduction

Polygonal terrain is one of the most common landscape features found in terrestrial polar environments (Mellon 1997a). These networks of interconnected trough-like depressions form through a process termed *thermal contraction cracking*—a result of complicated interactions between climatological and rheological processes (Lachenbruch 1962)—and often signify the presence of shallow subsurface ice deposits in the form of ice wedges (Mackay 1999).

Large polygonal patterns on the surface of Mars discovered by the Mariner missions were originally of great interest as they, too, were thought potentially to be implicit of ground ice deposits (Carr and Schaber 1977). However, subsequent analysis concluded that polygons with diameters ranging from 2-10km were too large to be associated with thermal contraction cracking and thus are now believed to be formed through a variety of other geological processes (e.g., Lane and Christensen 2000).

More recently, though, Mars Global Surveyor's Mars Orbiter Camera (MOC) had been used to identify and map polygons of much smaller size, revealing that these small-scale geometric networks are scattered throughout Mars' mid- to high-latitudes in both hemispheres (Kuzmin & Zabalueva 2003). With sizes ranging from 10–200 m, they are much more comparable to terrestrial polygons; as such, analysis of these features has prompted a revisiting of their analogical value.

Because polygons on Mars are often located in close proximity to other landforms thought to be representative of ground ice presence (e.g., Soare et al. 2007) and display strong visual similarities to terrestrial polygons, (Isaev and Abramenko 2003; Mangold 2005), the presence of these patterns on Mars has been used to suggest the possibility of near-surface ground ice deposits (e.g., Mellon 1997b; Seibert and Kargel 2001; Mangold et al. 2004).

Previous descriptions of polygonal terrain have tended to be qualitative in nature, and thus require some degree of subjectivity to analyze. However, by using quantitative techniques to describe polygonal geometry, it is possible to categorize various groups of networks and relate them to other factors.

Our goal for this study was to apply a statistical technique to surface patterns on the Martian surface, attempting to answer two overarching research questions pertaining to Martian polygonal terrain: "*is their geometry related to proximity to other periglacial landforms*?" and "*how similar are they to polygons found on Earth*?".

In essence, this study seeks not only to map the spatial distribution of polygonal terrain occurrence in relation to other features thought to be indicative of ground ice, but also to quantify the similarities and differences displayed between the geometry of the polygonal terrain observed on Earth and Mars.

Research Context

Terrestrial polygonal terrain and ice wedges

A detailed explanation of polygon formation via thermal contraction cracking is provided in the seminal works

performed by Lachenbruch (1962), Pewe (1966), and Black (1974), summarized below. When tensile stresses due to seasonal decreases in surface and subsurface temperatures exceed the tensile strength of frozen ground, vertical cracks develop in order to relieve the stress. Over time, numerous cracks begin to join or intersect, resulting in closed polygonal geometrical shapes. As temperatures warm, the open cracks are filled with surface meltwater and groundwater that freezes when it reaches the permafrost within the crack. The vertical vein of ice that results represents the early stages of an "ice wedge."

As the surrounding climate warms later in the year, movements of near-surface soils induced by thermal expansion promote the formation of shoulder-like ridges bounding a linear depression in the ground above the wedge. Eventually, the cracks close again and the buildup of stresses due to freezing reinitiates the following winter. By repeating the process over hundreds or thousands of years, the ice wedge continues to thicken and the polygonal topographic patterns at the surface become more enhanced.

Martian polygons = ground ice?

It is conceivable that polygons found on Mars represent analogous geocryological systems to those found on Earth, based on converging lines of evidence suggesting that Martian polygons may be indicative of near-surface ground ice.

For example, it is possible that both terrestrial and Martian polygons are formed by similar processes. Mellon (1997a,b) showed that the conditions required for thermal contraction cracking could be exhibited poleward of 30 degrees latitude. Subsequently, Seibert & Kargel (2001) demonstrated that ice wedge cracking was potentially responsible for their formation.

In addition, polygons tend to be located in areas otherwise believed to be rich in ground ice. Mangold et al. (2004) noted that the majority of polygonal terrain is located poleward of 55 degrees, within the zone predicted to contain stable ice and spatially coincident with regions where Odyssey's Neutron Spectrometer detected near surface hydrogen enrichment (Boynton et al. 2002). Moreover, Langsdorf & Britt (2004) and Soare et al. (2007) showed that polygons are often found in close proximity to other landforms potentially associated with ground ice deposits (Fig. 1)

Comparing polygonal terrains on Earth and Mars

The apparent lack of quantitative comparisons between the geometry of terrestrial and Martian polygonal terrain may be a result of how polygonal ground has been categorized on either planet. On Mars, various combinations of geographical distribution, proximity to nearby landforms, and polygon size have been used to group polygonal networks (Kuzmin and Zabalueva 2003; Langsdorf and Britt 2004; Mangold 2005). On Earth, however, polygons tend not to be classified by their geometry, but rather by their relation to permafrost aggradation or degradation (Mackay 2000).

A selection of previous researchers have attempted to use statistical analysis in their description of polygon morphology (e.g., Rossbacher 1986; Plug and Werner 2001; Yoshikawa 2003). Unfortunately, a universally accepted method to compare polygonal terrain on Earth and Mars has yet to be determined.

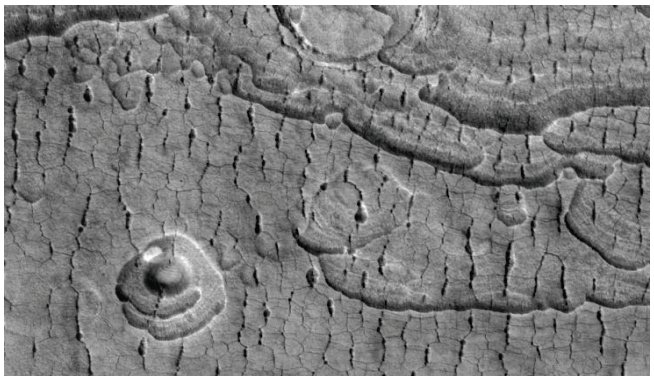

Figure 1: Example of polygons appearing within pitted and scalloped terrain (MOC image: R0301203). Image is approximately 3.5 km across.

Refined statement of objectives

Through previous work, we have introduced the utility of a particular statistical method – Spatial Point Pattern Analysis – for quantifying a variety of polygonal terrain morphologies observed on Earth and Mars (Haltigin et al. 2007). We have now begun to apply the method more systematically to investigate differences in polygon morphology on a regional (rather than global) scale.

Therefore, our specific objectives for the present study are to: (1) explore variations in observed polygon morphologies displayed in the Utopia Planitia region of Mars, and; (2) compare the observed morphologies with a selection of those present in the Canadian High Arctic. By satisfying these objectives, it is possible that the inferred similarities and differences can be used to interpret some of the processes responsible for their formation.

Study Areas

Mars: Utopia Planitia

Utopia Planitia is a major topographic depression situated in the northern plains of Mars (Fig. 2). Although Odyssey's Gamma Ray Spectrometer (GRS) has revealed that this area is relatively free of hydrogen in the near-surface (Boynton et al. 2002), the large spatial resolution of GRS pixels may not be capable of identifying local ground ice occurrence.

A variety of geomorphic indicators do, in fact, suggest the presence of ground ice in Utopia Planitia. For example, small-sized polygons throughout the region and possible thermokarst features such as pitted terrain and scalloped terrain (Fig. 1) has led to the suggestion that this region contains ice-rich sedimentary deposits, whose emplacement could well be atmospheric and relatively recent (Costard & Kargel 1995; Soare et al. 2007).

Earth: Axel Heiberg Island

Fieldwork was conducted at four polygonal terrain sites near the McGill Arctic Research Station (M.A.R.S.) (79.383N, 91.067W). The region is set within a polar desert climate, having a mean annual air temperature of approximately -15°C and total annual precipitation of <100 mm (Bigras et al. 1995).

Although polygonal terrain is widespread throughout Axel Heiberg Island, the four sites near the mouth of Expedition Fjord were selected based on geomorphological considerations after a preliminary reconnaissance field campaign in 2005.

Specifically, the sites chosen display differing morphologies, but are located in extremely close proximity to each other (three of the four are separated by <1 km, while the fourth is <10 km away). Such a small geographical range removes variation in the two primary factors known to affect polygon geometry: surface age (Sletten et al. 2003) and climate (Mackay 1999).

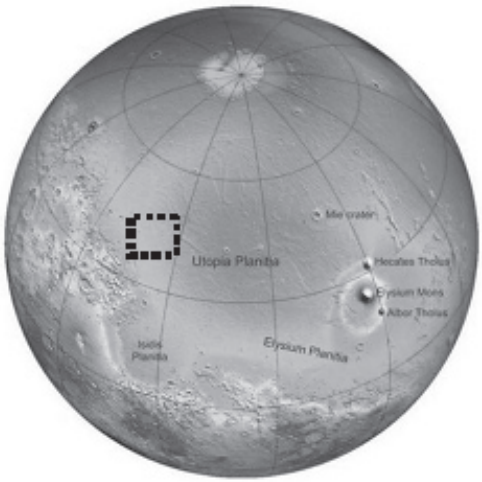

Figure 2: Topographic map of Mars centered on Utopia Planitia based on Mars Orbiter Laser Altimeter (MOLA) data. Dashed inset represents approximate region of interest for current study (Credit: MOLA Science Team, NASA, MOLA image gallery).

Methodology

Data collection

(a) Mars imagery

A systematic survey of all available Mars Global Surveyor MOC Narrow Angle images was performed for the region within Utopia Planitia between 80–90E and 40–50N. Images were downloaded from the online MOC database and visually inspected for the presence of polygonal terrain. The images selected represent a broad diversity of polygon morphologies, and thus are an ideal template upon which to examine the applicability of a statistical technique to detect and quantify geometrical variation. Of the 52 images on which polygonal terrain was identified, a subset of 22 images between 80–90E and 40–45N were selected for spatial analysis.

(b) Aerial photography

Prior to aerial photograph collection, the field sites were prepared by demarcating transects on the ground with a series of Ground Control Points (GCP)—a series of brightly colored markers that are easily identifiable on the photos. Depending on the width of the area required to be imaged, four to six transects spaced 40m apart were lined with alternating brightly-colored ground markers to provide readily visible flightlines for the helicopter pilot.

Vertical aerial photographs were taken from the helicopter using a Nikon D200 digital SLR camera equipped with a 50 mm Zoom-Nikkor lens. Images taken from an altitude of approximately 300 m resulted in image widths of approximately 100 m at sub-decimeter resolution. Between 15 and 20 photos were collected per transect, totaling 75–100 individual images per site.

(c) GPS surveys

A Trimble 5700 differential Global Positioning System (dGPS) was used to measure the spatial coordinates of the GCPs and selected polygon trough intersection point using the Post-Processed Kinematic survey method (Lantuit & Pollard 2005). Standard coordinate correction algorithms were applied using Trimble's TG-Office software. Processed dGPS coordinates were subsequently used to spatially reference the aerial images (see *Data analysis* section).

Data analysis

(a) MOC image processing

Each MOC image was imported into a Geographic Information System (GIS; ArcMap 9.1) and placed within an arbitrary coordinate system (units=meters); x-y coordinates of (0.00, 0.00) were assigned to the bottom left-hand corner of the image, while the remaining three corners were scaled according to the image height and width provided in the file's metadata.

Because of temporal and computational constraints, it was infeasible to perform the spatial analysis on the entire MOC image. Therefore, an initial visual inspection was performed in order to designate a representative area of the observed polygonal terrain. Within the selected area, all discernible polygon trough intersections were manually identified and digitized. Coordinates of the digitized points were exported and used for the statistical analysis.

(b) Aerial photo processing

Individual photos were imported into the GIS to be spatially referenced. Processed dGPS coordinates were assigned to the corresponding point on the images, causing the photos to be stretched and rotated to be oriented within Universal Transverse Mercator coordinate space. By performing this "georeferencing" on all images for a given site, an oriented and scaled photo mosaic was produced. Finally, all trough intersection points were manually digitized, with the coordinates exported for spatial analysis.

(c) Spatial point pattern analysis

A full explanation of spatial point patterns is provided by Diggle (2003). Tables of x-y coordinates for both the MOC and field images were analyzed using a customized code written for the statistical software package SAS. After the analysis area was defined, the analysis yields two key outputs: (1) a range of predicted nearest-neighbor distances (NND) that would satisfy the null hypothesis of a completely random distribution, and; (2) a table of observed NND for each trough intersection point.

By plotting a cumulative frequency distribution curve of the observed NND values, it is possible to determine whether the observed spatial distribution of trough intersection points is clustered, random, or regular, and the degree to which they are so designated.

Results and Discussion

Distribution of polygonal terrain in Utopia Planitia

Locations displaying polygonal terrain are spread quite evenly throughout the area within the transition zone grading from the cratered uplands to the basin below (Fig. 3a). Although the simple *occurrence* of polygons is widespread in the entire study area, the appearance of polygons in conjunction with other thermokarst features may be a function of surface elevation.

Specifically, the majority of instances where polygons appear independently of other features are found at higher elevations (lower left portion of Fig. 3a-c), with 10 of 14 cases found well above the basin floor. Furthermore, polygons in the vicinity of scalloped terrain appear primarily at lower elevations than do those found containing pitted chains. It is unsurprising, then, that a band of images displaying *both* pits and scallops is located in the zones of intermediate elevation.

Spatial point patterns of Utopia Planitia polygons

A great variation in polygon size is displayed clearly amongst the assorted terrains throughout the study area, with median NND span from 25.5 m to 64.4 m (Fig. 3b). The overall range of NND varied greatly as well, with minimum values ranging from 15.1 m to 32.8 and maximum values ranging from to 39.6 to 154.2 m.

A diversity of morphology is also evidenced by an examination of the observed spatial point patterns. Of particular interest is the recognition that in no cases are the observed patterns clustered; rather, the sites display varying degrees of randomness and regularity (Fig. 3c).

Sites were determined to be "primarily random" if at least 50% of the observed NND fell within the envelope predicted by the spatial point pattern analysis to satisfy the null hypothesis of complete randomness. Sites were identified as "mixed" if between 25% and 50% of the observed points satisfied this requirement and "primarily regular" if less than 25% of the observed NND satisfied the requirement.

In general, the majority of sites that displayed primarily regular patterns possessed the lowest median NND values

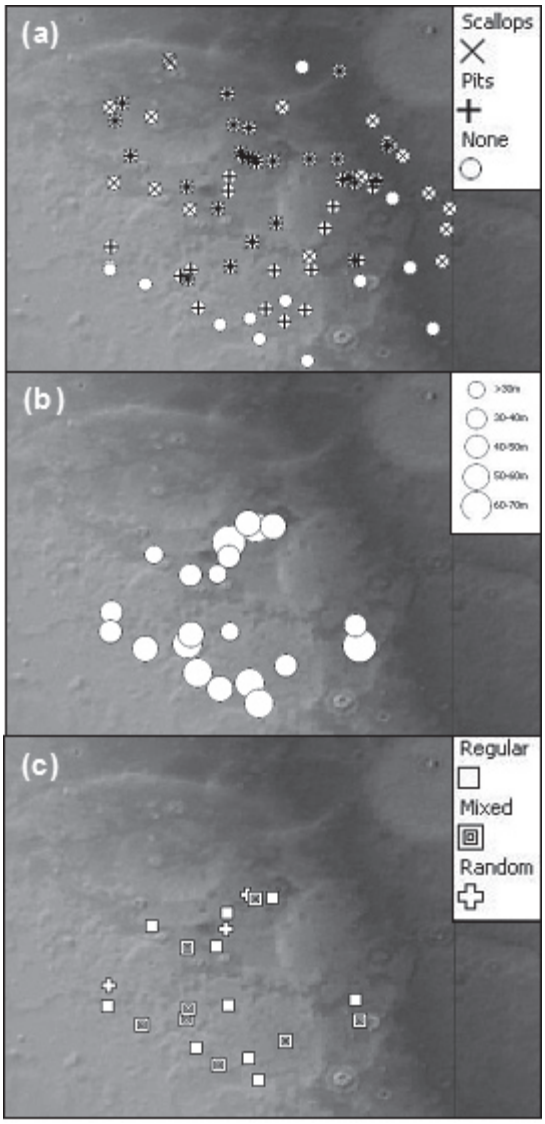

Figure 3: (a) Occurrence of polygonal terrain in relation to other periglacial features; (b) Median NND and (c) observed spatial point pattern of polygonal terrain field.

(averaging approximately 30 m), indicating that smaller polygons tend to be more regular. Conversely, the three sites determined to be primarily random had average median NND values of 40 m. Thus, a positive relationship can be inferred between polygon size and randomness of the network's geometry.

More trends emerge when comparing the observed spatial point patterns to proximity to other landforms. In particular, it is interesting to note that all three of the sites displaying primarily random geometry are found in conjunction with the pitted chains. In only one case each were pits found for sites with regular or mixed geometry, respectively. In addition, all sites that displayed scalloped terrain were found to contain regular patterning. No clear trend was apparent for sites with polygonal terrain appearing in the absence of other landscape features, having virtually an equal number of instances that were considered either mixed (5/9) or regular (4/9).

Spatial point patterns of Axel Heiberg polygons

As with the MOC images discussed above, size variation is displayed with the terrestrial polygons. It appears, though, that the terrestrial polygons are somewhat smaller. Median NND values range from 6.2 m to 19.5 m. Minimum NND values are comparable for the 4 sites, ranging from 2.2 m to 5.3 m; maximum NND values vary greatly, ranging from 15.2 m to 110 m.

Similar to the MOC images, in no cases did the terrestrial sites display a clustered distribution. However, while the MOC images tended mostly to vary between regular and random distributions, two of the four terrestrial sites were considered completely random.

It appears that a decrease in overall randomness occurs with decreasing polygon size for the field sites. Specifically, the two sites that were completely random had larger median NND than did the primarily regular sites.

Factors influencing polygon morphology

For both Martian and terrestrial polygonal terrain, spatial point pattern analysis was able to quantify variations in observed polygon morphologies. In both cases, polygons with smaller NND tended to be more regular, with increasing randomization occurring as the NND became greater. It is possible, then, that similar processes are responsible for polygon formation on both planets.

The two most well-documented factors influencing polygonal geometry are the surrounding climate (Mackay, 1999) and the amount of time that the polygons have been developing (Sletten et al. 2003). Given that the Utopia sites spanned a reasonably large range of elevation, it is evident that both climate and surface age of each site may not have been constant. As a result, it plausible that climate and age determinants may be responsible for the variations in observed polygonal size and regularity.

However, the same cannot be said for the Axel Heiberg sites. Because the polygonal terrain fields examined in this study are located so close together, climatic forcing would necessarily have been equal for each. Moreover, because their elevations are <10 m of each other, the estimated emergence age of the sites would also be virtually equal. Therefore, it is evident that some other factor must be responsible for the variation in observed morphologies.

We believe that substrate material may be as important as climate and age in determining the appearance of the polygons. Although polygonal terrain can develop in any type of ice-bonded sediment (Black 1974), varying substrate types have different rheological properties (Sletten et al. 2003). Namely, a soil's thermal contraction coefficient dictates the ground's response to thermally induced stresses (Lachenbruch 1962), and thus it will also determine the dimensions of the tension cracks and the rate and magnitude of surface sediment redistribution.

After a qualitative examination, it is possible that the sites' sediment distributions can be correlated with the polygonal morphology. In general, a decrease in maximum sediment size is associated with both a decrease in nearest neighbour distance and an increase in polygon regularity.

The use of spatial point patterns to analyze the distribution of trough intersection points may yield insight into the effects of age and substrate. As described by Lachenbruch (1962), the spacing of cracks depends on the local strength of the material and on the ground's ability to dissipate stress through the cracking process. Given that cracks initiate at local weaknesses that, theoretically, are randomly distributed throughout a particular field site, the earliest cracks to form (and thus the earliest intersections) should also be randomly distributed. Therefore, observations of random spatial distributions may indicate that the polygonal terrain under investigation is relatively young.

Similarly, point patterns may also be reflective of subsurface grain size distribution. Because cracking initiates at weaknesses, it is plausible that a more heterogeneous substrate would contain more randomly distributed points of weakness. Conversely, a more homogeneous substrate should have a more regular distribution of weaknesses. By using trough intersections as proxy indicators of the cumulative stress field that has acted over time on the site, more regular spatial point patterns may be used to infer a more uniform distribution of grain sizes in the ground.

Summary and Conclusions

The occurrence of polygonal terrain within Utopia Planitia, Mars, was characterized according to: (i) elevation; (ii) proximity to other landforms possibly indicative of ground ice, and; (iii) randomness/regularity of the spatial distribution of trough intersections.

Polygons found independently of other features tend to be located at the highest elevations, while polygons found within scalloped terrain tends to be located at lower elevations that those containing thermokarst pits. Generally, polygons within scalloped terrain are more regular than those found within pitted terrain.

Certain similarities were observed between terrestrial and Martian polygonal terrain. On both Earth and Mars, the polygons examined displayed varying degrees of regularity and randomness, but in no cases were the observed patterns considered statistically clustered.

Polygon "regularity" was found overall to have a negative relationship with polygon size. By examining the terrestrial analogue sites, a relationship was found between surface sediment size and the observed spatial point patterns. At the field sites, larger sediments were associated with larger, more irregular polygons. It is possible that similar characteristics could be evident on Mars.

The techniques outlined in this research can be applied to thousands of MOC images displaying polygonal terrain on the Martian surface, and would likely be even more effective on incoming HiRISE images. Potentially, spatial point patterns could be used to classify polygons found throughout the planet and provide a common platform by which to compare numerically the patterns observed on Mars and Earth.

Acknowledgments

Funding for this work was provided by the Canadian Space Agency's CARN program, NSERC, and ArcticNet. Logistical support in the field was provided by the Polar Continental Shelf Project (PCSP). Many thanks to Maude Oullet, Bimal Patel, and Geoff Pearce for painstakingly examining the MOC database in search of polygons. Finally, the authors acknowledge the use of the Mars Orbiter Camera images processed by Malin Space Science Systems that are available at http://www.msss.com/moc_gallery/.

References

Black, R.F. 1974. Ice-wedge polygons of northern Alaska. In D. Coates (ed.) *Glacial Geomorphology*. Binghampton, NY: State University of New York, 247-275.

Bigras, C., Bilz, M., Grattan, D.W. & Gruchy, C. 1995. Erosion of the geodetic hills fossil forest, Axel Heiberg Island, Northwest Territories. *Arctic*, 48(4): 342-353.

Boynton, W.V. & the GRS Team. 2002. Distribution of hydrogen in the near-surface of Mars: Evidence for subsurface ice deposits. *Science*, 297: 81-85.

Carr, M.H. & Schaber, G.G. 1977. Martian permafrost features. *Journal of Geophysical Research* 82: 4,039-4,054.

Costard F.M. & Kargel, J.S. 1995. Outwash plains and thermokarst on Mars. *Icarus* 114: 93-112.

Diggle, O. 2003. *Statistical Analysis of Spatial Point Patterns*. London, UK: Arnold.

French, H.M. 1996. *The Periglacial Environment*. Longman Group, Essex: 341pp.

Haltigin, T.W., Osinski, G.R., Pollard, W.H. & Dutilleul, P. 2007. Using spatial point patterns to quantify polar desert polygonal geometry. *Lunar and Planetary Science* XXXVIII: Abstract 1635.

Isaev, V.S. & Abramenko, O.N. 2003. Demonstration of polygonal ice-wedges [*sic*] terrain on the Tazovsky Peninsula in the Weastern [*sic*] Siberia and some polygonal patterns on the [*sic*] Mars. *Microsymposium on Comparative Planetology* 38, MS001, 1-2.

Kuzmin, R.O. & Zabalueva, E.V. 2003. Polygonal terrains on Mars: Preliminary results of global mapping of their spatial distribution. *Lunar and Planetary Science*, XXXIV: Abstract 1912.

Lachenbruch, A.H. 1962. Mechanics of thermal contraction cracks and ice-wedge polygons in permafrost. *Special paper to the Geological Society of America* 70: 69pp.

Lane, M.D. & Christensen, P.R. 2000. Convection in a catastrophic flood deposit as the mechanism for giant polygons on Mars. *Journal of Geophysical Research* 105: 17,617-17,627.

Langsdorf, E.L. & Britt, D.T. 2004. Periglacial processes in the southern hemisphere of Mars. *Lunar and Planetary Science* XXXV: Abstract 2115.

Lantuit, H. & Pollard, W.H. 2005. Temporal stereophotogrammetric analysis of retrogressive thaw slumps on Herschel Island, Yukon Territory. *Natural Hazards and Earth System Sciences* 5: 413-423.

Mackay, J.R. 1999. Periglacial features developed on the exposed lake bottoms of seven lakes that drained rapidly after 1950, Tuktoyaktuk Peninsula area, Western Arctic coast, Canada. *Permafrost and Periglacial Processes* 10: 39-63.

Mackay, J.R. 2000. Thermally induced movements in ice-wedge polygons, Western Arctic Coast: A long-term study. *Geographie Physique et Quaternaire* 54(1): 41-68.

Mangold, N. 2005. High latitude patterned grounds on Mars: Classification, distribution and climatic control. *Icarus* 174: 336-359.

Mangold, N., Maurice, S., Feldman, W.C., Costard, F. & Forget, F. 2004. Spatial relationships between patterned ground and ground ice detected by the Neutron Spectrometer on Mars. *Journal of Geophysical Research* 109(E08001).

Mellon. M.T. 1997a. Thermal contraction cracks in Martian permafrost: Implications for small-scale polygonal features. *Lunar and Planetary Science* (XXVIII): Abstract 1495.

Mellon, M.T. 1997b. Small-scale polygonal features on Mars: Seasonal thermal contraction cracks in permafrost. *Journal of Geophysical Research* 102(E11): 25,617-25,628.

Pewe, T.L. 1966. Ice wedges in Alaska – classification, distribution, and climatic significance. In *International Permafrost Conference Proceedings*: pp.76-81. *NAS-NRC Publication 1287*, National Academy of Science, Washington DC.

Plug, L.J. & Werner, B.T. 2001. Fracture networks in frozen ground. *Journal of Geophysical Research*, 106(B5): 8,599-8,613.

Rossbacher, L.A. 1986. Nearest-neighbour analysis: A technique for quantitative evaluation of polygonal ground patterns. *Geografiska Annaler, Series A, Physical Geography* 68(1/2): 101-105.

Seibert, N.M. & Kargel, J.S. 2001. Small-scale Martian polygonal terrain: Implications for liquid surface water. *Geophysical Research Letters* 28(5): 899-902.

Sletten, R.S., Hallet, B. & Fletcher, R.C. 2003. Resurfacing time of terrestrial surfaces by the formation and maturation of polygonal patterned ground. *Journal of Geophysical Research*, 108(E4): 8044, doi:10.1029/2002JE001914.

Soare R. J., Kargel J. S., Osinski G. R. & Costard F. 2007. Gully formation, periglacial processes and evidence of near-surface ground-ice in Utopia and western Elysium Planitia. *Icarus* in press.

Yoshikawa, K. 2003. Origin of the polygons and the thickness of Vastis Borealis formation in western Utopia Planitia on Mars. *Geophysical Research Letters* 30(12): 1603, doi:10.1029/2003GL017165.

Thermal and Water Conditions of the Active Layer after the 2002 Tundra Fire, Seward Peninsula, Alaska

Koichiro Harada
School of Food, Agricultural and Environmental Sciences, Miyagi University, Sendai, Japan
Yuki Sawada
Institute of Low Temperature Science, Hokkaido University, Sapporo, Japan
Kenji Narita
Faculty of Education and Human Studies, Akita University, Akita, Japan
Masami Fukuda
Institute of Low Temperature Science, Hokkaido University, Sapporo, Japan

Abstract

In order to clarify the effects of a tundra fire on the thermal and water conditions of permafrost and active layer, field observations were carried out on the Seward Peninsula, Alaska, between 2005 and 2007, where a 2002 tundra fire had burned up to a road that acted like a firebreak. Ground temperatures at burned sites were 4°C–5°C higher than those at unburned sites. Measurements of soil water content showed no significant tendency, increase or decrease. The depth of the active layer was significantly greater on the burned (60 cm) than the unburned (40 cm) side of the firebreak in 2005 and 2006. In 2007 the depths were 80 cm and 50 cm, respectively. The effect of fire on permafrost reaches only to the layer near ground surface, the active layer or upper part of the permafrost. Apparent electrical resistivity values up to 1 m at burned sites were relatively low. Resistivity values of unfrozen mineral soil in the active layer were calculated, and there was no significant difference of unfrozen soil between burned and unburned sites. The variation of calculated resistivity was small at burned sites, which may show the small variation of water content along the survey line due to the fire.

Keywords: active layer; permafrost; resistivity; wildfire.

Introduction

Due to its heat and disappearance of vegetation in the Arctic, wildfire affects the ground surface condition of permafrost and may cause its degradation. This degradation yields the emission of methane gas from the permafrost, which furthers global warming. Due to predicted warmer and dryer summers the area burned by tundra fire is expected to increase by as much as twice (Rupp et al. 2000), although current tundra fire activity is less frequent than the wildfires in boreal forests (Racine et al. 1985). Tundra fire disturbance and corresponding vegetation changes bring heat balance on the ground surface, and these may yield degradation of permafrost (Racine et al. 2004).

On the Seward Peninsula, large tundra fires occurred in 1971, 1997, and 2002, and a discontinuous permafrost area burned widely near the Kougarok River. In this area permafrost surveys were carried out in 2005, 2006, and 2007. The final goal of this study is to clarify effects of tundra fire on the thermal and water conditions of permafrost and active layer, and on vegetation recovery.

Study Area

Field observations were carried out in the Kougarok region, interior Seward Peninsula, Alaska (Fig. 1). There permafrost is discontinuously distributed and is considered to be sensitive to global and local climate changes. Mean annual air temperatures measured in this area range between –2.9°C and –5.5°C in 2000–2006 (Liljedahl et al. 2007).

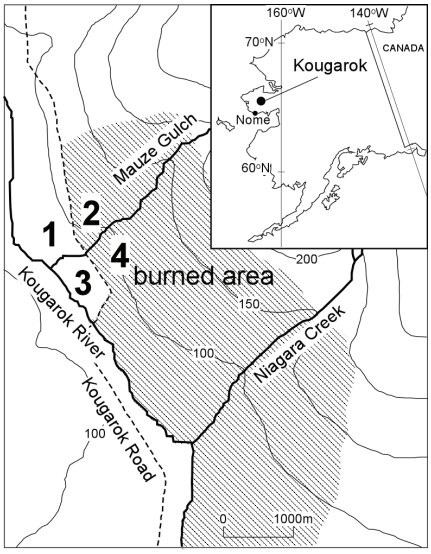

Figure 1. Location map of study sites.

In 2002, a wildfire occurred near Niagara Creek and Meuze Gulch. The fire began to burn at the east side of Kougarok Road and was stopped by the road, so the west side of the road did not burn and was considered to be undisturbed by the fire. Thus, four study sites were established near Meuze Gulch to compare the differences of thermal and moisture conditions in the active layer on the burned and unburned sides. The four sites in Figure 1 represent: unburned south-

Table 1. Average, minimum, maximum and median values of active layer thickness in 2005, 2006 and 2007.

	2005				2006				2007			
	average (cm)	minimum (cm)	maximum (cm)	median (cm)	average (cm)	minimum (cm)	maximum (cm)	median (cm)	average (cm)	minimum (cm)	maximum (cm)	median (cm)
1: US	40	24	59	40	37	24	60	34	44	28	66	44
2: BS	64	52	83	65	66	46	84	67	69	52	82	68
3: UN	40	22	62	41	39	16	66	38	52	27	79	52
4: BN	62	44	80	63	61	26	90	61	81	69	102	80

facing (Site 1: US), burned south-facing (Site 2: BS), unburned north-facing (Site 3: UN) and burned north-facing (Site 4: BN). It is assumed that vegetation cover was similar at all sites before the fire. Unburned sites (Sites 1 and 3) are now covered by tussock-shrub tundra.

Field Observations

In order to monitor present thermal and water conditions, ground temperatures, soil water contents, and thermal conductivities in the active layer were measured by pit excavations to the permafrost table at all four sites in July and August 2005, August 2006, and August 2007. The volumetric water content was measured by the TDR method, and the thermal conductivity by the thermal probe method. Depths of active layer were also measured by using a steel rod from the ground surface. We made 50 measurements within a 10 x 10 m area at each site.

Electromagnetic soundings were carried out in order to estimate the permafrost thickness in August 2005, which was 20–30 m at north-facing sites (Sites 3 and 4), but was not detected at south-facing sites (Sites 1 and 2) due to the shallow bedrock (Sawada et al. 2005).

Electrical resistivity values of the active layer and upper part of the permafrost (1 m deep) were obtained using the DC electrical sounding method. 2D measurements were conducted at all four sites. The electrode interval, the maximum depth, and the length of survey line were set to 1 m, 5 m, and 29 m, respectively.

Observational Results

In Figure 2, typical soil profiles to the permafrost table, obtained from pit surveys conducted in August 2007 at each site, are shown. The mineral soil consists mainly of clayey soil. The thickness of the organic layer ranges widely between 0 cm and 30 cm at each site.

The significant difference between burned and unburned sites is the presence or absence of a moss layer. The moss layer is not present at burned sites due to the fire. The thermal conductivities measured in 2007 in the moss, organic, and mineral layers were 0.1–0.5 W/mK, 0.3–1.2 W/mK and 0.5–1.3 W/mK, respectively. As the moss layer has a low thermal conductivity, this layer has an important role as a heat insulator and controls the depth of the active layer.

Thus, the measured active layer thicknesses were significantly different between the burned and unburned sites, about 60 cm and 40 cm in 2005 and 2006, and about 80 cm and 50 cm in 2007 (Table 1). Statistical analyses were also made and showed the availability of data (not shown here). The thickness at the burned sites was more than 20cm deeper than that at the unburned sites. This deep active layer at the burned sites was caused by the lack of the moss layer. Comparing the active layer thickness in 2005 and 2006, there is no significant increase. However, the thickness in 2007 at north-facing sites was more than 10–20 cm deeper than those in 2005 or 2006.

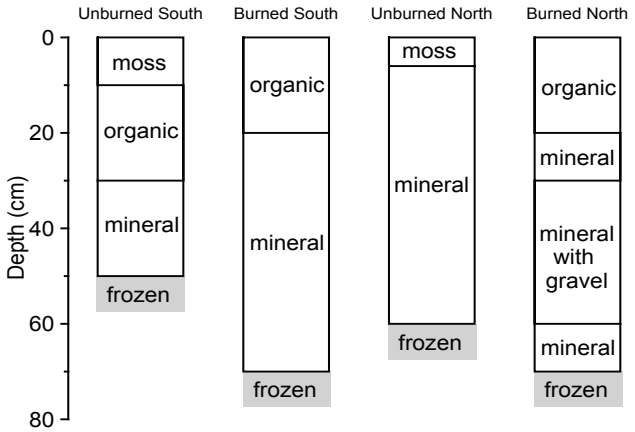

Figure 2. Typical soil profile at four sites in study area.

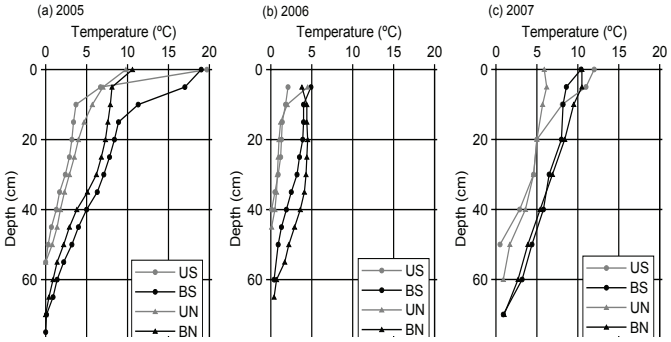

Figure 3. Ground temperature profiles in (a) 2005, (b) 2006 and (c) 2007.

Figure 3 shows the ground temperature profiles measured using soil pits. The ground temperatures at the burned sites (black lines in Fig. 3) were 4°C–5°C higher than those at the unburned sites (gray lines in Fig. 3). The volumetric water contents of soil at the burned sites were higher than those at the unburned sites in 2005, but lower in 2006 (Fig. 4). The data observed in 2007 was complicated, and may have been affected by the rain fall just before the observations.

Apparent resistivity values up to 1 m deep obtained from 2D soundings conducted in 2006 are shown in Figure 5. There is an obvious difference between the burned and unburned sites. The apparent resistivity value at the burned sites was much lower than at the unburned sites.

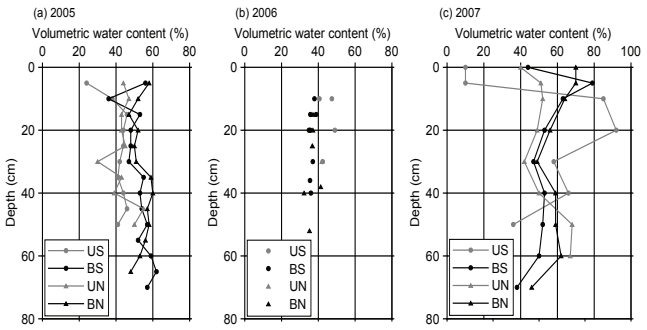

Figure 4. Volumetric water content at study sites in (a) 2005, (b) 2006 (point measurement) and (c) 2007.

Discussion

After the tundra fire, the thickness and ground temperature of the active layer at burned sites changed drastically due to the destruction of the surface moss layer. However, it is estimated that permafrost thickness has not changed between the burned and unburned sites (Sawada et al. 2005). These results suggest that the effect of fire on permafrost reaches only to the layer near ground surface, the active layer or upper part of the permafrost. In future, the active layer thickness may increase year by year, or the increase of active layer thickness will stop after recovery of surface vegetation. Thus, a continuous monitoring of ground temperature and a numerical calculation is needed to clarify the effect of fire on permafrost.

In 2007, the active layer thickness increased more than 10–20 cm, and this result with the other data (e.g. air temperature) should be discussed, but has yet to be. And more measurement will be needed to clarify the change of thickness of the active layer after a wildfire.

After the tundra fire, no significant tendency of change of water content was observed in this area, there was no drastic increase or decrease. As the water content is also an important factor

in solving the permafrost's degradation or recovery, it is also necessary to measure water content continuously.

Here, as a resistivity value of soil depends on soil water content (e.g. Harada and Fukuda 2000), an estimation of the water condition was made using measured apparent resistivity values. Generally, an apparent resistivity value obtained from the DC sounding is produced from the combination of a true resistivity value and the thickness of the layer. In this study, relative low apparent resistivity values were obtained at the burned sites (Fig. 5). As a resistivity value of soil also depends on temperature, and the value of resistivity in the active layer or unfrozen material is conductive (e.g. Harada and Fukuda 2000), a thick active layer condition shows a low apparent resistivity value (Fig. 6). An apparent resistivity value strongly depends on the thickness of the active layer, so this apparent resistivity value does not affect the true resistivity value in the active layer directly.

In order to obtain the true resistivity value of the unfrozen mineral layer in the active layer, a simple calculation was

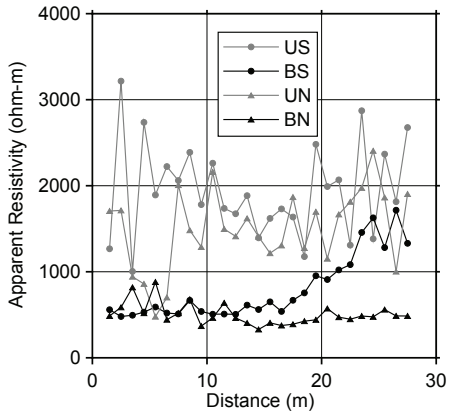

Figure 5. Apparent resistivity values up to 1 m deep along the 2D electrical sounding line conducted in August 2006. Horizontal axis shows the distance from the starting point of electrical sounding.

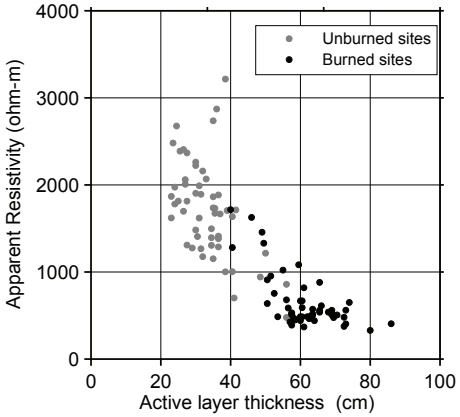

Figure 6. Relationship between active layer thickness and apparent resistivity measured in August 2006.

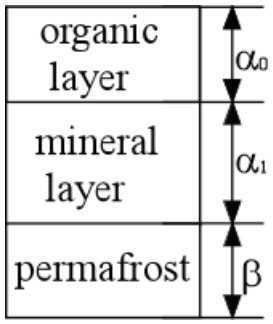

Figure 7. Estimation model for resistivity of unfrozen mineral layer.

carried out using the apparent resistivity value measured in 2006. The model used here is shown in Figure 7, and it was assumed that an apparent resistivity up to 1m, ρ_a, was produced from a resistivity value and thickness of each layer shown in Fig. 7, unfrozen organic layer, unfrozen mineral layer and permafrost,

$$\frac{1}{\rho_a} = \frac{\alpha_0}{\rho_0} + \frac{\alpha_1}{\rho_1} + \frac{\beta}{\rho_2} \quad (1)$$

$$\alpha_0+\alpha_1+\beta=1 ,$$

where ρ_0, ρ_1, and ρ_2 are true resistivity of the organic layer,

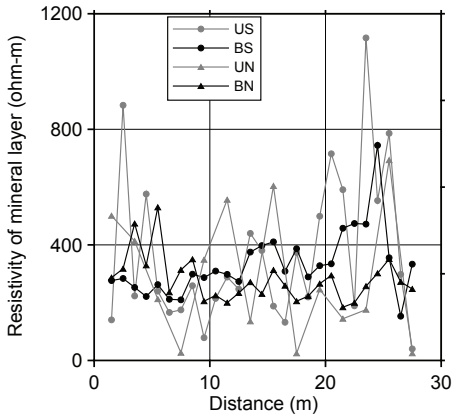

Figure 8. Estimated resistivity value of unfrozen mineral layer in 2006.

the mineral layer, and the permafrost, and α_0, α_1, and β are the thickness of each layer, respectively. Here, ρ_0 and ρ_2 were given as assumed values of 5000 and 10,000 ohm-m, respectively, and α_0, α_1, and β were given using measured thickness values were used. Then, the true resistivity value of unfrozen mineral layer ρ_1 was estimated using equation (1).

Figure 8 shows the calculated result of the true resistivity value of the unfrozen mineral layer in 2006. Comparing calculated values between the burned and unburned sites, there was no significant difference of the unfrozen mineral soil. Furthermore, the values ranged widely at the unburned sites, and a variation of resistivity was small at the burned sites. This may show the small variation of water content along the survey line due to the fire. In the future, a calibration between soil water content and resistivity will made, and this model will be developed to monitor the ground water content using the DC electrical sounding method.

Conclusions

Permafrost surveys were carried out in order to monitor the permafrost conditions after a wildfire at the discontinuous permafrost area on the Seward Peninsula, Alaska.

After a 2002 tundra fire, thermal conditions of the active layer at the burned sites changed drastically due to the destruction of the surface moss layer. The measured active layer thicknesses were significantly different between the burned and unburned sites, by more than 20 cm. There is no obvious increasing of the thickness between 2005 and 2006, however, the thickness in 2007 at north-facing sites was more than 10–20 cm deeper than those in 2005 or 2006.

The effect of fire on permafrost reaches only to the layer near ground surface, the active layer, or the upper part of permafrost.

The ground temperatures at the burned sites were 4°C–5°C higher than those at the unburned sites. Measurements of soil water content show no significant tendency, increasing or decreasing.

Measured apparent resistivity values at the burned sites show a lower value than those at the unburned sites, which was caused by the thick active layer. Using the estimation model, the true resistivity value of the unfrozen mineral layer was calculated, and there was no significant difference between burned and unburned sites. The resistivity values ranged widely at unburned sites, and the variation of resistivity was small at burned sites, which may show the small variation of water content along the survey line due to the fire.

Acknowledgments

We would like to express our sincere thanks to Prof. L. Hinzman, R. Busey, A. Liljedahl, and K. Yoshikawa of the University of Alaska Fairbanks for their support with the fieldwork. This research was financially supported by the Japan Aerospace Exploration Agency.

References

Harada, K. & Fukuda, M. 2000. Characteristics of the electrical resistivity of frozen soils. *Seppyo* 62: 15-22 (in Japanese with English Abstract).

Liljedahl, A., Hinzman, L., Busey, R. & Yoshikawa, K. 2007. Physical short-term changes after a tussock tundra fire, Seward Peninsula, Alaska. *Journal of Geophysical Research* 112: F02S07, doi: 10.1029/2006JF000554.

Racine, C.H., Patterson III, W.A. & Dennis, J.G. 1985. Tundra fire regimes in the Noatak River Watershed, Alaska: 1956–1983. *Arctic* 38: 194-200.

Racine, C.H., Jandt, R., Meyers, C. & Dennis, J. 2004. Tundra fire and vegetation change along a hillslope on the Seward Peninsula, Alaska, U.S.A. *Arctic, Antarctic, and Alpine Research* 36: 1-10.

Rupp, T.S., Chapin III, F.S. & Starfield, A.M. 2000. Response of subarctic vegetation to transient climatic change on the Seward Peninsula in north-west Alaska. *Global Change Biology* 6: 541-555.

Sawada, Y., Harada, K., Hinzman, L.D. & Fukuda, M. 2005. Permafrost degradation after the tundra fire in Seward Peninsula, Alaska - a perennial study-. *Proceedings of the 6th International Conference on Global Change: Connection to the Arctic (GCCA-6), Tokyo, Japan, December 12-13, 2005*: 148-151.

The Fate of Terrestrial Carbon Following Permafrost Degradation: Detecting Changes Over Recent Decades

Jennifer W. Harden and Christopher C. Fuller
U.S. Geological Survey, Menlo Park CA, USA
Martin Wilmking
University Greifswald, Greifswald, Germany
Isla Myers-Smith
University of Alberta, Edmonton, Alberta, Canada
Susan E. Trumbore
Univ. California, Irvine, CA, U.S.A.
Jill Bubier
Mount Holyoke College, South Hadley, MA, USA

Abstract

As boreal and arctic regions of North America have been undergoing considerable warming since the 1950s, a key question remains as to the fate of permafrost and carbon over this important time period. We used ^{137}Cs as an age constraint for soil carbon that has accumulated since the first occurrence of ^{137}Cs in 1954. We tested this approach by comparing profiles of $\Delta^{14}C$ to ^{137}Cs for soils of different plant communities near Delta Junction, central Alaska. Both isotopes indicate upward accumulating, organic systems that have little evidence for mixing or leaching. We then used inventories of these isotopes to normalize the C storage between frozen and thawed site-pairs. To date, we identified a net loss of carbon from a tundra-forest transition in northern Alaska. We measured net increases of C resulting from forest-bog and forest-fen transition in Alaska and Canada.

Keywords: boreal; carbon storage**;** discontinuous permafrost zone; peat; permafrost; soil carbon; thermokarst.

Introduction

Boreal regions in general and central Alaska in particular, encompass a broad range of ecosystems that are underlain by permafrost. There is an abundance of upland terrain with sporadic or discontinuous permafrost. Lowland terrain is also underlain by discontinuous permafrost, often with thicker peat deposits and ice-rich permafrost. Further nested within these landscapes are highly patchy vegetation and soil conditions that result from frequent fires. In central Alaska, recent results indicate that 7% of the landscape has undergone thermokarst, 47% has permafrost, 27% is unfrozen without a recent permafrost history, and 19% of the area has an uncertain thermal status (Jorgenson et al. 2005).

Permafrost degradation has been observed for the past decades when remotely-sensed and field observations have noted associated changes in vegetation (Vitt et al. 2000; Camill et al. 2001, Jorgenson et al. 2001, Turetsky et al. 2002, Christensen et al. 2004). Changes in air temperature, ground ice content, winter snowfall, and fire contribute to stabilization and destabilization of near-surface permafrost (Osterkamp & Romanovsky 1999). Discontinuous permafrost in Alaska may by particularly sensitive to climate warming in areas where soils are not blanketed by loess and ice-rich seasonal frost (Swanson 1996). Since 1949, thermokarst in the Tanana floodplain of Interior Alaska has increased by 21% and may result in the disappearance of permafrost in these landscapes (Jorgenson et al. 2001).

Thawing of near-surface permafrost has been associated with changes in patterned ground (Osterkamp et al. 2000) and conversion of forests to wetlands (Osterkamp et al. 2000, Jorgenson et al. 2001, Jorgenson & Osterkamp 2005). Permafrost thaw can also lead to the development of an open talik, or drained soil layer, involving shifts toward drier landscapes and ecosystems, for example, from moss- to lichen-dominated ground covers (Burn, 1998, Schuur et al, 2007).

Recent changes in northern climate systems have led to a piqued awareness of carbon stocks residing in near-surface permafrost and of their vulnerabilities to climate change. Since the 1960s, significant changes in air and surface temperatures have been documented for northern regions (see http://www.gtnp.org/pdf/icoppostergtnp). Upon significant warming, permafrost degradation can lead to either net accumulation or loss of carbon via shifts in ecosystems and C processing, and it is likely that both effects occur concurrently, yet heterogeneously, across the landscape. Evidence for net increases in carbon resulting from thermokarst, for example, include wetlands (Turetsky et al. 2007). Conversely, in systems that are becoming drier, there is the potential for aerobic respiration to reduce terrestrial carbon stocks.

Detecting changes in C storage using trace gas exchange requires long-term monitoring to decipher interannual variations from significant trends (Dunn et al. 2007). CO_2 budgets are particularly problematic because sources of respiration are numerous, and because detecting small changes in decomposition relative to large signals of

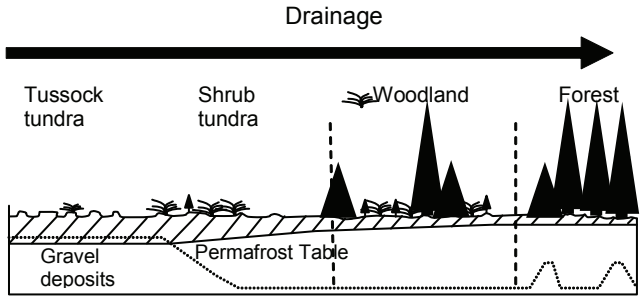

Figure 1a. Schematic drawing of permafrost degradation leading to drainage. Active layer in tundra on floodplain terrace deepens and leads to drainage of water through gravel deposits. Based on Wilmking et al. 2006.

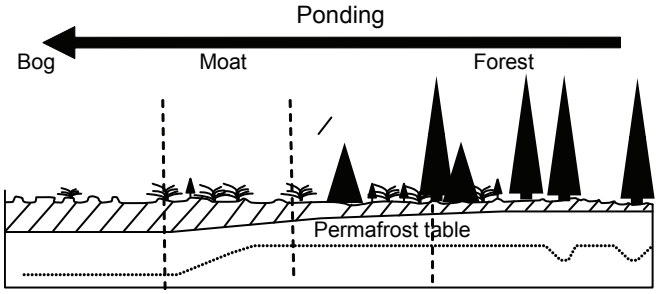

Figure 1b. Example of permafrost degradation leading to ponding. Based on Meyers-Smith et al. 2007.

respiration is difficult. Detecting changes in the solid carbon phase (e.g., vegetation and soil) is also challenging, owing largely to long-term variations in frozen ground, plant cover, and fire history (Harden et al. 2000).

Significantly, the recent warming trend in northern latitudes has been accompanied by atmospheric labeling by radiocarbon and radiocesium as a result of aboveground weapons testing. Such labeling of organic matter lends itself to assessments of carbon that has been fixed in recent decades. In context of landscape changes, such assessments can help to decipher the fate of carbon in the recent phase of northern latitude warming.

Approach

In Interior Alaska, the fate of terrestrial carbon over the next few decades likely will be determined by shifts in hydrology following permafrost thaw. Water plays a critical role in governing C cycling processes, including plant production (NPP), combustion (F), decomposition (kC or Rh), and leaching (DOC). Our goal is to test this hypothesis at the site scale, using radioisotopes of carbon and cesium to identify carbon stored in the past 50 years.

We examined a variety of ecosystems in Interior Alaska and northern Canada, including black spruce forests, tussock tundra, *Sphagnum* bogs, and a rich fen. We paired sites according to our interpretations of their near-surface permafrost and histories of thermokarst, and analyzed soils for radioisotopes.

Site scale measures of C stocks and isotopes are particularly helpful at establishing C accumulation rates over the last 50 years. ^{137}Cs is a product of uranium fission produced by weapons testing. The first significant atmospheric fallout occurred in 1952 with the maximum delivery occurring between 1963 and 1964. It can be used as a tracer for soil materials if the following conditions are met: (1) total cesium inventories are conserved in the soil, and (2) there is no significant movement of ^{137}Cs. These conditions are examined for a variety of soils before testing our hypotheses.

Radiocarbon was also produced by weapons testing and has been used as a tracer for carbon turnover in soils (Trumbore 2006). The main differences between Δ^{14}C and ^{137}Cs are: (1) Whereas fallout of ^{137}Cs declined precipitously after 1963, fallout of Delta^{14}C declined slowly owing to terrestrial C exchange with the atmosphere and fossil fuel emissions, And (2). Whereas ^{137}Cs is conserved in soil and sediment, Delta^{14}C can be retained via slow decomposition or effective stabilization or lost via rapid decomposition or combustion. ^{137}Cs in the atmosphere is generally bound to particulates, whereas Delta^{14}C in the atmosphere is present in gas phase. Isotopes of Cs and C therefore have different input mechanisms to the land surface.

Methods

In order to test the feasibility of using these isotopes to estimate recent changes in C storage, we first examined variations in soil ^{137}Cs and ^{14}C for patterns of storage, remobilization, and accumulation. Four sites were located in Interior Alaska near Delta Junction. Vegetation at all sites contained black spruce, but varied in tree density and abundance, owing mainly to variations in soil moisture and temperature (for more detail see Manies et al. 2004). Groundcover varies from a feather moss/lichen mix to feather moss.

In order to interpret the response of C storage to thaw, we sampled organic soils at sites with and without near-surface permafrost, interpreting sites as pairs of frozen and thawed landscapes. In Manitoba, Canada a frozen palsa was found adjacent to a collapse bog, a collapse fen, and a rich fen (Bubier et al. 1998, Trumbore et al. 1999). We assumed that the collapse fen originated as part of the palsa complex based on new collapse features on the side of the palsa that slumped into the fen. There was no direct evidence that the bog or rich fen had formed directly from the palsa, but cores at 2m depth were composed of *Sphagnum* peat and woody peat.

In Alaska, we sampled organic soils at permafrost/thawed pairs of soils in two locations. In the case of sites near the Kugururok River near treeline, sites from a tundra and a forest site (Wilmking et al. 2006) were used as frozen and thawed pairs. These sites were separated by shrub and shrub tundra ecosystems that were invaded by trees over the past 40 years; a deepening active layer along the tundra-forest transition indicates a transition from moderate to well-drained soil conditions (Fig. 1a). In the case of sites along the Tanana River near Fairbanks, a forest system underlain by permafrost was directly observed to burn and within a year to collapse into a wetland bog in 2001 (Myers-Smith et

al. 2007). Environmental reconstructions from charcoal and diatoms indicated previous cycles of fire-induced collapse.

We used ^{137}Cs and Δ^{14}C to identify organic matter that accumulated since about 1964, a time when atmospheric enrichment from aboveground weapons testing reached a maximum. Radiocarbon was measured on bulk organic matter at the UC Irvine W. M. Keck Carbon Cycle AMS facility (KCCAMS) and at the Lawrence Livermore Laboratory following correction and calibration procedures (Trumbore et al. 1999). Splits of the same samples were analyzed for ^{137}Cs, total ^{210}Pb and ^{226}Ra activity by gamma spectrometery at the USGS Sediment Radioisotope Laboratory in Menlo Park (Fuller et al. 1999). ^{210}Pb data is not presented and is being evaluated as a chronometer for these profiles.

For samples from both Manitoba and Alaska, we calculated inventories of radiocarbon and Cs to compare C stocks and accumulation rates represented in the upper layers of the organic soils. Inventories were calculated as:

$$\Sigma(i*fC*\ BD*\ th)_{horizons} \quad (1)$$

where i is the concentration of isotope in fraction modern (^{14}C) in soil; fC is the fraction organic C used for FM only; BD is bulk density (g m^{-3}); and th is the thickness of each horizon (m).

Soil horizons labeled by bomb-enriched concentrations of isotopes are defined by concentrations >0.04 pCi/g for ^{137}Cs, which represents the detection limit of the instrument, and concentrations >FM 1.0 for radiocarbon, where FM = Delta^{14}C/1000 + 1. In the case of Alaska samples, we assumed that the bomb-enriched layers were 50 years old (sampled in 2004; enriched by fallout since 1954). In the case of Manitoba samples collected in 1994, we used radiocarbon peak 1963 to estimate peat ages of 30 years (Trumbore et al. 1999). Inventories included only organic soil horizons.

Results

Depth profiles of both isotope profiles reach maximum and pre-bomb values at approximately the same depths in each core. Maximum values in both isotopes likely represent the time around 1963, when weapons testing reached peak-output to the atmosphere (Fig. 2). Deep soil horizons with radiocarbon values <1.0 FM likely indicate pre-bomb ages. These layers are essentially free of ^{137}Cs (Fig. 2), likely indicating that Cs was not re-mobilized from shallow to deeper layers. It also is possible, but unlikely, that ^{137}Cs and radiocarbon could have mobilized in tandem.

Mean ^{137}Cs inventories were 3.3 +/- 1.3 pCi/cm2 and mean Δ^{14}C inventories were 0.6 +/- 0.2 Delta^{14}C /cm^2 (data not shown). Variability in inventory of fallout materials among ecosystems in a given region ranged from 40 to 30% of the mean inventory for ^{14}C and Cs, respectively.

C inventories in bomb-labeled soil layers

Based on the site pairing where thermokarst led to drainage, there was a 64% loss of C in the near-surface soil (Table 1, example 1). Based on the examples where thermokarst led to ponding and formation of wetlands, there was a mixed response. In Manitoba, thaw resulted in -70% (loss) to +80% (gain) in C stocks in which fens accumulated C and the bog lost C (Table 1, examples 3–7). In Alaska, C stocks increased by 11% .Based on inter-site variations in Cs stocks (above), changes less than 30% are likely not significant.

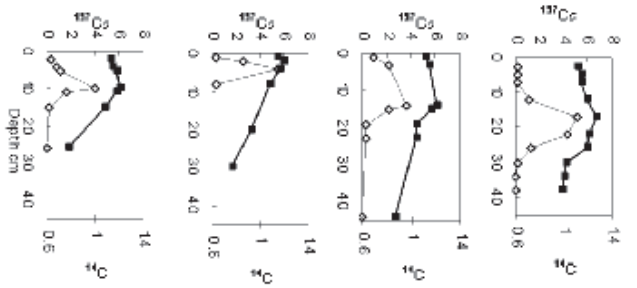

Figure 2. Radiocarbon (closed symbols) and radiocesium (open) concentrations versus basal horizon depths from 4 soils of differing ecosystem settings from the area around Delta Junction, Alaska. From left to right, profiles correspond to mature forest stands, sites DFTC6 (well-drained), DFTC23 (well-drained), DFCC15 (permafrost at ~50cm), DFDC1 (permafrost at 41 cm) from Manies et al. 2004. Samples collected in 2002. Cs measured in 2006.

Table 1. Recent soil carbon labeled with bomb-enriched isotopes and stored in pairs of frozen and unfrozen ground. Comparison 1: Frozen tundra (1Tundra) Unfrozen, drained forest soils (2Forest) based on Wilmking et al. 2006 using ^{14}C; Comparison 2: Frozen forest (3Forest) Unfrozen, ponded wetland bog (4WetlandBog) based on Myers-Smith et al, in press using ^{137}Cs. Comparison 3: Frozen palsa (5P) Unfrozen wetland bog (6WBog) Unfrozen wetland fen (7,8WFen) using ^{14}C. C stocks in g C m^{-2} Rates in gC m-2yr-1 calculated over 30 *(sites 7,8)* to 50 yrs *(sites 1–6)*.Changes calculated as difference in stock or rate between frozen and thawed state, divided by frozen state.

Site Pair		C Stock	Rate	Stock Change	Rate Change
1Frozen	1Tundra	10363	259		
Thawed	2Forest	3703	93	-64%	-64%
2Frozen	3Forest	5477	137		
Thawed	4Wetland Bog	6065	151	+11%	+11%
3Frozen	5Palsa	5413	258		
Thawed	6WetlandBog	1811	58	-67%	-77%
Thawed	7WetlandFen	9768	349	+80%	+35%
Thawed	8Wetland	9153	277	+69%	+8%

Table 2. Long-term total C stocks. Sites underscored in Table 1.

	Stock g m-^{2}	Age Yr BP	Rate g m^{-2}yr^{-1}	Rate Change	Stock Change
1Tundra	19772	680	29		
2Forest	8649	635	14	-56%	-53%
3Forest	13933	585	24		
4Wetland	20701	25	84	+49%	+255%

C inventories of total soil profiles

Changes in total carbon stocks for the full soil profiles showed a net decrease in C stock where thermokarst led to drainage, and a net increase in C stocks where thermokarst resulted in wetlands.

Discussion

Based on Cs and C isotopes, it appears that either isotope may be used as labels for C that has entered the soil since about the 1950s when above-ground weapons testing introduced significant sources of ^{137}Cs and $\Delta^{14}C$. We interpret depth profiles of these isotopes (Fig. 2) as evidence for "upward accumulating" systems with little or no vertical mixing. As noted above, the soils from Delta Junction showed little or no sign that Cs was mobilized in the soil profile based on the agreement in depths where (1) peak values and (2) pre-bomb values of both ^{137}Cs and $Delta^{14}C$ occurred. However, data from the Fairbanks site (Myers-Smith et al. in press) did show signs of remobilization in the deepest organic layers, based on a comparison to radiocarbon ages.

Albeit a preliminary finding with no replication, we found that soil C was lost (C source) where thaw water was drained and that there was a mixed response for C where thaw water was ponded. It is likely that drainage of thawed water resulted in aerobic decomposition, which outweighed plant production and resulted in a C source to the atmosphere. By contrast, where thaw resulted in ponding, changes from frozen state to anaerobic conditions for decomposition and changes in plant production may result in a mixed response, resulting in a C sink or C source.

There are at least three important limitations of this isotopic approach that limit our ability to constrain changes in carbon storage. First, mobilization of either radiocarbon or radiocesium would impact results of this approach. Input and decomposition of organic matter into and out of the soil layers causes most of the depth variations, because peaks and attenuations of both isotopes are coincident for 4 very different soil types. Nevertheless, some amount of both isotopes could move together through the profile via leaching or mixing. Second, any estimates of recent net carbon accumulation are overestimates, because C loss via decomposition of deep soil layers is not accounted for by this approach. Based on assessments by Rapalee et al. (1998), this overestimate may be quite small because decomposition rates are very slow in saturated systems. By the same logic, recent carbon losses resulting from thermokarst are underestimated, again because deep decomposition is not accounted for in this approach. Where systems are converting frozen and large C stocks to aerobic decomposition, such underestimates could be quite large. For example, turnover time in well-drained soil of 100 years applied to a carbon stock of the tundra soil of 10000 gC m^{-2} amounts to 100 gC m^{-2} yr^{-1}. Third, the time of initial thermokarst formation is not known for any of these sites. Therefore, if rates of C accumulation change over time-since-thermokarst, C accumulation rates should not be compared directly without finding a way to stratify the data according to post-thaw successional age.

In order to address these important limitations to our labeling approach, we recommend that C stocks be assessed for post-bomb labels, particularly in newly-formed thermokarst features of known age. Moreover, C inventories should be replicated for a variety of ecosystems. Methods also should be developed to account for the contribution that deep decomposition may make to offset near-surface accumulations of C. Owing to its powerful greenhouse potential and sensitivity to the water table, the role of methane in the trace gas budget of these systems will vary according to the fate of water upon thaw. For example, saturated collapse scars have significantly higher CH_4 emissions than palsas or non-permafrost wetlands (Wickand et al. 2006, Turetsky et al. 2002). As permafrost wetlands are dominant sources of CH_4, yet make up a small proportion of the total landscape, quantifying total green house gas emissions from remote sensing is a challenge that must be met for these boreal regions (Bubier et al. 2005).

Conclusions

Detection of change

Cesium and radiocarbon inventories lead us to expect 30 to 40% variability, respectively, in fallout inventories within a given region. Therefore, C stocks need to be >50% different from the control or baseline in order to be a significant detection of change. During the time period since the 1950s when the atmosphere warmed significantly, it is likely that significant soil C losses accompanied conversion of tundra to forest in our study site in Interior Alaska. By contrast, significant soil C uptake accompanied the conversion of black spruce forest to wetland in our study site in northern Manitoba.

Acknowledgments

Thanks go to Hugo Veldhuis for field insights; Ted Schuur, Peter Kuhry, and Jon O'Donnell for reviews; Ag. Canada NASA BOREAS; NSF Carbon-Water (solicitation no. NSF 06-514); and USGS (Earth Surface Dynamics Program) for funding.

References

Bubier, J.L., Crill, P.M., Moore, T.R., Savage, K. & Varner, R.K. 1998. Seasonal patterns and controls on net ecosystem CO_2 exchange in a boreal peatland complex. *Global Biogeochemical Cycles* 12: 703-714.

Bubier, J., Moore, T., Savage, K. & Crill, P. 2005. A comparison of methane flux in a boreal landscape between a dry and a wet year. *Global Biogeochemical Cycles* 19, GB1023, doi: 10.1029/2004GB002351.

Burn, C.R. 1998. The response (1958-1997) of permafrost and near-surface near-surface ground temperatures to forest fire, Takhini River valley, southern Yukon Territory. *Canadian Journal of Earth Sciences* 35(2):184-199.

Camill, P., Lynch, J.A., Clark, J.S., Adams, J.B. & Jordan, B. 2001. Changes in biomass, aboveground net primary production, and peat accumulation following permafrost thaw in the boreal peatlands of Manitoba. *Canada Ecosystems* 4: 461-478.

Christensen, T.R., Johansson, T., Åkerman, H.J., & Mastepanov, M.2004. Thawing sub-arctic permafrost: Effects on vegetation and methane emissions. *Geophys. Res. Lett.* 31: 1-4, doi 10.1029/2003GL018680.

Dunn, A.L, Barford, C.C., Wofsy, S.C., Goulden, M.L. & Daube, B.C. 2007. A long-term record of carbon exchange in a boreal black spruce forest: means, responses to interannual variability, and decadal trends. *Global Change Biology* 13(3): 577-590.

Fuller, C.C., vanGeen, A., Baskaran, M. & Anima, R. 1999. Sediment chronology in San Francisco Bay defined by 210Pb, 234Th, 137Cs, and 239,240Pu. *Marine Chemistry* 64: 7-27.

Harden, J.W., Trumbore, S.E., Stocks, B.J. Hirsch, A., Gower, S.T., O'Neill, K.P. & Kasischke. E.S. 2000. The role of fire in the boreal carbon budget. *Global Change Biology* 6(suppl.1): 174-184.

Jorgenson, M.T., Racine, C.H., Walters, J.C. & Osterkamp, T.E. 2001. Permafrost degradation and ecological changes associated with a warming climate in central Alaska. *Climatic Change* 48: 551-579.

Jorgenson, M.T. & Osterkamp, T.E. 2005. Response of boreal ecosystems to varying modes of permafrost degradation. *Can. J. Forest Res*. 35: 2100-2111.

Manies, K.L., Harden, J.W., Silva, S.R., Briggs, P.H. & Schmid, B.M. 2004. Soil data from Picea mariana stands near Delta Junction, AK of different ages and soil drainage type. U.S. Geological Survey Open File Report 2004-1271, 19 pp

Myers-Smith, I.H., Harden, J.W., Wilmking, M., Fuller, C.C., McGuire, A.D., Chapin, F.S.III. In press. Wetland succession in a permafrost collapse: interactions between fire and thermokarst. *European Biogeosciences*.

Osterkamp, T.E. & Romanovsky V.E. 1999. Evidence for warming and thawing of discontinuous permafrost in Alaska. *Permafrost Periglac*. 10: 17-37.

Osterkamp, T.E., Viereck, L., Shur, Y., Jorgenson, M.T., Racine, C., Doyle, A.,& Boone, R.D. 2000. Observations of thermokarst and its impact on boreal forests in Alaska, U.S.A. *Arctic Alpine Res*. 32: 303-315.

Rapalee, G., Trumbore, S.E., Davidson, E.A., Harden, J.W. & Velhuis, H. 1998. Scaling soil carbon stocks and fluxes at the BOREAS Northern Study Area. *Global Biogeochemical Cycles* 12(4): 687-701.

Schuur, E.A.G., Crummer, K.G., Vogel, J.G. & Mack. M.C. 2007. Plant productivity and species composition following permafrost thaw and thermokarst in Alaskan tundra. *Ecosystems,* doi:10.1007/s10021-007-9024-0.

Swanson, D.K. 1996. Susceptibility of permafrost soils to deep thaw after forest fires in Interior Alaska, U.S.A., and some ecological implications. *Arctic Alpine Res.* 28: 217-227.

Trumbore, S.E. 2006. Carbon respired by terrestrial ecosystems—recent progress and challenges. *Global Change Biology* 12: 141-153, doi:10.1111/j.1365-2486.2005.01067.x.

Trumbore, S.E., Bubier, J. Harden, J.W. & Crill, P.M. 1999. Carbon Cycling in Boreal Wetlands: A Comparison of Three Approaches. *Jour Geophys. Res. Atm.* 104: 27,673-27,682.

Turetsky, M.R., Wieder, R.K., & Vitt, D.H. 2002. Boreal peatland C fluxes under varying permafrost regimes, Soil Biol. *Biochem.* 34: 907-912.

Turetsky, M.R., Wieder, R.K., Vitt, D.H., Evans, R. & K. D. Scott. 2007. The disappearance of relict permafrost in boreal regions: effects on peatland carbon storage and fluxes. Global Change Biology 13: 1-13.

Vitt, D.H., Halsey, L.A. & Zoltai, S.C. 2000. The changing landscape of Canada's western boreal forest: the current dynamics of permafrost. *Can. J. Forest Res*. 30: 283-287.

Wickland, K.P., Striegl, R. G., Neff, J.C. & Sachs, T. 2006. Effects of permafrost melting on CO2 and CH4 exchange of a poorly drained black spruce lowland. *Jour. Geophys. Res.* 111:G02011, doi:10.1029/2005JG000099.

Wilmking, M., Harden, J. & Tape, K. 2006. Effect of tree line advance on carbon storage in NW Alaska. Journal of Geophysical Research 111:G02023, doi:10.1029/2005JG000074.

—Plenary Paper—

Recent Warming of European Permafrost: Evidence from Borehole Monitoring

Charles Harris
School of Earth, Ocean and Planetary Sciences, Cardiff University, Cardiff, CF10 3YE UK
Ketil Isaksen
Norwegian Meteorological Institute, P.O.Box 43 Blindern, NO-0313 Oslo, Norway

Abstract

Here we present a review of recent ground thermal data derived largely from the continent-scale network of instrumented boreholes within mountain permafrost established between 1998 and 2001 by the European Union PACE project. More recently, networks of intermediate and shallow boreholes in Switzerland, Norway, and Iceland have been added. A large number of complex variables determine permafrost temperatures, including altitude, topography, net radiation, and snow distribution. Thus, modeling the above-ground climate signal from observations of permafrost temperatures and coupling downscaled climate models to assess future permafrost thermal responses to climate forcing remain major research goals. Boreholes drilled in areas of steep mountain topography may penetrate complex three-dimensional thermal fields, making interpretation of thermal profiles in terms of changes in the upper thermal boundary extremely challenging. However, in the lower relief settings of the Scandinavian and Svalbard PACE boreholes, observed warm-side deviation in thermal profiles strongly suggests a period of sustained surface warming in the latter half of the 20th century and in the early 21st century. The significance of short-term extreme thermal events is illustrated with reference to the record-breaking summer of 2003 in the Alps and the anomalously warm winter-spring-summer period in 2005–2006 in Svalbard. It is concluded that such events may initially be more significant than the longer-term underlying trends in climate. Permafrost thermal responses to climate change occur at markedly different time scales, with changes in active layer thickness being more or less immediate, modification of thermal profiles below the depth of zero amplitude taking decades or centuries, and basal melting associated with progressive permafrost thinning requiring millennial time scales. However, as illustrated here by the example of Icelandic permafrost, where the frozen ground layer is thin and warm and the geothermal heat flux rates are high, permafrost decay and disappearance may be much more rapid.

Keywords: borehole monitoring; climate change; Europe; permafrost temperatures.

Introduction

In the present paper we review current evidence for permafrost warming within the European sector. In the mid-latitude high relief setting of the Alps, ground temperatures are only a few degrees below zero and permafrost may be thin near the lower permafrost boundary. Permafrost warming in alpine mountain slopes increases the risk of landslides, debris flows, and rockfalls (Noetzli at al. 2003, Gruber & Haeberli 2006). However, predicting the thermal response of mountain permafrost to climate change is challenging because of spatially complex topography and substrate properties (e.g. Hoezle et al. 2001). In contrast to the Alps, permafrost is continuous in the Arctic archipelago of Svalbard, outside the glaciated areas. Ocean-atmosphere coupling results in the climate being particularly sensitive to variations in sea-ice cover (Benestad et al. 2002, Isaksen et al. 2007b). Observed and predicted reductions in sea-ice (Stroeve et al. 2007, Serreze et al. 2007) suggest the onset of a rapid climate transition, with increasing frequency of anomalously high temperatures (Christensen et al. 2007, Isaksen et al. 2007b). The thermal response of permafrost may therefore exceed recent historical experience. Finally, the maritime setting of Iceland results in permafrost being restricted to higher elevations, and here geothermal heat flux increases the sensitivity of permafrost to changes in the upper boundary condition (Farbrot et al. 2007). This diversity of permafrost settings within Europe provides a background for this paper.

European Borehole Monitoring

A major stimulus to European permafrost research was provided by the PACE project (Permafrost and Climate in Europe), which commenced in 1997 (see Harris et al. 2001), and much of the more recent research reported here is a legacy of this program (Harris et al. submitted). Primary data have been collected through instrumented permafrost boreholes; the main borehole network of six instrumented bedrock boreholes drilled 100 m or more in depth was established between 1998 and 2001 through the PACE project (Fig. 1). The longest continuous European permafrost temperature time series is from the 32 m deep Murtèl Corvatsch borehole in Switzerland (Fig. 1) which was drilled in 1987, in an ice-rich rock glacier (Vonder Mühll and Haeberli 1990, Hoelzle et al. 2002). This borehole has been incorporated into the PACE network.

Over the past decade, the number of intermediate and shallow (less than 25 m) depth monitoring boreholes has increased steadily, particularly in Switzerland, where permafrost monitoring is coordinated by the PERMOS programme (Vonder Mühll et al. 2004, 2007). In Norway and Svalbard the IPY project "Thermal State of Permafrost" (TSP) (Christiansen this volume) has also instigated a

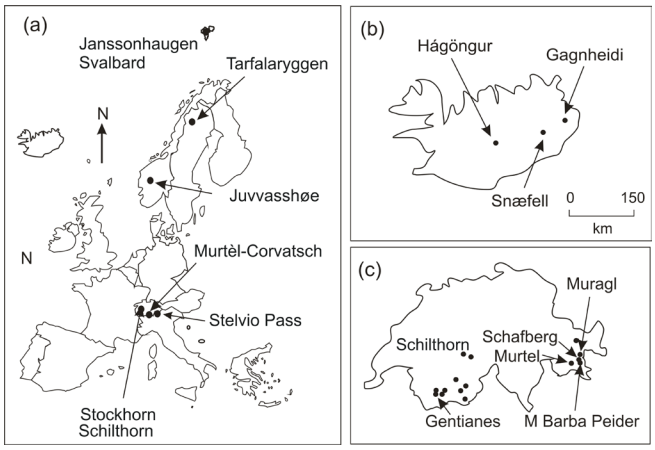

Figure 1. Distribution of boreholes mentioned in text. (a) PACE borehole network, (b) Icelandic boreholes, (c) Swiss boreholes.

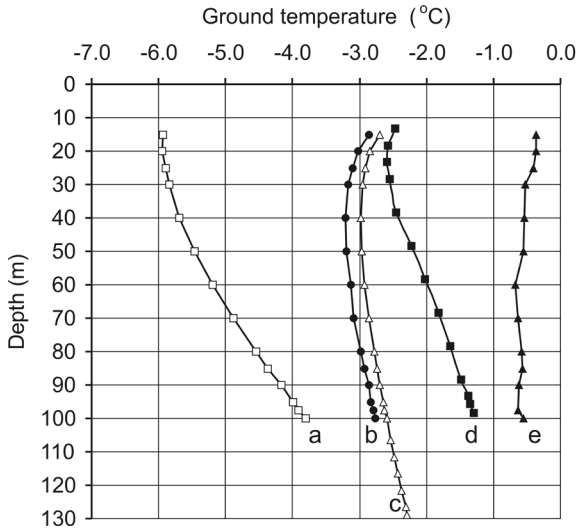

Figure 2. Ground temperature profiles in permafrost below 15 m at (a) Janssonhaugen, (b) Tarfalaryggen, (c) Juvvasshøe, (d) Stockhorn, (e) Schilthorn, and (f) Murtèl-Corvatsch. Data recorded 22 April 2005 (temperature profile at Juvvasshøe below 100 m depth recorded manually 1 October 2000).

program of permafrost monitoring through shallow boreholes. A total of 66 boreholes are listed from the European sector in the GTNP database (http://www.gtnp.org/); 31 of these are in Switzerland, 18 in Norway and Svalbard, and between 3 and 6 in Iceland, Italy, Spain, and Sweden. Not all are continuously monitored, and many have only short time series.

Instrumentation generally utilizes automatic logging of thermistor strings within cased boreholes. Recommendations on instrument specification, spacing, and logging frequencies may be found in the PACE Manual (see Appendix B, Vonder Mühll 2004), but all thermistors should be retrievable to allow periodic recalibration. In most PACE boreholes a second 15–20 m deep borehole was drilled adjacent to the deeper hole to allow more detailed higher frequency monitoring of the near surface (Isaksen et al. 2001, 2007a, Gruber et al. 2004c). In other borehole monitoring programs, a multimeter may be used to record thermistor temperatures periodically, or the borehole may be equipped with single-channel miniloggers, which are retrieved annually for downloading. Alternative approaches to monitoring the thermal status of permafrost include active layer thickness (e.g., the Circumpolar Active Layer Monitoring (CALM) program), and measurement of the Bottom Temperature of Snow (BTS) (e.g., Vonder Mühll et al. 2004, 2007).

Permafrost Geothermal Profiles

Since heat advection by ground water or air circulation is often negligible, permafrost geothermal profiles are primarily a function of heat conduction from the Earth's interior and heat fluxes at the ground surface. The annual ground surface thermal cycle penetrates to 15–20 m (the depth of zero amplitude), but larger perturbations of longer periodicity may penetrate much deeper and take much longer to do so (e.g., Lachenbruch & Marshall 1986). Perturbation of the thermal gradient below the depth of zero annual amplitude may provide direct evidence of thermal trends at the permafrost table during preceding decades or centuries (e.g., Cermak et al. 2000, Osterkamp & Romanovsky 1999). Where permafrost is thin (<100m), such thermal perturbation may extend to the base, causing basal melting, but in thicker permafrost, deeper penetration of climatically forced thermal cycles is likely to require millennial time scales.

In mountain permafrost, the thermal field is often strongly three-dimensional (Noetzli et al. 2007) and the thermal offset between mean ground surface temperature and mean permafrost table temperature reflects spatial heterogeneity in active layer composition and snow distribution, the latter also being subject to large inter-annual variations (Gruber et al. 2004c). Thus, modeling the above-ground climate signal from observations of permafrost temperatures, and coupling downscaled climate models to assess future permafrost thermal responses to climate forcing, remain major research goals (Harris et al. submitted). The greater altitudinal range and more complex topography in the Alps lead to greater variability in permafrost temperatures recorded by Swiss boreholes than those in Scandinavia and Svalbard. Figure 2 shows ground temperature profiles from PACE boreholes recorded in April 2005.

Ground temperatures in the Alpine boreholes Stockhorn and Schilthorn are highly disturbed by topography. Gruber et al. (2004c) have shown that for Stockhorn, marked differences in thermal gradient occur over short distances in response to a strongly three-dimensional temperature field. At Schilthorn, permafrost temperatures are very close to 0ºC and are influenced by latent heat effects and convective heat transfers by water as well as topographic effects. In contrast, the three Nordic boreholes have low relief within 100–200 m of the monitoring sites, relatively uniform bedrock and thin snow cover, suggesting that the climate signal dominates the observed geothermal gradients (Isaksen et al. 2007b). At greater depths than the boreholes, the effect of larger-scale relief may be significant and may in part explain

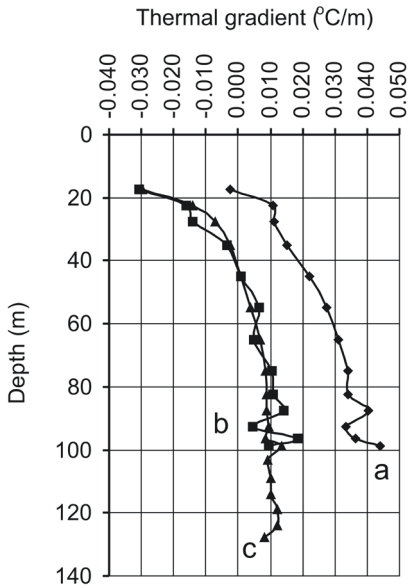

Figure 3. Thermal gradients at (a) Janssonhaugen, (b) Tarfalaryggen, (c) Juvvasshøe, calculated from profiles presented in Figure 2.

the low thermal gradients observed at Tarfalaryggen and Juvvasshøe (Fig. 3). All three boreholes show a significant warm-side deviation in their thermal profiles to 70 m depth, with marked increases in thermal gradient with depth. Just below the depth of zero amplitude, gradients are negative (Fig. 3). These characteristics probably reflect surface warming since the mid 20th century (Harris et al. 2003, Isaksen et al. 2001, 2007a) and extrapolation to the surface of temperature gradients between 30–20 m depths and 70–100 m suggests surface warming of ~1.4°C, ~1.1°C and ~1.0°C for Janssonhaugen, Tarfalaryggen, and Juvvasshøe respectively.

Recent Trends in Permafrost Temperatures

Permafrost temperatures at depths of around 10 m in Swiss and Norwegian boreholes are illustrated in Figure 4(a) and (b). At Murtèl-Corvatsch in Switzerland, marked warming was recorded between 1987 and 1995 (Vonder Mühll & Haeberli 1990, Vonder Mühll et al. 1998, 2002, 2007, Hoelzle et al. 2002), but this was reversed in the winter of 1995–96 and more markedly so in 1996–97. Since then, at Murtèl and other Swiss boreholes, no marked overall warming trend is apparent, with periods of rising ground temperatures being cancelled out by marked winter cooling in 2002–03 and 2006–07. Harris et al. (2003) showed that snow-poor early winter periods rather than markedly lower atmospheric temperatures were largely responsible for these ground cooling events.

In the three Nordic boreholes, deflation maintains relatively thin snow cover in winter, so that ground temperatures are strongly coupled to atmospheric temperatures (Isaksen et al. 2007a). At Janssonhaugen especially, temperature records at 10 m depth show pronounced fluctuations and large inter-annual variability, making identification of longer-

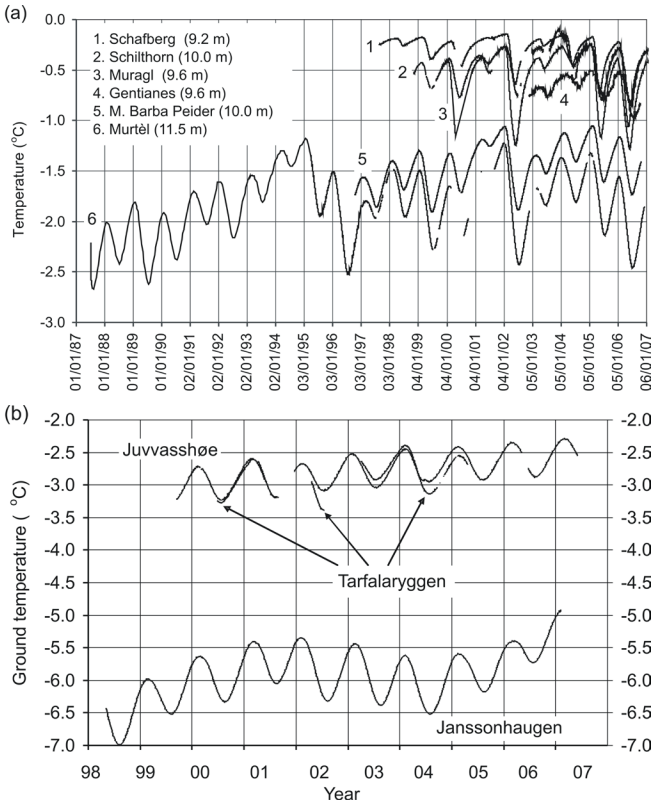

Figure 4. Permafrost temperature time series from around 10 m depth. (a) selected Swiss PERMOS boreholes. (b) Nordic PACE boreholes. For locations of boreholes, see Figure 1.

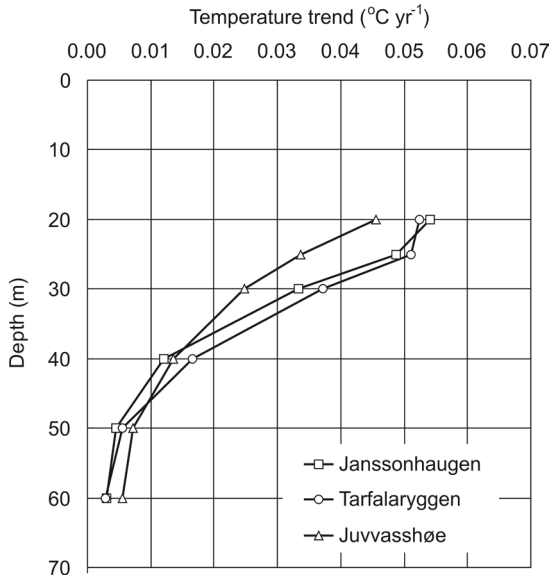

Figure 5. Observed linear trends in ground temperature as a function of depth. Time series at start in 1999 at Janssonhaugen, 2001 at Tarfalaryggen, and 2000 at Juvvasshøe, and they last for 6, 4, and 5 years, respectively.

term trends more difficult. However, recorded ground temperature changes below the zero annual amplitude provide direct evidence of thermal trends at the ground surface during recent decades. At all three sites a clear trend towards warming ground temperatures is detected (Fig. 5). For instance, at 30 m depth, present warming rates are

in the order of 0.025 - 0.035°C yr^{-1}. Isaksen et al (2007a) demonstrated that statistically significant ground warming may be detected to 60 m depth, the rate of warming being greatest at Tarfalaryggen and Janssonhaugen (Fig. 5).

The Significance of Extreme Events

Climate warming in the 20th and 21st centuries is likely to increase active layer thicknesses. However, an associated increase in frequency of high-temperature anomalies with sustained higher than normal temperatures may well dominate active layer evolution. Two examples of such extreme periods are discussed below: summer 2003 in the Alps, when temperatures during June, July, and August were approximately 3°C higher than the 1961–1990 average (Gruber et al. 2004c) and Svalbard in 2005–6 when anomalously high winter spring and summer temperatures caused significant permafrost warming (Isaksen et al. 2007b).

At the bedrock borehole of Schilthorn, Switzerland, active layer thickness ranged from around 4.4 m to around 4.9 m in the five years prior to 2003, but increased to nearly 9 m (Fig. 6a) during the 2003 extreme summer. In subsequent years the thickness has been around 4.8 m. At Stockhorn the active layer increased from around 3 m in the previous few years to 4.27 m in 2003. Numerical modeling has shown that in 2003 Alpine active layers were thicker than in the previous 21 years and were probably the greatest for several centuries (Gruber at al. 2004b). Rapid warming and thawing of bedrock containing ice-bonded joint planes led to a marked increase in rockfall events (Keller 2003) particularly on north-facing slopes where the effects of elevated atmospheric temperatures are greatest, and permafrost most widely distributed (Gruber et al. 2004b, Noetzli et al. 2007). The sharply increased depth of thaw during the summer of 2003 far outweighed the direct effect of gradually rising temperatures on the stability of the uppermost few metres of rock in most Alpine rock walls (Gruber et al. 2004c, Gruber & Haeberli 2006).

In contrast, active layer thickness changed much less dramatically at the ice-rich rock glacier of Murtèl-Corvatsch (Fig. 6b) in Switzerland where latent heat demand during thaw at the permafrost table provides an effective heat sink, limiting the active layer thickening. The general trend since 1987 has been towards increasing active layer thickness and in 2003 it reached 3.51m, around 11 cm thicker than in the previous summer and the greatest value since monitoring began in 1987. However, once thawed, meltwater drains away, leaving a thicker active layer with much lower ice content and therefore latent heat demand than the underlying permafrost. Thus, despite a much cooler summer in 2004, the active layer reached the same thickness as in 2003, and in 2005, which was cooler again, thaw penetration was only a few cm less than in 2003 (Vonder Mühl et al. 2007).

The winter-spring-summer period in 2005–6 on Svalbard provides a remarkable example of extreme atmospheric temperatures. The mean air temperature between December and May 2005–2006 was as high as −4.8°C, which is 8.2°C above the 1961–1990 average and 2.8°C higher than the previous record from 1954, amounting to an offset of 3.7 standard deviations from the mean (Isaksen et al. 2007b). The anomaly coincided with a marked reduction in sea-ice cover and an unusually large extent of marine open water around Svalbard during winter, spring, and summer 2005–2006. The warm winter was followed by warmer than average summer temperatures, which were around 2°C above the 1969–1990 normal. For calendar year 2006, the cumulative negative ground temperature at the permafrost table in the Janssonhaugen borehole (2 m depth) showed a 40% reduction compared with the average of the previous six years.

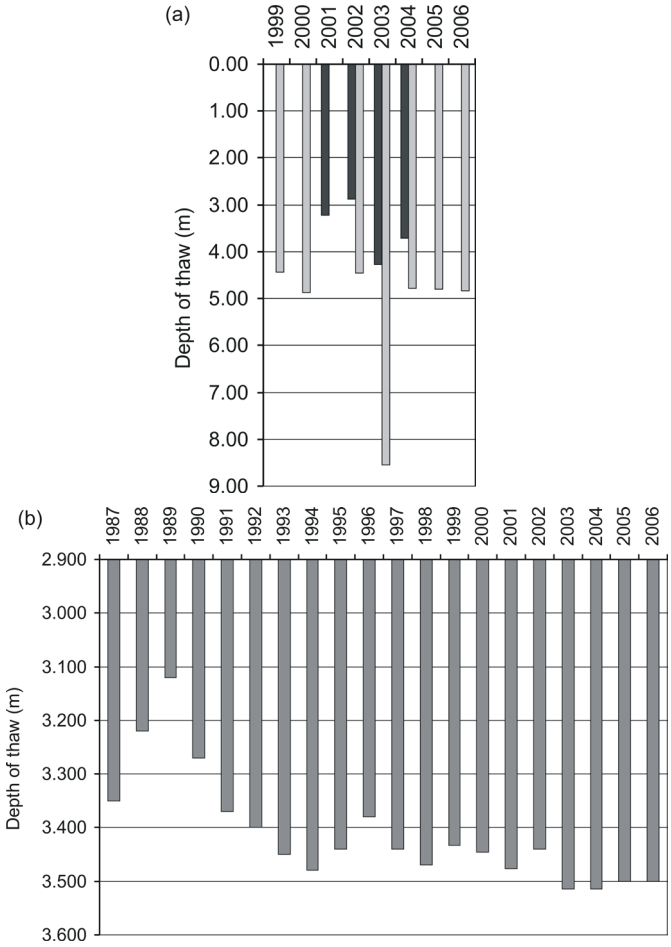

Figure 6. Active layer thickness: (a) Schilthorn (light bars) and Stockhorn (dark bars); (b) Murtèl-Corvatsch.

The effect on permafrost temperatures at Janssonhaugen is most clearly captured by considering the 12-month period from 1 December 2005 to 30 November 2006 (Isaksen 2007b). Plotting mean ground temperatures over this period, for instance the uppermost 3 meters, shows temperatures at the permafrost table 1.8°C above the 1999–2005 average, with the thermal anomaly traceable to a depth of at least 15 m. The start of active layer thawing was the earliest in the 8-year record and active layer thickness was 1.8 m, exceeding the mean of the previously recorded years by 0.18 m (an 11% increase).

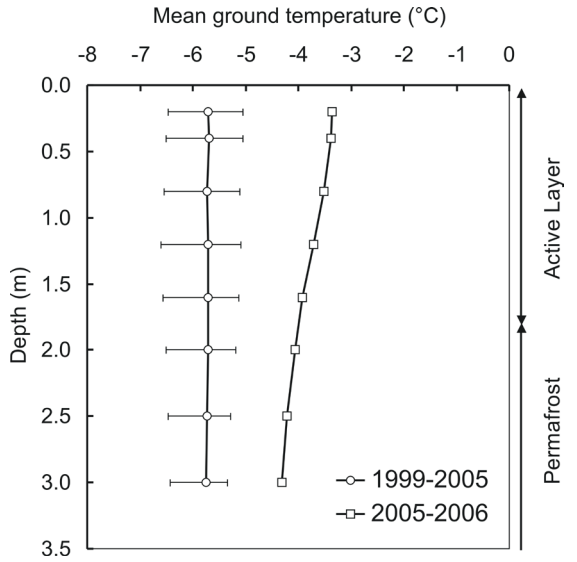

Figure 7. Mean ground temperature profile at Janssonhaugen for 2005–2006 compared with the mean for 1999–2005. Horizontal bars show the absolute variations of the previous years.

In order to place this anomaly into the context of climate change, Isaksen et al. (2007b) compared the accumulated degree day air temperature curve for 2006 at Svalbard airport with equivalent curves derived from empirical-statistical downscaling based on the multi-model World Climate Research Programme (WCRP) Coupled Model Intercomparison Project (CMIP3) of the most recent Intergovernmental Panel on Climate Change (IPCC) assessment in which atmospheric CO_2 reaches 720 parts per million by 2100. The 2006 accumulated degree day curve lay well within the range of the predicted scenarios for 2071–2100. Since 1999, accelerated warming has been observed at Janssonhaugen, the calculated rate at the top of the permafrost being in the order of 0.6–0.7°C/decade (Isaksen et al. 2007a). Thus the extreme temperatures of 2005–2006 were superimposed on a significant warming trend. If the frequency of such high temperature anomalies increases, then near-surface permafrost warming will be irregular rather than gradual and punctuated by rapid warming events such as that in 2005–2006.

Sensitivity to Geothermal Heat Flux

In Iceland, maritime conditions give cool summers and mild winters. The MAAT for 1961–1990 is around 4°–5° C in the south, and 2°–3°C in the north in lowland areas (Farbrot et al. 2007). Extensive non-glaciated mountain areas have MAAT below -3°C, indicating a potential for permafrost where snow cover is thin or absent. A regional model, calibrated against borehole thermal data and rock glacier inventories, suggests the presence of permafrost above around 800m a.s.l. in the north and above 1000m in the south (Etzelmüller et al. 2007, Etzelmüller et al. 2008), with the thickness of snow strongly modulating permafrost distribution.

Four monitoring boreholes in central and northeastern Iceland were established in 2004 (Farbrot et al. 2007, Etzelmüller et al. 2007, Etzelmüller et al. this volume), at altitudes of between 890–930 m a.s.l. (Fig. 1b). All boreholes are shallow (12–22 m deep) and penetrate thin sediment into basaltic bedrock. Permafrost was absent at the Vopnafjörður site due to excess snow cover, but at Snæfell and Gagnheiði it was estimated to be 30–35 m thick (Fig. 8b, c), with active layers around 2 m and 4 m respectively. At the Hágöngur borehole, permafrost was thin and the active layer thick (around 6 m) and permafrost temperatures close to zero degrees C (Fig. 7a). Meteorological data indicate that mean annual ground surface temperatures for the past few years in Iceland have been 0.5–1°C higher than those for the 1961–90 period (Etzelmüller et al. 2007). At the Gagnheiði and Snæfell boreholes, temperature profiles show warm-side deviation from steady state, suggesting recent rises in the upper boundary temperature (Fabrot et al. 2007).

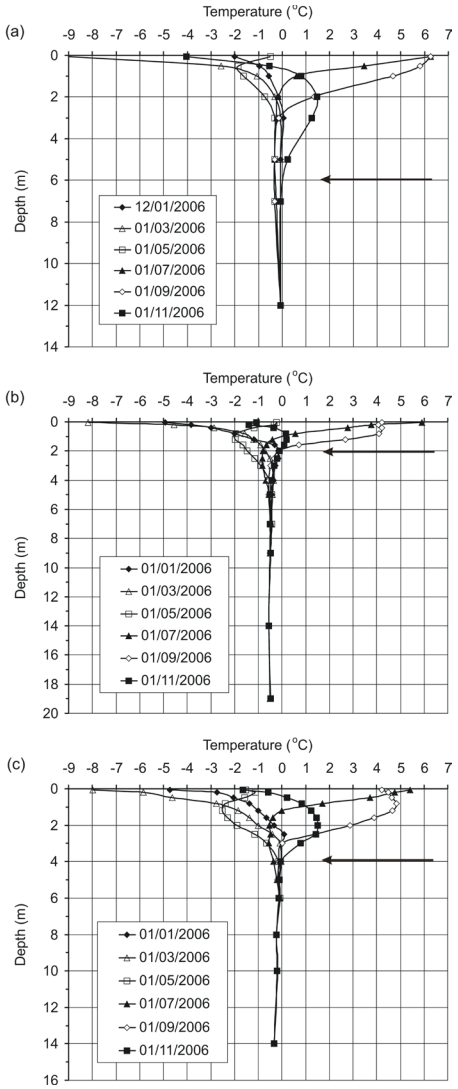

Figure 8. Temperature profiles in boreholes during 2006: (a) Hágöngur, (b) Snæfell, (c) Gagnheiði. Active layer thickness during the 2006 summer season indicated by arrows.

Using a one-dimensional thermal model, Farbrot et al. (2007) showed that increases in mean daily surface air temperatures of (a) 0.01°C a^{-1} and (b) 0.03°C a^{-1} would

cause permafrost to disappear at Snæfell in 160 and 100 yr respectively and at Gagnheiði in 125 and 75 yr respectively, the slower thermal response at Snæfell reflecting higher ice contents. Modeled temperature evolution since 1955 suggested that the present-day permafrost thicknesses reflect cooling in the late 1960s/early 1970s. This rapid permafrost thermal response is in part a reflection of the shallowness of the permafrost layer, but it is also due to the influence of high geothermal heat fluxes, which at Snæfell are around 170 mW m^2, approximately five times the values at the Scandinavian PACE borehole sites.

Conclusions

The spatial complexity of European mountain permafrost makes the representativeness of data from the small number of monitored boreholes extremely difficult to assess. The time series of borehole temperatures are mainly less than 10 yr, apart from Murtél-Corvatsch.

The addition of new boreholes provides the opportunity to sample a wider diversity of terrain and substrate character. However, prediction of permafrost distribution and response to climate change in European mountains requires further progress in physically-based numerical modeling coupled with remotely sensed data on relief, ground cover, and substrate characteristics.

PACE boreholes in Norway, Sweden, and Svalbard provide firm evidence for significant and accelerating ground warming. In addition, the importance of short-term extreme thawing events is emphasized. These have included the three-month period of sustained high temperatures during summer 2003 in the Alps, when active layers thickened significantly in bedrock sites and, in Svalbard, the anomalously warm year of 2005–6 when marked warming of permafrost occurred. Comparison of 2006 air temperatures in Svalbard with downscaled model scenarios of warming associated with enhanced greenhouse gases in the 21st century indicates that 2005–6 was well within the range predicted for the period 2071–2100, suggesting that the Svalbard archipelago may be in a critical location, with potential for particularly rapid climate change.

Given the variability of climate in the past and evidence for continued and possibly accelerated change in the future, permafrost is clearly in a transient state. More or less immediate response to extreme annual temperature variations may be anticipated in active layer thickness, while thermal profiles extending to several decimeters below the depth of zero amplitude reflect changes over many decades or centuries. Permafrost warming and basal melting are, however, likely to take several millennia, except where permafrost is thin and — as is the case in Iceland — where geothermal heat flux is unusually high.

Acknowledgments

The authors wish to thank Jeannette Noetzli, Dani Vonder Mühll, and Bernd Etzelmüller for supplying data presented in this paper.

References

Benestad, R.E., Førland, E.J. & Hanssen-Bauer, I. 2002. Empirically downscaled temperature scenarios for Svalbard, Atmosheric. *Science Letters* 3: 71–93, doi.10.1006/asle.2002.005.

Cermak, V., Safanda, J., Kresl, M., Dedecek, P. & Bodri, L. 2000. Recent climate warming: Surface air temperature series and geothermal evidence. *Studia geophysica et geodaetica* 44, 430–441.

Christensen, J.H. et al. 2007. Regional climate projections, in Climate Change 2007: The Physical Science Basis. Contribution of Working Group I to the Fourth Assessment Report of the Intergovernmental Panel on Climate Change, edited by S. Solomon et al., 849–940, Cambridge Univ. Press, New York.

Christiansen, H.H., Berthling, I., Blikra, L.H., Dehls, J., Etzelmuller, B., Farbrot, H., Humlum, O., Isaksen, K., Juliussen, H., Lauknes, T-R., Midttømme, K. & Rønning, J. 2008. Permafrost Observatory Project: A Contribution to the Thermal State of Permafrost in Norway and Svalbard, TSP NORWAY. Proceedings, *Ninth International Conference on Permafrost,* Fairbanks, Alaska, July 2008.

Etzelmüller, B., Farbrot, H., Guðmundsson, A., Humlum, O., Tveito, O.E. & Björnsson, H. 2007. The Regional Distribution of Mountain Permafrost in Iceland. *Permafrost and Periglacial Processes* 18: 185–199. DOI: 10.1002/ppp

Etzelmüller, B., Schuler, T.V., Farbrot, H. & Guðmundsson, Á. 2008. Permafrost in Iceland: Distribution. Ground Temperatures and Climate Change Impact. Proceedings, *Ninth International Conference on Permafrost,* Fairbanks Alaska, July 2008.

Farbrot, H., Etzelmüller, B., Gudmundsson, A., Schuler T.V., Eiken, T., Humlum, O. & Björnsson, H. 2007. Thermal characteristics and impact of climate change on mountain permafrost in Iceland. *Journal of Geophysical Research* 112, F03S90, doi:10.1029/2006JF000541.

Gruber, S. & Haeberli, W. 2007. Permafrost in steep bedrock slopes and its temperature-related destabilization following climate change. *Journal of Geophysical Research*, 112, F02S18, doi:10.1029/2006JF000547.

Gruber, S., Hoelzle, M. & Haeberli, W. 2004a. Permafrost thaw and destabilization of Alpine rock walls in the hot summer of 2003, *Geophysical Research Letters* 31: L13504, 4pp.

Gruber, S., Hoelzle, M. & Haeberli, W. 2004b. Rock wall temperatures in the Alps-modelling their topographic distribution and regional differences. *Permafrost and Periglacial Processes* 15(3): 299-307.

Gruber, S., King, L., Kohl, T., Herz, T., Haeberli, W. & Hoelzle, M. 2004c. Interpretation of geothermal profiles perturbed by topography: the Alpine permafrost boreholes at Stockhorn Plateau, Switzerland. *Permafrost and Periglacial Processes* 15(4): 349-357.

Harris, C., Haeberli, W., Vonder Mühll, D. & King, L. 2001. Permafrost monitoring in the high mountains of Europe: the PACE project in its global context. *Permafrost and Periglacial Processes* 12(1): 3-11.

Harris, C., Vonder Mühll D., Isaksen K., Haeberli W., Sollid J. L., King L., Holmlund P., Dramis F., Guglielmin M. & Palacios D. 2003. Warming permafrost in European mountains. *Global and Planetary Change* 39: 215-225.

Harris, C., Arenson, L.U., Christiansen, H.H., Etzelmüller, B., Frauenfelder, R., Gruber, S., Haeberli, W., Hauck, C, Hölzle, M., Humlum, O., Isaksen, K, Kääb, A., Lehning, M., Lütschg, M.A., Matsuoka, N., Murton, J.B., Nötzli, J., Phillips, M., Ross, N., Seppälä, M., Springman, S.M. & Vonder Mühll, D. Submitted. Permafrost and climate in Europe: geomorphological impacts, hazard assessment and geotechnical response Earth Science Reviews.

Hoelzle, M., Mittaz, C., Etzelmüller, B. & Haeberli, W. 2001. Surface energy fluxes and distribution models of permafrost in European mountain areas: an overview of current developments. *Permafrost and Periglacial Processes* 12(1): 53-68.

Hoelzle, M., Vonder Mühll, D. & Haeberli, W. 2002. Thirty years of permafrost research in the Corvatsch-Furtschellas area, Eastern Swiss Alps: a review. *Norwegian Journal of Geography* 56(2): 137-145.

Isaksen, K., Holmlund, P., Sollid, J.L & Harris, C. 2001. Three deep alpine-permafrost boreholes in Svalbard and Scandinavia. *Permafrost and Periglacial Processes* 12: 13-25.

Isaksen, K., Sollid, J.L., Holmlund, P. & Harris, C. 2007a. Recent warming of mountain permafrost in Svalbard and Scandinavia. *Journal of Geophysical Research* 112, F02S04, doi:10.1029/2006JF000522.

Isaksen, K., Benestad, R.E., Harris, C. & Sollid, J.L. 2007b. Recent extreme near-surface permafrost temperatures on Svalbard in relation to future climate scenarios Geophysical Research Letters, 34, L17502, doi:10.1029/2007GL031002, 2007.

Lachenbruch, A.H. & Marshall, B.V. 1986. Changing climate: Geothermal evidence from permafrost in the Alaskan Arctic. *Science* 234: 689-696.

Noetzli, J., Hoelzle, M. & Haeberli, W. 2003. Mountain permafrost and recent Alpine rock-fall events: a GIS-based approach to determine critical factors.

Noetzli, J., Gruber, S., Kohl, T., Salzmann, N. & Haeberli, W. 2007. Three-dimensional distribution and evolution of permafrost temperatures in idealized high-mountain topography. *Journal of Geophysical Research* 112,: F02S13, doi:10.1029/2006JF000545.

Osterkamp, T.E. & Romanovsky V.E. 1999. Evidence for Warming and Thawing of Discontinuous Permafrost in Alaska. *Permafrost and Periglacial Processes* 10: 17–37.

Serreze, M.C., Holland, M.M. & Stroeve, J. 2007. Perspectives on the Arctic's shrinking sea-ice cover,. *Science* 315: 1533, doi:10.1126/ science.1139426.

Stroeve, J., Holland, M.M., Meier, W., Scambos, T. & Serreze, M.C. 2007. Arctic sea ice decline: Faster than forecast. *Geophysical Research Letters* 34: L09501, doi:10.1029/2007GL029703.

Tveito, O. E. et al. 2000. Nordic temperature maps, report, 28 pp., Norwegian Meteorological Institute, Oslo.

Vonder Mühll, D. & Haeberli, W. 1990. Thermal characteristics of the permafrost within an active rock glacier (Murtèl/Corvatsch, Grisons, Swiss Alps). *Journal of Glaciology* 36(123): 151-158.

Vonder Mühll, D., Noetzli, J., Makowski, K. & Delaloye, R. 2004. Permafrost in Switzerland 2000/2001 and 2001/2002, Glaciological Report (Permafrost) No. 2/3 of the Glaciological Commission (GC) of the Swiss Academy of Sciences (SAS) and Department of Geography, University of Zurich, 86 p.

Vonder Mühll, D., Noetzli, J., Makowski, K. & Delaloye, R. 2007. Permafrost in Switzerland 200/2003 and 2003/2004, Glaciological Report (Permafrost) No. 4/5 of the Glaciological Commission (GC) of the Swiss Academy of Sciences (SAS) and the Department of Geography, University of Zurich.

Vonder Mühll, D., Stucki, T. & Haeberli, W. 1998. Borehole temperatures in Alpine permafrost: a ten years series, in Proceedings Seventh International Conference on Permafrost, Yellowknife, Canada, 23-27 June 1998, edited by A.G. Lewkowicz, and M. Allard, pp. 1089–1095, Centre d'Etudes Nordiques, Universite Laval, Collection Nordicana 57.

Full-Scale Physical Modeling of Solifluction Processes Associated with One-Sided and Two-Sided Active Layer Freezing

Charles Harris
School of Earth, Ocean and Planetary Sciences, Cardiff University, Cardiff CF10 3YE,UK
Martina Kern-Luetschg
School of Earth, Ocean and Planetary Sciences, Cardiff University, Cardiff CF10 3YE,UK
Julian Murton
University of Sussex, Dep tment of Geography, Brighton, BN1 9SJ, UK
Marianne Font
UMR CNRS 6143 M2C and University of Caen, Rue des Tilleuls, Caen, 14 032, France
Michael Davies
Faculty of Engineering, University of Auckland, Auckland 1142, New Zealand
Fraser Smith
School of Engineering, University of Dundee, Dundee, DD1 4HN, UK

Abstract

In this paper we present data from one typical cycle of freezing and thawing, derived from a 17-cycle full-scale experiment to simulate solifluction processes associated with two-sided active layer freezing and one-sided seasonal ground freezing. Two adjacent 12° slope models, each 5 m long, 1.5 m wide , and 35 cm thick were constructed using the same silt-rich natural soil. In the one-sided freezing model, the slope was formed above a sand substrate in an open hydraulic system, and the slope thawed completely between freezing cycles. The second model was constructed on a refrigerated plate that maintained permafrost in the lowermost 5 cm of soil and promoted bottom-upward soil freezing in addition to the top-down freezing induced by air temperature cycles. In the two-sided freezing model, downward moisture migration during the thaw period resulted in ice segregation immediately above and within the permafrost table. In the seasonally frozen slope model, ice segregation was greatest in the near-surface zones and decreased with depth. This contrasting distribution of soil ice caused marked differences in patterns of heave, thaw settlement, timing and style of downslope soil movement.

Keywords: one-sided freezing; physical modeling; solifluction; two-sided freezing.

Introduction

Here we present preliminary results from a three-year full-scale simulation experiment designed to investigate the influence of the distribution of segregation ice on the style and timing of periglacial solifluction (gelifluction and frost creep). These experiments form part of a larger program in which physical modeling coupled with field monitoring will provide detailed validation and calibration data for numerical modeling of solifluction processes (see also Kern-Luetschg et al. 2008).

Although the literature on periglacial solifluction is extensive, it is largely focused on areas with seasonally frozen ground or warm permafrost, where freezing takes place from the surface downwards. Field measurements (e.g., Washburn 1967, Benedict 1981, Smith 1988, Kinnard & Lewkowicz 2005, Jaesch et al. 2003) and laboratory simulations (Coutard et al. 1988, Harris et al. 1995, 1997) have shown that in seasonally frozen frost-susceptible soils, winter frost heave is followed by solifluction movements during summer thaw consolidation. Ice contents often decrease with depth, as do rates of soil movement. In cold permafrost regions, two-sided active layer freezing is observed, with freezing from the bottom upwards and the top downwards (Mackay 1981, Cheng 1983, Lewkowicz & Clark 1998, Schur 1988, Shiklomanov & Nelson 2007), and this commonly leads to a zone of ice segregation at the base of the active layer and top of the permafrost, termed the "transient layer" by Schur et al. (2005).

In Garry Island, Canada, Mackay (1981) described late summer plug-like solifluction, associated with displacement over the ice-rich zone at the base of the active layer. He showed that ice within this basal zone forms by early winter upward advance of a freezing front from the permafrost table, augmented by ice lensing in late summer as water migrates downward across the thaw front and into still-frozen basal active layer and upper permafrost. Similar observations of slow, annual downslope active layer movement over a deforming basal zone are reported by Lewkowicz & Clark (1998) and Matsuoka & Hirakawa (2000). Thaw consolidation may reduce the unfrozen thickness of this basal deforming zone, and resulting shear strains, accumulated over many annual freeze-thaw cycles, have been implicated in the reduction of local soil shear strength over time, promoting active layer detachment slides during anomalously warm summers (Harris & Lewkowicz 2000).

Table 1. Average test soil properties. *PL* is Plastic Limit, *LL* is Liquid Limit, c_v is coefficient of consolidation, and *k* is permeability.

% clay	% silt	% sand	PL %	LL %	ø degrees	c_v m^2/yr	k m/sec
25	65	10	22	33	26	18.4	4.4×10^{-8}

An early experiment to investigate the significance of ice distribution within the thawing active layer was reported by Rein & Burrous (1980), who used a tilting box containing a 25 cm thick layer of frost susceptible silt-loam. Two experiments were conducted, first with high ice contents in the mid profile, second with high ice contents at the base. Thaw consolidation and solifluction were shown to be concentrated within these ice-rich layers, with little shear strain occurring elsewhere in the profile. In the present paper we seek to test the hypothesis that similar processes of soil shear strain occur close to the surface in seasonally frozen ice-rich soil and at the base of the active layer in permafrost regions where two-sided freezing is associated with an ice-rich basal layer.

Experimental Design

Two identical 12° slope models were constructed adjacent to each other within a 5 m square freezing chamber, using the same frost susceptible soil (Fig. 1). Models were 5 m long, 1.5 m wide, and 35 cm thick. Soil properties are similar to those of many solifluction soils reported in the literature (see, for instance, the review by Harris, 1982) and are summarized in Table 1. Air temperatures were lowered to between -8°C and -12°C to simulate winter freezing, and were subsequently raised to between +15°C and +20°C to simulate the summer thaw period.

The two-sided freezing model was constructed above a refrigerated plate that maintained a 5-–6 cm thick permanently frozen layer (permafrost) at the base of the model, with basal temperatures around -2.5°C during simulated summer conditions. Freezing was from the bottom upwards and the top-down (two-sided) during simulated winter cycles. Since the maximum thaw depth was only around 30 cm, active layer thickness was much less than in most field situations. When the active layer had reached its full thickness, water was added at the surface via a fine spray. Downward moisture migration led to basal ice segregation, simulating summer frost heave (e.g., Mackay 1983) and increasing the basal ice content. The one-sided freezing slope model was formed above a sand substrate in an open hydraulic system (basal water supply). Moisture contents prior to initiation of winter freezing averaged around 25% by weight in the two-sided freezing model, but were slightly higher in the one-sided model.

In this paper we present results of one freeze-thaw cycle from the final sequence of 8 cycles and contrast the soil response in the two-sided model with that in the one-sided model.

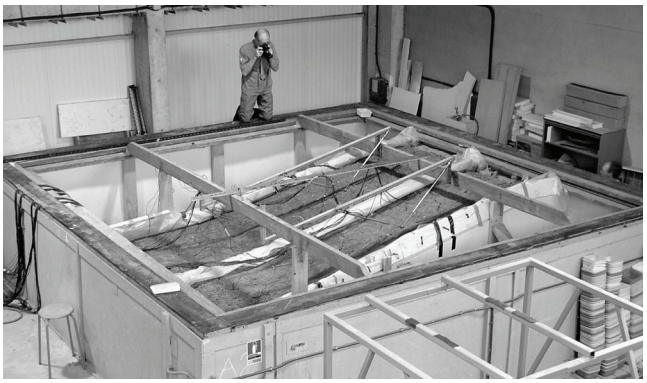

Figure 1. Two parallel slope models, far side, two-sided freezing model, near side, one-sided freezing model. Cross beams support pairs of LVDTs which form fixed base triangles, the apex of which is attached to a Perspex footplate embedded in the soil surface.

Instrumentation

Data were collected at half-hourly intervals via a PC-based data logging system. Instrumentation was similar to that used in earlier experiments (see Harris et al. 1997). Temperatures were measured using an array of stainless steel thermistor probes measuring to within ±0.38°C, (supplied by Campbell Scientific Ltd.) located at the surface and depths of 0 cm, 5 cm, 15 cm, 25 cm, and 35 cm in the central zone of each slope model. Pore water pressure monitoring used Druck PDCR 81 miniature pore pressure transducers consisting of stainless steel cylinders of diameter 6 mm and length 12 mm with a porous stone tip. Transducers were filled with low viscosity silicon oil and had a range of 350 mb, combined non-linearity and hysterics of ±0.2%, and thermal sensitivity of 0.2% of reading per °C. Pore pressure data are not included here but will be fully discussed in later papers.

Soil surface motion was recorded using pairs of longstroke (300 mm) captive guided armature linear variable differential transformers (LVDTs) with spherical
end bearings supplied by RDP Electronics Ltd, UK. Pairs of LVDTs formed a fixed base triangle mounted on a slotted track parallel to the slope above each model, supported by a beam (Fig. 1). Both LVDTs were connected to an 8 cm square Perspex footplate embedded in the soil surface, forming the apex of the triangle. Frost heave, thaw consolidation, and downslope displacements of the soil surface were registered by changes in LVDT length and were resolved as orthogonal vectors perpendicular and parallel to the soil surface. Soil displacement profiles were observed through re-excavation of Rudberg columns.

Results

Soil temperatures

Typical responses of both slope models to cyclic freezing and thawing are illustrated below by reference to Cycle 16, between 20 April and 7 June 2007. For convenience, all soil depths are given here for the equivalent unfrozen soil. When frozen, soil depths increase as a result of frost heave, but this varies from one cycle to another. Contrasting thermal

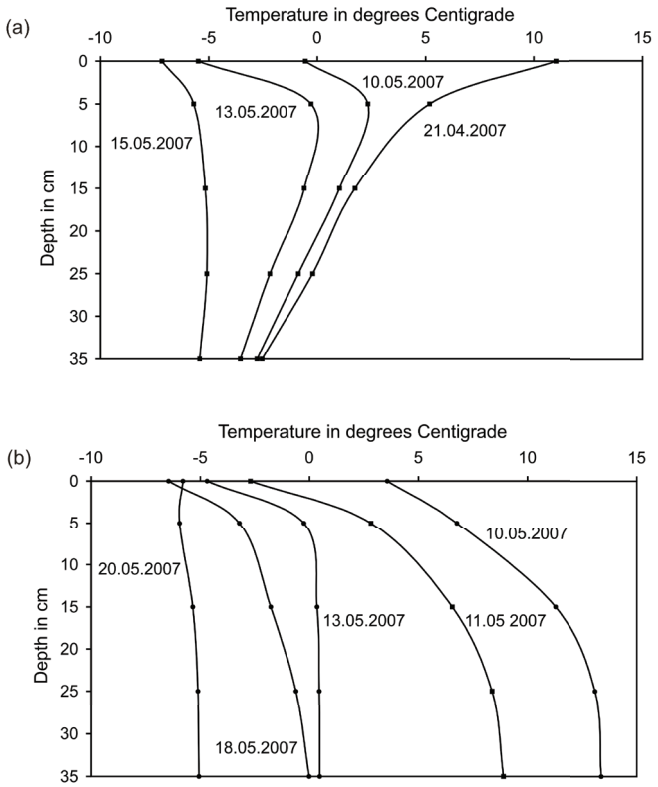

Figure 2. Thermal profiles during freezing. (a) two-sided freezing model, (b) one-sided freezing model.

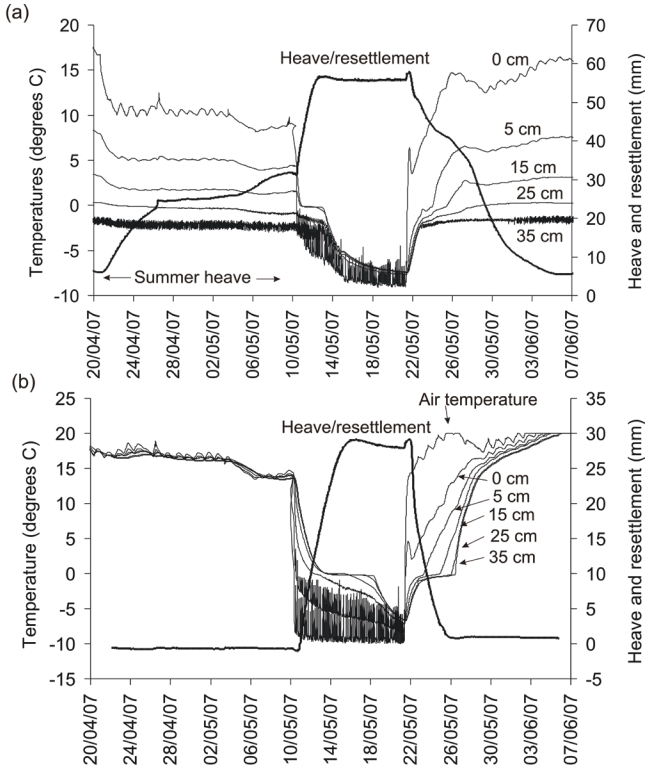

Figure 3. Frost heave followed by thaw settlement (heavy line) shown with soil temperatures through each model. (a) Two-sided freezing experiment. (b) One-sided freezing experiment.

regimes were observed during the freezing phase, reflecting the presence of permafrost in the two-sided freezing model, but its absence in the one-sided model (Figs. 2a, b). The basal temperature in the two-sided (permafrost) model was maintained at around -2.5°C, and active layer thickness was around 26 cm until air temperatures were lowered to approximately -10°C on May 10th. Winter freezing occurred over the next three days, with freezing fronts advancing from the permafrost table upwards and from the surface downwards. In the one-sided model downward freezing from the surface was initiated by the fall in air temperatures on May 10th and lasted some 5 days.

Frost heave and thaw settlement

A fall in surface temperatures of around 6°C on April 20, 2007, coupled with the addition of 5 litres of water sprayed across the entire surface, initiated the first phase of basal freezing in the two-sided freezing model and 18 mm of "summer heave" was recorded by April 26th (Fig. 3a). Further surface cooling on May 3rd, and the addition of 5 liters of water caused a second phase of ice segregation at the base of the active layer with an additional 6 mm of summer heave. Finally, the phase of two-sided freezing from May 10th–13th was associated with approximately 25 mm of frost heaving.

Surface downward frost penetration in the one-sided model, initiated on May 10th, led to a uniform rate of heaving with approximately 28 mm of surface frost heave recorded by May 16th (Fig. 3b) after which heave virtually ceased. The freezing front had penetrated to an unfrozen depth of between 15–20 cm by May 16th, so that little heave occurred during freezing of the lower 15 cm of the model. This was due to closure by freezing of the basal water supply tubes at the top of the model.

Thawing in both models was initiated by raising air temperatures to around 20°C on May 20, 2007. In the two-sided model the rate of thaw penetration increased through the uppermost 5 cm, was at a maximum between 5 and 15 cm depth, and then progressively decreased (Fig. 4a). Average thaw penetration rates are shown in Table 2. In the one-sided model, thaw penetration accelerated through the thaw period (Fig. 4b, Table 2) and was complete some 12 days before the maximum thaw depth was reached in the two-sided model.

By coupling the rate of thaw penetration with the rates of surface thaw settlement, and assuming that surface settlement during a given period was due to consolidation of the layer that thawed in that period, we were able to reconstruct ice contents within the thawing models (Table 2). Average heaving ratios (HR defined as frost heave divided by frozen thickness) were calculated from the amount of settlement recorded over a given soil depth range, divided by the frozen thickness. In the two-sided model, ice content was lowest within an ice-poor zone between unfrozen depths of 5 cm and 15 cm (HR 0.03), and highest in the basal zone between unfrozen depths of 25 cm and 26 cm (HR 0.66). In contrast, segregation ice was concentrated between 0 cm and 5 cm unfrozen depths in the one-sided freezing model, where the average heaving ratio was 0.25, and decreased to virtually zero in the lowermost 10 cm of the model.

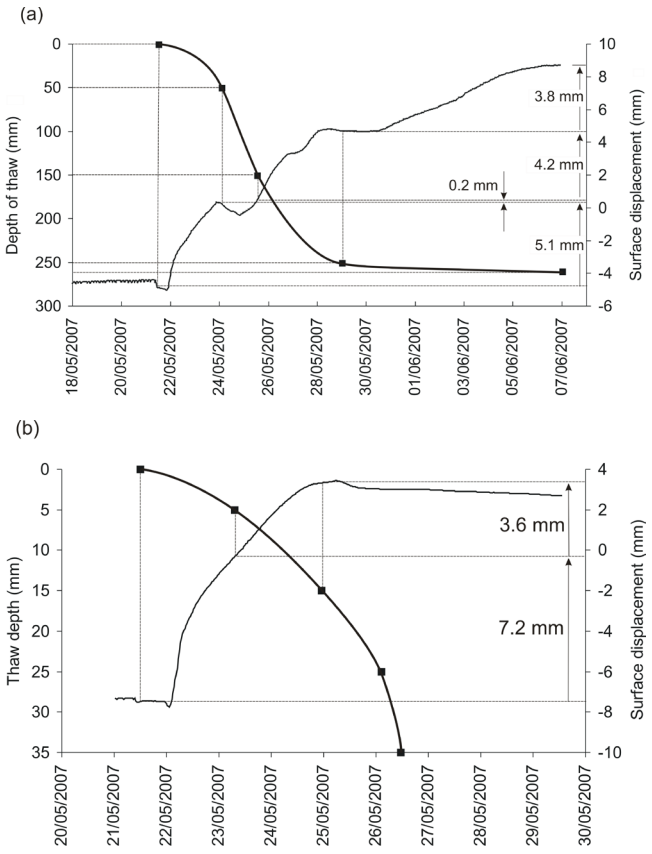

Figure 4. Rate of thaw penetration (heavy line) and measured surface downslope displacements. (a) Two-sided freezing model. (b) One-sided freezing model.

Downslope soil displacement

The distribution of soil shear strain within each model was assessed for the single thaw phase described here by attributing measured surface downslope surface displacement over a given time period to shear strain within the layer of soil that thawed over the same time period. In Figure 4(a) and (b), downslope surface displacement is plotted on a common time axis with the penetration of the thaw front. In the two-sided model, thawing of the upper 5 cm unfrozen thickness of soil was associated with some 5.1 mm downslope displacement, but thawing of the ice-poor region between 5 cm and 15 cm unfrozen depth caused virtually no net downslope movement, the recorded displacements probably reflecting changes in moisture status of the already thawed soil layer. As the thaw front penetrated to below 15 cm unfrozen depth, surface movement was again recorded, continuing over the prolonged period when the very ice-rich zone between 25 cm and 26 cm (unfrozen depths) thawed. In contrast, surface displacement in the one-sided model occurred only as the uppermost 15 cm of the model thawed, with displacement of 7.2 mm during thaw of the upper 5 cm, and 3.6 mm during thaw between 5 cm and 15 cm unfrozen depths.

Synthetic displacement profiles were generated for each model on the basis that the measured surface movements were attributed to the corresponding thawing soil layer. For

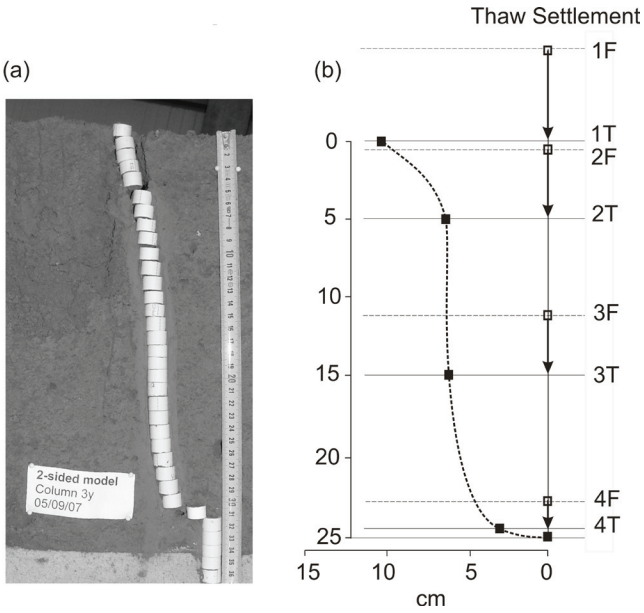

Figure 5. Soil displacement profiles, two-sided freezing model. (a) observed displacement profile after 8 cycles of freezing and thawing. (b) synthetic model derived from thaw penetration and displacement data (Figure 4[a]). Labels show levels of layer boundaries (surface, 5 cm, 15 cm, 25 cm and 26 cm) in frozen (1–4F) and thawed (1–4T) states.

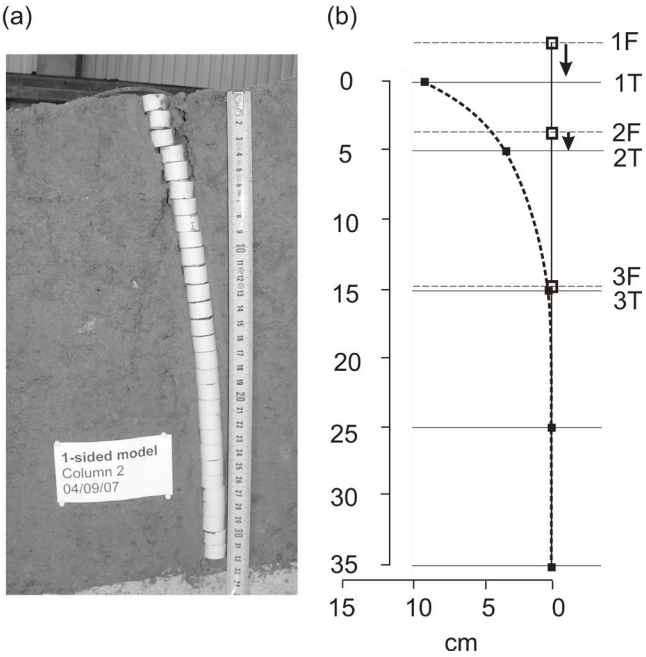

Figure 6. Soil displacement profiles one-sided freezing model. (a) observed displacement profile after 8 cycles of freezing and thawing. (b) synthetic model derived from thaw penetration and displacement data (Figure 4[a]). Labels show levels of layer boundaries (surface, 5 cm, 15 cm, 25 cm and 26 cm) in frozen (1–4F) and thawed (1–4T) states.

clarity, displacements are multiplied by 8, to give the synthetic profiles that would arise following eight identical cycles of freezing and thawing in each model. These are compared with observed displacement profiles from excavated Rudberg Columns following the last eight freeze-thaw cycles of the

Table 2. Details of model freezing and thawing.

Model	Unfrozen depth mm	Unfrozen thickness mm	Frozen thickness mm	Thaw settlement mm	Heaving Ratio	Time to thaw hr	Thaw rate mm/hr
Two-sided	0						
	50	50	62.85	12.85	0.20	38	1.65
	150	100	102.65	2.65	0.03	35	2.93
	250	100	115.59	15.59	0.13	83	1.39
	260	10	29.85	19.85	0.66	240	0.12
One sided	0						
	50	50	66.48	16.48	0.25	43.5	1.53
	150	100	109.23	9.23	0.08	39.5	2.77
	250	100	101.99	1.99	0.02	27.5	3.71
	350	100	100.03	0.03	0.0003	9	11.11

modeling program (Figs. 5, 6). Clear similarities are revealed between synthetic profiles and observed profiles.

Discussion and Conclusions

The thaw consolidation theory of Morgenstern & Nixon (1971) and Nixon & Morgenstern (1973) provides a theoretical basis for prediction of pore water pressures induced during thawing of ice-rich soils, and in our experiments, maximum shear strains were observed within the ice-rich layers where thaw consolidation was greatest. However, since the rate of thaw penetration was governed largely by soil ice contents (which determined latent heat required for phase change), thaw consolidation ratios (R) were actually highest where ice contents were least and thaw penetration fastest (central active layer zone, two-sided freezing experiment, $R = 0.37$ and basal zone, one-sided experiment, $R = 0.26$). Conversely, the slower thaw penetration in the ice-rich layers in both models resulted in the release of more meltwater and induced more soil deformation, but was reflected in lower thaw consolidation ratios.

Although the model of two-sided active-layer freezing did not strictly represent the annual cycle of the lower thermal boundary, we were able to successfully simulate segregation ice distributions. The distribution of segregation ice within the two-sided freezing model was similar to field observations in natural permafrost active layers. For instance, Mackay (1981, Fig. 15, p. 1674) clearly illustrated a desiccated central zone within the active layer in Garry Island very similar to that observed here. In addition, continuous monitoring of a permafrost slope in Svalbard during 2005–2006 (Harris et al. 2006) has also demonstrated an ice-poor zone in the central part of the active layer, with very little thaw settlement or downslope movement being recorded as this layer thawed. As in the experimental results discussed here, the majority of movement at the Svalbard field site occurred during thaw of the ice-rich basal zone. Progressive soil freezing from the surface down and from the permafrost table upwards forms a closed hydraulic system within the central zone of the active layer, both in the field and in our model. Water migration towards the respective freezing fronts reduces moisture contents in the central zone, and pore water suction increases effective stress and hence unfrozen shear strength.

In this paper we have presented initial results from one freeze-thaw cycle in a series of 17 such cycles undertaken during a three-year laboratory simulation of solifluction processes. More detailed papers are in preparation in which data from all cycles will be considered and recorded pore water pressures discussed. The initial hypothesis was that solifluction-induced shear strain results from thaw consolidation of ice-rich soil, and that the distribution of segregation ice within a frozen profile largely determines where greatest thaw strain will occur. Continuous monitoring of heave, settlement, and surface displacement of identical slope models subjected to contrasting thermal regimes has provided compelling evidence, supporting the initial hypothesis and confirming that thawing of the basal ice-rich zone within the permafrost model generated basal shearing and "plug-like flow" similar in character to field observations.

Acknowledgments

This research was funded by the British Natural Environment Research Council (Grant NER/B/S/2003/00748). Laboratory assistance from Gerard Guillemet and Anthony Dubois is gratefully acknowledged.

References

Benedict, J.B. 1970. Downslope soil movement in a Colorado alpine region: rates, processes, and climatic significance. *Arctic and Alpine Research* 2: 165-226.

Cheng, G. 1983. The mechanism of repeated segregation for the formation of thick-layered ground ice. *Cold Regions Science and Technology* 8: 57–66.

Coutard, J-P., Van Vliet- Lanoe, B. & Auzet, A.V. 1988. Frost heaving and frost creep on an experimental slope: results for soil structures and sorted stripes. *Zeitschrift für Geomorphologie, Supplementband* 71: 13-23.

Harris, C. 1981. *Periglacial Mass Wasting: A Review of Research.* BGRG Research Monograph. Norwich: Geo Books. 204 pp.

Harris, C., Davies, M.C.R. & Coutard, J.-P. 1997. Rates and processes of periglacial solifluction: an experimental approach. *Earth Surface Processes and Landforms* 22: 849-868.

Harris, C. & Lewkowicz, A.G. 2000. An analysis of the stability of thawing slopes, Ellesmere Island, Nunavut, Canada. *Canadian Geotechnical Journal*, 37: 465-478.

Harris, C., Luetschg, M., Murton, J.B., Smith, F.W., Davies, M.C.R., Christiansen, H.H. & Ertlen-Font, M. 2006. Solifluction processes in arctic permafrost: results of laboratory and field experiments, *EOS Transactions AGU* 87(52), Fall Meeting Supplement, Abstract C43A-03.

Kern-Luetschg, M.A., Harris, C., Cleall, P., Li, Y. & Thomas, H. 2008. Scaled centrifuge modeling of solifluction in permafrost and seasonally frozen soils. *Proceedings of the Ninth International Conference on Permafrost, Fairbanks, Alaska, June 29–July 3, 2008* (this proceedings).

Kinnard, C. & Lewkowicz, A.G. 2006. Frontal advance of turf-banked solifluction lobes, Kluane Range, Yukon Territory, Canada. *Geomorphology* 73: 261-276.

Lewkowicz, A.G. & Clark, S. 1998. Late summer solifluction and active-layer depths, Fosheim Peninsula, Ellesmere Island, Canada. In: A.G. Lewkowicz & M. Allard (eds.), *Proceedings of the Sixth International Conference on Permafrost, Yellowknife, Canada*. Centre d'Etude Nordiques, Université Laval, Sainte-Foy: 641-666.

Mackay, J.R. 1980. The origin of hummocks, western Arctic coast, Canada. *Canadian Journal of Earth Sciences* 17: 996-1006.

Mackay, J.R. 1981. Active layer slope movement in a continuous permafrost environment, Garry Island, Northwest Territories, Canada. *Canadian Journal of Earth Sciences* 18: 1666-1680.

Mackay, J.R. 1983. Downward water movement into frozen ground, western arctic coast, Canada. *Canadian Journal of Earth Sciences* 20: 120-134.

Matsuoka, N. & Hirakawa, K. 2000. Solifluction resulting from one-sided and two-sided freezing: field data from Svalbard. *Polar Geoscience* 13: 187-201.

Matsuoka, N. 2001. Solifluction rates, processes and landforms: a global review. *Earth-Science Reviews* 55: 107-133.

McRoberts, E.C. & Morgenstern, N.R. 1974. The stability of thawing slopes. *Canadian Geotechnical Journal* 11: 447-469.

Morgenstern, N.R. & Nixon, J.F. 1971. One-dimensional consolidation of thawing soils. *Canadian Geotechnical Journal* 8: 558-565.

Rein, R.G. & Burrous, C.M. 1980. Laboratory measurements of subsurface displacement during thaw of low-angle slopes of frost-susceptible soil. *Arctic and Alpine Research* 12: 349-358.

Schur, Y.I. 1988. The upper horizon of permafrost soils. *Proceedings of the Fifth International Conference on Permafrost,.(e Tapir, Trondheim*,: 867-871.

Schur, Y.I., Hinkel, K.M. & Nelson, F.E. 2005. The transient layer: implications for geocryology and climate change science. *Permafrost and Periglacial Processes* 16: 5-17.

Shiklomanov, N.I. & Nelson, F. 2007. Active layer processes. In.: S.A. Elias (ed.), *Encyclopedia of Quaternary Science* Vol. 3, Elsevier, Oxford, 2138-2146

Smith, D.J. 1988. Rates and controls of soil movement on a solifluction slope in the Mt. Rae area, Canadian Rocky Mountains, *Zeitschrift für Geomorphologie, Supplementband* 71: 25-44.

Washburn, A.L. 1967. Instrumental observations of mass-wasting in the Mesters Vig district, Northeast Greenland. *Meddelelser om Grønland* 166: 318 pp.

Wireless Sensor Networks in Permafrost Research: Concept, Requirements, Implementation, and Challenges

Andreas Hasler
Glaciology, Geomorphodynamics, Geochronology; Geography Department, University of Zurich, Switzerland
Igor Talzi
Computer Science Department, University of Basel, Switzerland
Jan Beutel
Computer Engineering and Networks Laboratory, ETH Zurich, Switzerland
Christian Tschudin
Computer Science Department, University of Basel, Switzerland
Stephan Gruber
Glaciology, Geomorphodynamics, Geochronology; Geography Department, University of Zurich, Switzerland

Abstract

In a joint project of computer- and geo-scientists, wireless sensor networks (WSNs) are customized for permafrost monitoring in alpine areas. In this paper, we discuss requirements for a rugged setup of such a network that is adapted to operation in a difficult environment. The experiences with a first deployment at Jungfraujoch (Switzerland) show that, beside hardware modifications of existing WSN platforms, special emphasis should be given to the development of robust synchronization and low-power data routing algorithms. This results from the fact that standard software tools are not capable in dealing with the high-temperature fluctuations found in high-mountains without compromising the power consumption and the network topology. Enhancements resulted in a second deployment at Matterhorn (Switzerland), from where we expect results in the near future. Once the technology of WSNs is a science-grade instrument, it will be a powerful tool to gather spatial permafrost data in near real-time.

Keywords: measurement; permafrost; PermaSense project; wireless sensor networks.

Introduction

Spatially distributed measurements of permafrost parameters over long periods are time consuming in deployment and maintenance, vulnerable to environmental impacts, and create inhomogeneous data sets, as no standard and easy applicable measurement devices exist. The project *PermaSense* addresses the development of a new generation of monitoring equipment for remote and harsh environments (Fig. 1). In this paper, we present the design and implementation of a wireless sensor network (WSN) to measure temperatures, dilatation, and diverse hydrological parameters in rock faces of alpine permafrost.

A WSN generally consists of distributed *network nodes* with attached sensors that communicate by local UHF radio within each other and that are up-linked by one (or several) *base stations* via mobile communication (e.g., UMTS, GPRS), internet, or other data transfer systems to a *data sink server* (Fig. 2). Each node contains a microprocessor, a radio transceiver, a sensor interface, some local memory, and an independent power supply. The network topology depends on the radio connectivity between the nodes. If data is transmitted via intermediate network nodes to the base station, this is called *multi-hop,* while a pure star-topology around the base station is called a *single-hop* network. Compared to existing logging systems using single radio-connected measurement devices, WSNs are designed to adapt their network topology dynamically according to the connectivity constraints, allowing observation of a larger area with multi-hop connection. While the dataflow is generally out of the network through the base station into the data sink, commands, network parameters or even executable programs can potentially be pushed into the network.

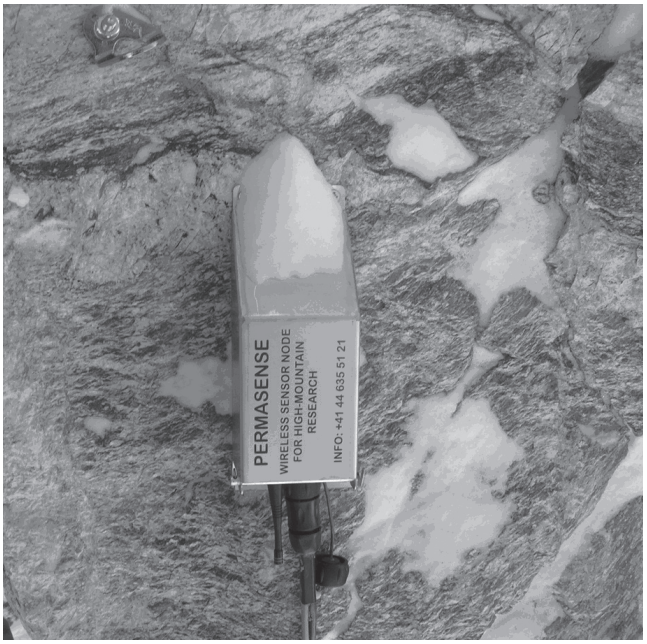

Figure 1. Network node at the field site Matterhorn – Hörnligrat.

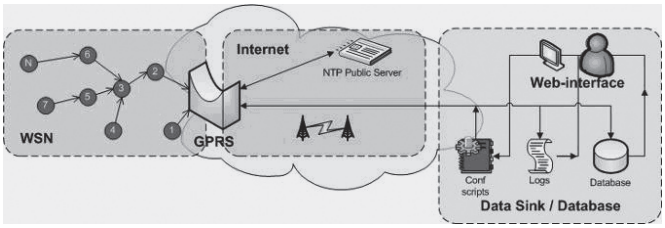

Figure 2. Framework of a WSN as used in our field deployments and test bed.

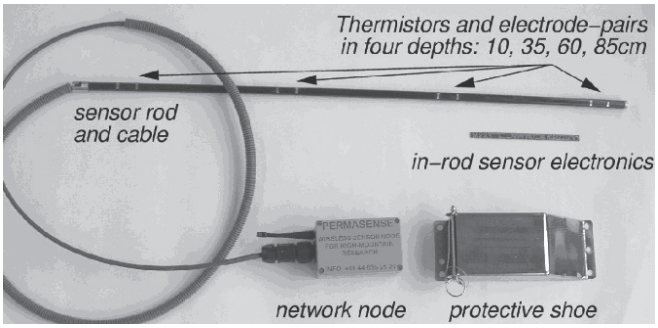

Figure 3. First-generation network node and customized sensor rod that measures temperatures and DC-resistivity as an indicator of liquid pore water at four different depths; the electronics and battery (lithium-thionyl) of the network node are mounted in a waterproof aluminum housing (125x80x57 mm) and protected from icefall and rockfall with a steel protective shoe. Measurement electronics are in the tip of the sensor rod to minimize temperature fluctuation errors.

Based on experiences with our first deployment on Jungfraujoch (3500 m a.s.l., Swiss Alps) during winter and spring 2006/2007, we specify requirements for yearlong stand-alone monitoring. WSN concepts and requirements for environmental use, and challenges for the implementation as well as the experiences from a second deployment generation are presented and discussed in this article.

Application of WSNs for Permafrost Research

Environmental WSNs

Environmental applications of WSNs have emerged in the past years following the general developments in mobile communication (Hart & Martinez 2006). Depending on the monitored variables and processes, the sensor networks differ in node size (e.g., from weather station to the futuristic "smart dust") as well as in spatial and functional extent of the network. In permafrost process research we are mainly interested in so-called localized multifunctional sensor networks. These systems are able to measure multiple parameters within an area of special interest. Despite the fast progress in the field of WSNs, only a limited number of application projects exists so far. The Projects *Glacsweb* (Martinez et al. 2004), *SensorScope* (http://sensorscope.epfl.ch/index.php), or the *Volcano monitoring project* (Werner-Allen et al. 2006) are such examples. A larger overview of existing environmental sensor network projects is given by Hart & Martinez (2006).

Potential of WSNs

For permafrost research and other remote environmental applications of WSNs, we identify the following potential:

- Once installed, maintenance and data acquisition is less time-consuming with WSNs than with standard logging systems, particularly at difficult accessible locations. The nodes inform the operator about battery level and functioning.
- Data is available all year-round at near real-time on a user interface. This is not only relevant for research, but can be very valuable for hazard monitoring.
- The data can be stored with redundancy, and not only locally on the logger. In case of destruction or loss of a sensor node, the data measured until this event is saved.
- Measurements are synchronous and arrive at one central database. No extensive manual post-processing and homogenization of the data is needed.
- Interval and mode of measurements do not require being statically predefined. They can be controlled by remote commands from the user interface or can be context-sensitive to other measurements of the network.

The project PermaSense

Wireless sensor networks have not yet been established for reliable, yearlong operation under cold climate and high alpine conditions. In PermaSense, computer- and geo-scientists upgrade in close cooperation the WSN platform *TinyNode* for permafrost research. Software for power-efficient operation of an adaptive multi-hop network topology is currently under development and being tested. Robust and reliable deployment hardware was designed, sensor interface hardware was developed, and software integration of sensors is being implemented. Customized sensors were manufactured, and compatible commercial sensors were evaluated and connected (Fig. 3). A detailed description of the network software of our first deployment, based on TinyOS, is given by Talzi et al. (2007).

Requirements for a permafrost WSN

Similar to standard logging systems for permafrost purposes, a WSN requires the following main features: Stable operation over a wide temperature range from -40°C to 40°C during at least one year or season, respectively (battery capacity). For analog measurements, a 12-bit analog-digital conversion (ADC) is generally sufficient, as the resulting resolution for temperature measurements over the indicated range is 0.02°C (a corresponding measurement accuracy can be reached with a zero-point calibration around 0°C). If pressure sensors are applied, a vibration wire (VW) compatible ADC, or frequency counter is of use. One or several digital interfaces (RS 232, RS 485, or SDI-12) for commercial sensors, allows the integration of diverse sensor types into the network. For power-intensive measurements (e.g., ERT), an incoming power supply line or solar panel control should be considered. All incoming and outgoing lines of this sensor interface should be lightning protected if the system operates at exposed locations.

As permafrost parameters typically change with slow rates, a temporal resolution of the measurements of some minutes to hours is required. Rarely, continuous measurements are needed (e.g., acceleration sensors), which is not further considered in this article. The mechanical setup should correspond to the operating conditions (e.g., Fig. 3).

WSN-specific requirements:

- The scale of the spatial extent ranges from decameters up to several hundred meters (depending on WSN limitations). To provide connectivity in complex alpine topography, a *multi-hop* system is preferable.
- Network topology is established automatically. A predefined topology is not applicable in practice and cannot adapt itself to a temporal lack of connection caused by snow cover, for example, of the devices.
- Connectivity through snow and ice is better with lower radio frequencies (<1GHz).
- Ultra low-power operation is supported. Sleeping cycles of the radio receiver, and consequently synchronization of the wake periods, are required.
- The measurements of different nodes are taken synchronically (in most cases, an accuracy of seconds is sufficient) and time-stamped.
- Nodes with no connectivity to neighbors store measured data locally on the node (capacity: 6 months).
- Data transmission capacity considers payload of the measured data with some margins to catch up data transmission from temporally invisible nodes. Generally, measured data does not exceed 2 kB per day.
- A *deployment mode* allows checking radio interconnectivity within the network during installation.
- A small form factor of the network node and a pluggable sensor interface ease the logistic effort for system maintenance.
- System health parameters (battery level, node temperature) inform the operator about network conditions and optimize the time of battery change.
- Command propagation into the network or context sensitivity allows to monitor periods of special interest in high resolution and to save power during less interesting periods.
- Data is stored in a database that provides metadata and has a safe backup strategy.
- A user interface supports the network maintenance (see above) and the database management.

Field Deployments

Energy balance models to estimate permafrost distribution and condition have recently been applied successfully to high-mountain topography (Gruber et al. 2004). Especially for steep and compact rock faces with little snow cover, modeling results correspond well with surface temperature measurements. Also mean annual subsurface temperature distribution and permafrost bodies are simulated satisfyingly with a 3D heat-conduction model (Noetzli et al. 2008). However, in such models processes of nonconductive heat transport are not considered despite their relevance for thawing depth and rate along fractures in the bedrock. The aim of our measurement site at Jungfraujoch is to quantify the spatial variability of thawing processes and heat transport in the near-surface layer.

First deployment: Jungfraujoch, winter 2006/2007

The influence of surface characteristics, fracturing, and meltwater availability is measured by eight of the above described sensor rods in gently steep (40°–70°) and fractured rock faces (general case in high alpine areas) around the Sphinx observatory at Jungfraujoch (ca. 3500 m a.s.l., Figs. 4, 5). Additionally, two thermistor chains are installed into the bordering ice faces.

The monitoring site consists of north and south faces of a ridge, which divide the network into two clusters with limited connectivity between them and differing thermal regimes (Fig. 4). Resulting from this topology, the thermal clock drift requires synchronization algorithms that let the node times converge even with such temperature deviations.

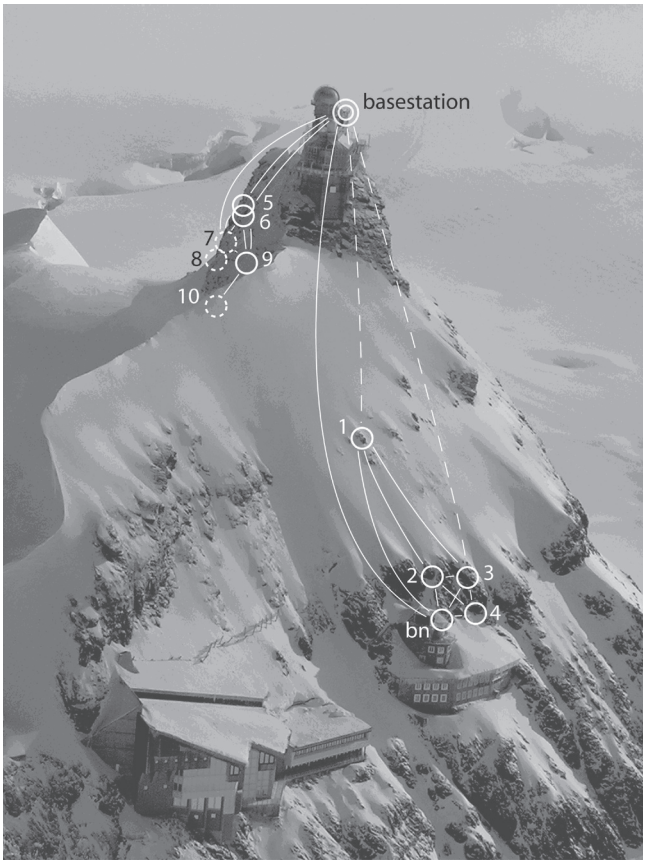

Figure 4. Deployment on Jungfraujoch (3500 m a.s.l., Swiss Alps) consisting of 10 sensor nodes with network topology; the base station is mounted on the Sphinx observatory. Each circle depicts a network node with its corresponding number. Lines indicate good radio connectivity between nodes; dashed lines indicate unstable connectivity; dashed circles are hidden nodes; and *bn* is a bridge node introduced to provide stable connection to the base station. The network is divided into to two clusters on the north-facing (left) and the south-facing (right) slopes of the ridge.

The initial installation of the sensors took place in fall 2006 after four months of system design and hardware production. We set up the first network at the same time, which, however, has not been successful due to the short development time and insufficient testing of the network software and hardware. In addition, a stability problem of the measurement values appeared under field conditions. After a debugging and testing phase over the winter of 2006/2007, first valid data could be gathered in April 2007 (Fig. 6). Yet no data transmission could be maintained over a period of more than two weeks. At this point, an extension of the project with the integration of network into a test bed prior to deployment was already planned for the second deployment in fall 2007. We decided to momentarily leave the network in a mode where data is stored locally to the node memory, and enhance and test the system for the second deployment.

Figure 5. Network node #4 and cable to the sensor rod, which is drilled one meter into the rock perpendicular to the surface. The network nodes can be easily exchanged and attached to the sensor by a waterproof plug.

Second deployment: Matterhorn "Hörnligrat" (3400 m a.s.l., Swiss Alps) in October 2007

Although public and research interests increased significantly following the hot summer of 2003, frost dynamics and natural hazards research in alpine permafrost areas has been discussed already a decade ago (e.g., Haeberli et al. 1997, Wegmann 1998). Frost weathering and rockfall activity is subject to yearlong field observations and measurements (e.g., Matsuoka & Sakai 1999, Matsuoka 2001) and lab experiments (Murton et al. 2006). These lab experiments have shown that ice segregation takes place also in solid (but porous) rock. Field data gave clear evidence for the contribution of temperature fluctuation and water to near-surface weathering and pebble fall. However, a direct physical linkage between temperature and rockfall disposition has not yet been demonstrated in the field. Different concepts of this linkage are discussed in Gruber & Haeberli (2007). The second deployment of PermaSense addresses this issue, to gather data of cleft ice and rock stability interaction.

The installation containing 13 sensor nodes with 6 sensor types, 2 bridge nodes, and 1 base station was made on the

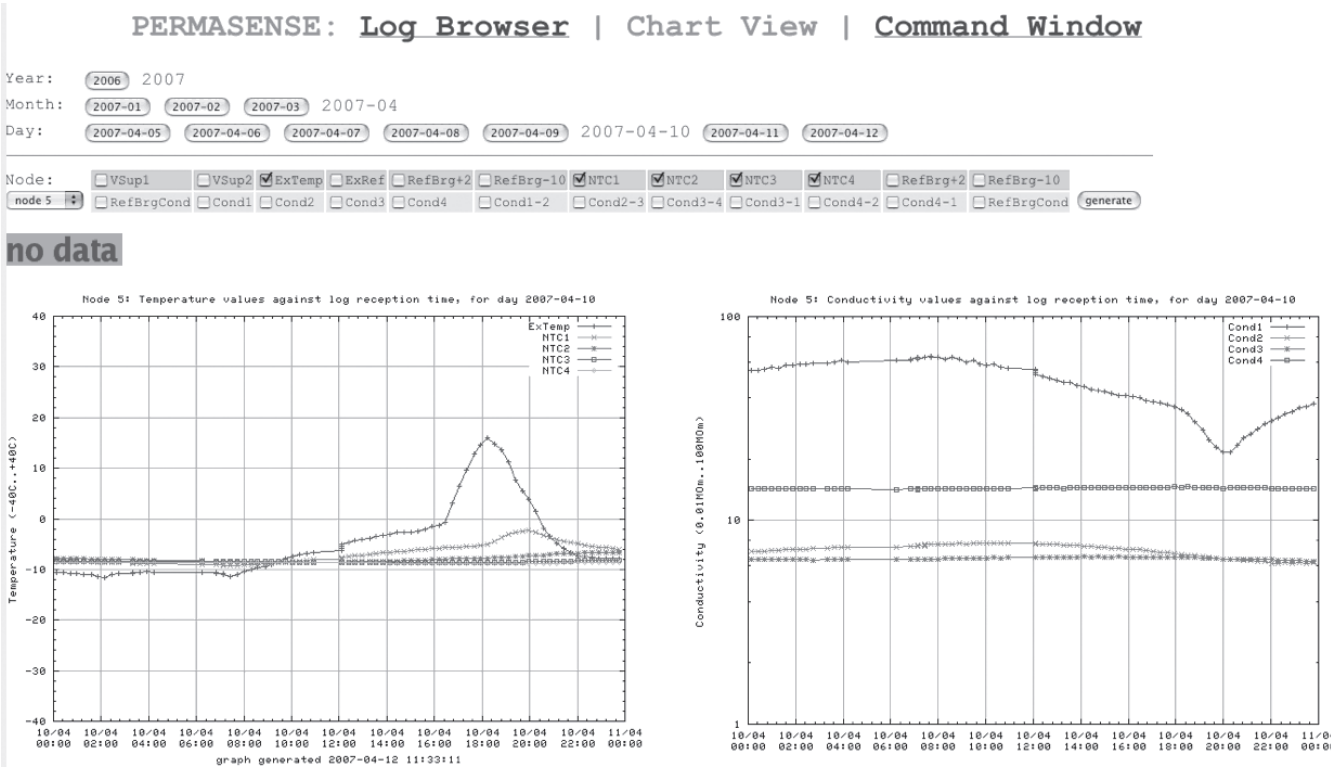

Figure 6. Screenshot of the user interface; direct visualization of one day of measurements from sensor rod #5 in the north-facing slope of the Sphinx. On the left, temperatures of the sensor rod thermistors (NTC1–NTC4) and the node temperature are plotted; the right diagram shows the corresponding rock resistivities. At the near-surface level (NTC/Cond 1), the temperature signal is clearly visible in the resistivity values.

northeast ridge of the Matterhorn at Hörnligrat in October 2007 (Fig. 7). At this site, a rockfall of some 1000 m^3 occurred in July 2003. Massive ice was observed at the surface of the detachment zone (Fig. 7) just after the event. This indicates the presence of stability-relevant ice-filled clefts in this area.

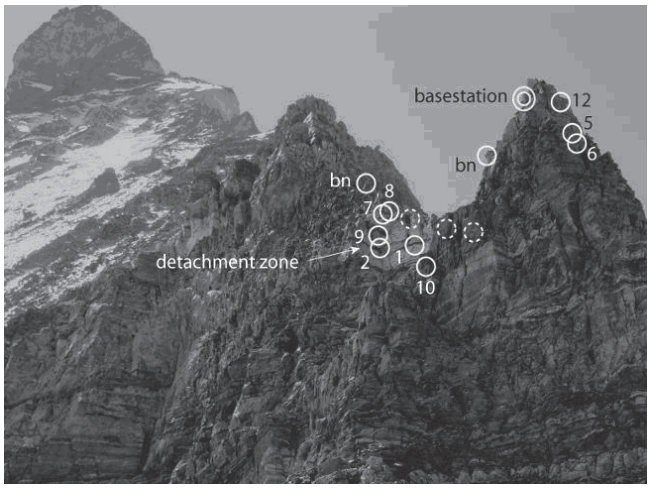

Figure 7. Deployment at Hörnligrat of the Matterhorn. Circles with numbers mark sensor nodes; dashed circles are sensors on the back (northwestern) side of the ridge; *bn* indicates bridge nodes.

Figure 8. Installation site with multiple sensors: At the bottom, two crack meters measure dilatation. Within the cleft, potential water pressure and ice stress, as well as temperatures at different depths, are measured. The tube between the two nodes is the reference air pressure measurement.

In addition to the sensors used on Jungfraujoch, we integrated commercial sensors with a newly designed *sensor interface board* (SIB) into our network. With these sensors we measure crack dilatation, water pressure, ice pressure, and water movements in the clefts. Thermistor chains are mounted into clefts to measure temperature profiles together with the mentioned parameters. One node and SIB has a combination of this sensors attached resulting in a multiple sensor network node. The installation of more than one network node at one spot allows a flexible combination of sensors adapted to the situation in the field (Fig. 8).

Discussion of Experiences and Challenges of PermaSense

In the initial phase of PermaSense until April 2007, diverse problems were critical for the function of the WSN and the subject of debugging. The quality of the measurements and the instable operation of the base station are two examples of early-stage and hardware-related problems. Other system parts, such as the mechanical setup or the battery type, appeared well adapted to the conditions met in the field over the winter and spring 2006/2007.

The network setup at Jungfraujoch at the end of April 2007 and the subsequent test runs at the test bed in Zurich showed two main topics remaining critical for stable, long-term operation:

1. Time synchronization of the nodes.
2. Stability and power efficiency of the data routing.

As described above, the conditions in the field make time synchronization challenging due to large temperature fluctuations and deviations between installation spots. Short radio receiving slots compared to the sleeping intervals due to power limitations require a high quality of synchronization. The fact that the clock quartz are generally optimized for 25°C and have high drifts at negative temperatures makes a precise synchronization of a permafrost WSN even more challenging. Software-based temperature-drift compensation could be a possible solution, but needs extensive testing before application.

The currently used statically predefined data transmission slots, the radio communication as a power intense component, are used in a rather inefficient way. To optimize power consumption and consequently increase battery life-time, a dynamic organization of the data transmission slots is promising. This could also increase the data transmission capacity in areas of the network where it is required and, as a consequence, support more stable data routing as well.

Conclusions

Based on the experience gained from technology development and two high-mountain deployments, we can draw the following main conclusions for the application of WSNs in mountain permafrost research:

For a successful application of WSNs in permafrost research and in other environmentally challenging situations, an adapted software design and extensive testing of the

network under realistic but well-monitored conditions are essential.

Due to large temperature fluctuations and large lateral temperature gradients, in combination with complex network topologies and power limitations, synchronization of the nodes is a very challenging task. Major algorithmic work, as well as specific testing, is needed here.

The power efficiency and the duration of operation without battery exchange in the field can be increased significantly with further software development.

Once we succeed in overcoming the current major problems, WSNs have the potential to become a powerful technology to gather spatially distributed field data in near-real time for permafrost research.

Acknowledgments

We would like to thank Sandro Schönborn, Roman Lim, and Mustafa Yücel for their contribution to PermaSense. The project is partly financed by the Swiss Federal Office for the Environment (FOEN) and the National Competence Center for Research – Mobile Information and Communication Systems (NCCR-MICS). We also acknowledge the helpful technical advice of Hansueli Gubler, ALPUG, in the initial phase of PermaSense.

References

Gruber, S. & Haeberli, W. 2007. Permafrost in steep bedrock slopes and its temperature-related destabilization following climate change. *Journal of Geophysical Research* 112. doi:10.1029/2006-JF000547.

Gruber, S., Hoelzle, M. & Haeberli, W. 2004. Rock wall temperatures in the Alps: Modelling their topographic distribution and regional differences. *Permafrost Periglacial Processes* 15(3): 299–307.

Haeberli, W., Wegmann, M. & Vonder Muehll D. 1997. Slope stability problems related to glacier shrinkage and permafrost degradation in the Alps. *Eclogae Geologicae Helvetiae* 90: 407–414.

Hart, J.K. & Martinez, K. 2006. Environmental sensor networks: A revolution in the earth system science? *Earth-Science Reviews* 78: 177–191.

Martinez, K., Hart, J.K. & Ong, R. 2004. Environmental sensor networks. *Computer* 37 (8): 50–56.

Matsuoka, N. 2001. Direct observation of frost wedging in alpine bedrock. *Earth Surface Processes and Landforms* 26: 601–614.

Matsuoka, N. & Sakai, A. 1999. Rockfall activity from an alpine cliff during thawing periods. *Geomorphology* 28: 309-328.

Murton, J.B., Peterson, R. & Ozouf, J-C. 2006. Bedrock fracture by ice segregation in cold regions. *Science* 314: 1127–1129.

Noetzli, J., Hilbich, C., Hauck, C., Hoelzle, M. & Gruber, S. 2008. Comparison of transient 2D temperature profiles with time-lapse electrical resistivity data at the Schilthorn Crest, Switzerland. *Proceedings.of the Ninth International Conference on Permafrost.*

Talzi, I., Hasler, A., Gruber, S. & Tschudin, C. 2007. PermaSense: Investigating permafrost with a WSN in the Swiss Alps. *In Proceedings for EmNets-07*: 8–12.

Wegmann, M. 1998. Frostdynamik in hochalpinen Feswänden am Beispiel der Region Jungfrau - Aletsch. Mitteilungen der Versuchsanstalt für Wasserbau, Hydrologie und Glaziologie an der ETH Zürich 161.

Werner-Allen, G., Lorincz, J., Johnson, J., Lees, J. & Welsh, M. 2006. Fidelity and yield in a volcano monitoring sensor network. *Proceedings of the 7th conference on USENIX Symposium on Operating Systems Design and Implementation* 7: 381–396.

A Four-Phase Model to Quantify Subsurface Ice and Water Content in Permafrost Regions Based on Geophysical Data Sets

Christian Hauck
Institute for Meteorology and Climate Research, University of Karlsruhe/Forschungszentrum Karlsruhe, Germany
Mathias Bach
Geophysical Institute, University of Karlsruhe, Germany
Christin Hilbich
Geographical Institute, University of Jena, Germany

Abstract

The indirect nature of geophysical soundings requires a relation between the measured variable (electrical resistivity, seismic velocity) and the rock/soil, water, air, and ice contents. In this contribution we present a model which determines the volumetric fractions of these four phases from tomographic electrical and seismic data sets. The so-called 4-phase model is based on geophysical mixing rules for electrical resistivity and seismic P-wave velocity. Observed resistivity and velocity data are used as input data on a two-dimensional grid; in the general case a porosity model has to be prescribed. First results confirm the good model performance, especially concerning the detection and quantification of ground ice as well as the detection of air cavities in the blocky surface layer. In addition, differences in ice content from time-lapse data can be determined. Examples from permafrost and non-permafrost sites with different morphologies (e.g., high mountain bedrock plateaus, scree slopes, moraines) are presented.

Keywords: electrical resistivity; four-phase model; geophysics; ice content; refraction seismics; water content.

Introduction

Based on the observational evidence of climate change in permafrost regions in recent years (e.g., Kääb et al. 2007, Marchenko et al. 2006, Fukui et al. 2007), it is now recognised that a detailed knowledge of the material composition of the subsurface in permafrost regions is required for (1) modeling of the future evolution of the ground thermal regime in permafrost areas, (2) a physically-based assessment of the hazard potential due to degrading permafrost, and (3) an optimal design of hazard mitigation measures. The important material properties in this context include the ice content, the unfrozen water content, and the porosity. The relative proportions between ice, water, and air content determines the thermal conductivity of the frozen material (e.g., Lachenbruch et al. 1982) which is needed for modeling of future thermal conditions of permafrost. Due to the commonly remote location of permafrost areas and corresponding logistical and financial difficulties in obtaining these properties from borehole logs, knowledge about the exact material composition of the subsurface in permafrost areas is scarce.

In frozen ground subsurface material may consist of four different phases: two solid phases (rock/soil matrix as well as ice), a liquid (unfrozen pore water), and a gaseous phase (airfilled pore space and cavities)(see Fig. 1). Except for laboratory and borehole data, the composition of the subsurface material can only be inferred through indirect geophysical investigations. Due to the complexity of the subsurface, a combination of complementary geophysical methods (e.g., electrical resistivity tomography and refraction seismic tomography) is often favoured to avoid ambiguities in the interpretation of the results (Maurer & Hauck 2007).

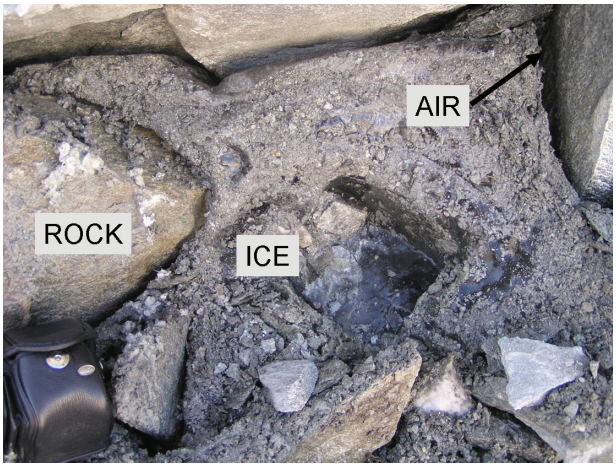

Figure 1. Photo of an ice-air-rock mixture within a rock glacier in the Swiss Alps. The camera in the lower left corner illustrates the scale.

However, the indirect nature of geophysical surveys requires a relation between the measured variable (electrical resistivity, seismic velocity) and the respective parts of the material composition (rock, water, air, ice). Such relations have been developed for the electrical properties; for example, the well-known relation between the electrical resistivity of the bulk material, the pore-water resistivity, the porosity and the saturation known as Archie's Law (Archie 1942), and for the elastic properties such as the mixing law for seismic P-wave velocities by Timur (1968).

In permafrost studies, quantitative combinations of electric and seismic data sets were introduced by McGinnis et al.

(1973) who used resistivity data for calculating the increase in seismic P-wave velocity due to the frozen layer. Oberholzer et al. (2003) used an index based on the ratio of resistivity and seismic P-wave velocity to differentiate between frozen and unfrozen morainic material in the Swiss Alps. However, up to now no physically-based relation between parameters commonly measured in surface geophysical surveys and the four phases present in permafrost material exists for practical applications in permafrost studies.

In the following a so-called 4-phase model (FPM) for explicit prediction of three of the four phases is presented which is based on two-dimensional tomographic electrical and seismic measurements. Results from the application of the 4-phase model to several periglacial morphologies will be shown to illustrate the performance of the model. In a further step the model is applied to time-dependent resistivity and seismic velocity data to determine the temporal change of ice and unfrozen water content between two measurement dates.

It is believed that the FPM serves as a useful tool for improved interpretation of geophysical data sets in frozen regions, and that it can be applied for determining quantitative information about the ice content and its temporal evolution.

Theory

The 4-phase-model is based on the well-known geophysical mixing rule for electrical resistivity (Archie 1942) and on an extension of the time-average formula for seismic P-wave velocities (Timur 1968) (Eqs. 1, 2):

$$\rho = a\rho_w \Phi^{-m} S_w^{-n} \tag{1}$$

$$\frac{1}{v} = \frac{f_w}{v_w} + \frac{f_r}{v_r} + \frac{f_i}{v_i} + \frac{f_a}{v_a} \tag{2}$$

where ρ and ρ_w are the electrical resistivities [in Ωm] of the bulk material and the pore water, respectively, Φ is the porosity, S_w is the saturation, n, m, and a are empirical constants, f_w, f_r, f_i, and f_a are the volumetric fractions of the water, rock, ice, and air content, and v, v_w, v_r, v_i, and v_a are the seismic P-wave velocities [in m/s] of the bulk material, water, rock, ice, and air, respectively. Under the condition

$$f_w + f_r + f_i + f_a = 1 \tag{3}$$

and using $\Phi = 1 - f_r$ and $S_w = f_w/\Phi$, equations for the ice, water, and air content can be derived as a function of the rock content (1-porosity):

$$f_i = \frac{v_i v_a}{v_a - v_i}\left[\frac{1}{v} - \frac{f_r}{v_r} - \frac{1-f_r}{v_a} + \left(\frac{a\rho_w(1-f_r)^n}{\rho(1-f_r)^m}\right)^{1/n}\left(\frac{1}{v_a} - \frac{1}{v_w}\right)\right] \tag{4}$$

$$f_a = \frac{v_i v_a}{v_i - v_a}\left[\frac{1}{v} - \frac{f_r}{v_r} + \frac{1}{v_i}(f_r - 1) - \left(\frac{a\rho_w(1-f_r)^n}{\rho(1-f_r)^m}\right)^{1/n}\left(\frac{1}{v_w} - \frac{1}{v_i}\right)\right] \tag{5}$$

$$f_w = \left(\frac{a\rho_w(1-f_r)^n}{\rho(1-f_r)^m}\right)^{1/n}. \tag{6}$$

Equations (4), (5), and (6) allow then to explicitly compute ice, air, and unfrozen water content for each model block on a 2D-grid from seismic P-wave velocity and electrical resistivity data if a suitable porosity model can be prescribed. In the absence of ice or if the ice and rock content are considered as one (solid) phase, Equations (1) to (3) can be rearranged to determine the porosity. The seismic velocities for air (330 m/s) and ice (3500 m/s) are known—further material properties such as the P-wave velocity of the host rock material, the resistivity of the pore water, or the so-called cementation exponent m and the saturation exponent n have to be specified. Whereas the former two parameters can be measured in the field, the latter are often assumed to equal 2 for many rock materials (e.g., Archie 1942, Keller & Frischknecht 1966). In a further step these model parameters can be determined by a Monte Carlo approach, the results of which are used additionally as indicator for the reliability of the model results (Bach 2008).

The model was tested using electric and seismic data sets from two active rock glaciers in the Swiss Alps, where borehole data were available to verify the performance of the FPM. Sensitivity studies indicate a strong dependence of the quantitative model results on the pore water resistivity, which should be measured directly in the field, wherever possible.

Data Sets

Seismic and ERT data sets from various field campaigns on different periglacial morphologies were used to test the model performance and evaluate the applicability of the FPM to different rates of ice, water, air, and water within the subsurface. The geophysical data stem from a number of different projects, including the EU PACE project (Permafrost and Climate in Europe) and the geophysical monitoring network within PERMOS (Hilbich et al. 2008) and are described in the respective publications (Table 1). Data inversions were performed using the geoelectric Res2DINV software and a seismic inversion algorithm by Lanz et al. (1998). In the following we will present data from an ice-rich, coarse-grained moraine material from the South-Shetland Islands, Maritime Antarctica (further details can be found in Hauck et al. 2007), poor-ice bedrock slope with superficial fine-grained material on Schilthorn, Swiss Alps (described in Hauck 2001), frozen and unfrozen bedrock material from a long gentle slope in Jotunheimen, Norway (Hauck et al. 2004) and a low-altitude, cold-ventilated scree slope in the Black Forest, Germany (Hauck & Kneisel 2008). Examples of rock glaciers will be discussed in detail

in a companion paper and will not be repeated here. Finally, a monitoring data set comprising measurements along the same survey line observed at two different times from the frozen bedrock plateau at Stockhorn, Swiss Alps (Hilbich et al. 2008) will be presented. The characteristics of the field sites are summarised in Table 1.

Four-Phase Model Results

Figure 2 shows inversion results for P-wave velocity and specific resistivity as well as the FPM results for the volumetric contents with a prescribed constant porosity model of 50% for a blocky moraine on Livingston Island, Maritime Antarctica. Ice, water, and air contents are normalised by the porosity showing the percentage of the pore space which is filled by the respective material. Resistivities are high below the uppermost 2 metres, and seismic velocities show a low-velocity zone in this region, indicating an active layer without any frozen material. Consequently, the result for the ice content shows values up to 100% below the uppermost 2 m meaning that 100% of the pore space is filled with ice below the active layer. Within the active layer, mostly air and only little water is present within the available pore space. The results indicate clearly that the moraine is ice-cored—similar results were obtained for the ice-rich rock glacier Murtèl in the Swiss Alps (not shown here).

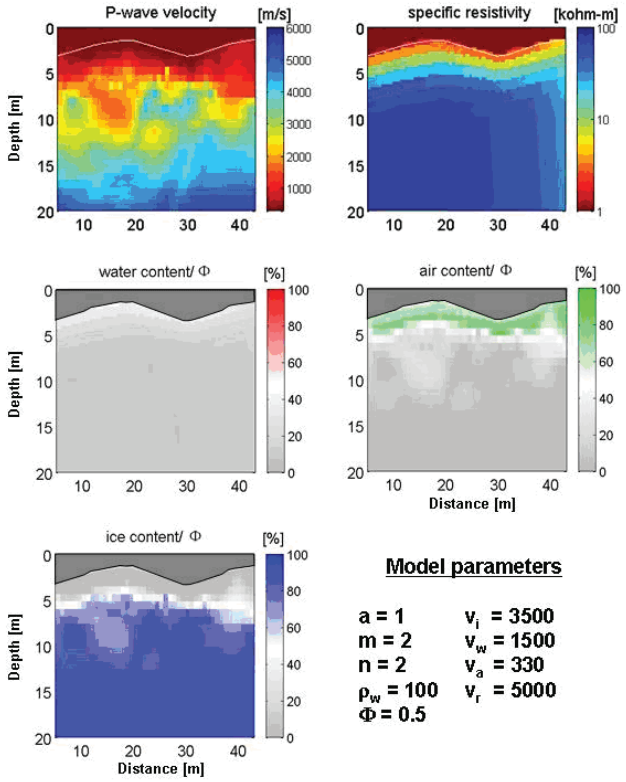

Figure 2. P-wave velocity and specific resistivity inversion results for the ice-cored moraine on Livingston Island, Maritime Antarctica. Ice, water, and air content are displayed relative to the available pore space of 50%.

Figure 3 summarises the results for the other landforms, i.e., the frozen bedrock sites at Schilthorn and Juvvasshøe, the unfrozen bedrock slope 600 m below the top of Juvasshøe, and the low-altitude scree slope at Präg. All examples except Schilthorn were computed with different but constant porosity models, which may limit the significance for interpreting absolute values, but which can be used as indication to what extent the pore space is filled with the respective material. Based on results from a drilling in 1998 (Vonder Mühll et al. 2000), a porosity model that decreases with depth was used for the Schilthorn site. Table 2 provides an overview of the model parameters used for the different field sites.

The results for the frozen bedrock at Juvvasshøe show high ice contents below a 4 m thick active layer, which is mainly "filled" with air but only little water. The sharp transition between active layer and permafrost at 4 m can be seen both in the resistivity and in the seismic data. The permafrost layer consists almost completely of rock and ice with only little air and water. These results agree well with borehole logs and borehole temperatures from this site (Isaksen et al. 2001, Harris et al. 2001).

In contrast, the results for the frozen bedrock at Schilthorn indicate a much lower ice content relative to the available pore space and a significantly higher unfrozen water content (see also Noetzli et al. 2008, Hilbich et al. 2008). These model results are caused by the much lower resistivity values

Table 1. Characterization of the field sites and data sets used in this study.

	Livingston Island, Maritime Antarctica	Juvvasshøe/Jotunheimen, Norway PACE borehole	Juvvass/Jotunheimen, Norway	Schilthorn, Northern Swiss Alps PACE borehole	Stockhorn, Western Swiss Alps PACE borehole	Präg/Black Forest, Germany
Site description	ice-cored moraine	flat bedrock	north facing bedrock slope	north facing bedrock slope	bedrock plateau	cold ventilated scree slope
Lithology	boulderly diamicton with sands and silts	quartz monzonorite, 3-5 m weathered layer	quartz monzonorite, thick debris cover (vegetated)	limestone schists 0 to several m debris cover	Albit-Muskowit schists, > 1m debris cover	large blocks, gneiss
Altitude (a.s.l.)	30 m	1894 m	1300 m	2910 m	3410 m	600 m
Profile length, investigation depth	35 m 15 m	60 m 15 m	65 m 20 m	58 m 10 m	94 m 15 m	168 m 25 m
Literature	Hauck et al. 2007	Hauck et al. 2004	Hauck et al. 2004	Hauck 2001	Hilbich et al. 2008	Hauck & Kneisel 2008

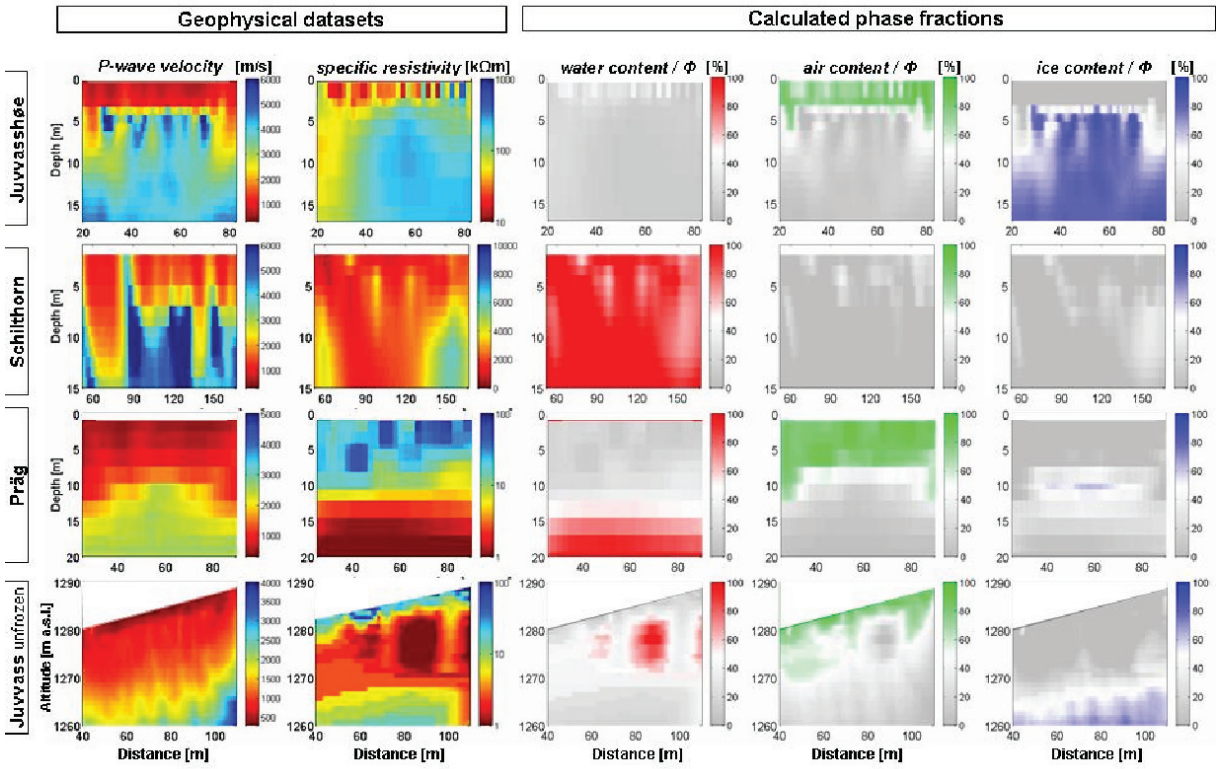

Figure 3. Geophysical data sets and 4-phase model results for four frozen and unfrozen mountain sites with different ice contents. Ice-, water- and air content are displayed relative to the available pore space Φ. The model parameters for the respective field cases are summarised in Table 2. Note, that the scales for seismic P-wave velocities and resistivities are different for the various sites.

yielding higher unfrozen water contents through Equation (1). Significant ice contents are found below a depth of 5 m, which agrees well with the observed active layer depth at the time of the measurements (Hauck 2001).

Blocky and ventilated scree slopes are known to sustain permafrost thermal regimes including substantial ground ice occurrences (Delaloye & Lambiel 2005). In the absence of excavations and boreholes, usually no indications are given as to whether ground ice is present or whether "dry permafrost conditions" prevail (Hauck & Kneisel 2008). Although the model results for the low-altitude scree slope at Präg indicate total ice contents of up to 25% (half of the available pore space of 50%) at around 10 m depth, this result has to be treated with care, as the model results for water and air show that the modeled ice-bearing zone is located right between the air-filled top layer (uppermost 7–10 m) and the ground water table at 12–15 m depth. Inversion results with a slightly deeper low-velocity top layer or a low-resistivity bottom layer reaching to slightly shallower depth would lead to a vanishing intermediate ice layer. Such inaccuracies in modeled layer depth are well within the uncertainty range of geophysical inversion models.

The unfrozen Juvvass slope is located along the northern slope of Juvvasshøe summit, but at an altitude where joint thermal and geophysical measurements proved the absence of permafrost (Hauck et al. 2004). The FPM results correctly predict no ice occurrences within the uppermost 10 m, where air is predominantly found in the upper 2 m with partly

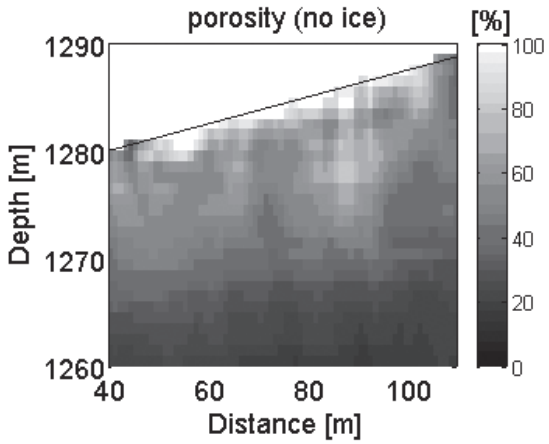

Figure 4. Calculated porosity for the unfrozen bedrock slope at Juvvass/Jotunheimen, Norway, under the assumptions of no ice and n = m = 2.

saturated conditions below. However, below a depth of 10 m modeled ice content values are increasing with depth. This obvious discrepancy to the thermal evidence has its causes in the increasing velocity and resistivity values measured at greater depth, which most probably corresponds to the bedrock layer. Assuming an ice content of zero and using the simplifications of n = m = 2, Equations (4)–(6) can be reformed to compute the porosity distribution over the model domain. In Figure 4 porosity values >50% are predicted for

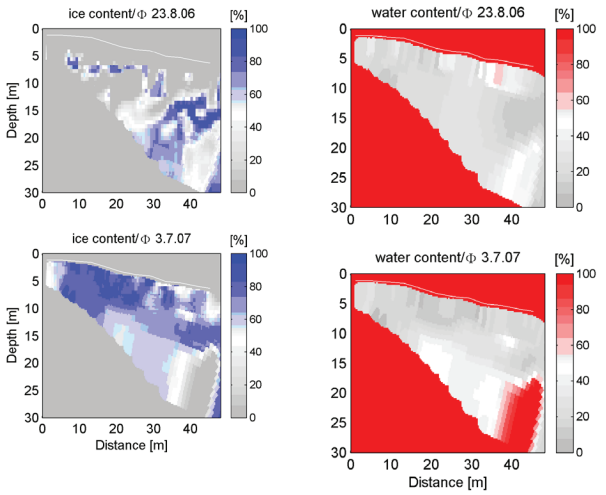

Figure 5. FPM Monitoring results for ice and water content at the bedrock plateau Stockhorn, Western Swiss Alps, for two measurement dates in summer 2006 and 2007.

the bouldery surface layer with decreasing porosity values below, indicating the more and more compacted rock material at greater depths. This much more probable scenario (no ice and decreasing porosity with depth as opposed to constant porosity and increasing ice content with depth) illustrates the main deficiency of the FPM in cases of low ice contents and unknown porosity distribution. Because rock and ice can exhibit similar seismic P-wave velocities and similarly high resistivity values, the differentiation between bedrock and ice occurrences is sometimes difficult, especially if no geological or glaciological *a priori* data are present.

Monitoring Results

The full potential of the FPM becomes evident for applications with time dependent data sets. Figure 5 shows the FPM results for two measurements at Stockhorn, Western Swiss Alps, where geoelectric and seismic measurements are regularly conducted within the geophysical monitoring network of PERMOS (Permafrost Monitoring Switzerland, see Hilbich et al. 2008). Due to different resolutions of seismic and ERT data sets, the coinciding model domain is triangular in this case.

Measurements were obtained in late summer 2006 and early summer 2007, representing different phases of the seasonal thawing of the active layer. The much higher ice contents in the uppermost 5 m in July 2007 compared to the ice-free conditions at the end of August 2006 are clearly visible in Figure 5. Furthermore, ice contents at greater depth (>15 m) are larger in August 2006 than in the beginning of July 2007, which may resemble the phase lag of winter temperatures. Corresponding water contents are generally low with maximum values near the surface in August and at greater depth in July. The saturated water anomaly in the lower right corner originates from a consistently occurring low-resistive anomaly in the ERT monitoring results, the cause of which has not yet been determined.

Table 2. Model parameters used for FPM calculations at the different field sites. In all cases the following values were used: a = 1, m = 2, n = 2, v_i = 3500 m/s, v_a = 330 m/s, v_w = 1500 m/s.

	ρ_w [ohm-m]	Φ	v_r [m/s]
Livingston Island,	100	0.5	5000
Juvvasshøe	100	0.2	6000
Schilthorn	300	0.5 – 0.25	4000
Präg	100	0.4	5200
Juvvass slope	100	0.5	6000
Stockhorn	100	0.3	5000

Conclusion

A new model for quantifying subsurface ice, water, and air contents in permafrost regions has been presented. The so-called 4-phase model (FPM) is based on tomographic specific resistivity and seismic P-wave velocity data sets and combines well-known petrophysical relationships of electric and elastic properties of the material on one hand and the relative phase fractions within the subsurface on the other hand. Field cases from a series of different permafrost sites were presented to evaluate the model performance. Key results from this study include:

- The model correctly delineates the ice, air, and water contents in cases of large ice occurrences such as ice-cored moraines and rock glaciers.
- Internal layers, especially the active layer, can be delineated because of strong contrasts in the vertical ice and air distribution. These contrasts can become more pronounced in the FPM results than in the original geophysical data, which facilitates the interpretation.
- Unfrozen water contents are generally low, except for the Schilthorn site, where modeled water content values are higher than the corresponding ice contents.
- In its present form, the absolute model results are strongly biased by the prescribed porosity model. As a consequence, phase fractions are shown relative to the available pore space. In a further step the free model parameters (including porosity) will be determined using a quasi Monte Carlo approach yielding more realistic porosity distributions.
- Deficiencies of the FPM have been found for cases of low ice contents in combination with an unknown porosity distribution. As rock and ice may exhibit similar seismic P-wave velocities and similar high resistivity values, the differentiation between bedrock and ice may become difficult, especially if no geological or glaciological *a priori* data are present.
- Promising results were obtained for geophysical monitoring data, where porosity remains unchanged and resistivity and velocity changes can unambiguously be related to changes in ice, air, and water content.

Acknowledgments

We would like to thank all field crews participating in the geophysical surveys, H. Maurer for providing the

seismic inversion code and M. Böttcher for her contribution in developing the FPM. Fieldwork was partly financed by the EU-PACE, PERMOS (BAFU, Switzerland) and Permamodel (Spanish Antarctic Program and University of Zürich) projects.

References

Archie, G.E. 1942. The electrical resitivity log as an aid in determining some reservoir characteristics. *American Inst. of Mining and Metallurgical Engineers* 146*:* 55–62.

Bach, M. 2008. Modellierung von Eis- und Wassergehalt im Untergrund mittels seismischer und geoelektrischer Tomographie. M.Sc. Thesis. University of Karlsruhe.

Delaloye, R. & Lambiel, C. 2005. Evidence of winter ascending air circulation throughout talus slopes and rock glaciers situated in the lower belt of alpine discontinuous permafrost (Swiss Alps). *Norwegian Journal of Geography* 59(2): 194-203.

Fukui, K., Fujii, Y., Ageta, Y. & Asahi, K. 2007. Changes in the lower limit of mountain permafrost between 1973 and 2004 in the Khumbu Himal, the Nepal Himalayas. *Global Planet. Change* 55(4): 251-256.

Harris C., Davies M.C.R. & Etzelmüller, B. 2001. The assessment of potential geotechnical hazards associated with mountain permafrost in a warming global climate. *Permafrost and Periglac. Process*. 12: 145-156.

Hauck, C. 2001. Geophysical methods for detecting permafrost in high mountains. PhD Thesis. ETH Zürich, Switzerland, *VAW-Mitteilung* 171, 204 pp.

Hauck, C., Isaksen, K., Vonder Mühll, D. & Sollid, J.L. 2004. Geophysical surveys designed to delineate the altitudinal limit of mountain permafrost: an example from Jotunheimen, Norway. *Permafrost and Periglac. Process*. 15 (3), 191-205.

Hauck, C., Vieira, G., Gruber, S., Blanco, J.J. & Ramos, M. 2007. Geophysical identification of permafrost in Livingston Island, maritime Antarctica. *J. Geophys. Res*. 112: F02S19, doi: 10.1029/2006JF000544.

Hauck, C. & Kneisel, C. 2008. Quantifying the ice content in low-altitude scree slopes using geophysical methods. In: C. Hauck & C. Kneisel (eds.), *Applied geophysics in periglacial environments*. Cambridge University Press, *in press*.

Hilbich, C., Hauck, C., Delaloye, R. & Hoelzle, M. (2008): A geoelectric monitoring network and resistivity-temperature relationships of different mountain permafrost sites in the Swiss Alps. *Proceedings of the Ninth International Conference on Permafrost, Fairbanks, Alaska, June 29–July 3, 2008* (this proceedings).

Isaksen K., Holmlund P., Sollid J.L. & Harris C. 2001. Three deep alpine-permafrost boreholes in Svalbard and Scandinavia. *Permafrost and Periglac. Process*. 12: 13-25.

Kääb, A., Frauenfelder, R. & Roer, I. 2007. On the response of rockglacier creep to surface temperature increase. *Global Planet. Change* 56 (1-2): 172-187.

Keller, G.V. & Frischknecht, F.C. 1966. *Electrical Methods in Geophysical Prospecting*, Pergamon Press, Inc.

Lachenbruch, A.H., Sass, J.H., Marshall, B.V. & Moses, T.H.J. 1982. Permafrost, heat flow and the geothermal regime at Prudhoe Bay, Alaska. *J. Geophys. Res.* 87(B11): 9301-9316.

Lanz, E., Maurer, H.R. & Green, A.G. 1998. Refraction tomography over a buried waste disposal site. *Geophysics* 63(4): 1414-1433.

Marchenko, S.S., Gorbunov, A.P. & Romanovsky, V.E. 2007. Permafrost warming in the Tien Shan Mountains, Central Asia. *Global Planet. Change* 56(3-4): 311-327.

Maurer, H. & Hauck, C. 2007. Geophysical imaging of alpine rock glaciers. *J. Glac.* 53(180): 110-120.

McGinnis, L.D., Nakao, K. & Clark, C.C. 1973. Geophysical identification of frozen and unfrozen ground, Antarctica. *Proceedings of the Second International Conference on Permafrost*, *Yakutsk, Russia:* 136-146.

Noetzli, J., Hilbich, C., Hauck, C., Hoelzle, M. & Gruber, S. 2008. Comparison of transient 2D temperature fields with time-lapse electrical resistivity data at the Schilthorn Crest, Switzerland. *Proceedings of the Ninth International Conference on Permafrost, Fairbanks, Alaska, June 29–July 3, 2008* (this proceedings).

Oberholzer, P., Vonder Mühll D. & Ansorge J. 2003. Shallow structure of the lower Rossboden Glacier and its moraine dam (Valais, Swiss Alps). *Eclogae Geologicae Helvetiae* 96(2): 299-312.

Timur, A. 1968. Velocity of compressional waves in porous media at permafrost temperatures. *Geophysics* 33(4): 584-595.

Vonder Mühll, D., Hauck, C. & Lehmann, F. 2000. Verification of geophysical models in Alpine permafrost using borehole information. *Annals of Glaciology* 31: 300-306.

—Plenary Paper—

Rationalizing Climate Change for Design of Structures on Permafrost: A Canadian Perspective

Don W. Hayley
EBA Engineering Consultants Ltd., Canada
Bill Horne
EBA Engineering Consultants Ltd., Canada

Abstract

The design engineer is challenged by uncertainty when determining how a plethora of published trends indicating a warming arctic climate can affect future permafrost stability. A process was developed in Canada in 1998 for screening projects in an attempt to rationalize the effects of climate change. Two case histories from the authors' files are used to illustrate the screening process. One project is a government building with complex foundation conditions but a defined service life. The second example is a site reclamation project that relies on permafrost for stability. Reclamation requires confirmation that the risk of thaw can be managed to an acceptable level over the long term. Climate change trends for structures on permafrost with a defined service life can reasonably be predicted from historical climate data and climate normals developed over a period of years (30 years). Global Climate Models (GCM) can be a better choice when longer term analyses are required. Both methodologies have limitations that must be balanced with appropriate risk assessment. A geothermal analysis that includes appropriate climate trend input, coupled with a failure modes and effects analysis, can provide a useful tool for evaluating alternatives where long term environmental risks must be managed.

Keywords: Canada; climate change; GCM; permafrost; site reclamation; thermal analysis; thermosyphons.

Introduction

Concern about global warming has added a new layer of uncertainty to the current practice of cold regions engineering. Recent studies have clearly shown that climatic warming trends are more severe at higher latitudes, and regional data from northern Canada has identified that the mean annual air temperatures are most affected by warmer than normal winter conditions. Structures that rely on properties of permafrost and ice for long-term stability can be at risk if design processes do not recognize and rationalize future uncertainty from changing climatic conditions. It is no longer an accepted procedure to adopt historic thirty-year climatic normals as design parameters in regions of permafrost.

This paper describes a risk-based process for screening projects sensitive to climatic warming that was developed in 1998 for application in Northern Canada. In this paper, the process is described in general terms, and two representative projects are used as case histories to illustrate the strengths and limitations of the process.

Project Screening Process

Engineering projects in the north usually depend on permafrost as a structural material for foundation support, seepage retention or as a barrier for contaminant flow. The ability of the frozen ground to carry out these functions depends on site conditions and meteorological parameters that sustain the permafrost. Environment Canada initiated a three year study to review and document the factors that require consideration when designing new structures on permafrost in 1995. The author was a contributor along with a number of government scientists and university researchers with permafrost interests. The product was a report titled "Climate Change Impacts on Permafrost Engineering Design" (Etkin et al. 1998). The report is no longer available in print but can be provided by the authors in .pdf form on request.

The report is ten years old and much has changed in our understanding of how climate change is affecting our practice. The value in the 1998 report is the recognition that not all structures are exposed to the same risk level. The process requires the designer to systematically consider the sensitivity of the site and type of structure to damage resulting from changes to the permafrost regime. Each project is screened to categorize its site sensitivity and the consequences of failure resulting from permafrost warming or thaw following the schematic in Figure 1. The probability and consequences feed into a risk table, Figure 2, where the risk level, identified as a scale with four levels, is used to determine a reasonable level of analyses appropriate for the project.

The analyses range from non-concern through application of professional judgement to detailed quantitative analyses using state-of-practice numerical models. A simple classification system for relating soil type and initial ground temperatures to site sensitivity is shown in Figure 3. A table of consequences linked to potential failure modes is included in Figure 4.

Project Examples

Application of the process can be illustrated with two projects from the authors' files. The first project has been chosen to illustrate a complex foundation design for a new municipal building with a defined service life. The

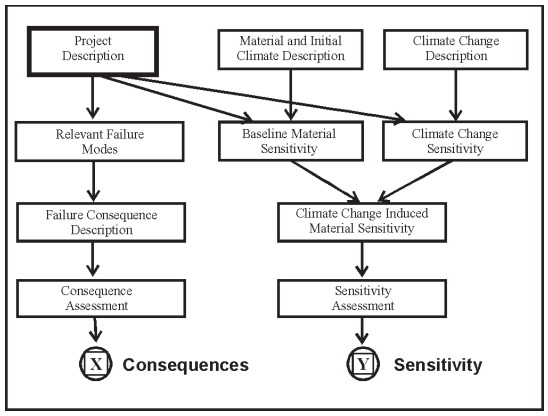

Figure 1. Screening process schematic.

Likelihood (Probability)	Consequence			
	Negligible	Minor	Major	Catastrophic
Frequent	C	A	A	A
Probable	C	B	A	A
Occasional	D	B	B	A
Remote	D	C	B	A
Improbable	D	C	C	B

Risk Level	Analysis Prescribed
D	Not Required
C	Qualitative
B	Semi-quantitative
A	Detailed Quantitative

Figure 2. Risk assessment table (adapted from Canadian Standards Association, CSA-Q634-91).

Type of Soil	Permafrost Temperature Zone			
	Zone 4 (T < -7°C)	Zone 3 (-7 ≤ T < -4°C)	Zone 2 (-4 ≤ T < -2°C)	Zone 1 (-2 ≤ T < 0°C)
Any Soil containing massive ice	M	H	H	H
Peat and Organic	L	M	H	H
Lacustrine (silt or clay)	M	M	M	H
Morainal soils (till)	L	L	L	M
Marine Soils with Salinity	M	M	H	H
Alluvial and Glaciofluvial (sand or gravel)	L	L	L	M
Frost-shattered rock	L	L	M	M

Figure 3. Classification of sensitivity by soil type and permafrost zone.

Failure Mode	Project Type				
	Tailings Ponds, Dams	Open Pit Mine	Roads	Foundations / Piles	Slopes, Embankments
Thaw Settlement	YES	NO	YES	YES	YES
Loss of strength / Creep	YES	YES	NO	YES	YES
Increased Permeability	YES	NO	NO	NO	NO
Accelerated frost effects	NO	NO	YES	YES	NO

Figure 4. Table of consequences linked to failure modes.

second project involves site reclamation that must address the implications of changes to the permafrost regime over the very long term. In both cases, the project cycle is well advanced such that they can be considered realistic case histories.

Inuvik Hospital

The Government of the Northwest Territories initiated replacement of the hospital in Inuvik with a new Regional Health Centre in the late 1990s. The chosen site was on the fringe of municipal development. The Inuvik area is typically covered with glacial materials with a high proportion of ground ice prevailing in continuous permafrost. The hospital site underlain by a granular soil with a relatively low ice content. Inuvik was developed as a new townsite in the 1950s, and the challenges of building on ice-rich permafrost were met at that time by establishing a procedure for installation of timber piles frozen into steamed holes (Philainen 1959). The construction could then proceed above the surrounding ground to provide a cold crawl space to allow natural air convection. These designs have functioned well but are now generally architecturally unacceptable for municipal and industrial buildings. The new hospital required its main floor to be on grade, with a crawl space excavated into permafrost soils. A thermosyphon heat exchange system was chosen to allow below grade foundation design.

The guideline screening process identified that Inuvik is a region of high sensitivity to climate warming and that the consequences of thaw-settlement on a structure of this type would be severe. Moreover, the lower Mackenzie Valley, in close proximity to the Beaufort Sea, is recognized as a "hot spot" for climatic extremes. An appropriate framework for design analyses was therefore state-of-practice geothermal modelling to select a thermosyphon configuration that would sustain the permafrost foundation soils. This must be coupled with consideration of the potential for future deformations attributed to permafrost warming. The building had a designated design life of thirty years; therefore, it was necessary to look forward to the year 2030 for climatic input to design analyses and to consider the probability that extreme events could upset the ground thermal regime during the thirty years of operation.

The building is a steel frame structure on concrete footings set below grade with a warm crawl space. The underlying permafrost is protected from thaw with a thick layer of rigid polystyrene insulation underlain by a horizontal looped thermosyphon system. Figure 5 shows the structure at the open foundation and framing stage in October 2001, and a foundation schematic is shown in Figure 6.

The thermal design requirements were to develop a combination of granular pad thickness, insulation thickness and thermosyphon spacing that would satisfy the design life requirements of preservation of the permafrost and minimal warming from initial ground temperatures. The design was based on two-dimensional finite element geothermal analyses that have been configured to include heat flux to a horizontal plane of thermosyphons (Hwang 1976). Heat is

Figure 5. Inuvik Hospital – open foundation and framing stage, October 2001.

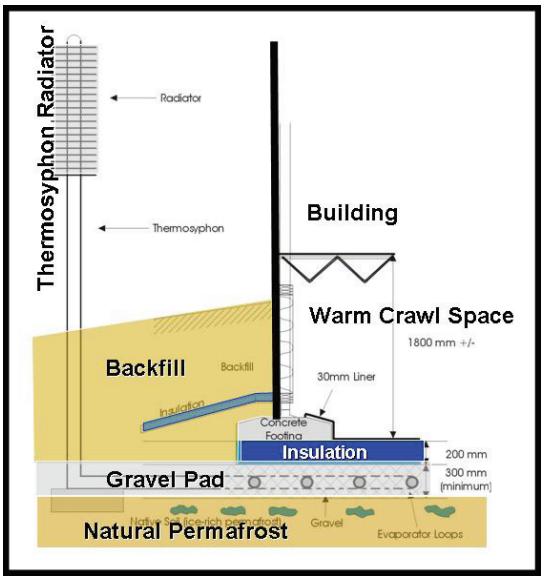

Figure 6. Foundation schematic.

removed from the foundation soils and dissipated to the air at the above-ground radiators whenever the air is colder than the ground below the building. The overall heat balance, therefore, becomes dependant on the outside air temperature and the efficiency of heat extraction process. That efficiency is expressed by a coefficient that can be determined from the literature (Haynes and Zarling 1988) or adapted from similar projects where performance records are available. The greatest uncertainty is the outside air temperature and wind velocity and how that might change in response to microclimatic effects from construction or macro-climatic effects from climate warming trends.

The foundation system was configured to satisfy thermal design criteria based on historic air temperature records for each of the following conditions:

- Five consecutive 1 in 5 warm years followed by a 1 in 100 warm year,
- Ten consecutive 1 in 5 years, and
- A linear warming trend over the life of the structure.

It was necessary to use the historical database to construct hypothetical annual air temperature inputs that were representative of each of the above conditions. A probabilistic analysis was carried out to determine the mean monthly temperatures representative of both the 1 in 5 and 1 in 100 return period warm years. The freezing and thawing indices for each of the years from 1957 to 2000 were calculated and ranked with a "best fit" linear regression on probability paper. The 1 in 5 and 1 in 100 warm indices were chosen and normal monthly air temperatures were scaled upward by the ratio of the respective freezing and thawing indices to their normals. These constructed new mean monthly air temperature annual cycles were considered representative of conditions with the chosen return periods.

The influence of a potential global warming trend was evaluated by starting at the mid-point of the thirty year Canadian Climate Normals available at the time (1961 to 1990) and ramping the mean annual temperatures upward in a linear function over the period from 1975 to 2030. The Environment Canada Report provided guidance for selecting either a best estimate case or a high sensitivity case global warming scenario and amplifying the effects based on season, and latitude. Inuvik lies at about 70°N latitude where the winter amplification increases the seasonal increase by a factor of 3 and the summer increases are attenuated by a factor of 0.5. The annual cycle is divided into four seasons of three months each and the air temperature increase applied for each month by cycle expressed as degree-C/month/decade was: Winter 0.95, Spring 0.66, Summer 0.16, and Fall 0.18. This allowed construction of a mean monthly air temperature representative of each year as the temperatures continued to increase in a linear fashion. The overall trend for the high sensitivity case chosen as a design basis could be expressed as a ramp increase in mean annual air temperature of 0.47°C/decade with most of the warming applied during the winter and spring months.

The resultant climatic design input is shown in Figure 7. The analyses and design were carried out in early 2001 using the best available information at that time. It is used here to illustrate a process rather than quantify climatic design parameters for the community of Inuvik. If the work were undertaken today, the most current data would be used. Figure 7 also shows mean annual air temperatures recorded in Inuvik since the design and construction was completed. The limited data suggests that with some excursions, the climate continues to warm following a near linear relationship that fits the extrapolated best fit line for the entire 50 year data set. That line falls slightly above and is parallel to the values chosen for design.

The ground temperatures below the warm crawl space under the structure have been monitored. Initial ground temperatures at a depth of 5 m were in the range of -2.6°C to -3.7°C and were predicted to rise slowly to -2.2°C over the thirty year term. Post-construction ground temperatures are reported elsewhere in these proceedings by Holubec et al, 2008. Performance has been better than design predictions for the first seven years of operation as the ground has been cooled by the thermosyphon system. There have been no movements reported for the foundations, although some water has migrated into the crawl space forming ice mounds under the insulation, and there has been some distress in the thermosyphon pipe attributed to manufacturing defects that are unrelated to the system design.

Reclamation of arctic military sites

Reclamation of decommissioned military defense sites across North America has been ongoing for the past twelve years. The most active program in Canada has been the Distant Early Warning (DEW) line of radar surveillance camps that stretched along the high arctic coastline from Baffin Island to Alaska. The sites typically lie about 69 degrees North Latitude where mean annual air temperatures range from -9°C to -15°C and corresponding ground temperatures range from -5°C to -12°C. The reclamation process often requires construction of secure landfills where contaminated soil is encapsulated in geomembrane liners and permafrost soils.

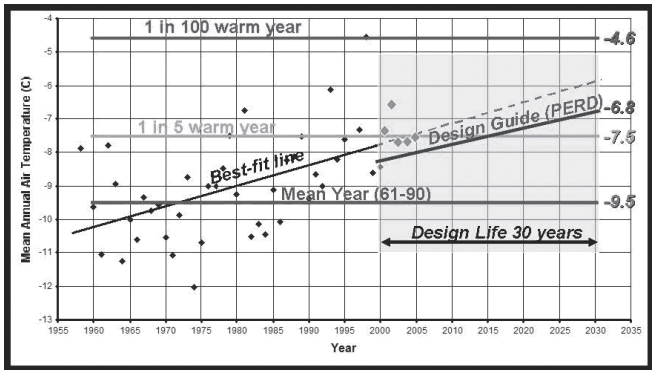

Figure 7. Mean annual air temperatures in Inuvik.

Unlike the Inuvik Hospital, these waste containment structures do not have a defined life but must function in perpetuity at a level of environmental risk that is acceptable to aboriginal people who use the nearby land for subsistence. Regulatory processes in the arctic require detailed technical review of all designs and consultation to ensure that best management practices are followed. Climatic uncertainty is therefore an important component in the design of waste containment structures that interface with permafrost. Stringent requirements must be met to achieve approvals.

A typical design developed jointly by EBA Engineering Consultants Ltd. (EBA) and UMA Engineering Ltd. for containment of contaminated soil is shown in Figure 8. The first defence against loss of contaminated pore fluid is a geomembrane liner. The second line of defence is the underlying ice-saturated permafrost soil. A final soil cover is configured to retain the active layer within the cover.

The screening process identifies most of these remote sites as moderate permafrost sensitivity; however, failure consequences could range from minor to major, depending on proximity to sensitive receptors. The risk posed from climatic warming is that the active layer thickness will increase with time allowing thaw to penetrate into the waste. A hypothetical worst-case failure mode could see the permafrost slopes supporting the liner thaw and slump,

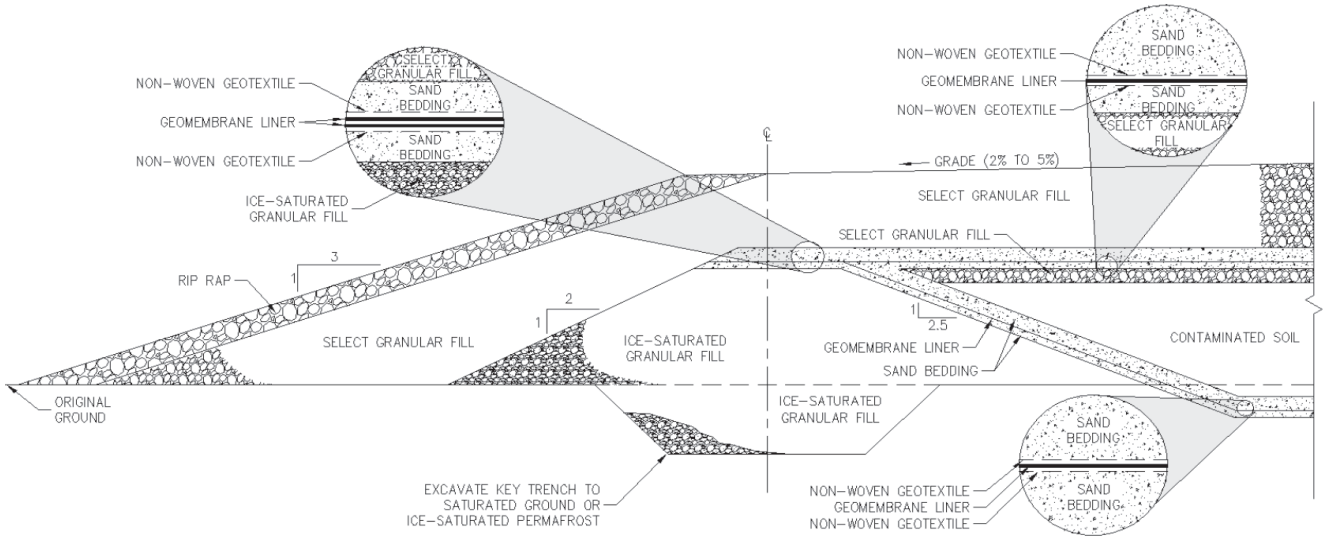

Figure 8. Design of soil containment landfill.

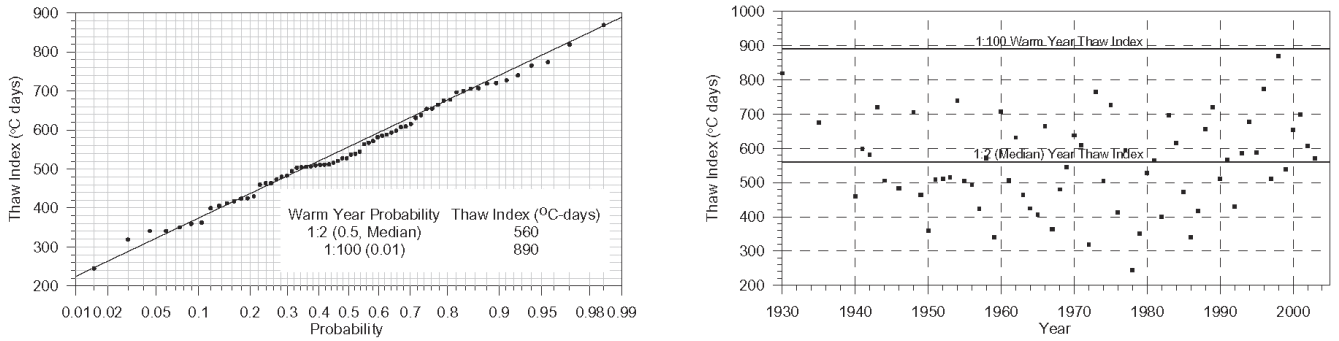

Figure 9. Historical thaw index probability.

resulting in failure of both the primary and secondary containment.

Geothermal analyses are required to substantiate the use of permafrost as a containment system for the landfills. Analyses are carried out to predict the short-term and long-term ground temperatures to determine the following:

- Length of time for landfill freezeback;
- Short-term thermal regime in the landfill;
- Long term thermal regime including an estimated amount of climate change; and
- Depth of annual thaw (active layer) in the cover material.

Geothermal analyses are carried out for each landfill using GEOTHERM, which is a proprietary two-dimensional finite element computer model developed by EBA. The model simulates transient, two-dimensional heat conduction with a change of phase for a variety of boundary conditions. The heat exchange at the ground surface is modelled with an energy balance equation considering air temperatures, wind velocity, snow depth, and solar radiation. The thermal analysis is calibrated to measured temperatures and/or observed active layers thicknesses.

Climatic data required for the thermal model include monthly mean air temperature, wind speed, solar radiation, and snow cover. Weather stations were maintained at the sites; therefore, climatic records dating back to the mid-1950s are available. The landfills are designed for mean conditions, warm conditions and long-term climate change.

Statistical analyses are carried out to determine mean monthly temperatures representative of a 1 in 100 warm year using the process described for the Inuvik Hospital. A historical thaw index probability analysis of a site is shown in Figure 9.

The influence of climate change on the landfill ground temperatures and active layer is evaluated by carrying out thermal analyses for a period of 100 years. The change in air temperature is estimated using a similar method, described in ACIA 2005. The air temperatures are estimated from Global Circulation Models, or GCMs. The GCMs are mathematical representations of the atmosphere, land surfaces, and oceans that have been developed to predict future climate behavior in response to changes in the composition of the atmosphere. Several scenarios have been developed to estimate the likely range of future emissions that may affect climate (IPCC 2000). Different GCMs have been developed, resulting in different degrees of projected climatic warming.

The outputs from various GCMs are posted on the web by the Canadian Climate Impact Scenario project (http://www.cics.uvic.ca/scenarios/index.cgi). Seasonal temperature changes are posted for the "B21 scenario" from four GCMs: a) CGCM2 (Canadian Centre for Climate Modelling and Analysis, Canada); b) GFDL-R30 (Geophysical Fluid Dynamics Laboratory, United States); c) ECHAM4 (Max-Planck Institute of Meteorology, Germany), and d) HadCM3 (Hadley Centre for Climate Prediction and Research, United Kingdom). Average seasonal changes in temperatures from the four GCMs for a central arctic site (69°N, 83°W) are listed in Table 1.

Table 1. Mean air temperature change (°C) over 110 years.

	December January February	March April May	June July August	September October November	Annual
Average of Four GCMs	6.4	4.2	3.8	5.1	4.9

Table 2. Predicted long-term maximum depth of thaw penetration into secure soil disposal landfills at a central arctic location.

Air Temperature Conditions	Predicted Active Layer Thickness (m)
After ten consecutive mean years	1.7
After one 1:100 warm year following ten mean years	2.2
After ten consecutive 1:100 warm years	2.4
After 100 years of global warming (average of four GCMs)	2.7
After 100 years of global warming plus one 1:100 warm year	3.3

The thermal analysis indicates that the permafrost remains during a 100-year period. The active layer depth continues to increase with time. Typical active layer thicknesses for a central arctic site are listed in Table 2 for the various climate conditions. The values are site specific. Thermal analysis are carried out for individual sites to take into account the local soil properties, ground temperatures, and climate.

The performance after 100 years becomes rather hypothetical because estimates of climate change scenarios seldom extend beyond 100 years. Longer term performance can only be bracketed by a range of climate potential climate extremes between 100 and 200 years. The project team has evaluated the following three alternatives:

- Air temperatures reach a stable condition and remain constant after 100 years;
- Warming rate continues on a linear ramp function similar the first 100 years; or
- Warming rate reduces to 50% of the 100 year warming rate.

Thermal analysis indicates that the permafrost at central arctic sites will be retained below a thickened active layer if the warming rate continues at a constant rate for a period of 200 years. The ground temperature warms at a rate similar to the air temperature at these sites. Degradation of the permafrost may begin to occur at sites that initially have warmer air and ground temperatures.

A failure modes effects analysis (FMEA) can be carried out to evaluate the effects climate change as well as other failure modes. Methods of FMEA are described by Nahir et al. 2005, and Roberson and Shaw, 2005. The FMEA considers the effects of retrogressive thaw of permafrost at a predicted rate on the performance of the landfill, including the potential for physical instability and contaminant flux out of the landfill. The potential consequences of these releases to the surrounding environment can then be considered.

The consequence of failure can be ranked as low,

minor, moderate, major or critical, relative to financial costs, ecosystem impact, and health and safety of the local population. Each proposed design must provide a balance between potential long term environmental impacts and legal obligations with the overall site remediation costs.

A geothermal design that includes a conservative climate change scenario coupled with an FMEA analysis will provide a basis for a rational decision on adoption of a landfill construction plan at a particular site.

Limitations and Conclusions

The screening process described in this paper has no official status as an adopted guideline in Canada. Nevertheless, it has received reasonable acceptance by Canadian regulators as an appropriate framework for identifying projects where climate change effects on permafrost can put the environment at risk. The study is now ten years old and has been tested with operating structures such as complex buildings, dams reliant on permafrost and industrial site reclamation. The process has been shown to add value to projects and streamline regulatory assessments. The inputs to the process must, however, evolve with time as scientific knowledge pertaining to the magnitude of warming trends matures.

The design engineer's toolbox comprises historical air temperature data and output from a range of GCMs that simulate hypothetical changes to the composition of the atmosphere. The application of these parameters as inputs to engineering analyses must be kept in perspective with the risks involved. Straight line extrapolation of historic air temperature data is not realistic beyond a thirty-year climate normal period and should never be used beyond the length of the period of record.

The failure of GCMs to predict current climate on a regional scale is a significant drawback to the use of these models for engineering analyses. All numerical models used by design engineers must be rationalized at the input stage by calibration to existing known conditions. The failure of many models to calibrate effectively sheds doubt on their use as predictive tools. At the current time, a practical option is to establish initial conditions at remote sites from limited site data and use the future trends predicted by GCMs with appropriate judgement.

It becomes a design engineer's unprecedented challenge to look more than 100 years into the future to establish climate change trends. Science seldom provides projections deep into the next century, and linear extrapolation from current conditions into that grey zone can have a serious adverse effect on decision-making for arctic resource development. Those projects must be based on best practices for risk assessment. That requires a coupling of appropriate ground thermal analyses with failure modes and effects analyses. We must always be prepared to weigh the consequences of a long term retrogressive system failure against general landscape degradation that could accompany many of the worst-case climate change scenarios that are currently being contemplated.

References

ACIA, 2005. *Arctic Climate Impact Assessment*. Cambridge University Press, 1042 pp.

Etkin, D. 1998. *Climate Change Impacts on Permafrost Engineering Design,* funded by Panel on Energy Research and Development Canada, Environment Canada, 42 pp.

Haynes, F.D. & Zarling, J.P. 1988. Heat transfer performance of commercial thermosyphons with inclined evaporator sections. *Proceedings of the Seventh International Conference on Offshore Mechanics and Arctic Engineering,* Vol. IV, 275-280.

Hwang, C.T. 1976. Predictions and Observations of the Behavior of a Warm Pipeline on Permafrost. *Canadian Geotechnical Journal,* Vol. 13. No. 4, pp. 452-480.

IPCC 2000. *Emissions Scenarios: A Special Report of the Intergovernmental Panel on Climate Change Working Group III.* Nebojsa Hakicenovic & Rob Swart (eds.). Cambridge, UK: Cambridge University Press, 570 pp.

Nahir, M., van Aanhout, M. & Reineche S., 2005. Application of Risk Management to Northern Affairs Program (NAP) Contaminated Sites in the North. Assessment and Remediation of Contaminated Sites in Arctic and Cold Climates, 189-198.

Philainen, J.A. 1959. Pile Construction in Permafrost. ASCE, *J. Soil Mechanics* Foundation Division., Vol. 85, No. SM6, Part I, 75-95.

Robertson, A. & Shaw, S. 2005. Enviromine. Failure Modes & Effects Analysis (FMEA). Ed. Shannon Shaw <http://robersongeoconsultants.com/rgc_enviromine/Issues/cls_FMEA.asp>

Terrestrial Carbon Dynamics Along a Permafrost-Dominated North-South Transect in the Tibetan Plateau

Jicheng He
Institute of Tibetan Plateau Research, Chinese Academy of Sciences, Beijing, P. R. China
Department of Earth & Atmospheric Sciences and Department of Agronomy, Purdue University, West Lafayette, Indiana
Qianlai Zhuang
Department of Earth & Atmospheric Sciences and Department of Agronomy, Purdue University, West Lafayette, Indiana
Tianxiang Luo
Institute of Tibetan Plateau Research, Chinese Academy of Sciences, Beijing, P. R. China

Abstract

We selected a north-south transect in the Tibetan Plateau, comprised of six alpine tundra ecosystems underlain with permafrost, to examine the terrestrial carbon dynamics with the Terrestrial Ecosystem Model (TEM) for the period from 1967 to 2000. We find that the ecosystems act as a carbon small source in the most northern site, Wudaoliang (-0.87 g C m^{-2} a^{-1}), while the other five sites act as a carbon sink at 0.31, 2.49, 5.19, 5.35, and 4.21 g C m^{-2} a^{-1} at Naqu, Tuotuohe, Anduo, Dangxiong, and Gandansi, respectively. From north to south, the number of months with carbon sink increases along the temperature and precipitation gradient. Due to warmer and wetter soil conditions, all sites in the transect acted as a carbon sink in the 1990s. The future warming climate may enhance ecosystem carbon sequestration due to increase of soil temperature and moisture associated with permafrost thawing in the Tibetan Plateau.

Keywords: net ecosystem production; permafrost; Tibetan Plateau; transect.

Introduction

The Tibetan Plateau, the largest geomorphologic unit on the Eurasian continent, almost covers an area of 2.6 million km^2, with an average altitude more than 4000 m above sea level, and accounts for 26.8% of China's landmass (Zhang et al. 2002). From the southeast to northwest, supplies of heat and water decrease gradually, and forest, meadow, steppe, and desert ecosystems are developed (Zheng 1996). Meanwhile, there exists the largest area of mountainous permafrost worldwide with an area of 1.5 million km^2 in the plateau. Climatic warming on the plateau in past decades has been evident from meteorological observation and ice core records (Liu & Chen 2000, Thompson et al. 2000). It has been shown that the annual mean temperature of the Tibetan Plateau has risen at a rate of 0.26°C per decade in the last 40 years, which was much higher than those of whole china and the world (Du 2001); the winter temperature rose about 0.32°C per decade from 1955 to 1996 (Liu & Chen 2000). Consequently, the region experienced widespread permafrost degradation, and the thickness of the active layer has increased in the last few decades. Future warming will likely result in an even more extensive and rapid permafrost degradation in the region. Thus, the knowledge of ecosystem responses to the changes of permafrost and active layer depths in the past will help understand the contribution of regional carbon dynamics to global carbon cycling. However, few studies have been conducted to quantify the inter-annual variations and changing trend in carbon fluxes for the terrestrial ecosystems in the plateau. On the plateau, heat and moisture increase gradually from north to south, and these gradients provide a good opportunity to examine the variation pattern of net ecosystem production (NEP) during the past decades. In this study, we select a north-south transect in the permafrost region in the plateau, including six field sites dominated by alpine tundra (Wudaoliang, Tuotuohe, Anduo, Naqu, Dangxiong, and Gandansi) to examine the terrestrial carbon dynamics during the past few decades with the Terrestrial Ecosystem Model (TEM), which is coupled with a permafrost model (Zhuang et al. 2001, 2002, 2003). Our aims are (1) to explore whether the terrestrial ecosystems in the permafrost region are sequestering or releasing carbon, (2) to examine the temporal trends of NEP for each site along the transect and their relations with soil temperature and moisture, and (3) to provide information for simulating the response of alpine tundra ecosystems to projected climate variability across the range of permafrost region on the plateau.

Methods

Data preparation

The six sites with high altitudes are located in plateau permafrost region (Fig. 1) with heat-moisture gradients from north to south (Table 1). To drive the TEM, the monthly temperature and precipitation data for each site are calculated from the nearest meteorological station. Considering the elevation differences between the field site and the nearest meteorological station site, we have recalculated the monthly temperature using the month-specific elevation lapse rate of temperature (Fang 1992). As for precipitation, we haven't done any recalculations and used meteorological data directly. The cloudiness data are extracted from the gridded data of the Climatic Research Unit, University of

Table 1. Locations and climatic, soil and vegetation characteristics for the six sites along the north-south transect in the plateau permafrost region.

	Longitude	Latitude	Altitude (m)	Annual temperature (°C)	Annual precipitation (mm)	Soil texture (sand:silt:clay)	Vegetation type
Wudaoliang	93.07°E	35.22°N	4,626	-5.4	273.1	91:6:3	Alpine needlegrass steppe
Tuotuohe	92.55°E	34.31°N	4,582	-4.2	273.4	97:2:1	Alpine needlegrass steppe
Anduo	91.81°E	32.46°N	4,871	-2.9	434.1	91:2:7	Alpine needlegrass steppe
Naqu	91.93°E	31.57°N	4,636	-1.3	429.8	62:28:10	Alpine kobresia meadow
Dangxiong	91.15°E	30.50°N	4,288	1.6	460.9	53:32:15	Alpine kobresia meadow
Gandansi	91.49°E	29.75°N	4,100	6.3	421.8	49:36:15	Alpine kobresia meadow

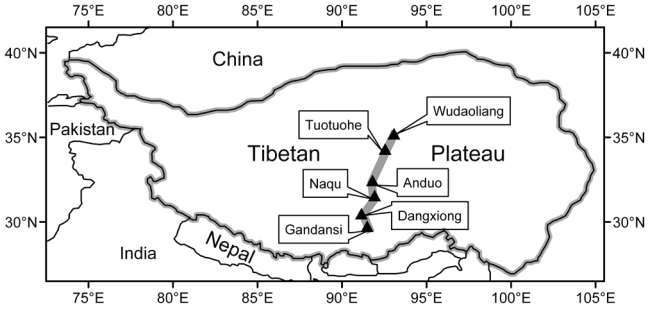

Figure 1. Locations of the north-south transect and field sites in the plateau permafrost region.

Norwich, U.K. (http://www.cru.uea.ac.uk/) based on the sites' geographic location. To parameterize model TEM, we have measured the net primary production (NPP), C in vegetation and soil, total N in vegetation and soil, and soil texture at Wudaoliang site (Luo et al., 2002a, b, 2004). We use the annual atmospheric CO_2 concentration data from Mauna Loa station (Keeling & Whorf 2005).

Model parameterization and simulations

As a process-based ecosystem model, the terrestrial ecosystem model (TEM) uses spatially referenced information on climate, elevation, soils, and vegetation to estimate the spatial and temporal distribution of major carbon and nitrogen fluxes and pool sizes at continental scales, and can be used to describe mechanistic processes of ecosystem carbon and nitrogen cycle and their dynamic responses to changes in environmental conditions. It was first applied to estimate the NPP of potential vegetation in South America (Raich et al. 1991) and then widely used in evaluating responses of terrestrial ecosystems to historical and projected changes in atmospheric CO_2 and climate for different spatial scales (Kicklighter et al. 1999, Tian et al. 2000, Schimel et al. 2000, Clein et al. 2000, McGuire et al. 2000, Clein et al. 2002), and modeling the carbon dynamics and emission of greenhouse gas in Alaska tundra ecosystems (Zhuang et al. 2007). In this study, we use version 5.0 of the model to quantify carbon dynamics for each field site along the north-south transect on the plateau permafrost region. We first parameterize TEM with the observations of vegetation and soil carbon and nitrogen and NPP for the alpine tundra ecosystem. The specific data used to parameterize the model

Table 2. Values and sources for estimated pools and fluxes used to parameterize the model for alpine tundra at Wudaoliang in the north-south transect. 93.1°E, 35.2°N. Elevation 4626 m.

Variable	Value*	Source and comments
C_v	347.5	Measured.
N_v	9.73	Measured.
C_s	2892	See Luo et al. (2004).
N_s	353	See Luo et al. (2004).
N_{av}	1.8	Based on 0.86%, the averaged N_{av}:N_s ratio from Wang et al. (2000) , Wang et al. (2006), Bai et al. (1999) and measured data of two Chinese Ecological Research Network's field stations.
GPP	233	Based on the NPP:GPP ratio in Table A1 by McGuire et al.(1992).
NPP	59.5	See Luo et al. (2004).
NPPSAT	119	Based on the NPP:NPPSAT ratio in Table A1 by McGuire et al.(1992).
NUPTAKE	1.24	Calculated from NPP_n, 75%NPP_n=NUPTAKE.

*Units for annual gross primary production (GPP), net primary production (NPP), and NPPSAT are g C $m^{-2}a^{-1}$. Units for annual N uptake by vegetation are g N $m^{-2}a^{-1}$. Units for vegetation carbon (C_v) and soil carbon (C_s) are g C m^{-2}. Units for vegetation nitrogen (N_v), soil N (N_s), and inorganic N (N_{av}) are g N m^{-2}.

are described in Table 2. The tundra parameterization of soil thermal dynamics in Alaska from our previous study is used for alpine tundra ecosystems in this study (Zhuang et al. 2003). The parameterization of carbon is verified with the observed data of NPP. Third, we simulate the monthly NEP from 1967 to 2000 for those six sites. Finally, we analyze the relationships between NEP, annual air temperature and precipitation, the averaged soil temperature in top 20 cm depth, and soil moisture.

Results

Temporal variation in simulated NEP

From 1967 to 2000, simulated annual NEP for Wuadaoliang, Tuotuohe, and Dangxiong decreased from -1.5, -11.3, and 13.2 to -3.3, -18.3, and 5.1 $g.C.m^{-2}.a^{-1}$, respectively. In contrast, annual NEP for Anduo and Gandansi increased from 3.3 and -10.2 to 30.9 and 16.4 $g.C.m^{-2}.a^{-1}$, respectively

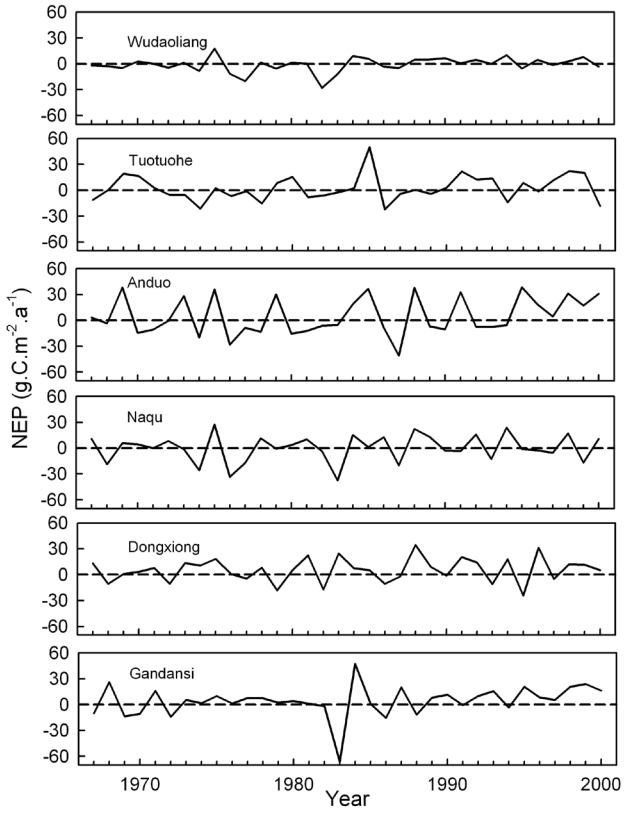

Figure 2. Changes in net ecosystem production (NEP) for the six sites along the north-south transect as simulated by the Terrestrial Ecosystem Model (TEM) during the period from 1967 through 2000.

(Fig. 2). During the past three decades, simulated NEP at the six sites differs in variation pattern, with small interannual variations in Wudaoliang and large variations in Anduo and Gandansi. The terrestrial ecosystem in Wudaoliang is a very weak carbon source with the average value of -0.87 g.C.m^{-2}.a^{-1}, while the terrestrial ecosystem in Naqu acts as a very weak sink with the value of 0.31 g.C.m^{-2}.a^{-1}. From north to south along the transect the terrestrial ecosystems in other the four sites are carbon sinks with values of 2.49, 5.19, 5.35 and 4.21 g.C.m^{-2}.a^{-1} in Tuotuohe, Anduo, Dangxiong and Gandansi, respectively.

Monthly variation in NEP

We calculate the mean monthly NEP from 1990–2000 and compare the seasonal variation patterns in NEP among the six sites (Fig. 3). From January to May, most sites along the transect act as a carbon source, except that Dangxiong and Gandansi are weak sinks in May with the values of 1.37 and 0.26 g.C.m^{-2}.month^{-1}, respectively. The NEP for all sites has switched from a net source to a net sink in June except for Tuotuohe. In October, the NEP for all sites has switched from a net sink to a net source except that Gandansi acts as a sink with the value of 5.99 g.C.m^{-2}.month^{-1}. From north to south along the transect, the number of months with carbon sink increased gradually from three months in Wudaoliang (from June through August) and Tuotuohe (from July through September), four months in Anduo and Naqu (from

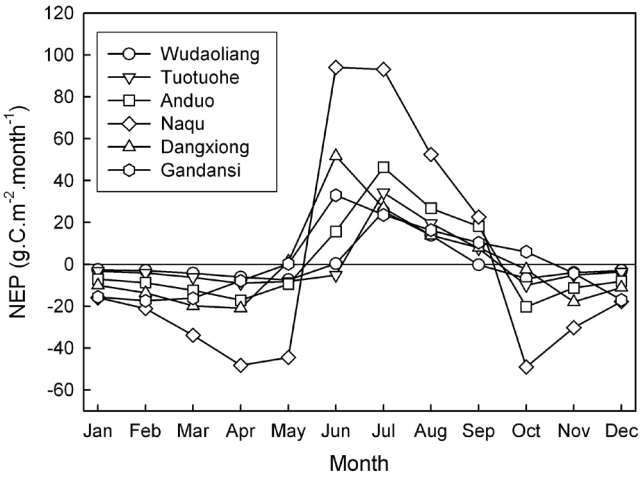

Figure 3. Mean monthly NEP values for the six sites along the north-south transect as simulated by the Terrestrial Ecosystem Model (TEM) during the period from 1990 through 2000.

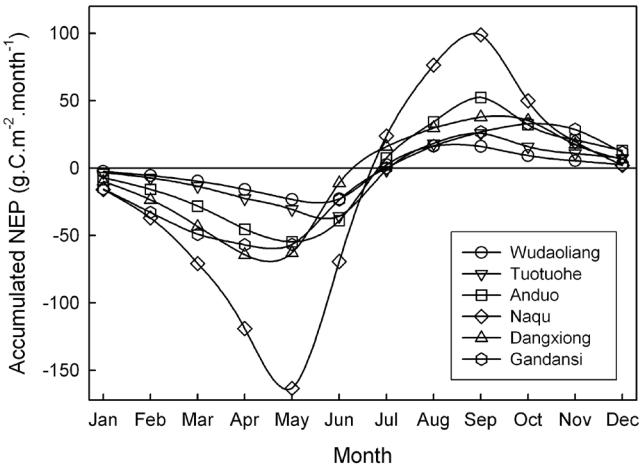

Figure 4. Accumulated mean monthly NEP values for the six sites along the north-south transect as simulated by the Terrestrial Ecosystem Model (TEM) during the period from 1990 through 2000.

June through September), five months in Dangxiong (from May through September), to six months in Gandansi (from May through October) due to water-heat increase trend from north to south along the transect. The mean NEP in months with sink increases from 13.18 g.C.m^{-2}.month^{-1} in Wudaoliang to 65.59 g.C.m^{-2}.month^{-1} in Naqu and then decreases to 14.97 g.C.m^{-2}.month^{-1} in Gandansi. For the inter-annual variation pattern, the estimates of monthly NEP for Naqu vary between -49.02 g.C.m^{-2}.month^{-1} in October and 94.13 g.C.m^{-2}.month^{-1} in June, and demonstrate considerably more variation than for other five sites. As for the inter-annual variation in accumulated NEP values (Fig. 4), the alpine tundra ecosystem in all sites has offset the amount of carbon released to atmosphere and sequestered carbon from atmosphere in July except for Tuotuohe, which begin to store carbon in ecosystem until August. In all sites, the ecosystem sequestering carbon activities occurred first in Dangxiong (Fig. 4). Similar to the intra-annual variation pattern in monthly NEP, the accumulated monthly NEP for

Table 3. The correlations between NEP and climatic factors in six sites along the north-south transect during 1967–2000.

	WDL	TTH	AD	NQ	DX	GDS
Air T	0.23	-0.21	0.20	0.08	0.05	0.34*
Air P	-0.03	0.15	-0.05	-0.16	0.13	0.49**
Soil T	0.24	-0.23	0.17	0.09	0.10	0.32
Soil M	-0.20	-0.54**	-0.52**	-0.26	0.14	0.23
Air $T_{5\text{-}9}$	0.35*	0.04	0.43*	0.37*	-0.07	-0.17
Air $P_{5\text{-}9}$	-0.01	0.04	-0.07	-0.17	0.15	0.49**
Soil $T_{5\text{-}9}$	0.47**	0.04	0.61**	0.35*	-0.04	-0.13
Soil $M_{5\text{-}9}$	-0.15	-0.30	-0.47**	-0.24	0.20	0.37*

WDL: Wudaoliang; TTH: Tuotuohe; AD: Anduo; NQ: Naqu; DX: Dangxiong; GDS: Gandansi; Air T: annual mean air temperature; Air P: total annual precipitation; Soil T (M): annual soil temperature (moisture) within 20 cm soil depth; Air $T_{5\text{-}9}$: mean temperature from May through September; Air $P_{5\text{-}9}$: total precipitation from May through September; Soil $T_{5\text{-}9}$ ($M_{5\text{-}9}$): mean soil temperature (moisture) within 20 cm soil depth from May through September; *indicates $p<0.05$, ** indicates $p<0.01$.

Naqu also shows considerably more variation than for the other five sites.

Temporal responses of NEP to climate

There are different temporal responses of NEP to temperature, precipitation, soil temperature, and moisture among the six sites. In general, climate in growing season (from May to September) plays a more important role than annual climate in affecting NEP in alpine tundra ecosystems (Table 3). For trends in annual climate during the past three decades (Table 3), simulated annual NEP and annual soil temperature within 20 cm depth are uncorrelated across six sites, and meanwhile simulated annual NEP and annual temperature and precipitation are also uncorrelated for all sites except for Gandansi. NEP trends are negatively correlated with annual soil moisture in Tuotuohe and Anduo. As for the relationships between NEP and climate in growing season (Table 3), estimates of annual NEP are positively correlated with the mean air temperature and soil temperature from May through September for Wudaoliang, Anduo, and Naqu. Mean soil moisture from May through September is negatively correlated with NEP for Anduo and positively with NEP in Gandansi. From the 1970s to the 1990s, mean temperature in growing season increased for all six sites (Fig. 5). In comparison to the 1970s, precipitation in growing season increased in the 1990s for all sites except for Tuotuohe in which the precipitation decreased by 36.32 mm. When both temperature and precipitation are considered, during the growing season five sites experienced warmer and wetter conditions over the three decades, and only one site (Tuotuohe) became warmer and drier (Fig. 5). In response to climatic change, NEP increased for all sites during the past three decades (Fig. 5). In the 70's, only two sites (Dangxiong and Gandansi) acted as a carbon sink, three sites (Tuotuohe, Naqu, and Dangxiong) became carbon sink in the 1980s, and all sites became carbon sink in the 1990s with the highest decadal NEP value of 11.20 in Gandansi.

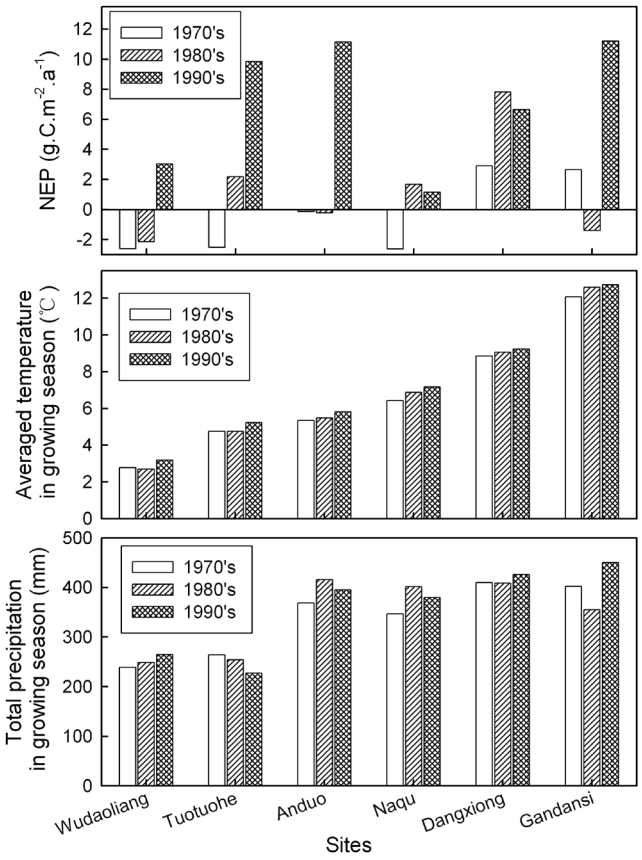

Figure 5. Mean NEP, averaged temperature and precipitation in growing season (May–September) in the 1970s, the 1980s and the 1990s for the six sites along the north-south transect.

Discussion

Using the TEM, we evaluate the NEP variation patterns in six sites dominated by alpine tundra in Tibetan permafrost region during the period from 1967 to 2000. Our results indicate that the alpine tundra ecosystems in the permafrost region mostly act as a carbon sink over the last three decades, which is consistent with the finding based on carbon flux measurements (Xu et al. 2005a, b, Zhao et al. 2005) and static closed chamber measurement data (Zhang et al. 2005) in other sites on the Tibetan plateau.

In the alpine shrub tundra ecosystem in Haibei of northeastern Tibetan plateau (101°19′E, 37°37′N, 3200 m), CO_2 flux observation data show that net CO_2 influx occurred from June to September, and net CO_2 efflux occurred from January to May and October to December with peak influx in August and peak efflux in April (Xu et al. 2005a, b). Our simulated NEP values show similar monthly variation pattern as that in Haibei. In our results, most sites along the transect acted as a carbon sink from June to September and had the lowest NEP in April and the highest NEP in June or July (Fig. 3). In comparison to the observation data in Haibei, our simulated mean NEP values during the 1990s for all sites, varying between 3.03 and 11.2 $g.C.m^{-2}.a^{-1}$ (Fig. 5), were less than 61.91 $g.C.m^{-2}.a^{-1}$ for alpine shrub ecosystem

(Xu et al. 2005a, b) and 76.91 g.C.m^{-2}.a^{-1} for alpine meadow ecosystem, close to 14.45 g.C.m^{-2}.a^{-1} for alpine shrub meadow ecosystem, and much higher than -130.36 g.C.m^{-2}.a^{-1} for alpine swamp meadow ecosystem (Zhao et al. 2005) in Haibei. These differences in NEP values may be due to higher altitude, lower temperature, shorter growth period, and different plant species in the transect. Our simulated mean NEP during the 1990s is also less than the value of 71.12 g.C.m^{-2}.a^{-1} for alpine grassland ecosystem, calculated from the empirical model between CO_2 emission amount and soil surface temperature in Pangkog (90.01°E, 31.23°N, 4800 m) on the Tibetan plateau (Zhang et al. 2005). This difference suggests that spatial variability in climate, soil, and vegetation is important in determining patterns of ecosystem NEP. Compared to the arctic tundra ecosystem, our estimates of mean NEP during the 1990s for Tuotuohe (9.85 g.C.m^{-2}.a^{-1}), Anduo (11.14 g.C.m^{-2}.a^{-1}), and Gandansi (11.20 g.C.m^{-2}.a^{-1}) are very close to the mean annual NEP of Pan-Artic (10 g.C.m^{-2}.a^{-1}) and substantially less than the value for moisture tundra in the Kuparuk River Basin, which fluctuated around 25 g.C.m^{-2}.a^{-1} (McGuire et al. 2000).

In the Pan-Arctic, simulated NEP in moisture tundra is more correlated with soil moisture than with air temperature (McGuire et al. 2000), and the same relationships are also found in Tuotuohe and Anduo in our study. For tundra in northwestern Alaska, NEP trends during 1981–2000 are negatively correlated with air temperature trends and positively correlated with precipitation trends (Thompson et al. 2005). In contrast, we didn't find the same correlations in this research. The results from Thompson et al. (2005) indicated that NEP for tundra in northwestern Alaska decreased in warmer and drier conditions or warmer and wetter conditions while in colder and wetter conditions, NEP would increase. In this study, the alpine tundra ecosystems in five sites experienced warmer and wetter conditions over the three decades and one (Tuotuohe) experienced warmer and drier conditions (Fig. 5). However, in comparison to the values in the 1970s, NEP increased for all sites during the past three decades (Fig. 5). Contrary to the results of Thompson et al. (2005), our study indicates that the warmer climate states result in increases in NEP, rather than decreases. Future warming will result in an even more extensive and rapid permafrost degradation in the permafrost region. The warmer and wetter condition in the Tibetan Plateau will likely enhance its carbon sequestration in the terrestrial ecosystems.

Conclusion

In this study, we evaluate the terrestrial carbon dynamics for six sites in permafrost region from 1967 to 2000 with the biogeochemistry TEM. We find that the alpine tundra ecosystems in most sites act as a carbon sink varying between 5.35 g.C.m^{-2}.a^{-1} in Dangxiong and 0.31 g.C.m^{-2}.a^{-1} in Naqu during the past three decades. As for the seasonal variation patterns in NEP among the six sites, from January to May, most sites along the transect act as a carbon source. The NEP for all sites switches from a net source to a net sink in June except for Tuotuohe. In October, the NEP for all sites switches from a net sink to a net source except for Gandansi. Moreover, there are different temporal responses of NEP to changes of air temperature, precipitation, soil temperature, and moisture among the six sites. Generally, climate in the growing season (from May to September) plays a more important role than annual climate in affecting NEP in alpine tundra ecosystems. In comparison to the 1970s, precipitation in the growing season increases in the 1990s for all sites except for Tuotuohe. So the alpine tundra ecosystems in five sites experienced warmer and wetter conditions over three decades, and one site (Tuotuohe) experienced warmer and drier conditions. In response to climatic change, NEP increased at all sites during the three decades. In the 1970s, only two sites (Dangxiong and Gandansi) acted as carbon sinks, three sites (Tuotuohe, Naqu and Dangxiong) became carbon sinks in the 1980s. All sites became carbon sinks in the 1990s. Our analysis suggests that the changes of soil temperature and moisture conditions due to changes in permafrost conditions have significant effects on terrestrial ecosystem carbon dynamics. The future quantification of carbon budget in the Tibetan Plateau should consider the NEP spatial variability induced by changes of soil temperature and moisture associated with permafrost dynamics.

Acknowledgments

This research was supported by K.C. Wong Education Foundation, Hong Kong.

References

Bai, K., Han, J. & Wang, P. 1999. The distribution and growing seasonal dynamics of soil nitrogen fractions on Russian wild rye grass pasture under different grazing intensities (in Chinese). *Acta Agrestia Sinica* 7: 308-318.

Clein, J.S., Kwiatkowski, B.L. & McGuire, A.D. 2000. Modeling carbon responses of tundra ecosystems to historical and projected climate: a comparison of a fine- and coarse-scale ecosystem model for identification of process-based uncertainties. *Global Change Biology* 6 (suppl. 1): 127-140.

Clein, J.S., McGuire, A.D. & Zhang, X. 2002. Historical and projected carbon balance of mature black spruce ecosystems across North America: the role of carbon-nitrogen interactions. *Plant and Soil* 242: 15-32.

Du, J. 2000. Change of temperature in Tibetan Plateau from 1961 to 2000 (in Chinese). *Acta Geographica Sinica* 56(6): 682-690.

Fang, J. 1992. Study on the geographic elements affecting temperature distribution in China. *Acta Ecologica Sinica* 12(2): 97-104.

Keeling, C.D. & Whorf, T.P. 2005. Atmospheric CO_2 records from sites in the SIO air sampling network. In *Trends: A Compendium of Data on Global Change.* Carbon Dioxide Information Analysis Center, Oak Ridge National Laboratory, U.S. Department of Energy, Oak Ridge, Tenn., U.S.A.

Kicklighter, D.W., Bruno, M. & Doenges, S. 1999. A first order analysis of the potential role of CO_2 fertilization to affect the global carbon budget: a comparison of four terrestrial biosphere models. *Tellus* 51B: 343-366.

Liu, X. & Chen, B. 2000. Climatic warming in the Tibetan Plateau during recent decades. *International Journal of Climatology* 20: 1729-1742.

Luo, T., Li, W. & Zhu, H. 2002b. Estimated biomass and productivity of natural vegetation on the Tibetan Plateau. *Ecological Applications* 12: 980-997.

Luo, T., Pan, Y. & Ouyang, H. 2004. Leaf area index and net primary productivity along subtropical to alpine gradients in the Tibetan Plateau. *Global Ecology and Biogeography* 13: 345-358.

Luo, T., Shi, P. & Luo, J. 2002a. Distribution patterns of aboveground biomass in Tibetan alpine vegetation transects. *Acta Phytoecologica Sinica* 26(6): 668-676.

McGuire, A.D., Clein, J.S. & Melillo, J.M. 2000. Modeling carbon responses of tundra ecosystems to historical and projected climate: sensitivity of pan-arctic carbon storage to temporal and spatial variation in climate. *Global Change Biology* 6 (suppl. 1): 141-159.

McGuire, A.D., Melillo, J.M. & Joyce, L.A. 1992. Interactions between carbon and nitrogen dynamics in estimating net primary productivity for potential vegetation in North America. *Global Biogeochemical Cycles* 6(2): 101-124.

Raich, J.W., Rastetter, E.B. & Melillo, J.M. 1991. Potential net primary productivity in South America: application of a global model. *Ecological Applications* 1(4): 399-429.

Schimel, D., Melillo, J.M. & Tian, H. 2000. Carbon storage by the natural and agricultural ecosystems of the US (1980–1993). *Science* 287: 2004-2006.

Thompson, C.C., McGuire, A.D. & Clein, J.S. 2005. Net carbon exchange across the arctic tundra-boreal forest transition in Alaska 1981-2000. *Mitigation and Adaptation Strategies for Global Change* 11: 805-827.

Thompson, L.G., Yao, T. & Mosley-Thompson, E. 2000. A high-resolution millennial record of the South Asian monsoon from Himalayan ice cores. *Science* 289: 1916-1919.

Tian, H., Melillo, J.M. & Kicklighter, D.W. 2000. Climatic and biotic controls on interannual variations of carbon storage in undisturbed ecosystems of the Amazon Basin. *Global Ecology and Biogeography* 9: 315-336.

Wang, C., Wan, S. & Xing, X. 2006. Temperature and soil moisture interactively affected soil net N mineralization in temperate grassland in Northern China. *Soil Biology & Biochemistry* 38: 1101-1110.

Wang, Q., Li, L. & Bai, Y. 2000. Field experimental studies on the effects of climate change on nitrogen mineralization of meadow steppe soil (in Chinese). *Acta Phytoecologica Sinica* 24: 687-692.

Xu, S., Zhao, X. & Fu, Y. 2005a. Characterizing CO_2 fluxes for growing and non-growing seasons in a shrub ecosystem on the Qinghai-Tibet plateau. *Science in China (series D)* 48 (supp. 1): 133-140.

Xu, S., Zhao, X. & Li, Y. 2005b. Diurnal and monthly variations of carbon dioxide flux in an alpine shrub on the Qinghai-Tibet plateau. *Chinese Science Bulletin* 50(6): 539-543.

Zhang, X., Shi, P. & Liu, Y. 2005. Experimental study on soil CO_2 emission in the alpine grassland ecosystem on Tibetan plateau. *Science in China (series D)* 48 (supp. 1): 218-224.

Zhang, Y., Li, B. & Zheng, D. 2002. A Discussion on the boundary and area of the Tibetan Plateau in China (in Chinese). *Geographical Research* 21(1): 1-8.

Zhao, L., Li, Y. & Zhao, X. 2005. Comparative study of the net exchange of CO_2 in 3 types of vegetation ecosystems on the Qinghai-Tibetan plateau. *Chinese Science Bulletin* 50(16): 1767-1774.

Zheng, D. 1996. The system of physico-geographical regions of the Qinghai-Xizang (Tibeta) Plateau. *Science in China* (Series D) 39(4): 410-417.

Zhuang, Q., Romanovsky, V.E. & McGuire, A.D. 2001. Incorporation of a permafrost model into a large-scale ecosystem model: Evaluation of temporal and spatial scaling issues in simulating soil thermal dynamics, *J. Geophys. Res*. 106(D24): 33,649-33,670.

Zhuang, Q., McGuire, A.D. & O'Neill, K.P. 2002. Modeling soil thermal and carbon dynamics of a fire chronosequence in interior Alaska. *Journal of Geophysical Research* 108: 8147, doi: 10.1029/2001JD001244.

Zhuang, Q., McGuire, A.D. & Melillo, J.M. 2003. Carbon cycling in extratropical terrestrial ecosystems of the Northern Hemisphere during the 20th century: a modeling analysis of the influences of soil thermal dynamics, *Tellus*, 55B: 751-776.

Zhuang, Q., Melillo, J.M. & McGuire, A.D. 2007. Net emissions of CH_4 and CO_2 in Alaska: implications for the region's greenhouse gas budget. *Ecological Applications* 17(1): 203-212.

Changes of Permafrost and the Cold-Region Environment in Northeastern China

Ruixia He, Huijun Jin, Lanzhi Lü, Shaopeng Yu, Shaoling Wang, Dongxin Guo
State Key Laboratory of Frozen Soils Engineering, Lanzhou, China 730000

Abstract

Extensive air-temperature inversions in the winter affect the development and distribution of permafrost in the Xing'anling Mountains, Northeastern China. Permafrost is thicker and colder in lower topographic positions. Wetlands and permafrost are interdependent. Permafrost conditions are closely related to surface coverage conditions. The cold-region environment has been greatly affected by climate warming and human activities during the past 50 years. Permafrost has been degrading as evidenced by the deepening active layer, thinning permafrost, rising ground temperatures, expanding taliks, disappearance of patches of permafrost, and the significant northward shift of the southern limit of permafrost. Under the projected climate warming, there would be significant degradation of permafrost and resultant environmental changes. In particular, degradation of permafrost would lead to land desertification on the Hulun Buir Plateau at the west flank of the Da Xing'anling Mountains and on the northern edge of the Songnen Plain, adversely affecting the regional sustainable development.

Keywords: assessment; cold-region environment; engineering projects; permafrost; urbanization; Xing'anling Mountains.

Introduction

Systematic geocryological studies in Northeastern China began in the early 1950s. Several important projects were conducted in the 1960s and 1970s, and the distribution and evolution of permafrost became better understood. In the 1970s, field expeditions, observations, and monitoring which focused on the development and distribution of permafrost, ground temperature, and ground ice were organized and sustained. The first map of permafrost (1: 3,000,000) was compiled based on engineering explorations, investigations, and climatic data (Guo et al. 1981, NECPRT 1983).

During the period from 1979 to 1980, the southern limit of permafrost was studied in detail through correlations of climatic variables and through field investigations along the delineated southern limit of permafrost from the correlations. From 1989 to 1992, the impact of forest fires on permafrost was observed and analyzed. The impact of climate warming on permafrost and its environmental effects also were investigated preliminarily. From 1990 to 2004, permafrost study was initialized to meet the needs for building civil infrastructures and because of increased environmental concerns. Since 2004, permafrost research has been re-activated by the Third-Term Knowledge Innovative Project of the Cold and Arid Regions Environmental and Engineering Research Institute, Chinese Academy of Sciences. The need for better understanding the frozen-ground conditions for the construction of the China-Russia crude-oil pipeline project from Skovorodino, Russia, via Mo'he, China, to Daqing, China, and the Mo'he Airport provided further incentive and funding for geocryology.

At present, the research mainly focuses on relationships among climatic and environmental changes in permafrost regions, interactions of permafrost, forested wetland and snow cover, and the changes of land use in the northern part of Northeastern China. This paper reviews the changes of permafrost and the cold-region environment in Northeastern China, in which the latest data obtained during the surveys and studies of permafrost conditions for the China-Russia Pipeline and Mo'he Airport projects, and field investigations on permafrost and periglacial phenomena in July–August 2007 are incorporated. It also includes the interactions between permafrost and human activities.

Although the degradation of permafrost in Northeastern China has been of considerable concern during recent decades, the research on the mechanisms and the processed-based modeling and prediction of permafrost degradation and its impacts on the cold-region environment are not well established. The Xing'anling Mountains contain the largest cluster of forests and wetlands and, consequently, the habitats and national reserves of many endangered species particularly sensitive to changes of permafrost, climate, and anthropogenic disturbances. Several national key construction projects, including the China–Russia crude-oil pipeline, Hei'he to Dalian Expressway, high-speed railway from Harbin to Dalian, require further investigations on frozen-ground engineering to provide a timely scientific base for frost hazard mitigation. Therefore, the studies on the degradation, mechanisms, trends, and environmental impacts of permafrost in the mountains under influences of climate warming and anthropogenic activities can provide scientific bases for regional environmental management and societal and economic development.

Study Region

Permafrost in Northeastern China is located on the eastern margin of the Eurasian Continent. The Xing'anling Mountains are located in the northern and western parts of Northeastern China (Fig. 1). The elevation of the Da Xing'anling Mountains ranges from 500 to 600 m in the northern section to 1,000 to 1,400 m in the middle section, and further to more than 2000 m in the southernmost section, with its highest peak (Huangganglian Mountains) at 2029

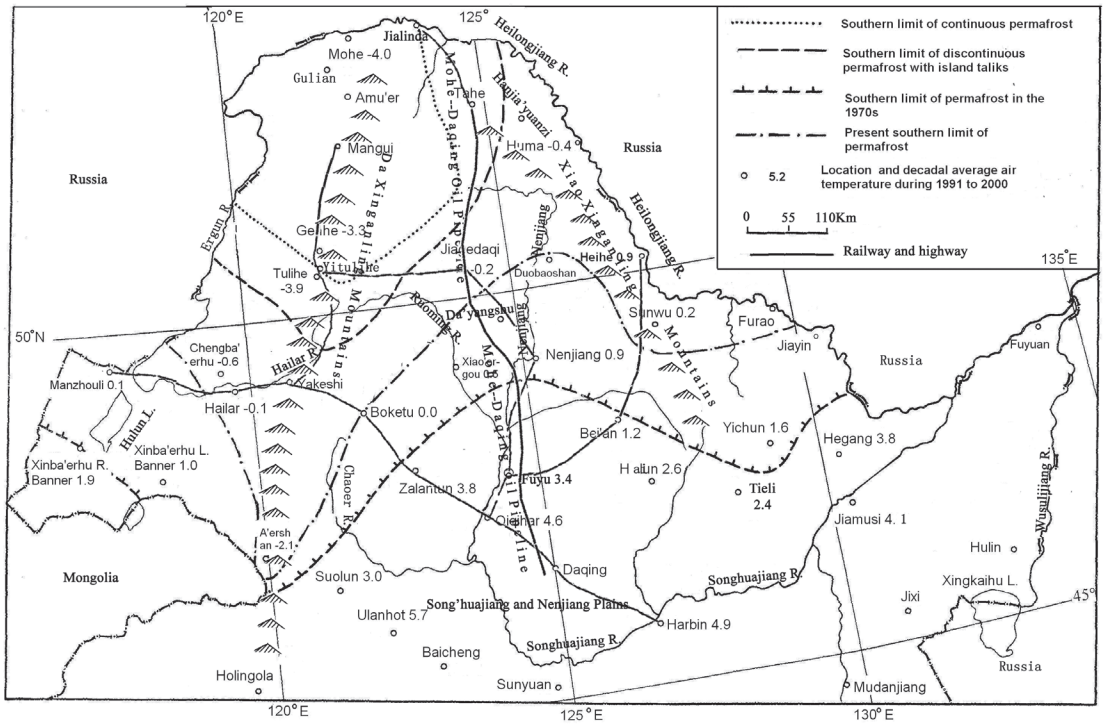

Figure 1. Study area map showing permafrost distribution and changes of the SLP in the Xing'anling (Hinggan) Mountains (revised from Jin et al. 2007a, with permission from the John Wiley & Sons, Ltd.).

m. In contrast, the Xiao Xing'anling Mountains are gentler in topography, with meandering river channels, elevations of 500 to 600 m, and few peaks higher than 800 m.

The mountains are comprised of Late Palaeozoic granites, and Cenozoic volcanic formations, with sporadic Paleozoic metamorphic and sedimentary rocks. Since the onset of the Quaternary, the mountains have been slowly and differentially uplifting, and have been subjected to long-term erosion and leveling. The slope deposits on the upper parts of the mountains are predominately angular gravel or sandy clay with gravel, generally only 1–2 m in thickness, and with a layer of humic topsoil 0.1–0.2 m in thickness. However, in piedmont areas, intermontane basins and valleys, deposits from debris flows, fluvial, and slope processes are as much as 10–15 m thick. In typical soil profiles, peat and humic soil are underlain by clayey sand and sandy clay with sand and gravel (Zhou et al. 2000).

The region is characterized by a temperate continental monsoonal climate with long, cold winters and short, hot summers. Mean annual air temperatures range from 0~+1°C in the south to -5~-6°C in the north. The average annual precipitation ranges from 500–700 mm in the southeast to less than 200 mm in the northwest. Rainfall in summers accounts for 80–90% of the annual precipitation. The Siberia high pressure in winter causes an extensive air temperature inversion which strongly affects the development and distribution of permafrost. A large part of the region is covered with dense forests, or shrubs, or wetlands.

The Hulun Buir Plateau is at the northwestern flank of the Da Xing'anling Mountains. It is gentler in topography with low relief and surrounded by hills. As a main body of the plateau, the Hailar platform is located in the central part. Loose Quaternary strata are widely distributed along the Hailar, Hui, and Wu'erxun Rivers. The upper part of soil profile is composed of silt and sand, generally its thickness varies from 20 to 50 m. The lower part consists of gravels, with thicknesses of 30–60 m. The landscape changes from forest to steppes to the west of the Yimin River.

Evidence of Permafrost Degradation

Although the features of permafrost are largely controlled by latitude, elevation, and longitude, they vary greatly within a relatively small area. The extensive air temperature inversion in winter greatly affects the development and distribution of permafrost. As a result, permafrost is thicker and colder in lower topographic positions than at higher elevations (Lu et al. 1981, Guo et al. 1981). Although the thickness of permafrost gradually increases northwards and northwestwards, it is further complicated by local geology, geography, snow cover, and vegetation. In addition, permafrost has been remarkably affected by anthropogenic activities.

Evidence of permafrost degradation

During the last few decades, permafrost has been remarkably affected by climate warming and increasing human activities. Permafrost degradation is shown by the deepening active layer, thinning permafrost, rising temperature, expanding taliks and the disappearance of permafrost patches (Zhou et al. 1996, Jin et al. 2006). The southern, or lower limit of permafrost has shifted significantly northward and upward (Jin et al. 2006, 2007a).

Northward shifts of the southern limit and areal reduction

Because of its marginal nature, permafrost in Northeastern China is very sensitive to external disturbances. Formation and degradation of permafrost has happened many times during the Pleistocene and Holocene (Guo & Li 1981). The main body of existing permafrost was formed during the Last Glaciation Maximum. There is a very statistically significant correlation between the mean annual air temperatures and the southern limit of permafrost (Guo et al. 1981). Based on the average air temperatures during 1991–2000, and extensive ground-truthing, the southern limit of permafrost has shifted evidently northwards, as much as 50–120 km in some areas (Jin et al. 2007a). The area of permafrost was reduced by 35%, from 390,000 km^2 in the 1970s (Lu et al. 1981) to 260,000 km^2 in the late 1990s (Jin et al. 2006, 2007a).

Deepening active layer and disappearing permafrost patches

The permafrost table has been lowering. The depths of maximum thaw have been increasing. For example, the depth of the active layer in the Amu'er area in the northern Da Xing'anling Mountains was less than 0.8 m during the 1970s. By 1991, it had increased to 1.2 m (Gu et al. 1994). Some patches of permafrost identified in the 1960s and 1970s have disappeared. For example, a permafrost island with the permafrost table at 1.7 m was observed near Jiagedaqi during railway construction in 1964, but by 1974 permafrost was absent under the rail roadbed. Many patches of permafrost from Dayangshu to Wuerqi, and even to Jiagedaqi, have disappeared according to the latest investigations and surveys in 2007.

Thinning and warming of permafrost

Borehole 14 at the former Yituli'he Permafrost Observatory is located in an undisturbed meadow on the first terrace of the northern bank of the Yituli'he River. The mean annual soil temperatures at shallow (<20 m in depths) have warmed as a result of the combined influence of rapid urbanization, disturbance from road construction and use, urban heat-island effects, and climate warming. Ground temperatures at 13 m increased by about 0.2°C between 1984 and 1997 (Jin et al. 2006). Permafrost degradation also has led to the change of its thermal stability types and the expansion of taliks. Some periglacial processes, such as thermokarsting and thaw-slumping, have been enhanced.

Factors Affecting Permafrost Degradation

Climate change

The main reason for extensive degradation of permafrost is climate warming (Gu et al. 1994, Jin et al. 2007). During the past century, the average temperature in Northeastern China had increased by 1.7°C. The mean annual air temperatures of the Da Xing'anling Mountains were increasing from 1954 to 1989 (Yan 1994). During the past 120 years, the mean annual air temperature in Heilongjiang Province has increased by 1.4°C; with the maximum increase in winter and spring (Pan et al. 2003). The warming during 1971–2000 was 1.4°C more than during the 30 years from end of the 19th century

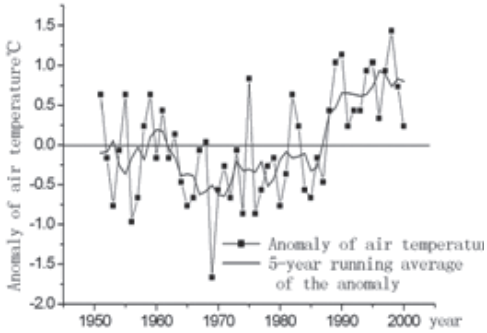

Figure 2. Changes of mean annual air temperature of the Da Xing'anling Mountains during 1961–2000.

to the early 20th century (Pan et al. 2003). Observations at 33 local stations confirmed a similar trend. The mean annual air temperatures during 1971–2000 were 0.9~2.2°C higher than those in the 1960s (Fig. 2) (Jin et al. 2007a). The intensity of warming in the north is more prevalent than that in the south, and the largest warming occurred in the northern Heilongjiang Province and eastern Inner Mongolia, where the mean increase rate was 0.08°C/year.

Increasing anthropogenic activities

There were few human activities in Northeastern China before the 19th century, and the natural environment was not significantly disturbed before the 20th century. During the 1930s to 1940s, the natural environments were devastated because of the Japanese occupation. Since the 1950s, the forest farming in Xing'anling Mountains has increased significantly. Town buildings, forestry, traffic, and transportation were constructed and expanded. In the late 1960s, large amounts of forests were felled for building the Nenlin Railway and the subsequent rapid expansion in population. Establishment and growths of new towns necessitated further deforestation. Long-term, illogical exploitation of forest resources has significantly reduced the forested areas, and remarkably and extensively changed the natural environments. The forested belts retreated northwards by as much as 150–200 km compared to those in the late 19th century. According to a forestry bureau in the Xiao Xing'anling Mountains, the percentage of local forest coverage decreased from 94% in 1957 to 10% in 1980 (Zhou et al. 2000). The extremely serious forest fire in May to June 1987 also changed the albedo of the ground surface and subsequent radiation balance, air and soil temperatures, and soil moisture, resulting in a significant change in the distribution and thickness of permafrost in the Da Xing'anling Mountains (Zhou et al. 1993).

There were about 20,600 people in the 1950s. This number increased to 540,000 by 1994 (Zhou et al. 2002). The population growth necessitated the construction of more infrastructures, such as railways, roads, and buildings. Engineering construction inevitably introduced disequilibrium in the thermal balance and temperatures of permafrost, resulting in various thawed zones, deepened active layers, and accelerated permafrost degradation. For example, in Yakeshi, Jiagedaqi, and Dayangshu near the southern limit of permafrost, there were patches of permafrost everywhere in the early 1950s and 1960s when the towns were

Table 1. Comparison of decadal average air temperature at the Gen'he (50°47′N, 120°30′E, 717 m) and Tuli'he (50°29′N, 120°04′°E, 733 m) meteorological stations during 1961–2000.

Station	Decadal average air temperature (°C)			
	1961–70	1971–80	1981–90	1991–2000
Gen'he	-5.5	-5.0	-4.0	-3.3
Tuli'he	-5.4	-5.0	-4.3	-3.9

Note: The average ground surface temperature at two stations from 1960–1980 was -4.1°C.

Table 2. Comparison of average of mean annual air temperature (AMAAT) and average ground-surface temperature (AGST), maximum frost depths (MFD), and date of thaw completion (DTC) at Gen'he and Tuli'he meteorological stations during 2000–2004.

Station	AMAAT (°C)	AGST (°C)	MFD (cm)	DTC
Gen'he	-3.4	-1.8	260	Late June
Tuli'he	-4.1	-2.6	300	Late July

booming. After 20–40 years of human activities, permafrost has been difficult to find. Urbanization and its "heat-island" effect on permafrost degradation were recognizable. The Gen'he and Tuli'he Forestry Bureaus were set up in 1953, in the discontinuous permafrost zone with natural *larch* forest. The mean annual and decadal average ground temperatures were little changed before 1980s. The Gen'he Forest Bureau had a population of 70,000 in the early 1990s. After the Gen'he City was founded in 1994, the population increased to 180,000 in an area of 19,929 km^2 (Zhou et al. 2002). The city dimensions are 3–4 times those of Tuli'he. It is apparent that the average temperature of Gen'he was 0.6°C higher than that of Tuli'he during 1991–2000 (Table 1). The depth of maximum seasonal frost penetration in Gen'he is 40 cm shallower than that in Tuli'he, and the completion of thawing of the seasonally frozen layer is 1 month ahead (Table 2).

Degradation of Permafrost and Environment

During recent decades, the rapid degradation of permafrost has led to a series of changes in local environments. The major impacts include wetlands degradation, grassland desertification, and shifts of forest types.

Permafrost degradation and changes in wetlands

Freshwater marshes and shallow lakes in Northeastern China, with a total area of 67,378 km^2, account for 17.5% of the total wetlands areas in China (Wang & Du 2006). Coexisting with permafrost, the wetlands in the Da Xing'anling Mountains, with a total area of 8,245 km^2, are mainly located in river valleys, on gentle slopes, and on divides of watersheds. The wetlands in the Xiao Xing'anling Mountains are mainly distributed in the wide valleys and the gulches adjacent to the watershed divides, more on the northern slopes than on the southern slopes.

The wetlands have been gradually shrinking due to the persistent climate warming and drying, permafrost degradation, deforestation, land reclamation, and other anthropogenic activities such as engineering construction and operation, urbanization, overgrazing, and land reclamation. According to a survey report, the area of rivers, marshes, and shrub wetlands in Wuma Forestry Bureau had decreased by 17.4 km^2 in 2001 compared to 1989 (Dai 2007). Further reduction in areal extent of herbaceous swamps was projected under climate change scenarios in the future.

Among the many factors contributing to the changes of wetland ecosystems in the Da Xing'anling Mountains, the single most important one was probably permafrost degradation . In permafrost regions, wetlands are developed in the active layer, which is the interactive interface for mass and heat transfers between permafrost and the external environments. The marsh vegetation layer and the underlying peat layer possess unique thermal properties for insulation and water conservation (Jin et al. 2007b). As a result, they facilitate the formation of permafrost and protect it.

At the meantime, the permafrost layer effectively withholds the downward infiltration of water into soil strata, resulting in ponding at ground surface. A variety of nutrients leached from the active layer enriched here is conducive to the growth of marsh plants. It again facilitates water collection on the surface and formation of an anaerobic environment with slow and decreased decomposition of organic matter.

The freeze-thaw processes have controlling effects on the development, distribution, and degradation of wetlands (Jin et al. 2007b). In recent decades, with the rapid degradation of permafrost, the frozen layer gradually has become thinner. When permafrost is less than 40 cm in thickness, it will be thawed by mid- to late April, before the marsh plants sprout in early May; the soil moisture quickly infiltrates and the ensued physiological drought of plants will adversely affect the swamp development (Zhao & Du, 1980). As a result, the degradation of permafrost inevitably leads to the shrinkage of wetlands, which degrades permafrost (Wang 1983).

Relationship between permafrost degradation and deterioration of the grassland ecosystem

The Hulun Buir Plateau consists of grasslands, wetlands, lakes, and deserts in a transitional zone between patchy permafrost and seasonally frozen ground. Located to the west of the Da Xing'anling Mountains, the Hulun Buir Sandy Land has an annual precipitation of about 350 mm but with good vegetation coverage. It is still considered one of the best pastoral areas in China. However, three sandy belts have developed and are expanding, eroding into the grasslands (Sun & Liu 2001).

According to the 3rd Grassland Resources Investigation, the total grassland area in the Hulun Buir was 112,980 km^2 during 1981–1985, in which the Aeolian-desertified area was 20,970 km^2. By the end of 2002, the area of existing grasslands was 100,878 km^2, with the sandy area of 38,828 km^2. About 12,102 km^2 of grasslands, or 10.7%, were lost during the past 20 years. The aeolian-desertified area increased from 20,970 km^2 (18.6%) in the 1980s to 38,828 km^2 (38.5%) in 2002 (Huang et al. 2003). A survey on desertification on the Hulun Buir Grassland indicates that

the total area of aeolian-desertified land has been expanded, to 11,413 km^2, which is about 3.3% more than that in the 1990s (Nie et al. 2005).

The deterioration of the Hulun Buir grassland ecosystem is attributed not only to natural causes, such as climate warming and permafrost degradation, but also to human activities, such as over-exploitation of water, land, and biological resources, among which the degradation of permafrost may have played an important role in the deterioration of the grasslands ecosystems.

Permafrost degradation could lead to deeper freezing and thawing, and resultant thermokarst, solifluction, and thaw-slump. Freeze-thaw cycles weaken soils structurally, and strengthen the frost weathering and mineralization of organics, resulting in intensifying damages to soil surfaces. The bare soil surface becomes material sources for desertification and is conducive to soil erosion. Permafrost degradation causes the reduction of soil moisture at the plant roots layer, drying of surface soils and wetlands, rising ground temperatures, and changes in soil structures and composition, facilitating grassland degradation. Therefore, permafrost, to a certain degree, constrains and impacts the trends and intensity of changes in the grassland eco-systems. In the permafrost zone, when vegetation coverage is reduced, surface heat absorption increases, ground temperatures rise, and depths of seasonal thaw penetration increase, accelerating permafrost degradation.

Changes of forest ecosystem

The Xing'anling Mountains are the northernmost and largest forested areas in China, with an area of 84,600 km^2. As the representative of bright-leaved taiga in Northern China, it belongs to the taiga area characterized by cold climate and simple forest structure, which mainly includes *Larix gmelinii*, *Pinus sylvestris var. mongolica,* primeval *Betula platyphylla* forests, and secondary forests and other underwood, and underherb (Zhang et al. 1995).

In the Da Xing'an Mountains, where about 81% of frozen ground has Xing'an *larch* forests, is the largest continual coniferous forest in China. Permafrost is necessary for the natural evolution of the Xing'an *larch*, which relies on the suprapermafrost water to keep growing in a shallow-rooted pattern over a long time, and to store freshwater with permafrost, forming a typical frost-forest environment.

Natural forests in permafrost regions are controlled by a frozen-ground environment. However, the degradation or disappearance of permafrost can result in ground subsidence, drunken forests, or dead woods. In a forest farm of Gen'he Forestry Bureau, 6,000 m^3 of woods fell and the thermokarstic subsidence hollow expanded at a rate of 10 m/year, resulting in the losses of woods (Zhou et al. 2003).

The degradation of permafrost and shifts in the southern limit of permafrost can cause a change of vegetative distribution and types (Tan & Li 1995). Patchy permafrost used to exist in Dayangshu in the 1960s, but it had disappeared by 1978. Primeval Xing'an *larch* forests disappeared gradually and were replaced by secondary *Populus davidiana* and *Betula platyphylla* forests, and further became *lespedeza* and *hazelnut* forests (Zhou et al. 2003). The enhanced air and ground temperatures had an impact on forest. As a result, the Xing'an larch forest belt moved northwards. For example, the Xing'an larch used to be common in Yakeshi in the west, but it is seldom sighted. In Nenjiang in the south, primeval forests have already been replaced by secondary forests (Tang & Li, 1995).

At present, the degradation of permafrost is accelerating. As a result, the areal extent of forests in permafrost regions is shrinking, and the vegetation system of the original Xing'an *larch* is being threatened because of human activities such as tree felling, land reclamation, mine exploitation, road construction and operation, anthropogenically-enhanced occurrences of forest fires, and influences of climate warming and permafrost degradation.

Conclusions

1. Due to the pronounced climate warming and increasing anthropogenic activities, permafrost has been degrading rapidly in Northeastern China as evidenced by the deepening active layer, thinning permafrost, rising ground temperatures, expanding taliks, and disappearance of permafrost patches.
2. A series of cold-region ecological and environmental changes were observed, some with adverse consequences.
3. It was estimated on the basis of changes in mean annual air temperatures, and partially verified by field investigations, that the southern limit of permafrost in Northeastern China has shifted significantly northwards, as much as 50–120 km in some areas, during the last 30 years. However, most of the surveys were made along major linear engineering corridors, which may have been more impacted by construction and operation of engineering infrastructures and other human activities.
4. Cold-region ecological environments have changed noticeably, such as vanishing wetlands, deforestation, desertifying grasslands and wetlands, and enhanced water and soil erosion.
5. Human activities, typically represented by rapid urbanization and engineered infrastructures, have cast significant influences on permafrost and the cold-region environment in Northeastern China, as many more people were supported there that other permafrost regions on earth.
6. The key to the study of environmental management and protection in the northern part of Northeastern China is to understand permafrost dynamics and the changes of permafrost environments under a changing climate and intense anthropogenic activities. Long-term, in-depth, and integrated research should be conducted to manage, protect and rehabilitate the damaged ecological environment, in order to healthily sustain the socio-societal and economic development in the cold region in the northern Northeastern China.

Acknowledgments

This study was supported by the CAS Cold and Arid Regions Environmental and Engineering Research Institute Third-term Knowledge Innovation Project "*Climatic and environmental changes in cold and arid northeastern China*

and their adaptation" (Grant No. O650445), National Science Foundation of China (NSFC) Glaciology and Geocryology Incubation Program "*Symbiosis and degradation of permafrost and wetlands ecosystems in northeastern China*" (Grant No. J0630966), and NSFC Project "*Symbiosis and degradation of Xing'an-type permafrost and peat bogs*" (Grant No. 40701031). Professor Max C. Brewer English-edited the paper. Two unidentified reviewers and Professor Douglas L. Kane provided insightful viewpoints and constructive advice for revisions. Their generous assistance is greatly appreciated and thus acknowledged.

References

Dai, B. 2007. Shallow analysis the current situation and protection of wetland in the Da Xing'anling Mountains. *Inner Mongolia Forestry Investigation and Design* 30(4): 68-73 (in Chinese).

Gu, Z., Zhou, Y., Liang, F., Liang, L. & Zhang, Q. 1993. Permafrost feature and their changes in Amuer Area, Da Xing'anling Moutains prefecture. *Journal of Glaciology and Geocryology* 15(1): 34-40 (in Chinese).

Gu, Z., Zhou, Y., Liang, F. & Liang, L. 1994. Permafrost features and their relationship to the environmental factors in Amuer, Da Xing'anling Mountains. *Impacts of Forest Fire on Environments in the Da Xing'anling Mountains and Their Mitigation*. Beijing, China: Science Press, 149-155 (in Chinese).

Guo, D. & Li, Z. 1981. Historical evolution and formation age of permafrost in northeastern China since the late Pleistocene. *Journal of Glaciology and Geocryology* 3(4): 1-6 (in Chinese).

Guo, D., Wang, S., Lu, G., Dai, J. & Li, E. 1981. Regionalization of permafrost in the Da- and Xiao-xing'anling Mountains in northeastern China. *Journal of Glaciology and Geocryology* 3(3): 1-9 (in Chinese).

Huang, G., Zhao, W. & Zhang, Z. 2003. Current situation and protection of grassland ecology in Hunlun Buir. *Inner Mongolia Prataculture* 15(4): 4-5 (in Chinese).

Jin, H., Yu, S., Lü, L., Guo, D. & Li, Y. 2006. Degradation of permafrost in the Da and Xiao Xing'anling mountains, Northeast China, and preliminary assessment of its trend. *Journal of Glaciology and Geocryology* 28(4): 467-475 (in Chinese).

Jin, H., Yu, Q., Lü, L., Guo, D., He, R., Yu, S., Sun, G. & Li, Y. 2007a. Changes of permafrost in the Da and Xiao Xing′anling Mountains, Northeastern China. *Permafrost and Periglacial Processes* 18(2): 245-258.

Jin, H., Yu, S., Jin, R. & Sun, G. 2007b. Symbiosis of marshes and permafrost in the Xing'anling Mountains, Northeastern China. *Chinese Geographical Science* 17(4): 376-382

Lu, G., Wen, B. & Guo, D. 1981. *Permafrost in Northeastern China*, Permafrost Expedition Team of Yakeshi Forestry Survey and Design Institute, Inner Mongolia, 69 pp. (in Chinese).

Nie, H., Yue, L. & Yang, W. 2005. Present situation, evolution trend and causes of sandy desertification in Hulunbuir Steppe. *Journal of Desert Research* 25(5): 635-639 (in Chinese).

Northeastern China Permafrost Research Taskforce (NECPRT). 1983. Major features of permafrost distribution in northeastern China. In *Proceedings of the Second Chinese Conference on Geocryology*. Lanzhou, China: Gansu People's Press, 36-42 (in Chinese).

Pan, H., Zhang, G. & Xu, N. 2003. A Preliminary analysis of climate warming in Heilongjiang Province since the 1980s. *Climatic and Environmental Research* 8(3): 348-355 (in Chinese).

Sun, J. & Liu, D. 2001. Desertification in the Northeastern China. *Quaternary Sciences* 21(1): 72-77 (in Chinese).

Tan, J. & Li, X. 1995. The study on the effects of the climate warming on permafrost degradation and *Larix gemillnii* northward shifts in the Da Xing'anling Mountains. *Inner Mongolia Forestry Investigation and Design* 1: 25-31 (in Chinese).

Wang, C. 1983. Relationships among freezing-thawing process swamp lands, and agriculture on the swampy Sanjiang Plain. *Proceedings of the Second Chinese Conference on Geocryology*. Lanzhou, China: Gansu People's Publishing House, 85-93 (in Chinese).

Wang, Q. & Du, M. 2006. Current situation and prospect of wetland restoration in Northeast China. *Forestry Investigate and Design* 140(4): 25-27 (in Chinese).

Yan, M.H. 1994. Climate changes in the Da Xing'anling Mountains in the recent 36 years. *Impacts of Forest Fire on Environments in the Da Xing'anling Mountains and Their Mitigation*. Beijing, China: Science Press, 143-148 (in Chinese).

Zhang, Y., Zhou, Y. & Ma, J. 1993. Insect taxonomy in forests in the Da Xing'anling Mountains and the impacts of forest fires on the insect taxonomy. *Impacts of Forest Fire on Environments in the Da Xing'anling Mountains and Their Mitigation*. Beijing, China: Science Press, 164-169 (in Chinese).

Zhao, Y. & Du, L. 1980. The study about the formation, type and distribution in the Da and Xiao Xing'anling Mountains. *Journal of Northeast Forestry University* 1: 27-34 (in Chinese)

Zhou, Y., Liang, L. & Gu, Z. 1993. Effects of forest fires on hydro-thermal regime of frozen ground, the Northern part of Da Xing'anling Mountains. *Journal of Glaciology and Geocryology* 15(1): 17-26 (in Chinese).

Zhou, Y., Guo, D., Qiu, G., Cheng, G. & Li, S. 2000. *Geocryology in China*. Beijing, China: Science Press, 171-194 (in Chinese).

Zhou, M., Yu, X. & Feng, L. 2002. Analysis on the driving forces of the permafrost degradation in the Da Xing'anling. *Journal of Arid Land Resources and Environment* 16(4): 44-47 (in Chinese).

Zhou, M., Yu, X. & Feng, L. 2003. Roles of permafrost and wetlands in forests in the Da Xing'an Mountains ecosystems. *Journal of Beijing Forestry University* 25(6): 91-93 (in Chinese).

A Geoelectric Monitoring Network and Resistivity-Temperature Relationships of Different Mountain Permafrost Sites in the Swiss Alps

Christin Hilbich
Department of Geography, University of Jena, Germany
Christian Hauck
Institute for Meteorology and Climate Research, University of Karlsruhe/Forschungszentrum Karlsruhe, Germany
Reynald Delaloye
Geosciences Department, Geography Unit, University of Fribourg, Switzerland
Martin Hoelzle
Glaciology, Geomorphodynamics and Geochronology, University of Zurich, Switzerland

Abstract

An Electrical Resistivity Tomography (ERT) monitoring network has been installed in different permafrost landforms in the Swiss Alps. Repeated ERT measurements yield information on changes occurring in the physical properties of the ground with changing temperature and time. Because the sensitivity of electrical resistivity to temperature is mainly due to the amount of unfrozen water in the pore space of the subsurface material, temporal resistivity changes can be related to freezing and thawing processes. The combined analysis of borehole temperature and ERT monitoring data is used to determine temporal changes of ice and unfrozen water. Key results from this approach include (a) the determination of site-specific total resistivity ranges (as a function of ice content) and amplitudes of seasonal resistivity changes, (b) the demonstration of 3D-topography effects on resistivity distribution in ridge situations, and (c) the identification of depth dependent resistivity-temperature relationships as a function of depth related unfrozen water contents.

Keywords: electrical resistivity tomography; monitoring; mountain permafrost; PERMOS; temperature.

Introduction

Within the context of climate change, the European Alps are affected by greater average warming than commonly projected for Europe as a whole (Beniston et al. 1997). The consequences of global warming for permafrost have been investigated and observed in polar regions for many years (e.g., Osterkamp et al. 1983, Nelson et al. 2001, Frauenfeld et al. 2004, IPCC 2007). In contrast to mainly flat polar lowlands, mountain permafrost is strongly influenced by topographic factors (aspect, slope angle, altitude) affecting net solar radiation and snow cover distribution (Hoelzle et al. 2001). Spatial and temporal heterogeneities of these factors cause complex permafrost distribution patterns that are complicated by heterogeneous subsurface material compositions (bedrock; fine- and coarse-grained debris). Consequently, also the ice content differs markedly between different permafrost landforms.

In addition to temperature, ice content is one of the most critical parameters for the evaluation of the impact of global warming on rockwall stability. Direct observations of ice content are scarce and difficult to obtain. Indirect information from Electrical Resistivity Tomography (ERT) has great potential for detecting the presence of ice, because the specific resistivities of frozen and unfrozen material are markedly different. With repeated ERT measurements under constant general conditions, temporal changes of resistivities are assessed and can be related to freezing and thawing processes (Hauck 2002, Hilbich et al. 2008).

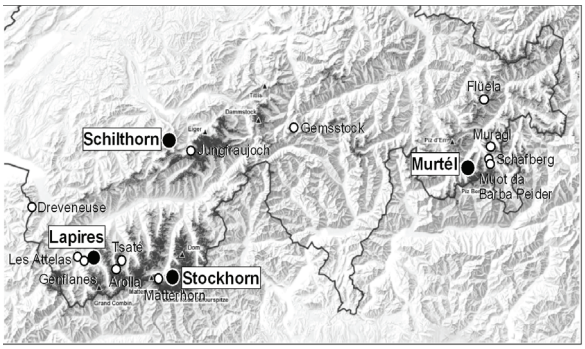

Figure 1. The PERMOS network in the Swiss Alps with borehole temperature monitoring sites (white dots) and combined borehole and ERT monitoring sites (black dots) (Map: BAFU 2007).

However, reliable and quantitative conclusions concerning climate-related changes in ice content can only be drawn when resistivity changes related to external water input (e.g., from precipitation, snowmelt, or lateral water flow) can be excluded (or distinguished from ice melt).

The newly installed ERT monitoring network within the Swiss permafrost monitoring network PERMOS (Fig. 1) provides a unique data set that facilitates study of the relations between measured resistivities and borehole tem

peratures in different permafrost landforms. Sites in the network include the *Schilthorn* (Bernese Alps) permafrost site, which has the longest (>8 years) record of ERT measurements (Hilbich et al. 2008). In this paper we analyze

the potential of coupled ERT and temperature monitoring to improve resistivity-based estimates of total amounts and temporal changes of ice content in permafrost regions.

Theory and Methods

Borehole temperatures

In existing European and Swiss permafrost monitoring networks (PACE21, PERMOS (Harris 2001, Vonder Mühll et al. 2004)), subsurface temperature data are obtained in a network of shallow and deep (down to 100 m) boreholes. The PERMOS programme started in 1999 and involves 16 permafrost borehole-monitoring sites with the longest time-series at rockglacier *Murtèl* (Upper Engadine), recording since 1987. However, long-term climate-related degradation processes in terms of thawing phenomena cannot necessarily be identified by thermal permafrost monitoring alone, as the ice content depends on temperature evolution, and also on the availability of unfrozen water during the freezing period (Hilbich et al. 2008).

Electrical Resistivity Tomography (ERT)

The electrical resistance of the ground can be determined by passing a current between two electrodes and measuring the resulting potential difference between two other electrodes coupled to the ground. Repeating this procedure along an electrode array for a number of different 4-electrode combinations (quadrupoles) with different center points and spacing reveals a two-dimensional distribution of electrical resistances within a subsurface section. By multiplying a geometric factor representing the distance between the four electrodes, the apparent resistivity ρ_a is obtained for each data point of a certain multi-electrode configuration. Using the software package RES2DINV (Loke & Barker 1995), a 2D model of specific resistivities ρ_s, i.e., the true resistivity distribution of the subsurface section, can be calculated from ρ_a by an iterative tomographic inversion process. All ERT data presented in this contribution were measured with the WENNER configuration, and the robust inversion scheme (Clairbout & Muir 1973) of the software RES2DINV was applied.

ERT monitoring

Within the ERT monitoring network a fixed electrode array was installed at four characteristic permafrost sites in the Swiss Alps. All electrodes of one array are permanently connected via cables to a contact box, which serves as an adaptor to a resistivity meter and can be accessed throughout the year (described in detail in Hilbich et al. 2008). Measurements can be carried out by only one person, even in winter, when the electrode array is covered with snow. ERT monitoring started in 1999 at the *Schilthorn* site, in 2005 at the *Murtèl* and *Stockhorn* sites, and in 2006 at the *Lapires* site (see section "Field Sites") and comprises roughly 10 measurements per site to date, except for *Schilthorn* with more than 100 measurements.

Dependence of resistivity on temperature

According to an empirical relationship called Archie´s Law, the resistivity of a medium (consisting of a rock or soil matrix and pore water) can be related to the resistivity of the water, the porosity, and the fraction of the pore space occupied by liquid water (Telford et al. 1990).

The sensitivity of electrical resistivity to temperature arises from different effects, above and below the freezing point. At positive temperatures, the resistivity of the pore water increases with decreasing temperature as a consequence of increasing viscosity of the pore water, which, in turn, decreases the mobility of the ions in the water. This can be quantitatively described as a linear function of the resistivity ρ_0 measured at a reference temperature T_0 and the temperature coefficient of resistivity α, which has a value of about 0.025 K^{-1} for most electrolytes (Telford et al. 1990):

$$\rho = \frac{\rho_0}{1 + \alpha (T - T_0)} \tag{1}$$

Below the freezing point, resistivities increase exponentially due to successive freezing of the pore water with decreasing temperatures. The subzero relationship between resistivity and temperature is given by:

$$\rho = \rho_0 \, e^{-b(T)} \tag{2}$$

where ρ_0 and b (in K^{-1}) are constants (e.g., Hauck 2002). The factor b controls the rate of decrease and can be determined from Equation (2) if resistivity data for different subzero temperatures are available.

Repeated ERT measurements therefore yield information on the changes occurring in the physical properties of the ground with changing temperature and time (Fortier et al. 1994). Plotting ground temperatures from boreholes (interpolated to the depths of the model blocks of the tomograms) against ρ_s extracted from ERT data at borehole positions (marked in Figs. 4–6) then allows comparison of the relation between T and ρ_s for different sites.

Field Sites

ERT monitoring sites have been chosen to represent different permafrost landforms, different climatic regions in the Swiss Alps, and with respect to the availability of deep boreholes (≥20 m). The landforms include the north-facing rock slope of *Schilthorn* (Bernese Alps), the rock plateau *Stockhorn* (Valais), the talus slope *Lapires* (Valais), and the active rock glacier *Murtèl* (Upper Engadine) (Fig. 1). All ERT profiles were placed close to at least one borehole to enable a calibration of the indirect geophysical measurements with direct observations of the subsurface material composition as made during drilling, and subsurface temperature records of the boreholes. A detailed description of the test sites is given in Table 1.

Results and Discussion

Eight-year ERT monitoring at Schilthorn

The ERT monitoring at *Schilthorn* started in September 1999 and comprises more than 100 datasets, making it the

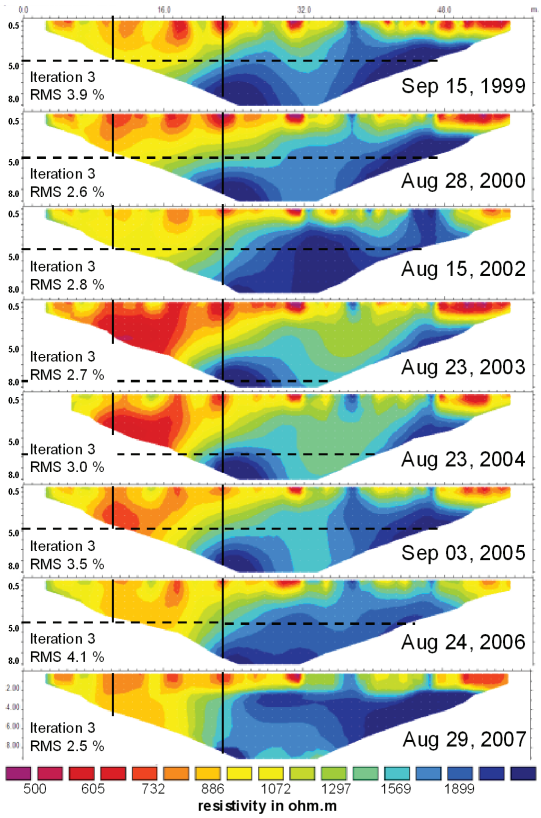

Figure 2. ERT monitoring results of Schilthorn: interannual comparison of late summer resistivity distribution (modified after Hilbich et al. 2008).

longest ERT monitoring record in mountain permafrost research. A comprehensive analysis of this time series is given in Hilbich et al. (2008). Figure 2 shows the interannual changes between measurements in late summer for each year except 2001.

One of the most prominent features of the dataset is the effect of the extraordinarily hot summer of 2003 on mountain permafrost in the European Alps. According to the borehole temperatures, the summer of 2003 caused an immense deepening of the active layer to almost twice the depth of the years before (horizontal dashed lines in Fig. 2). But, in contrast to the subsurface temperatures, which returned rapidly to almost "normal" conditions in 2004, measured resistivities took about 4 years to recover to pre-2003 conditions. As stated before, temporal resistivity changes are assumed to be caused by freezing and thawing processes that are themselves controlled by temperature. The close relation between temperature and resistivity is evident from Figure 3, where borehole temperatures and specific resistivities at the borehole position are shown for the upper four meters and for a one year period (September 1999 to 2000).

ERT monitoring at different landforms

First results from ERT monitoring in different permafrost landforms reveal pronounced differences in total resistivity values and the amplitude of seasonal resistivity dynamics. The first is due mainly to site-specific material characteristics

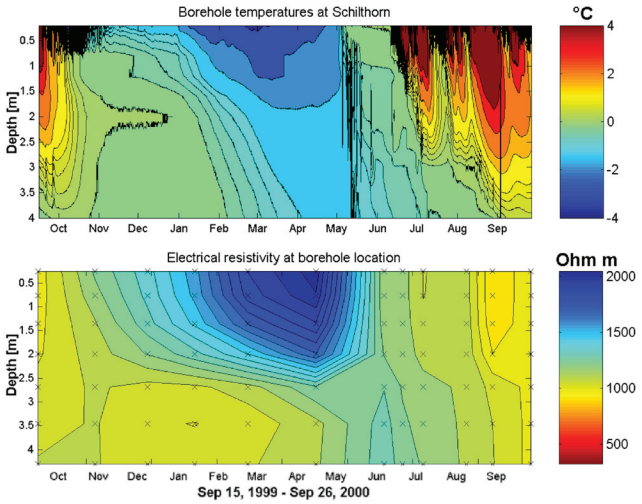

Figure 3. Comparison of temperatures (top) and interpolated resistivities at borehole location (bottom) for September 1999–September 2000 at *Schilthorn*. Resistivity data points used for interpolation are shown as black crosses.

(lithology, pore volume, fractions of pores filled with air, ice, and unfrozen water, etc.), but the latter can have different causes. Besides local climatic effects controlled by altitude, aspect, snow regime, etc., such morphological characteristics as differences in substrate, active layer thickness, thermal conduction in the active layer, etc. play an important role for the amount to which seasonally variable atmospheric forcing is transferred into the ground. This becomes evident not only from the site-specific subsurface temperature regime but also from the resistivity changes throughout a year. Figures 4, 5, and 6 show tomograms with typical summer (top) and winter (bottom) resistivity distributions for the bedrock (*Stockhorn*), rockglacier (*Murtèl*) and talus slope (*Lapires*) sites. From the qualitative comparison, the most important site-specific characteristics are discussed qualitatively in the following paragraphs:

Stockhorn

The Stockhorn profile is located on a plateau between the steep (>80°) northern rock face, and the steeply inclined southern slope. Permafrost distribution is therefore assumed to be affected by 3D topography effects as described by Gruber et al. (2004) and Noetzli et al. (2008). Three-dimensional effects become evident in the ERT monitoring data by pronounced active layer freezing (increasing resistivities during winter) in the northern part, while similar characteristics are missing in the southern part. This corresponds well with observations of the snow cover, which is usually thicker and persists longer in the northern part. In general, the site is exposed to pronounced resistivity changes in the whole subsurface section (to about 20 m depth), which is attributed to 3D topographic effects of the ridge, influencing radiation and turbulent heat transfer to the ground.

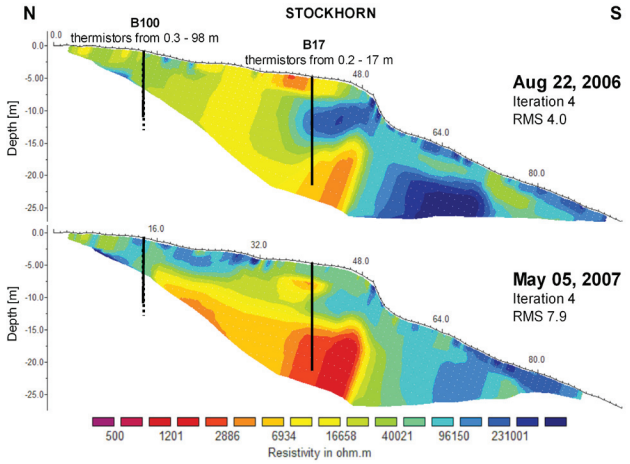

Figure 4. ERT tomogram for typical summer (top) and winter (bottom) conditions at rock plateau *Stockhorn*.

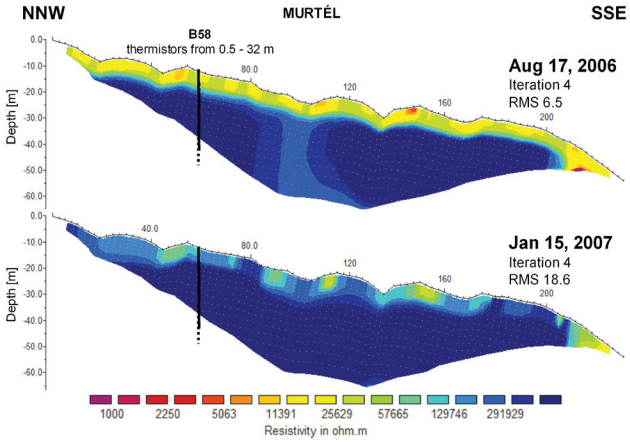

Figure 5. ERT tomogram for typical summer (top) and winter (bottom) conditions at rockglacier *Murtèl*.

Murtèl

Rock glacier Murtèl is generally characterized by extremely high resistivities (300 kΩm to > 2 MΩm) in the interior part caused by the large volume of massive ice. The air in the blocky top layer effectively isolates the ice core from summer heating. Consequently, seasonal resistivity changes are only observed in the active layer (ca. 3–3.5 m) and the tongue. Although changes in the inverted resistivities of the ice core can be quite high (not resolved by the color scale), no systematic seasonal change or trend can be observed from the monitoring data so far. Due to a limited sensitivity of the inversion model to high resistive zones at greater depth, spatial or temporal variations of such high resistivities on the order of MΩm should not be over-interpreted (Marescot et al. 2003). An exception concerns the slightly less resistive vertical zone below the depression at 100–105 m horizontal distance, which is observed in all ERT data (see upper panel in Fig. 5). In summer this resistivity contrast is usually more pronounced than in winter. Due to the uncertainties mentioned above, this zone with decreased (but still very high) resistivities is difficult to interpret but may be an indication of a slightly higher amount of unfrozen

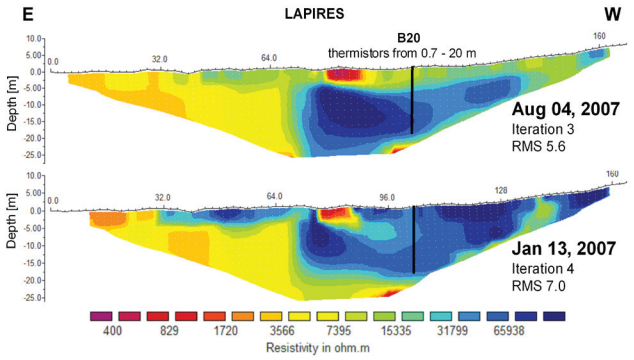

Figure 6. ERT tomogram for typical summer (top) and winter (bottom) conditions at talus slope *Lapires*.

water (under subzero temperature conditions), possibly indicating water flow or a zone of higher debris content.

Lapires

The *Lapires* site can be characterized as a talus slope thermally influenced by internal ventilation with a special pattern of permafrost and ground ice occurrence partially reflecting of this internal air circulation (reported in detail by Delaloye & Lambiel 2005). The highly resistive feature in the central part of the tomogram indicates the zone where ground ice is likely to be present. In general, such high resistivities (here >40 kΩm) can be caused by high amounts of ice or air within the pore space of the blocky talus slope (Hauck & Kneisel 2008). ERT monitoring results reveal substantial seasonal changes in resistivities within this zone, possibly indicating a change in material properties over the course of the year. In combination with direct observations during drilling of the borehole and subsurface temperature records, decreasing resistivities at the bottom of this feature during winter and increasing resistivities in summer appear to be related to the air circulation. This may indicate ice formation in summer and thawing processes in winter, but the process remains difficult to understand physically. However, the resistive anomaly can also be influenced by the presence of a cable car pylon in the middle of the profile, represented by very low resistivities in the upper few meters. This low resistive anomaly may cause a low confidence of the resistivity measurement and the inversion process beneath. Further tests are necessary to judge the significance of resistivity changes as indication for changes in material properties.

Active layer freezing during winter (up to 4 m) is, however, clearly evidenced at this site.

Resistivity-temperature relationships

Resistivity-temperature (ρ-T) relationships are plotted for all four test sites in Figures 7 and 8. Figure 7 shows the results for *Schilthorn* (active layer from 0–4.3 m depth), where the largest data set is available. For temperatures above the freezing point results agree well with theory (Eq. 1) with slightly but continuously increasing resistivities with decreasing temperature.

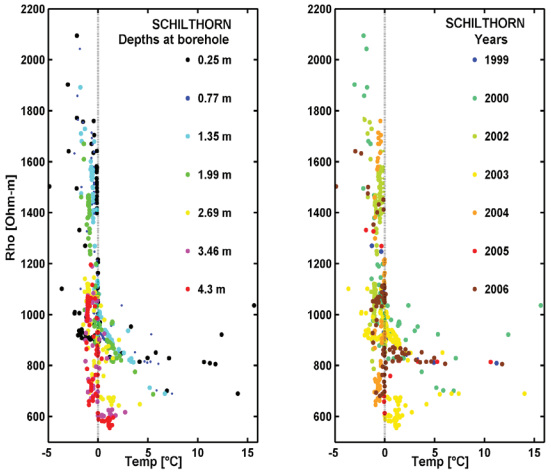

Figure 7. Resistivity at borehole location against subsurface temperatures for the 8-year *Schilthorn* dataset. Colors highlight depths (left panel) and years (right panel). Note that temporal resolution and number of measurements per year are not regular.

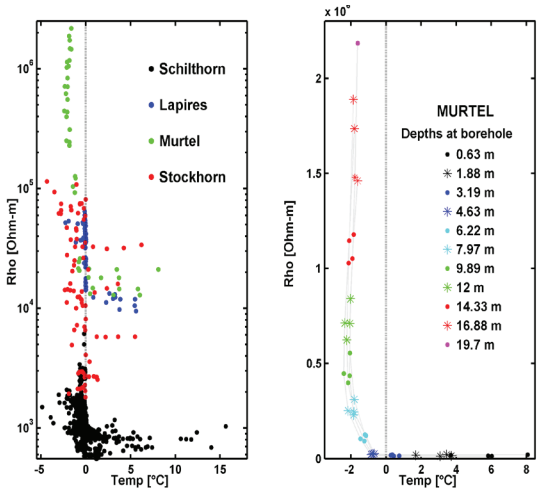

Figure 8. Left panel: comparison of amplitudes of resistivity-temperature relationships for all sites. Right panel: ρ-T relation for 4 different measurement dates at *Murtèl* with colors highlighting different depths. Note that temporal resolution and number of measurements per year are not regular.

At subzero temperatures the reverse effect is visible at all sites: starting at temperatures slightly below the freezing point; resistivities increase exponentially while temperature decrease is almost negligible. Comparing the ρ-T relationship for different depths it is apparent that although the shape of the curves is similar the resistivities are decreasing with depth, indicating higher amounts of unfrozen water at greater depths of the active layer (according to Archie's Law). During freezing unfrozen water contents remain higher in the deeper parts represented by the still lower resistivities (Hauck 2002). Analyzing the same data set with respect to different years, the exceptional low resistivity values of 2003 and the following years become evident as being completely below the main part of the ρ-T curve, again confirming the hypothesis of substantial ground ice degradation at *Schilthorn* in the summer of 2003.

Figure 8 shows the data from all monitoring sites. The amplitude of the resistivity increase for subzero temperatures differs significantly between the sites. While values approximately duplicate at *Schilthorn* from ca. 800 Ωm in unfrozen state to 1600–2000 Ωm in frozen state, they rise over more than an order of magnitude from <100 kΩm to >2 MΩm at *Murtèl*. Unfrozen values at *Lapires* and *Stockhorn* are similar to *Murtèl*, reflecting the blocky active layers, but frozen values are significantly lower due to the lower ice contents. Unfrozen resistivity values of *Stockhorn* cover a wide range due to high variations between dry and wet surface conditions.

The right panel in Figure 8 shows the ρ-T relationships for different measurement dates (lines) and depths (colors) at *Murtèl*. In contrast to *Schilthorn*, values are constant over time, showing almost the same relationship at all temporal reference points. This high degree of repeatability highlights the thermally inert role of the rockglacier and further confirms the reliability of the ERT monitoring approach, even on blocky and highly resistive terrain. A striking feature is the clear dependence of the ρ–T relation on depth. At *Murtèl* (and also at *Stockhorn* and *Lapires*, not shown here) the reverse pattern of *Schilthorn* is visible: Values increase with increasing depths. In contrast to *Schilthorn* (Fig. 7), values in Figure 8 mainly represent conditions below the permafrost table and are therefore interpreted as being due to decreasing unfrozen water contents with depth. However, also decreasing intensity of weathering, higher density and less pore space with depth may be contributing parameters.

Conclusion

Results from an ERT monitoring network at four sites in the Swiss Alps are presented and analyzed in combination with borehole temperature data. Key results from the landform-specific approach can be summarized as follows:

- Both total resistivity ranges and amplitudes of temporal resistivity changes differ markedly for the observed landforms. This is due to site-specific differences of material properties (lithology, pore volume, contents of air, ice and unfrozen water within the pore space, etc.), seasonal dynamics, temperature ranges and the hierarchy of dominating factors.
- Three-dimensional topographic effects influence radiation and turbulent heat transfer to the ground in ridge situations and complicate the pattern of resistivity distribution and seasonal changes, as shown by the example of the rock plateau *Stockhorn*.
- Small seasonal changes are recorded at the *Murtèl* site due to thermally inert characteristics of rockglaciers as opposed to high seasonal dynamics at the other sites as a consequence of internal ventilation (*Lapires* talus slope), high unfrozen water and low ice contents (*Schilthorn*) and 3D effects (*Stockhorn*).
- From the ρ-T relationships a significant dependence on depth becomes evident, with opposite behavior observed

in the active layer (at *Schilthorn*) and below the permafrost table (*Stockhorn*, *Lapires*, *Murtèl*) due to differences in unfrozen water content.

A long-term continuation of the ERT monitoring in the scope of PERMOS is intended and aims at a site-specific assessment of climate related ground ice degradation.

Acknowledgments

We thank Schilthornbahn AG, Zermatt Bergbahnen AG and Corvatsch AG for logistical, and the PERMOS network (BAFU, Switzerland) for financial support, and all students who helped in the field.

References

Beniston, M., Diaz, H.F. & Bradley, R.S. 1997: Climatic change at high elevation sites: An overview. *Climatic Change* 36(2): 233-251.

Bundesamt für Umwelt BAFU 2006. *Hinweiskarte Permafrost Schweiz*. http://www.bafu.admin.ch.

Claerbout, J.F. & Muir, F. 1973. Robust modeling with erratic data. *Geophysics* 38: 826-844.

Delaloye, R. & Lambiel, C. 2005. Evidences of winter ascending air circulation throughout talus slopes and rock glaciers situated in the lower belt of alpine discontinuous permafrost (Swiss Alps). *Norwegian Journal of Geography* 59(2): 194-203.

Fortier, R., Allard, M. & Seguin, M.K. 1994. Effect of physical properties of frozen ground on electrical resistivity logging. *Cold Regions Science and Technology* 22: 361-384.

Frauenfeld, O.W., Zhang, T. & Barry, R.G. 2004. Interdecadal changes in seasonal freeze and thaw depths in Russia. *Journal of Geophysical research* 109: 1-12.

Gruber, S., Hoelzle, M. & Haeberli, W. 2004. Permafrost thaw and destabilization of Alpine rock walls in the hot summer of 2003. *Geophysical Research Letters* 31: 1-4.

Harris, C. 2001. Permafrost and Climate in Europe (PACE), *Permafrost and Periglacial Processes* 12(1): 156.

Hauck, C. 2002. Frozen ground monitoring using DC resistivity tomography. *Geophysical Research Letters* 29(21): 2016.

Hauck, C. & Kneisel C. 2008a. *Applied geophysics in periglacial environments*. Cambridge: Cambridge University Press, in press.

Hilbich, C., Hauck, C., Hoelzle, M., Scherler, M., Schudel, L., Völksch, I., Vonder Mühll, D. & Mäusbacher, R. 2008. Monitoring of mountain permafrost evolution using electrical resistivity tomography: A seven-year study of seasonal, annual and long-term variations at Schilthorn, Swiss Alps. *Journal of Geophysical Research* 113: F01S90.

Hoelzle, M., Mittaz, C., Etzelmüller, B. & Haeberli, W. 2001. Surface energy fluxes and distribution of permafrost in European mountain areas: an overview of current developments. *Permafrost and Periglacial Processes* 12: 53-68.

Intergovernmental Panel on Climate Change (IPCC) 2007. *Climate change 2007: The physical science basis. Summary for policy makers.* http://www.ipcc.ch/.

Loke, M.H. & Barker, R.D. 1995. Least-squares deconvolution of apparent resistivity. *Geophysics* 60: 1682-1690.

Marescot, L., Loke, M.H., Chapellier, D., Delaloye, R., Lambiel, C. & Reynard, E. 2003. Assessing reliability of 2D resistivity imaging in mountain permafrost studies using the depth of investigation index method. *Near Surface Geophysics* 1.2: 57-67.

Nelson, F.E., Anisimov, O.A. & Shiklomanov, N.I. 2001. Subsidence risk from permafrost thaw. *Nature* 410: 889-890.

Noetzli, J., Hilbich, C., Hauck, C., Hoelzle, M. & Gruber, S. 2008. Comparison of Transient 2D Temperature Fields with Time-Lapse Electrical Resistivity Data at the Schilthorn Crest, Switzerland. *Proceedings of the Ninth International Conference on Permafrost, Fairbanks, Alaska, June 29–July 3, 2008* (this proceedings).

Osterkamp, T.E. 1983. Response of Alaskan permafrost to climate. *Proceedings of the Fourth International Conference on Permafrost, Fairbanks, Alaska*: 145-152.

Telford, W.M., Geldart, L.P. & Sheriff, R.E. 1990. *Applied geophysics*. 2nd edition, Cambridge: Cambridge University Press, 770 pp.

Vonder Mühll, D., Noetzli, J. Makowski, K. & Delaloye, R. (eds.) 2004. *Permafrost in Switzerland 2000/2001 and 2001/2002*. Glaciological Report (Permafrost) of the Glaciological Commission of the Swiss Academy of Sciences 2, 3.

Spatial and Interannual Patterns of Winter N-Factors Near Barrow, Alaska

Kenneth M. Hinkel
Department of Geography, University of Cincinnati, Cincinnati, OH 45221-0131 USA
Anna E. Klene
Department of Geography, University of Montana, Missoula, MT 59812 USA
Frederick E. Nelson
Department of Geography, University of Delaware, Newark, DE 19716 USA

Abstract

A 150-km^2 area near Barrow, Alaska, was monitored at hourly intervals between 2001 and 2005 using ~70 data loggers recording air and near-surface soil temperature as part of the Barrow Urban Heat Island Study. Data records for the winter period were used to calculate site-specific *n-factors*, the ratio between seasonally cumulated degree days at the ground surface to those at standard screen height at corresponding locations. Winter n-factors have similar magnitudes between sites and across years, with typical averages of 0.65-0.70. However, n-factor magnitudes are generally lower and their spatial variability much higher near the urbanized area, owing to heterogeneous snow accumulation and the effects of drifting snow.

Keywords: Alaska; air temperature; n-factor; permafrost; snow cover; urbanization.

Introduction

The surface energy balance in Arctic tundra is highly variable over relatively short distances owing to the localized effects of snow, vegetation, soil moisture content, and substrate properties. These variables affect the amount of heat conducted to depth and therefore have considerable influence on the soil thermal regime. In permafrost terrain, energy inputs in summer develop the active layer, which itself exhibits a high degree of spatial variability. One method to parameterize the surface energy balance and simplify calculations over longer time periods is the *n-factor*. Originally proposed by Carlson (1952), this is a simple ratio of seasonal degree days (°C-days) at the ground surface to seasonal degree days in the air over the same time period (Lunardini 1981). The n-factor's geographic variability has been analyzed at a variety of spatial scales. Shur & Slavin-Borovskiy (1993) examined summer n-factor patterns in western Siberia across more than 25 degrees of latitude, and noted a general increase in n-factors poleward. At the local plot scale, Klene et al. (2001) observed significant variation in summer n-factors between natural landscape-vegetation types, but relative consistency within the units.

This study was conducted at an intermediate scale, and uses a relatively dense network of temperature-measurement sites to map winter patterns of the n-factor. The purposes are to (1) quantify the degree of regularity in seasonal n-factor magnitude and spatial patterns between different years; and (2) identify conditions that influence winter n-factors at the scale of the study.

Study Area and Background

Barrow is a coastal village on the Chukchi Sea at 71.3°N, 156.5°W. With a mean annual temperature of -12.0°C (National Climate Data Center [NCDC] 2003), the area lies in the continuous permafrost zone, with permafrost thickness extending to depths of nearly 400 m. Active-layer thickness averages around 35 cm (Hinkel & Nelson 2003), but is highly variable between landscape types (Klene 2005). The snow cover is typically established by mid-September and averages about 40 cm in depth at the end of winter.

Barrow has a population of around 4600, with an urban settlement pattern typical of the U.S. Building density is relatively high in the older village center, while suburban-style housing of lower density dominates recent developments around the village's periphery and extends as a band along the coast for several km.

Most buildings are single-story and built atop piles driven into the underlying permafrost. The local road network consists of gravel berms elevated 1-2 m above the natural terrain. The urbanized area constitutes an artificial topography that exceeds the natural relief of the surrounding coastal plain and has significant impacts on snow-drift patterns, snow depth, and retention of water at the surface. Each of these factors, in turn, influences the n-factor.

As part of a larger study concerned with evaluating the impact of Barrow's urban heat island on soil temperatures and permafrost stability, HoboPro® data loggers were installed across a 150-km^2 area beginning in 2001. Fifty loggers were deployed in 2001, and by 2003 the network had expanded to nearly 70 loggers. About half were deployed in urban settings, with the remainder dispersed across the hinterland in a loose grid pattern (Hinkel et al. 2003, Hinkel & Nelson 2007). The two-channel loggers have an accuracy of ±0.2°C and precision of 0.02°C at the freezing point. Loggers were mounted on an instrument mast with one thermistor inside a radiation shield at standard screen height (1.8 m) to measure air temperature, and the other thermistor positioned 5 cm below the ground surface to measure near-surface soil temperature. Loggers were synchronized to record hourly measurements. The rate of instrument attrition was around

10% yearly, owing primarily to animal activity and logger failure.

Methodology

Because the date of snowmelt in spring and snow cover development in autumn varies between sites and years, it was first necessary to define seasonal boundaries. For each site, the mean daily air and soil temperature traces were plotted. Using these records in combination with graphs of daily soil temperature range, we defined the winter snowcover period as 15 Sept to 15 May (243 days; 244 days on leap year).

For each site with a complete record for the seasonal period, average daily air and soil temperatures were cumulated. The n-factor was then calculated for each site, summary statistics generated, and seasonal maps produced using a simple kriging algorithm (Golden Software 2002) to interpolate site values over the study area.

Sites were defined as urban or rural depending on whether they were within 30 m of any building, road, or other "built" structure.

Table 1. Winter air temperature (°C) summary statistics based on daily average for sites with a complete record over the period; winter is 15 Sept to 15 May.

	Winter-2001-02	Winter-2002-03	Winter-2003-04	Winter-2004-05
N	31	39	52	42
Mean	-17.98	-15.75	-17.89	-16.76
Median	-17.91	-15.60	-17.79	-16.63
Minimum	-19.09	-17.70	-19.00	-17.63
Maximum	-17.05	-15.05	-17.08	-16.20
Std_Dev	0.52	0.54	0.51	0.36

Table 2. Summary statistics for winter n-factors. Snow depth (cm) averages measured in either April or May.

	2001-02	2002-03	2003-04	2004-5
N	31	39	52	42
Minimum	0.36	0.34	0.32	0.28
Maximum	0.90	0.91	0.87	0.90
Range	0.54	0.57	0.55	0.63
Mean	0.66	0.66	0.65	0.66
Median	0.68	0.68	0.68	0.69
StdDev	0.13	0.15	0.13	0.16
Snow (cm)	31	30	38	31

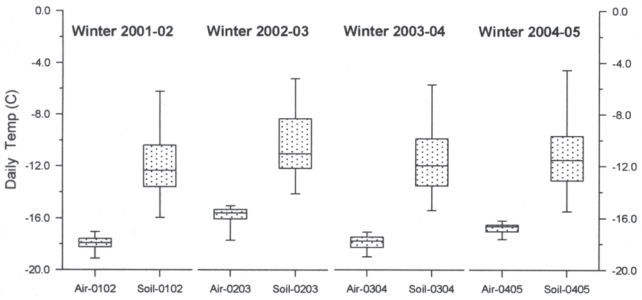

Figure 1. Box-and-whisker plots of average winter air and near-surface temperature for all valid sites.

Results and Discussion

In a region of relatively even and continuous tundra vegetation such as Barrow, winter n-factors can initially be treated as a homogenous group for analysis. N-factors near unity indicate close coupling between the soil and air temperature. Conversely, lower magnitudes indicate relatively warmer soil temperature in winter that reflects the insulating effects of the snow cover. Strong decoupling is induced by deep snow, with n-factors falling toward zero.

Annual summary statistics

Summary winter air temperature statistics are given in Table 1. The number of sites used in the calculations varied between winters owing to lost or partial records. Winter 2002-03 was about 2°C warmer than other years; this is also apparent in Figure 1, which shows the distribution of the daily air and soil temperature averages by winter period. There is limited variation in average daily air temperature in all winters, as can be expected within such a relatively small area. By contrast, the variability in near-surface soil temperature is substantial, and is related to local edaphic, vegetation, and snow conditions.

Summary n-factor statistics are given by winter period in Table 2, and the range of n-factors by year is shown in Figure 2. Winter n-factors have very similar measures of central tendency (0.65-0.69 for mean and medians), indicating little interannual variation. Winter snow-cover depth, measured each year at the 121 grid nodes of the ARCSS/CALM 1-km^2 grid within the study area, was consistently around 31 cm, except during the winter of 2003-04 when it averaged 38 cm. The thicker snow cover does not appear to impact the mean, median, or range of n-factors in that year, although values appear somewhat more clustered around the median (Fig. 2). Direct interannual comparison is difficult, however, because the number of operational sites varied between years.

Annual spatial patterns

Maps of the winter n-factor are shown in Figure 3. The winter pattern of n-factors demonstrates relatively consistent geographic patterns with (1) higher magnitudes (>0.70) near the coast, especially in the vicinity of Elson Lagoon; (2) lower magnitudes (<0.55) near the urban center, and (3) much higher spatial variability near the urbanized areas. This last point can be best appreciated by separating the urban and rural sites, and calculating summary statistical parameters of n-factors (N=164) for the two groups (Table 3). The urban sites have a lower mean and median n-factor (by about 0.10), and vary more around the measures of central tendency; the range is wider and the standard deviation is greater by a factor of two. A plot of the histograms for the two groups of sites (Fig. 4) verifies this interpretation and clearly illustrates the tight clustering of rural n-factors around the mean and median centered on 0.7.

In Barrow, strong winter winds (averaging ~11 knots or 5.5 m s^{-1}) are consistently from the NNE and snow drifting is common. Deflation of snow by wind on the northeastern

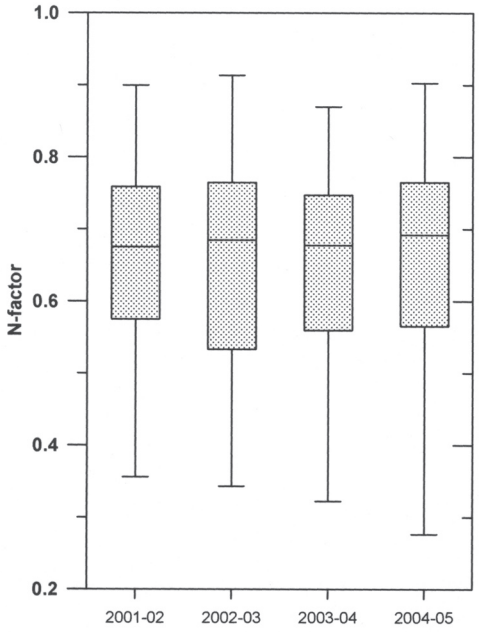

Figure 2. Box-and-whisker plots of winter (15 Sept-15 May) n-factor by year.

coast would tend to increase the winter n-factor at affected sites. Conversely, relatively large accumulations of snow in the lee of buildings, plowed roadways, and snow fences (Hinkel & Hurd 2006) reduce the magnitude of the n-factor and promote spatial variability. Because the number of sites used to construct these maps differs substantially, more detailed comparison is not prudent.

Forcing factors

During winter, snow depth and thermal properties have been found to be the dominant factors determining ground temperature in rural and urban environments (e.g., Gold 1967, Goodrich 1982, Woo & Debreuil 1983). In some environments, this is closely tied to vegetation, which traps snow in the canopy layer (Sturm et al. 2001). In Barrow, however, the relatively short tundra vegetation (seldom more than 20 cm and usually much less) reduces the importance of this factor. This study found snow to be the main determinant of winter soil temperatures and n-factors, with the artificial topography inducing snow accumulation and drifting, thus impacting the magnitude and variability of winter n-factors in the urban setting. Other urban factors that may complicate

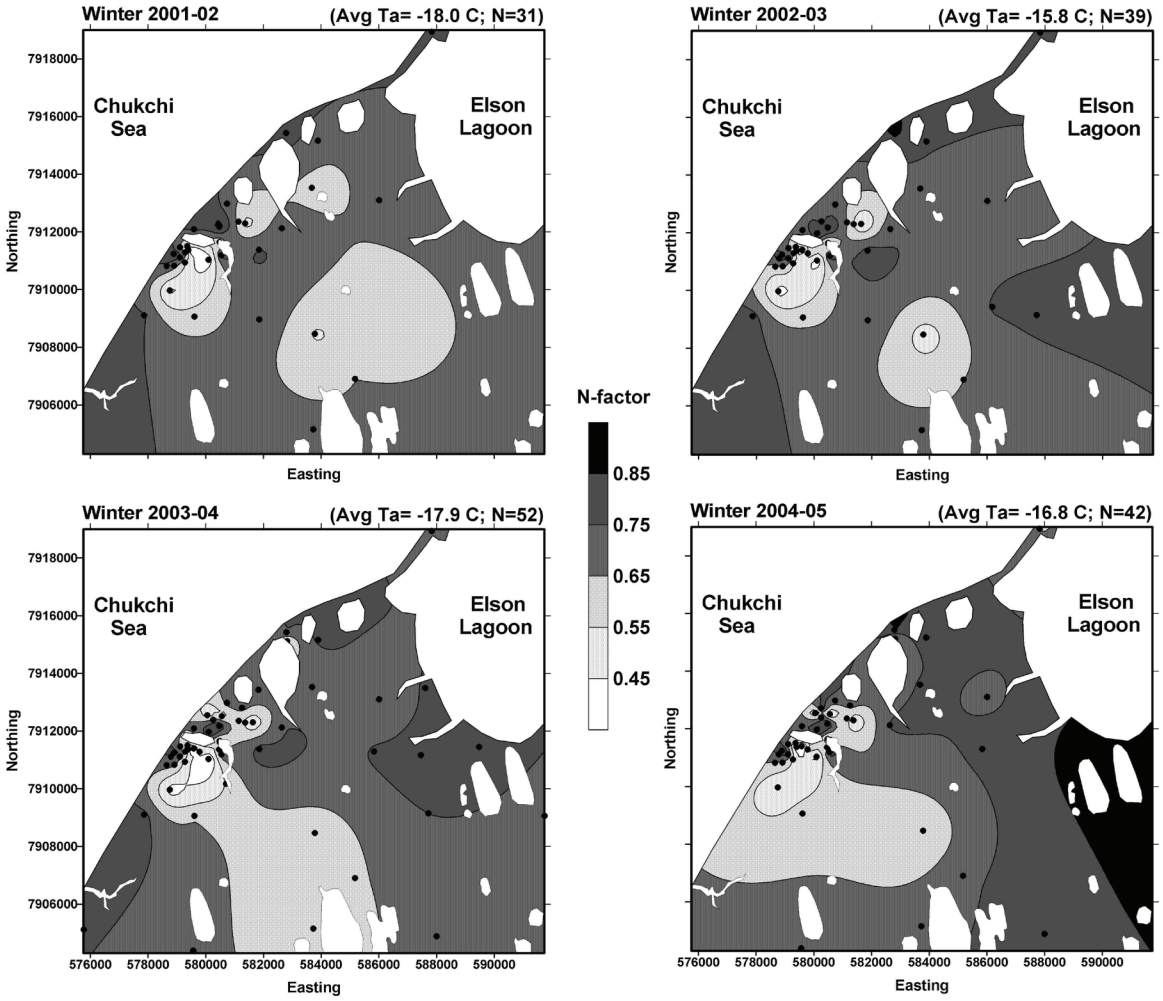

Figure 3. Isarithmic maps of winter n-factors; seasonal average air temperature and N indicated in upper right corner. Dots show instrument sites.

Table 3. Summary statistics of all winter n-factors (N=164) separated into either urban or rural setting.

	Urban	Rural
N	112	52
Minimum	0.28	0.50
Maximum	0.91	0.90
Range	0.64	0.41
Mean	0.63	0.71
Median	0.64	0.73
Std_Dev	0.16	0.08

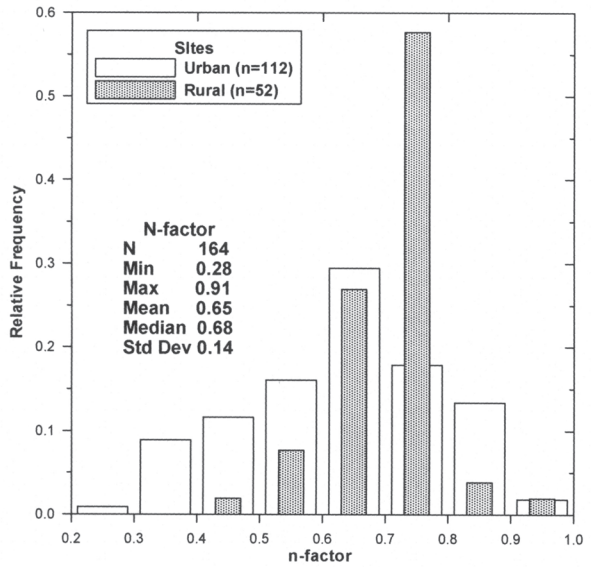

Figure 4. Histogram of n-factors by setting, with summary statistics for all sites.

the ground thermal regime include changes in subsurface soil water flow caused by construction of permafrost-stabilized road berms. Particularly in the newer subdivisions of Barrow, roads form a grid pattern that inhibits lateral meltwater runoff in spring and causes ponding. This results in such intensive flooding that tanker trucks proceed from block to block, pumping water to be dumped elsewhere. Other urban factors, such as the effects of dust on snow albedo (Dutton & Endres 1991), can also have an impact in this environment. Separation of n-factor regimes by rural and urban regions provides a useful first-approximation explanation.

Compared to results from previous studies, the rural values reported here are somewhat higher than those found by Taylor (1995), Karunaratne & Burn (2003, 2004) and Kade et al. (2006). Taylor (1995), for example, reported winter n-factors of 0.12–0.45 for forested sites in the Mackenzie River Valley. Karunaratne and Burn (2003) examined winter n-factors at several sites in the Yukon (forested, burned, meadow, snow fence, and cleared) between 1997 and 2000. They reported winter n-factors at the cleared sites (0.5) that were similar to those observed in the forested site, while the burned and snow fence sites had n-factors of ~0.3 and the meadow site had an intermediate value. Kade et al. (2006) examined n-factors in barren nonsorted frost circles and vegetated tundra along a climate gradient consisting of three sites in northern Alaska. They calculated tundra n-factors of about 0.3, 0.6, and 0.9 at Happy Valley, Franklin Bluffs, and Howe Island, respectively. This generally shows the impact of reduced snow depth, vegetation height, and soil organic layer thickness as one moves poleward from the Arctic Foothills towards the Arctic Ocean. Carlson (1952) calculated winter n-factors of 0.25-0.33 for three sites of differing land-covers (trees, shrubs, vegetation removed) with an undisturbed snow cover. At "urban" sites that were cleared of snow, he found n-factors of 0.62-0.76 at sites with a gravel surface and n-factors of 0.65–0.84 associated with concrete and asphalt surfaces. The high n-factors observed at Barrow likely reflect the effects of the relatively thin snow cover and tundra vegetation.

Conclusions

This study of n-factor magnitudes and spatial patterns is somewhat different from those conducted in the past in that (1) the analysis was performed at a spatial scale intermediate between the plot- and regional-scale studies reported in the literature; (2) it utilizes a relatively dense network of data loggers; and (3) the study took place over several years to examine the annual variability of winter n-factors. The spatial and temporal consistency of n-factors over a series of winters has been demonstrated empirically in the rural environment.

Conversely, individual sites within the urban environment were of lower magnitude and show greater variability. The anthropogenic impact on snow accumulation and drifting patterns induced by buildings, plowed roads, and snow fences is the likely cause. This indicates that n-factors may exhibit high variability across short distances in natural terrain of high relief, and merits further investigation. Other studies may focus on the impact of engineered structures or climate-induced vegetation changes. Spatial and temporal analysis of summer n-factors would likely require implementing a land cover classification scheme to fully understand the complex patterns (Klene et al. 2003, Hinkel et al. 2004).

Acknowledgments

This work was supported by the National Science Foundation (NSF) under grants OPP-9529783, 9732051 and 0094769 to KMH and OPP-0095088 and 0352958 to FEN. Any opinions, findings, conclusions, or recommendations expressed in this material are those of the authors and do not necessarily reflect the views of the NSF. Mention of any product does not constitute endorsement. We are grateful for support from the Barrow Arctic Science Consortium, the Ukpeagvik Inupiat Corporation, and the many Barrow residents who allowed us to use their backyards and parking lots. R. Beck, J. Bell, B. Jones, and C. Tweedie assisted in this study. Our thanks to an anonymous reviewer.

References

Carlson, H. 1952. Calculation of depth of thaw in frozen ground. In: *Frost Action in Soils: A Symposium*, pp. 192-223. *Highway Research Board Special Report 2* Washington, DC: National Research Council.

Dutton, E.G. & Endres, D.J. 1991. Date of snowmelt at Barrow, Alaska, U.S.A. *Arctic and Alpine Research* 23: 115-119.

Gold, L.W. 1967. Influence of surface conditions on ground temperature. *Canadian Journal of Earth Sciences* 4: 199-208.

Golden Software 2002. *Surfer 8 User's Guide: Contouring and 3D Surface Mapping for Scientists and Engineers*. Golden, CO: Golden Software.

Goodrich, L.E. 1982. The influence of snow cover on the ground thermal regime. *Canadian Geotechnical Journal* 19: 421-432.

Hinkel, K.M. & Nelson, F.E. 2003. Spatial and temporal patterns of active layer depth at CALM sites in Northern Alaska, 1995-2000. *Journal of Geophysical Research-Atmospheres* 108(D2), 10.129/2001JD000-927.

Hinkel, K.M., Nelson, F.E., Klene, A.E. & Bell, J.H. 2003. The urban heat island in winter at Barrow, Alaska. *International Journal of Climatology* 23: 1889-1905.

Hinkel, K.M., Klene, A.E. & Nelson, F.E. 2004. The summer climate of an arctic coastal village: Preliminary observations from the Barrow Urban Heat-Island study. *Polar Geography* 28(3): 197-221.

Hinkel, K.M. & Hurd, J.K., Jr. 2006. Permafrost destabilization and thermokarst following snow fence installation, Barrow, Alaska, U.S.A. *Arctic, Antarctic and Alpine Research* 38(4): 530-539.

Hinkel, K.M. & Nelson, F.E. 2007. Anthropogenic heat island at Barrow, Alaska, during winter: 2001-2005. *Journal of Geophysical Research-Atmospheres* 112, D06118, doi:10.1029/2006JD007837.

Kade, A., Romanovsky, V.E. & Walker, D.A. 2006. The n-factor of nonsorted circles along a climate gradient in Arctic Alaska. *Permafrost and Periglacial Processes* 17(4): 279-289.

Karunaratne, K.C. & Burn, C.R. 2003. Freezing n-factors in discontinuous permafrost terrain, Takhini River, Yukon Territory, Canada. In *Proceedings of the 8th International Conference on Permafrost. Zurich: University of Zurich-Irchel*: 519-524.

Karunaratne, K.C. & Burn, C.R. 2004. Relations between air and surface temperature in discontinuous permafrost terrain near Mayo, Yukon Territory. *Canadian Journal of Earth Sciences* 41: 1437-1451.

Klene, A.E., Nelson, F.E. Shiklomanov, N.I. & Hinkel, K.M. 2001. The N-factor in natural landscapes: Variability of air and soil-surface temperatures, Kuparuk River Basin, Alaska. *Arctic, Antarctic, and Alpine Research* 33(2): 140-148.

Klene, A.E., Hinkel, K.M. & Nelson, F.E. 2003. The Barrow heat island study: Soil temperatures and active-layer thickness. In *Proceedings of the 8th International Conference on Permafrost. Zurich: University of Zurich-Irchel*: 555-560.

Klene, A.E. 2005. *Climate and Urbanization in Barrow, Alaska*. Dissertation, Department of Geography. Newark, DE: University of Delaware.

Lunardini, V.J. 1981. *Heat Transfer in Cold Climates*. New York, NY: Van Nostrand Reinhold Company.

National Climate Data Center (NCDC) 2003. URL: http://www5.ncdc.noaa.gov [Available online at http://www5.ncdc.noaa.gov /pubs/publications.html#CLIM81.] "Monthly Normals (Climatography of the U.S. #81 and "SOD -Daily Surface Data (TD3200/3210 combined) for W. Post and W. Rogers Airport, Barrow, Alaska."

Shur, Y.L. & Slavin-Borovskiy, V.B. 1993. N-factor maps of Russian permafrost region. In *Proceedings of the Sixth International Conference on Permafrost, Vol.* 1. Wushan Guangzhou, China: South China University of Technology Press: 564-568.

Sturm, M., McFadden, J.P., Liston, G.E., Chapin, F. S. III, Racine, C.H. & Holmgren, J. 2001. Snow-shrub interactions in Arctic tundra: A hypothesis with climatic implications. *Journal of Climate* 14: 336-344.

Taylor, A.E. 1995. Field measurements of n-factors for natural forest areas, Mackenzie Valley, Northwest Territories. In *Geological Survey of Canada, Current Research,* 1995-B: 89-98.

Woo, M.-k. & Dubreuil, M.-A. 1983. Effects of an Arctic settlement on the snowpack. *40th Annual Meeting of the Eastern Snow Conference* 28: 143-156.

Spatial and Temporal Variation of Soil Temperatures and Arctic Hydrology in the Kuparuk River Basin, Alaska

Larry D. Hinzman
University of Alaska Fairbanks, International Arctic Research Center
Robert E. Gieck
University of Alaska Fairbanks, Water and Environmental Research Center
Douglas L. Kane
University of Alaska Fairbanks, Water and Environmental Research Center

Abstract

A series of environmental studies have been carried out in the northern foothills of the Brooks Range and the Arctic Coastal Plain in the Kuparuk River Basin, Alaska, to develop a better understanding of the physical and climatic dynamics of an arctic ecosystem. As part of these studies, soil temperature and snow depth measurements along a transect from near the Beaufort Sea coast across the Coastal Plain to the Brooks Range foothills were made continuously at three locations. Summarized here are trends observed in soil temperature spanning the last 15 years in this area. Soil temperature measurements were made in the active layer and permafrost to depths exceeding 10 meters. Data collection began at these sites in 1993. These datasets are of sufficient temporal length and quality to begin showing long-term trends in arctic soil temperature and the relationship between snow depth and winter soil temperature. All locations within the permafrost show a warming trend (average annual temperature) over the period of observations (depths greater than 50 cm at Franklin Bluffs and Sagwon Hill and 90 cm at Imnavait Ridge). Maximum soil temperatures in the active layer above the permafrost, however, show a slight cooling trend at all three sites. Minimum soil temperatures in the permafrost at each site are increasing as are average annual soil temperatures; maximum annual temperatures in the permafrost are mixed with Sagwon Hills decreasing. There is no significant overall trend in snow water equivalent (SWE) at the three sites. There is considerable variation in SWE and snow depth from year-to-year, which clarifies the dependence of the soil thermal regime on snow. The hydrologic cycle in these catchments has yet to show any response that can be documented.

Keywords: active layer; Alaska; climate change; hydrology; permafrost; soil temperature.

Introduction

Since 1985, continuous hydrologic research studies have been ongoing on the North Slope of the Alaskan Arctic (Fig. 1) in watersheds within and adjacent to the north-flowing Kuparuk River Basin (Kane et al. 2000). The hydrologic response of these basins is related to the major physical properties of the basin such as topography, soils, vegetation, and thermal state In this case the thermal state is probably the most important, as the area is underlain by continuous permafrost 250 to >600 m deep. It is clear from the published papers that the environment of this region is transitioning to a warmer climate (Serreze et al. 2000, Hinzman et al. 2005, and others). Heat and mass water fluxes in any environment are closely intertwined. Therefore, if the climate is warming, the hydrology of these Arctic basins will also be impacted. One could foresee greater precipitation with less spatial and temporal sea ice extent (sources of precipitable water increasing); perhaps increased evapotranspiration (ET) from land surfaces with increases in precipitation and air temperature; and the runoff response is debatable, depending upon what happens with precipitation. One of the major controversial areas is what will happen to the active layer and vegetation, as this has long-term implications to the hydrologic cycle of the Arctic.

Two decades ago, Lachenbruch and Marshall (1986)

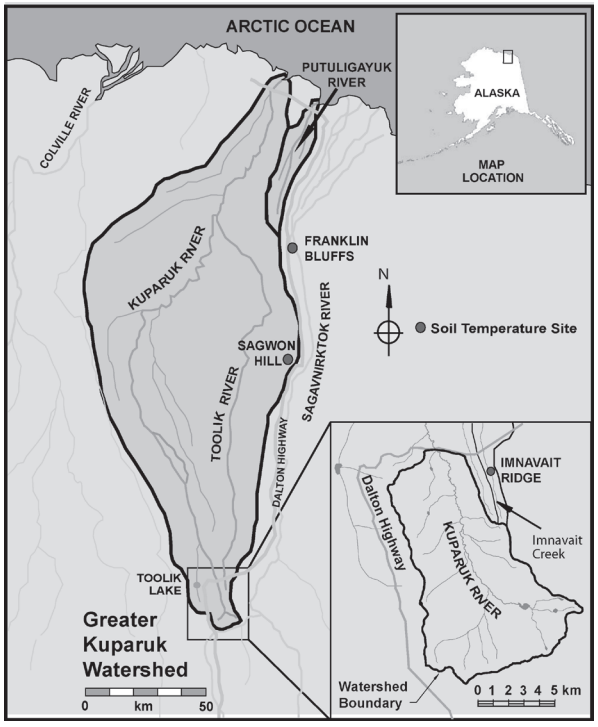

Figure 1. Map of the monitored watersheds and the borehole observations sites on the North Slope of Alaska, USA.

showed that permafrost on the North Slope of Alaska was warming. Clearly it took thousands of years for the permafrost to form, and it is not going to totally disappear for some time (except where it is quite warm and thin, but that is not the case in northern Alaska). Presently, the active layer in the Kuparuk basin is on average about 40 to 60 cm deep (Hinzman et al. 1998), greater in well-drained sites, and shallower in poorly drained sites. There is evidence, however, that change is ongoing near the ground surface. Sturm et al. (2001) described the increase in shrubs in the present tundra environment on the North Slope of Alaska; hydrologically this has implications for trapping snow, ET and soil moisture, and possibly runoff. A warmer climate should result in a deeper active layer initially, though there are some who would argue that shrubs will invade and provide ground shading and thus lower ground surface temperatures. It is more complex than this, however, as different plant communities have different soil water demands (drier soils typically have deeper active layers because less energy is needed for phase change). Overduin and Kane (2006) have shown that over a three-year period, no increase in the active layer thickness was observed for a site on the North Slope of Alaska from relative depth measurements at summer's end. However, more detailed analyses showed that areal ground surface subsidence rates of 2 to 5 cm/yr were due to the melting of ice at the base of the active layer, although not detected in simple active layer depth measurements relative to the surface with a probe.

Presented here are the results of 15 years of borehole data collected at sites on a north-south transect in the Kuparuk River basin. Most of the discussion will concentrate on three sites: Franklin Bluffs, Sagwon Hill, and Imnavait Ridge. At these three sites, measurements were made at depths greater than 10 m. Several thermistor strings were also installed at numerous other sites in the shallow active layer.

Setting

Four nested watersheds on the North Slope of Alaska, USA (Fig. 1), are instrumented with hydrologic and meteorological stations that support hydrologic and related process studies and data to complete water balance computations (Kane et al. 2004, Lilly et al. 1998, Kane et al. 2008a). These studies were initiated in 1985 in Imnavait Creek (2.2 km^2), 1993 in the Upper Kuparuk (142 km^2) and entire Kuparuk River (8,140 km^2), and in 1999 in the Putuligayuk catchment (471 km^2). The U.S. Geological Survey (USGS) started gauging the entire Kuparuk River near Deadhorse in 1971, and the record is continuous. They also started gauging the Putuligayuk River in 1971; however, in the 1980s some years of data are missing, and then they switched it to a crest gauge. During the early years of gauging by the USGS, there was very little complementary hydrologic data collected until this study was initiated.

The north draining Kuparuk basin transitions the northern extremities of the Brooks Range, through the foothills and finally into the Arctic Ocean after crossing the low-gradient Coastal Plain. The permafrost thickness increases from 250 m in the headwaters to 600 m along the coast. The active layer is generally about 40 to 60 cm deep, although it is quite variable, depending upon slope, aspect, soils, organic cover, etc. Vegetation is essentially continuous over the area, starting with alpine communities in the headwaters, tussock tundra in the foothills, and sedges and grasses on the Coastal Plain. Shrubs (~1 m high) can be found throughout the basin except at the high elevations and the northern extremes. More detailed description of these basins can be found in Kane et al. (2000).

Results

Franklin Bluffs is located approximately 25 miles south of the Arctic Ocean coastline in the Coastal Plain (Fig. 1). The terrain is low gradient and poorly drained. The daily soil temperatures are plotted since 1993 in Figure 2 (there is one gap in the dataset). Soils at this site displayed a cooling of the summer maximum annual temperature in the active layer and a warming of the permafrost soils (Fig. 3, Table 1). The winter minimum annual soil temperature showed a cooling trend for active layer soils and a warming trend of permafrost soils (Fig. 4). Overall the average annual soil temperature (Fig. 5) demonstrated a trend of cooling of the active layer soils and a warming of permafrost soils. With cooling of the active layer and warming of the permafrost, there was a convergence of the average annual temperature at each depth. Three winters had above-average SWE (Fig. 6) at this site after 2000; this would decrease deep winter cooling and delay ablation in the spring, thus possibly shortening summer.

The Imnavait Ridge site is located in the Imnavait Basin in the upland of the foothills of the Brooks Range near Toolik Lake (Fig. 1). The site is located on a well drained ridgeline on a gentle west facing slope.

Discussion

It is clear that the hydrology of the Kuparuk River Basin is dominated by deep continuous permafrost. First, the permafrost acts as an aquitard, and there is no hydraulic connectivity between the surface and the subsurface permafrost groundwater (Yoshikawa et al. 2007). In some neighboring watersheds, there are springs of subpermafrost groundwater origin that have apparently been flowing for thousands of years. The thick, ice-rich permafrost severely limits subsurface storage to just the active layer, where the volume of storage is quite close to the average total precipitation for just one year. Because of this limited storage, runoff ratios for these basins are much higher than found in more temperate climates (Kane & Yang 2004) for both snowmelt and rainfall

Kane et al. (2003a) discuss the impact of surficial permafrost features on the runoff response of arctic catchments. In general, these features (polygons, thaw lakes, strangemoor ridges, beaded drainage, etc.) reduce the hydrologic runoff response of these watersheds. However, as an example, the conversion of low-centered polygons to high-center polygons

Table 1. Trend line slopes (1993 to 2007) of annual maximum, minimum, and average temperature at two depths in boreholes on the North Slope of Alaska. *P*-values are in parentheses. The *p*-value represents a decreasing index of the reliability of a result (Brownlee 1960). The lower the *p*-value, the more we can believe that the trend line is significantly different from zero. A *p*-value of 0.01 implies the slope of the trend line is significantly different from zero at the 99% confidence level.

Annual	Imnavait Ridge		Sagwon Bluffs		Franklin Bluffs	
	20 cm	800 cm	20 cm	850 cm	20 cm	850 cm
	°C·yr^{-1}		°C·yr^{-1}		°C·yr^{-1}	
Average	0.03 (0.7377)	0.17 (<0.0001)	0.05 (0.6052)	0.04 (0.2231)	-0.01 (0.9206)	0.12 (0.0011)
Minimum	0.16 (0.5771)	0.14 (0.0004)	0.29 (0.1961)	0.09 (0.0189)	0.20 (0.3145)	0.13 (0.0058)
Maximum	-0.14 (0.0338)	0.13 (0.0013)	-0.27 (0.0026)	-0.02 (0.6161)	-0.19 (0.0128)	0.11 (<0.0001)

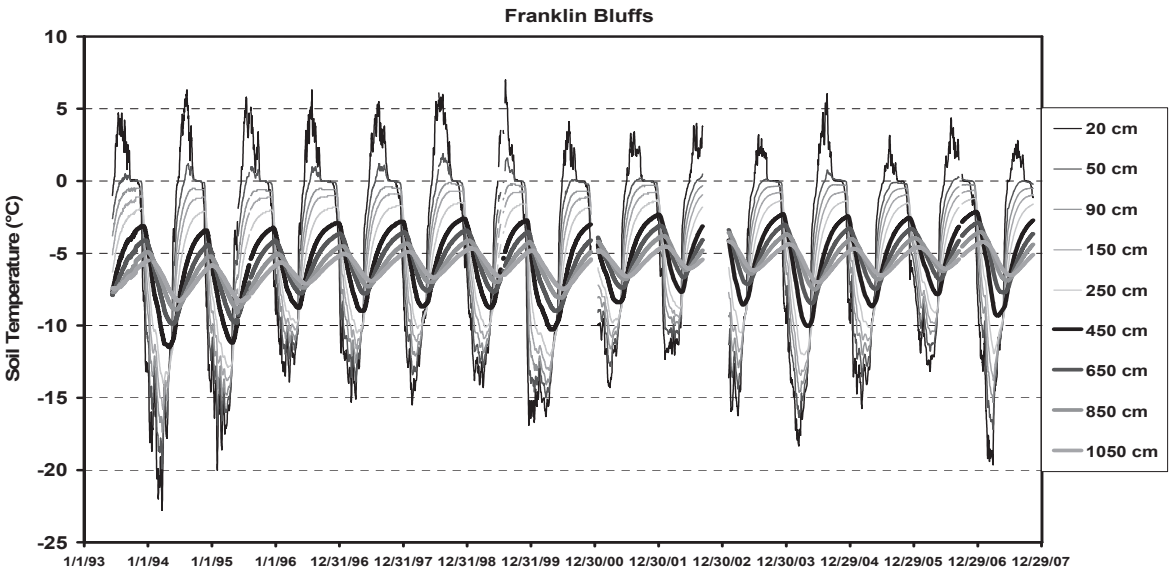

Figure 2. Daily variations in soil temperatures observed in a borehole near Franklin Bluffs, Alaska, from the surface down to 10.5 m from 1993 to 2007.

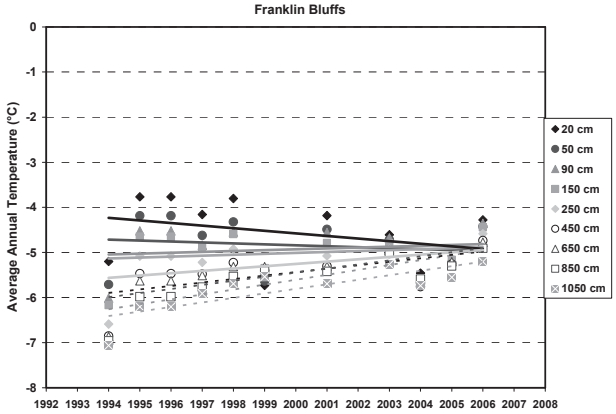

Figure 3. Trends observed in the average annual soil temperature profile of the borehole near Franklin Bluffs, Alaska.

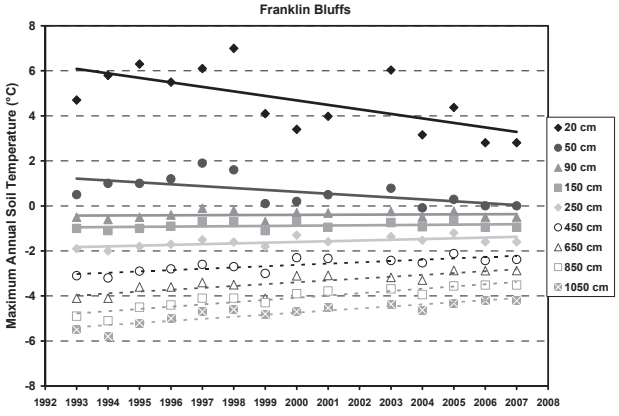

Figure 4. Trends observed in the maximum annual soil temperature profile of the borehole near Franklin Bluffs, Alaska.

could significantly increase the hydrologic runoff response of a watershed, including sediment yield. This process has been observed in several areas by the authors along the Dalton Highway outside the studied basin. McNamara et al. (1999) hypothesized that headwater drainages (water tracks) in the Arctic are immature channels that have not fully developed because of the underlying permafrost. The suggestion that permafrost is limiting channel maturity has many implications to the hydrologic response of arctic catchments in a changing climate, including runoff response and sediment (suspended and bed) yields.

In response to some imposed disturbance, such as a tundra fire or climatic warming, massive ice-rich permafrost may differentially thaw, creating irregular surface topography. Depressions forming on the surface soon form ponds, accelerating subsurface thaw through lower albedo and additional heat advected into the pond through runoff. In time, a talik (a layer of unfrozen soil above the permafrost and below the seasonally frozen soil) may form below such ponds as the depth of water becomes greater than the amount

that can refreeze during the winter. If the talik grows to a size that completely penetrates the underlying permafrost or connects to a subsurface layer that allows continued drainage, the pond may then begin to drain. Over the past three to five decades, increased pond formation and shrinking have been observed in Alaska (Yoshikawa & Hinzman 2003, Jorgensen et al. 2001), Canada (Smol & Douglas 2007), and Siberia (Smith et al. 2001).

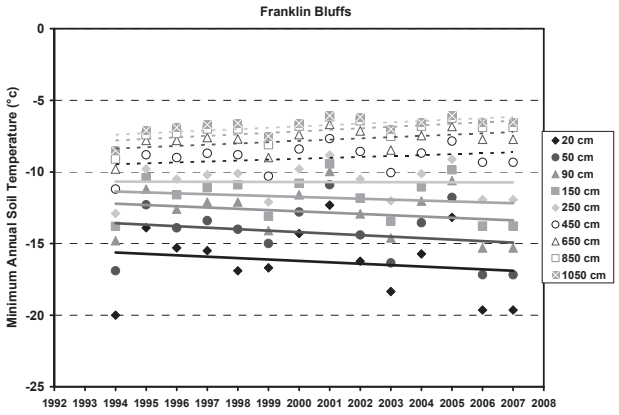

Figure 5. Trends observed in the minimum annual soil temperature profile of the borehole near Franklin Bluffs, Alaska.

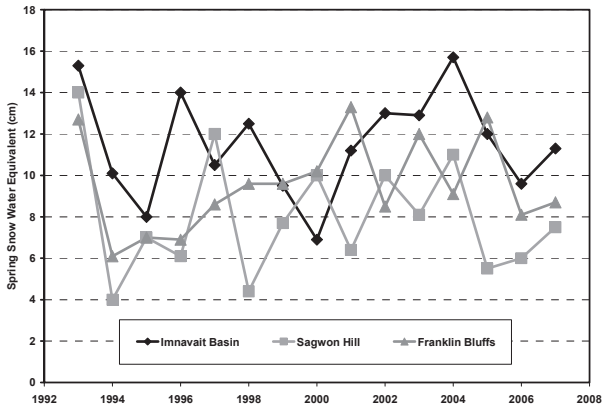

Figure 6. Annual variations in the maximum snowpack water equivalent measured near borehole sites just prior to spring melt.

Summary

The general trend of the thermal regime at the three research sites is one of overall warming; this is in agreement with other studies (Romanovsky et al. 2002). The warming was strongly statistically significant at the 850 cm depths for the minimum annual temperatures at all three sites. The deeper temperature probes (>400 cm) displayed significant warming in average, minimum, and maximum annual temperatures at Imnavait Creek and Franklin Bluffs, but was not consistent at Sagwon. To date, we do not see measurable responses of arctic hydrology to climate change in the form of changes in precipitation, runoff, soil moisture, storage, and ET. Clearly the permafrost is warming, thermokarsting is evident, and

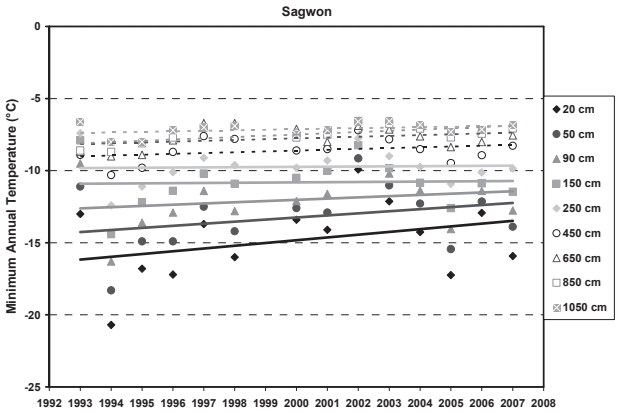

Figure 7. Daily variations in soil temperatures observed in a borehole near Sagwon Bluffs, Alaska, from the surface down to 10.5 m from 1993 to 2007.

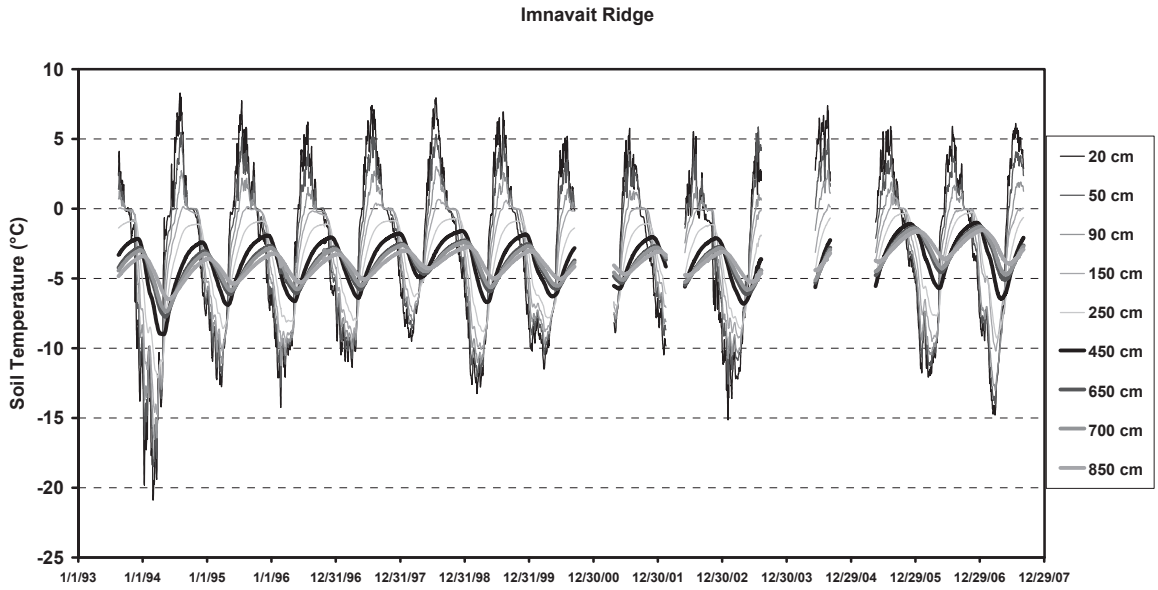

Figure 8. Daily variations in soil temperatures observed in a borehole near Imnavait Creek, Alaska, from the surface down to 8.5 m from 1993 to 2007.

thawing of the top of the ice-rich permafrost is ongoing. In an area of the world where frozen ground plays a dominant role in the physical structure of a watershed, this should be viewed ominously. Why do we not presently see this impact on arctic hydrology? First, it may not be extensive enough to reach a threshold value at the watershed scale. Second, changes in the hydrology will not be evident until the soil has progressed from frozen to thawed. Although warming is occurring, it appears that the small amount of thawing that has occurred at the base of the active layer has not significantly increased the available storage due to subsidence concurrent with thawing. Third, there is considerable natural variability in these hydrologic processes, plus we still struggle to make accurate estimates of hydrologic fluxes and stores. The natural variability in hydrological variables may be much greater than the subtle differences induced by a warming climate. We hypothesize that continued warming of the permafrost will bring significant changes to the hydrology of this region as we presently know it.

Acknowledgments

This paper is based on work supported by the National Science Foundation, Office of Polar Programs (Grants OPP-9814984, OPP-009615, OPP-0327664, and OPP-0335941), and the U.S. Army CRREL for borehole drilling support.

References

Hinzman, L.D. Bettez, N.D., Bolton, W.R., Chapin, F.S., Dyurgerov, M.B., Fastie, C.L., Griffith, B., Hollister, R.D., Hope, A., Huntington, H.P., Jensen, A.M., Jia, G.J., Jorgenson, T., Kane, D.L., Klein, D.R., Kofinas, G., Lynch, A.H., Lloyd, A.H., McGuire, A.D., Nelson, F.E., Oechel, W.C., Osterkamp, T.E., Racine, C.H., Romanovsky, V.E., Stone, R.S., Stow, D.A., Sturm, M., Tweedie, C.E., Vourlitis, G.L., Walker, M.D., Walker, D.A., Webber, P.J., Welker, J., Winker, K.S. & Yoshikawa, K. 2005. Evidence and implications of recent climate change in Northern Alaska and other Arctic regions. *Climatic Change* 72(3): 251-298.

Hinzman, L.D., Goering, D.J. & Kane, D.L. 1998. A distributed thermal model for calculating temperature profiles and depth of thaw in permafrost regions. *Journal of Geophysical Research – Atmospheres* 103(D22): 28,975-28,991.

Jorgenson, M.T., Racine, C.H., Walters, J.C. & Osterkamp, T.E. 2001. Permafrost degradation and ecological changes associated with a warming climate in central Alaska. *Climate Change* 48: 551-579.

Kane, D.L., Hinzman, L.D., McNamara, J.P., Zhang, Z. & Benson, C.S. 2000. An overview of a nested watershed study in Arctic Alaska. *Nordic Hydrology* 4/5: 245-266.

Kane, D.L., Gieck, R.E. & Bowling, L.C. 2003a. Impacts of surficial permafrost landforms on surface hydrology. *Proceedings of the Eighth International Conference on Permafrost, Zurich, Switzerland, 21–25 July 2003*, M. Phillips et al. (eds.). Lisse, The Netherlands: A.A. Balkema Publishers: 507-512.

Kane, D.L., McNamara, J.P., Yang, D., Olsson, P.Q. & Gieck, R.E. 2003b. An extreme rainfall/runoff event in Arctic Alaska. *Journal of Hydrometeorology* 4(6): 1220-1228.

Kane, D.L., Gieck, R.E., Kitover, D.C., Hinzman, L.D., McNamara, J.P. & Yang, D. 2004. *Hydrologic Cycle on the North Slope of Alaska*. International Association of Hydrological Sciences, IAHS Publication 290, 224-236.

Kane, D.L. & Yang, D. 2004. *Northern Research Basins Water Balance*. International Association of Hydrological Sciences, IAHS Publication 290, 271 pp.

Kane, D.L., Gieck, R.E. & Hinzman, L.D. 2008a. Water balance for a low-gradient watershed in Northern Alaska. *Proceedings of the Ninth International Conference on Permafrost, Fairbanks, Alaska, June 29–July 3, 2008* (this proceedings).

Kane, D.L., Hinzman, L.D., Gieck, R.E., McNamara, J.P., Youcha, E.K. & Oatley, J.A. 2008b. Contrasting extreme runoff events in areas of continuous permafrost. *Arctic Alaska. Hydrology Research* (in press).

Lachenbruch, A.H. & Marshall, B.V. 1986. Changing climate: geothermal evidence from permafrost in the Alaskan Arctic. *Science* 234: 689-696.

Lilly, E.K., Kane, D.L., Hinzman, L.D. & Gieck, R.E. 1998. Annual water balance for three nested watersheds on the North Slope of Alaska. *Proceedings of the Seventh International Conference on Permafrost*, *Yellowknife, Canada, June 1998*, A.G. Lewkowicz & M. Allard (eds.): 669-674.

McNamara, J.P., Kane, D.L. & Hinzman, L.D. 1999. An analyses of an Arctic channel network using a digital elevation model. *Geomorphology* 29: 339-353.

Overduin, P. P. & Kane, D.L. 2006. Frost boils and soil ice content: Field observations. *Permafrost and Periglacial Processes* 17: 291-307.

Romanovsky, V.E., Burgess, M., Smith, S., Yoshikawa, K. & Brown, J. 2002. Permafrost temperature records: indicators of climate change. *EOS* 83(50): 589 & 593-594.

Serreze, M. C., Walsh, J.E., Chapin, F.S. III, Osterkamp, T., Dyurgerov, M., Romanovsky, V., Oechel, W.C., Morison, J., Zhang, T. & Barry, R.G. 2000. Observational evidence of recent change in the northern high latitude environment. *Climate Change* 46: 159-207.

Smith, L.C., Sheng, Y., MacDonald, G.M. & Hinzman, L.D. 2005. Disappearing Arctic lakes. *Science* 308: 1429, (3 June 2005).

Smol, J.P. & Douglas, M.S.V. 2007. From controversy to consensus: Making the case for recent climatic change in the Arctic using lake sediments. *Frontiers in Ecology and the Environment* 5: 466-474.

Sturm, M., Racine, C. & Tape, K. 2001. Increasing shrub abundance in the Arctic. *Nature* 411: 546-547.

Yoshikawa, K. & Hinzman, L. 2003. Shrinking thermokarst ponds and groundwater dynamics in discontinuous permafrost. *Permafrost and Periglacial Processes* 14(2): 151-160.

Yoshikawa K., Hinzman, L.D. & Kane, D.L. 2007. Spring and aufeis (icing) hydrology in Brooks Range, Alaska *J. Geophys. Res*. 112: G04S43, doi:10.1029/2006JG000294.

Factors Controlling Periglacial Geodiversity in Subarctic Finland

Jan Hjort
Department of Geography, University of Helsinki, Helsinki, Finland
Miska Luoto
Thule Institute, University of Oulu, Oulu, Finland Department of Geography, University of Oulu, Oulu, Finland

Abstract

The aim of this study was to determine the environmental factors controlling the diversity of periglacial landforms on the landscape scale. The study was performed using an empirical dataset of periglacial landforms from an area of 600 km^2. Both distribution and abundance of landform diversity were modeled. The utilized statistical method was generalized linear modeling (GLM). A total of 40 different periglacial landform types and subtypes were identified. The number of different types in the 25-ha modeling squares varied from zero to nine. Based on GLM, the diversity of periglacial features increased with increasing moisture variability and altitude. Moreover, slope angle was an important correlate with cubic term; the diversity was highest on flat ground sites (0–2°) and on rather steep slopes (8–12°). The employment of GLM proved to be a useful approach to estimate the role of environmental factors in determining the periglacial geodiversity.

Keywords: generalized linear modeling (GLM); geodiversity; periglacial geomorphology; prediction; subarctic.

Introduction

Periglacial domain covers different features from large pingos to small sorted circles (French 2007). On a regional scale, the variety of periglacial phenomena can be substantial including several tens of features (e.g. Åkerman 1980). While the diversity of periglacial landforms is a well-known issue, rather few have studied the environmental factors behind the feature variability. One potential reason for the lack of research may be the difficulty in analyzing complex processes in extensive regions. The recent developments in combining the Geographic Information System (GIS), remote sensing (RS) data, and statistical techniques have improved the possibility of surveying extensive regions and studying different aspects of periglacial geomorphology (Luoto & Hjort 2005, 2008, Etzelmüller et al. 2006, Brenning et al. 2007, Hjort & Luoto, in press).

It would be profitable to develop spatial analysis techniques to map the sites of high geodiversity, because knowledge on the variability of geomorphological processes and landforms is important to conservation managers, engineers, and scientists (Walsh et al. 1998). Furthermore, in the context of geodiversity, the interest in variability on non-living nature has risen recently (e.g., Gray 2004). The concept of geodiversity is less well-appreciated in geomorphology, but is now developing momentum of its own. Geodiversity conservation is increasingly seen as important in its own right and as an essential support to biodiversity and cultural conservation programs (Gray 2004).

Here we examine the applicability of GIS-based datasets and generalized linear modeling (GLM) in determining the factors controlling the diversity of periglacial landforms on the landscape scale (Luoto & Hjort 2004, Hjort et al. 2007). The study is performed using an empirical dataset of periglacial landforms from an area of 600 km^2 at a 25-ha resolution (n = 2249). This rather coarse resolution was chosen based on data exploration and attempts to reduce the potential problems of spatial autocorrelation in statistical modeling (McCullagh & Nelder 1989). Both distribution (high- vs. low-diversity sites) and abundance (number of different types) of landform diversity were analyzed. Especially, we seek answers to the questions: (i) can we spatially predict the diversity of periglacial landforms and (ii) which environmental factors control the diversity in subarctic Finland on the landscape scale?

Study Setting

Background: factor-process-landform relationship

The complex relationship between environmental factors affecting the activity and presence of periglacial processes is presented in Figure 1A. In general, the most important environmental drivers are climate, topography, material, moisture conditions, snow and ice cover as well as vegetation (Washburn 1979, French 2007). Climatological conditions affect, for example, freeze-thaw cycles and moisture distribution and thus, all periglacial processes (Fig. 1B). Moreover, the wind has a significant role in snow redistribution, which affects ground temperatures and moisture conditions. Soil moisture, along with temperature, is one of the most important determinants of frost processes (e.g., Matthews et al. 1998). Soil material affects the moisture distribution and activity of periglacial process. Topography, snow cover, and vegetation influence the processes through the main factors: temperature and soil moisture (Fig. 1). However, topography directly affects slope phenomena, and vegetation on the slope as well as aeolian processes. Most of these environmental factors have a positive relationship with the process activity. Nonetheless, some factors (e.g., soil moisture) may reduce the activity of periglacial processes (e.g., aeolian phenomena).

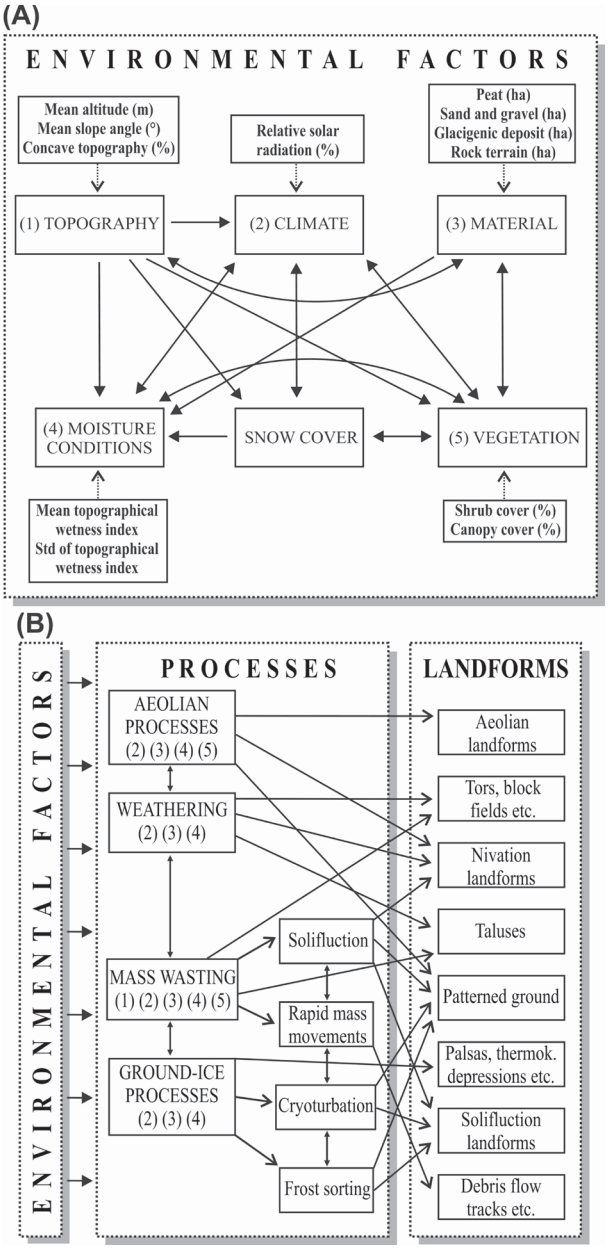

Figure 1. (A) The main interactions between environmental factors affecting periglacial processes and landforms on a regional scale. The environmental predictors and surrogates of factors used in this study are shown in outermost boxes. (B) Simplified conceptual model of the relationships between environmental factors, periglacial processes, and periglacial landforms commonly found from northern Fennoscandia (e.g., Lundqvist 1962, Harris 1982, Seppälä 2005). The main factors affecting processes are indicated with numbers (1 = topography, 2 = climate, etc.).

Study area

The study area is located in the northernmost Finnish Lapland within the zone of discontinuous permafrost (Fig. 2). The landscape of the area is characterized by rather rounded fells with elevations ranging from 110 to 641 m above sea level. The bedrock (ca. 1.9 billion-year-old) is covered by glacigenic till and peat, as well as sand and gravel deposits (Meriläinen 1976). Moreover, silty sediments are prevalent in the wide flat-bottomed valleys. The climate of the area is subarctic: the mean annual air temperature is -2.0°C, and mean annual precipitation ca. 400 mm (*Climatological Statistics in Finland 1961–1990* 1991). The vegetation of the area is characterized by subalpine mountain birch forests (*Betula pubescens* ssp. *czerepanovii*) and alpine heaths (*regio alpina*).

Modeling data

Periglacial landforms. The landforms were mapped and converted to grid-based modeling data in four steps (for details see Hjort 2006). First, a detailed stereoscopic interpretation of black-and-white aerial photographs (1:31,000) was performed to identify the potential sites of periglacial features. Second, the features were mapped utilizing pre-mapping results and a Global Positioning System (GPS) device (Garmin eTrex personal navigator with an accuracy of ca. 10 m) in the field during the summers of 2002 and 2003. Third, the field-mapping results were digitized in a vector format on orthorectified aerial photographs (ground resolution = 1 m) utilizing GIS software. Both active and inactive landforms were grouped together because the determination of activity of some feature types would have been a complicated task without several year-round field measurements. Finally, the created geomorphological database was used to produce two types of response datasets at the 25-ha resolution. In the first case, the datum was divided to the sites of high (coded 1) and low (coded 0) diversity using threshold values from 4 to 6 (e.g., high diversity ≥4 landform types present in the modeling square, low diversity <4 types present). In the second case, landform diversity was determined based on the number of different landform types in the modeling squares. The first type of datum was used to model the occurrence of high and low sites of diversity (distribution modeling) and the second type was used to analyze the intensity of diversity (abundance modeling).

Explanatory data. Taking into account the study aims, modeling resolution, and the complex relationships between environmental factors, periglacial processes, and periglacial landforms (Fig. 1), the explanatory variables (i.e., predictors) were compiled from commonly used and accessible information sources, namely a digital elevation model (DEM) (20-m grid size) (Hjort 2006), biotope database (Anonymous 2002), and digital soil map (Hjort 2006). Six topographical parameters (mean altitude, mean slope angle, mean and standard deviation of topographical wetness index, proportion of concave topography, and relative solar radiation), 4 soil-type variables (glacigenic deposit, sand and gravel, peat, as well as rock terrain cover), and 2 vegetation factors (shrub and tree cover) were computed using Arc/Info GRID at the 25-ha resolution (Fig. 1).

Data split. The final modeling data included 2249 squares, which were randomly divided into model- calibrating (50%, n = 1125) and model-evaluation sets (50%, n = 1124) (Guisan & Zimmerman 2000). A total of 151 squares were excluded due to the abundant water cover and deficiency in the explanatory data.

Figure 2. Location of the study area in northern Fennoscandia. Permafrost conditions are indicated with shades of gray: continuous (darkest), discontinuous, and sporadic (modified after Brown et al. 1998).

Generalized linear modeling

Generalized linear models (GLMs) are mathematical extensions of traditional least square (LS) regression models that do not force data into unnatural scales; they allow for nonlinearity and nonconstant variance (heteroscedasticity) structures in the data (McCullagh & Nelder 1989). In this study, the model calibration was performed utilizing the statistical package R version 2.3.0, with standard GLM function. The probability of curvilinear relationships between the explanatory and response variables was examined by including the quadratic and cubic terms of the predictors in the models (Crawley 1993). The variables were selected using a statistically focused backward elimination approach (see Crawley 1993). Elimination was based on a strict criterion ($p < 0.001$) for variable exclusion. The percentage of deviance explained [(null deviance – residual deviance / null deviance) * 100] was calculated for the final GLMs to gain an overall picture of the success of the fitting (for details see Hjort 2006).

Model evaluation. The distribution models were assessed utilizing evaluation data and the area under the curve (AUC) values of a receiver operating characteristic (ROC) plot (e.g., Pearce & Ferrier 2000). The AUC values range from 0.5 for models with no discriminative ability to 1.0 for models with perfect discrimination. Swets (1988) proposed a rough guide for classifying the AUC measures of the models: 0.50–0.70 = low model accuracy, 0.71–0.90 good model accuracy, > 0.90 = high model accuracy. The predictive ability of the abundance model was assessed by calculating Spearman's rank correlation coefficient (R_s) between the predicted and observed diversity using evaluation data (Guisan & Zimmermann 2000).

Results

Periglacial landforms

A total of 40 different periglacial landform types and subtypes were identified (Table 1). The most common landforms, if calculated by occupied modeling squares, were earth hummocks (n = 1636), peat pounus (n = 702), sorted nets (n = 631) and sorted sheets (n = 431). The rarest features were non-sorted lobes (n = 10), slushflow tracks (n = 4) and braking blocks (n = 4), respectively.

Table 1. Periglacial landforms mapped from the study area and their prevalence at the 25-ha modeling resolution (x = not determined).

Periglacial landforms	Present squares (%)
Palsas (4 subtypes)	134 (5.4%)
Thermokarst ponds	69 (2.8%)
Circles	
- convex non-sorted circles	229 (9.2%)
- stony earth circles	245 (9.8%)
- earth hummocks	1636 (65.4%)
- peat pounu	702 (28.1%)
- sorted stone circles	81 (3.2%)
- stone pits	252 (10.1%)
- debris islands	38 (1.5%)
Polygons	
- non-sorted polygons	18 (0.7%)
- sorted polygons	50 (2.0%)
Nets	
- sorted nets	631 (25.2%)
Boulder depressions	73 (2.9%)
Steps	
- non-sorted steps	111 (4.4%)
Stripes	
- non-sorted stripes	36 (1.4%)
- sorted stripes	198 (7.9%)
Debris flow slopes	17 (0.7%)
Slush flow tracks	4 (0.2%)
Solifluction features	
- non-sorted terraces	275 (11.0%)
- non-sorted lobes	10 (0.4%)
- ploughing blocks	15 (0.6%)
- braking blocks	4 (0.2%)
- sorted sheets (2 subtypes)	431 (17.2%)
- sorted terraces	74 (3.0%)
- sorted lobes	68 (2.7%)
- sorted streams	244 (9.8%)
Talus slopes	19 (0.8%)
Block fields	34 (1.4%)
Tors	127 (5.1%)
Nivation sites	x
Stone pavements	15 (0.6%)
Sand dunes (3 subtypes)	99 (4.0%)
Deflation sites (2 subtypes)	295 (11.8%)

The number of different periglacial landform types in the 25-ha modeling squares varied from 0 to 9 (Fig. 3). A total of 247 (9.9%) squares were without any periglacial features and 2253 (90.1%) sites were occupied by at least 1 landform type. Squares with only 1 landform type were commonly occupied by extensive fields of earth hummocks, peat pounus, palsas, or sorted nets. Considerably many of the modeling squares included 2 to 4 different landform

types, which is mainly caused by the presence of feature continuums. Over 6 landform types were observed from only 58 (2.3%) squares.

Diversity GLMs

The results of the diversity modeling are summarized in Table 2. In distribution modeling, the amount of explained deviance varied between 16% and 18%. The abundance model was able to explain 21% of the deviance change. In model evaluation, the AUC measures of the distribution models ranged from 0.76 to 0.78, indicating fair discrimination ability between the sites of high and low diversity. The abundance model was moderate in predicting the number of different periglacial landforms present in the analysis squares (R_s = 0.52).

The number of the environmental factors varied from 2 to 4 in the final GLMs (Table 2). The most important correlates for both the distribution of high-diversity sites (≥4 landforms present) and abundance of landform types were mean altitude, mean slope angle, and soil moisture variability. The slope angle variable was included in 3 of the 4 models with cubic term, indicating that the diversity was highest on flat ground sites (0–2°) and on rather steep slopes (8–12°) (Fig. 4). Moreover, canopy and peat cover were shown to be connected to the diversity (Table 2).

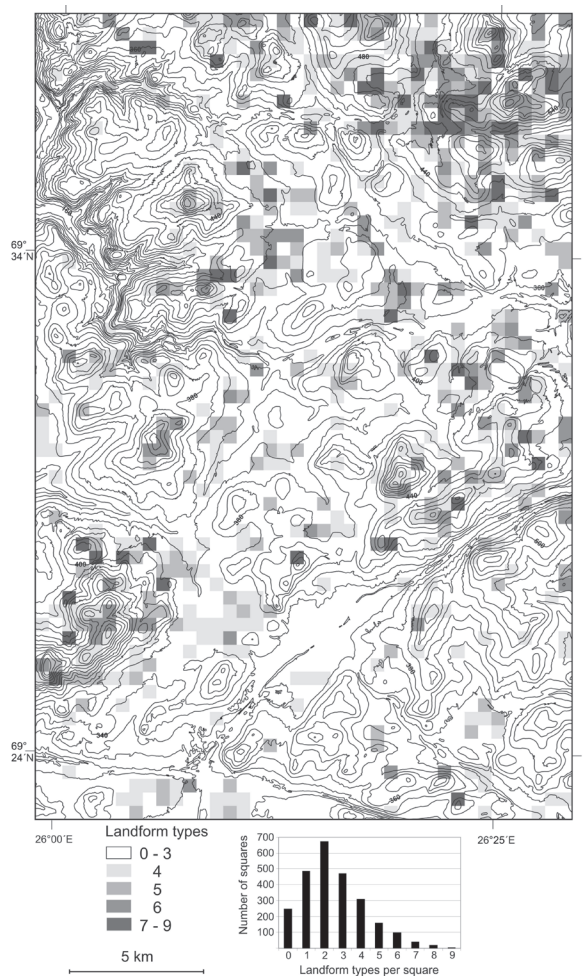

Figure 3. Number of different periglacial landform types at the 25-ha modeling resolution. The vertical interval of contours is 20 m (© National Land Survey of Finland).

Discussion

In general, knowledge on the diversity of geomorphological phenomena could be useful for academic, applied and economic applications (Gray 2004). In the context of global change, spatial models of geodiversity could be used to assess the impacts of changing environmental conditions on periglacial processes (Fronzek et al. 2006, Johansson et al. 2006). One would expect that declining frost conditions would decrease the feature variability, but the short-term effects of climate change on periglacial processes are rather unclear. For example, increasing temperature decreases frost severity. However, increasing precipitation could increase frost activity because moisture availability has shown to be one of the most important determinants for the occurrence

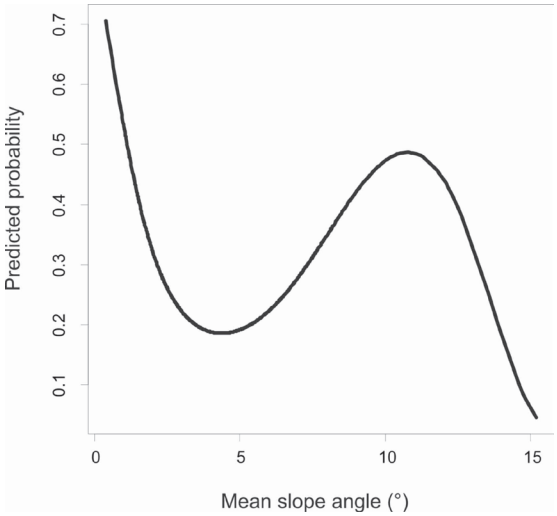

Figure 4. Relationship between diversity of periglacial landforms and slope angle. The predicted probability of diversity is derived from the distribution GLM (threshold value = 4) relating slope variable separately to the response variable.

Table 2. Summary of the final distribution (D_x) and abundance (A) models (x indicates the utilized threshold value in distribution modeling).

GLM	Mean altitude	Mean slope angle	Std of wetness index	Mean canopy cover	Peat cover	AUC cal / eval $R_{(s)}$ cal / eval
D_4	↗	− + −	↗	↘		0.79 / 0.76
D_5	↗	− + −	↗			0.78 / 0.76
D_6	↗		↗			0.79 / 0.78
A	↗	− + −	↗		∩	*0.48 / 0.52*

The direction of the effect of environmental factor ($p < 0.001$) is indicated with symbols (↗ = positive correlate, ↘ = negative correlate, ∩ = second-order correlate with a humped response curve, − + − = third-order correlate with a recumbent S-shaped response curve). The area under the curve (AUC) values and Spearman's rank correlation coefficient (R_s) were calculated with the calibration (cal) and evaluation (eval) data.

and activity of frost processes on a local (e.g., Matthews et al. 1998) and regional (Luoto & Hjort 2004) scale. Moreover, climate warming will probably increase the vegetation cover in sparsely vegetated arctic and subarctic regions (e.g., Liston et al. 2002). This would affect the periglacial processes, because feature occurrences have shown to be connected to shrub abundance, both positively and negatively, depending on the process type (Hjort 2006).

Periglacial phenomena have been mapped from numerous cold climate regions, but environmental factors controlling diversity have not been analyzed statistically previously (e.g. Lundqvist 1962, Karte 1979, Åkerman 1980, Harris 1982, Hjort 2006). Based on the modeling conducted in this study, the diversity of periglacial landforms was connected to altitude and soil moisture variability on the landscape scale. Moreover, the most diverse sites were either flat areas (0–2°) or rather steep slopes (8–12°). Different patterned ground features occur on flat topography, whereas moderate slopes are covered by sorted and non-sorted solifluction landforms. In proportion, gentle slopes are less suitable for most of the observed periglacial feature types (cf. Washburn 1979, French 2007).

The prediction and explanation power of the models were only on a moderate level (cf. Brenning & Trombotto 2006, Hjort et al. 2007). This is partly due to the complex process-environment relationships when landforms of different origin are grouped. Several different processes are responsible for the genesis of the observed periglacial landforms, and it is a challenging task to generate spatial datasets of causal factors of periglacial processes (Luoto & Seppälä 2002). Moreover, the correlation between environmental factors and periglacial landforms may be blurred by the fact that an environmental factor may be a positive or a negative correlate, depending on the feature type. On the other hand, the employment of a multivariate method and GIS-based data helped to draw a conclusion of factors affecting periglacial geodiversity, an issue that may be a complicated task using traditional descriptive methods.

Despite the fact that the prediction and explanation abilities of the models were rather low, the models were robust and gave parallel results. Therefore, the inferences of important environmental factors lie on fairly solid ground. However, the data-related limitations and method-based weaknesses may bias the modeling results, and the model outcomes should not be interpreted uncritically. In the context of geomorphological modeling, these important issues have been discussed, for example by Guzzetti et al. (1999) as well as Luoto & Hjort (2006).

Conclusions

The employment of GLM and GIS-based data proved to be a useful way to estimate the role of environmental factors in determining the diversity of periglacial features. However, the prediction and explanation power of the models were comparatively low due to the complex process-environment relationships when landforms of different genesis were grouped. Thus, there remains considerable room for further improvements in modeling the diversity of periglacial geomorphology. Improved models could be applied in geodiversity and environmental change studies.

Acknowledgments

The Kevo Subarctic Research Institute provided outstanding facilities during the field surveys. J. Hjort was funded by the Finnish Cultural Foundation.

References

Åkerman, J. 1980. Studies on periglacial geomorphology in West Spitsbergen. *Meddelanden Från Lunds Universitets Geografiska Institution, Avhandlingar* 89, 297 pp.

Anonymous, 2002. *Digital Biotope Data*. Helsinki: Metsähallitus.

Brenning, A. & Trombotto, D. 2006. Logistic regression modeling of rock glacier and glacier distribution: Topographic and climatic controls in the semi-arid Andes. *Geomorphology* 81: 141-154.

Brenning, A., Grasser, M. & Friend, D.A. 2007. Statistical estimation and generalized additive modeling of rock glacier distribution in the San Juan Mountains, Colorado, United States. *Journal of Geophysical Research* 112: F02S15.

Brown, J., Ferrians, O.J.J., Heginbottom, J.A. & Melnikov, E.S. 1998 (revised February 2001). *Circum-Arctic map of permafrost and ground-ice conditions*. Boulder, CO: National Snow and Ice Data Center/ World Data Center for Glaciology. Digital Media.

Climatological Statistics in Finland, 1961–1990. 1991. Supplement of meteorological yearbook of Finland. Helsinki: Finnish Meteorological Institute, 125 pp.

Crawley, M.J. 1993. *GLIM for Ecologists*. Oxford: Blackwell Scientific Publications, 379 pp.

Etzelmüller, B., Heggem, E.S.F., Sharkhuu, N., Frauenfelder, R., Kääb, A. & Goulden, C. 2006. Mountain permafrost distribution modelling using a multi-criteria approach in the Hövsgöl area, northern Mogolia. *Permafrost and Periglacial Processes* 17: 91-104.

French, H.M. 2007. *The Periglacial Environment* (3rd ed.) Chichester: Wiley, 458 pp.

Fronzek, S., Luoto, M. & Carter, T.R. 2006. Potential effect of climate change on the distribution of palsa mires in subarctic Fennoscandia. *Climate Research* 32: 1-12.

Gray, M. 2004. *Geodiversity. Valuing and Conserving Abiotic Nature*. Chichester: Wiley, 434 pp.

Guisan, A. & Zimmermann, N.E. 2000. Predictive habitat distribution models in ecology. *Ecological Modelling* 135: 147-186.

Guzzetti, F., Carrara, A., Cardinali, M. & Reichenbach, P. 1999. Landslide hazard evaluation: a review of current techniques and their application in a multi-scale study, Central Italia. *Geomorphology* 31: 181-216.

Harris, C. 1982. The distribution and altitudinal zonation of periglacial landforms, Okstindan, Norway. *Zeitschrift für Geomorphologie* 26: 283-304.

Hjort, J. 2006. *Environmental Factors Affecting the Occurrence of Periglacial Landforms in Finnish Lapland: A Numerical Approach*. Shaker Aachen: Verlag, 162 pp.

Hjort, J. & M. Luoto (In press). Can abundance of geomorphological features be predicted using presence-absence data? *Earth Surface Processes and Landforms* 33.

Hjort, J., Luoto, M. & Seppälä, M. 2007. Landscape scale determinants of periglacial features in subarctic Finland: a grid-based modelling approach. *Permafrost and Periglacial Processes* 18: 115-127.

Johansson, M., Christensen, T.R., Åkerman, J.H. & Callaghan, T.V. 2006. What determines the current presence or absence of permafrost in the Torneträsk region, a sub-arctic landscape in Northern Sweden? *Ambio* 35: 190-197.

Karte, J. 1979. Räumliche Abgrenzung und regionale Differenzierung des Periglaziärs (in German with English summary). *Bochumer Geographische Arbeiten* 35: 211 pp.

Liston, G.E., McFadden, J.P., Sturm, M. & Pielke Sr., R.A. 2002. Modelled changes in arctic tundra snow, energy and moisture fluxes due to increased shrubs. *Global Change Biology* 8: 17-32.

Lundqvist, J. 1962. Patterned ground and related frost phenomena in Sweden. *Sveriges Geologiska Undersökning, Serie C, Avhandlingar och Uppsatser* 583. 101 pp.

Luoto, M. & Hjort, J. 2004. Generalized linear models in periglacial studies: terrain parameters and patterned ground. *Permafrost and Periglacial Processes* 15: 327-338.

Luoto, M. & Hjort, J. 2005. Evaluation of current statistical approaches for predictive geomorphological mapping. *Geomorphology* 67: 299-315.

Luoto, M. & Hjort, J. 2006. Scale matters: A multi-resolution study of the determinants of patterned ground activity in subarctic Finland. *Geomorphology* 80: 282-294.

Luoto, M. & Hjort, J. 2008. Downscaling of coarse-grained geomorphological data. *Earth Surface Processes and Landforms* 33: 75-89.

Luoto, M. & Seppälä, M. 2002. Modelling the distribution of palsas in Finnish Lapland with logistic regression and GIS. *Permafrost and Periglacial Processes* 13: 17-28.

Matthews, J.A., Shakesby, R.A., Berrisford, M.S. & McEwen, L.J. 1998. Periglacial patterned ground on the Styggedalsbreen glacier foreland, Jotunheimen, southern Norway: micro-topographic, paraglacial and geoecological controls. *Permafrost and Periglacial Processes* 9: 147-166.

McCullagh, P. & Nelder, J.A. 1989. *Generalized Linear Models* (2nd ed.) New York: Chapman & Hall, 511 pp.

Meriläinen, K. 1976. The granulite complex and adjacent rock in Lapland, northern Finland. *Bulletin of Geological Survey of Finland* 281. 129 pp.

Pearce, J. & Ferrier, S. 2000. Evaluating the predictive performance of habitat models using logistic regression. *Ecological Modelling* 133: 225-245.

Seppälä, M. 2005. Periglacial environment. In: M. Seppälä (ed.), *The Physical Geography of Fennoscandia*. Oxford: Oxford University Press, 349-364.

Swets, J.A. 1988. Measuring the accuracy of diagnostic systems. *Science* 240: 1285-1293.

Walsh, S.J., Butler, D.R. & Malanson, G.P. 1998. An overview of scale, pattern, process relationships in geomorphology: a remote sensing and GIS perspective. *Geomorphology* 21: 183-205.

Washburn, A.L. 1979. *Geocryology: A Survey of Periglacial Processes and Environments*. London: Arnold, 406 pp.

Borehole and Ground Surface Temperatures and Their Relationship to Meteorological Conditions in the Swiss Alps

Martin Hoelzle
Glaciology, Geomorphodynamic, & Geochronology, University of Zurich
Stephan Gruber
Glaciology, Geomorphodynamics & Geochronology, University of Zurich

Abstract

In Switzerland, several boreholes are monitored within the framework of the Permafrost Monitoring Switzerland (PERMOS). Three of these boreholes, at Murtèl, at Schilthorn, and at Stockhorn, are at least 60 m deep. In addition, a number of shorter boreholes (c. 6 m deep) were drilled in other projects and have been continuously observed over several years. Results on long- and short-term behavior of these boreholes are presented and compared to standard meteorological components, such as air temperatures and snow cover, measured directly at these borehole sites or nearby. First analyses show the importance of the snow cover duration and thickness; more important on a local scale are different surface and subsurface characteristics influencing heat transfer by conduction and heat capacity. The concept of different offsets between atmosphere and lithosphere is discussed, and data reflecting these offsets are presented for typical alpine conditions.

Keywords: alpine permafrost; borehole temperatures; meteorological measurements; surface offset; thermal offset; total offset.

Introduction

Climatic and microclimatic factors control the surface temperature. In turn, the surface temperature is one of the major factors influencing the ground thermal regime. Usually, once the surface temperature regime is known, the thermal regime in the ground, provided it is homogenous, can be analyzed without further consideration of climate. However, snow cover as well as ground thermal properties that depend on surface and near-surface characteristics often strongly modify heat and energy fluxes in the ground (Brown & Péwé 1973, Harris & Brown 1978).

Since the early 1980s, climate–permafrost relationships in high-alpine areas have been in the focus of Alpine permafrost research (cf. Keller 1994, Haeberli et al. 1998, Hoelzle et al. 1999, Hoelzle et al. 2001, Hoelzle et al. 2003, Mittaz et al. 2000, Stocker-Mittaz et al. 2002). In recent years, mountain permafrost research has developed considerably. Main efforts are concentrated on improved modeling and attempting to couple regional climate models with local scale models (Salzmann et al. 2006, Noetzli et al. 2007, Salzmann et al. 2007). There is, however, still a considerable lack in process understanding of the complex interactions between atmosphere and lithosphere in high- mountain areas. This is mainly caused by the complex topography and the high variability of the spatial and temporal influences of snow and surface characteristics (Gruber et al. 2004, Hanson & Hoelzle 2005). The model-concept describing the offset between mean annual air temperature (MAAT) and temperature at the top of permafrost (TTOP) has been developed by several authors (Burn & Smith 1988, Smith & Riseborough 1996, Smith et al. 1998, Henry & Smith 2001, Riseborough 2002) and is a useful simplification to overcoming the problem of physically coupling the atmosphere and the ground. However, snow and surface/subsurface conditions in alpine areas differ quite strongly from the ones in the Arctic. First attempts to apply the concept of TTOP to mountain areas were made by Herz et al. 2003 and Juliussen & Humlum 2007. In the concepts of Lachenbruch & Marshall 1986, Burn & Smith 1988, and Smith & Riseborough 1996, the total offset between MAAT and TTOP is often expressed first by a surface offset between MAAT and the mean annual ground surface temperature (MAGST) and MAGST and TTOP. In reality, the surface offset consists of two separate offsets: one between MAAT and the mean annual surface temperature (MAST) and one between the MAST and MAGST. These two offsets are often treated as one, because they are hardly ever separately measured. The MAST can be expressed as the radiative surface skin temperature, which can be measured by an IR thermometer (see Table 1) measuring the thermal infrared radiating temperature of the ground surface in its field of view. This temperature is measured always at the variable current surface of the corresponding season; e.g., in winter mainly the snow surface and in summer mainly the bedrock surface.

Until today, no reliable information about long-term values of these offsets for alpine areas have been available that are based on long-term measurements. The long-term measurements presented in this paper should help to provide first approximations of the various offsets and a description of the general relationship between MAAT, snow depth, MAGST, and TTOP. This study also reveals the importance of long-term monitoring to improve our process understanding, which is required to develop useful but simple model concepts.

Measurements at Murtèl-Corvatsch and Schilthorn

Meteorological measurements at Murtèl-Corvatsch

The Murtèl-Corvatsch and Chastelets borehole sites are located northwest of the Murtèl cable car station within the ski area Silvaplana – Piz Corvatsch. The area is situated in the Upper Engadine (Eastern Swiss Alps). A steep northwest-facing rock wall surrounds the area, and the slopes below the rock walls are covered by several meters of loose debris. Several rock glaciers and protalus ramparts are situated at the foot of the slope below the ridge. The area is inside the periglacial belt with strong weathering intensity on the headwalls resulting in a large amount of debris feeding the active rock glaciers below.

One of these rock glaciers is the Murtèl rock glacier (46°26´N, 9°49´E), which has been well-investigated over many years (Hoelzle et al. 2002). A borehole was drilled in 1987 and has provided a ground temperature data record since then. In 1997 a first micrometeorological station was installed at the Murtèl-Corvatsch site (Mittaz et al. 2000). Such long-term micrometeorological studies at the borehole locations (Harris et al. 2003) are needed for process understanding, model development, and calibration (Hoelzle et al. 2001). They provide data on heat fluxes between the atmosphere and the active layer, and between the active layer and the underlying permafrost. Therefore, they have been included in the concept of the permafrost monitoring network Switzerland (PERMOS).

Air temperature, radiation, and wind speed among others have been measured directly at the borehole site on the rock glacier since January 1997. In addition, there is a meteorological station on the summit cable car station that has been run by MeteoSwiss since 1983. With the help of this meteorological station the air temperature at Murtèl-Corvatsch was reconstructed from 1997 back until 1987, which is when the ground temperature measurements started. The same reconstruction is made for the surface temperature measurements, which have been recorded since 2001 by an IR thermometer. Since 1972, snow depths have been continuously measured in winter (October to May) at the middle station of the Corvatsch cable car by the Snow and Avalanche Research Institute in Davos. These data are compared and adjusted to the direct measurements made at the Murtèl-Corvatsch station, which allowed a continuous reconstruction of snow depth for the period 1988ñ2007. These reconstructions were necessary to have a continuous data record directly at the measurement site of the Murtèl borehole.

Table 1. Sensors used in this study.

Variables	Sensors (Company)	Sensor Type	Range	Accuracy
Air temperature	MP-100A (Rotronic)	RTD PT-100 1/3-Din ventilated	-40 - +60°C	±10 %
Snow height	SR50 (Campell)	Ultrasonic Electrostatic Transducer	0.5 – 10 m	±0.01 m
Surface temperature	Infrared thermometer	IRt/c.5	-35 – 10°C	±1.5°C
Ground temp. Murtèl-Schilthorn-Stockhorn boreholes	YSI 44006 Yellow Springs Instruments	NTC-Thermistors	-20 - +40°C	±0.02 °C
Ground temp. Active layer	UUB31J1 Fenwal	NTC-Thermistors	-20 - +40°C	±0.02 °C
Chastelets boreholes	YSI 44006 Yellow Springs Instruments	NTC-Thermistors	-20 - +40°C	±0.02 °C
Rocklogger	M-Log Geoprecision	PT1000	-55 - +85°C	±0.01°C

The micrometeorological station measures air temperature, wind speed and direction, humidity, snow depth, as well as all components of the radiation balance every 10 minutes which is logged every half-hour as a 30-minute mean (cf. sensor description in Table 1). Meteorological measurements in high-alpine environments are difficult because of the harsh climatic conditions. This results in many periods without data. Such periods are caused by lightning, avalanches, rime-ice, or burying of the instrumentation by snowfall.

Ground temperature masurements at Murtèl-Corvatsch

The Murtèl borehole from 1987 was drilled down to 58 m, but in this study only the uppermost thermistors, down to 6 m, are analyzed. The measuring interval is 24 hours.

Seven thermistors were placed in the uppermost 90 cm of the active layer less than 2 m from the microclimate station and in close vicinity of the borehole. Five thermistors are placed 5 cm deep in the boulders, while two thermistors are hanging in cavities between the boulders, thus measuring the ambient air temperatures. They are described in detail by Hanson & Hoelzle 2003, 2004. Temperatures were registered every minute and logged as a 5-minute mean. All thermistors were calibrated before their placement and are annually indirectly calibrated by the zero curtain in spring.

In the Chastelets area, five boreholes were drilled in the year 2002. These boreholes are described in detail by Hanson & Hoelzle 2005. The boreholes were selected using the criteria that aspect and climatic conditions should be the same and that only the surface characteristics are different, such as, for example, coarse debris or bedrock.

Meteorological measurements at Schilthorn

The study area in the Schilthorn massif is situated at the transition between the Prealps in the north and the principle chain of the Bernese Alps, which exceed 4000 m a.s.l. The Schilthorn summit reaches 2970 m a.s.l. and is located at 46°34′N, 7°50′E.

Today, only perennial snow patches can be found, which have been shrinking considerably as a consequence of the warm 1980s and 1990s (Imhof 2000).

Due to its geographic situation (exposed to moist western winds), the climate in the Schilthorn massif is of almost maritime alpine character; i.e., with fairly abundant precipitation, showing a distinct summer maximum. The mean annual accumulation in Lauterbrunnen (valley floor) is 1234 mm, whereas about 2700 mm were estimated on the highest summits, where about 90% of the precipitation falls as snow (Imhof 2000). Consequently, the surface is snow-covered for longer than in most of the comparable regions of the central Alps.

The microclimatological station was installed about 100 m to the northwest of the Schilthorn summit at 2900 m a.s.l. in 1998.

Ground temperature measurements at Schilthorn

Also in 1998, a 14-m deep borehole was drilled into bedrock a few meters to the northwest of the climate station and equipped with a thermistor chain. Two additional boreholes were drilled in the year 2000: a vertical one with a depth of 100 m and a horizontal one with a depth of 92 m. The borehole data show that the active layer reaches, in general, to a depth of about 5 m, and that the MAGT at 14 m depth is around -0.5 to -0.7°C. Thus, permafrost is present at the drill sites but is rather warm.

Results

Meteorological measurements at Murtèl-Corvatsch and Schilthorn

Tables 2 and 3 show the mean monthly values for the three variables (1) air temperature, measured 2 m above the ground, (2) snow height, and (3) ground temperature at 3.6 m and 5.0 m below surface at the top of permafrost.

As ground temperature data for Murtèl-Corvatsch exist from 1987 onwards, air temperature and snow depth were reconstructed as needed.

Schilthorn meteorological and ground temperature data recording started in 1998/99. The mean ground temperature at 3.6 m depth represents the TTOP. Air temperature has an annual peak amplitude at Murtèl-Corvatsch of 15.4°C and at Schilthorn of 13.5°C. Mean snow depth at Schilthorn is approximately double that of Murtèl-Corvatsch.

These values indicate that Murtèl-Corvatsch has a more continental climate than Schilthorn. Schilthorn is situated around 300 m higher than Murtèl-Corvatsch. Despite this elevation difference, the ground temperatures at Murtèl-Corvatsch are by far -1.2°C colder.

TTOP at Schilthorn is at a depth of around 5 m; however, in the year 2003, the active layer thickness increased to around 9 m. This was caused by the heat wave of 2003 which lead to warmer TTOP temperatures than normal. This can also be recognized in Figure 2.

Time series of air temperature, snow depth, and ground temperatures at Murtèl-Corvatsch

Figure 1 displays the continuous mean monthly data set from 1988 to 2007 for air temperature, snow depth, and ground temperature at TTOP 3.6 m below surface. The time series illustrates the influence of snow cover on the TTOP. The winters 1993/94, 1996/97, 2000/01, and 2002/03 had snow depths that far exceeded normal conditions. As a result, the TTOP were very warm, even in the year 2002/03 which had very cold winter air temperatures. In contrast, the winters 1988/89 and especially 2001/02 had below-average snow conditions, which resulted in very cold TTOP. An exception was the winter 2006/07, which had the lowest snow depth since the beginning of the snow measurements in 1972. It did not result in the coldest TTOP, because winter air temperatures were the warmest ever recorded at the meteorological stations in the Corvatsch area.

Table 2. Mean monthly values of different meteorological measurements at the Murtèl-Corvatsch site from 1988 to 2006.

Monthly mean 1988-2006	Air temperature [°C]	Snow height [m]	Borehole temperature (depth = 3.6 m) [°C]
January	-7.42	0.64	-2.24
February	-8.79	0.70	-2.84
March	-6.91	0.82	-3.20
April	-5.06	0.94	-3.57
May	0.24	0.67	-2.87
June	3.59	0.21	-0.75
July	6.50	0.02	-0.42
August	6.65	0.01	-0.29
September	2.81	0.02	-0.20
October	-0.09	0.08	-0.18
November	-5.31	0.32	-0.26
December	-7.38	0.52	-1.16
Average	**-1.76**	**0.41**	**-1.50**

Table 3. Mean monthly values of different meteorological measurements at the Schilthorn site from 1999 to 2007.

Monthly mean 1999-2007	Air temperature [°C]	Snow height [m]	Borehole temperature (depth = 5 m) [°C]
January	-9.60	1.10	-0.10
February	-9.27	1.12	-0.26
March	-7.62	1.25	-0.60
April	-4.79	1.48	-0.87
May	-0.33	1.59	-0.92
June	2.74	1.20	-0.77
July	3.87	0.29	-0.46
August	3.93	0.03	-0.25
September	2.6	0.02	0.07
October	-0.98	0.22	0.03
November	-5.86	0.50	-0.04
December	-7.88	0.88	-0.08
Average	**-2.77**	**0.81**	**-0.35**

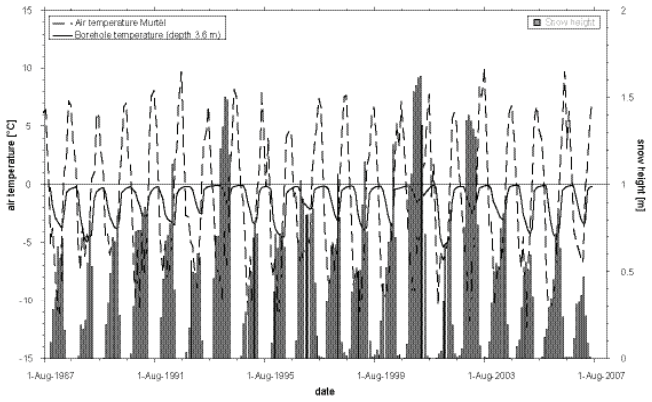

Figure 1. Monthly air temperature, snow depth and ground temperature at TTOP in 3.6 m depth at Murtèl-Corvatsch (borehole 2/87).

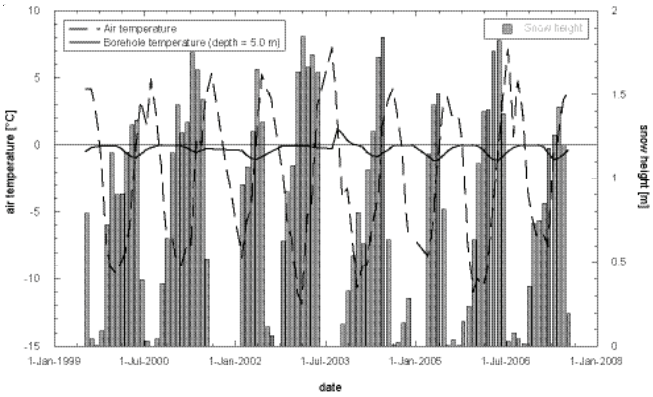

Figure 2. Monthly air temperature, snow depth and ground temperature at TTOP in 5.0 m depth at Schilthorn (borehole 51/98).

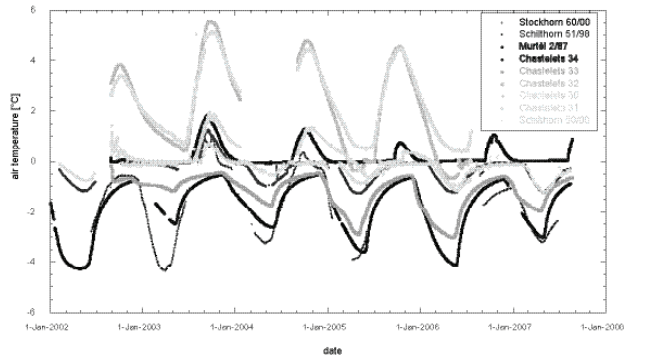

Figure 3. Daily ground temperatures in all boreholes at 5 m depth.

Time series of air temperature, snow depth, and ground temperature at Schilthorn

Figure 2 shows the mean monthly data set from 1999 to 2007 for air temperature, snow depth, and ground temperature at TTOP in a depth of 5.0 m. The time series from the Schilthorn does not reflect the influence of the snow cover on the TTOP temperature as well as the Murtèl-Corvatsch series does. The winter snow cover at Schilthorn shows less variability than at Murtèl-Corvatsch.

In general, winter snow cover at Schilthorn starts earlier and reaches greater snow thicknesses than at Murtèl-Corvatsch. This results in stronger warming than at Murtèl-Corvatsch. Additionally, the surface layer at the Schilthorn is composed of fine-grained material containing more unfrozen water and resulting, therefore, in reduced cooling because of latent heat effects.

Table 4. Surface offset (temperature at 0.5 m depth – air temperature) and total offset (including thermal offset) 1) temperature at 2.5 m depth – air temperature; 2) temperature at 4.5 m depth – air temperature) for different boreholes and years. The rows in grey show the values for the permafrost boreholes.

Borehole	Measurement period	Surface offset	Total offset 1	Total offset 2
Murtèl 2/87	1997/98	1.50	0.33	-0.12
Murtèl 2/87	2001/02	0.26	-0.33	-0.50
Murtèl 2/87	2002/03	1.33	0.02	-0.37
Murtèl 2/87	2003/04	1.40	0.73	0.28
Murtèl 2/87	2004/05	0.41	0.10	-0.37
Murtèl surface block	2003/04	2.08		
Murtèl surface block	2004/05	1.24		
Murtèl below surface block	2003/04	1.39		
Murtèl below surface block	2004/05	0.50		
Chastelets B30	2002/03	4.57	3.63	3.35
Chastelets B31	2002/03	2.89	1.85	1.38
Chastelets B32	2002/03	4.66	3.79	3.32
Chastelets B33	2002/03	2.49	0.62	0.32
Chastelets B34	2002/03	3.37	2.22	1.36
Chastelets B30	2004/05	3.52	3.62	4.06
Chastelets B31	2004/05	1.51	2.14	2.02
Chastelets B32	2004/05	3.41	3.56	3.72
Chastelets B33	2004/05	1.11	0.00	0.36
Chastelets B34	2004/05	2.21	2.11	1.94
Murtèl rock	2003/04	4.61		
Murtèl rock	2004/05	4.08		
Murtèl rock	2005/06	3.98		
Schilthorn 51/98	1999/00	2.49	2.70	2.49
Schilthorn 51/98	2005/06	2.85	2.72	2.66
Schilthorn 50/00	2005/06	2.90	2.88	2.77
Stockhorn 60/00	2002/03	-1.28	4.98	3.72

Time series of different ground temperatures at all investigation sites

Figure 3 shows the temperature development since 2002 within all boreholes investigated in this study. After the very warm summer 2003, a slight cooling trend is observed within all boreholes. This effect can mainly be attributed to less winter snow (see also Fig. 1).

Offset data at all sites

Table 4 shows the surface offset and total offset for several years and borehole sites. These selected data only include years that have less than 10% data gaps. The data show that at most permafrost sites the surface offset is less than at per-

mafrost-free sites. The range of surface offset at the permafrost sites varies from less than 0 up to 2.9°C, but between 3.41 and 4.6°C at permafrost-free sites. Borehole 34 lies in between and should be treated as a special case, because this site is at the edge of a rock glacier within fine material and the lowest temperature sensor at 6 m depth is close to 0°C, indicating permafrost below but not in this borehole.

In Figures 4 and 5, the surface offset and thermal offset, including the offset between MAAT and MAST, are shown as an average over the whole measurement period for Murtèl-Corvatsch (Fig. 4) and Schilthorn (Fig. 5). The offset data reveal that the mean difference between MAAT and MAST is 1.12°C at Murtèl-Corvatsch and 1.24°C at Schilthorn, respectively. The offset between MAST and MAGST is 3.62°C at Murtèl-Corvatsch and 3.99°C at Schilthorn.

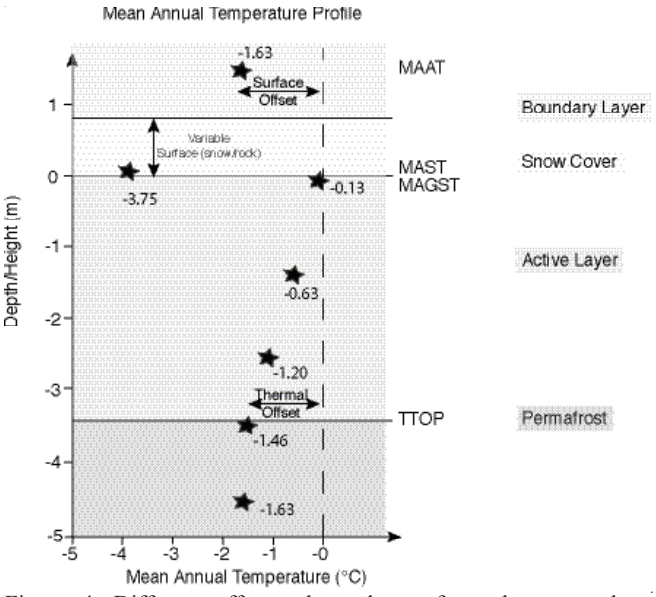

Figure 4. Different offset values shown from the mean data measured at the Murtèl-Corvatsch.

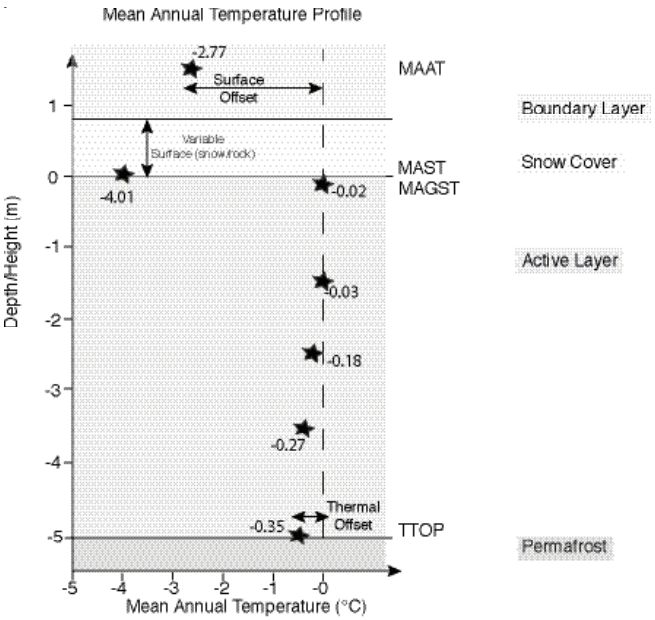

Figure 5. Different offset values shown from the mean data measured at the Schilthorn.

The offset usually called *surface offset* (MAGST – MAAT) is 1.50°C at Murtèl-Corvatsch and 2.75°C at Schilthorn. The offset usually called *thermal offset* (TTOP –MAGST) is 1.53°C at Murtèl-Corvatsch and 0.33°C at Schilthorn. The total offset (TTOP – MAAT) at Murtèl-Corvatsch with a value of 0.17°C is considerably smaller than at Schilthorn with 2.42°C.

Discussion and Conclusions

The long-term data sets collected in the last 20 years within the monitoring project PERMOS, together with the additional data, form a unique archive that is becoming more and more valuable. The time series at Murtèl-Corvatsch and Schilthorn not only reveal how the TTOP are related to snow cover and air temperature, but they also show the different behavior at the different investigation sites mainly caused by variable surface and subsurface characteristics.

However, the variability of the offsets between the permafrost sites is high. As an example, the surface offset at Murtèl-Corvatsch is more or less compensated by the thermal offset in the ground, which results in a very small total offset of only 0.17°C. In contrast, at Schilthorn the surface offset is dominating and the thermal offset is very small, resulting in a larger total offset of 2.42°C.

In the future, the concept of working with different offset values, based on long-term measurements, may help to better understand the processes between atmosphere and mountain permafrost and, therefore, will help to build up simple relationships for modeling mountain permafrost (Noetzli et al. this volume) and to better interpret the development of temperature and related ice content in the ground (Hilbich et al. this volume).

Acknowledgments

We would like to acknowledge the continuous support of the Permafrost Monitoring of Switzerland (PERMOS), the Corvatsch cable car company, and all students and colleagues at the University of Zurich. The very constructive review of the referees is kindly acknowledged.

References

Brown, R.J.E. & Péwé, T.L. 1973. Distribution of permafrost in North America and its relationship to the environment, a review 1963-1973. *Proceedings of* the *Second International Conference on Permafrost*, *Yakutsk, USSR*: 71-100.

Burn, C.R. & Smith, C.A.S. 1988. Observations of the 'thermal offset' in near-surface mean annual ground temperatures at several sites near Mayo, Yukon Territory Canada. *Arctic* 41: 99-104.

Gruber, S., King, L., Kohl, T., Herz, T., Haeberli, W. & Hoelzle, M. 2004. Interpretation of geothermal profiles perturbed by topography: The Alpine permafrost boreholes at Stockhorn Plateau, Switzerland, *Permafrost & Periglacial Proc.* 15(4): 349-357.

Haeberli, W., Hoelzle, M., Kääb, A., Keller, F., Vonder Mühll, D. & Wagner, S. 1998. Ten years after drilling through the permafrost of the active rock glacier Murtèl, Eastern Swiss Alps: Answered questions and new perspectives. *Proceedings of the Seventh International Conference on Permafrost*, *Yellowknife, Canada*: 403-410.

Hanson, S. & Hoelzle, M. 2003. The thermal regime of the coarse blocky active layer at the Murtèl rock glacier in the Swiss Alps. *Eighth International Conference on Permafrost, Zürich, Extended Abstracts*: 51-52.

Hanson, S. & Hoelzle, M. 2004. The thermal regime of the active layer at the Murtèl rock glacier based on data from 2002. *Permafrost & Periglacial Proc.* 15(3): 273-282.

Hanson, S. & Hoelzle, M. 2005. Installation of a shallow borehole network and monitoring of the ground thermal regime of a high alpine discontinuous permafrost environment, Eastern Swiss Alps. *Norwegian Journal of Geography* 59: 84-93.

Harris, C., Vonder Mühll, D., Isaksen, K., Haeberli, W., Sollid, J.L., King, L., Holmlund, P., Dramis, F., Guglielmin, M. & Palacios, D. 2003. Warming permafrost in European mountains. *Global and Planetary Change* 39: 215-225.

Harris, S.A. & Brown, R.J.E. 1978. Plateau Mountain: a case study of Alpine permafrost in the Canadian Rocky Mountains. *Proceedings of the Third International Conference on Permafrost*, *Edmonton, Canada*: 385-391.

Henry, K. & Smith, M. 2001. A model-based map of ground temperatures for the permafrost regions of Canada, *Permafrost and Periglacial Processes* 12: 389-398.

Herz, T., King, L. & Gubler, H. 2003. Thermal regime of coarse debris layers in the Ritigraben catchment, Matter valley, Swiss Alps. *Eighth International Conference on Permafrost, Zürich, Extended Abstracts*.

Hilbich, C., Hauck, C., R., D. & Hoelzle, M. 2008. Geoelectric monitoring network and resistivity-temperature relationships of different mountain permafrost sites in the Swiss Alps. *Proceedings of the Ninth International Conference on Permafrost, Fairbanks, Alaska (*this volume).

Hoelzle, M., Wegmann, M. & Krummenacher, B. 1999. Miniature temperature dataloggers for mapping and monitoring of permafrost in high mountain areas: First experience from the Swiss Alps. *Permafrost & Periglacial Proc.* 10(2): 113-124.

Hoelzle, M., Haeberli, W. & Stocker-Mittaz, C. 2003. Miniature ground temperature data logger measurements 2000-2002 in the Murtèl-Corvatsch area. *Proceedings of the Eighth International Conference on Permafrost*, *Zürich*: 419-424.

Hoelzle, M., Mittaz, C., Etzelmüller, B. & Haeberli, W. 2001. Surface energy fluxes and distribution models of permafrost in European mountain areas: an overview of current developments. *Permafrost & Periglacial Proc.* 12(1): 53-68.

Imhof, M. 2000. Permafrost investigation in the Schilthorn massif, Bernese Alps, Switzerland. *Permafrost & Periglacial Proc.*, 11(3): 189-206.

Juliussen, H. & Humlum, O. 2007. Towards a TTOP Ground Temperature Model for Mountaneous Terrain in Central-Eastern Norway. *Permafrost & Periglacial Proc.* 18: 161-184.

Keller, F. 1994. *Interaktionen zwischen Schnee und Permafrost - Eine Grundlagenstudie im Oberengadin*, Dissertation thesis, ETH Zürich, Zürich, 145 pp.

Lachenbruch, A.H. & Marshall, B.V. 1986. Changing climate: geothermal evidence from permafrost in the Alaskan Arctic. *Science* 234: 689-696.

Mittaz, C., Hoelzle, M. & Haeberli, W. 2000. First results and interpretation of energy-flux measurements of Alpine permafrost. *Annals of Glaciology* 31: 275-280.

Noetzli, J., Gruber, S., Kohl, T., Salzmann, N. & Haeberli, W. 2007. Three-dimensional distribution and evolution of permafrost temperatures in idealized high-mountain topography. *J. of Geophysical Res.*, 112 (F02S13): doi:10.1029/2006JF000545.

Noetzli, J., Hilbich, C., Hauck, C., Hoelzle, M. & Gruber, S. this volume. Comparison of transient 2D temperature profiles with time-lapse electrical resistivity data at the Schilthorn crest, Switzerland. *Proceedings of the Ninth International Conference on Permafrost, Fairbanks, Alaska* (this volume).

Riseborough, D.W. 2002. The mean annual temperature at the top of permafrost, the TTOP model, and the effect of unfrozen water. *Permafrost & Periglacial Proc.* 13: 137-143.

Salzmann, N., Frei, C., Vidale, P.L. & Hoelzle, M. 2006. The application of Regional Climate Model output for the simulation of high-mountain permafrost scenarios. *Global & Planetary Change* 56: 188-202.

Salzmann, N., Noetzli, J., Hauck, C., Gruber, S., Hoelzle, M. & Haeberli, W. 2007. RCM-based ground-surface temperature scenarios in high-mountain topography and their uncertainty ranges. *J. of Geophysical Res.* 112 (F02S12): doi:10.1029/2006JF000527.

Smith, C.A.S., Burn, C.R., Tarnocai, C. & Sproule, B. 1998. Air and soil temperature relations along an ecological transect through the permafrost zones of Northwestern Canada. *Proceedings of the Seventh International Conference on Permafrost, Yellowknife, Canada*: 1009-1015.

Smith, M.W. & Riseborough, D.W. 1996. Ground temperature monitoring and detection of climate change. *Permafrost & Periglacial Proc.* 7: 301-310.

Stocker-Mittaz, C., Hoelzle, M. & Haeberli, W. 2002. Permafrost distribution modeling based on energy-balance data: a first step. *Permafrost & Periglacial Proc.* 13(4): 271-282.

Soil Temperature and Thaw Response to Manipulated Air Temperature and Plant Cover at Barrow and Atqasuk, Alaska

Robert D. Hollister
Department of Biology, Grand Valley State University, 1 Campus Drive, Allendale, Michigan 49401-9403, USA
Patrick J. Webber
P.O. Box 1380, Ranchos de Taos, NM 87557-1380, USA
Robert T. Slider
Department of Biology, Grand Valley State University, 1 Campus Drive, Allendale, Michigan 49401-9403, USA
Fredrick E. Nelson
Department of Geography, University of Delaware, Newark, DE 19716-2541, USA
Craig E. Tweedie
Department of Biology and the Environmental Science and Engineering Program, University of Texas at El Paso, 500 University Avenue, El Paso, Texas 79968-0513, USA

Abstract

This paper examines the response of tundra systems to more than a decade of experimental warming, using International Tundra Experiment (ITEX) open-top chambers (OTCs) in wet and dry vegetation types near Barrow and Atqasuk, Alaska. The magnitude of chamber warming varied by site and changed over time. Maximum thaw depth varied little between OTC and control plots, except in recent years. To understand how vegetation controls air-soil heat exchange, we denuded the vegetation to bare ground in two chambers and added the removed vegetation to adjacent chambers to provide enhanced thermal insulation. Soil temperatures were coolest in chambers to which litter had been added. The difference between air and soil temperatures was similar between the chambers with added litter and chambers that had been in place for nine years. This experiment indicates that changes in vegetation due to a warmer climate may result in cooler soils.

Keywords: experimental warming; ITEX; open-top chamber, soil temperature; thaw depth; tundra; vegetation.

Introduction

Open Top Chambers (OTCs) have been used by the International Tundra Experiment (ITEX) since the early 1990s to simulate warmer snow-free growing conditions, which are expected to occur in the Arctic with climate change (Henry & Molau 1997, Arft et al. 1999, Hollister et al. 2005a, Walker et al. 2006). Recent studies have shown that the effect of OTCs on air and soil warming varies across sites of differing vegetation type (Marion et al. 1997, Hollister et al. 2006). Related studies document increased plant growth, changes in plant species composition and abundance, and an accumulation of leaf litter in response to warming (Hollister 2003, Hollister 2005a, b, Walker et al. 2006). This study aims to understand how changes in vegetation can alter the air-soil heat exchange properties of warmed plots and potentially explain the differential response of some vegetation types to OTCs.

We manipulated vegetation by removing the canopy and adding the clipped plant matter to adjacent plots to directly explore the impact of the plant canopy on air-soil heat exchange in a manner similar to Ng and Miller (1977). The relationship between air and soil warming is driven by soil type and vegetation (Gross et al. 1990, Walker et al. 2003). While dead plant litter is not a true substitute for a denser living plant canopy, it is easily manipulated and may provide insights into the insulating effect of the vegetation on soil temperature.

Study Area and Methods

Study sites were established in different years (see Table 1) in wet and dry plant communities near the villages of Barrow (71°18′N, 156°40′W) and Atqasuk (70°29′N, 157°25′W), Alaska. Barrow and Atqasuk are on the coastal plain of Alaska's North Slope and lie within the zone of continuous permafrost. Seasonal thaw varies with landscape position and is generally less than 1 meter (Nelson et al. 1998, Hinkel & Nelson 2003). Atqasuk is 100 km south and inland from Barrow and is on average 5°C warmer in July than Barrow (Haugen & Brown 1980). The Barrow dry (BD) site lies on a former raised beach ridge. The soil is a moderately well drained xeric pergelic cryaquept underlain with fine silt, sand, and gravel. The vegetation is a dry heath dominated by prostrate shrubs and lichens. The Barrow wet (BW) site lies on the edge of a drained thaw lake basin. The soil is a poorly drained histic pergelic cryaquept underlain by fine silt. The vegetation is a wet meadow dominated by graminoids and mosses. The Atqasuk dry (AD) site lies on a raised rim of a drained thaw lake basin. The soil is a well drained pergelic cryopsamment underlain with aolian sand. The vegetation is a dry heath dominated by lichens and prostrate shrubs. The Atqasuk wet (AW) site lies on a pond margin. The soil is a poorly drained histic pergelic cryaquept underlain with aolian sand and silt. The vegetation is a wet meadow dominated by mosses and graminoids.

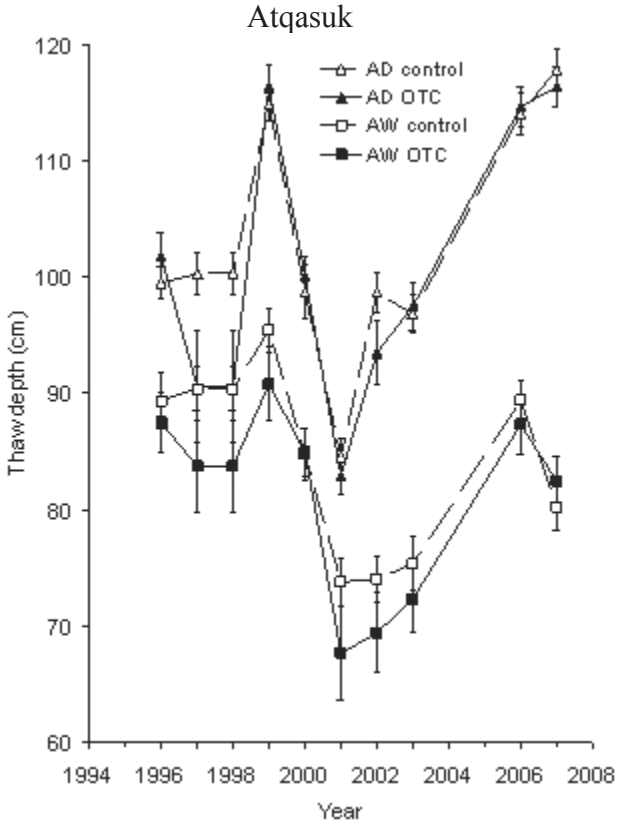

Figure 1. Mean annual maximum depth of thaw below OTC plots (filled symbols) and control plots (open symbols) at Atqasuk (left) and Barrow (right). Note the change in scale between locations; lines between readings for each year to allow for ease of delineating sites and treatments. Data were not collected in 2004 and 2005. Error bars represent the standard error of the mean and most sample sizes were 24.

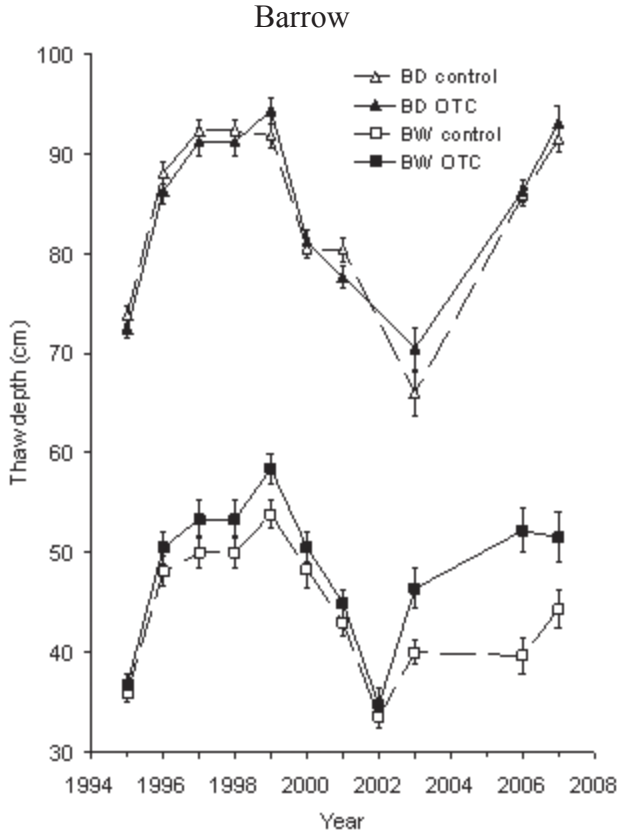

Figure 2. Mean July temperature (°C) of air at +13 cm (circles) and soil at depths of 10 cm (triangles) and 45 cm (squares) in OTC plots (filled symbols) and control plots (open symbols) at the four study sites. Error bars represent the standard error of the mean (n=2). Missing data are represented by an M; a dot above and below the value to represent missing error bars.

Table 1. Years that sites were established, temperature and thaw measurements were initiated, and number of years in operation. Sites of 24 OTC and 24 control plots were established in different years. Plots where temperatures were recorded were established in the same year.

Site	Established		No. years	
	Site	Temp	Temp	Thaw
Atqasuk dry (AD)	1996	1998	9	11
Atqasuk wet (AW)	1996	1998	9	11
Barrow dry (BD)	1994	1998	9	13
Barrow wet (BW)	1995	1998	9	12

Each of the study sites consists of 24 OTC and 24 control plots in which standardized annual measurements, such as summer thaw depth, are made. The hexagonal OTCs are constructed of Sun-Lite HPTM fiberglass (Solar Components Corporation, Manchester, New Hampshire) to passively warm study plots. Chambers are approximately 35 cm high, 103 cm across at the base, and 60 cm across at the top (Molau 1993, Hollister 2003). The OTC and control plots cover an area of approximately 1 m^2. The magnitude of warming in the OTCs is driven by solar intensity and wind conditions (Marion et al. 1997, Hollister et al. 2006). For example, on calm sunny days the passive OTCs can warm the plant canopy up to 10°C above the ambient temperature. OTCs were installed soon after snowmelt and removed in mid to late August at the end of each field season. The length of the growing season and snow depths were not altered by the experimental manipulation. Additional plots for destructive sampling and sensor installation have been set up since the sites were established.

At each site two plots per treatment were established in 1998 to provide more detailed information on the effects of the OTCs on the air and soil microclimate. Since 1998 soil temperature has been measured at depths of 0 cm , 10 cm, and 45 cm using TP101M temperature probes (Measurement Research Corporation, Gig Harbor, Washington) connected to Campbell Scientific CR10X dataloggers. Prior to 2005, aerial sensors were housed in radiation shields placed within the plant canopy at approximately 13 cm above the ground surface and connected to HOBO® or StowAway™ loggers (Onset Computer Corporation, Pocasset, Massachusetts). In 2005 air temperatures were measured with Campbell 107 temperature probes connected to the CR10X at each site. The accuracy of each probe varies with temperature but is generally within 0.2°C. Temperatures were measured every 10 to 80 minutes. Averages and standard errors were

calculated by averaging values for each plot and then comparing plots.

To explore the influence of the plant canopy on OTC performance between sites, two new treatments with two replicates each were established in 2007 at each site. In one treatment the plant canopy was removed down to bare ground in a 20 cm diameter circle in the center of the plot during late June. The removed vegetation was added to adjacent plots, forming a loose layer of litter that mixed in the existing plant canopy. This additional material may generally be considered as litter because the plants were unattached, although it contained lichens, mosses and vascular plants that remained green and appeared vigorous. These two new treatments of OTC plots were in place for one field season. Temperature was monitored in these plots at +13 cm, -1 cm, and -10 cm using StowAway™ loggers.

Depth of thaw was measured to the nearest cm by inserting a graduated metal rod into the ground until the ice-rich permafrost table was reached, usually in mid-August, at each of the 24 plots per treatment.

Results

Mean annual maximum thaw depth

Mean annual maximum thaw depth generally varied little between the OTC and control plots (Fig 1). Thaw was deeper at Atqasuk than Barrow and was deeper in dry sites than in wet sites. Thaw was deeper in warmer years (see mean July temperatures in Fig 2). Thaw in this study's wet sites, which are subject to periodic inundation and have thick insulating moss layers, is somewhat shallower than in dry sites, but large relative to thaw depths recorded in other land cover types in the region. At the dry sites the difference between OTC and control plots was generally indistinguishable. At the wet sites the average difference between OTC and control plots was more consistent across years. At the AW site the control plots generally showed deeper average thaw than OTCs, while at the BW site thaw was consistently deeper in the OTC plots compared with control plots. This difference was more pronounced in recent years.

Air and soil temperature

Mean July air temperatures were between 0.3°C and 4.3°C warmer within the OTC plots. The magnitude of this warming varied by site and over time, with the most pronounced warming in later years (Fig 3). The effect of OTCs on soil temperature varied by site and year. The OTCs cooled the soils at the AW site and warmed them at the AD site. At Barrow, OTCs warmed the soils in early years and cooled them in later years. The effect of OTCs on soil temperature diminished with depth.

The change from soil warming to cooling over time at Barrow warranted further examination. Table 2 represents the average difference in temperature between the control and OTC plots over the course of the experiment. Winter temperatures were consistently warmer under the OTC plots and this difference intensified over time. In summer, soil temperatures became increasingly cooler over time in the OTCs.

Table 2. Mean seasonal differences in soil temperature (°C) between OTC and control plots at the BD and BW sites. Differences were calculated by subtracting the mean of the control plots from that of the OTC plots.

	BD site			BW site		
Year	0 cm	-10 cm	-45 cm	0 cm	-10 cm	-45 cm
			Winter (September–May)			
1998	0.5	0.5	0.3	0.1	0.1	0.2
1999	0.7	0.7	0.4	0.5	0.2	0.2
2000	0.3	0.4	0.3	0.3	0.1	0.2
2001	0.4	0.5	0.2	0.5	0.1	0.1
2002	0.5	0.5	0.3	0.4	0.0	0.1
2003	0.4	0.4	0.3	0.4	0.1	0.2
2004	0.5	0.6	0.3	0.4	0.2	0.2
2005	0.3	0.4	0.2	1.0	0.1	0.2
2006	0.3	0.4	0.3	---	---	---
2007	0.7	0.7	0.5	---	---	---
			Summer (June–August)			
1998	-0.1	-0.1	0.1	0.3	0.3	0.4
1999	0.2	0.2	0.1	1.3	0.6	0.3
2000	-0.2	0.1	0.1	0.6	0.3	0.2
2001	-0.1	0.3	0.1	0.0	0.0	0.1
2002	-0.8	0.2	0.2	0.0	0.1	0.2
2003	-0.7	0.0	0.1	-0.3	-0.2	0.1
2004	-1.1	0.0	0.2	-1.6	-0.9	0.0
2005	-0.9	0.0	0.1	-0.6	-0.8	0.1
2006	-1.5	-0.1	0.0	---	---	---
2007	-2.0	-0.1	0.1	---	---	---

--- no data due to instrument malfunction

Note: recording begun in Aug of 1998 and data are missing between Aug 2004–June 2005 at the BW site.

Vegetation manipulation

The difference between air temperature and soil temperature at a depth of 10 cm was least in the control plots (Table 3). Regardless of whether or not the OTCs cooled or warmed the soils, the pattern across the three warming treatment types (bare ground, added plant matter, 9 years of warming) was consistent. Within the OTCs the soil temperatures were coolest under the plots receiving additional plant matter. The soils under the OTCs which had been in place for nine years were either warmer or similar in temperature to soil under OTCs where the vegetation was removed. The difference between air (13 cm height) and soil (10 cm depth) temperature within the OTCs was greatest in OTCs where plant matter was added, and this difference was similar to the OTCs which had been in place for 9 years.

Discussion

Previous studies have found that temperature enhancement by the OTCs varied significantly in different plant communities (Marion et al. 1997, Hollister et al.

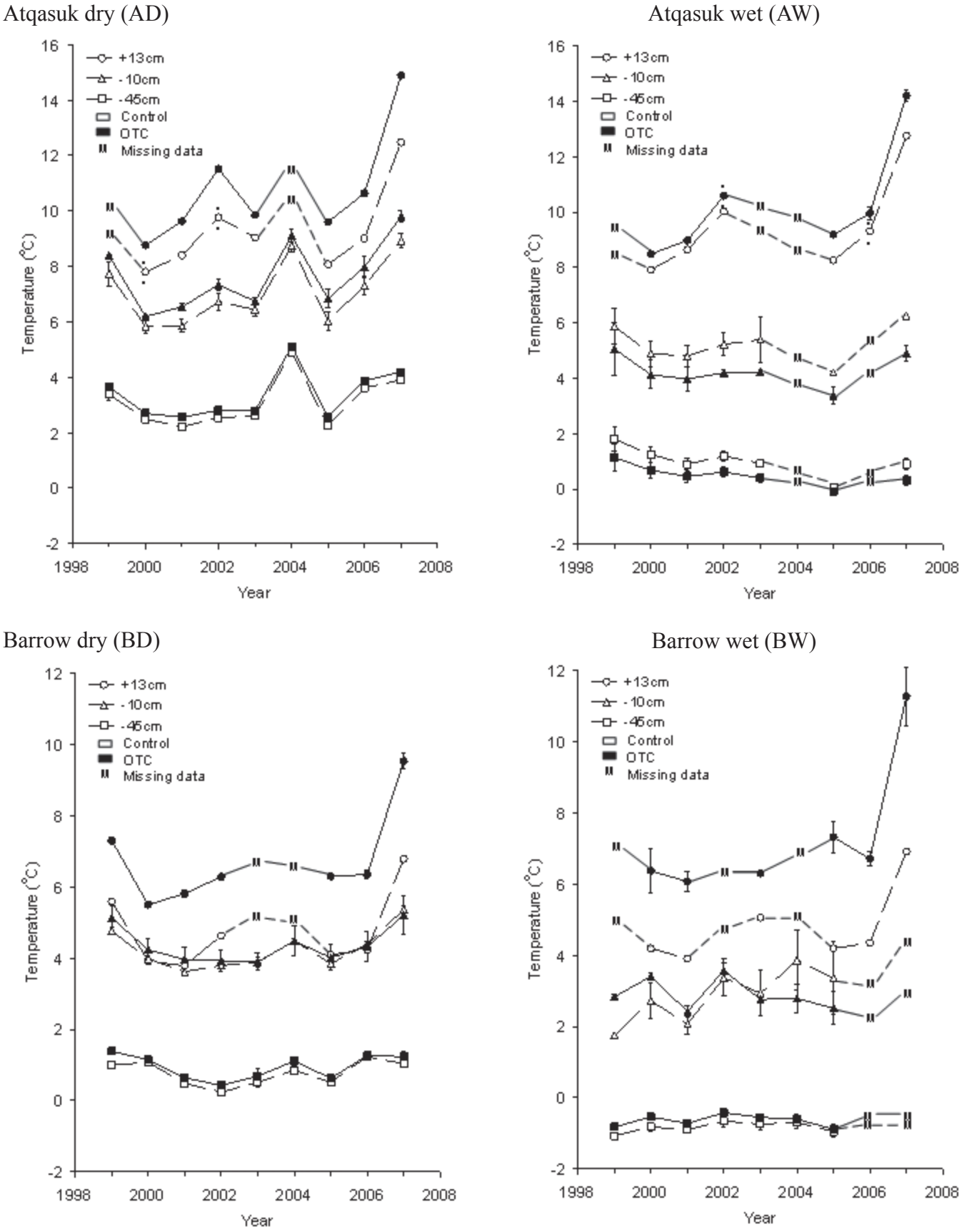

Figure 3. Mean July temperature (°C) of air at +13 cm (circles) and soil at depths of 10 cm (triangles) and 45 cm (squares) in OTC plots (filled symb ols) and control plots (open symbols) at the four study sites. Error bars represent the standard error of the mean (n=2). Missing data are represented by an M; a dot above and below the value to represent missing error bars.

Table 3. The effect of plant removal and addition on mean July canopy and soil temperature within the study plots (°C). Plots included control plots (Control) and OTC plots in place for 9 years (9 years) or in place for one year where the surface vegetation was removed to expose bare ground (Bare) and where the removed vegetation was added (Added) at the four study sites. Measurements were made at canopy height (+13), within 1 cm of the ground surface (0) and at a depth of 10 cm (-10). The difference between the temperature at the plant canopy and at a depth of 10 cm is shown (Diff). Values in parentheses represent the standard error of the mean (n=2).

		OTC		
	Control	**Bare**	**Added**	**9 Years**
		Atqasuk dry (AD)		
+13	12.5 (0.1)	13.4 ---	14.3 (0.2)	14.9 (0.0)
0	14.4 (0.4)	12.8 (0.3)	11.1 (0.3)	15.6 (1.8)
-10	8.9 (0.3)	9.8 (0.1)	8.9 (0.3)	9.8 (0.2)
Diff	**3.5 (0.2)**	**3.7 ---**	**5.4 (0.5)**	**5.1 (0.2)**
		Atqasuk wet (AW)		
+13	12.8 (0.1)	10.1 (2.9)	13.4 (0.1)	14.2 (0.2)
0	12.8 (1.1)	6.7 ---	7.2 (0.5)	11.1 (0.7)
-10	6.3 (0.1)	4.5 (0.1)	3.8 (0.3)	4.9 (0.3)
Diff	**6.5 (0.1)**	**5.6 (2.8)**	**9.7 (0.4)**	**9.3 (0.5)**
		Barrow dry (BD)		
+13	6.8 (0.1)	8.6 (0.0)	8.4 --	9.5 (0.2)
0	10.4 (0.4)	8.2 (0.4)	4.5 (0.9)	8.2 (1.1)
-10	5.4 (0.1)	5.4 (0.1)	3.1 (0.6)	5.2 (0.5)
Diff	**1.4 (0.0)**	**3.2 (0.1)**	**4.7 --**	**4.3 (0.3)**
		Barrow wet (BW)		
+13	6.8 (0.1)	8.9 (0.6)	9.7 (0.0)	11.0 (0.8)
0	--- ---	10.3 (2.3)	4.6 (0.8)	11.5 ---
-10	--- ---	3.7 (0.3)	3.0 ---	4.4 ---
Diff	**--- ---**	**5.3 (0.3)**	**6.7 ---**	**6.3 ---**

--- no data due to instrument malfunction

2006). The consistency of results from this study across sites indicates that the sites share a common response to changes in vegetation. At all sites the difference between air temperature and soil temperature measured at a depth of 10 cm was greatest in the OTC plots and greatest in either the OTC plots in place for 9 years or where plant matter was added. It appears, therefore, that vegetation is influencing both soil temperatures beneath the plots and long-term changes in the vegetation layer, such as increased leaf area index (Hollister 2003). Moreover, these significant changes resulting from experimental warming occurred over a period of less than ten years. The most likely explanation for the increase in soil temperature is increased insulation provided by enhanced vegetation growth and plant litter. This result is in agreement with that of the classic Ng and Miller (1977) experiment and modeling exercise, in which increased canopy and litter layers led to a cooling of the soil and a reduction of the active layer. The small size of the plots in this study probably reduced the impact on thaw depth.

These findings indicate that vegetation also plays a role in OTC warming. There was a tendency toward more warming in later years of the experiment, and the OTCs in place for nine years were warmer than the newly installed OTC plots where vegetation was manipulated. Presumably the vegetation minimizes heat loss from the warmed interior of the chamber. Vegetation becomes taller and denser over time, creating warmer conditions that are more conducive to tundra plant growth. Through this process the OTCs retain progressively more heat, leading to greater seasonal average differences between the OTCs and the control plots.

The increase in thaw depth at the BW site in later years of the experiment and the concomitant soil cooling during the summer months warrant further investigation. The two data sets were collected from different plots (temperature from 2 plots per treatment established in 1998 and thaw from 24 plots per treatment established in 1996). The change in temperature diminished with depth and was not significant at the depths near maximum thaw. It is also possible, although unlikely, that minor movements of the sensors due to cryoturbation may have influenced soil temperatures.

Taken together, the long-term warming experiment and short-term vegetation manipulation within the warming experiment demonstrate that vegetation is one of the dominant determinants of air-soil heat exchange at shallow depth at these sites, and that differences in OTC performance at the sites are strongly influenced by vegetation. As the vegetation responds to warming with increased growth, these changes appear to dampen air-soil heat exchange. Not only does this study reaffirm the importance of vegetation in influencing patterns of air-soil heat exchange in tundra regions, it also highlights the value of long-term experimental observations and how these can facilitate our understanding of how climate change may affect tundra ecosystem structure and function.

Acknowledgments

We thank the US National Science Foundation, Office of Polar Programs, Arctic System Science Program for its support of this work (OPP #9714103, #0632263), student assistants responsible for data collection, two anonymous reviewers, and our many ITEX colleagues for sharing their insights and constructive criticism. Any opinions, findings, conclusions, or recommendations expressed in this paper are those of the authors and do not necessarily reflect the views of the National Science Foundation. Identification of specific products and manufacturers in the text does not imply endorsement by the National Science Foundation.

References

Arft, A.M., Walker, M.D., Gurevitch, J., Alatalo, J.M., Bret-Harte, M.S., Dale, M.R.T., Diemer, M.C., Gugerli, F., Henry, G.H.R., Jones, M.H., Hollister, R.D., Jónsdóttir, I.S., Laine, K., Lévesque, E., Marion, G.M., Molau, U., Mølgaard, P., Nordenhall, U., Raszhivin, V., Robinson, C.H., Starr, G., Stenström, A., Stenström, M., Totland, Ø., Turner, P.L., Walker, L.J., Webber, P.J., Welker, J.M. & Wookey, P.A. 1999. Responses of tundra plants to experimental warming: Meta-analysis of the international tundra experiment. *Ecological Monographs* 64: 491-511.

Gross, M.F., Hardisky, M.A., Doolittle, J.A. & Klemas, V. 1990. Relationships among depth of frozen soil, soil wetness,and vegetation type and biomass in tundra near Bethel, Alaska. *Arctic and Alpine Research* 22 (3): 275-282.

Haugen, R.K. & Brown, J. 1980. Coastal-inland distributions of summer air temperature and precipitation in northern Alaska. *Arctic and Alpine Research* 12(4): 403-412.

Henry, G.H.R. & Molau, U. 1997. Tundra plants and climate change: The International Tundra Experiment (ITEX), Introduction. *Global Change Biology* 3(Suppl. 1): 1-9.

Hinkel, K.M. & Nelson, F.E. 2003. Spatial and temporal patterns of active layer thickness at circumpolar active layer monitoring (CALM) sites in northern Alaska, 1995–2000. *Journal of Geophysical Research-Atmospheres* 108: 81688168, DOI:10.1029/2001JD000927, 2003.

Hollister, R.D., Webber, P.J. & Bay, C. 2005a. Plant response to temperature in northern Alaska: Implications for predicting vegetation change. *Ecology* 86: 1562-1570.

Hollister, R.D. 2003. *Response of Tundra Vegetation to Temperature: Implications for Forecasting Vegetation Change.* Ph.D. Thesis. East Lansing, Michigan, USA: Michigan State University.. 385+XXIV pp.

Hollister, R.D., Webber, P.J., Nelson, F.E. & Tweedie, C.E. 2006. Soil thaw and temperature response to air warming varies by plant community: Results from an open-top chamber experiment in northern Alaska. *Arctic Antarctic and Alpine Research* 38: 206-215.

Hollister, R.D., Webber, P.J. & Tweedie, C.E. 2005b. The response of Alaskan arctic tundra to experimental warming: Differences between short- and long-term responses. *Global Change Biology* 11: 525-536.

Marion, G.M., Henry, G.H.R., Freckman, D.W., Johnstone, J., Jones, G., Jones, M.H., Lévesque, E., Molau, U., Mølgaard, P., Parsons, A.N., Svoboda, J. & Virginia, R.A. 1997. Open-top designs for manipulating field temperature in high-latitude ecosystems. *Global Change Biology* 3(Suppl. 1): 20-32.

Molau, U. (ed) 1993. *International Tundra Experiment (ITEX) Manual*. Copenhagen, Denmark: Danish Polar Center. 29+XV pp.

Nelson, F.E., Outcalt, S.I., Brown, J., Hinkel, K.M. & Shiklomanov, N.I. (1998). Spatial and temporal attributes of the active-layer thickness record, Barrow, Alaska, U.S.A. *Proceedings of the Seventh International Conference on Permafrost*. Québec: Centre d'études nordiques, Université Laval, Publication No. 57: 797-802.

Ng, E. & Miller, P.C. 1977. Validation of a model of the effect of tundra vegetation on soil temperatures. *Arctic and Alpine Research* 9 (2): 89-104.

Walker, D.A., Jia, G.J., Epstein, H.E., Raynolds, M.K., Chapin, F.S., III, Copass, C., Hinzman, L.D., Knudson, J.A., Maier, H.A., Michaelson, G.J., Nelson, F., Ping, C.L., Romanovsky, V.E. & Shiklomanov, N. 2003. Vegetation-soil-thaw-depth relationships along a low-Arctic bioclimate gradient, Alaska: Synthesis of information from the ATLAS studies. *Permafrost and Periglacial Processes* 14: 103-123.

Walker, M.D., Wahren, C.H., Hollister, R.D., Henry, G.H.R., Ahlquist, L.E., Alatalo, J.M., Bret-Harte, M.S., Calef, M.P., Callaghan, T.V., Carroll, A.B., Epstein, H.E., Jónsdóttir, I.S., Klein, J.A., Magnusson, B., Molau, U., Oberbauer, S.F., Rewa, S.P., Robinson, C.H., Shaver, G.R., Suding, K.N., Thompson, C.C., Tolvanen, A., Totland, Ø., Turner, P.L., Tweedie, C.E., Webber, P.J. & Wookey, P.A. 2006. Plant community responses to experimental warming across the tundra biome. *Proceedings of the National Academy of Sciences of the United States of America* 103: 1342-1346.

Flat Loop Evaporator Thermosyphon Foundations: Design, Construction, and Performance in the Canadian Permafrost Regions

Igor Holubec
I. Holubec Consulting Inc.
John Jardine
Arctic Foundations of Canada Inc.
Bill Watt
Arctic Foundations of Canada Inc.

Abstract

Climate change is rapidly warming permafrost in the Arctic, with the result that the traditional sand-slurry piles foundation may not be applicable for new structures with a design lifespan of 50 years or so. One foundation design that may be suitable for the warming trend of permafrost is the thermosyphon foundation design with flat loop evaporator pipes. There is limited published information on the design and performance of this foundation. To address the above points, the performance of several thermosyphon foundations with horizontal evaporator piping at several locations with varied climate conditions, foundation designs, and construction history is presented. Thermosyphon foundations presented herein are all located in Canada in Inuvik, NT, Iqaluit, and Pangnirtung, NU, and Kuujjuaq, QC. Mean annual air and ground temperatures are given for these projects along with design, construction schedule, and ground-temperature changes.

Keywords: flat-looped; foundation; performance; permafrost; thermosyphon.

Introduction

The design and construction of foundations for buildings is a challenge in permafrost with high ice content. The heat from the buildings may warm and thaw the frozen ground resulting in settlement of building; jacking of piles in raised buildings due to the annual freezing of the active layer; and settlement of piles due to creep of high ice-rich soils. There are limited windows for construction during the year, and a construction schedule is influenced by the availability of materials and equipment. Finally, the site and drainage conditions may change due to the construction that may impact the thermal conditions of the site.

The challenges have been increased by climate warming that is rapidly increasing the ground temperature in Arctic regions. The most recent Intergovernmental Panel on Climate Change (IPCC 2007) made the following statements: a) warming of the climate system is unequivocal; b) average Arctic temperatures increased at almost twice the global average rate; and c) temperatures at the top of the permafrost layer have generally increased since the 1980s in the Arctic by up to 3°C. Global air temperature increases since 1975 to 2001 and the future changes predicted by various models are shown in Figure 1. This figure illustrates two points that should be considered in the design of future foundations in permafrost: a) air temperature has increased appreciably since about 1975, and b) this rate of temperature increase will likely continue to about 2100.

Holubec (2007) looked at the mean annual air temperature (MAAT) records at 24 weather stations across the Canadian permafrost regions to obtain MAAT and establish the warming rate at these stations from 1985 on. Data were interpreted by means of linear trend lines to smooth out the MAAT variations from year to year. This provides an estimate of the present mean climate warming rate and allows determining MAAT for a specific year over the next 100 years. Mean annual ground temperatures (MAGT) were estimated for the same locations by assuming that the MAGT was 4.4°C warmer than the MAAT (Smith & Burgess 2000). Results grouped into four general Canadian areas with permafrost are given in Table 1.

Results in Table 1 indicate that permafrost will warm significantly and will start to thaw in most of Canada's mainland permafrost region in less than 50 years, which is the normal design period for new buildings.

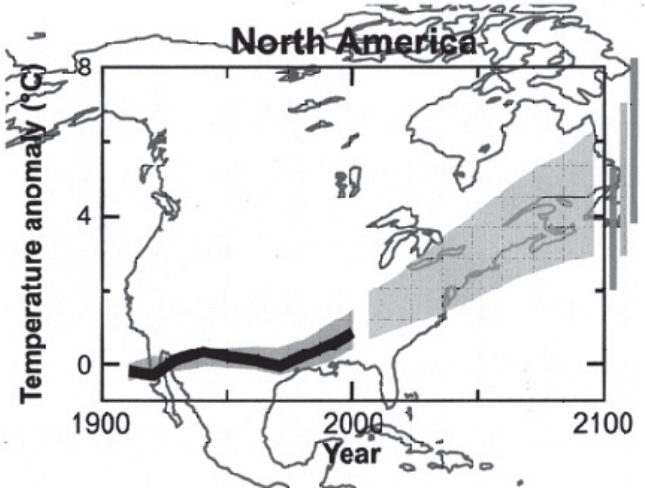

Figure 1. Global air temperature changes (IPCC Climate Change 2007: The Physical Science Basis).

Table 1. Climate conditions across Canadian Arctic in 2006.

Region [a]	MAAT [b] deg C	MAGT [b] deg C	Warming rate [c] deg C/10years
Western Arctic	- 3 to -9	1 to -5	0.7
Central Mainland Arctic	-9.8	-5.4	1.1
Eastern Arctic	-5.8	-1.4	1.7
Arctic Islands	-14.1	-9.7	0.9

a) Results based on average of 3 to 4 climate stations in each Region. b) MAAT & MAGT in 2006. c) Warming rate since 1985

The MAGT's at Inuvik, NT, and Iqaluit, NU, were at about -3.0°C in 2006. These are in general agreement with ground-temperature measurements. The -3°C is the ground temperature at which Johnston (1981) suggests that a passive cooling system should be considered for building foundations. The fact that most of the Canadian mainland permafrost region is in the range of 0 to -5°C and the climate warming rate is about 1°C every decade suggests a cooling system should be considered for building foundations.

Flat Loop Thermosyphon Design

Thermosyphon cooling is a passive thermal system that was first used in Alaska in 1960. Its benefit was clearly demonstrated on the Alaska pipeline, where over 120,000 thermosyphon tubes were installed within pipe piles (Heuer et al. 1985). Thermosyphon is a closed pipe, charged with a gas that is maintained in two phases: liquid and gas.

A thermosyphon continuously transfers heat during winter by evaporation and condensation of a liquid and gas, respectively. Heat transfer occurs when the top of the tube (radiator/condenser) is in an environment colder than the bottom part of the tube (evaporator) located in the ground. A vertical thermosyphon design, normally called thermopile/thermoprobe, expanded into sloped evaporator thermosyphon in 1978; and then in 1994, the flat loop thermosyphon design evolved. The three thermosyphon designs used in building foundations are illustrated in Figure 2.

Brief descriptions of the three designs are:

a) Buildings are supported on thermopiles with a 0.6 m to 1 m air space between the ground and building.
b) Conventional sloping evaporator (CSE) has an evaporator-condenser pipe that slopes beneath the building. The slope allows the condensate to flow to the bottom of the pipe. The building rests on a granular pad, and the evaporator pipes are covered with insulation to retard heat flow into the ground.
c) Flat looped evaporator (FLE) has a looped pipe (evaporator pipe) beneath the building that connects to a larger-diameter riser that functions as the condenser. Evaporator pipes are installed within a granular pad and covered with insulation and granular bedding. The building may be supported directly on the insulation or columns resting on footings on the bedding.

The principle of the flat looped evaporator thermosyphon is illustrated in Figure 3. The FLE design is a relatively recent development (Yarmak & Long 2002). Its performance was tested during the winter of 1993–1994 in Winnipeg, where it was observed to be 1.4 more efficient that the CSE. The FLE started to be installed in 1994 in Alaska and Canada.

The use of the FLE has been much greater in Canada than in Alaska because of different availability of access. The prevalent thermosyphon foundation design in Alaska is the thermopile because of ready access in most locations for large equipment to drill the large holes for these piles. The FLE design is more common in Canada because of the smaller weight of material that needs to be transported to the site and requires only small equipment for installation. Furthermore, the FLE protects a large building footprint at relatively low installation cost.

Since 1994 some 80 FLE systems have been constructed in Canada. Of these, 10 FLE have been placed at the bottom of dams to keep the foundation frozen and 70 FLE under buildings. The FLE system has been used in two configurations: either below slab-on-grade, where the lower building is founded on a gravel/insulation/evaporator pipe system, or the base of the building has a crawl-space that is followed by the gravel/insulation/evaporator pipe system. The majority of FLE have the buildings supported on the slab grade-on design.

The two foundation systems have different requirements for the installation of water and grey water pipes. In the slab-on-grade design, the services are installed in insulated conduits or utilidors below the floor slab. In the crawl-space design; the services are hung from the floor beams. The slab-

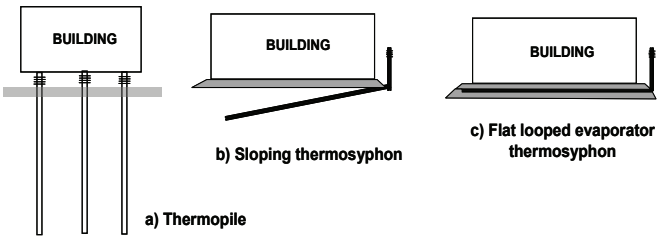

Figure 2. Three thermosyphon designs.

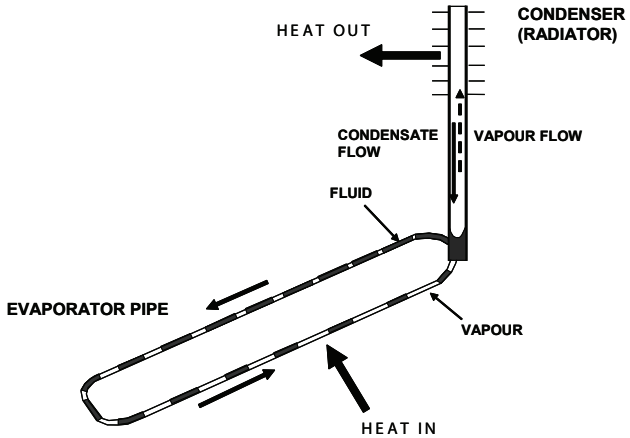

Figure 3. Operation of a flat looped thermosyphon.

on-grade may make repairs or changes to the services more difficult.

The foundation of the flat looped thermosyphon system consists of following basic components: a) 1- to 2-m thick compacted gravel pad; b) evaporator pipes; c) 150 mm bedding below and above the pipes; d) 100 to 200 mm rigid insulation; and e) a vertical radiator. A typical layout of the evaporator pipes and the location of the radiators for a flat looped thermosyphon installation is shown in Figure 4.

Performance

Only limited-performance information is available, because many installations are small buildings constructed on slab-on thermosyphon foundations. Due to the small size of the buildings and the remoteness of the sites, the installations are poorly monitored. Difficulties of the foundations are only noticed if drywalls in the building start to crack or if it is difficult to open or close doors. It appears that the majority of slab-on-grade thermosyphons are working well by the small number of known complaints.

Information on the facilities, their locations, temperatures at time of installation, and type of foundation discussed herein are given in Table 2.

Aurora College

The best performing flat looped thermosyphon foundation, with no problems and having ground-temperature records, is the Aurora College in Inuvik constructed in 2002. This is a slab-on-grade installation with a thick granular pad below the evaporator pipes and good surface drainage control. The natural ground before construction consisted of 0.5 m of granular fill, followed by nearly 2 m of peat and highly ice-rich soil with numerous ice lenses. A reference ground-temperature cable indicates the MAGT to have been about -2.5°C in 2002.

The native ground was excavated to about 3 m and replaced with compacted non-frost susceptible granular fill. Evaporator pipes were installed within a bedding layer and covered with 100 mm rigid insulation. The evaporator pipes were spaced at about 0.8 m. The excavation and granular backfill were completed in May 2002. This was followed by installing the thermosyphon system, charging it with carbon dioxide, and covering the evaporator pipes with insulation and about 1.25 m granular. This was completed in early June. Ground temperature performance from June 2002 to July 2003 is shown by means of ground-temperature profiles in Figure 5.

Ground-temperature profiles illustrate that the granular foundation started to cool right after it was covered with insulation and about 1.2 m of gravel. The thermosyphons started to cool and freeze the granular fill and natural ground below the evaporator pipes in mid-October and completed the conversion of all pore water to ice early in December. The coldest temperature at 6 m of -4.4°C was reached in May 2003; this warmed to -2.3°C on December 9, 2003. The warmest temperature at the base of the evaporator pipes (depth 0 m), -0.2°C, was reached in mid-September 2003.

One set of ground temperatures measured in September 2007 showed the ground temperature at the evaporator pipes and at 6 m depth to be -0.2°C and -3°C, respectively. The first temperature indicates the maximum ground temperature reached in 2007. However, the second is not representative of the MAGT because data for a whole 12 months is not available.

Inuvik Hospital

This case history has several aspects that are of interest. This is a flat looped thermosyphon foundation with a heated crawl space. The base of the foundation was excavated about 2 m below the ground surface and backfilled with 0.5 m granular fill. The evaporator pipes were installed within 300 mm of bedding and subsequently covered with 200 mm of rigid Styrofoam insulation. The insulation was covered with a membrane liner and 19 mm cement boards to protect the liner. Height from the cement board to the base of the main floor slab is about 1.9 m. The base of the crawl space is about 1 m below the outside ground level. Finally, the excavation between the natural ground and basement wall was backfilled with free draining granular material that was

Figure 4. Typical thermosyphon flat loop, slab on ground installation at Pangnirtung, NU.

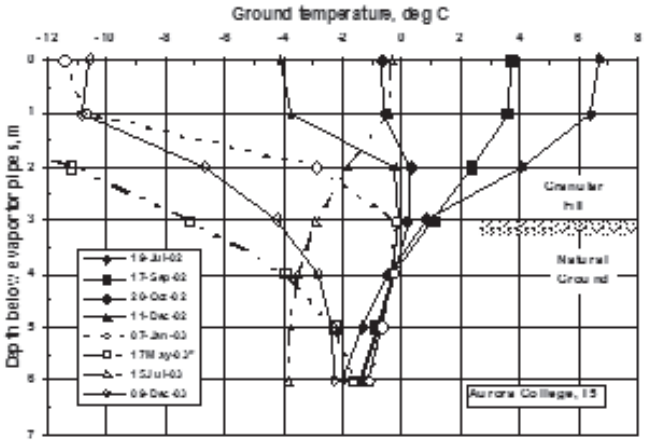

Note: Depth measured from evaporator pipe

Figure 5. Ground temperature profiles after installation of thermosyphon foundation at Aurora College.

Table 2. Information on facilities discussed in this paper.

Name	Aurora College	Hospital	RCMP Office	Pangnirtung Health Centre	Service Building	Air Terminal
Settlement Territory	Inuvik NT	Inuvik NT	Iqaluit NU	Pangnirtung NU	Kuujjuaq QC	Kuujjuaq QC
Year installed	2002	2001	2006	2006	1986	2006
Freezing Index, degree-days	4200	4200	3546	3400	3200	2568
MAAT °C @ installation	-7.5	-7.5	-7.3	-6.7	-5.2	-3.5
Estimated MAGT, °C	-3.1	-3.1	-2.9	-2.3	-0.8	+0.9
Insulation thickness ,mm	100	200	150	150	100	150
MAGT @ evaporator pipes, °C	-0.1	-1.0	-1.5	-2.0	-0.1	-0.6
Avg MAGT @ ~ 5m, °C	-4.3	-4.1	-6.1	-3.0	-2.5	-1.2
Max depth of MAGT readings, m	6	5	5.85	4.8	7.8	7.6
Avg MAGT at max'm depth, °C	-4.0	-4.1	-5.8	-3.0	-1.0	-0.4
Range of MAGT at maximum drill hole depth. °C	1.3 to -7.0	2.9 to -5.4	-2.9 to -7.6	-1.7 to -5.5	-0.5 to -2.1	-0.2 to -7.6
MAGT @ 5m colder than natural ground	1.2	1.0	3.2	0.7	1.7	2.1

Notes: MAAT – Mean annul air temperature, MAGT – Mean annual ground temperature.

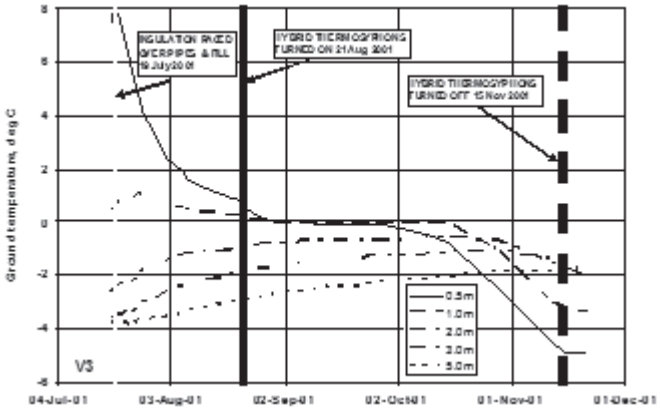

Figure 6. Ground cooling by hybrid system at Inuvik Hospital.

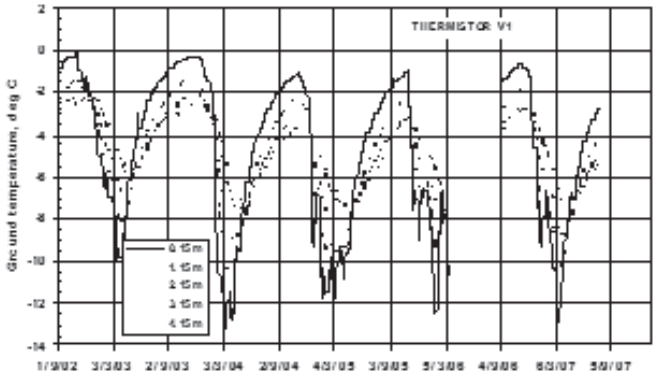

Figure 7. Ground temperature changes below evaporator pipes at Inuvik Hospital.

not covered with a low permeability soil zone to prevent surface water infiltrating the granular fill.

Excavation, granular fill, evaporator pipe, and insulation placement were completed by 19 July 2001. Since the project desired to have the ground below the thermosyphon foundation frozen as early as possible before pouring the footings, a hybrid thermosyphon system was installed. This consisted of cooling coils around the conductor pipes that were cooled by a mechanical refrigeration plant. The cooling plant was activated on 21 August 2001 and switched off permanently on 15 November 2001, when the foundations were completely frozen with a cold reserve. Ground cooling of the foundation by the hybrid system is illustrated in Figure 6. This shows that thaw within the natural ground did not exceed more than about 1 m below the base of the excavation, and the ground was completely frozen by 17 October 2001. The hybrid system was turned off on 15 November 2001, and the passive thermosyphon system started to operate.

The vertical thermistors at the hospital started to be monitored again in mid-September 2002. The changes in ground temperature, at five depths from this date on, are shown in Figure 6.

Graphs presented in Figures 7 and 8 show the warmest and coldest ground temperatures below the evaporator pipes during five years of operations.

Figure 8 illustrates that, for the first two years, the maximum ground temperature 0.15 m below the evaporator pipes was at about -0.3°C, and thereafter it varied between -0.6 and -1.0°C. At a depth of 4.15 m the ground temperature was about -2.5°C for the first two years and then cooled to about -3.5°C.

The minimum ground temperatures varied greatly just below the evaporator pipes, as expected, but steadied at 4.15 m depth after one year at about -7.5°C (Fig. 9).

Two problems developed at Inuvik Hospital. First, the mill that provided the evaporator pipes shipped defective welded A53B pipes that were found to leak slowly at the manufacturer's seam welds. This developed after the evaporator pipes were cooled when the thermosyphons started to operate, and resulted in a loss of refrigerant and

some of the thermosyphon loops having to be recharged annually. Since that installation, the installer has used only seamless A104 pipe.

The second problem was caused by surface water penetrating the surface granular zone above the evaporator pipes during the summer. This water froze in the fall when the thermosyphons start to operate and produced localized ice boils between the top of gravel and insulation.

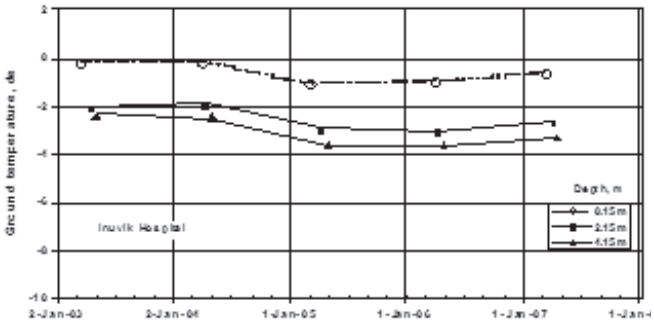

Figure 8. Maximum ground temperatures measured below the evaporator pipes.

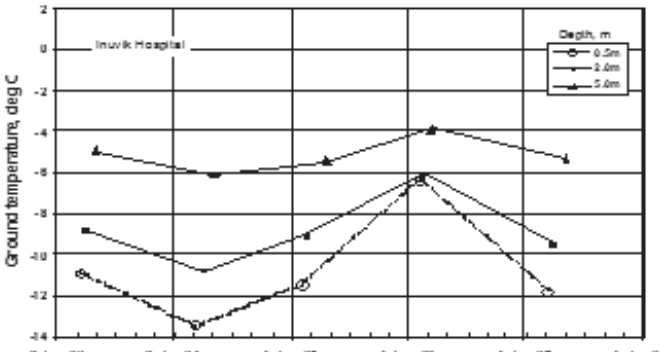

Figure 9. Minimum ground temperatures measured below the evaporator pipes.

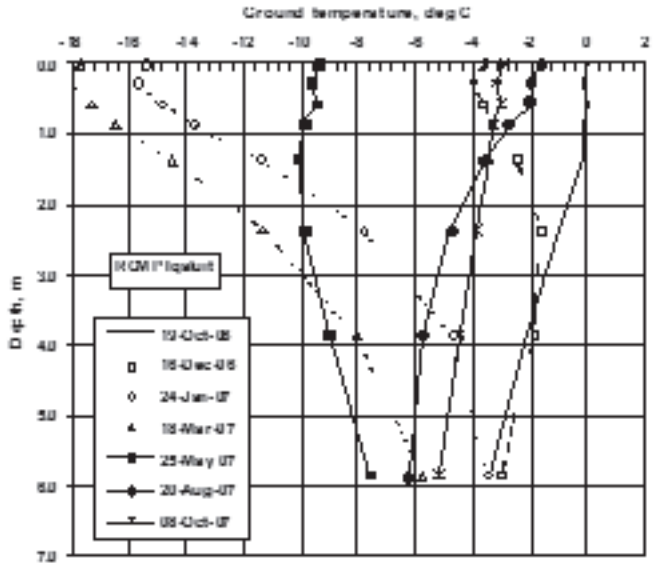

Figure 10. Ground temperature profiles after installation of thermosyphons at RCMP site, Iqaluit, NU.

Other troubled installations

Problems have been observed at three other flat loop thermosyphon installations: 1) In 1994 a FLE foundation with a crawl was constructed under a small Visitor Centre in Inuvik, NT. The central portion of the building started to settle, which is believed to be caused by locating the insulation above the base of the footing and not insulating the concrete columns that conducted heat to the frozen ground. 2) Another above-FLE foundation with crawl space constructed in Rankin Inlet, NU, in 1996 had routed extra heat from a power plant through trenches into the crawl space of the building. It is believed that the heat from the pipes and surface water infiltration through the trenches resulted in settlement of columns. Finally, 3) A Female Young Offender Facility constructed with slab-on-ground FLE foundation in Inuvik, NT, in 2001 exhibited considerable settlement under the eastern portion of the building. It appears that poor foundation cooling in this area was the result of introducing channel bends in the evaporator pipes during construction to accommodate a service piping trench. It is postulated that the four right-angle bends to accommodate the services reduced the efficiency of liquid/gas movement.

Construction scheduling

The normal practice in the construction of buildings on a FLE foundation has been to allow the FLE to operate over the first winter before putting up the structure of the building. The desire to start construction of the building the same year as the thermosyphon was built led to employing mechanical freezing during the summer (hybrid system) at the Inuvik Hospital. Three case histories of thermosyphon construction at Iqaluit, NU (RCMP), Pangnirtung, NU (Health Centre), and Kuujjuaq, QC (Air Terminal) illustrate the time required to develop permafrost with different construction schedules, MAAT, and soil type. Summary of relevant information and ground temperatures attained are given in Table 2.

The RCMP installation demonstrates the benefit in constructing the thermosyphon foundation in early summer. With this schedule, the subgrade froze completely by mid-October (Fig. 10). Since the foundation was left over the winter before adding the building, the absence of a heated slab during the first winter resulted in the coldest foundation at -6.1°C at 5 m below the evaporator pipes.

At Pangnirtung (Health Centre), the foundation with the thermosyphon and insulation was not completed until 24 August 2006. At this site complete freezing was attained in mid-December, and the building was enclosed and started to be heated mid-January 2007. In early October 2007, when thermosyphon cooling began again, the ground at the evaporator pipes was still frozen at -2.0°C, and the ground at 5 m depth was at -4°C.

The Air Terminal at Kuujjuaq differs from the previous two case histories because it has a higher MAGT and a smaller freezing index, and the soil is predominantly silt with higher water content. The thermosyphon installation at this location was completed at the end of August 2006, but was not completely frozen until mid-February 2007. It is estimated the MAGT was -1.2°C at 5 m depth.

Ground temperature regime with longer record of data is available from an earlier installation with sloped evaporator design (Service Building) in Kuujjuaq (Fig. 11). This installation was constructed in 1986, and ground temperatures are available to 1995. It needs to be noted that the MAAT was warmer in 1986, -5.5°C, and about -4.5°C in 1995 and only 100 mm of insulation was used. It is estimated that the MAGT at 5 m depth was about -2.5°C.

Conclusions

1. A majority of the 80 flat loop thermosyphon foundations have demonstrated that this design provides an economical foundation system that will function for some time even with climate warming affecting the permafrost.
2. Problems encountered in four installations were not associated with the flat loop evaporator thermosyphon concept. The problems were due to a) defective pipes provided by the mill; b)inadequate insulation around concrete columns; c)incorporating right angle channel geometry (in section) in the evaporator pipes to accommodate services; and d) allowing surface water into the evaporator granular pad.
3. The air terminal installation in Kuujjuaq shows that frozen ground can be developed, or maintained at MAAT at locations that are not conducive to permafrost. The effectiveness of the flat loop thermosyphon can be increased by increasing insulation thickness, decreasing evaporator spacing, and increasing condenser size.
4. A review of existing FLE installations show a past history of poor granular pad design and construction control, and insufficient attention has been given to surface water control around the building.

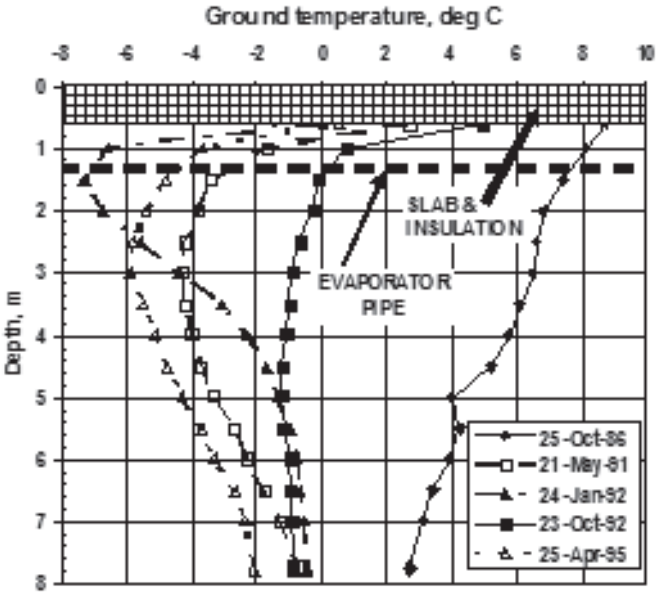

Figure 11. Ground temperature changes at FLE slab-grade at Service Building in Kuujjuaq, BC.

Acknowledgments

The authors would like to thank the Public Works and Services of Northwest Territories in providing information on the projects constructed in Inuvik, and other clients in providing ground-temperature data at their projects.

References

Heuer, C.E., Long. E.L. & Zarling J.P. 1985. Passive techniques for ground temperature control. Thermal Design Consideration in Frozen Ground Engineering. *Technical Council on Cold Regions Engineering Monogram*.

Holubec, I. 2007. Design requirements for climate warming in permafrost. *Yellowknife 2007 Symposium*. May 24, 2007 (unpublished).

IPCC 2007. Climate change 2007: The physical science basis. *Working Group I. Summary for Policymakers.* Published by WMO & UNEP, February 5, 2007.

Smith, S. & Burgess, M. 2000. Geological survey of Canada. *Open File Report 3954*, October 2000.

Yarmak, E. Jr. & Long, E.L. 2002. Recent developments in thermosyphon technology. *Proceedings of the Eleventh International Conference on Cold Regions Engineering, Anchorage, Alaska, May 2002*.

Thermal and Mechanical Erosion Along Ice-Rich Arctic Coasts

Md. Azharul Hoque
Department of Geography, McGill University, 805 Sherbrooke St. W, Montreal, QC, H3A 2K6, Canada
Wayne H. Pollard
Department of Geography, McGill University, 805 Sherbrooke St. W, Montreal, QC, H3A 2K6, Canada

Abstract

Block failure and retrogressive thaw slump activity are significant modifiers of Arctic costal morphology. This study investigates these erosional processes along ice-rich bluffs of the southern Beaufort Sea coast through a series of analytical models. Block failure potential is linked with different permafrost features like ice wedges and thermo-erosional niches. Failure often occurs along the ice wedge axis when wave erosion undercuts the base of the cliff. Model results indicate that low cliff heights tend to exhibit overturning failure, whereas high cliffs display sliding failure. Headwall retreat of retrogressive thaw slumps are also analyzed using parametric model calculations that incorporate energy balance activity to model melting ground ice. Model findings for block failure and headwall retreat are supported by field observations made in 2007 and previous studies. Using the approaches discussed in this paper, long-term morphologic patterns along Arctic coasts can be estimated using the spatial and rheological nature of permafrost materials and meteorological inputs.

Keywords: arctic coast; block failure; ice wedge; permafrost; retrogressive thaw slump.

Introduction

Coastal erosion in polar environments involves the synergistic interaction of wave-, thermal-, and gravity-induced mechanisms. The theory behind wave-induced erosion processes are reasonably well understood, and given the short open-water season that typically occurs in the Arctic, the magnitude of these effects are thought to be limited. However, the roles of morphologic and climatic coastal erosion processes are not as clearly understood. For example, field evidence indicates that mass wasting processes can occur almost year-round through gravity-driven processes, as large sediment blocks have been observed resting on sea ice as well as within shallow water. Similarly, thermal erosion processes, such as thermokarst, are readily observed when solar radiation raises ice-rich sediment surface temperatures above 0°C in spite of sub-0°C ambient temperatures. Ice-rich bluffs along the Yukon north coast display rates of coastal retreat that cannot be explained by wave action alone. The literature frequently refers to block collapse and retrogressive thaw slump activity as significant coastal erosion processes (Aré 1988, Walker 1988).

In this paper, we examine the potential role of two non-wave related erosional processes: block failure and thermokarst. The mechanics of block failure are studied through analytical models. The safety factor approach to slope-stability analysis is based on a series of widely recognized analytical and numerical solutions (Carson 1971, Chowdhury 1978). In this study, we apply different failure planes and mechanisms for a range of permafrost rheological characteristics, specifically exploring the role of ice wedge and thermo-erosional niche development in block failure. Strength parameters related to ice content and temperatures for coastal bluffs are then used to predict the failure potential for site-specific conditions. Additionally, we analyze the thermal erosion of exposed ground ice in retrogressive thaw slump headwalls through a computational model based on energy balance. Solar radiation and heat flux components are calculated to quantify the ablation of exposed ground ice as well as headwall retreat. The sensitivity of various factors affecting thermal and mechanical erosion of ice-rich coastal cliffs is examined. The complex processes of block failure and retrogressive thaw retreat of frozen cliffs are examined in a series of numerical solutions for a range of input conditions. We also discuss the implications of climate change on block failure and retrogressive thaw slumps and how the findings of this study can be used to predict long-term associated morphologic change under these conditions.

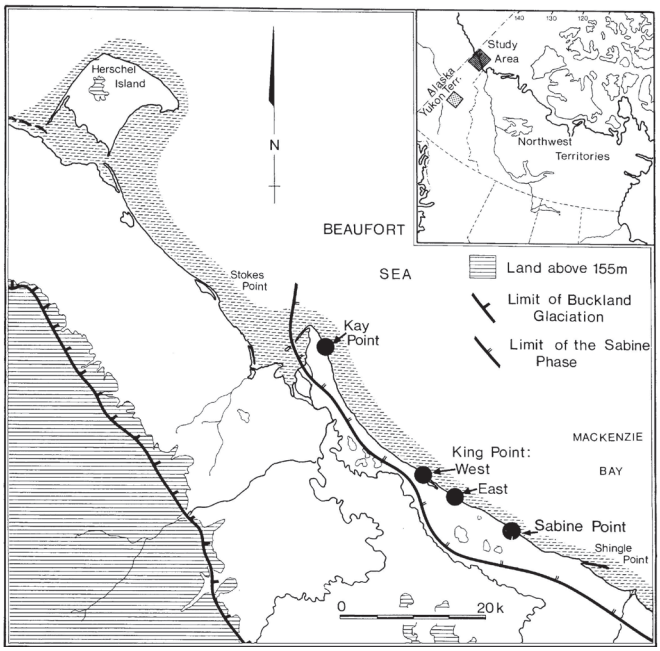

Figure 1. Study area: southern Beaufort Sea Coast.

Study Area

Our study focuses mainly on the southern Beaufort Sea coast (Fig. 1). The Beaufort Sea and its coastal region are the focus of considerable interest for a number of reasons, including human history, land claims, potential oil and gas development, permafrost and ground ice characteristics, and climate change. Extensive segments of the Beaufort Sea coast are characterized by bluffs ranging from 3–30 m in height (Solomon 1995). A previous study near King Point on the Beaufort Sea coast found an apparent spacing of modern ice wedges extending up to 15 m (Harry et al. 1985). This study also reported that most wedges have minimum heights between 4.5 m and 6.0 m. Other studies have described ground ice exposures and thermokarst activity (de Krom & Pollard 1988). Numerous recent block failures and active retrogressive thaw slumps were observed in this area during reconnaissance in 2007.

Block Failure

Model description

Two key features cause block failure along Arctic coasts: 1) the occurrence of horizontal thermo-erosional niches at the base of a bluff, and 2) the presence of ice wedges in backshore permafrost. Block failure is initiated by the development of an underlying niche, while ice wedge geometry determines the block size. The distance between two ice wedges along the coastline determines the length of the block. Figure 2 shows a two-dimensional cross section of a cliff with an ice wedge and horizontal niche. The cliff is characterized by H_c (cliff height), x_n (horizontal depth of the niche), z_n (height of the niche at the cliff face), and x_w (distance of ice wedge from the cliff face).

As a niche is formed at the base of a cliff, the toe of the cliff shifts from its initial position *P* to the new position *O*. According to the Culmann method of slope stability, the failure surface is a plane passing through the toe of the slope (Carson 1971). Following Culmann's assumption, Carson (1971) showed that the potential failure plane is inclined with an angle $\theta = (\alpha/2+\phi/2)$, where α is the slope angle of the cliff face and ϕ is the angle of internal friction of soil materials. In the areas where ice wedges are present, failure usually occurs along the ice wedge (Walker 1988). When an ice wedge and a thermo-erosional niche both are present, there are two possible modes of block failure: sliding and overturning.

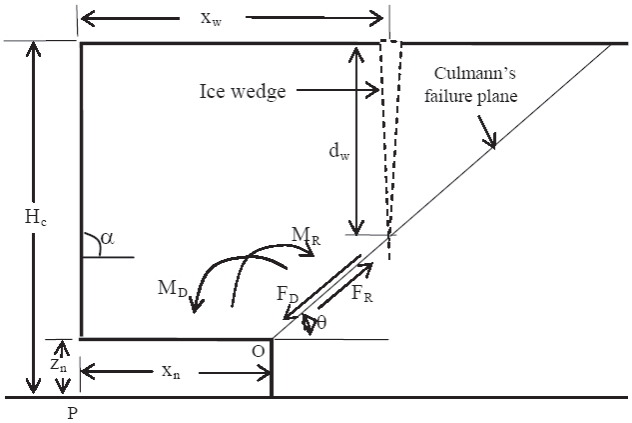

Figure 2. Two-dimensional cross section of a vertical cliff.

Sliding failure occurs when a block of frozen soil slides down the cliff on a relatively planar surface. The sliding mass is assumed to translate as a rigid body down the surface; it does not undergo rotation. When we apply a static balance of forces, the factor of safety against sliding is then defined as the ratio of resisting force to driving force. The driving force consists of the downslope component induced by weight, and the resisting force is the shear strength existant along the failure plane. The latter is comprised of two components: (1) cohesive strength of the soil, and (2) frictional forces derived from the angle of internal friction and the weight component perpendicular to the shear plane. If F_D is the driving force and F_R is the total resisting force, then the factor of safety against sliding is expressed as:

$$F_S = F_R / F_D \quad (1)$$

On the other hand, the cantilever action of the overhanging bluff induces an overturning moment (M_D) at the toe of the bluff. The resisting moments (M_R) are due to the weight of landward portion of the block and to the tensile strength (f_t) of the ice-rich permafrost soil. Overturning failure occurs if the overturning moment exceeds the resisting moment. In this case, the factor of safety against overturning is expressed as:

$$F_O = M_R / M_D \quad (2)$$

Strength of permafrost soils

The long-term strength of perennially frozen soils is of great importance in the evaluation of bluff stability. The strength of a frozen soil depends on its temperature, moisture content, mineral composition, and structure (Tsytovich 1975). Ground ice acts as cement in frozen soil; hence the widely used term "ice bonded." Temperature impacts ground ice physical properties, and therefore, in cases where ice contents are high, it influences soil strength. Tsytovich (1975) reported that the long-term compressive strength of frozen ground strongly depends on negative temperatures and can be expressed as:

$$\sigma_c = a + b(\theta)^n \quad (3)$$

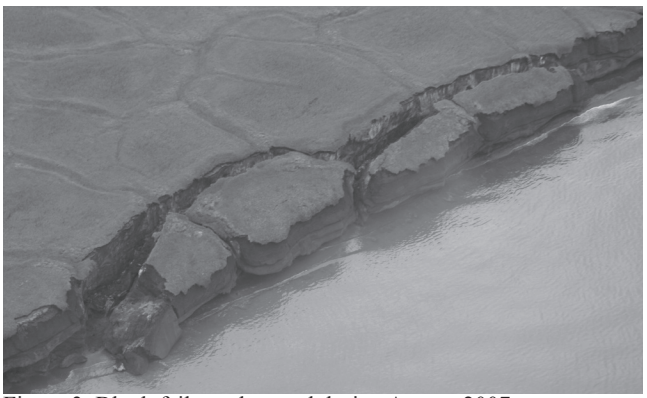
Figure 3. Block failure observed during August 2007.

where, *a*, *b,* and *n* are empirical parameters that depend on frozen soil types and θ is the absolute value of the negative temperature.

Long-term cohesion is expressed as $c = \sigma_c / 3^{0.5}$ (Vyalov 1966). There is limited information on long-term tensile strength of frozen soils, with the majority of available information related to compressive strength. The tensile strength of a frozen soil is substantially lower than its compressive strength (by a factor of 2–6) (Tsytovitch 1975). Based on Vyalov's experiment, Tsytovitch (1975) reported the long-term tensile strength for soils ranging from 30–180 kPa with temperature ranges of -0.2°C to -4.6°C.

Model calculations and discussions

For a given set of rheological conditions, block failures will be governed by the wave-eroded niche depth as well as the depth, location, and orientation of ice wedges. Aerial surveys along the Yukon coast revealed that failure usually occurs within the ice wedge (Fig. 3). Accordingly, the present study includes ice wedges as part of the block failure analysis. In this case, the ice wedge is assumed to have a recent thermal contraction crack and, therefore, no pressure or resisting force along the failure plane within the ice wedge. Thermal expansion pressure at the face of the ice wedge is also considered to be negligible.

Model calculations are performed for different cliff heights, ice wedge locations (distance from the bluff), and niche depths to: (1) obtain critical combinations of input parameters to induce cliff failure and (2) determine associated modes of failure (i.e., overturning vs. sliding). Permafrost soil strengths used in model calculations are based on Tsytovich's (1975) experimental results. A sample calculation using c=100 kPa, f_t=35 kPa, $\phi=20^0$, x_w=4 m indicates that cliff heights up to about 7.5 m exhibit overturning, whereas larger cliffs displayed sliding failure. Calculations using a range of input conditions show that for a given set of soil strength parameters and ice wedge distance, smaller cliffs are subjected to overturning whereas larger cliffs are subjected to sliding. The model is in general agreement with field conditions, as observed block failure in bluffs 3–6 m high were predominantly overturning-type failure. These results are supported by their mechanical nature: in smaller cliffs the sliding force exerted by the weight of soil is less than the total resisting force exerted by the cohesive strength of the soil. Therefore, block failure occurs when the niche extends to a critical distance causing overturning due to cantilever effect of the overhanging mass. The critical niche depth necessary for an overturning failure increases with the cliff height. This is because any increase in niche depth increases overturning moment (M_D) and decreases resisting moment (M_R). This agrees with the findings of Are′ (1988), in which the critical niche depth is calculated from the formula of curvature for an overhanging mass of frozen sediment.

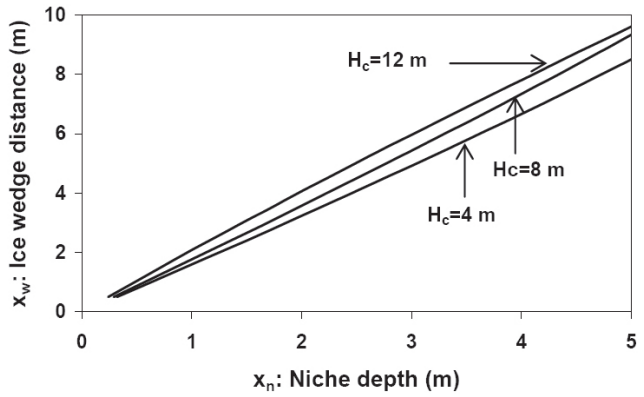

Figure 4. Ice wedge location and niche depth required for failure of cliffs of 4 m, 8 m, and 12 m heights.

Figure 4 depicts the model calculations for different cliff heights using c=200 kPa, f_t=70 kPa, $\phi=20^0$. It can be seen that, for a given cliff height and soil strengths, the relationship between niche depth and ice wedge distance is linear. It should be noted, however, that when ice wedges are closer to the shoreline, the critical niche depths are close for different cliff heights. In the present discussion, the maximum cliff height for overturning failure is denoted as H_0. Figure 5 shows the variation in H_0 with permafrost soil strength. Calculations are performed for niche dimensions x_n=2 m and z_n=1 m. Results indicate that H_0 increases with cohesive strength, meaning that higher cohesive strength increases the range of cliff heights subjected to overturning. The relationship between H_0 and cohesive strength are linear, meaning that the non-dimensional parameter given by $\gamma H_0/c$ can be considered constant for a given set of rheological properties of cliff materials. Model calculations with cohesive strength ranging from 100 kPa to 400 kPa, ϕ = 0, and an ice wedge distance x_w ranging from 2 m to 10 m show that the values of non-dimensional parameter $\gamma H_0/c$ varies from 0.95 to 1.1.

The calculations discussed above are for cases where the ice wedge depth intersects Culmann's failure plane. Calculations show that overturning can also occur for ice wedges with depths (d_w) less than the depth of Culmann's failure plane (d_{cl}). However in such cases, the ice wedge distance required for failure is less than that previously obtained. Calculations were performed for a cliff height of 10 m using niche dimensions and strength parameters as follows: z_n=1 m, x_n =2 m, c=200 kPa, f_t=70 kPa, and ϕ =20^0. Figure 6 shows variations in critical d_w that produce overturning under a varying x_w and displays that overturning can occur for a d_w less than the depth of Culmann's failure

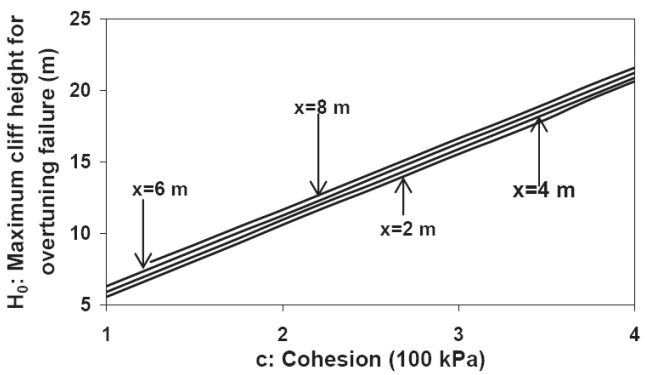

Figure 5. Ice wedge distance required for various cliff heights and material strength.

plane. In such cases, it is found that failure occurs along the plane passing through the toe of the slope and the bottom of the ice wedge and that the critical d_w for overturning increases with x_w.

Retrogressive Thaw Slumps

Model description

Retrogressive thaw slumps are a form of back-wasting slope retreat due to thawing ice-rich permafrost and are frequently observed in thermokarst landscapes. Their morphology consists of (i) a vertical headwall, (ii) a steeply inclined headscarp of ice-rich sediment, and (iii) a lobate mudflow at the base of the slump (de Krom 1989, Lantuit and Pollard 2005). Headwall retreat has previously been linked to thawing degree days (Robinson 2000) and net radiation flux (Lewkowicz, 1986b). Retrogressive thaw slumps have been the focus of several studies involving the field measurement of headwall retreat (e.g., French 1974, French & Egginton 1973, Lamothe & St Onge 1961, McRoberts & Morgenstern 1974), and additional studies have attempted to create empherical models for headwall retreat using energy flux (Lewkowicz 1986b), global radiation and degree-days (Egginton 1976), and thawing degree-hours (Kerfoot 1969). However, most of these cases are based on limited data. The present study formulates a computational model for headwall retreat using energy balance terms.

Headwall retreat can be calculated using the ablation rate of ground ice at the exposed face. The energy available for ground-ice ablation is represented by the following energy balance equation (Lewkowicz 1986a):

$$Q_m = Q_s + Q_l + Q_h + Q_e + Q_g + Q_p + Q_w \quad (4)$$

where, Q_m is energy flux available for ground ice ablation, Q_s is net shortwave radiation, Q_l is net long-wave radiation, Q_h is air convection (sensible heat), Q_e is vapor condensation (latent heat), Q_g is ground heat conduction, Q_p is the heat flux from precipitation, and Q_w represents the heat flux from water flowing down the headwall. Fluxes are measured as energy per time per unit area of the exposed surface (kJ/m^2-sec).

The summation of all sources of energy represents the total amount of energy (Q_m) available to melt the ground ice. The amount of headwall retreat *(R)* through ablation of ground ice can be expressed as:

$$\frac{dR}{dt} = \frac{Q_m}{c_i L B} \quad (5)$$

where, c_i is volumetric ice content in the headwall, L is volumetric latent heat of fusion of ground ice (kJ/m^3), B is thermal quality of the ground ice (e.g., ratio of heat required to melt a unit weight of the ground ice to that of ice at °C). The melting face consists of a mixture of ice, free water, and soil particles. The latent heat for fusion of ground ice is less than that of pure ice. This is because the relative proportion of the ice determines the thermal quality of ground ice. The relationship between ice content and volumetric latent heat reported by Lewkowicz (1986b) shows that latent heat decreases with lower ice contents.

Net shortwave radiation is an important source of ground ice ablation and consequentially, headwall retreat. The amount of energy available from the absorption of shortwave radiation for ground ice ablation is given by:

$$Q_s = (1-\alpha)\, I_i \quad (6)$$

where α is the albedo of ice-rich headwall soils and I_i is the incident solar radiation.

The longwave radiation component (Q_l) consists of the radiation emitted from the headscarp to the atmosphere (resulting in a net energy loss on clear days) and back-radiation reflected by the atmosphere and cloud cover. Longwave radiation (Q_a) from headscarp materials to the atmosphere can be expressed in accordance with the Stefan-Boltzman law:

$$Q_a = \varepsilon\sigma\, T_s^4 \quad (7)$$

where ε is the emissivity of headscarp materials, σ is the Sefan-Boltzman constant (5.735x10-11 kJ/m^{2}sK^4), and T_s is the temperature of melting face (°K).

The transmission of back-radiation (Q_b) is a complex process based on experimental data and various assumptions. Snow investigations show that the downward longwave radiation can be adequately expressed by a single air temperature function as: $Q_b = 0.67\sigma\, T_s^4$ for clear skies and $Q_b = \sigma\, T_s^4$ for

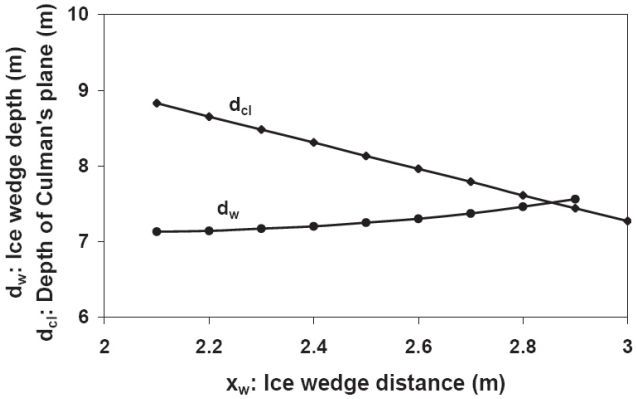

Figure 6. Critical ice wedge depth for failure under varying ice wedge distance.

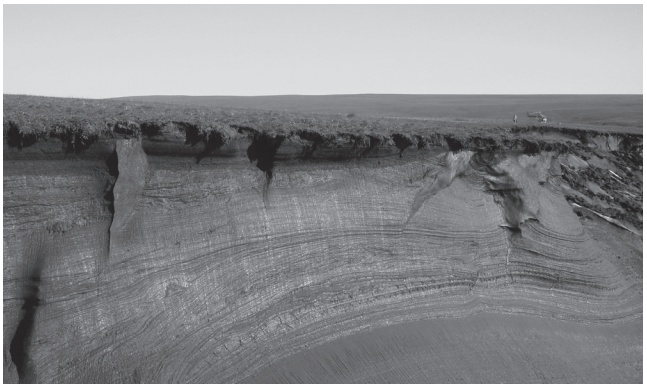

Figure 7. Headwall of an active retrogressive thaw slump on Herschel Island (photo taken on 11 August 2007).

cloud or forest cover (USACE 1998). By combining the findings from incoming and outgoing longwave radiation, the net longwave radiation can be determined using the following equation:

$$Q_l = Q_a - Q_b \tag{8}$$

Turbulent exchange, by convection (Q_h) and condensation (Q_e), varies widely depending on climate and local weather conditions. Following Gray & Prowse (1992), the sensible and latent heat transfer are expressed as:

$$Q_h = D_h u_z (T_a - T_s) \tag{9}$$

$$Qe = D_e u_z (e_a - e_s) \tag{10}$$

where D_h is the bulk transfer coefficient for sensible heat transfer (kJ/m^3 °C), u_z is the wind speed (m/s) measured upslope of the slump headwall at a chosen height, T_a is the air temperature (°C), T_s is the temperature at the melting face (°C), D_e is the bulk transfer coefficient for latent heat transfer (kJ/m^3 Pa), e_a is the vapor pressure of the air surface (Pa), and e_s is the vapor pressure at the melting ice face (Pa).

During periods of retrogressive thaw slump activity, it is reasonable to assume that T_s at melting face is 0°C and that e_s is the saturation vapor pressure at 0°C (6.108 mbar). This allows for the measurement of air temperature and vapor pressure at a single height to apply the bulk transfer method. According to Male & Gray (1981) there is wide range in variation in the bulk transfer coefficients reported by researchers, and these values are typically determined experimentally. However, Lewkowicz (1986a) considered the coefficients to be the same for both sensible and latent heat through the use of a psychrometer constant (mbar/°C), thereby allowing for the application of the bulk transfer method without obtaining field measurements for the coefficients.

Q_g is very small compared to the overall energy budget (USACE 1998). Using the measured ground temperature gradient, ground heat flux can be calculated by solving the one-dimensional, steady state conduction equation:

$$Q_g = -k\,(dT_g/dx) \tag{11}$$

where k is the thermal conductivity of the permafrost soil, dT_g/dx is the temperature gradient, and x is the depth to ground ice.

Q_p is encountered as precipitation falls upon and runs down the ice face(USACE 1998) and can be expressed as:

$$Q_p = C_p \rho_w P\,(T_r - T_s) \tag{12}$$

where C_p is the specific heat of rain (kJ/kg °C), ρ_w is the density of water (kg/m^3), P is the rainfall intensity (mm/unit time), T_r is the rain temperature (°C), and T_s is the temperature of the ice face (°C). The temperature of the rain is assumed to be air temperature or, if available, the wet bulb temperature.

As the temperature of the meltwater flowing down the headwall is close to the melting face temperature (0°C), the conductive heat transfer term Q_w in Eq. (4) is considered to be negligible compare to the overall energy budget.

Model calculation and discussions

Equation 5, supplemented by Equations 6–12, can be solved using a first-order explicit finite difference method in time to calculate the temporal variation of headwall retreat. Model calculations have applied hourly weather data obtained from King Point, Yukon Territory, Canada. Net shortwave radiation is calculated by assuming an albedo of 0.15 for the headscarp based on a regression analysis of field measurements reported by Lewkowicz (1986b). The coefficient for sensible heat transfer component (Q_h) was taken from Lewkowicz (1986b). The energy exchange components Q_e and Q_g are ignored in the present model calculations, as Lewkowicz (1986b) reported that these components are small compare to the total energy flux. Sample calculations are performed for the incoming shortwave radiation ranging from 0 to 400 W/m^2 on the sloping face of a headwall, a wind speed of 20 km/hr, and air temperatures of 2°C and 6°C. Results from model calculations are provided in Figure 8. For a given incoming shortwave radiation, higher temperatures correspond to higher retreat rates, which are due to the melting component of Q_h. Model calculations are on the same order of magnitude reported by other studies in the Arctic (e.g., Lewkowicz 1986a, 1986b).

Headwall retreat calculations were undertaken using data from King Point, Yukon Territory, over a 60-day

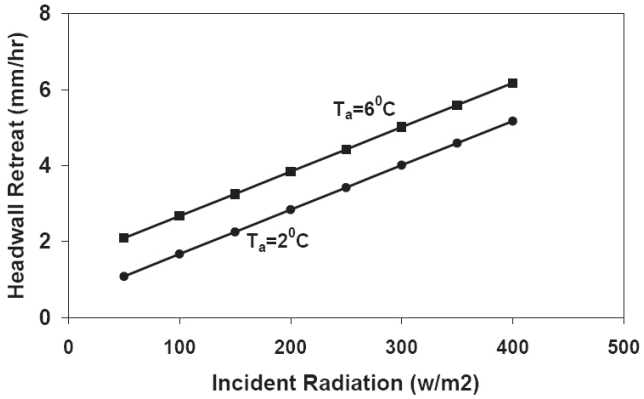

Figure 8. Headwall retreat rates for 2°C and 6°C under different incoming shortwave radiation.

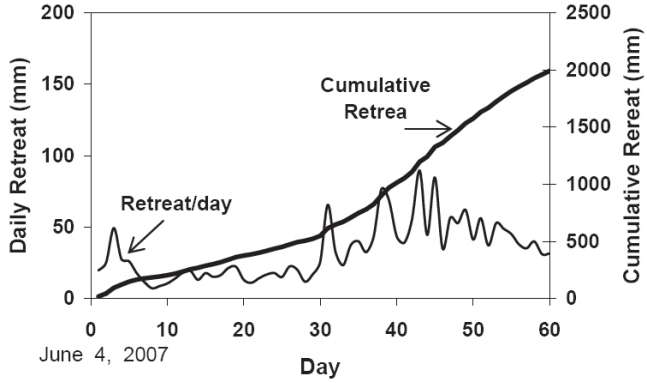

Figure 9. Calculated cumulative retreat using meteorological data at King Point.

period beginning June 4, 2007. Estimated values of daily and cumulative retreat are shown in Figure 9. July retreat is higher than that for June in response to increased solar energy and air temperatures. The calculated values of 34 mm and 90 mm of retreat for average and maximum daily retreat and 2 m of cumulative retreat over a 60-day period is an excellent average approximation of observed retrogressive thaw slump activity in this region.

Concluding Remarks

The present study provides computational models for two important erosion processes common to ice-rich Arctic coastal cliffs: (1) block failure, and (2) headwall retreat of retrogressive thaw slumps. Model calculations (supported by field observations) offer the following conclusions:

a) Block failure typically occurs along Culmann's failure plane, where ice wedges intersect Culman's plane. If ice wedge depth is less than the depth of Culmann's failure plane, failure occurs along the plane passing through the bottom of the wedge and the toe of the overhanging cliff.
b) Low cliffs are subjected to overturning failure, whereas the higher cliffs are subject to sliding failure.
c) In cases where ice wedges intersect the Cullman's failure plane, the maximum cliff height exhibiting overturning failure is dependent on the strength of cliff materials and can be expressed as a constant non-dimensional parameter $\gamma H_0/c$ for a given internal friction angle.
d) Headwall retreat of retrogressive thaw slump is governed by net shortwave radiation. Calculated headwall retreat based on weather data from King Point, Yukon Territories, gives an average value of 34 mm/day during summer 2007.

The block failure model is being enhanced by further quantifying the effects of ice content and ice wedge morphology. Field measurements of headwall retreat and microclimate data are being conducted for final model calibration and validation. Improvement of the thaw model will involve coupling with a slope irradiance model. Further studies relating block failure and headwall retreat are also needed to determine which process is predominant in specific permafrost regions. These models provide insight into morphological processes of Arctic coastlines and suggest potential responses to changing climate conditions by predicting changes in permafrost integrity and retrogressive thaw slump activity.

References

Are′, F.E. 1988. Thermal abrasion of sea coasts. *Polar Geography and Geology* 12(2): 87-155.

Carson, M.A. 1971. *The Mechanics of Erosion* (Monographs in spatial and environmental systems analysis). London: Pion Publisher, 174 pp.

Chowdhury, R.N. 1978. Slope Analysis. *Development in Geotechnical Engineering,* 22: Elsevier, 423 pp.

de Krom, V. & Pollard, W.H. 1989. The occurrence of ground ice slumps on Herschel Island Yukon Territory. *Musk-Ox* 37: 1-7.

French, M.H. 1974. Active thermokarst processes, eastern Banks Island, western Canadian Arctic. *Canadian Journal of Earth Science* 11: 785-794.

French, H.M. & Egginton, P. 1973. Thermokarst development, Bank Island, Western Canadian Arctic. In: *Permafrost: the North American Contribution*, *2nd International Conference*, *Yukutsk, USSR*. Washington, DC: National Academy of Sciences, Publication 211: 203-212.

Kerfoot, D.E. 1969. *The Geomorphology and Permafrost Conditions of Garry Island, N.W.T.*, Ph. D. Thesis. Vancouver, B.C.: The University of British Columbia.

Harry, D.G, French, H.M. & Pollard, W.H. 1985. Ice wedge and permafrost condition near King Point, Beaufort Sea Coast, Yukon Territory. In: *Current Research, Geological Survey of Canada* 85 (1A): 111-116.

Lamothe, C. & St Onge, D.A. 1961. A note on a periglacial erosional process in the Iscachen area, N.W.T. *Geological Bulletin* 16: 104-113.

Lantuit, H. & Pollard, W.H. 2005. Temporal stereo photogrammetric analysis of retrogressive thaw slumps on Herschel Island, Yukon Territory. *Natural Hazards and Earth System Sciences* 5: 413-423.

Lewkowicz, A.G. 1986a. Headwall retreat of ground-ice slumps, Banks Island, Northwest Territories. *Canadian Journal of Earth Sciences* 24: 1077-1085.

Lewkowicz, A.G. 1986b. Rate of short-term ablation of exposed ground ice, Bank Island, Northwest Territories, Canada. *Journal of Glaciolog* 32 (112): 511-519.

Male, D.H. & Gray, D.M. 1981. Snowcover ablation and runoff. In: D.M. Gray & D.H. Male (ed.), *Handbook of Snow: Principles, Processes, Management and Use*. Pergamon Press, 360-436.

McRoberts, E.C. & Morgenstern, N.R. 1974. The stability of thawing slopes. *Canadian Geotechnical Journal* 11: 447-469.

Robinson, S.D. 2000. Thaw slump derived thermokarst near Weather Creek, Ellesmere Island, Nunavut. *Geological Survey of Canada Bulletin* 529: 335-345.

Solomon, S.M. 1995. *Impact of the September 1993 Storm on the Beaufort Sea,* Geological Survey of Canada, Atlantic Geoscience Center, Nova Scotia, Canada

Tsytovitch, N.A. 1975. *The Mechanics of Frozen Ground*. George K. Swinzow (ed.), US Army Cold Regions Research and Engineering Laboratory. New York: McGraw-Hill, 426 pp.

USACE (U.S. Army Corps of Engineers). 1998. *Runoff from Snowmelt.* Engineering Manual, No.-110-2-1406.

Vialov, S.S., Gorodetskii, S.E., Ermakov V.F., Zatsarnaya, A.G., & Pekarskaya, N.K. 1966. *Method of Determining Creep, Long-term Strength and Compressibility Characteristics of Frozen Soils*. (Technical translation 1364, National Science Library, NRC, Canada) Moscow: Nakua Publisher, 106 pp.

Walker, H.J. 1988. Permafrost and coastal processes. *Proceedings of the Fifth International Conference on Permafrost* 3: 35-42.

The 2005 Mt. Steller, Alaska, Rock-Ice Avalanche: A Large Slope Failure in Cold Permafrost

Christian Huggel, Stephan Gruber
Glaciology, Geomorphodynamics & Geochronology, Department of Geography, University of Zurich
Jaqueline Caplan-Auerbach
Geology Department, Western Washington University, Bellingham WA, USA
Rick L. Wessels
U.S. Geological Survey, Alaska Science Center - Alaska Volcano Observatory, Anchorage AK, USA
Bruce F. Molnia
U.S. Geological Survey, Reston VA, USA

Abstract

This paper describes and analyzes the exceptionally large rock-ice avalanche of 40 to 60 million m³ volume that occurred in 2005 from the south face of Mt. Steller (Bering Glacier region, Alaska), which has steep glaciers at the summit. Analysis of seismic signals revealed a series of precursory rock/icefalls and a special sequence interpreted as slip and deformation in glacier ice. Reconstruction of the thermal conditions based on regional climate and radiosonde data yielded mean annual ground surface temperatures of -10 to -15°C for the failure area. Because the slope failure was at depths of meters to decameters we also performed numerical modeling of a 2D temperature profile across the mountain. Results showed that the existence of a hanging glacier in the summit area induces a deep-seated thermal anomaly. We subsequently outline a number of processes that may be effective for slope destabilization with the given thermal conditions.

Keywords: cold permafrost; Mt. Steller, Alaska; rock-ice avalanche; seismic signals; steep glacier; thermal modeling.

Introduction

A large rock-ice avalanche of 40 to 60 million m3 occurred on 14 September 2005 from the southern flank of Mt. Steller in the Bering Glacier-Bagley Ice Field region. The initial failure from a maximum elevation of 3100 m a.s.l. involved significant volumes of both rock and ice from steep glaciers. The avalanche mass travelled for almost 10 km and was deposited on Bering Glacier. As we will show, the failure was from areas in cold permafrost conditions, with the area of failure being thermally disturbed by an overlying steep glacier. Understanding of such large slope failures is important in the context of atmospheric warming and the potentially severe consequences in case of similar events in populous regions.

Increasing temperatures can destabilize frozen rock (Gruber & Haeberli 2007). Recent studies have demonstrated that not only rock surface temperatures but also temperature distribution at depth should be considered for slope stability, and have simulated the effects of projected climate change on the thermal regimes of different mountain topography (Noetzli et al. 2007). In Alaska, atmospheric warming and a related increase of permafrost temperatures have been generally strong in the 20th century. According to borehole observations in low-land areas, permafrost temperatures in the 20th century warmed by 2–4°C by the early 1980s (Lachenbruch & Marshall 1986) and up to 2–3°C during the past two decades (Osterkamp & Romanovsky 1999, Osterkamp 2007). The rise of permafrost temperatures, however, has not been as consistent as the rise of air temperatures in Alaska, mainly because of the influence of local factors (e.g., snow cover) on the energy balance (Osterkamp 2007). Knowledge on the evolution of permafrost temperatures in Alaskan high-mountain areas is scarce.

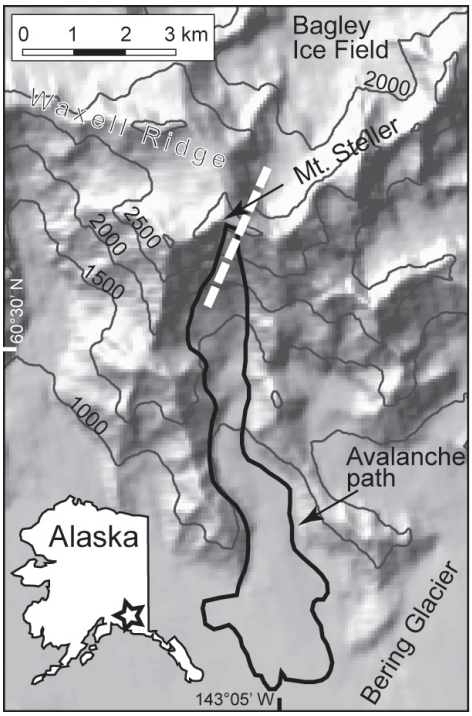

Figure 1. Map showing Mt. Steller and the extent of the 2005 rock-ice avalanche (dashed line indicates the cross section used for thermal modeling, cf. Fig. 5).

Steep glaciers in mountain walls can induce complex thermal anomalies in perennially frozen bedrock. A limited number of studies have shown that even in cold permafrost conditions, overlying glaciers can create temperatures close to phase equilibrium at the ice-bedrock interface (Wegmann et al. 1998, Haeberli et al. 1999). Because on-site access to large high-mountain walls is very limited and often impossible, investigations are typically restricted to remotely based measurements and modeling, although systematic rock temperature measurements exist in the Alps where site access is comparably easy (Gruber et al. 2004).

Seismometers have been used to study rapid mass movements resulting from slope failures (e.g., Weaver et al. 1990, Norris 1994). More recently, seismology has been used as a tool to analyze slope failure processes up to two hours before avalanche initiation (Caplan-Auerbach et al. 2004, Caplan-Auerbach & Huggel 2007), thus revealing new possibilities for the investigation of slope failures.

This study aims at reconstructing the 2005 failure and avalanche at Mt. Steller and the factors that led to this event. Although the site geology is fundamental for the slope failure we will concentrate here on the thermal conditions at the failure site and related transient effects such as atmospheric warming and overlying glaciers. More generally, we want to improve our understanding of large slope failures in steep terrain in cold permafrost and discuss the possible influence of thermal disturbance.

The 2005 Mt. Steller Avalanche

Mt. Steller (3236 m a.s.l., 60°13′N, 143°05′W) is part of the Waxell Ridge, a bedrock massif that separates the Bagley Ice Field from Bering Glacier (Fig. 1). Climatically, Mt. Steller is located close to the divide between the warmer and more humid climate of coastal Alaska and the drier and colder interior of Alaska. Geologically, the Steller S-face consists of tertiary sedimentary rocks that are layered sub-parallel to the surface slope in the failure zone.

The Waxell Ridge is a very remote area with difficult access conditions and almost only visited from the air. The 14 September 2005 rock-ice avalanche from Mt. Steller was identified because its associated seismic signals were recorded at seismometers throughout Alaska and around the world. The Alaska Earthquake Information Center reported that the event had an equivalent local magnitude of 3.8, while analysis of global long period waves yielded a magnitude of 5.2 (G. Ekstrom, personal communication, 2005). Due to the complicated access conditions of Mt. Steller, we based the reconstruction of the rock-ice avalanche on available remotely operating systems such as satellite imagery, airborne observations, and seismic recordings. We used a Landsat ETM+ scene taken a few hours after the avalanche on 14 September 2005 and photographs from a fixed-wing flight the day immediately after the event, repeated in Summer 2006 and 2007. Topographic information was derived from the USGS NED (2 arc sec, ~60 m) digital elevation model (DEM) and available topographic maps. Data from climate stations and radiosonde measurements in the region were used for temperature reconstruction at the Steller site.

Figure 2. Upper section of the avalanche failure zone. The summit hanging glacier failed on a width of ~500 m and an elevation range of ~200 m. The ice thickness is in the range of 20–30 m. Note the liquid water on the exposed rock failure surface, and the large hollow-like cavity at the right margin, possibly indicating the existence of water (photo courtesy of Ruedi Homberger).

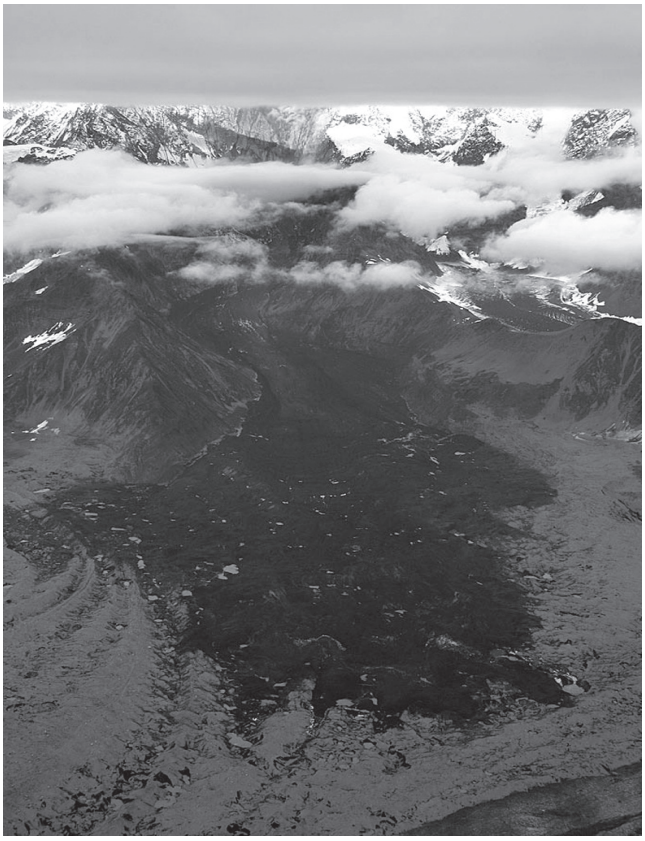

Figure 3. Photo showing the flow path through the glacial valley and the runout area of the rock-ice avalanche on the Bering Glacier For scale, refer to Fig. 1 (photo courtesy of Ruedi Homberger).

The 2005 rock-ice avalanche initiated in the S-face of Mt. Steller that has an average slope of 45° and an elevation drop of 1600 m. At the uppermost section, this face is covered by steep glacier ice which extends over the ridge to the northern side. At the time of the avalanche, the S-face of Mt. Steller was extensively covered by snow, as is typical

of mountain walls in this region. The photographs taken the day after the event show that a significant part of the hanging glacier, along with large volumes of bedrock, was involved in the avalanche (Fig. 2). We estimate that 3 to 4.5 million m^3 of glacier ice with ice thickness of 20 to 30 m failed. The failure volume of rock is difficult to assess without precise topographic data. It is evident that almost the entire S-face was affected by the avalanche, but it is not clear which bedrock areas actually failed and which ones were only affected by the passing avalanche. We estimate that bedrock failed between 2500 and 3100 m a.s.l. und crudely estimate the initial rock volume at 10 to 20 million m^3. Additionally, another 2 million m^3 of snow may have been involved in the initial avalanche.

The rock and ice mass from the Mt. Steller avalanche impacted the glacier at the toe of the S-face that extends from ~1700 m a.s.l. towards the south, and eroded several millions of m^3 of glacier ice. The avalanche then traveled on the glacier surface in a laterally confined valley for about 4 km until it reached the relatively flat surface of Bering Glacier where the mass spread and stopped on the debris-covered ice (Fig. 3). The total horizontal run out distance was 9 km, whereas the drop height was 2430 m, with the uppermost failure point at ~3100 m a.s.l. and the lowest run.out point at 670 m a.s.l. The total avalanche volume deposited on Bering Glacier can be reconstructed with an area of 4 km^2 and an average deposit thickness of 10 to 15 m using the undulating topography of the moraine ridges that were filled by the avalanche deposits as a height reference. This yields a total avalanche volume of 40 to 60 million m^3; and thus, the 2005 Mt. Steller avalanche ranges among the largest avalanches observed in recent decades worldwide. These volume estimates furthermore indicate that the initially failed glacier ice made up about 10% of the total avalanche volume, and that probably about 5 to 30 million m^3 of ice, snow, and debris were entrained along the avalanche path.

Seismic Response

Seismic recordings played a particularly important role in the detection and analysis of the 2005 Mt. Steller avalanche. First analyses of seismic signals recorded at several Alaskan stations showed spindle-shaped seismograms typical of mass movements such as rockfall and debris avalanches (Weaver et al. 1990, Norris 1994, Caplan-Auerbach et al. 2004) or snow avalanches (Suriñach et al. 2001). Based on the duration of these signals and the horizontal runout distance, we estimated an avalanche speed of ~100 m/s or possibly even more. It is not completely clear why the avalanche produced such a large seismic signal that was recorded all over the world, but the steep topography with the high S-face and the resulting strong impact at the toe of the face must have contributed to this. The large size of the seismic signal also supports our estimate that a very large mass of >20 million m^3 was involved in the initial failure

Another remarkable aspect of the seismic signal analysis

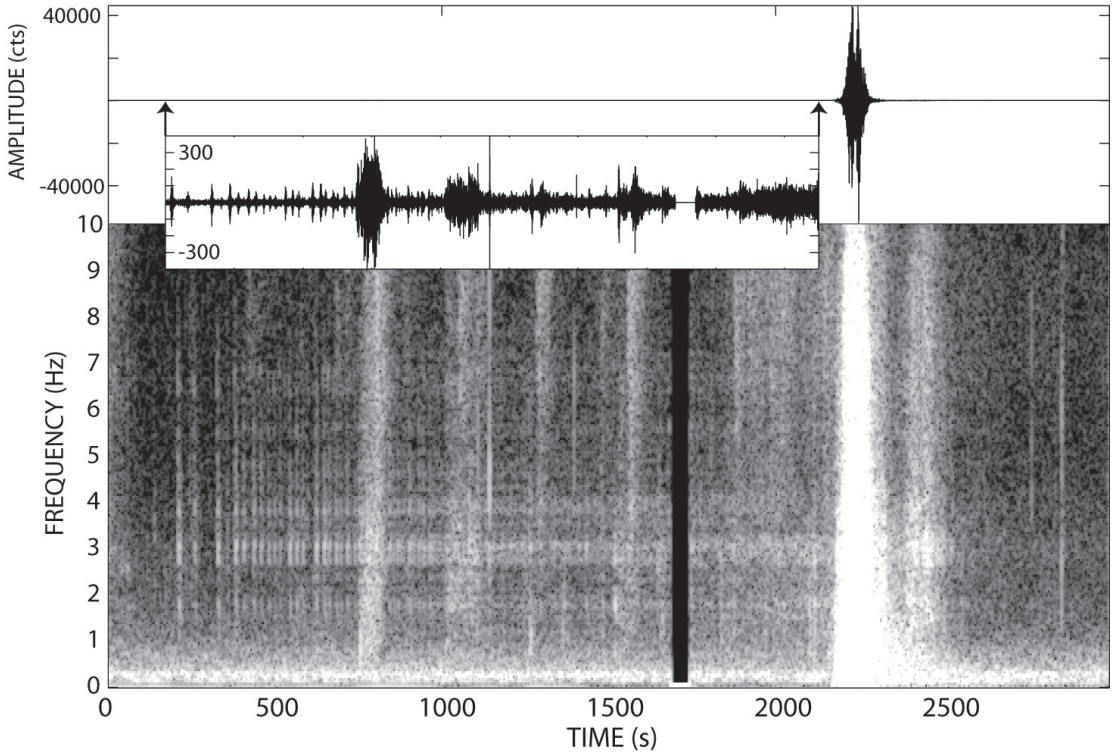

Figure 4. Seismic signal surrounding the 2005 avalanche at Mt. Steller. The top panel shows the time series of groundshaking as recorded at station KHIT, 12 km to the SW of Mt. Steller. The bottom panel is a spectrogram representing signal strength at different frequencies for the time series, with white representing stronger signals. The avalanche is visible at ~2150 seconds into the record. Because the amplitude of the avalanche is so large, a close-up of the precursory time series is shown in the inset. Note the different vertical scales on the two time series. (We acknowledge the Alaska Earthquake Information Center for operating the network and providing the data.)

at Mt. Steller was an unusual precursory seismic sequence occurring up to 30 minutes prior to failure. It should be noted that avalanches initiating in snow or rock have not been observed to exhibit precursory seismicity (Norris 1994, Suriñach et al. 2001, Caplan-Auerbach et al. 2004). Recent studies at Iliamna Volcano (3050 m a.s.l., 60.03°N, 153.09°W) in the Cook Inlet region of Alaska, however, have demonstrated that such precursory signals do occur with avalanches that initiate in ice or at the ice-bedrock interface (Caplan-Auerbach & Huggel 2007). The Mt. Steller precursory seismic signals mimic those at Iliamna in that they exhibit a series of discrete earthquakes which increase in occurrence rate for ~15 minutes before they gradually transform into a continuous ground-shaking (Fig. 4). The 15–20 minute continuous signal eventually culminates in a strong, broadband, spindle-shaped signal believed to represent the actual avalanche. At Iliamna, Caplan-Auerbach & Huggel (2007) interpreted the precursory seismic signals as deformation and slip movement in the ice with slip rates accelerating as failure approaches, and we propose the same mechanism for the Mt. Steller event. The evidence for relating the precursory seismic signals to failure in ice and not in rock supports a model in which the ice of the subsequently failed hanging glacier began to move over 30 minutes prior to failure. This, however, does not necessarily imply that the Mt. Steller avalanche initiated in ice and not in rock. Closer observation of the seismic signal (Fig. 4) shows that a number of smaller avalanches, represented by broadband, spindle-shaped signals, occurred prior to and during the precursory slip events. While the signals of these precursory slip events are well-defined at specific frequencies (i.e., at ~2, 3 and 4 Hz, Fig. 4) the smaller avalanches are identifiable by their broadband spectrum (i.e., all the way up to 10 Hz and more) at ~750, 1000, 1200 and 1500 seconds (Fig. 4). This suggests that the first stages of failure included rock, and that these initial slope failures could have triggered slip along the base of the hanging glacier. Unfortunately, because of the small (<M1) magnitude of the events and sparse nature of the regional seismic network, precise epicentral locations cannot be calculated for the precursory seismicity. However, examination of S-P times at station KHIT suggests a location at a distance consistent with a source at Mt. Steller.

Permafrost Analysis and Failure Interpretation

The purpose of this section is a first estimate of the permafrost conditions at the failure site, including the thermal regime at depth. Our thermal model presented here provides some general and basic insights but may have limitations compared to real conditions at Mt. Steller. We highlight the thermal interaction of permafrost with glacier ice and possible relations to slope stability and failure.

The reconstruction of the thermal ground conditions at the failure site was chiefly based on radiosonde data from Yakutat, located 270 km SE of Mt. Steller, and the closest regional meteorological stations (Cordova, Yakutat,

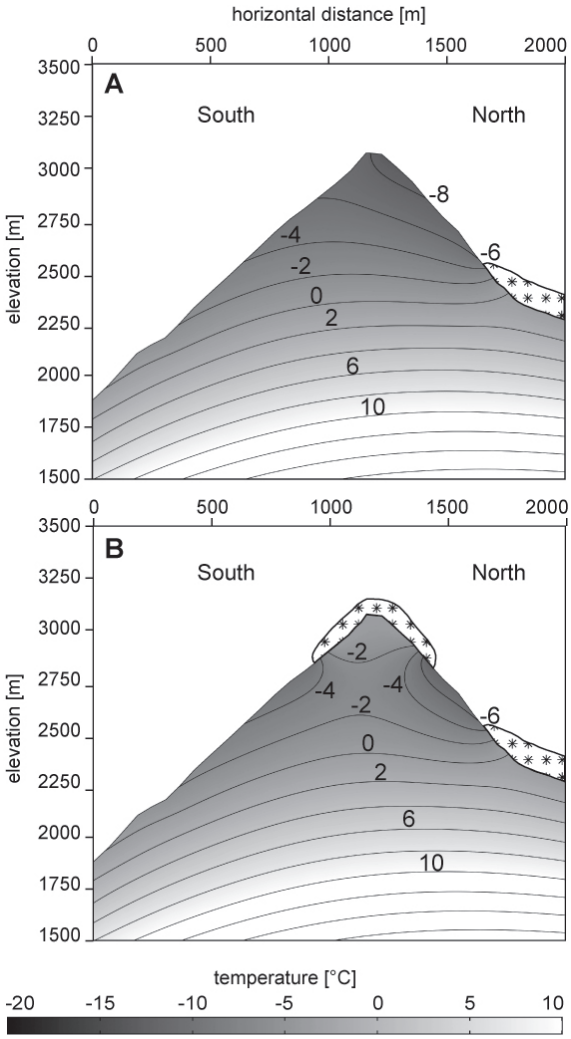

Figure 5. 2D rock temperature distribution in a N-S cross section of Mt. Steller. Distance and elevation a.s.l. are in meters, isotherms in °C. A: Rock temperature without considering overlying glaciers. B: Rock temperature with overlying glaciers (ice depth not in scale). Note the temperature differences at the summit area for A and B.

McCarthy, Chitina, Ernestine, and Thompson Pass, 3 to 760 m a.s.l.). The Yakutat radiosonde data yielded a mean annual air temperature (MAAT) of -10.5°C at 3000 m a.s.l. considering the period 1994–2007. However, vertical temperature extrapolation from the closest meteorological stations in the warmer and more humid climate of the Alaskan S-coast using a lapse rate of 0.0065°C m^{-1} derived from radiosonde data resulted in a MAAT of -15.5°C at the 3000 m a.s.l. level. Some, but not all, of this temperature difference may be explained by the fact that the MAAT extrapolated from ground-based climate stations was derived from a 50-year record and, therefore, does not fully reflect the recent warming in Alaska. For subsequent assessment and thermal modeling, we applied the radiosonde-based MAAT value since it may reasonably be assumed that the temperature record of the more homogeneous troposphere is a more accurate approximation of conditions at Mt. Steller than are local ground stations. We set the mean annual ground

surface temperature (MAGST) 3°C warmer than MAAT for the S-face and 1°C warmer than MAAT for the N-face of Mt. Steller (Haeberli et al. 2003, Gruber et al. 2004).

Our analysis of thermal conditions at Mt. Steller was concerned with the temperature distribution at the surface and at depth since the failure depth reached meters to decameters depth. Recent studies using a modeling scheme with surface temperature (Gruber et al. 2004) and 3D subsurface heat conduction calculation (Noetzli et al. 2007) have demonstrated the distribution of temperature for idealized 3D topography such as ridges. For Mt. Steller, we calculated a 2D temperature profile along a N-S cross section. Subsurface temperatures were simulated using a steady-state, two-dimensional, finite-element, heat conduction model of 10.5 km width having a base 2000 m below sea level. The upper boundary condition was given by estimated surface temperature (see above), and an inward heat flux of 0.08 W/m^2 was set at the lower boundary. The thermal conductivity for rock was assumed to be homogeneous and isotropic at 2.5 W/m/K, a reasonable average value for sedimentary rock. Noetzli et al. (2007) have shown that realistically small variations of the thermal conductivity do not significantly affect the model result. Transient model runs were not considered because the corresponding boundary conditions for this remote area are poorly known and would introduce additional uncertainty.

We first modeled a temperature profile assuming there was no summit glacier on Mt. Steller (Fig. 5A). Results show steeply inclined isotherms at the summit area with heat flux from S to N, and less inclined isotherms below the summit. Studies in the Alps have demonstrated that steep glaciers in conditions with MAAT of about -5 to -10°C have a cold-based front frozen to the ground but can show much warmer or even phase-equilibrium temperatures at the upper part (Haeberli et al. 1997, 1999). This is due to latent heat dissipation from percolating and refreezing meltwater in the snow and firn layer. For the second model, which includes the summit glacier ice (Fig. 5B), we, therefore, assumed cold ice for the front of the S-face glacier; entirely cold ice conditions for the N-face glacier; and temperate ice for the upper part of the summit ice apron, as well as for the glaciers at lower elevations of the N and S face. Model results show the deep-seated thermal anomaly induced by the glacier ice with bedrock temperatures at the summit region close to phase transition up to several decameters depth (Fig. 5B). Exposed bedrock in the S-face below the hanging glacier is several degrees colder.

Based on our assumptions, the existence of temperate ice and liquid water at the Mt. Steller summit area is possible. Relatively large amounts of liquid water on the bedrock of the formerly glacier-covered failure zone (Fig. 2) photographed a few hours after the avalanche in cloudy weather conditions likely also hint at this; however, this water could also stem from immediate snow/ice melting after the event. Irrespective of the source of liquid water (i.e., from the base of the glacier and/or subsurface rock, or from recent snow/ice melting), it is evidence of quite significant melting conditions at the ~3000 m a.s.l. level at Mt. Steller.

Despite incomplete information, we hypothesize a temperature-related destabilization, with a likely influence of the strong recent warming in Alaska. A MAAT increase of 2–4°C during the past decades could have penetrated several decameters into the bedrock; additionally, the Mt. Steller summit glacier likely experienced a transition to warmer temperatures where infiltration has become more frequent and has warmed large portions of the glacier, possibly to phase equilibrium temperatures. The Yakutat radiosonde data, in fact, is evidence that temperatures above freezing repeatedly persisted at elevations of the Mt. Steller summit in the past few years as late as September. The ~10 days prior to the 2005 failure were characterized by particularly warm temperatures above freezing; and correspondingly enhanced melting could likely have contributed to the slope failure.

A system of well-developed cracks is observable in air photos and could have experienced corresponding effects of hydrostatic pressure variations. However, the 2005 slope failure also involved large parts of bedrock at lower elevation that was not glacier-covered but was in cold permafrost conditions (Fig. 5). It is not clear which mechanisms contributed to the slope failure in this zone, but an effect of the upper warmer part is imaginable. For instance, variations of hydrostatic pressure and effective stress induced by the upper part could cause micro fractures and progressive failure in the lower part (Eberhardt et al. 2004).

Discussion and Conclusions

We have described the 2005 rock-ice avalanche from Mt. Steller in the Bering Glacier region, Alaska, which was one of the world's largest slope failures and avalanches of the past decades. We have focused on the conditions of failure, with a particular eye on the surface and subsurface thermal regime. Seismic signals contributed to an improved understanding of the failure mechanism by providing evidence of precursory rock/ice-falls and indication of deformation and slip of the overlying glacier ice. It is only recently that such processes in glacier ice prior to failure were discovered in seismic signals and more investigation is needed to better constrain the involved mechanisms.

The MAGST reconstruction at the failure zone was mainly based on radiosonde data and yielded temperatures of about -4 to -8°C. Numerical modeling allowed us to estimate the subsurface temperature distribution at Mt. Steller, demonstrating the deep-seated thermal effect of overlying steep glaciers on bed rock temperatures at depth. The radiosonde data should well reflect the recent strong warming in Alaska, and, according to these temperatures, the assumption of polythermal and temperate ice in the S-face and on the summit is reasonable. Nevertheless, there is an uncertainty in the boundary conditions of the thermal model which may range within ~2–3°C.

Our understanding of temperature-driven slope destabilization processes at mountains with permafrost is still very incomplete. So far, based on this study and a

number of recent similar slope failures (Haeberli et al. 2003, Huggel et al. 2005, Fischer et al. 2006), we conclude that the existence of steep glaciers in cold permafrost mountains is an important and quickly changing factor of slope stability.

Acknowledgments

These studies were partly supported by funds of the Swiss National Science Foundation and the USGS Mendenhall Postdoctoral Program. We very much thank R. Homberger and P.& D. Claus for providing photographs. Helpful comments by P. Deline, M. Wegmann, and the editor D. Kane are acknowledged.

References

Caplan-Auerbach, J., Prejean, S.G. & Power, J.A. 2004. Seismic recordings of ice and debris avalanches on Iliamna Volcano (Alaska). *Acta Vulcanologica* 16: 9-20.

Caplan-Auerbach, J. & Huggel, C. 2007. Precursory seismicity associated with frequent, large avalanches on Iliamna Volcano. *Alaska. Journal Glaciology* 53: 128-140.

Eberhardt, E., Stead, D. & Coggan, J.S. 2004. Numerical analysis and progressive failure in natural rock slopes - the 1991 Randa rockslide. *International Journal of Rock Mechanics & Mining Sciences* 41: 69-78.

Fischer, L., Kääb, A., Huggel, C. & Noetzli, J. 2006. Geology, glacier retreat and permafrost degradation as controlling factors of slope instabilities in a high-mountain rock wall: the Monte Rosa east face. *Natural Hazards and Earth System Science* 6: 761-772.

Gruber, S., Hoelzle, M. & Haeberli, W. 2004. Rock wall temperatures in the Alps: Modelling their topographic distribution and regional differences. *Permafrost and Periglacial Processes* 15: 299-307.

Gruber, S. & Haeberli, W. 2007. Permafrost in steep bedrock slopes and its temperature-related destabilization following climate change. *Journal of Geophysical Research* 112:F02S18, doi:10.1029/2006JF000547.

Haeberli, W., Wegmann, M. & Vonder Mühll, D. 1997. Slope stability problems related to glacier shrinkage and permafrost degradation in the Alps. *Eclogae Geologicae Helvetia* 90: 407- 414.

Haeberli, W., Huggel, C., Kääb, A., Polkvoj, A., Zotikov, I. & Osokin, N. 2003. Permafrost conditions in the starting zone of the Kolka-Karmadon rock/ice slide of 20 September 2002 in North Osetia (Russian Caucasus), *Proceedings of the 8th International Conference on Permafrost, Zürich, Switzerland, July, 2003*, *Extended Abstracts*: 49-50.

Haeberli, W., Kääb, A., Hoelzle, M., Bösch, H., Funk, M., Vonder Mühll, D. & Keller, F. 1999. Eisschwund und Naturkatastrophen im Hochgebirge. Zürich: VDF Hochschulverlag an der ETH Zürich, 190 pp.

Huggel, C., Zgraggen-Oswald, S., Haeberli, W., Kääb, A., Polkvoj, A., Galushkin, I. & Evans, S.G. 2005. The 2002 rock/ice avalanche at Kolka/Karmadon, Russian Caucasus: assessment of extraordinary avalanche formation and mobility, and application of QuickBird satellite imagery. *Natural Hazards and Earth System Sciences* 5: 173-187.

Lachenbruch, A.H. & Marshall, B.V. 1986. Changing climate: geothermal evidence from permafrost in the Alaskan Arctic. *Science* 234: 689-696.

Noetzli, J., Gruber, S., Kohl, T., Salzmann, N. & Haeberli, W. 2007. Three-dimensional distribution and evolution of permafrost temperatures in idealized high-mountain topography. *Journal of Geophysical Research* 112: F02S13, doi:10.1029/2006JF000545.

Norris, R. D. 1994. Seismicity of rockfalls and avalanches at three Cascade Range volcanoes: implications for seismic detection of hazardous mass movements, *Bulletin Seismological Society of America* 84: 1925-1939.

Osterkamp, T.E. 2007. Characteristics of the recent warming of permafrost in Alaska. *Journal of Geophysical Research* 112:F02S02.

Osterkamp, T.E. & Romanovsky, V.E. 1999. Evidence for warming and thawing of discontinuous permafrost in Alaska. *Permafrost and Periglacial Processes* 10: 17-37.

Suriñach, E., Furdada, G., Sabot, F., Biescas, B. & Vilaplana, J.M. 2001. On the characterization of seismic signals generated by snow avalanches for monitoring purposes. *Annals of Glaciology* 32: 268-274.

Weaver, C. S., Norris, R. D. & Jonientz-Trisler, C. 1990. Results of seismological monitoring in the Cascade Range, 1962–1989: earthquakes, eruptions, avalanches and other curiosities. *Geoscience Canada* 17: 158-162.

Wegmann, M., Gudmundsson, G. & Haeberli, W. 1998. Permafrost changes and the retreat of Alpine glaciers: A thermal modelling approach. *Permafrost and Periglacial Processes* 9: 23-33.